EXPLORING METABOLIC VULNERABILITY AND THERAPEUTIC POTENTIAL IN CANCERS WITH ISOCITRATE DEHYDROGENASE MUTATIONS

INGVILD COMFORT HVINDEN

DEPARTMENT OF CHEMISTRY

UNIVERSITY OF OXFORD

SUBMISSION MICHAELMAS 2022

A THESIS SUBMITTED TO THE BOARD OF THE MATHEMATICAL, PHYSICAL AND LIFE SCIENCES DIVISION AT THE UNIVERSITY OF OXFORD IN PARTIAL FULFILMENT OF THE REQUIREMENTS FOR THE DEGREE OF DOCTOR OF PHILOSOPHY

I. Abstract

Treatment of mutant isocitrate dehydrogenase 1 (IDH1) glioma remains challenging; targeted allosteric inhibitors currently provide limited clinical effect. Resistance to mutIDH1 inhibitors has also emerged in other cancers with mutant *IDH1*. IDH1 catalyses the decarboxylation of isocitrate to 2-oxoglutarate (2-OG) and concomitant reduction of $NADP^+$ to NADPH. Upon mutation, the enzyme instead reduces 2-OG to (*R*)-2-hydroxyglutarate (2-HG) with NADPH. 2-HG accumulates to high levels in cells and is thought to promote tumorigenesis by *e.g.,* disrupting DNA and histone methylation and impairing DNA repair. Altered central carbon, amino acid and lipid metabolism, as well as redox homeostasis, has been linked to expression of $mutIDH1^{R132H}$ and presence of high levels of 2-HG. Yet, the understanding of the mechanisms by which 2-HG affects metabolism, and what capacity those metabolic changes have to drive tumorigenesis, remains limited. A more detailed comprehension of the metabolic changes in mutIDH1 glioma and how they relate to 2-HG abundance would improve understanding of tumorigenesis and potentially uncover new therapeutic targets. The aim of this thesis was therefore to investigate mutIDH1 glioma metabolism by comparison to a matched wild-type (wt) IDH1 model and with metabolic inhibitors targeting the mutated enzyme or substrate availability.

The glioblastoma cell line LN18 with mutant *IDH1* expressed via lentiviral vector was compared to wtIDH1 LN18 cells and treated with mutIDH1 inhibitors (AG-120, AG-881, BAY 1436032, GSK864 and FT2102) or glutaminase (GLS) inhibitor (CB-839) to investigate mutIDH1 glioma metabolism. Anion exchange chromatography (IC) and reverse phase liquid chromatography (RPLC), both coupled to mass spectrometers (MS) were used to measure metabolites in samples. Cell viability was measured by colorimetric assay. Univariate and multivariate statistical analyses were performed to identify altered metabolites and reveal correlative relationships to 2-HG abundance. Untargeted pathways analysis was used to assess metabolic changes at the pathway level.

The abundance of 2-HG was significantly elevated in $mutIDH1^{R132H}$ LN18 cells and glutamine was the main carbon source. Amino acids and metabolic intermediates, nucleotides, lipid-related metabolites, *N*-acetylaspartylglutamate (NAAG) and B-citryl-L-glutamate (B-CG) were significantly altered in the mutant cell line. On the pathway level, amino acid

metabolism (lysine degradation, BCAA catabolism, glutamate, arginine & proline and aspartate & asparagine), butanoate & propanoate and vitamin B1 and vitamin C were significantly altered between the wtIDH1 and mutIDH1^{R132H} LN18 cells. Certain metabolites required 2-OG or NADPH for biosynthesis, while others did not, suggesting that 2-HG affected metabolism both directly (*e.g.,* competitive inhibition) or indirectly (*e.g.,* altered transcription of enzymes).

MutIDH1 inhibitors were capable of significantly decreasing 2-HG abundance in mutIDH1^{R132H} LN18 cells. AG-120, AG-881 and GSK864 were also capable of inhibiting wtIDH1; isocitrate accumulated in treated cells. AG-881 was inferior in ability to decrease 2-HG abundance and reached a maximum inhibition threshold at far lower concentration than the other three mutIDH1 inhibitors. None of the mutIDH1 inhibitors had a substantial impact on cell viability. Mutant cells treated with mutIDH1 inhibitors were metabolically more similar to wtIDH1 cells. Several metabolites correlated with 2-HG abundance. Nevertheless, it was difficult to determine the extent 2-HG abundance affected other metabolites due to concurrent inhibition of wtIDH1. GLS inhibition was assessed as an alternative treatment strategy; it indirectly decreased substrate availability by decreasing glutamate abundance. Cell viability was decreased significantly compared to treatment with mutIDH1 inhibitors. Despite 2-OG abundance decreasing, 2-HG levels were maintained. However, this effect was used to determine which metabolites were affected by 2-HG only or and which were also dependent on 2-OG.

Amino acid metabolism was suggested to be affected by competitive inhibition by 2-HG. Amino acids are key for cell proliferation by providing energy and are substrates for anaplerosis and redox-active compounds. B-CG had a particularly strong correlative relationship to 2-HG abundance and the effect was likely indirect. The function of B-CG in human metabolism is not well understood, but its proposed redox protective abilities suggest a tumorigenic role in maintaining redox homeostasis. Collectively, the experiments in this thesis revealed that 2-HG abundance correlated consistently with certain metabolic changes and that altered metabolism was due to a combination of direct and indirect effects by 2-HG. Future work should focus on the potential contributions to tumorigenesis and therapeutic potential of B-CG and amino acid metabolism in mutIDH1 glioma.

II. Declaration

The work in this thesis was carried out under the supervision of Professor James S. O. McCullagh. All work described herein is my own, unless stated otherwise, and material from other sources have been fully acknowledged. I confirm that no part of this thesis has been submitted, either partially or in full, for qualification at this University or any other institution.

In chapter 1, **section 1.1, 1.2, 1.3** and the conclusion in **section 1.6** are a modified version of a literature review published in Cell Reports Medicine [1] where I was first author. It has been reproduced here with the permission of the publisher Elsevier (Copyright © 1969, Elsevier) under a Creative Commons (CC BY 4.0) license.

Ingvild Comfort Hvinden
Balliol College, University of Oxford
Michaelmas 2022

III. Acknowledgements

I would like to thank my supervisor professor James S. O. McCullagh for taking me on as a DPhil student in your group and offering me such an interesting and challenging project. Your time, guidance and encouragement were invaluable support throughout my work. I'm grateful for everything I've had the opportunity to learn by being a part of the McCullagh group. I would also like to thank the Anne Grete Eidsvig and Kjell Inge Røkke's Foundation for Education for an Aker Scholarship, enabling me to pursue this degree.

Thank you to Dr John Walsby-Tickle for teaching me the art of tissue culture, helping me when the instruments threw fits, and answering my many questions. I would not be the analytical chemist I am today without your patience and willingness to teach me new skills. Thank you to Dr Chiara Bardella for kindly gifting the cell lines that made my work possible. Professor Christopher Schofield and Schofield group members working on the *IDH1*

mutation have provided me with all kinds of opportunities to expand my own work and knowledge, and I am grateful for the collaborations. Thank you to Dr Raphael Reinbold for including me in your research on resistance to mutIDH1 inhibitors, which led to me developing experimental methods that benefitted my other work as well.

Thank you to the members of the McCullagh group for your friendship and support. Dr Thomas Cadoux-Hudson and Dr David Hauton provided broad insight into cancer and human metabolism. Dr Judith Ngere and Elisabete Pires provided technical support, laboratory know-how and a good chat when needed. My fellow DPhils, thank you for your encouragement and willingness to discuss all matter of research questions. To the master's students past and current, thank you for keeping me on my toes and my knowledge fresh. Your eagerness to learn and develop as scientists has been inspiring. I would especially like to thank the master's students I co-supervised and who whose work pushed the study of mutIDH1 metabolism forward: Polly Thisdell, Becky Clarke and Adam Harward. Finally, I'd like to thank John, Becky and Rachel Williams for so kindly taking the time to help proofread my thesis.

My friends at Balliol college and back home in Norway have been never ending in their support and believing in me when I had my own doubts. Thank you to my parents for teaching me the importance of trying my best rather than seeking perfection. Without your love and care I would not be where I am today. Thank you to my brother and sister for their love, kind words and being only a phone call away. Finally, thank you to my partner Tor Jan. You have been my rock and put up with me through the good, the bad and the ugly during this degree. I'm forever grateful for your patience, encouragement and willingness to listen to me ramble on about experiments and data analysis.

Ingvild Comfort Hvinden

Friday January 13th, 2023

IV. Abbreviations

2-HG	2-hydroxyglutarate
2-HGDH	2-HG dehydrogenases
2-OG	2-oxoglutarate
3M2OV	3-methyl-2-oxovalerate
3PHP	3-phosphohydroxypyruvate
ABAT	4-aminobutyrate aminotransferase
ADP	adenosine diphosphate
AML	Acute myeloid leukaemia
AMP	adenosine monophosphate
AQC	6-aminoquinolyl-N-hydroxysuccinimidyl carbamate
ASNS	Asparagine synthetase
ASSC2	Acyl-coenzyme A synthetase short-chain family member 2
ATP	Adenosine triphosphate
BCAT	Branched chain amino transferase
B-CG	beta-citrylglutamate
CA	Correlation analysis
CE	Capillary electrophoresis
CNS	Central nervous system
CoS	Correlation score
CS	Citrate synthase
CSE	Cystathionine-γ-lyase
CV	Coefficient of variation
D- or LHGA	D- or L-hydroxyglutarate aciduria
dADP	Deoxyadenosine diphosphate

DC	Direct current
DERA	Deoxyribose 5-phosphate aldolase
dGDP	Deoxyguanosine diphosphate
DMEM	Dulbecco's modified Eagle's medium
DNPH1	2’-deoxynucleoside 5’-phosphate N-hydrolase 1
DR5P	Deoxyribose 5-phosphate
EASE	Expression Analysis Systematic Explorer (software application)
EC	Empirical compound
EIC	Extracted ion chromatogram
EM	Electron multiplier
FBS	Foetal bovine serum
FC	Fold change
FDA	USA Food and Drug Administration
FET	Fishers exact test
G6PD	Glucose 6-phosphate dehydrogenase
GABA	γ-aminobutyric acid
GAD-1	Glutamate decarboxylase
GBM	Glioblastoma
GC	Gas chromatography
GDP	Guanosine diphosphate
GLS	Glutaminase
GLUD	Glutamate dehydrogenase
GLUT	Glucose transporter
GOPOD	glucose oxidase/peroxidase
GOT	Glutamate oxaloacetate transaminase

GPCho	Glycerophosphocholine
GPE	Glycerophosphoethanolamine
HEK	Human embryonic kidney
HEPES	4-(2-hydroxyethyl-1-piperazineethansulfonic acid
HILIC	Hydrophilic interaction chromatography
HMDB	Human Metabolome Database
HMGCR	3-hydroxy-3-methyl-glutaryl CoA reductase
HOG	Human oligodendroglioma
HOT	Hydroxyacid oxoacid trans-hydrogenase
HRMS	High resolution mass spectrometer
IC	Ion exchange chromatography
IC50	Half maximal inhibitory concentration
ICC	Intrahepatic cholangiocarcinoma
IDH	Isocitrate dehydrogenase
IPP	Isopentenyl pyrophosphate
IQR	Interquartile range
kDA	kilo Dalton
KEGG	Kyoto Encyclopaedia of Genes and Genomes
LC	Liquid chromatography
LDH	Lactate dehydrogenase
LOOCV	Leave-one-out cross validation
LRMS	Low resolution mass spectrometer
LV	Latent variable
m/z	mass-to-charge ratio
MCT	Monocarboxylate transporter

MCTe	Multiple comparison test
MDH2	Malate dehydrogenase
ME	Malic enzyme
MeOH	Methanol
MRS	Magnetic resonance spectroscopy
MS	Mass spectrometry
mut	Mutant
MWCO	Molecular weight cut-off (filter)
NAD	Nicotinamide dinucleotide
NADP	Nicotinamide dinucleotide phosphate
NAM	*N*-acetylmethionine
NAMPT	Nicotinamide phosphoribosyl transferase
Naprt1	Nicotinate phosphoribosyl transferase 1
NHA	Normal human astrocytes
NMR	Nuclear magnetic resonance spectroscopy
Nrf2	Nuclear factor erythroid 2-related factor
NAA	N-acetylaspartate
NAAA	N-acetylated amino acids
NAAG	N-acetylaspartylglutamate
ODC	Ornithine decarboxylase
OGDH	2-oxoglutarate dehydrogenase
oxPPP	Oxidative pentose phosphate pathway
PBS	Phosphate buffered saline
PC	Pyruvate carboxylase
PC	Principal component

PCA	Principal component analysis
PCho	Phosphocholine
PDH	Pyruvate dehydrogenase
PDX	Patient derived xenograft
PE	Phosphoethanolamine
PGD	6-phosphogluconate dehydrogenase
PHGDH	Phosphoglycerate dehydrogenase
PI	Phosphatidylinositol
PLS-DA	Partial least squares-discriminant analysis
PPP	Pentose phosphate pathway
PTB	Patient tumour biopsy
RF	Radio frequency
ROS	Reactive oxygen species
RP	Reverse phase
RPMI	Roswell Park Memorial Institute
RTK	Receptor tyrosine kinase
SREBP2	Sterol regulatory element-binding protein 2
SSADH	Succinate semialdehyde dehydrogenase
TCA	Tricarboxylic acid cycle
UDP	Uridine diphosphate
UMP	Uridine monophosphate
VIP	Variable importance in projection
WHO	World Health Organisation
wt	Wild type

V. Table of contents

VI. List of figures

Figures 1.2.3, 2.5.1, 2.5.2, 2.5.3 and **2.5.4** were created with Biorender.com under a student license.

VII. List of tables

Chapter 1. Introduction

1.1. Isocitrate dehydrogenase and its role in cancer

1.1.1. The discovery of *IDH1* and *IDH2* mutations and the 'oncometabolite' *R*-2-hydroxyglutarate

Metabolic alterations are a hallmark of cancer, however, their role in tumorigenesis is not well understood [2, 3]. Point mutations in the gene for the metabolic enzyme isocitrate dehydrogenase 1 (*IDH1*) were first discovered in glioma in 2008 [4, 5] and in acute myeloid leukaemia (AML) in 2009 [6]. Analogous points mutations were also found in *IDH2* [7-9]. Now *IDH1* and *IDH2* mutations have been found in at least 20 different cancers. *IDH1* and *IDH2* mutations are prevalent in grade II and III gliomas (> 70%) and secondary glioblastomas (GBMs) (55-88%), but not primary GBMs (5-14%) [4, 5, 9-13]. The mutations are also prevalent in certain cartilaginous and bone tumours (20-80%) [14-21], AML (15-30%) [6, 8, 22-28], intrahepatic cholangiocarcinoma (ICC) (6-30%) [29-37], angioimmunoblastic T-cell lymphoma (20-30%) [38-41], sinonasal undifferentiated carcinoma (35-80%) [42-44], and solid papillary carcinoma with reverse polarity (>77%) [45, 46]. In the remaining cancer types in which *IDH1* or *IDH2* mutations are reported, the incidence rates are low (< 5%). Interestingly, with rare exceptions [10, 22, 28], mutations of *IDH1* and *IDH2* appear to be mutually exclusive [10, 13, 27]. All reported frequency rates are summarised in **Table 1.1.1**.

Table 1.1.1. Reported frequency of canonical IDH1 and IDH2 mutations in cancers and benign tumours. IDH1/2 mutations were determined using DNA sequencing and antibodies. IDH1 or IDH2 mutations other than the missense mutation causing substitution at IDH1 R132 and IHD2 R172 or R140, known as non-canonical mutations, are also listed (other mutIDH1/2). Table reproduced from Hvinden et al. [1].

Cancer type	Reported occurrence (%)			Source
	mutIDH1 (R132)	mutIDH2 (R172 or R140)	Other mutIDH1/2	
Central nervous system neoplasm				
Grade II and III glioma	> 70	5	0.3-2.3	[4, 5, 9-12, 47, 48]
Secondary GBM (grade IV)	55-88	3.4	-	[4, 5, 9, 12, 13]
Primary GBM (grade IV)	5-14	0.5	-	[5, 9-13, 49]
Myeloid and lymphoid neoplasms				
Acute myeloid leukaemia	6-13	8-20	0.6	[6-8, 22-28]
B-cell acute lymphoblastic leukaemia	1.7	-	-	[50]
Angioimmunoblastic T-cell lymphoma	-	20-33	-	[38-41]
Peripheral T-cell lymphoma	-	< 5	-	[41]
Myelodysplastic syndrome	< 4	< 4	-	[26, 51]
Myeloproliferative neoplasm – chronic- or fibrotic-phase	< 3	< 1.5	-	[52, 53]
Myeloproliferative neoplasm – blast-phase	5-12	2-9	-	[52, 53]
Paediatric acute myeloid leukaemia	<1.5	<2.5	-	[54, 55]
Paediatric acute lymphoblastic leukaemia	0.4	0	-	[55]
Bile duct neoplasms				
Intrahepatic cholangiocarcinoma	6.5-32	1-9	0.3	[29-37]
Extrahepatic cholangiocarcinoma/Clear cell extrahepatic cholangiocarcinoma	0-10	< 4	-	[29, 30, 35, 56]
Cartilage and bone neoplasms				
Chondrosarcoma	12-54	5-16	-	[14-16, 18-21, 57]
Giant-cell tumour of the bone/Osteoclastoma	-	80	25	[17]
Osteosarcoma	-	28	-	[58]
Ewing sarcoma family tumours	3.3	3.3	-	[59]
Ollier disease and Mafucci syndrome related neoplasms				
Ollier related enchondroma and chondrosarcomas	>80	3		[60, 61]
Mafucci related enchondroma and chondrosarcomas	>80	-	-	[60, 61]
Mafucci syndrome related haemangioma	1 reported case	-	-	[61]
Mafucci syndrome related spindle cell haemangioma	70	-	-	[60]

Table 1.1.1. continued.

Cancer type	Reported occurrence (%)			Source
	mutIDH1 (R132)	mutIDH2 (R172 or R140)	Other mutIDH1/2	
Other neoplasms				
Breast cancer (other)	**0.2**	**-**	**-**	**[62]**
Solid papillary carcinoma with reverse polarity – rare breast cancer subtype	**-**	**>77**	**-**	**[45, 46]**
Gastric adenocarcinoma	**2.7**	**-**	**-**	**[63]**
Irritable bowel syndrome–associated intestinal adenocarcinoma	**13**	**-**	**-**	**[64]**
Melanoma metastasis	**1.3**	**-**	**-**	**[65]**
Non-small cell lung cancer	**0.6**	**0.4**	**-**	**[66]**
Paraganglioma	**1.5**	**-**	**-**	**[67]**
Prostate cancer	**0.3-2.7**	**-**	**-**	**[50, 68]**
Sinonasal undifferentiated carcinoma	**-**	**35-80**	**-**	**[42-44]**
Spindle cell haemangioma	**28**	**7.1**	**3.6**	**[69]**
Thyroid cancer	**-**	**-**	**8-16**	**[70, 71]**
Wilms tumour	**-**	**-**	**10**	**[72]**

The importance of *IDH1/2* mutations in glioma is reflected by the fact that since 2016 they have featured as diagnostic criteria in the World Health Organisation's (WHO) categorisation of central nervous system (CNS) tumours [73]. The updated 2021 WHO classification of CNS tumours further emphasizes the importance of the *IDH1/2* mutations by reducing the number of types of adult diffuse glioma to three, *i.e.* astrocytoma, oligodendroglioma and glioblastoma, with both astrocytoma and oligodendroglioma now requiring the presence of an *IDH1/2* mutation for diagnosis [74].

Early reports suggested cancer-associated *IDH1* mutations caused 'simple' loss of the ability to catalyse conversion of isocitrate to 2-oxoglutarate (2-OG) [9], also known as α-ketoglutarate, and that wild type (wt) IDH1 was dominantly inhibited by forming a heterodimer with mutant (mut) IDH1 [75]. In a seminal study, Dang *et al.* found that mutIDH1^{R132H} catalyses production of the metabolite *R*-2-hydroxyglutarate (*R*-2-HG), also referred to as D-2-HG, showing apparent oncogenic selection for the production of a specific metabolite [76]. Soon after it was demonstrated that mutIDH2^{R172K} and mutIDH2^{R140Q} also catalyse enantioselective production of *R*-2-HG [8]. Both the *R*- and *S*-2-HG enantiomers are present at low μM levels in healthy individuals [77-79], but their roles in normal metabolism are poorly understood. For the common mutations of *IDH1* and *IDH2* found in cancer, intracellular and extracellular *R*-2-HG levels are substantially increased [8, 76].

Mutation of *IDH1* and *IDH2* are reported to occur early in the development of solid tumour cells [12, 80], but not hematopoietic malignancies [53, 81, 82]. The current view is that in nascent tumour cells elevated *R*-2-HG may dysregulate multiple enzymes, including some 2-OG dependent dioxygenases and metabolic enzymes, leading to altered cellular metabolism presumed to support or promote tumorigenesis [83-85]. In myeloid cancers, mutations in *IDH1/2* are considered important for disease progression via similar mechanisms [82]. The presence of mutIDH1 or mutIDH2 in cell models results in alteration of covalent post-oligomerisation modifications (*e.g.,* methylation) to both the nucleic acid and histone components of chromatin ('epigenetic' modifications) [86, 87].

1.1.2. Wild-type functions of IDH 1, IDH2 and IDH3

There are three isoforms of human IDH, the closely related homodimeric IDH1 and IDH2, and the heterotetrameric IDH3, all of which catalyse conversion of isocitrate to 2-OG and CO_2. IDH3 simultaneously reduces nicotinamide adenine dinucleotide (NAD^+) to produce NADH, whereas IDH1 and IDH2 reduce nicotinamide adenine dinucleotide phosphate ($NADP^+$) to NADPH [88]. IDH1 and IDH2 can catalyse the reverse reaction, *i.e.* reductive carboxylation of 2-OG with CO_2 [89, 90], but IDH3 is reported not to do this under physiological conditions [91].

The human IDH isoforms have distinctive roles in 'normal' cellular metabolism. IDH1 localises to the cytosol and peroxisomes, while IDH2 and IDH3 localise to the mitochondrial matrix [92-95]. IDH1 normally provides the cytosol and peroxisomes with NADPH, which is used in fatty acid synthesis or to protect from oxidative damage [96-98]. In cells with damaged mitochondria, or those in hypoxia for example, IDH1 can indirectly provide acetyl-CoA for fatty acid synthesis by catalysing the reductive carboxylation of glutamine-derived 2-OG to isocitrate; isocitrate is isomerised to citrate and then ATP citrate lyase cleaves it to acetyl-CoA and oxaloacetate [99, 100].

IDH2 functions similarly to IDH1, but in the context of the mitochondrial matrix. It provides NADPH to help protect mitochondria against oxidative damage [101, 102] and also synthesises isocitrate under hypoxia by reductive carboxylation of glutamine-derived 2-OG [103]. IDH3 takes part in mitochondrial respiration by catalysing oxidation of isocitrate in

the tricarboxylic (TCA) cycle, producing NADH for ATP production [91, 94]. The metabolic roles of IDH1, IDH2 and IDH3 are summarised in **Figure 1.1.1**.

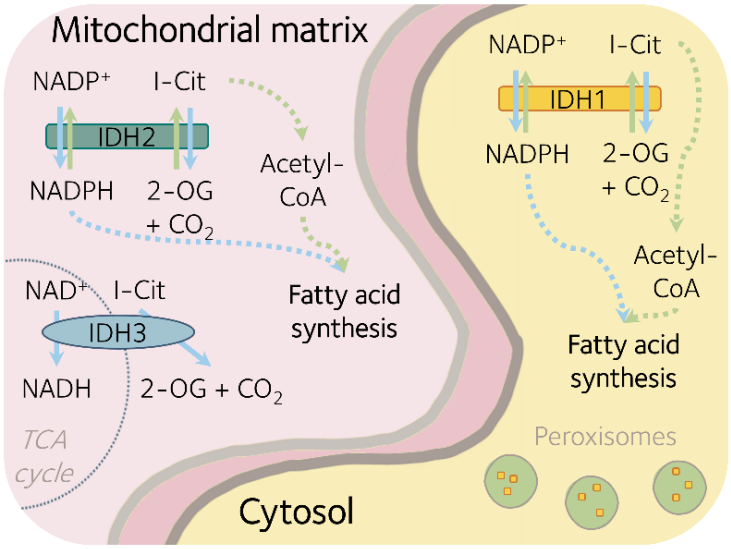

Figure 1.1.1. Normal function of IDH1, IDH2 and IDH3. IDH1 is located in the cytosol and peroxisomes, while IDH2 and IDH3 is located in the mitochondrial matrix. IDH1 and IDH2 catalyse the oxidative decarboxylation of isocitrate (I-Cit) to 2-oxoglutarate (2-OG) and CO_2 with concurrent reduction of $NADP^+$ to NADPH. The reverse reaction is also possible. IDH3 can only catalyse oxidative decarboxylation of isocitrate to 2-OG and CO_2 with concurrent reduction of NAD^+ to NADH. Figure reproduced from Hvinden *et al.* [1].

1.1.3. Biosynthesis of 2-hydroxyglutarate in non-mutant IDH cells

The role of 2-HG in healthy metabolism is not well understood, but both *R*- and *S*-2-HG enantiomers occur in low µM concentrations in plasma [104, 105] and urine (low mmol per mole creatinine [78] for adults and low µmol per mmol of creatinine in neonates [77]). 2-HG can be formed by multiple processes in cells. For example the *R*-2-HG enantiomer results from metabolism of 5-hydroxy-*L*-lysine [106] and by a coupled reaction involving oxidation of a hydroxyacid and reduction of an oxoacid by hydroxyacid oxoacid *trans*-hydrogenase (HOT) (*e.g.* coupling of γ-conversion of hydroxybutyrate to succinic semialdehyde and 2-OG to *R*-2-HG) [107, 108]. *R*-2-HG and *S*-2-HG can also be formed by 'promiscuous' reactions catalysed by phosphoglycerate dehydrogenase (PHGDH) and mitochondrial malate dehydrogenase (MDH2), respectively [109, 110]. In hypoxia the production of *S*-2-HG increases, at least in part catalysed by 'promiscuous' reactions of lactate dehydrogenase A (LDHA), MDH2 and cytosolic malate dehydrogenase (MDH1) [111]. It is proposed that *S*-2-HG supports the regulation of cellular redox homeostasis under conditions of cell stress, *e.g.* hypoxia [112]. The increased *S*-2-HG seen in hypoxia is

likely due to the increased efficiency in the 'promiscuous' reactions by LDH and MDH under acidic conditions (pH 6.0-6.8) [113, 114]. Similarly, PHGDH leads to increased production of *R*-2-HG under acidic conditions [113].

Levels of both 2-HG enantiomers are normally regulated by 2-HG dehydrogenases (2-HGDH), which convert 2-HG to 2-OG. Inborn errors of metabolism, arising from mutations to the genes for *R*- and *S*-2-HGDH, are known as D- or L-2-HG aciduria (D- or LHGA). DHGA can also be caused by mutation of *IDH2* [115]. Loss of *R*-2-HG or *S*-2-HG dehydrogenase catalysis causes accumulation of *R*- or *S*-2-HG to high levels in urine, plasma, and cerebral spinal fluid [115-120]. Both D- or L-2-HG aciduria are associated with neurological abnormalities including developmental delay, epilepsy and cerebral ataxia, as well as cardiomyopathy for DHGA patients [116-121]. Interestingly, there appears to be a lack of association between DHGA and cancer types commonly reported to have mutations in *IDH1* and *IDH2* [122]. There are also a small number of reported cases of central nervous system tumours developing in LHGA patients [123, 124], but it is not always clinically observed [125]. All reactions are summarised in **Figure 1.1.2**.

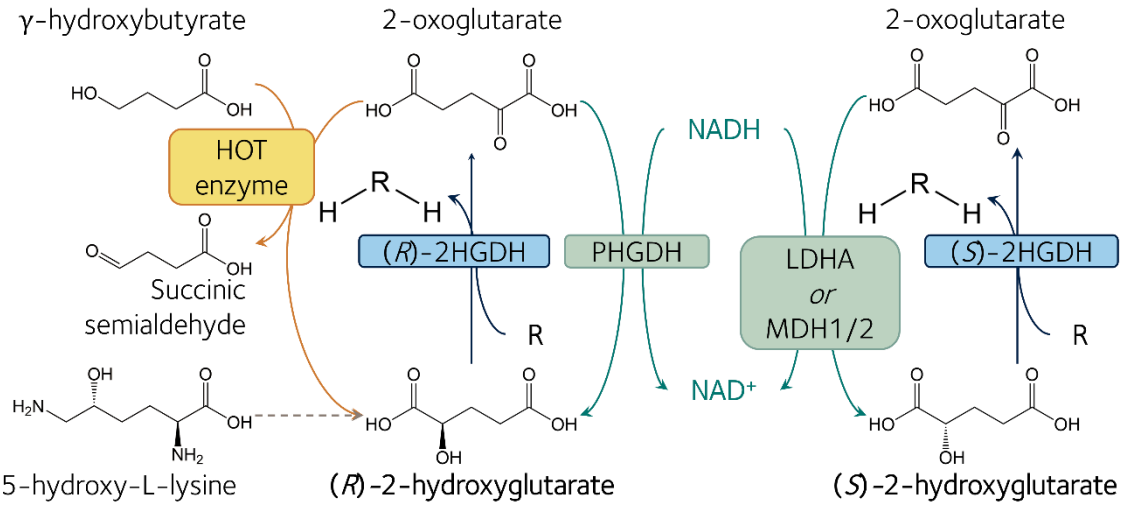

Figure 1.1.2. Enzymatic reactions other than mutIDH1&2 leading to biosynthesis of *R*-2-HG and *S*-2-HG. Solid lines indicate direct reactions, while dotted lines indicate multiple reactions. Abbreviations: HOT = hydroxyacid oxoacid *trans*-hydrogenase, PHGDH = phosphoglycerate dehydrogenase, LDHA = lactate dehydrogenase A, MDH = malate dehydrogenase, and 2HGDH = 2-HG dehydrogenase. Figure reproduced from Hvinden *et al.* [1].

1.1.4. *R*-2-hydroxyglutarate synthesis is linked to IDH1 & IDH2 mutations

IDH1 and *IDH2* point mutations in cancer are heterozygous and occur most frequently at, or close to, their active sites. In IDH1, R132 is the most commonly substituted residue; in IDH2 either the analogous residue R172, or R140, are the most commonly altered. For all three of these mutation sites, the specific substituted residue is often linked to a particular cancer type. Histidine is the most common residue substitution for R132 in mutIDH1 in glioma [4, 5, 9-12], whereas cysteine is more common for chondrosarcoma [14, 15, 19-21] and ICC [30, 31], and in AML both histidine and cysteine occur at a similar frequency [6, 7, 22-25]. Residue R140 in mutIDH2 is most commonly substituted with glutamine in AML [22, 23]. Substitution of R172 in mutIDH2 is usually by serine in chondrosarcoma [14, 15, 19-21], lysine or tryptophan in ICC [30, 31], and lysine in glioma [9, 10].

Kinetic and structural analyses of the mutIDHs have revealed that substitution of an active site arginine (R132 IDH1) correlates with a lowered affinity for isocitrate and the NADPH dependent ability to reduce 2-OG to *R*-2-HG [8, 75, 76, 126]. However, it has also been shown that, when observed with NMR-based enzyme assays [127] rather than fluorescence-based assay [128], mutIDH1^{R132H} is capable of producing *R*-2-HG from isocitrate [127] (see **Figure 1.1.3**). Cytosolic mutIDH1 is reported to rely on co-expression with wtIDH1 to elevate intracellular 2-HG [129-131], but substrate (2-OG and NADPH) is likely not channelled from wtIDH1 to mutIDH1 in a heterodimer [131]. At least in studied cases, mutIDH2 does not appear to bind to, or dominantly inhibit, wtIDH2 [132] and does not require wtIDH2 or IDH3 to produce *R*-2-HG [129]. WtIDH1 and wtIDH2 can produce small amounts of *R*-2-HG from 2-OG [8, 126], though the reaction is limited because isocitrate binding is more efficient than of 2-OG [126]. The ability of wtIDH1 to produce *R*-2-HG is not pH-dependent unlike some other metabolic enzymes with similar 'promiscuous' reactions [113].

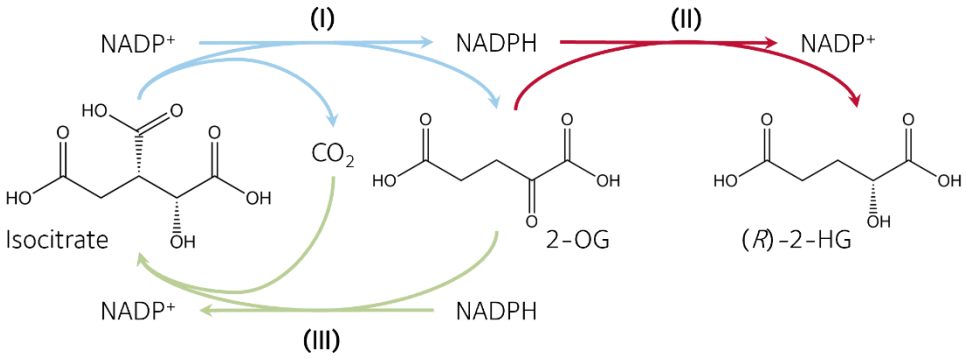

Figure 1.1.3. Reactions occurring with wild type and mutated IDH. WtIDH1/2 carry out reaction (I) in normoxic conditions and reaction (III) in hypoxic conditions. Reaction (II) can also be carried out by wtIDH1, but to a far smaller extent than reaction (I) and (III). MutIDH1/2 carry out reaction (II) and it has been shown that mutIDH1 can also do reaction (I). Reaction (III) appears to be lost upon mutation. Figure adapted from Hvinden *et al.* [1] and Liu *et al.* [127].

The extent of *R*-2-HG accumulation may in part depend on the residue and position that the active site arginine is replaced with. Studies on rare IDH1 substitutions, *e.g.* R132L/S/G, report significantly higher *R*-2-HG levels in glioma tumour tissue compared to mutIDH1^{R132H} and mutIDH1^{R132C} [133, 134]. In cell models with mutIDH2^{R172}, *R*-2-HG levels were significantly higher than models with mutIDH2^{R140Q} or mutIDH^{R132H} [129, 135]. It is noted, however, that in HEK293T cells where mutIDH1^{R132H} was co-overexpressed with wtIDH1, the intracellular *R*-2-HG levels were similar to those of HEK293T cells expressing mutIDH2^{R172K} [129]. Furthermore, when mutIDH1^{R132H} was expressed in the mitochondria of HEK293T cells, rather than the cytosol, *R*-2-HG levels were again comparable to HEK293T cells expressing mutIDH2^{R72K} [129].

1.2. Metabolic changes in mutant isocitrate dehydrogenase cancers

1.2.1. IDH mutant and wild-type cancer models

Developing robust pathophysiological models to study metabolism in mutant *IDH1/2* glioma has been challenging. Early attempts to establish a stable patient-derived mutIDH1 glioma cell line proved difficult [136] and it was reported that the mutant allele was lost after a small number of passages (< 10) [136, 137]. It has been suggested that cells with prior loss of the mutIDH1 allele have a selective growth advantage in tissue culture [138]. However, loss of either the mutant allele [138] or the wild-type allele can occur during *in vitro* culturing [138-141].

Most studies, where insights into altered metabolism are reported using cell models, use genetically engineered cells that overexpress the mutant enzyme, such as in immortalised glioblastoma cell lines (*e.g.,* U87, U251, LN18 or LN229), human oligodendroglioma (HOG) cells, or immortalized normal human astrocytes (NHA) [142-148]. These cell lines provide relatively stable models to study the effects of mutIDH1/2 enzymes, but do not account for some genetic, and subsequently metabolic, differences between wtIDH and mutIDH1/2 gliomas [149-151]. Nevertheless, the models are useful in studying the metabolic effect of mutIDH1/2 alone and can be considered the first of several steps of investigating research questions. Findings from genetically engineered cell lines should be corroborated with other models and patient derived samples.

A limited number of glioma cell lines that endogenously express mutant *IDH1* have been successfully cultured from grade II astrocytomas [152], grade III gliomas and what were formerly known as secondary GBMs [139, 152-155]. Patient derived xenograft (PDX) mouse models bearing patient-derived cells with *IDH1/2* mutations are potentially more physiologically relevant than cell culture using immortalised cell lines [150, 156, 157]. Several PDX-specific mutIDH1 glioma cell lines have been established [157-159], but in comparison to cultured cells these can be less practical and straightforward to work with [reviewed in 150].

In contrast with glioma cells bearing *IDH* mutations, there are several cell lines derived from chondrosarcomas that harbour endogenous mutIDH1 or mutIDH2 with little to no stability issues, *e.g.,* HT1080 and L835 ($IDH1^{R132C}$), JJ012 ($IDH1^{R132G}$), CS1 ($IDH2^{R172S}$) and SW1353 ($IDH2^{R172K}$) [129, 160-166]. Both JJ012 and CS1 have been successfully propagated in mice [165]. For AML, it has been common to use human primary AML cells, either as grafts in mice [167] or cultured cells [168, 169]. Transfected commercially available mutIDH1 cell lines have also been established (HL60 with $mutIDH1^{R132H}$) [170]. There are at least two ICC cell lines with endogenous *IDH1* mutations, RBE ($IDH1^{R132S}$) and SNU-1079 ($IDH1^{R132C}$), that have genetic characteristics comparable to biopsies from patients with ICC [36]. Inducing *IDH1* or *IDH2* mutations has also been achieved in intrahepatic biliary organoids [171], as well as hepatoblasts and adult mouse liver [172], to study how the mutations promote tumorigenesis. However, despite the wide variety of non-glioma cell lines with endogenous *IDH1/2* mutations, there are very few comprehensive studies addressing metabolic

changes in these models. The literature has predominantly focussed on metabolic studies of glioma, using engineered or endogenous cell lines, PDX mouse models and patient tumour biopsies (PTBs).

1.2.2. Altered metabolite levels in mutIDH glioma cancer cell and tumour models

Although there is a lack of comprehensive studies on broader metabolism in mutant *IDH1/2* cancers, there have been numerous reports on elevated *R*-2-HG levels. Comparison of wtIDH1/2 and mutIDH1/2 cells has revealed >100-fold change (FC) in *R*-2-HG levels for chondrosarcoma cells (HT1080) [161], glioma cells (LN18) [148], glioma PDX mouse models [157] and glioma PTBs [76]. A > 50 FC increase in *R*-2-HG levels in mutIDH1/2 AML patient-derived cells, when compared to wtIDH1/2 cells, has also been reported [7]. Multiple studies report significant differences, but no specific FC, in *R*-2-HG levels between wtIDH1/2 and mutIDH1/2 glioma cells (U251, NHA, U87, HOG) [144, 147, 173-175], chondrosarcoma cells (L835, JJ012, SW1353, L2975) [176, 177], glioma PDX mouse models [158], glioma, chondrosarcoma and AML PTBs [8, 142, 178-181], and in ICC patient plasma [182].

Studies investigating altered metabolite levels in mutIDH1/2 when compared to wtIDH glioma cell lines, PDX mouse models and PTBs, using a range of analytical approaches (gas chromatography-mass spectrometry (GC-MS), liquid chromatography (LC)-MS, MS imaging (MSI), nuclear magnetic resonance spectroscopy (NMR), magnetic resonance spectroscopy (MRS)), have reported significantly altered metabolite levels [142, 144, 147, 148, 158, 174, 175, 178, 181, 183]. Comparison of metabolite levels is usually made between the wtIDH1/2 and mutIDH1/2 samples; often the difference is reported as a relative difference or FC rather than absolute concentrations. In contrast with *R*-2-HG, the abundance changes associated with other metabolites appear to be more context dependent [142, 144, 147, 148, 158, 174, 175, 181].

There are conflicting reports of altered lactate levels in *IDH1/2* variant-bearing cells compared to wild type. For example, studies with mutIDH1^{R132H} and wtIDH1 HOG cell line, PDX mouse models and PTBs, using capillary electrophoresis (CE)-, GC- or LC-MS or MSI, report no change in lactate levels [142, 158, 175, 181] (**Table 1.2.1**). However, three other studies report lower lactate levels in mutIDH1^{R132H} U87, NHA and LN18 cells and PDX mouse

models compared to wild-type cells [144, 148, 183]. Lactate levels in mutIDH1^{R132H} U87 glioblastoma cells were reported as significantly increased [174]. An MRS study on patients with mutIDH1^{R132H} and mutIDH2^{R172K} (grade II and III glioma) reported increased lactate compared to wtIDH1/2 gliomas [178]. In mutIDH2^{R172K} HOG and U87 cells, lactate levels have been reported as being unchanged [175] or decreased [174], respectively. A potential confounding issue with regards to reporting lactate levels, and indeed other metabolite levels including *R*-2-HG, is whether extracellular and intracellular pools of metabolites have been combined (*e.g.* when tissue samples are homogenised) or not (*e.g.* when 2-D tissues culture cells are harvested and metabolites extracted). For example, in the studies using cultured cells extracellular lactate was largely removed prior to intracellular metabolite extraction and analysis [144, 148, 174, 175]. In studies using PTBs or PDX mouse models, the extracts were from whole tissue [142, 158, 181] or used methods that are unlikely able to distinguish intracellular and extracellular lactate levels, *i.e.* MSI [158] or *in vivo* MRS [178, 183].

Pyruvate, as measured by LC-MS and MSI in mutIDH1^{R132H} glioma tissue and PDX mouse models, as well as in mutIDH1^{R132H} expressing LN18 or HOG cell lines, showed no significant differences in abundance when comparing *IDH1* wild type and mutant samples [142, 148, 158, 175]. No significant changes in pyruvate levels were observed between mutIDH2^{R172K} and wtIDH2 expressing HOG cells [175]. Two studies reported pyruvate to be significantly decreased in abundance in mutIDH1^{R132H} PTBs compared to wtIDH1 PTBs [158, 181].

Table 1.2.1. Analysis of glycolysis intermediates and related metabolites in mutIDH glioma samples. Changes in metabolite level in mutIDH glioma samples relative to wtIDH glioma samples. — = not significantly different; ▼ = significantly lower in mutIDH1; ▲= significantly higher in mutIDH1. PTB = patient tissue biopsy; PDX = patient-derived mouse xenograft; CL = cell line; suppl = from supplementary information. Table reproduced from Hvinden *et al. [1].*

Metabolite	Change	Mutation	Model type	Analysis Method	Reference
Glucose-1-phosphate	—	$IDH1^{R132H}$	PTB	CE-MS	[142]
	—	$IDH1^{R132H}$	CL (LN18)	IC-MS	[148]
Glucose-6-phosphate	—	$IDH1^{R132H}$	PTB	CE-MS	[142]
	—	$IDH1^{R132H}$	PTB	GC-MS/LC-MS	[181]
	▼	$IDH1^{R132H}$	CL (U87)	NMR	[174]
	—	$IDH2^{R172K}$	CL (U87)	NMR	[174]
6-phospho-gluconate	—	$IDH1^{R132H}$	PTB	CE-MS	[142]
	▼	$IDH1^{R132H}$	PTB	GC-MS/LC-MS	[181]
Ribulose-5-phosphate	—	$IDH1^{R132H}$	PTB	CE-MS	[142]
	▼	$IDH1^{R132H}$	CL (LN18)	IC-MS	[148]
	▼	$IDH1^{R132H}$	CL (U87)	NMR	[174]
	▲	$IDH2^{R172K}$	CL (U87)	NMR	[174]
Ribose-5-phosphate	—	$IDH1^{R132H}$	PTB	CE-MS	[142]
	—	$IDH1^{R132H}$	PTB	GC-MS/LC-MS	[181]
	▼	$IDH1^{R132H}$	CL (LN18)	IC-MS	[148]
Seduheptulose-7-phosphate	—	$IDH1^{R132}$	PTB	CE-MS	[142]
	—	$IDH1^{R132H}$	PDX	MSI/LC-MS	[158]
	▼	$IDH1^{R132H}$	CL (LN18)	IC-MS	[148]
Fructose-1,6-bisphosphate	▼	$IDH1^{R132H}$	PTB	GC-MS/LC-MS	[181]
	—	$IDH1^{R132H}$	CL (LN18)	IC-MS	[148]
Fructose-6-phosphate	—	$IDH1^{R132}$	PTB	CE-MS	[142]
	—	$IDH1^{R132H}$	PTB	GC-MS/LC-MS	[181]
	—	$IDH1^{R132H}$	CL (LN18)	IC-MS	[148]
	—	$IDH1^{R132H}$	CL (U87)	NMR	[174]
	—	$IDH2^{R172K}$	CL (U87)	NMR	[174]
Dihydroxyacetone phosphate	—	$IDH1^{R132H}$	PTB	CE-MS	[142]
Glyceraldehyde-3-phosphate	—	$IDH1^{R132H}$	PTB	CE-MS	[142]
	▲	$IDH1^{R132H}$	CL (LN18)	IC-MS	[148]
Phosphoenolpyruvate	—	$IDH1^{R132H}$	PTB	CE-MS	[142]
	▼	$IDH1^{R132H}$	PTB	GC-MS/LC-MS	[181]
	▲	$IDH1^{R132H}$	CL (LN18)	IC-MS	[148]
3-phospho-glycerate	—	$IDH1^{R132H}$	PTB	CE-MS	[142]
	▼	$IDH1^{R132H}$	PTB	GC-MS/LC-MS	[181]
	▼	$IDH1^{R132H}$	CL (LN18)	IC-MS	[148]
Acetyl-CoA	▲	$IDH1^{R132H}$	CL (HOG)	LC-MS	[175]
	▲	$IDH2^{R172K}$	CL (HOG)	LC-MS	[175]
Pyruvate	—	$IDH1^{R132H}$	PTB	CE-MS	[142]
	—	$IDH1^{R132H}$	PDX	MSI/LC-MS	[158]
	—	$IDH1^{R132H}$	CL (HOG)	LC-MS	[175]
	—	$IDH1^{R132H}$	CL (LN18)	IC-MS	[148]
	▼	$IDH1^{R132H}$	PTB	GC-MS/LC-MS	[181]
	▼	$IDH1^{R132H}$	PTB	LC-MS	[158] (suppl.)
	—	$IDH2^{R172K}$	CL (HOG)	LC-MS	[175]

Table 1.2.1. continued.

Metabolite	Change	Mutation	Model type	Analysis Method	Reference
Lactate	—	**IDH1^{R132H}**	**PTB**	**CE-MS**	**[142]**
	—	**IDH1^{R132H}**	**PTB**	**GC-MS/LC-MS**	**[181]**
	—	**IDH1^{R132H}**	**PTB**	**LC-MS**	**[158] (suppl.)**
	—	**IDH1^{R132H}**	**PDX**	**MSI/LC-MS**	**[158]**
	—	**IDH1^{R132H}**	**CL (HOG)**	**LC-MS**	**[175]**
	▼	**IDH1^{R132H}**	**PDX**	**MRSI**	**[183]**
	▼	**IDH1^{R132H}**	**CL (U87)**	**NMR**	**[144]**
	▼	**IDH1^{R132H}**	**CL (NHA)**	**NMR**	**[144]**
	▼	**IDH1^{R132H}**	**CL (LN18)**	**IC-MS**	**[148]**
	▲	**IDH1^{R132H}**	**CL (U87)**	**NMR**	**[174]**
	—	**IDH2^{R172K}**	**CL (HOG)**	**LC-MS**	**[175]**
	▼	**IDH2^{R172K}**	**CL (U87)**	**NMR**	**[174]**

The TCA cycle intermediates 2-OG, citrate, cis-aconitate, isocitrate and fumarate are reported to be either decreased or unchanged in all model types comparing mutIDH1^{R132H} with corresponding wtIDH1 samples (**Table 1.2.2**) [142, 147, 148, 158, 174, 175, 181]. Succinate, oxaloacetate and malate are the only TCA cycle intermediates with reports of increased levels in mutIDH1^{R132H} compared to wtIDH1, in cultured cells [147, 174, 175]. Other studies on succinate, oxaloacetate and malate, using either PTBs, PDXs or cultured cells, report decreased relative levels [148, 158, 175] or no significant change in abundance [142, 158, 174, 181]. Two independent studies reporting on relative levels of TCA cycle intermediates (using different cell lines and different analytical methods; LC-MS and NMR respectively), for mutIDH2^{R172K} cells (HOG and U87), report decreased succinate levels [174, 175].

Table 1.2.2. Analysis of TCA cycle intermediates in mutIDH glioma samples. Changes in metabolite level in mutIDH glioma samples relative to wtIDH glioma samples. — = not significantly different; ▼ = significantly lower in mutIDH1; ▲= significantly higher in mutIDH1. PTB = patient tissue biopsy; PDX = patient-derived mouse xenograft; CL = cell line; suppl = from supplementary information. Table reproduced from Hvinden *et al. [1].*

Metabolite	Change	Mutation	Model type	Analysis Method	Reference
2-OG	—	$IDH1^{R132H}$	PTB	CE-MS	[142]
	—	$IDH1^{R132H}$	CL (U87)	NMR	[174]
	—	$IDH1^{R132H}$	CL (U251)	LC-MS	[147]
	▼	$IDH1^{R132H}$	PTB	GC-MS/LC-MS	[181]
	▼	$IDH1^{R132H}$	PTB	LC-MS	[158] (suppl.)
	▼	$IDH1^{R132H}$	PDX	MSI/LC-MS	[158]
	▼	$IDH1^{R132H}$	CL (LN18)	IC-MS	[148]
	▼	$IDH1^{R132H}$	CL (HOG)	LC-MS	[175]
	—	$IDH2^{R172K}$	CL (HOG)	LC-MS	[175]
	▼	$IDH2^{R172K}$	CL (U87)	NMR	[174]
Oxaloacetate	—	$IDH1^{R132H}$	PTB	GC-MS/LC-MS	[181]
	▲	$IDH1^{R132H}$	CL (U87)	NMR	[174]
	▼	$IDH2^{R172K}$	CL (U87)	NMR	[174]
Citrate	—	$IDH1^{R132H}$	PTB	CE-MS	[142]
	—	$IDH1^{R132H}$	PTB	GC-MS/LC-MS	[181]
	—	$IDH1^{R132H}$	PTB	LC-MS	[158] (suppl.)
	—	$IDH1^{R132H}$	PDX	MSI/LC-MS	[158]
	—	$IDH1^{R132H}$	CL (U87)	NMR	[174]
	—	$IDH1^{R132H}$	CL (LN18)	IC-MS	[148]
	—	$IDH1^{R132H}$	CL (U251)	LC-MS	[147]
	▼	$IDH1^{R132H}$	CL (HOG)	LC-MS	[175]
	▲	$IDH2^{R172K}$	CL (HOG)	LC-MS	[175]
	▼	$IDH2^{R172K}$	CL (U87)	NMR	[174]
Cis-aconitate	—	$IDH1^{R132H}$	PTB	CE-MS	[142]
	▼	$IDH1^{R132H}$	CL (HOG)	LC-MS	[175]
Isocitrate	—	$IDH1^{R132H}$	PTB	CE-MS	[142]
	▼	$IDH1^{R132H}$	PTB	GC-MS/LC-MS	[181]
Succinate	—	$IDH1^{R132H}$	PTB	CE-MS	[142]
	—	$IDH1^{R132H}$	PTB	LC-MS	[158] (suppl.)
	—	$IDH1^{R132H}$	PDX	MSI/LC-MS	[158]
	▼	$IDH1^{R132H}$	CL (LN18)	IC-MS	[148]
	▲	$IDH1^{R132H}$	CL (HOG)	LC-MS	[175]
	▲	$IDH1^{R132H}$	CL (U251)	LC-MS	[147]
	▲	$IDH1^{R132H}$	CL (U87)	NMR	[174]
	▼	$IDH2^{R172K}$	CL (U87)	NMR	[174]
	▼	$IDH2^{R172K}$	CL (HOG)	LC-MS	[175]
Fumarate	—	$IDH1^{R132H}$	PTB	CE-MS	[142]
	—	$IDH1^{R132H}$	PTB	GC-MS/LC-MS	[181]
	—	$IDH1^{R132H}$	CL (U87)	NMR	[174]
	—	$IDH1^{R132H}$	CL (U251)	LC-MS	[147]
	▼	$IDH1^{R132H}$	CL (HOG)	LC-MS	[175]
	▼	$IDH1^{R132H}$	CL (LN18)	IC-MS	[148]
	—	$IDH2^{R172K}$	CL (U87)	NMR	[174]
	▼	$IDH2^{R172K}$	CL (HOG)	LC-MS	[175]

Table 1.2.2. continued.

Metabolite	Change	Mutation	Model type	Analysis Method	Reference
Malate	—	**IDH1^{R132H}**	**PTB**	**LC-MS**	**[158] (suppl.)**
	—	**IDH1^{R132H}**	**CL (U87)**	**NMR**	**[174]**
	▼	**IDH1^{R132H}**	**PDX**	**MSI/LC-MS**	**[158]**
	▼	**IDH1^{R132H}**	**CL (LN18)**	**IC-MS**	**[148]**
	▼	**IDH1^{R132H}**	**CL (HOG)**	**LC-MS**	**[175]**
	▲	**IDH1^{R132H}**	**CL (U251)**	**LC-MS**	**[147]**
	—	**IDH2^{R172K}**	**CL (U87)**	**NMR**	**[174]**
	▼	**IDH2^{R172K}**	**CL (HOG)**	**LC-MS**	**[175]**

Changes in amino acid abundances have often been reported for mutIDH cell models; but as with the aforementioned metabolites, other than *R*-2-HG, the abundance changes are generally not consistent across studies or model types (**Table 1.2.3**) [142, 144, 174, 175, 181, 183], with comprehensive analyses only being reported in a small number of studies [142, 174, 175]. Only cysteine and proline, out of the 20 amino acids measured, were reported to have the same relative abundances between wtIDH1 and mutIDH1^{R132H} in two studies including them [142, 175]. Despite a lack of agreement in abundance changes across models and techniques, the consistent modulation of amino acids in the context of *IDH1* mutations does merit further study.

Table 1.2.3. Analysis of amino acids in mutIDH glioma samples. Changes in metabolite level in mutIDH glioma samples relative to wtIDH glioma samples. — = not significantly different; ▼ = significantly lower in mutIDH1; ▲= significantly higher in mutIDH1. PTB = patient tissue biopsy; PDX = patient-derived mouse xenograft; CL = cell line; suppl = from supplementary information. Table reproduced from Hvinden *et al. [1].*

Metabolite	Change	Mutation	Model type	Analysis Method	Reference
Glutamate	—	$IDH1^{R132H}$	PTB	GC-MS/LC-MS	[181]
	—	$IDH1^{R132H}$	PDX	MRSI	[183]
	▼	$IDH1^{R132H}$	PTB	CE-MS	[142]
	▼	$IDH1^{R132H}$	PTB	LC-MS	[158] (suppl.)
	▼	$IDH1^{R132H}$	PTB	NMR	[184]
	▼	$IDH1^{R132H}$	CL (U87)	NMR	[174]
	▼	$IDH1^{R132H}$	CL (HOG)	LC-MS	[175]
	▼	$IDH1^{R132H}$	CL (U87)	NMR	[144]
	▼	$IDH1^{R132H}$	CL (NHA)	NMR	[144]
	▲	$IDH1^{R132H}$	CL (U251)	LC-MS	[147]
	—	$IDH2^{R172K}$	CL (HOG)	LC-MS	[175]
	▲	$IDH2^{R172K}$	CL (U87)	NMR	[174]
Aspartate	—	$IDH1^{R132H}$	PTB	CE-MS	[142]
	—	$IDH1^{R132H}$	PTB	GC-MS/LC-MS	[181]
	—	$IDH1^{R132H}$	CL (NHA)	NMR	[144]
	▼	$IDH1^{R132H}$	PTB	LC-MS	[158] (suppl.)
	▼	$IDH1^{R132H}$	CL (HOG)	LC-MS	[175]
	▼	$IDH1^{R132H}$	CL (U87)	NMR	[144]
	▼	$IDH2^{R172K}$	CL (HOG)	LC-MS	[175]
Alanine	—	$IDH1^{R132H}$	PTB	CE-MS	[142]
	▼	$IDH1^{R132H}$	PTB	GC-MS/LC-MS	[181]
	▼	$IDH1^{R132H}$	CL (U87)	NMR	[174]
	▲	$IDH1^{R132H}$	CL (HOG)	LC-MS	[175]
	▼	$IDH2^{R172K}$	CL (U87)	NMR	[174]
	▲	$IDH2^{R172K}$	CL (HOG)	LC-MS	[175]
Arginine	—	$IDH1^{R132H}$	PTB	CE-MS	[142]
	▲	$IDH1^{R132H}$	CL (HOG)	LC-MS	[175]
	▼	$IDH2^{R172K}$	CL (HOG)	LC-MS	[175]
Asparagine	▼	$IDH1^{R132H}$	PTB	CE-MS	[142]
	▲	$IDH1^{R132H}$	PTB	GC-MS/LC-MS	[181]
	▲	$IDH1^{R132H}$	CL (HOG)	LC-MS	[175]
	▲	$IDH2^{R172K}$	CL (HOG)	LC-MS	[175]
Cysteine	—	$IDH1^{R132H}$	PTB	CE-MS	[142]
	—	$IDH1^{R132H}$	CL (HOG)	LC-MS	[175]
	—	$IDH2^{R172K}$	CL (HOG)	LC-MS	[175]
Glutamine	—	$IDH1^{R132H}$	PTB	GC-MS/LC-MS	[181]
	—	$IDH1^{R132H}$	PTB	LC-MS	[158] (suppl.)
	—	$IDH1^{R132H}$	CL (NHA)	NMR	[144]
	▼	$IDH1^{R132H}$	PTB	CE-MS	[142]
	▼	$IDH1^{R132H}$	CL (U87)	NMR	[144]
	▲	$IDH1^{R132H}$	PDX	MRSI	[183]
	▲	$IDH1^{R132H}$	CL (HOG)	LC-MS	[175]
	▲	$IDH2^{R172K}$	CL (HOG)	LC-MS	[175]

Table 1.2.3. continued.

Metabolite	Change	Mutation	Model type	Analysis Method	Reference
Glycine	—	$IDH1^{R132H}$	PTB	CE-MS	[142]
	▼	$IDH1^{R132H}$	PTB	GC-MS/LC-MS	[181]
	▼	$IDH1^{R132H}$	CL (U87)	NMR	[174]
	▲	$IDH1^{R132H}$	CL (HOG)	LC-MS	[175]
	▼	$IDH2^{R172K}$	CL (U87)	NMR	[174]
	▲	$IDH2^{R172K}$	CL (HOG)	LC-MS	[175]
Histidine	—	$IDH1^{R132H}$	PTB	CE-MS	[142]
	▲	$IDH1^{R132H}$	CL (HOG)	LC-MS	[175]
	—	$IDH2^{R172K}$	CL (HOG)	LC-MS	[175]
Isoleucine	—	$IDH1^{R132H}$	PTB	CE-MS	[142]
	▼	$IDH1^{R132H}$	CL (U87)	NMR	[174]
	▲	$IDH1^{R132H}$	CL (HOG)	LC-MS	[175]
	▲	$IDH2^{R172K}$	CL (HOG)	LC-MS	[175]
	▲	$IDH2^{R172K}$	CL (U87)	NMR	[174]
Leucine	—	$IDH1^{R132H}$	PTB	CE-MS	[142]
	▼	$IDH1^{R132H}$	CL (U87)	NMR	[174]
	▲	$IDH1^{R132H}$	CL (HOG)	LC-MS	[175]
	▼	$IDH2^{R172K}$	CL (U87)	NMR	[174]
	▲	$IDH2^{R172K}$	CL (HOG)	LC-MS	[175]
Lysine	—	$IDH1^{R132H}$	PTB	CE-MS	[142]
	▲	$IDH1^{R132H}$	CL (HOG)	LC-MS	[175]
	▲	$IDH2^{R172K}$	CL (HOG)	LC-MS	[175]
Methionine	—	$IDH1^{R132H}$	PTB	CE-MS	[142]
	▲	$IDH1^{R132H}$	CL (HOG)	LC-MS	[175]
	▲	$IDH2^{R172K}$	CL (HOG)	LC-MS	[175]
Phenylalanine	▼	$IDH1^{R132H}$	PTB	CE-MS	[142]
	▼	$IDH1^{R132H}$	CL (U87)	NMR	[174]
	▲	$IDH1^{R132H}$	CL (HOG)	LC-MS	[175]
	▼	$IDH2^{R172K}$	CL (U87)	NMR	[174]
	▲	$IDH2^{R172K}$	CL (HOG)	LC-MS	[175]
Proline	—	$IDH1^{R132H}$	PTB	CE-MS	[142]
	—	$IDH1^{R132H}$	CL (HOG)	LC-MS	[175]
	▼	$IDH2^{R172K}$	CL (HOG)	LC-MS	[175]
Serine	▼	$IDH1^{R132H}$	PTB	GC-MS/LC-MS	[181]
	▲	$IDH1^{R132H}$	CL (HOG)	LC-MS	[175]
	—	$IDH2^{R172K}$	CL (HOG)	LC-MS	[175]
Threonine	—	$IDH1^{R132H}$	PTB	CE-MS	[142]
	▼	$IDH1^{R132H}$	CL (U87)	NMR	[174]
	▲	$IDH1^{R132H}$	CL (HOG)	LC-MS	[175]
	▲	$IDH2^{R172K}$	CL (U87)	NMR	[174]
	▲	$IDH2^{R172K}$	CL (HOG)	LC-MS	[175]
Tryptophan	—	$IDH1^{R132H}$	PTB	CE-MS	[142]
	▲	$IDH1^{R132H}$	CL (HOG)	LC-MS	[175]
	▲	$IDH2^{R172K}$	CL (HOG)	LC-MS	[175]
Tyrosine	—	$IDH1^{R132H}$	PTB	CE-MS	[142]
	▲	$IDH1^{R132H}$	CL (HOG)	LC-MS	[175]
	▲	$IDH2^{R172K}$	CL (HOG)	LC-MS	[175]

Table 1.2.3. continued.

Metabolite	Change	Mutation	Model type	Analysis Method	Reference
Valine	—	**IDH1^{R132H}**	**PTB**	**CE-MS**	**[142]**
	▼	**IDH1^{R132H}**	**CL (U87)**	**NMR**	**[174]**
	▲	**IDH1^{R132H}**	**CL (HOG)**	**LC-MS**	**[175]**
	▲	**IDH1^{R132H}**	**CL (U87)**	**NMR**	**[144]**
	▲	**IDH1^{R132H}**	**CL (NHA)**	**NMR**	**[144]**
	▲	**IDH2^{R172K}**	**CL (U87)**	**NMR**	**[174]**
	▲	**IDH2^{R172K}**	**CL (HOG)**	**LC-MS**	**[175]**

Comparisons of mutIDH1$^{R132H/C}$, mutIDH2$^{R172K/W/G}$ and wtIDH1 glioma using *in vivo* MRS in human patients, has shown that *N*-acetylated amino acids (NAAAs) are consistently decreased in all tumour types measured compared to healthy tissue [178, 185, 186]. Orthotopic mutIDH1^{R132H} and wtIDH1 glioma PDX mouse models similarly show lower levels of NAAAs compared to healthy tissue [158, 183]. In one study comparing the abundance of NAAAs in mutIDH1^{R132H} to wtIDH1 glioma patients, MRS revealed that total NAAAs were slightly higher in mutIDH1^{R132H} than wtIDH1 gliomas [178]. However, it was found that specific NAAAs were depleted in mutIDH1^{R132H} cells compared to wtIDH1 cells [148, 175] (**Table 1.2.4**). These differences may be linked to concomitant differences in amino acid abundance *in vivo* and *in vitro*, but this link requires further confirmation.

Table 1.2.4. Analysis of *N*-Acetylated amino acids in mutIDH glioma samples. Changes in metabolite levels in mutIDH glioma samples relative to wtIDH glioma samples. ▬ = not significantly different; ▼ = significantly lower in mutIDH1; ▲= significantly higher in mutIDH1. PTB = patient tissue biopsy; PDX = patient-derived mouse xenograft; CL = cell line; suppl = from supplementary information. NAAA = N-acetylated amino acids; NAAG = N-acetylaspartylglutamate; NAA = N-acetylaspartate. Table reproduced from Hvinden *et al. [1].*

Metabolite	Change	Mutation	Model type	Analysis Method	Reference
Total NAAA	▲	$IDH1^{R132H}$ $IDH2^{R172K}$	PTB	MRS	[178]
	▬	$IDH1^{R132H}$	PDX	MRS	[183]
NAAG	▲	$IDH1^{R132H}$	PTB	LC-MS	[158] (suppl.)
	▬	$IDH1^{R132H}$	PDX	MSI	[158]
	▼	$IDH1^{R132H}$	CL (HOG)	LC-MS	[175]
	▼	$IDH1^{R132H}$	CL (LN18)	IC-MS	[148]
	▼	$IDH2^{R172K}$	CL (HOG)	LC-MS	[175]
NAA	▼	$IDH1^{R132H}$	PTB	CE-MS	[142]
	▼	$IDH1^{R132H}$	PTB	LC-MS	[158] (suppl.)
	▬	$IDH1^{R132H}$	PDX	MSI	[158]
	▼	$IDH1^{R132H}$	CL (HOG)	LC-MS	[175]
	▼	$IDH2^{R172K}$	CL (HOG)	LC-MS	[175]
N-acetylalanine	▼	$IDH1^{R132H}$	CL (HOG)	LC-MS	[175]
	▼	$IDH2^{R172K}$	CL (HOG)	LC-MS	[175]
N-acetylglutamine	▼	$IDH1^{R132H}$	CL (HOG)	LC-MS	[175]
	▬	$IDH2^{R172K}$	CL (HOG)	LC-MS	[175]
N-acetylglutamate	▼	$IDH1^{R132H}$	PTB	CE-MS	[142]
	▼	$IDH1^{R132H}$	CL (HOG)	LC-MS	[175]
	▼	$IDH2^{R172K}$	CL (HOG)	LC-MS	[175]
N-acetylglycine	▲	$IDH1^{R132H}$	CL (U87)	NMR	[174]
	▼	$IDH2^{R172K}$	CL (U87)	NMR	[174]
N-acetylhistidine	▼	$IDH1^{R132H}$	PTB	CE-MS	[142]
N-acetylmethionine	▼	$IDH1^{R132H}$	CL (HOG)	LC-MS	[175]
	▬	$IDH2^{R172K}$	CL (HOG)	LC-MS	[175]
N-acetylserine	▼	$IDH1^{R132H}$	CL (HOG)	LC-MS	[175]
	▼	$IDH2^{R172K}$	CL (HOG)	LC-MS	[175]
N-acetylthreonine	▼	$IDH1^{R132H}$	CL (HOG)	LC-MS	[175]
	▼	$IDH2^{R172K}$	CL (HOG)	LC-MS	[175]

Glutathione, in its thiol or disulphide forms, is reported to be decreased in mutIDH1/2 compared to wtIDH1/2 cultured cells, in four studies [144, 148, 174, 175], except for mutIDH1^{R132H} U87 cells (increased) [174] and mutIDH1^{R132H} NHA cells (unchanged) [144] (**Table 1.2.5**). Interestingly, a different study, also using mutIDH1^{R132H} U87 cells, reported lower glutathione disulphide levels compared to wtIDH1 U87 cells [144]. Both U87 studies used NMR measurements and both expressed mutIDH1 and wtIDH1 using a lentiviral vector; it is unclear why different relative glutathione levels were observed [144, 174]. The one study reporting on glutathione levels in tissues did not find a significant difference

between mutIDH1^{R132H} and wtIDH1 PDX samples or PTBs [158]. Few studies have reported on levels of other redox metabolites directly, *e.g.,* NADP/NADPH or NAD/NADH, or energy 'currency' compounds, *e.g.,* creatine, AMP/ADP/ATP [144, 148, 158, 174].

Table 1.2.5. Analysis of other metabolites in mutIDH glioma samples. Changes in metabolite level in mutIDH glioma samples relative to wtIDH glioma samples. ▬ = not significantly different; ▼ = significantly lower in mutIDH1; ▲= significantly higher in mutIDH1. PTB = patient tissue biopsy; PDX = patient-derived mouse xenograft; CL = cell line; suppl = from supplementary information. Table reproduced from Hvinden et al. [1].

Metabolite	Change	Mutation	Model type	Analysis Method	Reference
Glutathione (oxidised)	▼	IDH1^{R132H}	CL (HOG)	LC-MS	[175]
	▼	IDH2^{R172K}	CL (HOG)	LC-MS	[175]
Glutathione (reduced)	▬	IDH1^{R132H}	PTB	LC-MS	[158] (suppl.)
	▬	IDH1^{R132H}	PDX	MSI/LC-MS	[158]
	▬	IDH1^{R132H}	CL (NHA)	NMR	[144]
	▼	IDH1^{R132H}	CL (HOG)	LC-MS	[175]
	▼	IDH1^{R132H}	CL (U87)	NMR	[144]
	▼	IDH1^{R132H}	CL (LN18)	IC-MS	[148]
	▲	IDH1^{R132H}	CL (U87)	NMR	[174]
	▼	IDH2^{R172K}	CL (U87)	NMR	[174]
	▼	IDH2^{R172K}	CL (HOG)	LC-MS	[175]
Cystathionine	▼	IDH1^{R132H}	PDX	MSI/LC-MS	[158]
Creatine	▬	IDH1^{R132H}	CL (NHA)	NMR	[144]
	▼	IDH1^{R132H}	CL (U87)	NMR	[174]
	▼	IDH1^{R132H}	CL (U87)	NMR	[144]
	▬	IDH2^{R172K}	CL (U87)	NMR	[174]
ATP	▬	IDH1^{R132H}	PTB	LC-MS	[158] (suppl.)
	▬	IDH1^{R132H}	CL (LN18)	IC-MS	[148]
	▼	IDH1^{R132H}	PDX	MSI/LC-MS	[158]
ADP	▬	IDH1^{R132H}	PDX	MSI/LC-MS	[158]
	▲	IDH1^{R132H}	CL (LN18)	IC-MS	[148]
AMP	▬	IDH1^{R132H}	PTB	LC-MS	[158] (suppl.)
	▬	IDH1^{R132H}	PDX	MSI/LC-MS	[158]
	▬	IDH1^{R132H}	CL (LN18)	IC-MS	[148]
NAD^+	▼	IDH1^{R132H}	CL (U87)	NMR	[174]
	▲	IDH2^{R172K}	CL (U87)	NMR	[174]
NADH	▲	IDH1^{R132H}	CL (LN18)	IC-MS	[148]

In summary, studies into altered metabolite abundances in the presence of mutIDH (all reported as significant) are inconsistent across model types (*e.g.* cultured cells versus PTB/PDX) and/or analysis methods (*e.g.* MS, NMR, MRS) (**Tables 1.2.1-1.2.5**). The differences in reported relative levels of metabolites likely results from multiple factors, including the varied genetic backgrounds of the multiple cell models used. The cell lines discussed are especially relevant in this respect as they represent a mixture of cancerous and non-cancerous cell types (*e.g.* NHA and HOG) or gliomas with different mutational

landscapes (*e.g.* U87, U251 and LN18). In addition, 'background' mutations also have the potential to contribute to metabolic differences observed between cell types for mutIDH1 and *R*-2-HG effects, previously highlighted by *e.g.* Carbonneau *et al.* [151].

It is unclear to what extent the altered metabolite levels directly result from raised *R*-2-HG levels (for example directly affected by *R*-2-HG mediated enzyme inhibition) or result from secondary effects (for example the consequence of altered redox equilibrium due to changes in NADPH production mediated by mutIDH). It is also possible that differences in cell proliferation rates lead to metabolic differences, as has been reported for a number of isogenic cell lines [187-190], which are commonly used when studying the effects of mutIDH1 in glioma. The slower proliferation rate of mutIDH1 cells (compared to wild-type) has also been reported for patient-derived glioma cells [137] and human leukemic cells exposed to *R*-2-HG [191]. Currently, other than for elevated *R*-2-HG, it is difficult to form clear conclusions about metabolic adaptions in mutIDH1/2 glioma based on changes in metabolite levels alone. However, when combined with information from additional techniques (*e.g*., isotopic tracer experiments, proteomics and transcriptomics data), and information about the cancer models, a somewhat clearer picture of metabolic changes and pathways in mutIDH1/2 models starts to emerge.

1.2.3. MutIDH1 glioma cells have been shown to be less glycolytic and have altered TCA cycle function compared to wild type cells

Recent studies, in which levels of metabolic enzymes were measured in PDX mice or PTBs, found that mutIDH1^{R132H} glioma appear to rely less on glycolysis and more on mitochondrial metabolism to alleviate mutIDH1-related metabolic stress [183, 192, 193]. These results support the proposal that some mutIDH1^{R132H} glioma use lactate and glutamate as anaplerotic substrates for TCA cycle metabolism [183, 192, 193]. In contrast, it has been proposed that wtIDH1 glioma are more dependent on glucose, glutamine and acetate as anaplerotic substrates [183, 192, 194, 195]. In mutIDH1 glioma, glutamate and lactate appear to be further metabolised by deamination of glutamate to 2-OG and carboxylation of pyruvate (from imported lactate) to give oxaloacetate, respectively [183, 192, 193]. The differences in metabolism between wtIDH1 and mutIDH1^{R132H} glioma are summarised in **Figure 1.2.1**.

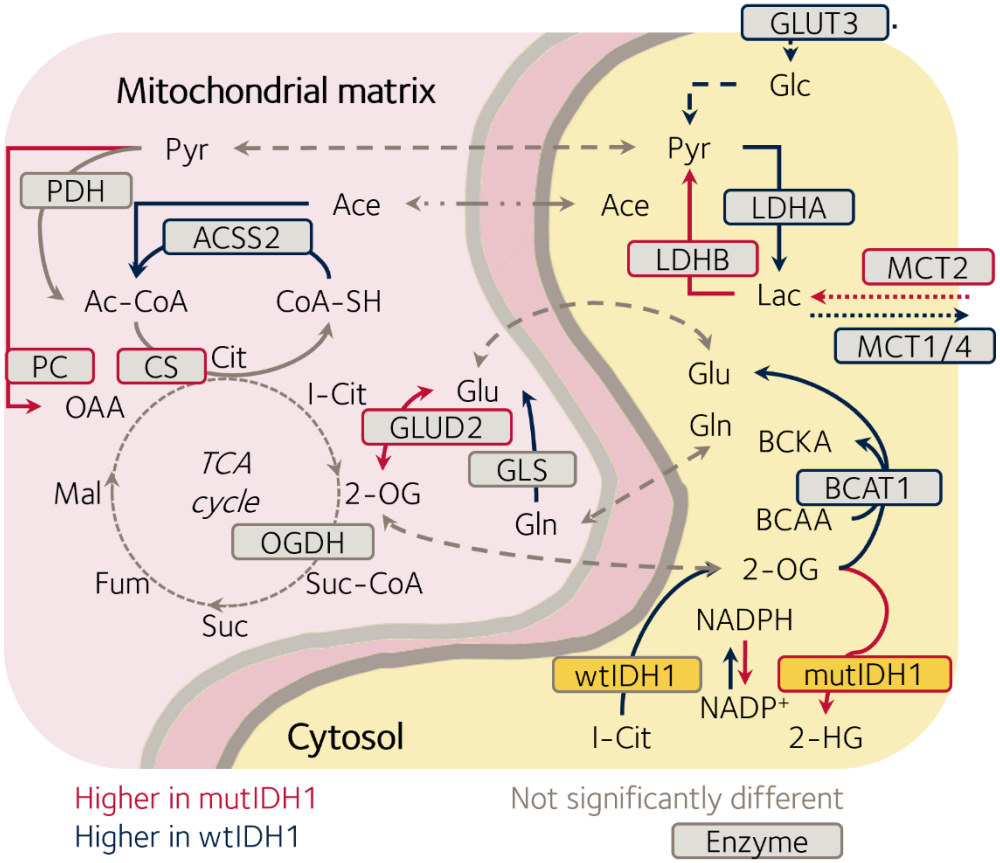

Figure 1.2.1. Overview of reported metabolic differences between wtIDH1 and mutIDH1 glioma. Mutant isocitrate dehydrogenase 1 glioma cells are less glycolytic and have altered TCA cycle function compared to wild type cells. In mutIDH1^{R132H} glioma cells, glutamate and lactate are favoured for anaplerosis of the TCA cycle, while wtIDH1 glioma are more glycolytic and use acetate and glutamate in anaplerosis of the TCA cycle. Abbreviations: PDH (pyruvate dehydrogenase), PC (pyruvate carboxylase), ACSS2 (acyl-coenzyme A synthetase short-chain family member 2), CS (citrate synthase), OGDH (2-oxoglutarate dehydrogenase complex), GLUD2 (glutamate dehydrogenase), GLS (glutaminase), GLUT3 (glucose transporter 3), LDHA and B (lactate dehydrogenase A and B), MCT1/2/4 (monocarboxylate transporter), BCAT1 (branched chain amino acid transferase) and IDH (isocitrate dehydrogenase). Cit (citrate), I-Cit (isocitrate), 2-OG (2-oxoglutarate), Suc-CoA (succinyl-CoA), Suc (succinate), Fum (fumarate), Mal (malate), OAA (oxaloacetate), Pyr (Pyruvate), Ac-CoA (acetyl-CoA), Ace (acetate), Glc (glucose), Lac (lactate), Glu (glutamate), Gln (glutamine), BCAA (branched chain amino acids), and BCKA (branched chain α-ketoacids). Figure reproduced from Hvinden *et al.* [1].

MutIDH1^{R132H} glioma are reported to have reduced glucose uptake compared to wtIDH1 gliomas [137, 183, 192]. Cultured mutIDH1^{R132H} NHA and glioma (BT142) cells have reduced expression of the mono-carboxylate exporters MCT-1 and MCT-4 compared to wtIDH glioma cells (NHA, U87) [196, 197], supporting the hypothesis that mutIDH1 gliomas are less glycolytic than wtIDH1 gliomas. LDHA, which catalyses oxidation of pyruvate to lactate, is downregulated in mutIDH1^{R132H} glioma cell, PDX (mouse) and PTBs [193, 197, 198], while LDHB (which converts lactate to pyruvate) has increased expression in mutIDH1^{R132H}-expressing BT142 cells, PTBs and PDX (mouse) glioma [183, 192, 193, 197]. Isotope tracer experiments show that production of intracellular lactate from

hyperpolarised [1-^{13}C]-pyruvate is significantly lower in mutIDH1^{R132H} versus wtIDH1 NHA cells [196]. A similar experiment comparing BT142 (mutIDH1^{R132H}) to U87 (wtIDH1) cells, in both cell culture and mouse tumour models, showed that there is significantly less labelled lactate in mutIDH1 compared to wtIDH1 cells after perfusion with hyperpolarised [1-^{13}C]-pyruvate [197]. However, levels of isotopically labelled lactate derived from [1-^{13}C]-glucose tracer experiments were reported as being both significantly lower in mtIHD1^{R132H} cells (NHA) [196] and unchanged in U87 mutIDH1^{R132H} and wtIDH1 cells [199]. It was reported that it can take a number of cell-growth cycles (passages) for sufficient promoter region hypermethylation of, *e.g.* the *LDHA* gene, to affect expression levels [198, 200]; therefore whether lactate level changes are particularly cell line dependent, or sensitive to passage number after induction of mutIDH1^{R132H}, remains to be determined.

As an anaplerotic substrate for the TCA cycle, pyruvate can be converted to oxaloacetate by pyruvate carboxylase (PC) and to acetyl-CoA by pyruvate dehydrogenase (PDH). In mutIDH1^{R132H} U87 and NHA cells, PC showed increased expression levels and activity, while PDH had reduced activity [143, 199]. Furthermore, the fractional flux of pyruvate through PC was increased in mutIDH1^{R132H} NHA cells compared to wtIDH1 cells, and the fractional flux of pyruvate through PDH was decreased [143]. Thus, by reducing PDH activity and increasing PC levels, mutIDH1^{R132H} glioma U87 and NHA cells have been shown to use pyruvate for the production of oxaloacetate, a process supported by separate studies [143, 199]. In general, there appears to be experimental agreement that gliomas with mutIDH1R^{R132H} are less glycolytic and rely more on oxidative phosphorylation than wtIDH1 gliomas [147, 157, 158, 183, 192, 197, 198].

1.2.4. Glutamate is an important anaplerotic substrate in mutIDH1 glioma cells

Glutamate dehydrogenase 1 and 2 (GLUD1&2), which catalyse oxidative deamination of glutamate to 2-OG, are significantly elevated in mutIDH1^{R132H} glioma compared with wtIDH1 glioma [183, 192, 193, 201, 202], indicating the potential for increased glutamate utilization by the TCA cycle. Moreover, increased expression of nerve-tissue specific GLUD2 leads to enhanced tumour growth in mutIDH1^{R132H} glioma murine models [201, 202].

Branched-chain amino acid transaminase 1 (BCAT1), which is located in the cytosol and widely expressed in the brain [203], is present at significantly lower levels in mutIDH1^{R132H}

glioma PTB and PDX, compared to wtIDH1 glioma samples [183, 192, 204]. BCAT1 catalyses transamination of valine, leucine, and isoleucine; the α-amino group is transferred to 2-OG, producing glutamate and branched-chain α-ketoacids [205]. High expression of BCAT1 may be counterproductive to glutamate in its role as an anaplerotic substrate of the TCA cycle in *IDH* mutant tumours. The reduced level of BCAT1 in mutIDH1^{R132H} cells is in part due to extensive hypermethylation of the promoter region of the *BCAT1* gene [192, 204]. However, other mutIDH1-related mechanisms may be involved in regulation of *BCAT1* expression, as expression of *mutIDH1* in immortalised human astrocytes caused *BCAT1* downregulation, but not by hypermethylation of its promoter region [204]. It is reported that *R*-2-HG can directly inhibit BCAT1 activity in mutIDH1^{R132H} HOG cells at high (millimolar) concentrations [173], although this was not the case in mouse brain detergent extracts exposed to millimolar *R*-2-HG [204].

Glutaminolysis, where glutamine is converted to TCA cycle intermediates, is a hallmark of metabolism in several types of cancers [reviewed in 206]. Inhibition of glutaminase (GLS), the enzyme catalysing conversion of glutamine to glutamate, decreased proliferation in certain cultured glioma cells (D54, U87) [142, 207], but had only a moderate antiproliferative effect on certain patient-derived cultured cell lines (BT142, TS603 and NCH1681) [208]. GLS expression is not significantly increased in mutIDH1^{R132H} patient samples [183, 192]. Furthermore, the reliance on glutaminolysis in cultured cells could be due to the high levels of cystine present in standard culture media. When a variety of cancer cell lines were grown in the presence of high levels of cystine, the xCT glutamate/cystine antiporter led to a depletion of glutamate in cells, which was ameliorated via glutaminolysis [209]. Cells grown in low cystine media were significantly less sensitive to inhibition of glutaminolysis as the xCT glutamate/cystine antiporter no longer exported glutamate from the cells [209]. Patient derived mutIDH1^{R132H} cell lines (BT142, TS603 and NCH1681) were also shown to have increased expression of asparagine synthetase (ASNS) and glutamate oxaloacetate transaminase (GOT) [208]. The enzymes allow the cells to circumvent GLS inhibition and produce glutamate via aspartate and glutamine (ASNS) or aspartate and 2-OG (GOT). The importance and therapeutic relevance of GLS in mutIDH1 glioma thus remains to be determined.

1.2.5. Other pathways involved in tricarboxylic acid cycle anaplerosis

Additional changes related to TCA cycle related metabolism reported in mutIDH1 cells include the γ-aminobutyric acid (GABA) shunt, lipid oxidation-derived acetyl-CoA and the 2-OG dehydrogenase complex [147, 170, 183, 210]; the disease significance of these changes is unclear. In the GABA shunt, glutamate is decarboxylated forming GABA (catalysed by glutamate decarboxylase (GAD-1)), followed by deamination to give succinic acid semialdehyde (catalysed by 4-aminobutyrate aminotransferase (ABAT)) and finally oxidation to succinate by succinate semialdehyde dehydrogenase (SSADH). Levels of the enzymes involved in the GABA shunt pathway are significantly elevated in glioma tissue in general [147] or mutIDH1^{R132H} glioma tissue specifically [183], but not in an orthotopic xenograft mouse model of mutIDH1^{R132H} glioma [183]. In U251 glioma cells the expression of mutIDH1, or treatment of wtIDH1 cells with exogenous *R*-2-HG, leads to a reduction in the pro-proliferative effects of GABA [147]. Further studies are needed to understand the effects of *R*-2-HG on enzymes in the GABA shunt and its role in glioma metabolism.

1.2.6. Altered redox homeostasis due to mutIDH1 consumption of NADPH

Cells must control reactive oxygen species (ROS) to limit damage to nucleic acids, proteins and lipids and to maintain ROS-based signalling pathways [211]. Antioxidants are central to regulating ROS; glutathione is a ubiquitous antioxidant tripeptide thiol requiring NADPH for its production [212]. Cells employ multiple pathways for NADPH production; in the cytosol major contributors to ROS regulation are IDH1, malic enzyme 1 (ME1) and glucose 6-phopshate dehydrogenase (G6PD)/6-phosphogluconate dehydrogenase (PGD) in the oxidative pentose phosphate pathway (oxPPP) [213, 214]. IDH1 is especially important for NADPH production in the brain [215]. IDH2 plays an important role in mitochondrial redox balance and in protection against ROS [101, 102], protecting tissues such as lung, kidney, heart and liver from mitochondrial oxidative damage [216-219]. MutIDH1&2 have a substantially reduced ability to produce NADPH compared to the wild-type and instead consume significant amounts of NADPH during *R*-2-HG production [161, 215, 220, 221]. This puts pressure on maintenance of the cellular NADPH/$NADP^+$ balance and redox homeostasis, potentially making mutIDH cells more vulnerable to ROS and metabolic stress [161, 220-225].

There is evidence that mutIDH1 cells employ compensatory pathways to ameliorate the increased use of NADPH for *R*-2-HG production. The pentose phosphate pathway (PPP) has been suggested to act in this role and there is evidence of increased flux through the PPP in mutIDH1^{R132H} HCT116 and NHA cells [221]. However, such increased flux was shown not to fully compensate for *R*-2-HG mediated NADPH consumption, especially when the mutIDH1^{R132H} cells were under metabolic stress [161, 221]. In mutIDH1^{R132H} U87 glioma, primary GBM and immortalized astrocytes cell lines, NADPH levels were partially restored by phosphorylating NAD^+ by NAD^+ kinase [220]. The upregulation of NAD^+ synthesis enzymes varies between immortalised astrocyte and GBM cell lines, as well as PTBs, indicating the changing role of mutIDH1 throughout tumorigenesis [220]. MutIDH1^{R132H} glioma xenograft cell lines have reduced NAD^+ levels, as well as lowered nicotinate phosphoribosyltransferase (Naprt1), an enzyme involved in NAD^+ salvaging pathway [226]. The mutIDH1^{R132H} glioma cells were sensitive to inhibition of nicotinamide phosphoribosyltransferase (NAMPT), the rate limiting enzyme of the NAD^+ salvaging pathway, which left the mutIDH1^{R132H} cells with fewer options to increase intracellular NAD^+ [226].

Glioma (BT142) cells rely on glutamate to boost redox homeostasis, both by increasing the NADPH/$NADP^+$ and reduced/oxidised glutathione ratios [224]. Induction of mutIDH1^{R132H} or mutIDH1^{R132C} expression in U251 glioma cell increases expression of glutathione biosynthesis enzymes [225]. The nuclear factor erythroid 2-related factor (Nrf2), which regulates the response to oxidative damage including glutathione biosynthesis, has enhanced activity in mutIDH1$^{R132C/H}$ U251 cells [225]. MutIDH1 astrocytoma cells have displayed critical reliance on cystathionine-γ-lyase (CSE) both *in vitro* and *in vivo* [141]; CSE provides cysteine for glutathione synthesis via lysis of cystathionine. The reliance on CSE was most pronounced under limited cysteine availability [141]. Glioblastomas also have upregulated wtIDH1 expression [227, 228] and gene knockdown or pharmacological inhibition of wtIDH1 has been shown to lead to decreased NADPH and glutathione levels, along with increased ROS expression and apoptosis [227, 228]. Collectively these observations suggest the importance of wtIDH1 activity in maintaining redox homeostasis.

1.2.7. Altered lipid metabolism in cells expressing mutant isocitrate dehydrogenase

The conversion of isocitrate to 2-OG by wtIDH1 provides NADPH that is subsequently available for fatty acid synthesis [96] and both wtIDH1&2 support fatty acid synthesis under hypoxic conditions by providing isocitrate that is converted to acetyl-CoA via citrate [99, 103] (**Figure 1.2.2**). Since mutIDH1^{R132H} loses both the ability to produce NADPH and to carry out reductive carboxylation [187, 229], it is reasonable to propose that cells carrying mutIDH1^{R132H} may have altered lipid metabolism compared to wtIDH1 cells.

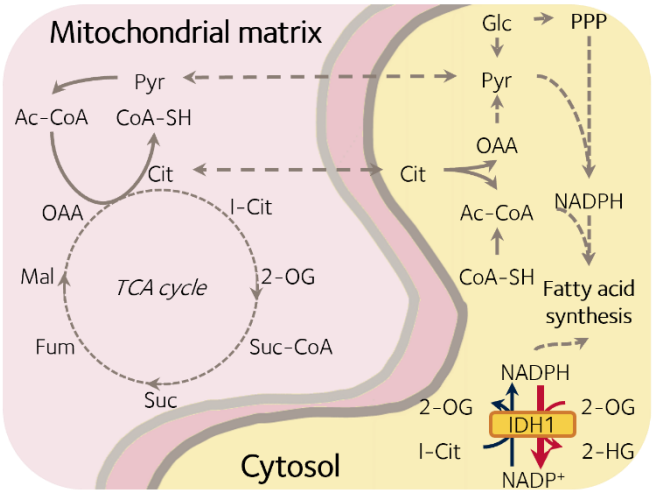

Figure 1.2.2. Overview of IDH related lipid biosynthesis. Lipid biosynthesis require NADPH, which is sourced from the oxidative pentose phosphate pathway (PPP), citric acid shuttle, and IDH1. When IDH1 is mutated, copious NADPH is used to synthesise 2-HG. Abbreviations: Cit (citrate), I-Cit (isocitrate), 2-OG (2-oxoglutarate), Suc-CoA (succinyl-CoA), Suc (succinate), Fum (fumarate), Mal (malate), OAA (oxaloacetate), Pyr (Pyruvate) and Ac-CoA (acetyl-CoA). Figure reproduced from supplementary material from Hvinden *et al.* [1].

In mutIDH1 glioma, alterations in phospholipid profiles have been observed in cultured cell models and tumours, as shown by LC-MS, MSI and ^{1}H and ^{31}P *in vitro* and *ex vivo* NMR and *in vivo* MRS [144, 158, 184, 230], in part summarised in **Table 1.2.6**. Independent studies using MRS/NMR show that phosphocholine (PCho) and glycerophosphocholine (GPCho) are increased in cultured glioma cells expressing mutIDH1^{R132H}, xenograft models, and PTBs when compared to equivalent wtIDH1 glioma samples [184, 230]. However, a study measuring PCho with LC-MS in cultured HOG cells expressing mutIDH1^{R132H} or mutIDH2^{R172K} found that PCho was significantly lower compared to HOG wtIDH cells [175] and reported GPCho as increased. In addition to PCho and GPCho, phosphoethanolamine (PE) was significantly lower in mutIDH1^{R132H} gliomas across all the sample types analysed [230]. In an MSI study, four putatively identified PE lipids were reported to be substantially increased in mutIDH1^{R132H} glioma mouse PDXs [158]. However, the NMR methods employed were insufficiently sensitive to differentiate between the different PEs.

Table 1.2.6. Analysis of phosphorylated lipids in mutIDH glioma samples. Change in metabolite level in mutIDH glioma samples relative to wtIDH glioma samples. — = not significantly different; ▼ = significantly lower in mutIDH1; ▲= significantly higher in mutIDH1. PTB = patient tissue biopsy; PDX = patient-derived mouse xenograft; CL = cell line. Table reproduced from Hvinden *et al. [1].*

Metabolite	Change	Mutation	Model type	Analysis Method	References
Phosphocholine	▲	$IDH1^{R132H}$	PTB	^{1}H NMR	[184]
	—	$IDH1^{R132H}$	PTB	^{31}P NMR	[230]
	—	$IDH1^{R132H}$	PDX	^{31}P MRI	[230]
	▲	$IDH1^{R132H}$	CL (U251)	^{31}P NMR	[230]
	▼	$IDH1^{R132H}$	CL (HOG)	LC-MS	[175]
	▼	$IDH1^{R132H}$	CL (U87)	^{1}H NMR	[144]
	▼	$IDH1^{R132H}$	CL (NHA)	^{1}H NMR	[144]
	▼	$IDH2^{R172K}$	CL (HOG)	LC-MS	[175]
Glycerophosphocholine	▲	$IDH1^{R132H}$	PTB	^{1}H NMR	[184]
	▲	$IDH1^{R132H}$	PTB	^{31}P NMR	[230]
	▲	$IDH1^{R132H}$	PDX	^{31}P MRI	[230]
	▲	$IDH1^{R132H}$	CL (U251)	^{31}P NMR	[230]
	▲	$IDH1^{R132H}$	CL (HOG)	LC-MS	[175]
	▲	$IDH1^{R132H}$	CL (U87)	^{1}H NMR	[144]
	—	$IDH1^{R132H}$	CL (NHA)	^{1}H NMR	[144]
	▼	$IDH2^{R172K}$	CL (HOG)	LC-MS	[175]
Phosphoethanolamine	—	$IDH1^{R132H}$	PTB	^{1}H MRI	[231]
	▼	$IDH1^{R132H}$	PTB	^{31}P NMR	[230]
	▼	$IDH1^{R132H}$	PDX	^{31}P MRI	[230]
	▼	$IDH1^{R132H}$	CL (U251)	^{31}P NMR	[230]
Glycerophospho-ethanolamine	—	$IDH1^{R132H}$	PTB	^{31}P NMR	[230]
	—	$IDH1^{R132H}$	PDX	^{31}P MRI	[230]
	—	$IDH1^{R132H}$	CL (U251)	^{31}P NMR	[230]
Phosphatidylinositol	▲	$IDH1^{R132H}$	PDX	MSI	[158]

In addition to PE and PCho, levels of phosphatidylinositol (PI) lipids are reported as being increased when comparing $mutIDH1^{R132H}$ and wtIDH1 glioma PDXs in mice [158]. When gliomas were analysed in patients using *in vivo* MRS measurements, no significant differences in ratios of PE/PCho, GPCho/glycerophosphoethanolamine (GPE) or (PCho+GPCho)/(PE+GPE), were detected between $mutIDH1^{R132H}$ and wtIDH1 glioma patients [231]. The apparently specific differences in lipid profiles in glioma may in part be due to cells compensating for loss of wtIDH1 activity [230] by increasing IDH2-enabled NADPH and lipid production. Cells from mouse PDXs of mutIDH1 glioma have been shown to have significantly higher mitochondrial density than corresponding wtIDH1 cells [157], an interesting observation given IDH2 localises to mitochondria. Additional mitochondria would also increase the lipid membrane content in cells, which could help explain the differences seen in the phospholipid composition of mutIDH1 and wtIDH1 gliomas [230].

Cholesterol metabolism in mutIDH1/2 glioma has received limited attention to date, but a recent study suggests it may be of therapeutic relevance [232]. It was found that cholesterol levels were lower in brains from both mutIDH1^{R132H} knock-in (KI) mice and mutIDH1^{R132H} expressing U87 and U251 cells, when compared to corresponding wtIDH1 samples [232]. MutIDH glioma cells had increased expression of *de novo* cholesterol synthesis enzymes 3-hydroxy-3-methyl-glutaryl CoA reductase (HMGCR) and sterol regulatory element-binding protein 2 (SREBP2). Inhibition of HMGCR by atorvastatin led to significant cell death in mutIDH1^{R132G}-expressing U87 and U251 cells, but had little effect on the wtIDH1-expressing U87 and U251 cells [232].

1.3. Treating mutIDH1 cancer: direct inhibition or utilise metabolic vulnerabilities?

The specificity of metabolic changes in mutIDH1 or mutIDH2 cancers, and the apparent lack of a critical metabolic role for *R*-2-HG in wtIDH cells, means mutIDHs are promising medicinal chemistry targets. Multiple small-molecule inhibitors have now been developed to target mutIDH and there are several current clinical trials underway for treatment of glioma, AML, chondrosarcoma, and ICC [55, 233-245]. The inhibitors are potent, for example three different mutIDH1 inhibitors (AG-120, BAY 1436032 and GSK864) report low nM half maximal inhibitory concentrations (IC_{50}) (12.0-15.2) for *in vitro* assays. The mutIDH2 inhibitor AG-221 has a slightly higher *in vitro* IC_{50} at 100 nM, but a cellular assay was on par with two of the mutIDH1 inhibitors: cellular $IC_{50\ AG\text{-}221}$ = 10-20 nM, $IC_{50\ AG\text{-}120}$ = 8 nM and $IC_{50\ BAY\ 1436032}$ = 13-73 nM [246-248]. The cellular assays were carried out with glioma and GBM cells lines either endogenously expressing mutIDH1 or engineered to express it. A pan mutIDH inhibitor (AG-881) capable of inhibiting both mutIDH1 and mutIDH2, reports *in vitro* IC_{50} values of 31.9 nM and 31.7 nM, respectively [249]. The IC_{50} values for the aforementioned inhibitors are summarised in **Table 1.3.1**.

Table 1.3.1. IC_{50} values reported for three mutIDH inhibitors, one pan mutIDH1 inhibitor (AG-881) and one mutIDH2 inhibitor (AG-221). Reported cell IC_{50}‡ values were for glioma or GBM cells, either harbouring $mutIDH1^{R132H}$ or engineered to express it. ‡Only cell EC_{50} data was found in the literature for treatment of engineered GBM cells with GSK864.

Inhibitor	Inhibits	IC_{50} (enzyme) (nM)	IC_{50} (cell) (nM)	Reference
AG-120	**mutIDH1**	**12.0**	**8**	**[246]**
AG-881	**mutIDH1**	**31.9**	**-**	**[249]**
	mutIDH2	**31.7**	**-**	**[249]**
BAY 1436032	**mutIDH1**	**15.0**	**13-73**	**[247]**
GSK864	**mutIDH1**	**15.2**	**-**	**[250]**
	mutIDH1	**-**	**191‡**	**[251]**
AG-221	**mutIDH2**	**100**	**10-20**	**[248]**

A variety of mutIDH1 and mutIDH2 inhibitors substantially decrease *R*-2-HG levels in *in vitro* and xenograft models [174, 176, 177, 226, 252-256], glioma patients [257] and in AML patients [258-261]. Some of these inhibitors are reported to initiate differentiation in AML and glioma cell lines and mouse models [253, 254]; differentiation of cancer stem cells has been suggested as a strategy to reduce treatment resistance and disease recurrence in cancer in general [reviewed in 262]. However, other glioma and chondrosarcoma cell lines did not have significant decreases in growth after treatment with mutIDH1 inhibitors, despite decreased 2-HG abundance [177, 226]. First generation therapeutic mutIDH-selective inhibitors were approved for AML treatment in 2018 by the USA Food and Drug Administration (FDA) [258, 261]. For solid tumours, promising initial results from clinical trials have been reported for advanced cholangiocarcinoma [245] and glioma [263]. Advanced mutIDH1 cholangiocarcinomas treated with the mutIDH1 inhibitor AG-120 (ivosidenib) report significantly increased progression-free survival (PFS) (p-value < 0.0001) and improved overall survival [245], while a different trial of ivosidenib in advanced mutIDH1 gliomas reported improved disease control and reduced tumour growth [263].

Resistance has been reported for these first-generation inhibitors (AG-120 and AG-221) [258, 264-266] which is generally categorized as primary or acquired and *R*-2-HG restoring or non-restoring [264-266]. Primary resistance to AG-120 and AG-221 (enasidenib), *i.e.,* where non-restoration of *R*-2-HG levels is manifest, has been reported in AML patients. The non-responding patients had a higher mutational burden compared to responders, either as baseline mutations in genes of the receptor-tyrosine kinase (RTK) pathway [266] or of the Ras pathway [258]. There have been two different types of acquired and *R*-2-HG restoring mechanisms described in the literature. The first type are second-site mutations that are proposed to reduce the binding affinity of the allosteric inhibitors AG-221 [264]

and AG-120 [266], in mutIDH2 and mutIDH1 respectively. The second type of acquired *R*-2-HG restoring mechanism is the emergence of the 'opposite' *IDH* mutation (isoform switching), *i.e.,* mutIDH1 arising in previously mutIDH2 patients or vice versa [265, 266].

Altered metabolism in mutIDH1&2 cancer cells after inhibitor treatment, beyond modulation of *R*-2-HG, has received limited attention to date. Three studies, all using NMR and two using cultured glioma cell lines (U87 and/or NHA, mutIDH1^{R132H}), and one using patient derived cultured cell lines (BT142, TS603, NCH1681), confirm that *R*-2-HG levels are significantly decreased upon treatment with either AG5198 [174, 208], AG-120 or AG-881 [255]. There is otherwise not necessarily a high degree of agreement between the studies with regards to changes in other metabolite levels. Lactate is reported as either unchanged [255] or significantly reduced [174] upon treatment. Glutamate was reported as being significantly increased after treatment for engineered cell lines (p-value < 0.001) [255] and certain patient derived cell lines (TS603 and NCH1681) (p-value < 0.05) [208]. Wen *et al.*, also using engineered cell lines, reported that there was no significant change in glutamate levels [174]. Only the study using patient derived cell lines reported on glutamine levels, which were significantly elevated in TS603 and NCH1681 after treatment with AG5198 [208]. In the two studies using the engineered cell line, both cell line (U87) and analysis method (NMR) were the same and therefore potentially the difference in glutamate response to treatment was due to the use of different cell media in the tissue culture experiments (Dulbecco's Modified Eagle's Medium (DMEM) [255] versus Roswell Park Memorial Institute (RPMI) Medium [174]). A third study using isogenic mutIDH1$^{R132H/C}$ clones of HCT116 cells reported that reductive carboxylation could not be rescued after treatment with mutIDH1 inhibitor IDH1iA [187].

In more clinically relevant models, two further studies investigated the effect of mutIDH1 inhibitors on the wider metabolism of mutIDH1 glioma cells [256, 257]. In orthotopic mouse tumours, either from mutIDH1^{R132H} U87 or patient-derived mutIDH1 BT257 (astrocytoma) and mutIDH1 SF10417 (oligodendroglioma), both inhibitors AG-881 and BAY1436032 were able to significantly decrease *R*-2-HG levels and significantly increase glutamate and the combined MRS signal of glutamate/glutamine [256]. Interestingly, NAA was significantly increased across all tumours and drug combinations, but only at the first measurement timepoint after treatment induction (7 days) and not the final timepoint (14-15 days). The

first measurement was made prior to changes in tumour volume [256]. Finally, a clinical trial of the mutIDH1 inhibitor 'IDH305' in glioma, studying 5 patients, one week of treatment (550 mg/day, orally) led to a significant reduction in 2-HG levels ($P < 0.05$) [257]. Furthermore, there was a trend towards increased lactate levels and an inverse correlation between glutathione and 2-HG levels. Glutamine/glutamate levels, however, were reported as being unchanged [257].

There has been some interest in alternative therapeutic approaches that take advantage of metabolic vulnerabilities in mutIDH [267]. For example, the apparent reliance of mutIDH1 cells on glutamine has been explored. Treatment with glutaminase inhibitors showed a greater reduction in viability for mutIDH1 compared with wtIDH1 glioma and AML cells [169, 207, 268, 269], although the antiproliferative effect has also been reported as cell line dependent for patient-derived mutIDH1 glioma cells [208]. There is an ongoing clinical trial using a glutaminase inhibitor (CB-839/telaglenastat) combined with radiation therapy and temozolomide for treatment of astrocytoma with mutIDH1 or mutIDH2 [270]. The use of glutaminase inhibitors in general would benefit from patient stratification to ensure that genetic mutations that confer vulnerability to glutamine starvation are present [271, 272]. As a single-agent treatment, it appears that telaglenastat stabilises disease rather than being cytotoxic [273].

Chloroquine, best known as an antimalarial agent [274] and autophagy inhibitor [275], is also capable of inhibiting nerve-specific GLUD2 [276]. MutIDH1 glioma cells are likely reliant on GLUD2 for glutamate-dependent anaplerosis of the TCA cycle [183, 201] and express GLUD2 at significantly higher levels than wtIDH1 glioma [183, 192, 193, 201, 202]. Treatment with chloroquine could potentially render mutIDH1 glioma cells more metabolically vulnerable by limiting their ability to utilise glutamate. Extracellular glutamate has been reported to increase redox potential in mutIDH1 glioma cells [224] and chloroquine could combine synergistically with a treatment that applies oxidative stress to cells, *e.g.,* radiation therapy. A preclinical study using wtIDH1 stem-like glioma cells demonstrated that treatment with chloroquine during radiation significantly increased cell death; however, in this context it was considered due to the autophagy inhibitory effects of chloroquine [277].

Unanswered questions remain in metabolism-focussed treatment of mutIDH1 glioma, including whether treatment with mutIDH1 inhibition alone is effective, whether it should be combined with other therapies, or whether potential metabolic vulnerabilities either originating from, or correlating with, the presence of the mutation should be targeted instead. A better understanding of the metabolic response to mutIDH1 inhibition is needed to make informed choices for therapeutic development. The wider metabolic effect after inhibition of mutIDH1 can inform on which parts of glioma metabolism are related to increase in 2-HG or mutIDH1 activity (i.e., altered redox state or increased 2-OG consumption) and can be used to inform on development and stratification of future therapeutic strategies. The next two sections will discuss the methodology that was used in this thesis to assess the wider metabolic effect of mutIDH1 and GLS inhibition in wtIDH1 and mutIDH1^{R132H} GBM cells.

1.4. Instrumentation for metabolomics analysis

Metabolomics is the comprehensive study of the metabolism of a given biological system. Metabolism is comprised of the collection of metabolites (≤ 1500 Da) and the reactions they partake in, within the given biological system. Metabolites are also considered the 'end-point' or output of a cascade of biochemical processes initiated in the genome, which collectively encompasses cellular function. Metabolomics analysis can be targeted, where a pre-defined set of metabolites are measured, or untargeted, where as many metabolite-features as possible are measured. Targeted analysis is usually hypothesis driven, where a specific group of metabolites are quantified to answer a defined biological question. Untargeted analysis is usually hypothesis generating, where as many features as possible are measured, then various statistical analyses are applied to elucidate potential biomarkers or changes in activity across a metabolic pathway or network of pathways. The two analysis types can be combined in a semi-targeted analysis workflow, in which metabolites are identified based on comparison to known standards, but the unknown features are still included to allow for more comprehensive analysis of the biological system under review. Regardless of whether targeted, untargeted or semi-targeted analysis is carried out, choice of instrumentation remains a central part of any metabolomics study.

MS and NMR are the most commonly used instruments for sample analysis in metabolomics. In MS, charged chemical species in the gas phase are separated based on the mass-to-charge ratio (*m/z*) prior to detection [278]. There are a large number of different instrumentation options for MS and it is commonly used in combination with other analysis techniques, e.g., chromatography. Which specific application is used depends on the sample and analyte(s) of interest. The relevant techniques for metabolomics will be described further below.

In NMR, the resonance frequency of nuclei in a constant and strong external magnetic field is measured. Only nuclei with angular momentum (spin) can be measured, as they can align with the external magnetic field and then be excited by pulses of electromagnetic radiation. The energy that is emitted as the nuclei return to a lower energy state is detected. The exact resonance frequency depends on the chemical and physical environment the nuclei is in, thus nuclei within a molecule can be distinguished from each other. Only nuclei with odd numbers of protons, neutrons or both have spin [279]. In biological applications, the most common nuclei to measure are ^{1}H, ^{13}C and ^{31}P and both liquid and solid samples can be analysed.

NMR is robust and provides repeatable analysis, but is currently lacking in coverage and sensitivity when compared to hyphenated MS techniques. MS alone is more sensitive than NMR, but without prior separation of metabolites there are issues with ion suppression and the annotation of isomeric compounds. Hyphenated MS was the main analytical technique used in the studies reported in this thesis and will be described in detail in this section. The technical aspects and considerations of MS instrumentation will be explained and the hyphenation of MS to liquid chromatography (LC) will be described. Finally, the different LC stationary phases most applicable to metabolomics study will be considered.

1.4.1. Mass spectrometry

The MS instrument is made up of components that allow for the introduction of sample (inlet) and ionisation of chemical species (ion source), the separation of charged species (mass analyser) and then detection (detector) [278]. The different types of sample inlet/ion source and mass analysers commonly used in metabolomics are described below.

Gaseous, liquid or solid samples can be analysed by MS. Their introduction to the ion source, and type of ion source used, depends on the physical state of the samples. Desorption techniques are most common for solid samples and there are a number of different techniques available [reviewed in 280, 281, 282]. In short, the sample is dispersed through a matrix and then analytes are freed from the matrix by high energy ions, neutral atoms or photons [278]. In the biological sciences, secondary ion MS (SIMS) and matrix assisted laser desorption ionisation (MALDI) MS are the most commonly used techniques [reviewed in 281, 282]. MADLI is suitable for the study of large, non-volatile molecules, e.g., intact proteins [reviewed in 280, 282], but it can also be used in metabolomics [158]. However, in MS-based metabolomics applications it is more common to have samples in the liquid or gas phase prior to introduction to the MS instrument. The introduction of gas phase sample, e.g., after gas chromatography (GC) analysis, simply requires letting a part of the gas stream into the ion source. Similar to solid samples, liquid samples require an inlet that transitions the analytes in the sample to the gas phase. The most commonly used technique is electrospray ionisation (ESI), but atmospheric pressure chemical ionisation (APCI) is also applicable [reviewed in 283, 284].

In ESI, the vaporisation of the liquid sample starts by passing it through a capillary tube with a high voltage applied (± 5 kV). At the other end of the ion source, the MS inlet, the opposite charge is applied. The charged liquid forms a cone at the end of the capillary tube and if high enough voltage is applied, a jet of liquid droplets forms. Heating can also be applied to the capillary tube to aid in droplet formation. Within the droplets, the analytes are either negatively or positively charged depending on the voltage applied to the capillary. A counter stream of gas, usually nitrogen, is directed at the droplet stream to help remove solvent. As droplets shrink from loss of solvent, the charge density increases and once the electrostatic forces are greater than the surface tension, the droplets break apart. This happens again and again until only gaseous charged species remain, known as the charge residue model. Ions can also be 'emitted' from a droplet when the field strength at the droplet surface is enough to overcome solvation forces. This known as the ion evaporation model. Both processes are believed to contribute to the formation of gaseous ions [reviewed in 285, 286]. The ESI source is schematically illustrated in **Figure 1.4.1**. The resulting ions from ESI are commonly protonated (positive mode) or deprotonated

(negative mode), but additional adducts with e.g., Na^+ or K^+ (positive mode) or Cl^- (negative mode) also occur. Protonation or deprotonation can be aided by adjusting the pH of the solution being introduced to the capillary.

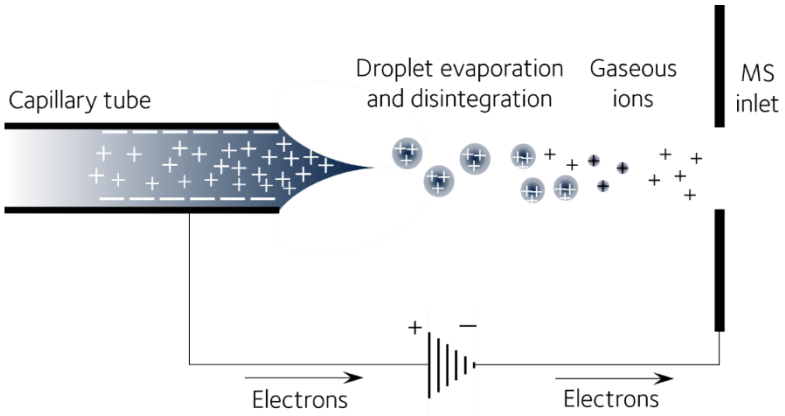

Figure 1.4.1. Schematic illustration of formation of gaseous ions from liquid phase by electrospray ionisation. The power supply is of high voltage, 2-5 kV. Figure adapted from [278].

ESI occurs at near atmospheric pressure, but mass analysers must operate at high vacuum. If not, there would be loss of ions by collisions with other gaseous species. Therefore, after the ion source, ions move through a series of ion guides by application of an electrical field. The geometry of the guide is such that neutral species cannot enter the mass analyser. Additionally, the acceleration ensures that the ions have the same kinetic energy, which is central to the performance of certain mass analysers.

There are many different types of mass analysers available and an important distinction between them is whether they provide high or low mass resolution. The mass resolution is the ability to separate peaks of two different *m/z* values. Mass resolution is generally described using the mass resolving power (R):

Equation 1.1

$$R = \frac{m}{\Delta m}$$

where m is the mass of an ion and Δm is the width of the peak of that ion, at a defined peak height, e.g. full-width half maximum [278]. Low resolution MS (LRMS) instruments usually have R ≤ 10,000, while high resolution MS (HRMS) instruments have R ≥ 60,000 [287]. HRMS instruments provide high enough accuracy in their mass measurements that molecular formulas can be determined. In semi- and untargeted metabolomics, this is invaluable information about the potential identity of a species and HRMS mass analysers are most commonly used. However, for tandem MS, where two mass analysers are connected sequentially, the first mass analyser does not need to be high resolution because the

resolving power ahead of detection is provided by the second mass analyser. The three mass analysers used extensively in this work are described below.

Quadrupole mass analyser

The quadrupole is a low-resolution mass analyser where ions are guided between four straight metal rods by an oscillating electric field. Fixed direct current (DC) is applied to two opposing rods and alternating radio frequency (RF) voltage through the other two. The electric field is adjusted by varying the RF and at certain frequencies ions of specific *m/z* have a trajectory that allows them to pass through the rods, schematically illustrated in **Figure 1.4.2**. The ions with an unstable trajectory collide with the rods and do not reach the detector. A range of *m/z* values can be scanned through to allow ions with different *m/z* to pass.

Three quadrupoles can be connected sequentially for MS-MS analyses, where the second quadrupole is used as a fragmentation chamber, after ion selection by the first quadrupole. The third quadrupole is used to separate the fragments before detection. In hybrid tandem MS, the quadrupole is usually the first of two mass analysers due to its low mass resolution (R ≤ 3,000) [278, reviewed in 288].

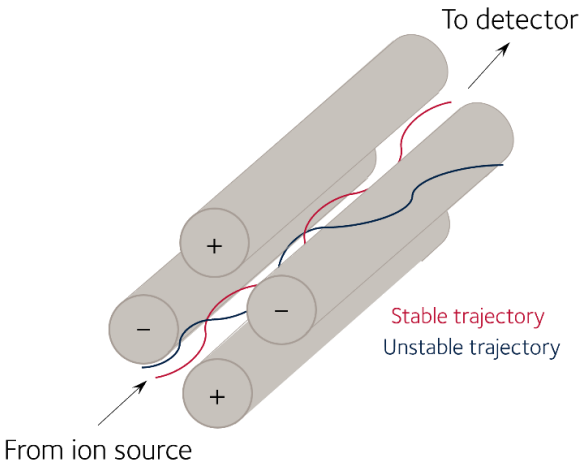

Figure 1.4.2. Schematic illustration of quadrupole mass analyser. Adapted from [278].

Time of Flight mass analyser

Time of flight (ToF) mass analysers separate ions based on the difference in velocity between ions of different mass that have been accelerated with the same amount of kinetic energy. The relationship between kinetic energy, mass and velocity is:

Equation 1.2

$$E_K = \frac{1}{2}mv^2$$

where E_K is kinetic energy, *m* is mass and *v* is the velocity. The kinetic energy applied to an ion is dependent on the charge of the ion and the electric potential (voltage) applied:

Equation 1.3 $$E_K = zU$$

where *z* is the charge of the particle, *U* is the electric potential. Finally, the relationship between velocity, time and distance is:

Equation 1.4 $$v = \frac{L}{t}$$

where L is distance travelled and t is time. Replacing E_K in equation 1.2 with Equation 1.3, and *v* in Equation 1.2 with equation 1.4, then rearranging, it follows that:

Equation 1.5 $$t = \frac{L}{\sqrt{2U}} \times \sqrt{\frac{m}{z}}$$

The distance travelled and voltage applied are the same for all ions entering the mass analyser, thus if two ions have the same charge, the heavier ion will have lower velocity than the lighter ion and take longer to reach the detector [278, reviewed in 288]. To increase the resolution, i.e., separation of ions, the flight length must be increased. This is both done by having longer flight tubes, but also by using reflectrons that turn ions around to travel down a second flight tube [reviewed in 288]. Commercially available HRMS ToF instruments generally have R = 60,000-70,000.

Orbitrap™ mass analyser

The Orbitrap™ consists of an inner spindle electrode and an outer barrel electrode, where an electric field is generated by applying a DC voltage between the two electrodes. Ions are collected and held in a modified quadrupole called a C-trap and then radially injected into the Orbitrap™ as a 'packet' of ions. The injection is achieved by ramping down the RF and applying short bursts of DC [289]. Once inside the Orbitrap™, the ions begin to oscillate around the spindle electrode and along it axially (z-axis). A schematic illustration of the Orbitrap™ mass analyser is provided in **Figure 1.4.3**. The oscillations frequency (ω) along the z-axis of the spindle electrode is related to the ion *m/z*:

Equation 1.6 $$\omega \propto \frac{1}{\sqrt{\frac{m}{z}}}$$

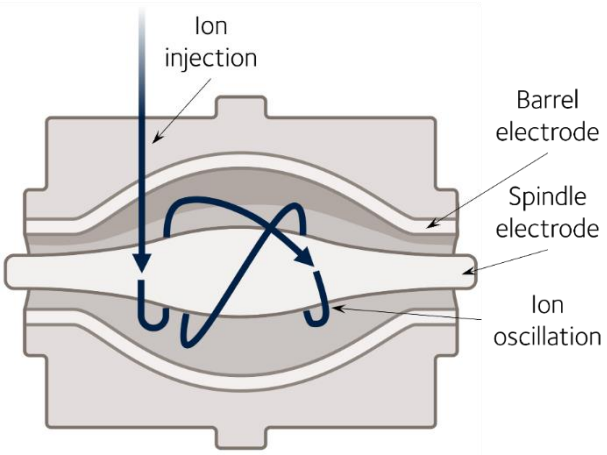

Figure 1.4.3. Schematic illustration of the Orbitrap™ mass analyser. Adapted from [290, 291].

The axial frequency is independent of the energy and spatial spread of ions, unlike the rotational and radial oscillation frequency. The axial oscillation induces a detectable image current that can be Fourier transformed to bring the time-domain signal to mass-to-charge frequency [290-292]. The commercially available Orbitrap™ mass analysers have R ≥ 100,000.

Direct detection of ions

The detection of ions is a part of the mass analysis of ions in the Orbitrap™, but the quadrupole and ToF mass analysers rely on direct detection of ions after they have passed through the mass analyser. The most common form of detector used for direct detection are electron multipliers (EM). In essence, the EM contains a dynode that, when hit with an ion with enough kinetic energy, emits electrons. The emitted electrons are directed such that they will cause more electrons to be emitted and a cascade ensues that increases the original signal a million-fold or more. The resulting current is processed and digitised for simple readout on a computer. There are different EM geometries, broadly split into either continuous or discrete dynodes. Either geometry is fine for a quadrupole mass analyser, but a ToF requires fast detection. A common EM geometry for ToF is therefore multichannel plates where the electron path is short and the resulting pulse width is narrow. The plates can be stacked to increase the signal [reviewed in 293].

1.4.2. Liquid chromatography

MS alone can separate ions based on their *m/z*, but coverage suffers when complex samples are analysed. There are many isomeric metabolites and they cannot be separated by MS. Therefore, it is common to hyphenate MS with either GC or LC. GC requires compounds that can be volatilised, which can be difficult to achieve with the many highly polar and ionisable compounds found in human metabolism. Derivatisation can be used to

achieve ionisation, but it adds additional sample preparation and sources of error. LC, with the use of ESI to achieve gas-phase ions prior to MS analysis, is better suited for the direct analysis of highly polar and ionised metabolites.

No practically feasible LC-MS technique is able to provide robust coverage of all metabolites within the cellular metabolome, as the diversity in chemical structure and functional groups is currently beyond the capabilities of a single LC-MS method. Usually multiple LC-MS techniques have to be employed, but analysis of polar metabolites remains challenging. There are a number of LC column chemistries available, the most commonly used in metabolomics studies being reversed phase (RP) and hydrophilic interaction chromatography (HILIC). RP normally uses carbon chains (C_2-C_{30}, C_{18} most common) as the stationary phase. Common mobile phases are water (polar, weak eluent) and methanol or acetonitrile (less polar than water, stronger eluent). Increasing the less polar fraction of the mobile phase reduces affinity to the stationary phases. The retention time of ionic and polar metabolites is generally poor on standard reversed phase columns [294, reviewed in 295], oftentimes requiring derivatisation to improve retention time [296, 297]. The derivatised RPLC-MS method employed here demonstrates the feasibility of this process, but as mentioned for GC, it adds time to sample preparation and is a source of error. More importantly, derivatisation is selective for a specific functional group and adds substantial complexity to the data analysis of untargeted metabolomics experiments. RP columns made specifically for more polar compounds are available, but in general it is challenging to reach adequate separation, i.e., retention for longer than the void volume of the column.

HILIC comes with a variety of stationary phases: polar non-charged (e.g., amide, cyano or diol), cationic, anionic, and zwitterionic. Different combinations of anion and cation are possible for zwitterionic columns (e.g., sulfobetaine or phosphorylcholine). Polar mobile phases such as water or methanol are the stronger eluent in HILIC, while less polar eluents such as acetonitrile are weaker. The mechanism of retention on a HILIC column is multimodal. Water is adsorbed to the stationary phase and forms an immobilised layer. Analytes be separated based on different degree of partitioning between the immobilised water and the mobile phase passing through the column. In addition, ionic and hydrogen bonding interactions with the stationary phase itself occurs as well [reviewed in 298, 299]. Buffers are added to the mobile phase to improve peak shape and retention time, as they

reduce the electrostatic interactions between charged solutes and charged stationary phase. Furthermore, buffers provide pH control to ensure appropriately charged analytes and charged stationary phase, if acidic/basic [reviewed in 298]. A ZIC stationary phase with immobilised water layer is schematically illustrated in **Figure 1.4.4**. HILIC is capable of separating many different polar compounds with different chemical characteristics [reviewed in 298, 299], but it is not considered as robust as RPLC-MS with regards to retention time stability and peak shape quality. Ion-exchange chromatography is a reliable alternative for the analysis of charged analytes, if coupled to an ion suppressor that is capable of removing eluent ions prior to coupling with MS.

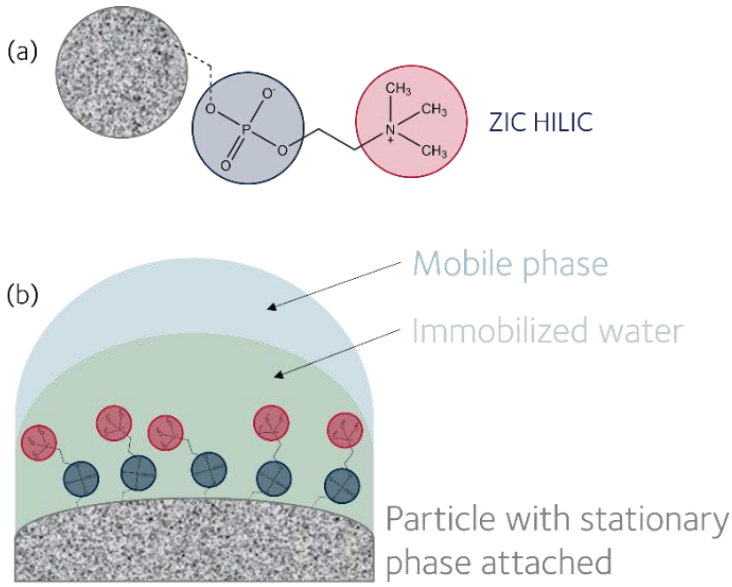

Figure 1.4.4. Schematic illustration of the HILIC stationary phase and immobilized water layer. Here with phosphorylcholine as the stationary phase.

In ion exchange chromatography, the stationary phase is charged (e.g., quaternary ammonium ion) and the mobile phase contains a counter ion (e.g., hydroxide ions). The analytes are separated based on the strength of their ionic interactions with the stationary phase. After the column, the elute is passed through the ion suppressor. The suppressor consists of a channel for eluent, which is flanked on each side by regenerant channels with flow counter to that of the eluent. Electrodes on the outside of the regenerant channels have a DC voltage applied to electrolyse water. The generated ions pass through an ion exchange membrane to the eluent. Depending on the type of ion suppressor, the membrane is either a cation exchange material, allowing hydronium ions through, or an anion exchange material, allowing hydroxide ions through. The hydronium or hydroxide ion

convert the eluent to a nonionised form. In anion exchange chromatography, the eluent is a sodium hydroxide, thus the membrane is a cation exchanger that only allows hydronium ions through to neutralise the hydroxide. Counter ions in the eluent are driven towards the opposite electrode and are removed from the eluent as well. Finally, the analytes are generally converted to their more conducive form [300]. A schematic illustration of the ion suppressor is provided in **Figure 1.4.5**.

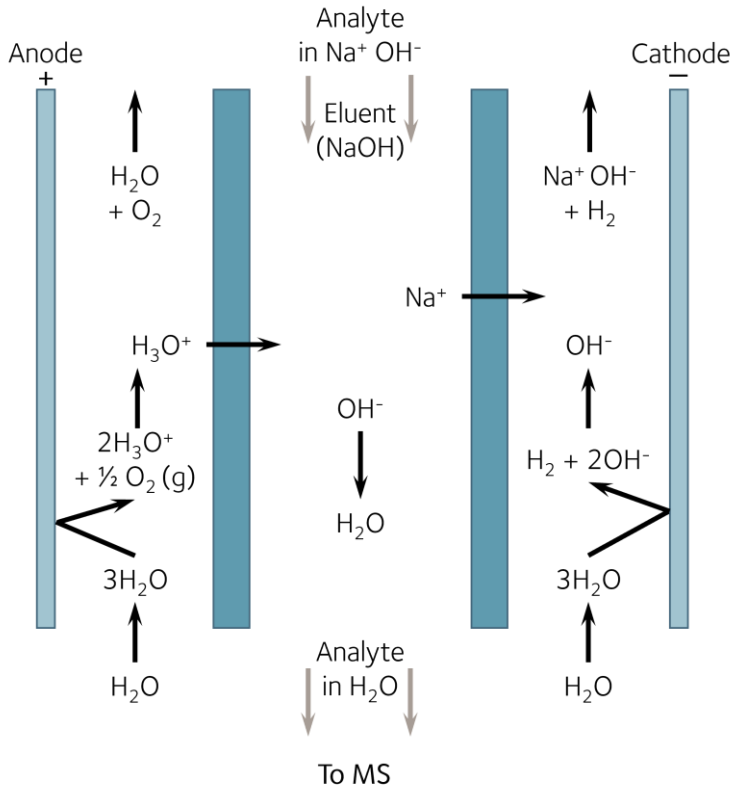

Figure 1.4.5. Schematic illustration of an ion suppressor operating for the eluent suppression of hydroxide ions from an anion exchange chromatographic analysis. Adapted from [300].

Despite the ability to separate highly polar compounds robustly, the technique has not been used widely in metabolomics to date. There is a relatively small number of papers reporting its application [301-305]. In work carried out by Dr John Walsby-Tickle (Services Manager, Mass Spectrometry Research Facility and former McCullagh Group member (DPhil in Metabolomics)), an anion exchange IC-MS method that provides robust separation of highly polar metabolites was established [148]. The method is suitable for measuring metabolites found in *e.g.,* glycolysis, pentose phosphate pathway, TCA cycle, nucleotides and other carboxylic acids. Retention time stability is excellent (± 0.1 min) [148] and peak shapes are generally symmetric with stable peak areas. No additional sample

preparation after filtration and sample normalisation (to DNA or protein concentration) is required. The method has been applied to a growing number of different metabolomics studies [127, 306-312]. Because of its coverage of highly relevant areas of mutIDH1 metabolism, excellent chromatographic capabilities and simple requirements to sample preparation, the method was used extensively in this thesis for semi-targeted metabolomics analysis.

1.5. Metabolic functional analysis using untargeted pathway analysis

Metabolomics data analysis usually includes univariate analyses, e.g., significance tests and calculation of FCs, as well as multivariate analyses, e.g., principal component analysis (PCA), partial least squares discriminant analysis (PLS-DA) or cluster analysis such as hierarchical cluster analysis (HCA). The statistical methods are appropriate for e.g., assessing similarities or differences between experimental groups and identifying biomarkers. However, they are focussed on individual variables or groups of variables without consideration of the pathways that the metabolites are a part of. Functional analysis is the analysis of whole pathways, but has traditionally been focussed on genes and genetic output like transcripts and proteins. The genome is studied to better understand how specific genes or gene products within a system contribute to the observed phenotype. Transcriptomics and proteomics provide closer links to the genome (DNA) than metabolites, but metabolites are more closely linked to the observed phenotype. The difficulty of using metabolites for functional analysis lies in their identification.

The gold standard of metabolite identification in LC-MS based metabolomics is matching retention time, *m/z*, isotopic pattern and preferably fragmentation pattern to a known standard. This is a time-consuming and expensive process, with some metabolites lacking commercially available standards. However, high resolution LC-MS still provides valuable information in *m/z* values with sufficient accuracy to determine molecular formulas and an additional dimension of information from retention time. The latter improves the feasibility of matching fragments and adducts that originate from the same compound. However, there can still remain a lot of potential metabolite annotations for the same *m/z* value, as noted by Li *et al.* [313]. The authors of Li *et al.* reason that metabolites in a pathway are not independent of each other and any true biological change would be clustered or

enriched in a specific area of a metabolic network. Thus, when assigning metabolites to LC-MS features, the ones that cluster together are more likely to be the correct identity than those distributed randomly across the network. Li *et al*. developed an algorithm that married functional analysis and metabolite annotation, by performing the processes together. In a later iteration, they added retention time as an additional option to improve the robustness of metabolite annotations [314].

The algorithm requires a list of all *m/z* measured ranked by p-value from a Student's t-test, and matching retention time if available. Two complementary analyses are carried out: module and pathway analysis. The results from both are combined for the final output. The module analysis is based on a metabolic network model (MNM) made by the authors using Kyoto Encyclopaedia of Genes and Genomes (KEGG), University of California San Diego (UCSD) Recon1 and the Edinburgh human metabolic network [315-318]. In module analysis, modules can form within and between pathways making it less biased than pathway analysis because it is not constricted to only pre-defined pathways. The significant features are used to search MNM for matched metabolites, identifying subnetworks of metabolites connected by reactions. From the subnetworks, structural modules with more connections than would be expected randomly are identified. The subnetworks and structural modules are considered candidate modules ($G_1, G_2, \ldots, G_N$), for which an activity score is calculated based the number of matched metabolites contributing and the degree of modularity. Li *et al*. defined the activity score for a candidate module *G* as follows [313, p. 3]:

Equation 1.7

$$A = Q \times \frac{N_{I,G}}{N_G}$$

where N_G is the number of metabolites in *G* and $N_{I,G}$ is the number of significant metabolites. *Q* is the Newman-Girvan modularity:

Equation 1.8

$$Q = \sqrt{\frac{N_I}{N_G}} \times \left(\frac{E_G}{m} - \sum_{i,j} \frac{k_i}{2m} \frac{k_j}{2m}\right), i, j \in G$$

where k_i was the network degree of metabolite *i*, *m* the total number of edges in the MNM, E_G the total number of edges in *G*, and N_I the number of "input metabolite" [313, p. 3]. Finally, Li *et al*. adjusted Q by the square root of N_I/N_G to decrease the bias towards larger

modules. Random models are made by sampling from the non-significant features with the same number of features as the significant list. The activity scores from the random samples are used to calculate a distribution that is then used estimate the significance of each module [313].

The significance of the pathway module is estimated with a similar method. Random samplings of the non-significant features, at the same length as the list of significant features, are matched to pre-defined pathways. A right-tailed Fishers exact test (FET) is performed. The FET p-value indicates whether the pathway is significantly enriched or not. The process of random sampling, matching to pathways and calculating FET right-tailed p-values is performed multiple times. The p-values are needed to calculate a distribution that is later used to adjust the p-values of the 'true' model. The true model is made with significant features only. In addition to a FET p-value, an EASE[1] score adjusted p-value is calculated as well. The EASE score adjustment involves removing one 'hit' from the pathway and then calculating the FET p-value [319].

The final output is a list of pathways found and the p-values calculated from module and pathway analysis. The number of significant empirical compounds (ECs) found per pathway is reported, together with a separate list of ECs matched to KEGG compound codes. The exact identity of the EC is not provided, as multiple KEGG codes can match to the same EC. The ECs and matching KEGG codes can be used to assess whether the putative annotations are reasonable considering the column chemistry used for analysis. For the biological interpretation, however, it is the whole pathway that is of interest and less so specific metabolites.

1.6. Summary and aim of study

In the study of *IDH1* and *IDH2* mutations in glioma, metabolomics has, in addition to proteomics, transcriptomics and techniques such as ^{13}C tracer experiments, shown that remarkably high intracellular and extra-cellular levels of *R*-2-HG are accompanied by apparently wide-ranging, potentially context dependent, effects on metabolism and redox homeostasis. It has been proposed that many of the metabolic changes observed in mutant

[1] Expression Analysis Systematic Explorer (EASE) is a software application.

IDH1/2 cells are a consequence of elevated *R*-2-HG, in particular via inhibition of specific enzymes, but direct evidence for this is only available in a relatively small number of cases.

Glioma cells harbouring mutIDH1 appear less glycolytic and rely to a greater extent on oxidative phosphorylation than their wtIDH1 counterparts. Altered metabolic flux in mutant *IDH1* cells appears to compensate for reduced production of NADPH by wtIDH1/2 and increased consumption by mutIDH1/2. However, the consumption of NADPH by mutIDH1/2 extends beyond upregulation of the PPP and the compensatory mechanisms are poorly understood. Glutathione metabolism is also modulated with likely pleiotropic effects on redox chemistry in cells. Amino acid and lipid metabolism are often reported to be altered in mutIDH1/2 cancer cells but the type and extent of changes appears to be highly context and disease-model dependent; a better understanding of what drives changes in amino acids levels in mutIDH1/2 cells is needed.

Selective inhibition of mutIDH1 or mutIDH2 has been demonstrated as a chemically and biologically tractable therapeutic approach and inhibition of mutIDH1/2 leads to a clear reduction in *R*-2-HG levels *in vitro* and *in vivo*. In terms of patient benefit, the inhibitors have mainly been tested for efficacy on patients with more advanced disease and provide relief from disease progression. To date relatively little focus has been given to targeting metabolic vulnerabilities other than elevated *R*-2-HG. This is likely in part due to a lack of consistency across different models and how well the models reflect relevant disease-specific targets.

A significant amount of research revealing altered metabolism in *mutIDH* cells has been conducted, but there needs to be a better understanding of the relationship between elevated 2-HG levels and other metabolic changes. Furthermore, it remains to be determined whether pursuing direct inhibition of the mutIDH1/2 enzymes using specific inhibitors, or modulating other metabolic targets, either alone or in combination with mutIDH1 inhibition, will lead to the most effective therapeutic approach for treatment of patients with mutIDH1/2 cancers.

In order to further our understanding of the effects of IDH mutations on cell function the objectives of this thesis were therefore to:

1. Investigate the metabolic effects of *IDH1* mutation and elevated 2-HG in glioblastoma cell models using a range of LC-MS-based metabolomics methods and asking the questions:
    i. How is 2-HG abundance altered in mutIDH1^{R132H} cells?
    ii. Are other metabolites altered in abundance in mutIDH1 cells?
2. Explore the effect of experimental and FDA approved mutIDH inhibitors on 2-HG levels in wtIDH1 and mutIDH1^{R132H} GBM cells.
    i. How do different mutIDH1 inhibitors compare in their ability to decrease 2-HG abundance in mutIDH1^{R132H} GBM cells?
3. Explore broader metabolic changes linked to treatment of cells with mutIDH1 inhibitors
    i. Are other metabolites modulated in wtIDH1 and mutIDH1^{R132H} GBM cells after treatment with mutIDH1 inhibitors?
    ii. Are abundance changes in other metabolites correlated to 2-HG abundance changes?
    iii. What can this pattern of changes tell us about altered metabolism?
4. Explore the metabolic effect of inhibiting GLS in wtIDH1 and mutIDH1^{R132H} cells:
    i. Is 2-HG abundance decreased with decreasing glutamate abundance?
    ii. Is the change in glutamine, glutamate or 2-HG levels correlated with additional metabolic modulation, and is there a difference in response between wtIDH1 and mutIDH1^{R132H} cells?

Chapter 2. Methods and materials

In chapter 2, the materials and experimental methods that were used to collect the data presented in chapter 3-6 are described. The first two sections (**2.1 and 2.2**) list the equipment, consumables, LC-MS systems and chemicals used. The next section (**2.3**) describes the solutions prepared for general use, tissue culture, as well as sample processing and analysis. The cell lines used throughout the thesis are described in **section 2.4**. How the cells were cultured, plated for specific experiments, and collected prior to further sample processing is presented in **section 2.6**. Preparation of standards, cell and media samples for LC-MS analysis is detailed in **section 2.6**. Sample analysis by LC-MS or plate reader is described in **section 2.7**, with data processing specifics provided in **section 2.8**.

2.1. Instrumentation

2.1.1. Equipment and consumables

Small instruments

Water purification was done with a Milli-Q Direct 8 system, equipped with a Millipak® Express 40 filter with pore size of 0.22 µM, both from Merck Millipore (Burlington, MA, USA).

Microscopy inspection of cells was done with a Motic AE31E trinocular microscope from Motic (Kowloon, Hong Kong). Cell counting was done with a Countess™ II FL Automated Cell Counter, using Countess™ Cell counting chamber slides, both from Thermo Fisher Scientific (Waltham, MA, USA). Spectroscopic measurements of samples were done with either a NanoDrop One microvolume UV-VIS spectrophotometer from Thermo Fisher Scientific (Waltham, MA, USA) or a CLARIOStar® Plus multi-mode plate reader (fitted with an LVis Plate) from BMG Labtech (Ortenburg, Germany). Sample centrifugation was carried out on a Megafuge 8R Small Benchtop Centrifuge from Thermo Fisher Scientific (Waltham, MA, USA), with either a 30-sample or 48-sample insert.

Consumables: tubes, filters and vials

Sterile polypropylene CryoPure tubes, 2mL, with QuickSeal screw cap were purchased from Sarstedt AG & Co. KG (Nümbrecht, Germany). Sartorius Minisart™ regenerated cellulose

(RC) syringe filters with 0.2 µm pore size and 15 mm filter diameter were acquired from Fisher Scientific (Waltham, MA, USA). Amicon® Ultra 0.5 mL RC filters with either 3 kDa or 10 kDa molecular weight (MW) cut-off were purchased from Merck (Darmstadt, Germany). LCGC clear glass total recovery vials with cap and pre-slit PTFE/silicone septum (1 mL volume) were acquired from Waters (Milford, MA, USA). Measurement of pH was done with pH-Fix 0-6 and pH-Fix 7-14 strips from Fisher Scientific (Waltham, MA, USA), as well as pH-Fix 6.0-7.7 strips from Macherey-Nagel (Düren, Germany).

Petri dishes and multi-well plates

Sterile polystyrene 60 mm and 100 mm petri dishes for adherent cells and with lids were from Sarstedt AG & Co. KG. Sterile, clear and flat-bottomed 12- and 96-well plates that were individually wrapped and had lids with condensation rings, were purchased from Scientific Laboratory Supplies (Galveston, TX, USA). Non-sterile, non-treated, clear, flat-bottomed, polystyrene 96-well assay plates with low evaporation lids were acquired from Corning Inc (Corning, NY, USA). The freezing container, a Mr. Frosty™, was from Thermo Fisher Scientific (Waltham, MA, USA).

Chromatographic columns

A Dionex™ IonPac™ AS11-HC column (2 × 250 mm, 4 µm particle size) was acquired from Thermo Fisher Scientific (Waltham, MA, USA). A SeQuant® ZIC®-cHILIC (2.1 × 150 mm, 3 µM particle size, 100 Å) column was purchased from Merck (Darmstadt, Germany). The four following columns were all purchased from Waters (Milford, MA, USA): AccQ·Tag™ ULTRA C18 (2.1 × 100, 1.7 µM particle size), Atlantis Premier BEH Z-HILIC (2.1 × 100 mm, 1.7 µm particle size), ACQUITY UPLC® BEH Amide (2.1 × 100 mm, 1.7 µm particle size) and CORTECS® UPLC® T3 C18 (2.1 × 100 mm, 1.6 µm particle size).

2.1.2. Chromatography systems and mass spectrometers

Two different systems from Waters (Milford, MA, USA) were used: The Xevo G2-XS QToF and the Vion IMS QToF. Both instruments were equipped with a Zspray™ ion source with LockSpray™ set to H-ESI mode. Furthermore, both were connected to Acquity UPLC® I-Class Pluss systems with flow-through needle (FTN) sample managers. The Xevo and the Vion had hybrid quadrupole and ToF mass analysers. The Vion also had a travelling wave ion mobility cell preceding the mass analyser.

The Q-Exactive HF, a hybrid quadrupole-Orbitrap, was equipped with a HESI II probe, connected to a Dionex ICS 5000+ HPIC system, fitted with a Dionex 500e ERS suppressor. The Q-Exactive HF and HESI II probe were from Thermo Fisher Scientific (Waltham, MA, USA), while the ICS 5000+ was from Dionex (Sunnyvale, CA, USA). The Orbitrap Exploris 240™, also a quadrupole-Orbitrap hybrid, was equipped with an EASY-IC™ ion source, both from Thermo Fisher Scientific (Waltham, MA, USA). The Exploris 240™was connected to an Ultimate-3000 UHPLC pump from Dionex (Sunnyvale, CA, USA).

2.2. Chemicals

2.2.1. General use chemicals

Water was purified on the MilliQ system to the requirements of type 1 water (resistivity 18.2 MΩ·cm and low total carbon content (2 ppb). Unless otherwise mentioned, all water used was type 1 water. Methanol (≥99.9%, for HPLC), acetonitrile (≥99.9%, for HPLC) and isopropanol (≥99.9%, for HPLC) were from Sigma Aldrich (Saint-Louis, MO, USA). Unless otherwise mentioned, all methanol, acetonitrile and isopropanol used throughout was HPLC purity.

2.2.2. Chemicals for cell culture

Cell medium and supplements

Non-USA origin foetal bovine serum (FBS) and liquid DMEM with phenol red, sodium bicarbonate (3.7 g/L), sodium pyruvate (1.0 mM), high (4500 mg/L) or low (1000 mg/L) glucose and without glutamine or HEPES (4-(2-hydroxyethyl-1-piperazineethansulfonic acid), were acquired from Sigma-Aldrich (Saint-Louis, MO, USA). Liquid Dulbecco's

phosphate buffered saline (PBS), without calcium chloride or magnesium chloride, BioXtra D-(+)-glucose (100 g/L in water), and trypsin-EDTA solution (2.5 g porcine trypsin and 0.2 g EDTA·4 Na per litre of Hank's Balanced Salt solution and phenol red) were also acquired from Sigma-Aldrich (Saint-Louis, MO, USA). L-glutamine (200 mM), L-glutamine-$^{13}C_5$ (98% ^{13}C) and D-glucose-[1,2]-$^{13}C_2$ (99% ^{13}C) was purchased from Merck Life Science (Darmstadt, Germany). Liquid DMEM without glucose, glutamine, sodium pyruvate or phenol red was purchased from Gibco, Thermo Fisher Scientific (Waltham, MA, USA). Sodium pyruvate (100 mM) and GlutaMAX™ (GM™) supplement (200 mM L-alanyl-L-glutamine in 0.85% NaCl) were also purchased from Thermo Fisher Scientific (Waltham, MA, USA). All purchased solutions and FBS were sterile filtered by the manufacturers.

Dimethyl sulfoxide (DMSO) (molecular biology grade, 99.9%) was purchased from Sigma Aldrich (Saint-Louis, MO, USA) and was sterile filtered in house with a 0.2 µm RC syringe filter. Trypan blue was included with the Countess™ cell counting chamber slides from Thermo Fisher Scientific (Waltham, MA, USA).

Metabolic inhibitors

MutIDH1 inhibitors BAY1436032, AG-120 and AG-881 were purchased from Enzo Life Sciences (UK) Ltd (Exeter, UK), all with purity 98% (HPLC), while GSK-864 (≥98%, HPLC) was purchased from Sigma-Aldrich (Saint-Louis, MO, USA) and FT2102 (98.35%) from MedChemExpress LLC (Monmouth, NJ, USA). Glutaminase (GLS1) inhibitor CB-839 (≥ 98%) was acquired from Cayman Chemical Company (Ann Arbor, MI, USA).

2.2.3. Chemicals for sample processing and analysis

AccQ-Tag™ Ultra derivatization kit containing sodium tetraborate decahydrate buffer, 6-aminoquinolyl-N-hydroxysuccinimidyl carbamate (AQC) reagent and acetonitrile was acquired from Waters (Milford, MA, USA). Amino acid standard (analytical standard) was purchased from Sigma Aldrich (Saint-Louis, MO, USA). MTS kits were purchased from Abcam PLC (Cambridge, CB2 0AX, UK) and Enzo Life Sciences (UK) Ltd. The D-glucose assay kit (glucose oxidase/peroxidase (GOPOD) format) was acquired from Megazyme/Neogen (Bray, Ireland and Lansing, MI, USA).

Formic acid (99%, for analysis) was purchased from Thermo Fisher Scientific (Waltham, MA, USA). Ammonium formate (Optima® LC-MS grade) was acquired from Fisher Scientific

(Waltham, MA, USA). Ammonium hydroxide solution (~ 25% NH_3, puriss), ammonium acetate (for MS, eluent additive for LC-MS), and ammonium bicarbonate (BioUltra, ≥ 99.5%) were from purchased Sigma Aldrich (Saint-Louis, MO, USA). The EGC 500 KOH potassium hydroxide eluent generator cartridge was from Dionex (Sunnyvale, CA, USA). AccQ-Tag™ Ultra Eluent A concentrate (1 L) containing phosphoric acid, triethylamine and sodium azide was purchased from Waters (Milford, MA, USA).

NAD^+, NADH, $NADP^+$ and NADPH (98%) standards were acquired from Roche Diagnostics GmbH (Mannheim, Germany).

2.3. Solutions

2.3.1. General use solutions

An 80% aqueous methanol solution (v/v) ($MeOH_{(aq)}$) was made by measuring the volumes of methanol (80 mL) and water (20 mL) separately in graduated cylinders before mixing in a glass Schott bottle. The solution was stored at 4 °C between use.

2.3.2. Solutions for cell culture

Cell culture stock solutions

Stock solutions of all inhibitors (AG-120, AG-881, BAY 1436032, FT2102, GSK864 and CB-839) were dissolved in DMSO to 5 mM concentration. D-glucose-[1,2]-$^{13}C_2$ was dissolved in water (50 mM) and L-glutamine-$^{13}C_5$ was also dissolved in water (200 mM). All stock solutions were sterile filtered with 0.2 µm Sartorius Minisart™ filters, before storage at -20 °C between use.

Cell medium and related solutions

PBS and trypsin-EDTA were used as supplied. The trypsin-EDTA was aliquoted (8-12 mL) and stored at -20 °C prior to use, once thawed it was stored at 4 °C and used within two weeks. PBS was kept at room temperature, both prior to and during use. Both high and low glucose (HG or LG) DMEM were supplemented with 10% (v/v) FBS and 1% (v/v) GM™,.

The DMEM without glucose, sodium pyruvate, glutamine or phenol red was used to make cell medium for several different experiments. In all experiments it was supplemented with 10% (v/v) FBS and 1.0% (v/v) sodium pyruvate (100 mM). It was then either supplemented

with 1.0% (v/v) BioXtra D-(+)-glucose and 1.0% GM™; 1.0% (v/v) BioXtra D-(+)-glucose and 0.1%, 0.5%, 1.0%, 1.5% or 2.0% (v/v) GM™; 1.0% (v/v) BioXtra D-(+)-glucose solution and 1.0% L-glutamine solution (200 mM); 1.0% (v/v) of 50 mM D-glucose-[1,2]-$^{13}C_2$ and 1.0% L-glutamine solution (200 mM); or 1.0% (v/v) BioXtra D-(+)-glucose solution and 1.0% (v/v) 200 mM L-glutamine-$^{13}C_5$. Final glucose concentration in all media compositions was 5 mM and the media with glutamine or GM™ had a final concentration of 2 mM.

Aliquots of FBS (50 mL) and GM™ (5 mL) were stored at -20 °C prior to use, non-supplemented medium was stored at 4 °C. The sodium pyruvate and glucose solutions were stored at 4 °C prior to first use and at -20 °C after opening. Once supplemented, the medium was stored at 4 °C between use and kept for a maximum of four weeks.

2.3.3. Solutions for sample harvest and processing

Routine and redox harvest solutions

Routine metabolomics harvests used the 80% $MeOH_{(aq)}$ solution described previously. Redox harvests used two solutions: extraction and neutralising. The extraction solution was made by mixing 40:40:20 of acetonitrile, methanol and water by volume. The volumes of each solvent were measured separately. Finally, pure formic acid was added to reach a final concentration of 0.1M. The neutralising solution was 15% (w/v) NH_4HCO_3 in water, made by dissolving 1.5 g NH_4HCO_3 in 10 mL water. Both solutions were stored at 4 °C between use.

Amino acid derivatisation reagent

The reagent was prepared with solutions from the AccQ-Tag™ Ultra derivatization kit. From bottle 2B, 1.000 mL of solvent (acetonitrile) was transferred to bottle 2A (powder 6-aminoquinolyl-N-hydroxysuccinimidyl carbamate). Bottle 2A was heated at 55 °C for 10 minutes or until all solids were dissolved. The solution was stored at room temperature and used within a week of preparation, as recommended by the manufacturer.

Acetonitrile solutions for denaturing and precipitating proteins in media samples

An acidic protein precipitation/denaturation solution was prepared by adding 1% (v/v) formic acid to 200 mL of acetonitrile. A basic protein precipitation/denaturation solution was prepared by 1% (v/v) $NH_{3\,(aq)}$ (~25 %) to acetonitrile. The solutions were stored at 4 °C in glass Schott bottles between use.

Glucose assay solutions

The GOPOD reagent buffer (*p*-hydroxybenzoic acid and 0.095% (w/v) sodium azide was diluted to 1.0L in a volumetric flask with water. The dry reagent powder, containing glucose oxidase plus peroxidase and 4-aminoantipyrine, was dissolved in 20 mL of the diluted reagent buffer and then transferred to the volumetric flask. The solution was protected from light, aliquoted and stored at -20 °C before use.

The concentration of the provided D-glucose standard solution was 1.0 µg/µL. Five dilutions were made to establish a calibration curve. The following dilutions were made: 0.750 µg/µL, 0.500 µg/µL, 0.250 µg/µL, 0.125 µg/µL and 0.05 µg/µL. The diluent was water.

2.3.4. Mobile phases and standards for chromatographic sample analysis

All mobile phases were stored at room temperature after preparation.

Mobile phases for amino acid analysis with derivatised RPLC-MS

AccQ·Tag™ Ultra Eluent A concentrate was diluted by mixing 1 part eluent A concentrate with 9 parts water, measured separately with graduated cylinders. Eluent B, which was 1.3% (v/v) formic acid in acetonitrile, was prepared by measuring the solvent and acid with graduated cylinders. Both mobile phases were mixed well prior to use by shaking. Eluent A was used within three months of preparation, eluent B was used within 6 months. Preparation of the amino acid standard is described in **section 2.6.2**.

Mobile phases and standards for non-derivatised RPLC-MS

Mobile phase A was 0.1% (v/v) formic acid in water and mobile phase B was 0.1% formic acid in methanol. Both solutions were made by measuring the solvent with a graduated cylinder and then adding formic acid to the bottle via a dispenser set to the appropriate volume. Both mobile phases were mixed well prior to use by shaking. Mobile phase A was used within a month of preparation, mobile phase B was used within 3 months.

Standards (1 µM) of the mutIDH1 inhibitors (AG-120, AG-881, BAY 1436032, GSK864) were made by diluting the stock solutions with 80% $MeOH_{(aq)}$. A 5 µM standard of GLS1 inhibitor CB-839 was prepared the same way.

Mobile phase buffers and standards for HILIC-MS

All volumetric measurements of solvents for mobile phase buffers were done with graduated cylinders. The mobile phases were kept in glass Schott bottles at room temperature after preparation. Buffers were used within a week of preparation. Seven different mobile phase buffers were prepared for the three different HILIC columns tested (amide (BEH amide), ZIC phosphorylcholine (ZIC® cHILIC), ZIC sulfobetaine (Z-HILIC)). In addition to the mobile phase buffers, pure acetonitrile was used as the second mobile phase. Adjustment of pH was done with ammonium hydroxide (25% w/v) or formic acid. The pH was measured using pH strips.

For the amide column, a mobile phase buffer consisting of 95:5 water:acetonitrile with 20 mM ammonium acetate and 20 mM ammonium hydroxide was prepared (pH 9). For the ZIC phosphorylcholine column two different mobile phases buffers were prepared: 20 mM ammonium acetate, one each at pH 6 and pH 9. Finally, for the ZIC sulfobetaine column, the following mobile phases were prepared: 20 mM ammonium acetate, one each at pH 6 and 9; 5 mM ammonium formate (pH 6); and 20 mM ammonium formate, one each at pH 3, 6, and 9.

Stock solutions of NAD^+, NADH, $NADP^+$ and NADPH were made up in water at approximately 1-2 mg/mL concentration by weighing out a known amount of standard and diluting with 1 mL water. Then the exact molar concentration was determined and the diluted standards were made using the redox extraction solution and neutralising solution. Per 100 µL of extraction solution, 8.7 µL of neutralising solution was added. A mix of all four metabolites was prepared at 50 µM, which was further diluted to 3.0 µM. A calibration curve with the following concentrations was prepared in the same manner: 1.0, 0.75, 0.50, 0.25, 0.10 and 0.05 µM.

2.4. Cell lines

The LN18 cell line was originally from ATCC (CRL-2610). The expression of mutIDH1^{R132H} was done with a stable lentiviral insert, carried out by Dr Chiara Bardella and colleagues at the University of Birmingham and kindly gifted. Two different 'generations' of LN18 wtIDH1 and mutIDH1 cells lines were used. The first-generation LN18 wtIDH1 cell line was untransmuted, while the mutIDH1^{R132H} LN18 cell line was established using the methods described in [148, 320]. In the second generation, a different lentiviral vector was used (pUltra-Chili) and wtIDH1 LN18 was transduced with an empty lentiviral vector. Two different *IDH1* mutant variants were provided: mutIDH1^{R132H} and mutIDH1$^{R132H+S280F}$. The methods for establishing the second generation are described by Reinbold *et al*. [312]. Unless otherwise noted, the second-generation wtIDH1 and mutIDH1^{R132H} cell line was used.

2.5. Tissue culture

The following chapter section details the methods used during cell culture and preparation of cell samples for metabolomics and cell-based assays. The methods applied in the different experiments were quite similar to each other, thus they are described in general terms in the sections outlined in **Figure 2.5.1**. A detailed overview of all metabolomics experiments carried out, with specific LN18 cell line variants, media composition and inhibitors, as well as harvesting methods are provided in **Table 2.5.7.1** and **Table 2.5.7.2** in **Section 2.5.7**. Throughout this chapter section, any reference to incubation of cells will at all times mean incubation at 37 °C and 5% CO_2 under normoxic conditions. With regards to media, LG DMEM supplemented with 10% (v/v) FBS and 1.0% (v/v) GM™ was used, unless otherwise specified. Finally, a biological replicate was defined as a sample consisting of cells or media from a single plate or well. An analytical replicate was a repeat measurement of e.g., a standard or a biological replicate.

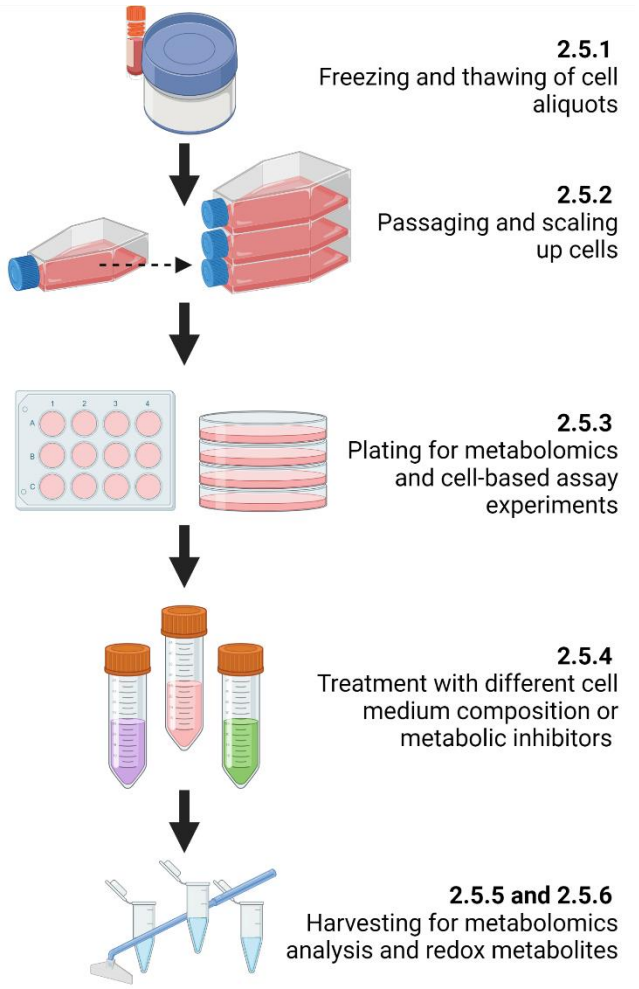

Figure 2.5.1. Overview of methods described in section 2.5.

2.5.1. Thawing and freezing of cell aliquots

Cell aliquots were thawed rapidly (2-3 minutes) in a heated water bath (35-40 °C) before transfer to a 15 mL Falcon tube with 10 mL of HG DMEM. The sample was centrifuged at 0.2 relative centrifugal force (rcf) for 2 minutes to gently pellet the cells. The supernatant

was removed and cells were resuspended in 5- or 10-mL fresh medium for transfer to a T25 or T75 flask, respectively. Media was replaced after 24 hours to remove cells that had not adhered after thawing.

Stocks of cell aliquots were prepared by mixing resuspended cells with an equal amount of HG DMEM with 16% (v/v) DMSO. The final concentration of DMSO was 8% (v/v). Aliquots of 1.0 or 1.5 mL were transferred to cryovials. The aliquots were frozen slowly by being placed in a Mr. Frosty™ freezing container with isopropanol, overnight, at -80 °C. Once fully frozen, the cell aliquots were stored at -80 °C until thawing.

2.5.2. Passaging and scaling up cells

Prior to detaching cells, media was removed from the flask by pouring and cells were washed with an equivalent volume of PBS (e.g., 5 mL PBS for a T25 flask). After the PBS was removed by aspiration, the cells were washed with trypsin-EDTA (0.5 mL for T25 flask, 1.0 mL for T75 flask and 2.0 mL for T175 flask). The flask was incubated until cell detachment (2-5 minutes). Once detached, the cells were washed with fresh media and aspirated to disperse the cells. Resuspended cells were diluted by transfer to a new flask with fresh media. Exact dilution ratios depended on cell line and confluency, and could range from 1:1 to 1:10. To increase the number of cells, e.g., for large experiments requiring many plates, the resuspended cells would be diluted at ratios from 1:1 to 1:10 into an increased number of and/or larger flasks.

2.5.3. Plating for metabolomics and cell-based assay experiments

Plating for metabolomics experiments

Plating cells and subsequent harvest for metabolomics analysis was done with 60 mm dishes or 12-well plates. Cells were resuspended as described for passaging and then counted with the Countess™ II FL Automated Cell Counter using Countess™ Cell counting chamber slides. Counting was done by mixing 11 µL of trypan blue dye with 11 µL resuspended cells in a 0.5 mL microtube and then transferring 10 µL of the mixture to each side of the slide.

Once counted, cells were either diluted down to the equivalent of the most dilute cell line being plated at the time or an appropriate number depending on plate/dish size and cell

line growth rate. For the 60 mm dishes the maximum number of cells plated was 300,000 cells/mL and for 12-well plates it was 200,000 cells/mL. Cells were counted again post-dilution. The dilution ratio of resuspended cells depended on the size of the plate/dish. For 60 mm dishes, 1.0 mL of re-suspended cells was mixed with 2.0 mL fresh media. For 12-well plates, 0.700 mL of resuspended cells were transferred to each well without further dilution. In a long time-course experiment, cells grown for timepoints 24 and 48 hours were plated as described for 12-well plates. Cells grown for timepoints 72 and 96 hours were diluted 1+1 and 1+3 (resuspended cells + fresh media) before transfer to individual wells. The final cell number after dilution for the 72- and 96-hour timepoint were 100,000 and 50,000 cells/mL, respectively.

Plating for colorimetric-based assays

Colorimetric cell-based assays were carried out in sterile, flat-bottom, clear-walled 96-well plates. The spaces between all wells were filled with 50 µL PBS. Cells were resuspended as when passaging, then counted as previously described and diluted to approximately 100,000 cells/mL. After dilution the count was repeated. The outer edge of wells (row A, row H, column 1 and column 12) were left empty. For each well containing cells, 100 µL of resuspended cells were transferred. The final number of cells per well was approximately 10,000. For the long time-course (L-TICO) colorimetric assay, cells grown for the 24- and 48-hour timepoints were plated as described, i.e., final cell number per well was approximately 10,000. The cells grown for the 72- and 96-hour timepoints were diluted to approximately 50,000 and 25,000 cells, respectively, with final number of cells per well 5,000 and 2,500.

2.5.4. Treatment with different cell medium composition or metabolic inhibitors

In all experiments, except for a metabolomics L-TICO treatment with mutIDH1 inhibitors, cells were incubated for a minimum of 24 hours after plating before treatment was added.

Treatment of cultured cells with metabolic inhibitors or different media composition: 60 mm dish

The 60 mm plates had a total media volume of 3 mL. After 24 hours of incubation, 1 mL of spent media was removed and 1 mL of fresh media containing 15 µM inhibitor was added, for a final concentration of 5 µM of drug. Control medium containing the drug stock solution solvent (DMSO) had DMSO added to the equivalence of the inhibitor media. For

all experiments in 60 mm dishes, the final amount of DMSO in the control media was 0.1% (v/v). Treatment and control medium were left on the cells for 24 hours. The only exception to this methodology was for the ^{13}C tracer experiment. All spent medium was removed after 24 hours and 3 mL of either media without labelling, media with ^{13}C-labelled glucose and unlabelled glutamine, or media with unlabelled glucose and ^{13}C-labelled glutamine was added. The cells were incubated for an additional 24 hours before harvest.

All experiments carried out in 60 mm dishes are listed in **Table 2.5.7.1**. The table summarises cell lines, inhibitors, treatment concentration and number of biological replicates.

Treatment with metabolic inhibitors: 12-well plate

For 12-well plates, all spent media (0.700 mL) was removed and replaced with media containing the appropriate concentration of drug after 24 hours of incubation. All media was made up with the same percentage (v/v) DMSO, i.e., media with lower concentration of inhibitor had DMSO added to match the DMSO percentage of the control media as well as the media with highest drug concentration. Media with the following concentration of mutIDH1 inhibitors (AG-120, AG-.881, BAY 1436032 and GSK864) were used: 0.05, 0.50, 5.00 and 10.0 µM, and 0.2% (v/v) DMSO. Media with the following concentrations of glutaminase inhibitor (CB-839) were used (in a separate experiment): 0.05, 0.10, 0.30, 0.70, 1.00, 3.00 and 5.00 µM, with 0.1% (v/v) DMSO. In all experiments, treatment was left on the cells for 24 hours, except the time-course experiments which are further described below. All experiments carried out in 12-well plates are listed in **Table 2.5.7.2**. The table summarises cell lines, inhibitors, treatment concentration and number of biological replicates.

Metabolomics time-course experiments

In both the L-TICO and short time-course experiments (S-TICO), mutIDH1 inhibitors AG-120, AG-881, BAY1436032 and GSK864 were used. The plate layout used for all timepoints in the short and long time-course experiment is shown in **Figure 2.5.1**.

Figure 2.5.2. Plate layout for short and long time-course experiments. Inhibitor concentration was 5.0 µM and control cell media had 0.1% (v/v) DMSO.

The S-TICO experiment had time points at 1, 2, 4, 8, 12 and 24 hours. After 24 hours initial incubation the spent media was completely removed and replaced with 0.700 mL of media with 5.0 µM inhibitor or 0.1% (v/v) DMSO. The cells were incubated for the duration of their timepoint.

In the L-TICO experiment, cells destined for 48, 72 or 96 hours of inhibitor exposure had treatment added to the resuspended cells before plating. Cells treated for 24 hours had treatment (inhibitor or DMSO only) added after 24 hours of incubation, as described for the other 12-well experiments. The cells treated with inhibitor for 48, 72 and 96 hours were further split into two groups: in group 1 where media was swapped completely every 24 hours until harvest, and in group 2 where media was left on for the duration of timepoint. Experimental group name, treatment length and number of media swaps is summarised in **Table 2.5.1**.

Table 2.5.1. Summary of experimental groups in the long time-course experiment, including total treatment length and number of media swaps.

Experimental group name	Total treatment length (hours)	Number of media swaps
A	24	1*
B1	48	1
B2	48	0
C1	72	2
C2	72	0
D1	96	3
D2	96	0

***Cells were plated without inhibitor and the media was swapped after 24 hours to media with inhibitors for a final 24 hours of incubation.**

Treatment with metabolic inhibitors: cell-based assay in 96-well plate

After plating, cells were incubated for 24 hours before spent media was removed and 200 µL of fresh media with inhibitor or DMSO was added. Two different cell-based assays were carried out: L-TICO with three inhibitor concentration levels (0.50, 5.00 and 10.0 µM) and glutaminase inhibitor (CB-839) concentration range (0.05-5.00 µM). The layout of each assay is illustrated in **Figure 2.5.3**.

For glutaminase inhibitor (CB-839) concentration range assays, DMEM without phenol red was used. The inhibitor concentrations were 0.05, 0.10, 0.30, 0.70, 1.00, 3.00 and 5.00 µM. All media, including control, had a DMSO concentration of 0.1% (v/v). The cells were incubated with inhibitor for 24 hours and the total incubation time after plating was 48 hours. Media aliquots (50 µL) were removed from each sample prior to performing the MTS assays.

For the L-TICO assay, media with inhibitor (AG-120, AG-881, BAY 1436032 or GSK864) was added to all plates after 24 hours of initial incubation. Inhibitor concentration was 0.50, 5.00 and 10.0 µM. All media, including control media, had a DMSO concentration of 0.2% (v/v). Media was left on for the duration of incubation, i.e., same as group 2 in the metabolomics experiment.

The MTS reagent was thawed at room temperature. Two wells (position 6A and 7H) were used for blanks with 200 µL unused media transferred into each. Then 10 µL MTS dye was transferred into each well, blank and containing cells. The plate was incubated for a minimum of 45 minutes at 37 °C and 5% CO_2 before any further measurements (described in **Section 2.7.5**).

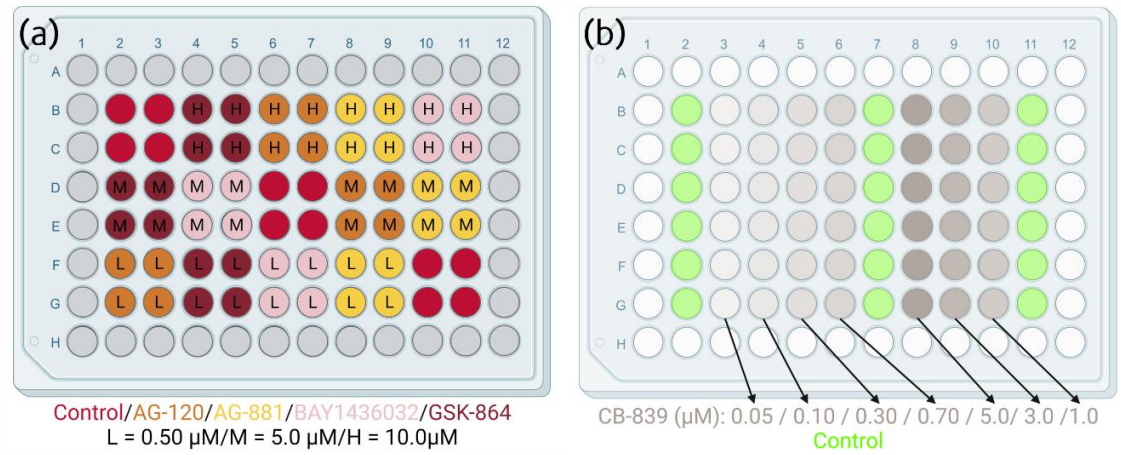

Figure 2.5.3. Layout of 96-well inhibitor assays. (a) L-TICO mutIDH1 inhibitor assay layout. Each well for the 24- and 48-hour timepoints was plated with 10,000 cells, the 72-hour timepoints with 7,500 cells and the 96-hour timepoints with 5,000 cells. Colour codes: control = red, orange = AG-120, yellow = AG-881, pink = BAY1436032 and maroon = GSK864. Inhibitor concentration: L = 0.50 µM, M = 5.0 µM and H = 10.0 µM. (b) CB-839 treatment assay layout. One plate each of mutIDH1^{R132H} and wtIDH1 LN18 cells was prepared. Each well was plated with 10,000 cells. Medium was swapped after 24 hours of incubation. Colour code: green = control, grey = CB-839. The inhibitor concentrations were 0.05, 0.10, 0.30, 0.70, 1.0, 3.0 and 5.0 µM.

2.5.5. Arresting metabolism and extracting metabolites: Routine harvest of metabolomics samples

In this project, the phrase 'cell harvest' included arresting cellular processes and extracting metabolites from cells plated on 60 mm dishes or in 12-well plates. Arrestment and extraction for each method will be described in detail below. Prior to any harvest, cells were briefly inspected with a Motic trinocular microscope (×4) magnification, phase contrast objective 0) and cell confluency and morphology were noted. All harvests from 60 mm dishes were done in randomised order. The random order was generated by assigning a random number between 0 and 1 in Excel (*=rand()*) to each sample name and then sorting from smallest to largest number. Harvest order within a 12-well plate was not randomised.

Harvesting cells from 60 mm dishes

Three dishes were taken from the incubator into the laminar flow hood at a time. Media aliquots were pooled for each experimental group from each dish, generally 50 or 100 µL from each plate. Then, one dish at a time, media was poured off and the dish was washed

with approximately 5 mL PBS twice. Excess PBS was removed by dabbing a tissue at the edge of the dish, taking care not to touch the cells. Finally, approximately 5 mL liquid nitrogen was poured into the dish to arrest metabolic activity.

Once the third dish was set with liquid nitrogen, the nitrogen in the first dish had boiled off. Subsequently 180 µL 80% $MeOH_{(aq)}$ was transferred to the first dish to extract metabolites and denature proteins to further arrest cellular processes. A cell scraper was used in circular motions, and then the cells were scraped down to one side of the plate. The plate was turned 90° counter-clockwise and the scraping was repeated. The solution and cell debris were transferred to a 1.5 mL microtube. The process of adding 80% $MeOH_{(aq)}$, scraping and transferring to microtube was repeated for the second and third dish. Samples were kept on ice until all dishes were done. If the liquid nitrogen boiled off a dish before 80% $MeOH_{(aq)}$ was added, the dish was placed on ice until its turn. Once the three samples were harvested, they were placed on dry ice until all samples were harvested. After harvest, samples were stored at -80 °C before further processing (described in **Section 2.6.1**).

Harvest from 12-well plates

One 12-well plate was harvested at a time. Media was aliquoted (50 µL), but only pooled for the glutaminase inhibitor concentration experiment. In all other 12-well metabolomics experiments, the media from each well was saved as a separate sample (0.700 mL). Media was removed row by row and kept on ice until the whole harvest process of the plate was completed. After removal of media for one row, PBS (0.700 mL) was added. Once all wells contained PBS, the process was repeated (remove PBS and replace with fresh PBS row by row). Final removal of PBS included an additional aspiration to remove any remaining PBS.

The plate was placed on dry ice and 100 µL of cold 80% $MeOH_{(aq)}$ was added to each well, except in the pilot 12-well experiment where 70 µL was added. The 80% $MeOH_{(aq)}$ was kept on dry ice. The combination of being on dry ice and adding cold 80% $MeOH_{(aq)}$ to the wells arrested metabolic activity. The 80% $MeOH_{(aq)}$ was also used to extract the metabolites from the cells. The cells were scraped loose in all wells and then the 12-well plate was tipped upwards. For each well, the solution was pipetted over the well surface, followed by transfer of solution and cell debris to a 1.5 mL microtube. The microtubes were kept on

ice. Wells were harvested column by column. Once all 12 wells were harvested, the cell and media were kept on dry ice until all plates were finished. After harvest, samples were stored at -80 °C before further processing (described in **Section 2.6.1**).

2.5.6. Arresting metabolism and extracting metabolites NAD^+, NADH, $NADP^+$ and NADPH: Redox harvest for analysis

Harvest for analysis of redox metabolites (NAD^+, NADH, $NADP^+$, NADPH) was only done from 60 mm dishes. The metabolite extraction protocol was adjusted to better preserve the redox metabolites (NAD^+, NADH, $NADP^+$, NADPH). Three plates were taken into the laminar flow hood at a time. Media aliquots were not taken. One plate at a time, media was poured off and the plate was washed with PBS twice; approximately 5 mL each time. Excess PBS was removed by dabbing a tissue at the edge of the plate, taking care not to touch the cells. Finally, ca. 5 mL of liquid nitrogen was poured into the dish, which arrested metabolic activity.

Once the third dish was set with liquid nitrogen, the nitrogen in the first dish had boiled off. Subsequently, 150 µL of extraction solution (40:40:20 ACN/MeOH/H_2O with 0.1M FA) was added to the dish. A cell scraper was used in circular motions, and then the cells were scraped down to one side of the plate. The plate was turned 90° counter-clockwise and the scraping was repeated. The solution and cell debris were then transferred to a 1.5 mL microtube. Then 13.1 µL of neutralising solution (15% $NaHCO_3$ in water (w/v)) was added to the tube. The process of adding extraction solution, scraping, transferring to microtube and then adding neutralising solution was repeated for the second and third dish. Samples were kept on ice until all dishes were done. If the liquid nitrogen boiled off a dish before extraction solution was added, it was placed on ice until its turn. Once the three samples were harvested, they were placed on dry ice until all samples were harvested. After harvest, samples were processed the following day (described in **Section 2.6.1**) and then stored at -80 °C if further analysis could not be carried out immediately after.

2.5.7. Summary of all metabolomics experiments carried out

In total, nine different metabolomics experiments were carried out. The 12-well plate layouts are illustrated in **Figure 2.5.4**, with exception for the time-course experiments

layouts, which are provided in **Figure 2.5.2** in **Section 2.5.4**. The experiments using 60 mm dishes are listed in **Table 2.5.2** and the experiments using 12-well plates are listed in **Table 2.5.3**. The tables include experiment name, LN18 generation and *IDH* mutational status, inhibitors used and concentration, percentage DMSO in media, treatment length and total incubation length, biological replicates per experimental group, total number of samples, harvest method (**Table 2.5.2** only) and notes on plate layout (**Table 2.5.3** only).

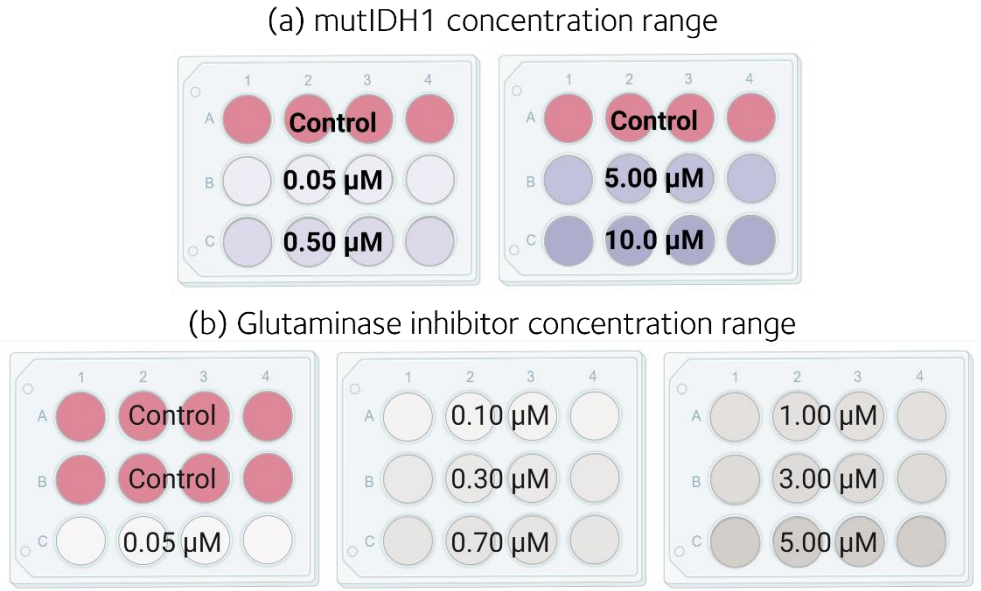

Figure 2.5.4. Plate layout for 12-well metabolomics experiments described in Table 2.5.2, **except time-course experiments. (a) Layout of 12-well plates for the mutIDH1 inhibitor concentration range experiment. For each inhibitor (AG-120, AG-881, BAY 1436032 and GSK864) this layout was used. (b) Layout of 12-well plates for the glutaminase inhibitor (CB-839) concentration range experiment. The layout was used for wtIDH1 and mutIDH1^{R132H} LN18 cells separately.**

Table 2.5.2. Summary of all metabolomics experiments carried out using 60 mm dishes. The table includes experiment name, LN18 generation and *IDH* mutational status, which inhibitors were used and concentration, percent DMSO in media, treatment and total incubation length, number of biological replicates per experimental group, total number of samples and harvest method. Routine harvest method was described in Section 2.5.5 and the redox harvest method was described in Section 2.5.6.

Experiment name	LN18 generation	*IDH* mutational status	Inhibitor(s) used	Inhibitor concentration (μM)	Percentage (v/v) DMSO	Treatment/ total incubation (h)	Biological replicates per experimental group	Total number of samples	Harvest method
mutIDH1 inhibitor single concentration, metabolomics	Second	wtIDH1 mutIDH1^{R132H}	AG-120 AG-881 BAY 1436032 GSK864	5.0	0.1	24/48	10 × treated 20 × control	120 (60 × 2)	Routine
Redox	Second	wtIDH1 mutIDH1^{R132H}	-	-	-	0/48	10 × wild type 10 × mutant	2a0	Redox
^{13}C tracer	First	wtIDH1 mutIDH1^{R132H}	*	-	0.0	0/24 12/36 24/48	3 × unlabelled media 5 × D-glucose-[1,2]-$^{13}C_2$ 5 × L-glutamine-$^{13}C_5$	58	Routine

*No inhibitor was added in the ^{13}C tracer experiment, but non-labelled media, or media with either [1,2-$^{13}C_2$]-glucose and unlabelled glutamine, or media with unlabelled glucose and [U-$^{13}C_5$]-glutamine was added.

Table 2.5.3. Summary of all metabolomics experiments carried out with 12-well plates. The table includes experiment name, LN18 generation and *IDH* mutational status, which inhibitors were used and concentration percent DMSO in media, treatment and total incubation length, number of biological replicates per experimental group, total number of samples and notes on plate layout. All samples were harvested with the routine harvest method described in Section 2.5.5.

Experiment name	LN18 generation	*IDH* mutational status	Inhibitor(s) used	Inhibitor concentration (μM)	Percentage (v/v) DMSO	Treatment/ total incubation (h)	Biological replicates per experimental group	Total number of samples	Plate layout
12-well pilot	First	wtIDH1 mutIDH1^{R132H}	-	-	0.0	0/48	12	12	One plate each of wtIDH1 and mutIDH1^{R132H}
Short time-course (S-TICO)	Second	mutIDH1^{R132H}	AG-120 AG-881 BAY 1436032 GSK864	5.0	0.1	1/24 2/26 4/28 8/32 12/36 24/48	4 × treated 8 × control	144	Shown in Figure 2.5.4.1.
Long time-course (L-TICO)	Second	mutIDH1^{R132H}	AG-120 AG-881 BAY 1436032 GSK864	5.0	0.1	24/48 48/48 72/72 96/96	4 × treated 8 × control	168	Shown in Figure 2.5.4.1.
MutIDH1 inhibitor concentration range	Second	mutIDH1^{R132H}	AG-120 AG-881 BAY 1436032 GSK864	0.05, 0.50, 5.0, 10.0	0.2	24/48	4 × treated 8 × control	96	Shown Figure 2.5.7.1 (a)
MutIDH1 inhibitor resistance	Second	wtIDH1 mutIDH1^{R132H} mutIDH1$^{R132H+S280F}$	AG-120 FT2102	5.00	0.1	24/48	4 × treated 4 × control	36	One row each of control, AG-120 and FT2102
Glutaminase inhibitor	Second	wtIDH1 mutIDH1^{R132H}	CB-839	0.05, 0.10, 0.30, 0.70, 1.0, 3.0, 5.0	0.1	24/48	4 × treated 8 × control	72	Shown Figure 2.5.7.1 (b)

2.6. Sample processing

2.6.1. The main steps in metabolomics cell sample preparation: filtration and sample normalisation

Samples harvested for metabolomics (routine or redox) were thawed on ice. The centrifuge was cooled to 4 °C prior to use. Cells were spun down at either 14,000 rpm for 25 minutes or at 12,900 rpm for 28 minutes, for the 30-sample or 48-sample inserts respectively. Molecular weight cut-off filters (3 or 10 kilo Dalton (kDA)) were washed once with 500 µL H_2O by centrifugation at the same settings as the cell samples. Remaining water in the filter was removed before further use. A fresh tube was used to collect cell sample filtrate. The entirety of sample supernatant was transferred to the filter before centrifugation at 4 °C and either 14,000 rpm for 25 minutes or at 12,900 rpm for 28 minutes, for the 30-sample or 48-sample inserts respectively.

The timing of measurement of DNA concentration differed for 60 mm dish versus 12-well plate samples. Dish samples were measured after pelleting of cell debris, but before filtration. 12-well plate samples were measured after filtration and sample was taken from the sample remaining in the filter. Either the NanoDrop One or the ClarioStar plate reader, equipped with a LVis plate, were used to measure dsDNA (ng/µL). Sample volume was 2.0 µL for measurements on the NanoDrop and 2.5 µL on the ClarioStar. The NanoDrop was cleaned by wiping with lint free wipes wetted with water prior to each measurement. It was blanked with 80% $MeOH_{(aq)}$ (2.0 µL). The ClarioStar LVis plate was wiped with lint free wipes and ethanol, checked for cleanliness (accepted at < 10 mOD difference) and then blanked with 80% $MeOH_{(aq)}$ (accepted at < 10 mOD difference). Blanking was only repeated when the instrument was used after a break or if repeated sample measurements were highly irregular. Each sample was measured at least twice when using the NanoDrop or ClarioStar. If the concentration of the second measurement differed more than 5-6 ng/µL or 10% of the total concentration of measurement 1, further measurements were taken.

After DNA concentration was measured and samples were filtered, the relative DNA concentration was used for diluting the samples. Final total volume of samples harvested from 60 mm dishes was 80 or 100 µL and for samples from 12-well plates it was 40-50 µL.

Samples were transferred to total recovery vials during dilution. Long-term storage (> 1 week) of samples was at -80 °C, short-term storage (up to 1 week) was at 4 °C.

2.6.2. Preparation of cell and media samples for amino acid analysis

Metabolomics samples prepared per **Section 2.6.1** were further processed for amino acid analysis using the Waters AccQ-Tag™ kit (Milford, MA, USA). For each standard or sample (media or processed cell lysate), 35 µL of borate buffer was mixed with 5 µL sample or amino acid standard to a total recovery vial. Following this, 10 µL amino acid derivatising reagent (described in **Section 2.3.3**) was added to the recovery vial and the mixture was heated for 10 minutes at 55 °C. The quality control sample was made by pooling 2-5 µL of each sample (not standard) in a total recovery vial after the samples had been heated and cooled down. A reagent blank was prepared by mixing 40 µL borate buffer with 10 µL derivatising reagent in a total recovery vial and heating for 10 minutes at 55 °C. Finally, a blank of just borate buffer was transferred to a 1.5 mL glass vial. All derivatised samples, standards and blanks were stored at room temperature for up to a week prior to analysis.

2.6.3. Preparation of media samples for underivatised RPLC-MS analysis

Media (supplemented DMEM) containing the mutIDH1 inhibitors AG-120, AG-881, BAY 1436032 or GSK864 were treated with acidic (1% (v/v) formic acid), neutral or basic (1% (v/v) ~25% NH_3 in water) acetonitrile. In the method development (described in **section 4.3**), 100 µL of media and 300 µL of extraction solvent were transferred to a microtube and placed at -20 °C overnight. All three extraction solvents (acidic, neutral and basic) were used. The samples were thawed at 4 °C and 200 µL of the top phase layer was transferred to a total recovery vial.

In the sample preparation of media from the concentration range experiment and S-TICO and L-TICO experiments, 100 µL of media and 200 µL of neutral acetonitrile were transferred to a microtube and placed at -20 °C overnight. The samples were thawed at 4 °C and 100 µL of the top phase layer was transferred to a total recovery vial.

2.6.4. Preparation of glucose quantification assay for measurement of glucose in media samples

Glucose concentration in media from the CB-839 concentration range experiment was measured. The original assay protocol was described for larger sample volumes (0.1 mL sample and 3.0 mL reagent solution) and was scaled down to fit into a 96-well plate format (8 µL sample and 240 µL reagent solution). Samples, standards and blanks (water) were transferred to non-sterile clear 96-well plates and mixed with 240 µL of reagent solution. The plate was incubated at 40 °C in the ClarioStar plate reader for 20 minutes.

2.7. Sample analysis

In the following section, the different LC-MS methods used throughout the thesis are described, organised by column chemistry and sample type. The final sub-section details the plate-reader settings used for the MTS and glucose assays. The method described in **section 2.7.1** and **section 2.7.3** were developed by Dr Walsby-Tickle [148, 321].

2.7.1. Anion-exchange chromatography-mass spectrometry (IC-MS)

Sample volume was 5.0 µL with partial-loop injection. The sample manager was set to 4.0 °C and column temperature was 30 °C. Flow rate was 0.250 m/min and the following hydroxide gradient was used: 0.0 min, 5 mM; 1.0 min, 5 mM; 15.0 min, 60 mM; 25.0 min, 100 mM; 30.0 min, 100 mM; 30.1 min, 5 mM; 37.0 min, 5 mM. Curve was set to 5 for all gradient steps. The ion suppressor was operated in external water mode with a 0.500 mL/min flow rate and a continuously regenerated trap column removed ionic contaminants from the eluent. The ion suppressor current was set to 62 mA.

Spray voltage was –3.60 kV (negative polarity), capillary temperature was 320 °C and the probe heater temperature was 350 °C. Gas flow rates were: sheath gas at 60, auxiliary gas was at 20 and spare gas at 0, all arbitrary units (a.u.). S-Lens RF level was set to 70.0%. The method was run with full MS and data dependent (dd) MS^2 and the mass range was from 60-900 *m/z*. The following settings were used for full MS: resolution 7.0×10^4; microscans, 2; AGC target, 1.0×10^6; and maximum IT, 120 ms. The following settings were used for $ddMS^2$: resolution, 1.75×10^3; microscans, 2; AGC target, 1.0×10^5; and maximum IT, 250 ms.

2.7.2. RPLC-MS for analysis of derivatised amino acids

Sample volume was 2.0 µL with flow-through needle injection. The sample manager was operated without temperature control (i.e., room temperature) and the column temperature was 50 °C. Flow rate was 0.600 mL/min and the following gradient was used, with percent eluent A: 0 min, 99.9%; 0.54 min, 99.9%; 5.74 min, 90.9%; 7.74 min, 78.8 %; 8.04 min, 40.4%; 8.05 min, 10.0%; 8.64 min, 10.0%; 8.73 min, 99.9%; 9.50 min, 99.9%. Curve was set to 6 for all steps except from 5.74-7-74 minutes, where it was set to 7.

The source type was ESI, polarity was positive and the analyser mode was set to 'sensitivity'. Capillary voltage was 2.00 kV, with sample cone voltage 40 V and source offset voltage 80 V. The source temperature was 130 °C and the desolvation temperature was 450 °C. Cone gas flow was 50 L/h and desolvation gas flow was 900 L/h. Mass range was 50-1000 *m/z* in high definition MS^E mode. The scan time was 0.200 s. Low collision energy was 6 V and the high energy collision ramp was 20-30 V. Intelligent data capture was not enabled. IMS was enabled with standard transmission mode. Lock mass correction was carried out every 5 minutes, using leucine enkephalin (50 pg/µL) as the reference.

2.7.3. RPLC-MS for analysis of non-derivatised samples

The reverse phase method was used on both the Xevo G2-XS QToF and the Vion IMS QToF systems. The same chromatographic parameters were used for both. The sample volume was 5.0 µL with flow-through needle injection for cell samples. The sample manager was to set 4.0 °C and the column was set to 40 °C. Flow rate was 0.300 mL/min and the following gradient was used, with percent indicating the amount of mobile phase A (0.1% FA in water): 0 min, 95.0%; 4.0 min, 50.0%; 12.0 min, 0.1%; 15.0 min, 0.1%; 15.1 min, 95.0%; 18.0 min, 95%; 30.0 min, 95.0%; 30.1 min, 95.0%. Curve was set to 6 for all steps.

The MS settings for the Vion IMS QToF were ESI source type, positive polarity and 'sensitivity' analyser mode. Capillary voltage was 2.50 kV, sample cone voltage was 40 V and source offset voltage was 80 V. The source temperature was 120 °C and the desolvation temperature was 250 °C. Cone gas flow was 50 L/h and the desolvation gas flow was 600 L/h. Mass range was 50-1000 *m/z* in high definition MS^E mode. The scan time was 0.500 s. Low collision energy was 6.0 eV and the high energy collision ramp was

20.0-40.0 eV. Intelligent data capture was not enabled. IMS was enabled with standard transmission mode. Lock mass correction was enabled with leucine enkephalin (50 pg/µL) as the reference.

The MS settings for the Xevo G2-XS QToF were ESI source type in positive polarity. Capillary voltage was 2.0 kV, sampling cone voltage was 40 V and source offset was 80 V. Source temperature was 130 °C and desolvation temperature was 600 °C. Cone gas was 50 L/h and desolvation gas was 900 L/h. Mass range was from 50-900 *m/z*, in sensitivity analyser mode and MS^E, with scan time of 0.5 s. The low collision energy was 6.0 eV and the high energy collision ramp was 20.0-40.0 eV.

2.7.4. HILIC-MS

The amide and ZIC phosphorylcholine column were only used with the Ultimate 3000 pump and Exploris 240™ MS, while the ZIC sulfobetaine column was used on both the Ultimate-3000 pump and Exploris 240™ MS and the Acquity UPLC® pump and Vion MS. In the following section, all of the methods for the Ultimate-3000 pump and Exploris 240™ are described first, followed by the methods for the Acquity UPLC® pump and Vion MS. Across both instruments the sample holders were kept at 4 °C and injection volume was 5.0 µL.

Ultimate-3000 pump and Exploris 240™ MS methods

The amide column temperature was 25 °C. Mobile phase A was the 95:5 water: acetonitrile buffer described in **section 2.3.4** and mobile phase B was acetonitrile. Flow rate was 0.200 mL/min. The gradient, based on the method reported by Lu *et al*. [322], was: 0 min, 90% B; 2 min, 90% B; 5 min, 50% B; 11 min, 0% B; 13.5 min, 0% B; 15 min, 90% B. The ion source was H-ESI and the MS was operated in negative mode. The spray voltage was -3.4 kV and the ion transfer tube was 320 °C, while vaporiser temperature was 0 °C. Sheath gas was 45, auxiliary gas was 7 and sweep gas was 3, all arbitrary units. Full scan at resolution 1.2×10^6 and scan range 400-800 *m/z* was used. The RF lens was at 65%. The internal mass calibration (EASY-IC™) was disabled.

The ZIC phosphorylcholine column temperature was 40 °C. Mobile phase A was 20 mM ammonium acetate at either pH 6 or 9 and mobile phase B was acetonitrile. Flow rate was 0.300 mL/min. The gradient, based on the method reported by Smith *et al*. [310], was: 0

min, 70% B; 1 min, 70% B; 10 min, 60% B; 10.5 min, 40% B; 15 min, 40% B; 15.5 min, 70% B; 19 min, 70% B. The ion source was H-ESI and the MS was operated in negative mode. The spray voltage was –3.4 kV and the ion transfer tube was 300 °C, while vaporiser temperature was 0 °C. Sheath gas was 50, auxiliary gas was 21 and sweep gas was 3, all arbitrary units. Full scan at resolution 1.2×10^6 and scan range 100-900 *m/z* was used. The RF lens was at 65%. The internal mass calibration (EASY-IC™) was disabled.

The ZIC sulfobetaine column temperature was 50 °C. Mobile phase A was acetonitrile and mobile phase B was either 5 mM ammonium formate (pH 6), 20 mM ammonium formate (pH 3, 6 or 9) or 20 mM ammonium acetate (pH 6 or 9). Flow rate was 0.400 mL/min. The gradient was: 0 min, 5% B; 1 min, 5% B; 9 min, 50% B; 13 min, 50% B; 13.5 min, 5% B; 18 min, 5% B. The ion source was H-ESI and the following parameters were used when operated in negative mode: spray voltage, – 3.5 kV; sheath gas, 20; auxiliary gas, 10; sweep gas, 0; scan type, full; resolution, 1.2×10^6 resolution; scan range, 350-850 m/z; RF lens, 65%. The internal mass calibration (EASY-IC™) was enabled. The ion transfer tube and vaporiser temperature were normally both set to 250 °C. Nine different combinations of temperatures were tested when using 20 mM ammonium formate (pH 9) as mobile phase B: low (200 °C), medium (250 °C) and high (300 °C). When the 20 mM ammonium formate buffer (pH 3) was used, the MS was operated in positive mode with the following parameters: spray voltage, 2.0 kV; sheath gas, 45; auxiliary gas, 11; sweep gas, 1; ion transfer tube, 300 °C; vaporiser temperature, 250 °C; scan mode, full; scan range, 100-1000 *m/z*; RF lens, 65%. The internal mass calibration (EASY-IC™) was enabled.

Acquity UPLC® pump and Vion MS methods

Seven chromatographic methods were tested with the ZIC sulfobetaine column. Mobile phase A was in each case the buffer. The base method, adapted from the method reported by Smith *et al*. [310], had flow rate 0.400 mL/min, column temperature of 40 °C and used 20 mM ammonium acetate (pH 6). The gradient was: 0.0 min, 30% A; 1.0 min 30% A; 10.0 min, 40% A; 10.5 min, 60% A; 15.0 min, 60% A; 15.5 min, 30% A; 20.0 min, 30% A. The base method was adjusted by changing the gradient, but leaving column temperature and flow rate same as before. The new gradient was as following: 0.0 min, 15% A; 1.0 min, 15% A; 9.0 min, 40% A; 9.50 min, 70% A; 14.0 min 70% A; 14.5 min, 15% A; 20.0 min, 15% A.

Mobile phase A (20 mM ammonium formate) at pH 6 and pH 9 were tested with the new gradient.

A shortened gradient was also tested: 0.0 min, 15% A; 1.0 min, 15% A; 4.0 min, 40% A; 4.50 min, 70% A; 9.0 min 70% A; 9.5 min, 15% A; 15.0 min, 15% A. The short gradient was also tested with higher flow rate (0.500 mL/min), higher column temperature (50 °C) and both higher flow rate and higher temperature. All four methods were only done with 20 mM ammonium acetate at pH 9.

The following MS parameters were used for the previously mentioned pump settings: ion source, H-ESI; polarity, negative; analyser mode, sensitivity; IMS, standard transmission; capillary voltage, –2.50 kV; sample cone voltage, 40 V; source offset voltage, 80 V; source temperature, 150 °C; desolvation temperature, 300 °C; cone gas, 50 L/h; desolvation gas, 750 L/h; mode, MS^E; mass range, 50-900 *m/z*; scan time, 1.0 s; collision energy low, 6.0 eV; collision energy high (ramp), 20.0-30.0 eV; intelligent data capture, enabled.

Based on the previous methods, a final method was devised. It had column temperature at 50 °C and flow rate at 0.500 mL/min, using 20 mM ammonium acetate (pH 9) and acetonitrile. The gradient was: 0.0 min, 5% A; 1.0 min, 5% A; 9.0 min, 50% A; 13.0 min, 50% A; 13.5 min, 5% A; 18.0 min, 5% A. The following MS parameters were used: ion source, H-ESI; polarity, negative; analyser mode, sensitivity; IMS, standard transmission; capillary voltage, –2.50 kV; sample cone voltage, 40 V; source offset voltage, 80 V; source temperature, 125 °C; desolvation temperature, 300 °C; cone gas, 50 L/h; desolvation gas, 750 L/h; mode, high definition MS^E; mass range, 50-900 *m/z*; scan time, 1.0 s; collision energy low, 6.0 eV; collision energy high (ramp), 20.0-30.0 eV; intelligent data capture, disabled.

2.7.5. Assay analysis with plate reader

The ClarioStar plate reader was used to measure the absorbance at specific wavelengths (defined below for each experiment) per well of a 96-well plate. In the MTS cell proliferation assay, absorbance of treated cell samples was considered relative to the absorbance of control cell samples. In the glucose quantification assay, the absorbance of

known standards was used to create a linear calibration curve based on the correlation of concentration of solution to its absorbance, as per Beer-Lamberts law:

Equation 2.1 $$A = \epsilon \times C \times p$$

Where A = absorbance, ε the molar extinction coefficient (mol^{-1} cm^{-1}), C is concentration (mol/L) and p is path length of the sample. In the glucose quantification assay, ε and p were the same for each sample as the absorbance of the same molecule was measured and each sample had the same volume (i.e., path length). The concentration range for the calibration curve was carried out based on the manufacturer's recommendations, i.e., within the linear range specified for the assay.

MTS cell proliferation assay

The ClarioStar plate reader was set to 37 °C and 5% CO_2 during MTS assays. Absorbance was measured at 490 nm and each well was orbital scanned (diameter 3 mm). The blank absorbance was subtracted from the absorbance of the sample wells. The L-TICO plates were measured once after 45 minutes of incubation. The glutaminase inhibitor (CB-839) concentration range 96-well plates were measured after 45 minutes of incubation, and then three additional times every 10-15 minutes.

Glucose quantification assay

After 20 minutes of incubation at 40 °C, samples were shaken (200 rpm) for 30s. The absorbance was measured at 510 nm and each well was orbitally scanned (diameter 3 mm). The blank absorbance was subtracted from the absorbance of the sample wells. Each plate was measured once. The plate layout mirrored that illustrated in **Figure 2.5.3**, with standards and blanks placed in the leftmost and rightmost columns.

2.8. Data processing and statistical analysis

2.8.1. Processing of raw instrument data and univariate statistical analysis of targeted LC-MS data

Processing of data acquired with HILIC-MS

Data processing was done in QualBrowser in XCalibur (Thermo Fisher Scientific (Waltham, MA, USA)) for data collected with the Exploris 240™ and UNIFI (Waters (Milford, MA, USA)) for data collected with the Vion IMS QToF. The most abundant adduct for all redox metabolites (NAD^+, NADH, $NADP^+$ and NADPH) was $[M-H]^-$ in both standard and cell samples. Integration in XCalibur was done manually with the "pick peak" tool. Integration in UNIFI was done with automatic peak width detection and detection threshold without smoothing. NAD^+ and NADH peak width was generally 30-60 s, $NADP^+$ and NADPH peak width was generally 5.0-6.0 minutes. Retention time varied depending on buffer composition.

Pre-processing data acquired with IC-MS

The isotope distributions of 2-HG in the ^{13}C-tracer experiment (see **Table 2.5.2**) were measured by manually integrating the peak areas of the EICs of the $[M-H]^-$ adduct of the different 2-HG isotopes (M+1, M+2, M+3, M+4 and M+5) with 5 ppm mass accuracy. The "pick peak" tool in XCalibur was used for the manual integration. The average retention time for all isotopes of 2-HG was 9.88 ± 0.02 min, which was within one minute of the retention time of the known standard. Peak width was set to 1.0 minute.

Pre-processing data acquired with underivatized RPLC-MS

For each inhibitor, the peak area of the most abundant adducts were determined using the extracted ion chromatogram (EIC). The EICs for extracted media samples were smoothed and integrated (peak-to-peak amplitude = 2,000) in MassLynx. The smoothing parameters were: window size (scans), 3; number of smooths, 2. The EICs for the cell samples (S- and L-TICO and mutIDH1 inhibitors concentration range) were integrated in Unifi (Waters (Milford, MA, USA)). Integration was done with automatic peak width detection and detection threshold without smoothing. For all inhibitors $[M+H]^+$ was the most abundant adduct; GSK864 in media samples also had a substantial $[M+Na]^+$ adduct and this was

included in the calculation of total peak area. The *m/z* of the most abundant adduct(s) and the retention time of each inhibitor are listed in **Table 2.8.1**.

Table 2.8.1. Adduct(s), *m/z* values and retention time (min) of inhibitors analysed with RPLC-MS.

Inhibitor Name	Adduct	*m/z*	Retention time (min)
AG-120	$[M+H]^+$	583.147	7.34 ± 10s
AG-881	$[M+H]^+$	415.087	8.64 ± 10s
BAY 1436032	$[M+H]^+$	490.231	8.35 ± 10s
GSK864	$[M+H]^+$	559.246	8.95 ± 10s
	$[M+Na]^+$	581.221	

Univariate statistics and regression analyses

All statistical analyses were performed in Prism 9.4.0 from GraphPad (San Diego, CA, USA). For single binary comparisons, an unpaired parametric Student's t-test was used. For multiple comparisons, one-way ANOVA followed with Tukey's, Šidák or Dunnett's multiple comparison tests (MCTe) was used. The Dunnett's test was used when a single group (control) was compared to a number of others (treated)). Šidák and Tukey's test were used when multiple comparisons were carried out, per recommendations by Prism. Simple linear regression was carried out without forcing the line through x = 0, y = 0.

2.8.2. Pre-processing of raw instrument data: semi-targeted analysis

Progenesis QI: Uploading data, alignment and peak picking

The raw files (Thermo for IC-MS data and Waters UNIFI for derivatised RPLC-MS data) were uploaded to the Progenesis QI from Nonlinear Dynamics/Waters (Langley-on-Tyne, Northumberland, UK/Milford, MA, USA). For the two different file formats, type of instrument was 'high resolution mass spectrometer' and data format was 'profile data'. Ionisation polarity was negative for IC-MS data and positive for Waters UNIFI data. The following adducts were chosen for samples analysed in positive ionisation mode: $[M+H]^+$, $[M+H-H_2O]^+$, $[M+2H]^{+2}$, and $[2M+H]^+$, while for negative ionisation mode the following adducts were chosen: $[M-H]^-$, $[M-H-H_2O]^-$, $[M-2H]^{-2}$ and $[2M-H]^-$.

After data was uploaded, all files were aligned based on a reference chromatogram chosen by the software. All runs (i.e., a LC-MS data file for the analysis of a single sample) were assessed for suitability, in which each run is compared to all of the others and the run with most similar alignment to all is chosen as the reference. Alignment was checked and generally accepted if it was ≥ 90% in agreement with the reference run. Next the software

picked peaks in all runs, i.e., found retention time and *m/z* pairs judged as a genuine peak/ion. The peak picking sensitivity was set to default, and the software used a noise estimation algorithm to decide between 'noise' and 'peak'. No minimum peak width or retention time limits were set. Peak picking also included peak integration, which was done with default settings.

Compound identification in Progenesis QI

Compound identification was completed using an in-house database. The IC-MS database is provided in **Table A.I.1** and the derivatised RPLC-MS database is provided in **Table A.I.2**, both in **Appendix I**. When searching the IC-MS database, maximum retention time deviation was set to 2.0 minutes, maximum precursor mass error tolerance was set to 5 ppm and maximum fragment mass error tolerance was set to 12 ppm. For the derivatised RPLC-MS database, maximum retention time deviation was set to 1.0 minutes and maximum precursor mass error tolerance was to 5 ppm. No fragmentation data was collected for the derivatised RPLC-MS data.

The following identification parameters were used during metabolite identification: retention time error, mass error, fragmentation score (IC-MS data only), isotope similarity, minimum coefficient of variation (CV) and maximum abundance. The different parameter cut-offs used to determine whether an identification was confident, putative or not accepted are given in **Table 2.8.1.2**. Retention time and mass error were used to decide whether an identification was confident or putative. Fragmentation score was used to differentiate between suggested identifications with otherwise similar retention time and mass error. The score was calculated with an algorithm developed by Progenesis QI, based on the cosine similarity method [323]. The fragmentation of a standard was compared to the feature of interest, and this was only available for data collected by IC-MS analysis. Isotope similarity could determine whether a metabolite identification was confident, putative or not accepted. Minimum CV and maximum abundance were used to rule out suggested identifications that were most likely noise, i.e., it was not used to decide between confident and putative identifications. An identification was also considered putative if more than one metabolite was suggested and all of the parameters (retention time error, mass error, fragmentation score and isotope similarity) were too close to call.

Table 2.8.2. Metabolite identification parameters and their cut-offs for confident, putative or unaccepted suggestions by Progenesis QI.

Data/ Acquisition Instrument	Identification considered	Retention time error (minutes)	Mass Error (ppm)	Isotope similarity (%)	Maximum abundance	Minimum CV%
IC-MS Acquired with QExactive	Confident	< 1.0	2.5	> 90	-	-
	Putative	< 2.0	5.0	> 85	-	30-50%
	Not accepted	-	-	< 85	< 50	> 50%
Derivatised RPLC-MS Acquired with Vion IMS QToF	Confident	< 0.5	2.5	> 90	-	-
	Putative	< 1.0	5.0	> 85	-	30-50%
	Not accepted	-	-	< 85	< 1.5	> 50%

The final output from Progenesis was a peak intensity table of all compound ions (*m/z* and retention time) for picked peaks. The raw data was used for further statistical analysis described in the next section.

2.8.3. Processing and statistical analysis of untargeted metabolomics data

The data was processed with R (version 4.0.5) in RStudio (2022.02.3 Build 492) [324] mainly using the following packages: MetaboAnalystR [325], tidyverse [326], ggplot2 [327], and rstatix [328]. Packages used within the tidyverse included dplyr, purrr, stringr, tibble, rio and pacman. Additional packages were used for supporting the tasks performed by the main packages: png [329], grid [324], gridExtra [330], memoise [331], plyr [332], scales [333], qpcR [334], fs [335], janitor [336], and rlist [324]. The R code used for data processing is provided in **Appendix X**. Prism 9.4.0 was used for additional plotting. The general workflow of data processing and statistical analysis is outlined in the flowchart in **Figure 2.8.1**. The workflow was applied to all data acquired with IC-MS and derivatised RPLC-MS.

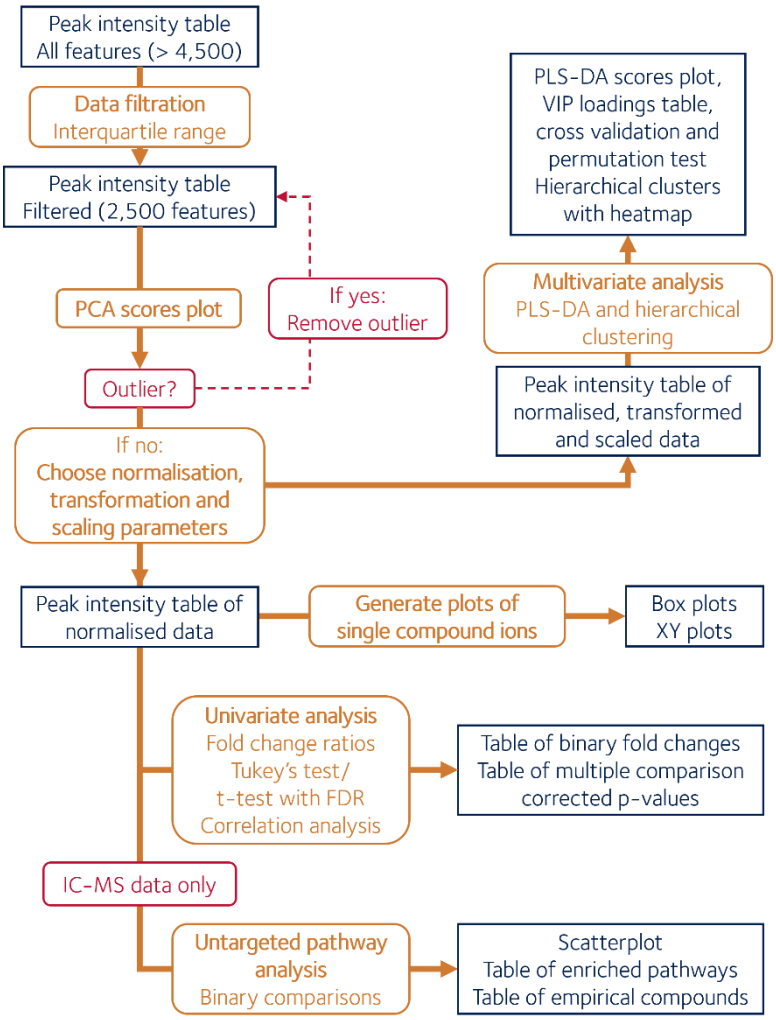

Figure 2.8.1. Overview of processing and statistical analysis of untargeted metabolomics data. The Progenesis output (peak intensity table with raw data) was filtered, then PCA scores plot (PC1 × PC2) was used to determine outliers. Then different combinations of normalisation (none, median, quantile and sum), transformation (none and log) and scaling (none, auto and pareto) were considered. The processed data table was used for multivariate (PLS-DA and hierarchical clustering) analysis. Filtered and normalised data, but not scaled/transformed, was used for univariate analysis (Tukey's significance test, t-tests with FDR adjustment (Benjamini-Hochberg), fold change calculations and correlation analysis), generation of box and/or line plots and untargeted pathway analysis.

Filtration, normalisation, transformation and scaling

All peak intensity tables were filtered by interquartile range, removing near-constant values and bringing total number of features down to 2,500. A PCA scores plot (PC1 × PC2) was generated and samples falling outside of the 95% confidence interval were considered outliers and removed. Then data normalisation, transformation and scaling were assessed by applying all possible combinations of none, median, sum and quantile normalisation, none or log transformation, and none, auto- or pareto-scaling. The mathematical operations of each normalisation, transformation and scaling parameter is described in

Table 2.8.3. The resulting peak intensity table of a specific combination of parameters was used to plot feature and sample distribution plots, and a heatmap of all features and samples. In the heatmap, the features were autoscaled and neither samples nor features were clustered.

Table 2.8.3. The mathematical operations performed when normalising, transforming and scaling peak intensity tables of metabolomics data. Notation: the peak intensity table (*D*) has rows (*X*) corresponding to samples (1, 2, …, *s*) and columns (*Y*) corresponding to metabolites (1, 2, …, *m*). Thus, X_m is a row of metabolites for a given sample and Y_s is a column of samples for a given metabolite. Any given ion count for a specific metabolite of a specific sample is x_i. After normalisation/transformation/scaling the ion count is denoted x_i^n. Standard deviation is σ. Notation and operations were based on van der Berg *et al.* and Wulff *et al.* [337, 338]. Description of quantile normalisation was based on Karaman [339].

Operation type	Parameter name	Mathematical operation
Normalisation	Sum	$x_i^n = x_i / \sum_{j=1}^{m} x_{ij}$
	Median	$x_i^n = x_i / median(X_m)$
	Quantile	1) Rank rows highest to lowest 2) Rank columns by highest to lowest 3) Calculate new row mean 4) Apply new mean to initial ranking of rows
Transformation	Log	$x_i^n = \log_{10}(x_i)$
Scaling	Auto	$x_i^n = x_i - mean(Y_s) / \sigma_{Y_s}$
	Pareto	$x_i^n = x_i - mean(Y_s) / \sqrt{\sigma_{Y_s}}$

All plots were assessed and the combination of parameters that provided normal (or as close to normal) distributions of features and samples, as well as even heatmaps without clear outlier columns, were chosen. After an appropriate choice of normalisation, transformation and scaling parameters was made, this was applied to the peak intensity table and the resulting data table was used for multivariate analysis (PLS-DA and hierarchical clustering). Untargeted pathway analysis and univariate analysis, as well as generation of box- or line-plots, was carried out with filtered and normalised data, but not transformed or scaled.

Univariate statistical analysis of processed untargeted metabolomics data

The univariate statistical analysis of processed untargeted metabolomics data included calculation of FC ratios, performing significance tests and correlation analysis (CA). The FC of individual features and identified metabolites were calculated as ratios, i.e., average normalised ion count of group 1 divided by average normalised ion count of group 2. The average was calculated as the mean, excluding any outliers identified in the data processing. FC was calculated with R code written for the task, see **Appendix X**.

The statistical significance tests were t-tests and ANOVA with appropriate correction applied when carrying out multiple comparisons. For binary comparisons of experimental groups, Tukey's test was used if the number of replicates was the same between two experimental groups (N ± 1). A two-sided unpaired t-test with FDR adjustment (Benjamini-Hochberg procedure) was used if the number of replicates were not the same between two experimental groups for a specific binary comparison. The two-sided t-tests were performed on identified metabolites only, generally between control and treated groups or between treated groups of the same inhibitor but different concentration or exposure time. The Tukey's test and t-test with FDR was calculated with R code written for the task, see **Appendix X.** The CA was performed on www.metaboanalyst.ca, where it is called PatternSearch or PatternHunter. Spearman rank correlation was used as the distance measure and correlation to the template and the FDR adjusted significance of that correlation were reported. The template was either 2-HG, 2-OG or isocitrate abundance.

Generating line plots of features and identified metabolites

Plots were either made with a self-written R script or in Prism 9.4.0. In the R script, the package ggplot2 was used. The concentration plots were made by calculating the mean and standard deviation of each feature or metabolite for each group, and plotting that as point and line plots with error bars. The code for generating line plots is provided in **Appendix X**.

Multivariate statistical analysis of processed untargeted metabolomics data

PCA, PLS-DA and HCA were generated on the website www.metaboanalyst.ca, using version 5.0 of MetaboAnalyst. PCA was also performed with the R package MetaboAnalystR, see **Appendix X** for code. The PCA and PLS-DA scores plots were generated with 95% confidence regions. For the PLS-DA specifically, variable importance in projection (VIP) scores were provided by the website. Cross validation (CV) was done for the first 5 components, using leave-one-out CV (LOOCV). R^2 (goodness of fit), Q^2 (predictive ability) and accuracy were reported for the CV. Finally, a permutation test with 2,000 repeats, using prediction accuracy during training as the test statistic, was performed.

Hierarchical cluster analysis (HCA) was performed with autoscaled features for standardisation, Euclidian distance measure and Ward's clustering method. Euclidian distance measures the shortest straight line between two data points and can be calculated

for n-dimensional data [340]. Ward's linkage method is based on calculating the error sum of squares (ESS) between clusters and clustering two groups that lead to the smallest increase in ESS [340]. The top 50 features ranked by one-way ANOVA (calculated by MetaboAnalyst) were used to generate clusters. In HCAs where the clustering of features was included, samples were not concomitantly clustered. Feature clusters also included a heatmap to show relative abundance.

Putative feature identification with the Human Metabolome Database

The multivariate statistical analyses of IC-MS data sometimes revealed features of interest. The LC-MS search function available on the Human Metabolome Database (HMDB) (www.hmdb.ca/spectra/ms/search) was used for putative identification. The ionisation mode was set to negative and mass error was set to 5 ppm. The following adducts were used during the search: $[M-H]^-$, $[M-H_2O-H]^-$, $[M-2H]^{-2}$, $[2M-H]^-$, $[M-3H]^{-3}$, and $[3M-H]^-$. Collision cross section values were not available and were therefore not included.

Untargeted pathway analysis of IC-MS data

Untargeted pathway analysis (UPA), called 'functional analysis' in the MetaboAnalystR package, was only carried out with IC-MS data. The wtIDH1 control and mutIDH1 control data were used for UPA. For each binary comparison, a Student's t test was performed for all 2,500 features in the peak list table, without multiple comparison correction. The Student's t test was from the package rstatix. The features in the peak list were ranked by p-value, and a file including *m/z*, retention time, p-value and t score was generated.

The file was then used to perform the UPA provided by the MetaboAnalystR package. The mass error was set to 5.0 ppm, MS mode was negative and retention time was in minutes. The algorithm used in the UPA was mummichog and the organism library was *Homo sapiens* MFN, a manually curated library originated from KEGG, BiGG and the Edinburgh model [313, 318]. The number of permutations was set to 100 (default) and the number of metabolites needed to consider a set of metabolites as a pathway was 3. Finally, per the recommendations of the MetaboAnalyst website, p-value cut-off was chosen such that ca 10% of all features were considered significant, usually p-value = 0.05. After the UPA had been carried out, additional R code matched ECs to KEGG codes from the output files provided by the MetaboAnalystR UPA. The R code is provided in **Appendix X**.

Chapter 3. Investigation of metabolic differences between wtIDH1 and mutIDH1^{R132H} glioma cells

3.1. Introduction

A hallmark of mutIDH1^{R132H} glioma is the production of substantial amounts of *R*-2-HG [reviewed in 1]. The mutation has also been shown to correlate with wider metabolic change such as increased anaplerosis of the TCA cycle; decreased glucose uptake, GABA shunt and BCAT1 activity; altered phospholipid and cholesterol metabolism; and redox metabolism under pressure of increased utilisation of NADPH [reviewed in 1]. However, surprisingly, there have been relatively few hypothesis-generating experiments that explore metabolic changes associated with IDH1 mutations using deep metabolome coverage. In this chapter, the LN18 cell model expressing mutIDH1^{R132H} via lentiviral overexpression is compared to the empty vector LN18 cell line and metabolic differences will be explored and discussed in the context of what has been reported previously for other glioma cell lines, mouse models and PTBs.

When reviewing previous published research (see **chapter 1**), a large degree of variability in significantly altered metabolite levels was found. It appeared to often, but not always, be dependent on the tissue model chosen. Although the metabolomic analysis of wtIDH1 and mutIDH1^{R132H} glioma presented in this chapter was limited to a single cell line, metabolic changes similar to those reported in the literature were explored in addition to changes in the wider metabolome. Multiple LC-MS approaches, including IC-MS, were used to validate the cell model and explore the scope of broader metabolite changes. Targeted and untargeted metabolomics data collected on wtIDH1 and mutIDH1^{R132H} LN18 cells will be explored using a variety of statistical analysis tools, including significance tests with MCTe, PLS-DA, HCA and functional analysis by UPA. The purpose was to expand our understanding of the metabolic effects associated with IDH1 mutations.

The aims of this chapter therefore are:

1. Measure 2-HG levels in mutIDH1 LN18 glioblastoma cells and compare difference with wtIDH1 cells.

2. Investigate other individual metabolite changes linked to *IDH1* mutation status, including a focus on redox metabolites.
3. Predict metabolic pathway changes associated with the IDH1 mutation and elevated 2-HG in mutIDH1^{R132H} LN18 cells.
4. Compare individual metabolite and pathway changes to those already reported in the literature for other glioma models.

3.2. 2-HG abundance significantly and substantially elevated in mutIDH1^{R132H} LN18 glioblastoma cells

The hallmark of mutIDH1 glioma is the high levels of 2-HG [reviewed in 1]. Therefore, it was essential that the glioma model used in this project, LN18 GBM cells expressing mutIDH1^{R132H} via lentiviral vector, had a substantially elevated 2-HG abundance.

Data processing and analysis

LN18 GBM cells stably transfected with either an empty lentiviral vector or one encoding for mutIDH1^{R132H} were used. The overexpression of mutIDH1^{R132H} in transfected cells was confirmed with quantitative reverse transcription polymerase chain reaction (qRT-PCR) in work carried out by collaborator Dr Bardella (University of Birmingham) [312]. Twenty biological of replicates each LN18 variant were grown in supplemented DMEM (1.0 g/L glucose) with 0.1% (v/v) DMSO and incubated for 48h. Cells from each sample were then harvested and samples processed, as described in **Section 2.5.3, 2.5.4** and **2.6.1.** The metabolite extracts were normalised by dilution to relative DNA concentrations (values provided in **Table A.II.1** in **Appendix II**). The samples were analysed by untargeted IC-MS [148], as described in **Section 2.7.1**. One wtIDH1 sample was not analysed with IC-MS due to an injection error, therefore N = 19 for wtIDH1 LN18 cell samples. The IC-MS data was processed in Progenesis QI (**section 2.8.2**) and 2-HG was identified by comparing retention time (-0.88 min), *m/z* (2.54 ppm), isotopic similarity (99.8%), and fragmentation pattern (81/100 similarity score) to a known standard, as described in **section 2.8.2**. Ion abundance was measured by integration of the identified peak in Progenesis QI.

Results

The ion abundance of 2-HG in cell samples were significantly and substantially higher in mutIDH1^{R132H} versus wtIDH1 LN18 cells (FC = 52.9 (MUT/WT) and p-value < 0.0001, Tukey's test). The box plot of median normalised 2-HG abundance is shown in **Figure 3.2.1.(a)**. The extracted ion chromatograms (EICs) of the most abundant 2-HG adduct, $[M-H]^-$ (147.0299 *m/z*), further illustrated the substantial difference in 2-HG abundance between the two different cell lines. To be able to observe the EICs from the wtIDH1 samples, the y-axis maximum had to be reduced 150-fold, as shown in **Figure 3.2.1.(b)** and **(c)**. IC-MS could not distinguish between the R and S isomers of 2-HG, but the level of *S*-2-HG is naturally

low [77-79]. The majority of 2-HG measured by IC-MS was therefore concluded to be *R*-2-HG, but it will be written as 2-HG when referring to measurements done by IC-MS.

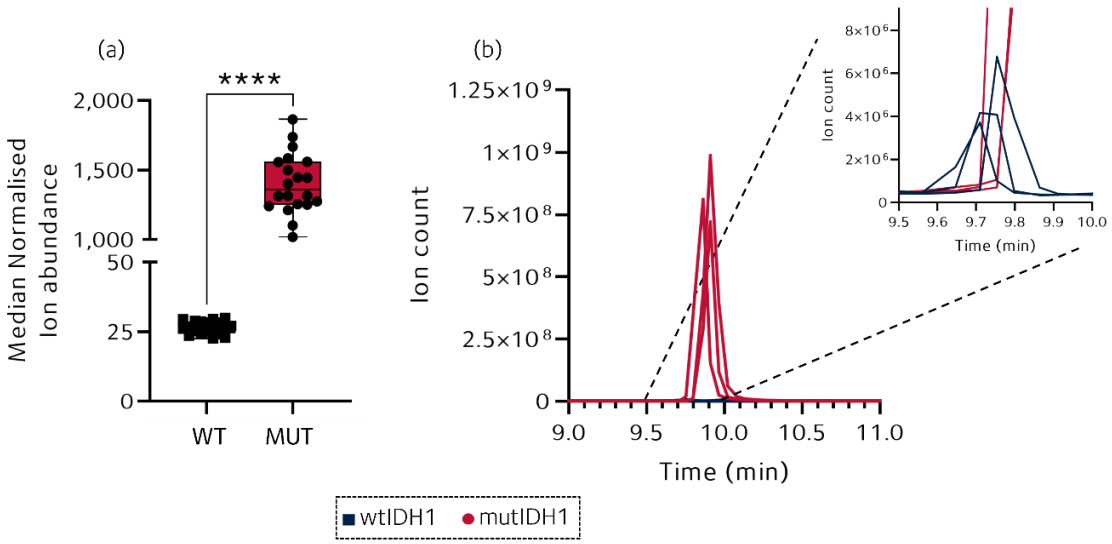

Figure 3.2.1. Abundance of 2-HG in wtIDH1 and mutIDH1^{R132H} LN18 cells. (a) Box plot of median normalised 2-HG abundance. Number of biological replicates was: N = 20 for mutIDH1^{R132H} and N = 19 for wtIDH1. ** = Tukey's test p-value < 0.0001. The box plot limits are the 25th and 75th percentile, the middle line is the data median. The whiskers are the minimum and maximum measured values. (b) EIC of [M-H]$^-$ adduct of 2-HG (147.0299 *m/z*) in mutIDH1^{R132H} and wtIDH1 LN18 cells. Enlarged area has lower maximum y-axis to show the 2-HG abundance in wtIDH1 cells. In (b-c) N = 3 biological replicates for both wtIDH1 and mutIDH1^{R132H} cell samples.**

3.3. Multivariate statistical analyses reveal metabolite changes beyond 2-HG in wtIDH1 and mutIDH1^{R132H} cells

After confirming the high levels of 2-HG in mutIDH1^{R132H} LN18 cells, it was of interest to compare the wider metabolome of the wild type and mutant cell lines. The ability of the IC-MS data to capture differences in metabolome composition between wtIDH1 and mutIDH1^{R132H} LN18 cells was explored with multivariate statistical analysis tools PLS-DA and HCA. PLS-DA is a supervised dimension reducing multivariate analysis based on finding components, also known as latent variables (LV), that maximise the covariance between the explanatory and response variables [341, 342]. HCA is an unsupervised multivariate statistical tool that is complimentary to PLS-DA. In HCA, data is separated based on distance between samples rather than covariance.

Data processing and analysis

The IC-MS method described in **section 2.7.1** and used to measure 2-HG abundance was also used for semi-targeted analysis of the wider cellular metabolome. From the IC-MS data, 6,645 compound-features were peak-picked and integrated (Progenesis QI) and 141 metabolite identifications were made (86 confident/55 putative). The metabolite identification process and criteria for confident versus putative identification are described in **Section 2.8.2**. A full list of identified metabolites and identification criteria are provided in **Table A.II.2**. Data filtration and processing was performed as described in **section 2.8.3**. The IC-MS data was median normalised and pareto scaled. Median normalisation was chosen as it most effectively minimised the small amount of systematic bias evident in the heatmap output, see **Figure A.II.1**. Pareto scaling was chosen for multivariate data analysis as it ensured that the feature distribution was normal, see **Figure A.II.1.** PLS-DA and HCA were performed as described in **section 2.8.3**. In the HCA, the top 50 features ranked by t-test scores were used.

Results

In the PLS-DA scores plot (component 1 × component 2), which shows the separation of samples along the LVs, there was complete separation of wtIDH1 and mutIDH1^{R132H} LN18 cell samples along the x-axis (first component/LV), see **Figure 3.3.1.(a)**. The separation in the scores plot indicated a metabolic difference between wtIDH1 and mutIDH1^{R132H} LN18 cells. However, before assessing which metabolites contributed to the separation, the model had to be validated by assessing goodness of fit (R^2 score), predictive ability (Q^2 score) and how the model performed under permutation. The validation was performed to assess whether the model was overfitted; an overfit model would have poor predictive ability and potentially emphasize noise. Leave-one out cross-validation (LOOCV) was used to calculate the R^2 and Q^2 score for the first five components of the model. Both scores were above 0.80 from the first component onward, and Q^2 was within 0.20 of R^2 at all components, which meant the model had a good fit and predictive ability. The accuracy score was 1.0 for all 5 components calculated suggesting the model was able to discriminate the two groups very effectively. The cross-validation results are summarised in **Figure 3.3.1.(b)**. In the permutation test, the model was calculated with sample labels applied randomly several times and the original model was compared to determine whether it had better predictive ability than random iterations. The permutation test of the wtIDH1 and mutIDH1^{R132H} model did not reach significance (p-value = 0.179). The test was done with prediction accuracy during training as test statistic and 2,000 permutations, plotted in **Figure 3.3.1.(c)**. The outcome of the permutation test meant that the original model did not perform significantly better than the randomly labelled data. In other words, the IC-MS data was not able to provide enough distinguishing features to confidently assign samples to the correct experimental group. Therefore, any features or metabolites that contributed to the PLS-DA model should be evaluated with additional statistical analyses.

The variable importance in projection (VIP) score of a feature reflects its contribution to an LV or, in other words, the degree of variation contributed to the LV [343, 344]. 2-HG was ranked highest by VIP scores for component 1 by a substantial margin, as shown in **Figure 3.3.1.(d)**. The VIP score of 2-HG was 38.07, while the second ranked feature (14.11_96.9695m/z) had a VIP score of 11.43. Additional identified metabolites in the top 15 features ranked by VIP score were B-citryl-L-glutamate (B-CG), *myo*-inositol,

N-acetylaspartylglutamate (NAAG), uridine 5'-diphosphate (UDP), adipate semialdehyde and uridine 5'-monophosphate (UMP). The first five had higher abundance in wtIDH1 than mutIDH1^{R132H} LN18 cells, while the latter two had lower abundance. Thus, the PLS-DA model revealed additional metabolites to 2-HG, with similar and opposite abundance profiles, which helps differentiate the metabolic phenotype of the two experimental groups.

Seven unidentified compound-features were among the top 15 features ranked by VIP score, as shown in **Figure 3.3.1.(d)**. Two of the features, *m/z* 101.0244 and neutral mass 104.0473, had the same retention time as 2-HG: 9.90 minutes. Both features were present at higher abundance in mutIDH1^{R132H} than wtIDH1 LN18 cells similar to 2-HG, and it was interpreted as fragments of 2-HG. A feature (neutral mass 217.0853) with the same retention time as B-CG (19.94 minutes) was present at higher abundance in wtIDH1 compared to mutIDH1^{R132H} LN18 cells, similar to B-CG and the feature was likely a fragment of B-CG. The remaining features did not match the retention time of previously identified metabolites. The *m/z* values were used to search HMDB as described in **section 2.8.3**. The feature with retention time 14.11 minutes and *m/z* 96.9695 was interpreted as the $[M-H]^-$ adduct of phosphate (1 ppm ME). The cells are washed with PBS prior to quenching with liquid N_2 during harvest, but the difference in free phosphate should not be due to difference in sample harvest or processing because the samples were handled in randomised order. Potentially there was more total phosphate present in the wtIDH1 samples and the free phosphate was from degradation of phosphorylated metabolites. Total phosphate amount would have to be measured to confirm this assumption, *e.g.*, with ^{31}P NMR. It was an otherwise useful observation, as this is a species unlikely to have been picked up with conventional chromatographic methods used in metabolomics such as *e.g.*, RP-LC or HILIC. The feature 15.65_607.0815n could be UDP *N*-acetyl-glucosamine ([M], 0 ppm ME), but the authentic standard had a retention time of 17.77 min (in-house database). Potentially it could be the isomer UDP *N*-acetyl-galactosamine. None of the remaining features (14.11_195.9536n, 3.36_242.0798m/z and 12.63_339.0737n) produced any database matches to HMDB.

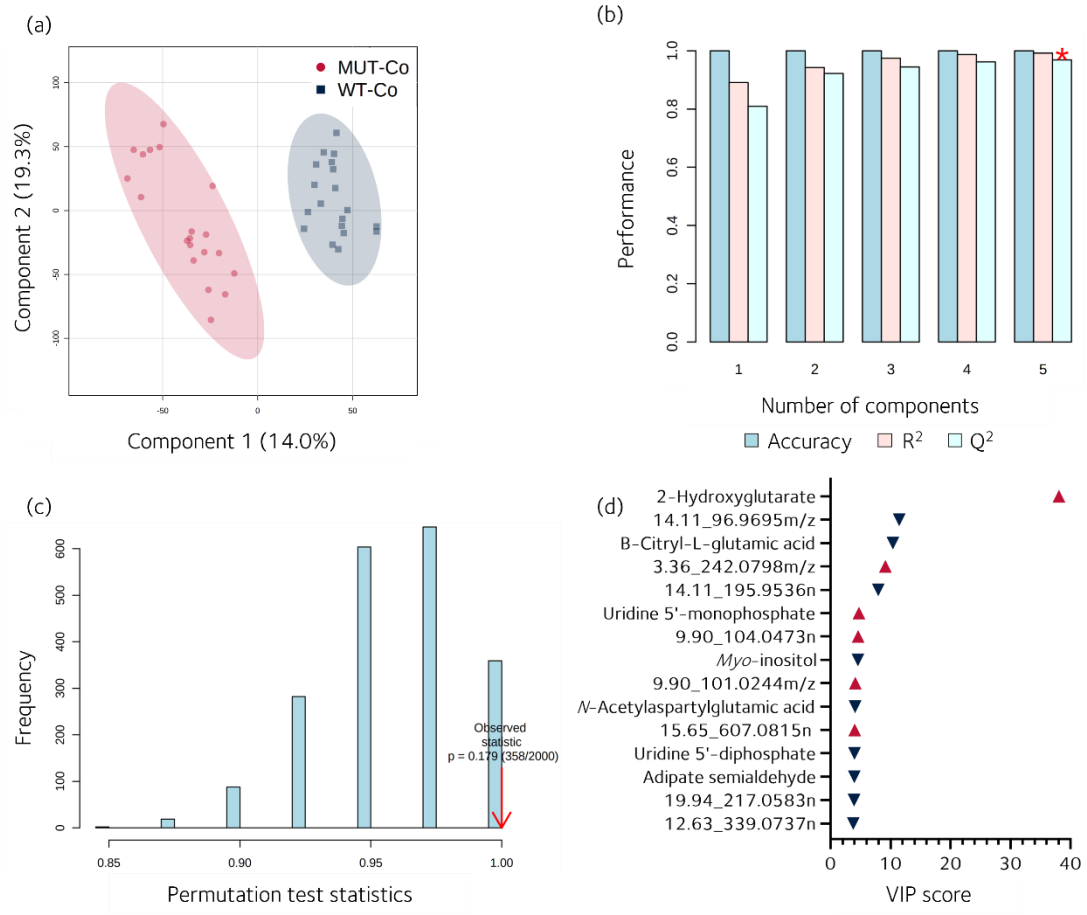

Figure 3.3.1. PLS-DA of IC-MS data of wtIDH1 and mutIDH1^{R132H} LN18 cells. (a) PLS-DA scores plot. (b) Top 15 metabolites and features ranked by VIP scores. Blue arrow indicates higher abundance in wtIDH1 cells and red arrows indicate higher abundance in mutIDH1^{R132H} cells. (c) LOOCV was carried out for 5 components. (d) Prediction accuracy during training was used as the test statistic in the permutation calculation, and a total of 2,000 permutations were performed. N = 20 for mutIDH1^{R132H} LN18 cell samples and N = 19 for wtIDH1 LN18 cell samples.

In the HCA, see **Figure 3.3.2**, 2-HG and adducts (retention time 9.90 min) dominated in one of the two main feature clusters (I). In the other main feature cluster (II), which had elevated metabolite abundance in wtIDH1 relative to mutIDH1^{R132H} cells, the following identified metabolites were present: B-CG, NAAG, *O*-phosphoserine, methylisocitrate and oxoadipate. Features with retention times matching B-CG (19.94 min) dominated otherwise. The domination of features with matching retention time to 2-HG and B-CG was likely due to the high abundance of both metabolites in the cell samples. The high abundance of the parent ions would allow different adducts (*e.g.* $[M\text{-}2H]^{-2}$, $[2M\text{-}H]^{-}$ or $[M\text{-}H_2O\text{-}H]^{-}$) and fragments to themselves be present at high enough abundance and with little enough variation that IQR filtering would not remove them and the statistical tests would not fail. From experience, the fragmentation and adduct formation in IC-MS is

usually scaled with parent ion abundance such that differences between experimental groups remains. Thus, a parent ion with a particularly significant difference between experimental groups, and with high enough abundance, can generate adducts and fragments that contribute to untargeted multivariate analyses, such as those performed here. The features could be removed to 'make space' for other features, but the multivariate analyses in this section were exploratory in nature and it was of interest to determine the contribution of the different features. Several of the features did not match the retention time to known compounds and were included in case they provided additional information about wtIDH1 and mutIDH1^{R132H} LN18 cells. The identified metabolites that were in common between the PLS-DA and HCA were 2-HG, B-CG, and NAAG.

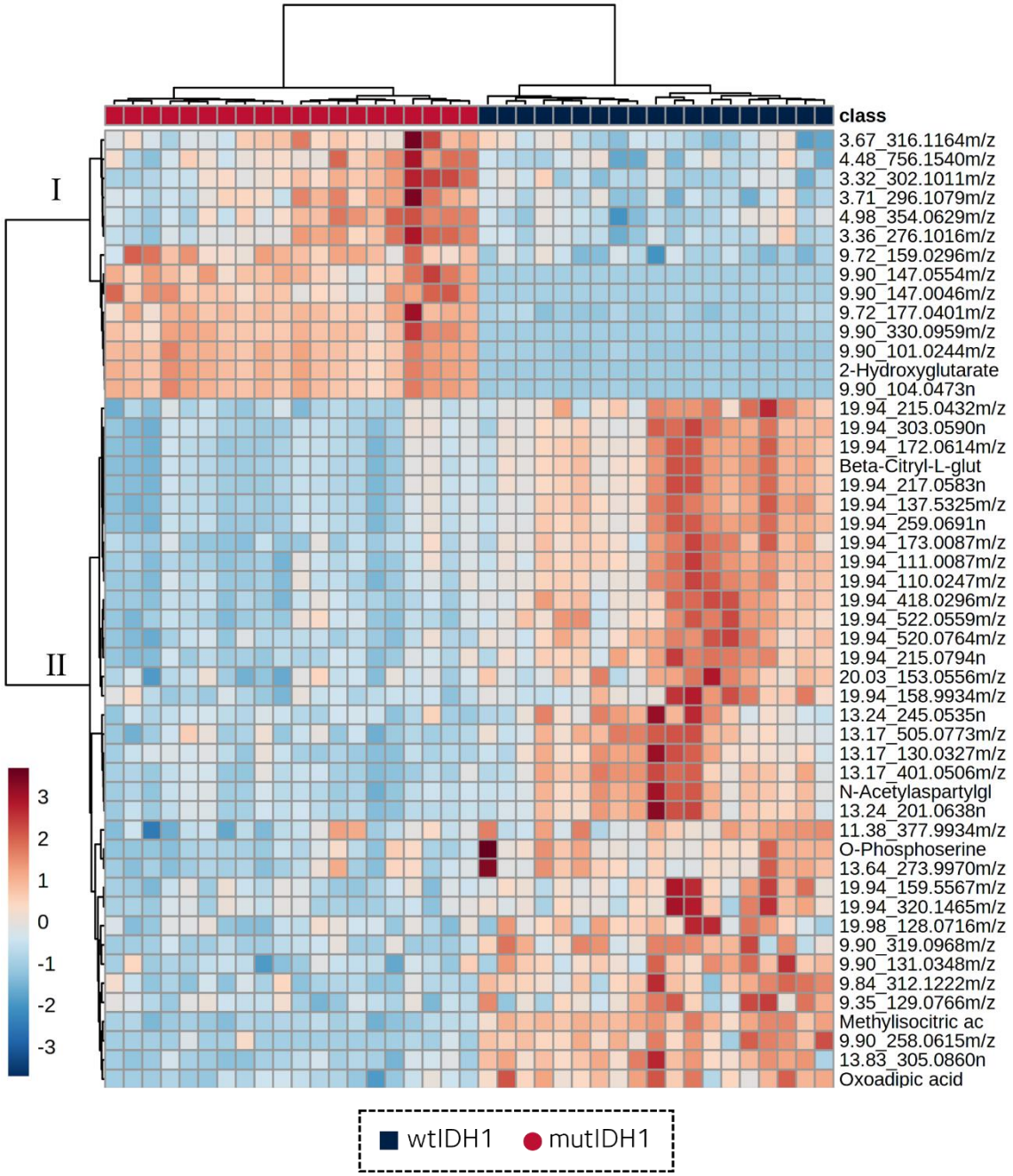

Figure 3.3.2. HCA of wtIDH1 and mutIDH1R^{132H} LN18 cell data collected by IC-MS analysis. The HCA was performed with top 50 features ranked by t-test (FDR adjusted), with Euclidian distance measure and Ward's clustering method. Both features and samples were clustered. The data was interquartile range filtered, median normalised and pareto scaled. The colour bar indicates relative ion abundance. N = 20 for mutIDH1^{R132H} LN18 cell samples and N = 19 for wtIDH1 LN18 cell samples.

In summary, 2-HG contributed substantially to separation between wtIDH1 and mutIDH1^{R132H} cells in PLS-DA and HCA. Additional metabolites also strongly differentiated the two groups as indicated in both supervised and unsupervised multivariate analyses. These features will be investigated further using univariate analysis in the next section.

3.4. Nucleotides, amino acids and related metabolites altered in abundance in mutIDH1^{R132H} LN18 cells

The multivariate methods used in **section 3.3** indicated that metabolites in addition to 2-HG had altered abundance in mutIDH1^{R132H} LN18 cells. To further probe metabolites beyond 2-HG, Tukey's significance tests were performed and FC ratios were calculated for all measured compound-features and identified metabolites. Identified metabolites from the IC-MS data were included, in addition to metabolites identified with the derivatised RPLC-MS method.

Data processing

Samples were prepared for RPLC-MS analysis by using the AccQ-Tag derivatisation kit, detailed in **section 2.6.2**. Aliquots of each sample were prepared as individual samples and analysed as described in **section 2.7.2**. From the derivatised RPLC-MS data, 53 metabolite identifications were made (34 confident/19 putative). The metabolite identification and criteria for confident versus putative identification are described in **Section 2.8.2**. A full list of identified metabolites and identification criteria are provided in **Table A.II.3**. The data was IQR filtered and median normalised prior to univariate analysis. Significance tests and FC calculations were carried with a bespoke R code written for efficient output, as the analyses were carried out for all 2,500 features in each dataset from IC-MS and derivatised RPLC-MS analysis, see **section 2.8.3** for further methodology details. A feature was considered significant if the Tukey's test p-value < 0.05 and the FC was considered appreciable if the FC ≥ 1.2 (WT/MUT or MUT/WT). Only the identified metabolites that fulfilled these criteria will be presented in this section.

3.4.1. Results

Based on the criteria, the IC-MS data yielded 15 appreciably and significantly altered identified metabolites, including 2-HG. The derivatised RPLC-MS data yielded 10 appreciably and significantly altered identified metabolites. The 25 metabolites and their FC and Tukey's test p-values are listed in **Table 3.4.1**.

Table 3.4.1. Overview of identified metabolites that were significantly and appreciably different between wtIDH1 and mutIDH1^{R132H} LN18 glioma cell samples. Significantly different was defined as Tukey's test p-value < 0.05 and appreciably different was defined as a FC ratio ≥ 1.2 (WT/MUT or MUT/WT). FC and Tukey's test was carried out on median normalised, but not scaled or transformed, data. Red FC = MUT/WT and blue FC = WT/MUT. P-values: * < 0.05, ** < 0.01, * < 0.001, **** < 0.0001.**

Measured by IC-MS			
Metabolite	**Higher in wtIDH1 (■) Higher in mutIDH1^{R132H} (●)**	**FC**	**p-value (Tukey's test)**
2-Hydroxyglutarate	●	52.9	****
2-Oxoglutarate	■	1.30	**
3-methyl-2-oxovalerate	■	1.35	**
B-Citryl-L-glutamate	■	1.77	****
Deoxyadenosine diphosphate	●	1.50	*
Deoxyribose 5-phosphate	●	1.27	*
Glycerate	■	1.26	**
Isopentenyl pyrophosphate	■	1.29	**
Methylisocitrate	■	1.84	****
***N*-Acetylaspartylglutamate**	■	1.92	****
***N*-Acetyl-L-methionine**	●	1.20	*
***N*-carbamoyl-L-aspartate**	●	1.46	*
***O*-Phosphoserine**	■	2.45	****
Oxoadipate	■	1.70	****
Uridine 5'-monophosphate	●	1.54	**
Measured by derivatised RPLC-MS			
2-aminoadipate	■	1.38	***
4-Hydroxyproline	●	1.27	*
Asparagine	●	1.26	*
B-Alanine	●	1.21	**
Cysteine	●	1.30	*
Histidine	●	1.21	**
Isoleucine	●	1.20	*
Methionine	●	1.24	*
Pipecolate	■	1.29	**
Putrescine	●	1.45	*

Considering all significant and appreciably elevated identified metabolites, different areas of metabolism become apparent as being affected in *IDH1* mutant cells compared to wild type: nucleotide metabolism, amino acid metabolism, lipid related metabolites, and metabolites that were not as easily categorised. Each area of metabolism will be presented more in-depth below.

Nucleotides and related metabolites elevated in mutIDH1^{R132H} cells

The purine metabolite deoxyadenosine diphosphate (dADP) was appreciably and significantly higher in abundance in mutIDH1^{R132H} than wtIDH1 cells (FC = 1.50 (MUT/WT) and p-value < 0.05, Tukey's test). None of the other identified purines (adenosine diphosphate (ADP), adenosine triphosphate (ATP), deoxyguanosine diphosphate (dGDP) and guanosine diphosphate (GDP)) had appreciably or significantly different in abundance between wtIDH1 and mutIDH1^{R132H} LN18 cells. The metabolite deoxyribose 5-phosphate (DR5P) was also appreciably and significantly higher in abundance in mutIDH1^{R132H} compared to wtIDH1 cells (FC = 1.27 and p-value < 0.05, Tukey's test), see **Figure 3.4.1.(a)**. DR5P is generally considered a part of the PPP, but it can also be released from purines by 2'-deoxynucleoside 5'-phosphate N-hydrolase 1 (DNPH1) [345]. DR5P can be further metabolised to acetaldehyde and glyceraldehyde 3-phosphate, the latter a glycolysis intermediate, by deoxyribose 5-phosphate aldolase (DERA) [346]. DERA can also catalyse the reverse reaction and is activated by polycarboxylic acids, of which citric acid was the most effective and 2-OG one of the least effective [347, 348]. It is not known whether DERA is activated by 2-HG, nor what that activation may mean with regards to which reaction would be favoured (breakdown or formation of DR5P).

The pyrimidine UMP was appreciably and significantly increased in mutIDH1^{R132H} compared to wtIDH1 LN18 cells (FC = 1.54 and 1.50, respectively). UDP was ranked in the top 15 compound features by VIP score in the PLS-DA, but there was no appreciable or significant difference in abundance between wtIDH1 and mutIDH1^{R132H} cells, see **Figure 3.4.1.(b)**. The pyrimidine metabolites B-alanine and *N*-carbamoyl-aspartate, which are up/downstream of UMP, were also significantly elevated in mutIDH1^{R132H} LN18 cells (FC = 1.21 and 1.46, respectively). The overall increase of pyrimidine metabolites in mutIDH1^{R132H} cells indicate a potential link to mutIDH1 activity and/or elevated 2-HG abundance.

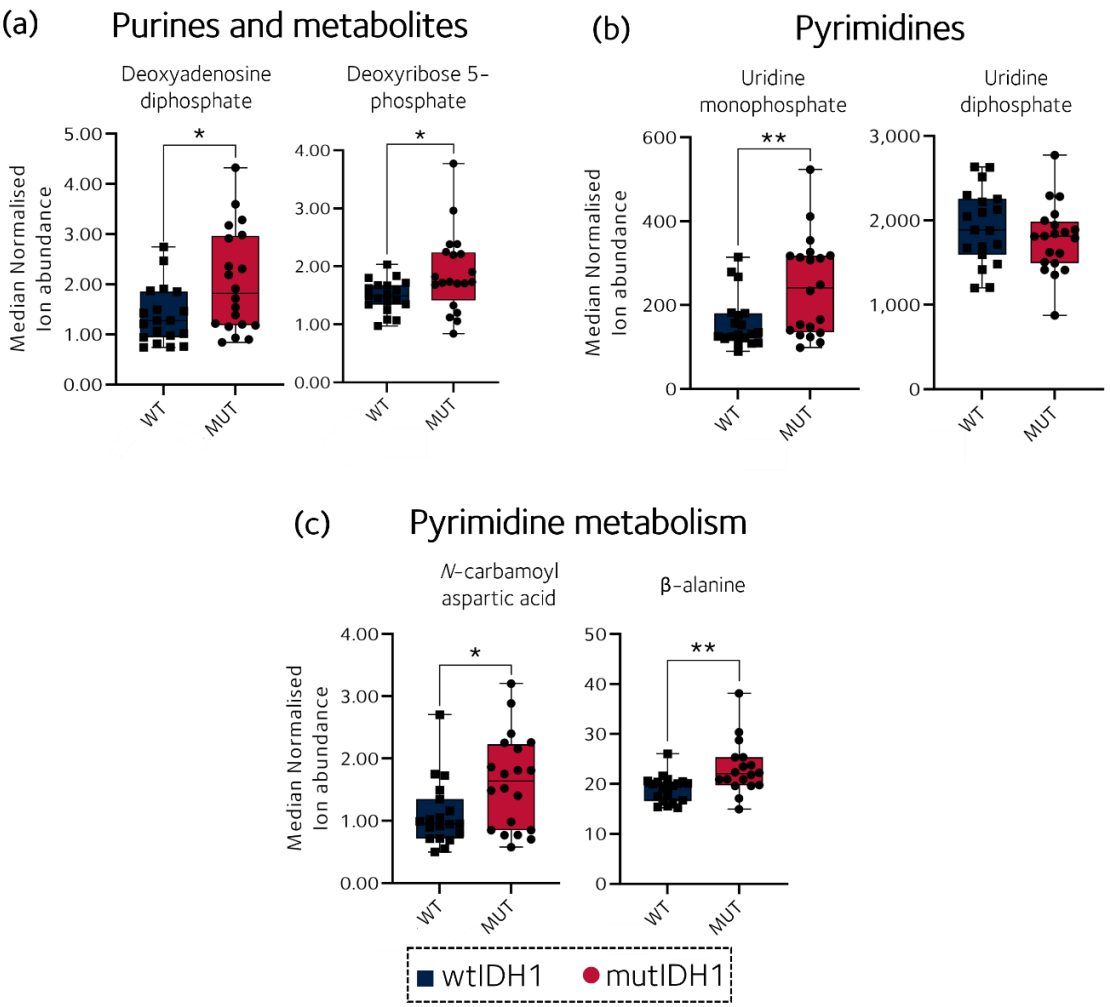

Figure 3.4.1. Box plots of normalised abundance of nucleotides and related metabolites in wtIDH1 and mutIDH1^{R132H} LN18 cells. The box plot limits are the 25th and 75th percentile, the middle line is the data median. The whiskers are the minimum and maximum measured values. * = p-value < 0.05 and ** = p-value < 0.01, calculated with a Tukey's test. For all metabolites, except B-alanine, number of biological replicates was N = 20 for mutIDH1^{R132H} and N = 19 for wtIDH1. For B-alanine N = 18 for mutIDH1^{R132H} and N = 20 for wtIDH1.

Altered amino acid abundances in IDH1 mutant cells

A number of amino acids and metabolic intermediates emerged from the univariate statistical analysis as significantly altered in abundance (see **Table 3.4.1**). It was noted that several depended on 2-OG for transamination. In transamination, an amine group is transferred from one amino acid to a free keto-acid to form another amino acid (*e.g.,* 2-OG, forming glutamate). There was an appreciable and significant decrease of 2-OG in mutIDH1^{R132H} compared to wtIDH1 LN18 cells (FC = 1.30 (WT/MUT) and p-value < 0.01, Tukey's test, see **Figure 3.4.2**), but far smaller than the increase in 2-HG. 2-HG was substantially accumulated in mutIDH1^{R132H} LN18 cells and it was speculated that the abundance of 2-OG could be decreased because of its role as a precursor for 2-HG.

Glutamate, which can be oxidised to 2-OG by GLUD, was not appreciably or significantly altered in abundance between wtIDH1 and mutIDH1^{R132H} cells. Both 2-OG and glutamate partake in many metabolic reactions [reviewed in 349, 350] and utilisation of 2-OG in 2-HG biosynthesis may be compensated for by other reactions.

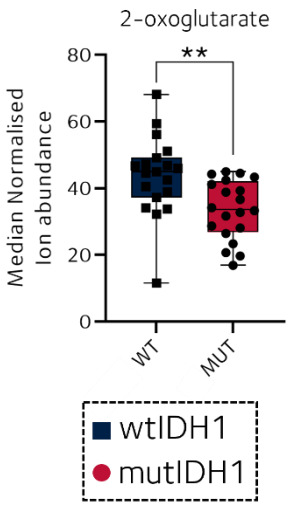

Figure 3.4.2. Box plot of normalised abundance of 2-OG in wtIDH1 and mutIDH1^{R132H} LN18 cells. The box plot limits are the 25th and 75th percentile, the middle line is the data median. The whiskers are the minimum and maximum measured values. ** = p-value < 0.01, calculated with a Tukey's test. Number of biological replicates was N = 20 for mutIDH1^{R132H} and N = 19 for wtIDH1.

The lysine degradation pathway has two transamination reactions that require 2-OG. Three intermediates of the lysine degradation pathway (pipecolate, 2-aminoadipate and oxoadipate) were all appreciably and significantly decreased in mutIDH1^{R132H} LN18 cells (FC = 1.38, 1.70 and 1.29 (WT/MUT), respectively. P-value < 0.01, Tukey's test)), see figure **3.4.3.(a)**. The lysine degradation pathway is split into the saccharopine pathway and the pipecolate pathway [reviewed in 351]. The saccharopine pathway requires 2-OG for transamination of lysine to L-2-aminoadipate-6-semialdehyde via formation of saccharopine, which involves loss of the ε-amine from lysine [352]. However, there was no appreciable or significant difference in lysine or saccharopine abundance between wtIDH1 and mutIDH1^{R132H} cells. In the pipecolic pathway, the α-amine is removed by oxidation rather than transamination, and α-keto-ε-caproic acid is formed [353]. The two pathways eventually converge at L-2-aminoadipate-6-semialdehyde, which is oxidised to 2-aminoadipate. A second 2-OG dependent step of lysine degradation then occurs, deaminating 2-aminoadipate to oxoadipate. Thus, it appeared that the pipecolic pathway branch and the end of the lysine degradation was affected by 2-HG/mutIDH1 activity due to the decreased abundance of pipecolate, 2-aminoadipate and oxoadipate in mutIDH1^{R132H} LN18 cells.

Isoleucine accumulated in mutIDH1^{R132H} LN18 cells (FC = 1.20 (MUT/WT) and p-value < 0.05, Tukey's test). The ketoacid that results from transamination of isoleucine, 3-methyl-2-oxovalerate (3M2OV), had lower abundance in mutIDH1^{R132H} than wtIDH1 LN18 cells (FC = 1.35 (WT/MUT) and p-value < 0.01, Tukey's test). Leucine was significantly

accumulated in mutIDH1^{R132H} LN18 cells (p-value < 0.05, Tukey's test), but the FC was small (FC = 1.17 (MUT/WT)). Valine abundance was not appreciably or significantly different between the two LN18 variants (FC = 1.13 (MUT/WT)). The ketoacids of leucine and valine had not been analysed with standards and it was therefore not known whether their abundance was affected in mutIDH1^{R132H} cells or not. See **Figure 3.4.3.(b)** for box plots of isoleucine and 3M2OV. Valine, Leu and Ile are all branched chain amino acids (BCAA) and BCAA metabolism also requires 2-OG for transamination. The BCAA transaminase enzyme, BCAT1, has previously been found to have decreased expression levels in mutIDH1^{R132H} glioma cells [reviewed in 1]. BCAT1 has been shown to be inhibited at millimolar levels of 2-HG, although that is disputed [reviewed in 1]. Nonetheless, the accumulation of isoleucine and decrease of 3M2OV suggests that BCAA metabolism is also affected in mutIDH1^{R132H} LN18 cells, potentially by a similar mechanism.

An additional related amino acid that was altered in abundance and is linked to 2-OG and/or glutamate metabolism is *O*-phosphoserine. However, the biosynthesis of *O*-phosphoserine requires glutamate to donate an amine group to 3-phosphate-hydroxypyruvate (3PHP). The abundance of *O*-phosphoserine was appreciably and significantly decreased in mutIDH1^{R132H} compared to wtIDH1 LN18 cells (FC = 2.45 (WT/MUT) and p-value < 0.0001, Tukey's test), see **Figure 3.4.3.(c)**. Serine had slightly higher abundance in mutIDH1^{R132H} cells than wtIDH1 cells (FC = 1.17 (MUT/WT) and p-value < 0.05, Tukey's test). The precursor of *O*-phosphoserine is from glycolysis and wtIDH1 glioma is considered more glycolytic than mutIDH1 glioma [reviewed in 1], so potentially there was more precursor available in the wtIDH1 than mutIDH1^{R132H} LN18 cells.

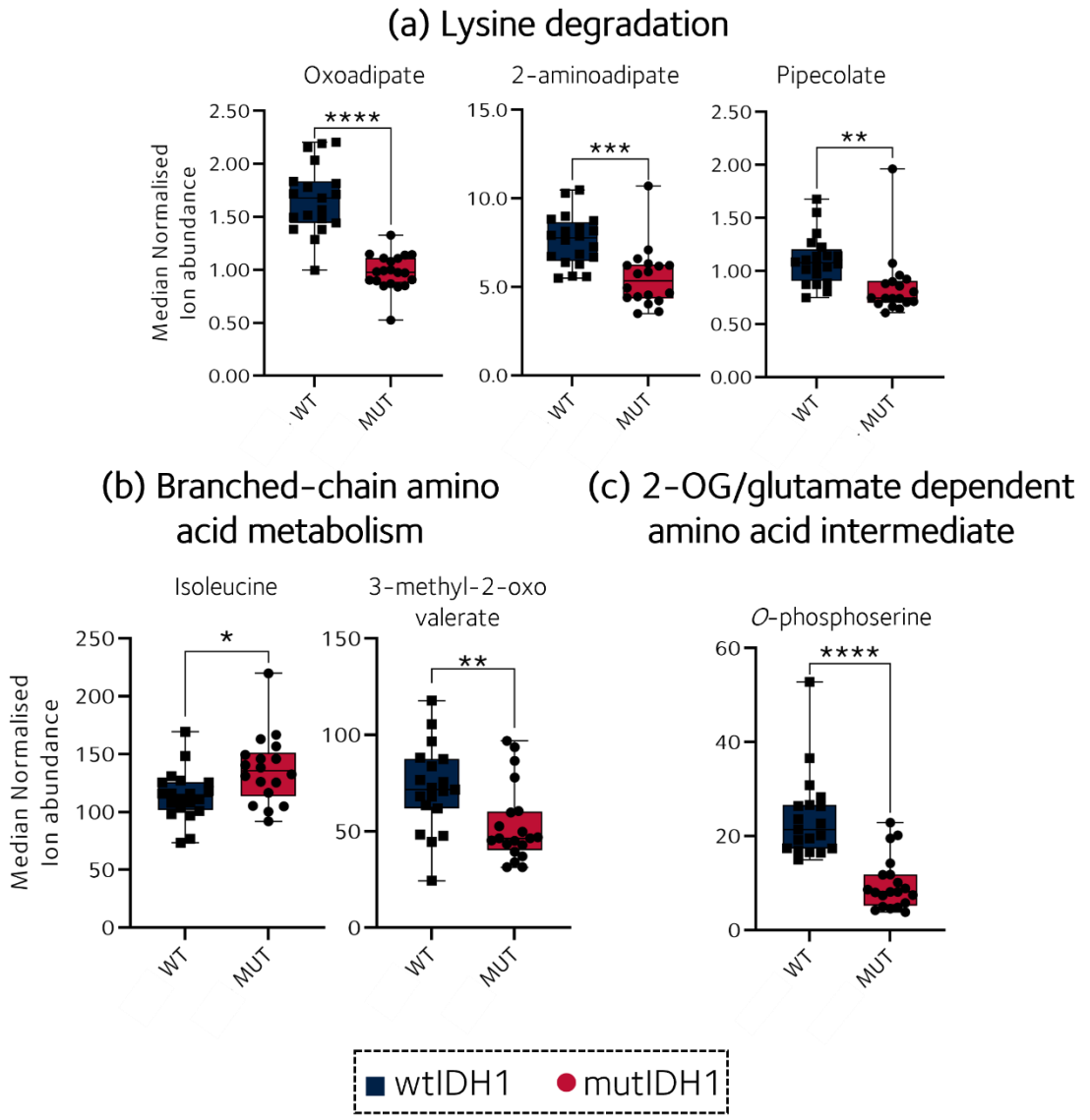

Figure 3.4.3. Box plots of amino acids and related metabolites in wtIDH1 and mutIDH1^{R132H} LN18 cells. (a) lysine degradation intermediates, (b) isoleucine and ketoacid, and (c) 2-OG/glutamate dependent amino acid intermediate. The box plot limits are the 25th and 75th percentile, the middle line is the data median. The whiskers are the minimum and maximum measured values. * = p-value < 0.05 and ** = p-value < 0.01, *** = p-value < 0.001 and **** = p-value < 0.0001, calculated with a Tukey's test. For oxoadipate, 3-methyl-2-oxo valeric acid, succinic acid semialdehyde and *O*-phosphoserine N = 20 for mutIDH1^{R132H} and N = 19 for wtIDH1. For 2-aminoadipate, pipecolate and isoleucine, N = 18 for mutIDH1^{R132H} and N = 20 for wtIDH1. N = biological replicates.

The other amino acids and metabolic intermediates were not as closely linked to 2-OG or glutamate. Cysteine and methionine abundance was appreciably and significantly increased in mutIDH1^{R132H} cells (FC = 1.30 and 1.24, respectively (MUT/WT) and p-value < 0.05, Tukey's test), see **Figure 3.4.4.(a)**. Cysteine is needed for biosynthesis of glutathione, together with glutamate and glycine. Glycine abundance was not appreciably or significantly different between wtIDH1 and mutIDH1^{R132H} LN18 cells. Methionine can be used to indirectly biosynthesise cysteine, via formation of L-homocysteine and then

cystathionine. The biosynthesis of 2-HG utilises large amounts of NADPH [161, 215, 220, 221], which affects the redox homeostasis of mutIDH1 glioma cells, as discussed in the introduction [reviewed in 1]. Potentially, increased cysteine and methionine indicate increased utilisation of the metabolites for glutathione biosynthesis, a key cellular antioxidant [reviewed in 354]. However, glutathione was not identified in this IC-MS data set and any abundance changes cannot be commented on.

Free methionine can also be rapidly acetylated to *N*-acetylmethionine (NAM) in a variety of brain derived cell types [355]. In this experiment, NAM was significantly increased in mutIDH1^{R132H} cells (p-value < 0.05, Tukey's test), but the difference to wtIDH1 cells was small (FC = 1.20 (MUT/WT)), see **Figure 3.4.4.(a)**. It has been suggested that the acetylation of methionine is either to produce an acetyl group donor or for maintaining a pool of methionine [355]. NAM can also be sourced from protein degradation. Due to the uncertainty in the metabolic role of NAM in healthy brain cells it remains unclear why it is accumulating in mutIDH1^{R132H} cells.

Putrescine is derived from arginine either via agmatine or ornithine, and was appreciably and significantly elevated in mutIDH1^{R132H} cells (FC = 1.45 (MUT/WT) and p-value < 0.05, Tukey's test), see **Figure 3.4.4.(b)**. Putrescine can be further metabolised to GABA, as a way for astrocytes to source GABA in addition to a pathway via glutamate [reviewed in 356]. The formation of GABA from putrescine does not require 2-OG, but further metabolization of GABA does. However, GABA abundance was not appreciably or significantly different between wtIDH1 and mutIDH1^{R132H} LN18 cells and it remains unclear how 2-HG or mutIDH1^{R132H} activity may be affecting putrescine levels.

The metabolite 4-hydroxyproline was appreciably and significantly elevated in mutIDH1^{R132H} cells (FC = 1.27 (MUT/WT) and p-value < 0.05, Tukey's test), see **Figure 3.4.4.(b)**. It is not directly derived from proline, but is instead formed during post-translational modification of proline in pre-collagen [reviewed in 357]. The modification is carried out by 2-OG dependent procollagen-proline dioxygenase, which can be inhibited by 2-HG at concentrations achieved by mutIDH1^{R132H} cells [84]. The presence of mutIDH1 and 2-HG has been shown to impair collagen maturation [358]. Increased 4-hydroxyproline indicates either increased production or decreased break down of mature collagen.

Increased production would be counterintuitive due the inhibitory effects of 2-HG on collagen maturation [358]. However, the breakdown of 4-hydroxyproline requires 2-OG to convert L-erythro-4-hydroxyglutamic acid to (*R*)-4-hydroxy-2-oxoglutarate and potentially the increased consumption of 2-OG for 2-HG biosynthesis is limiting the breakdown of 4-hydroxyproline.

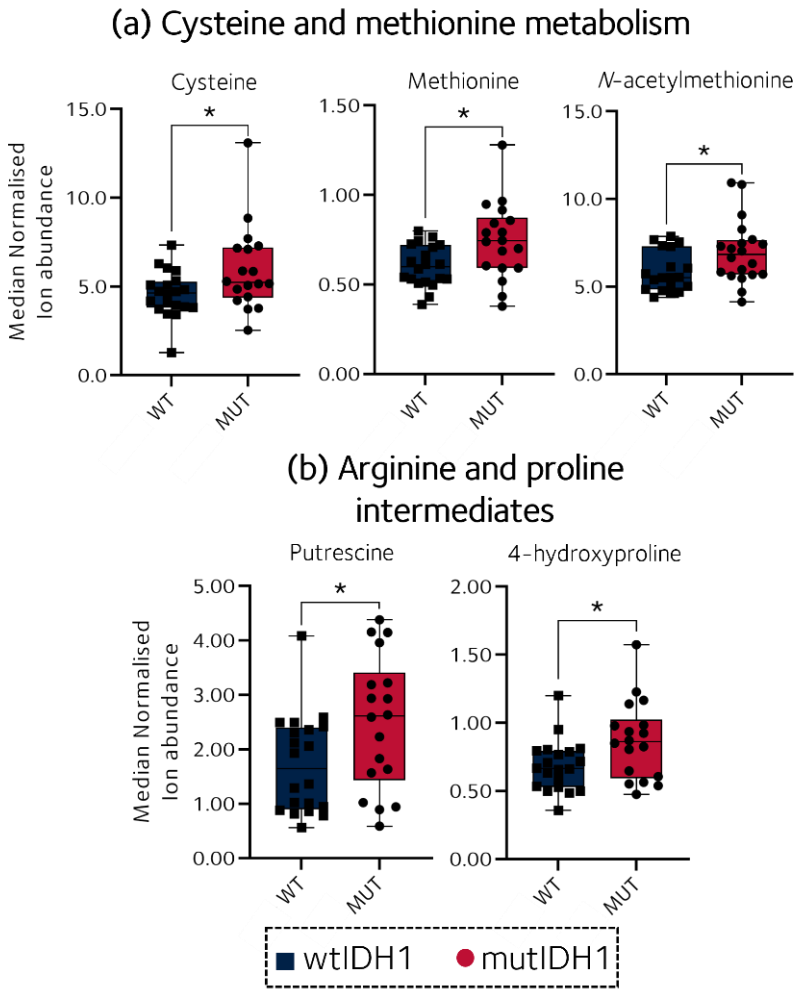

Figure 3.4.4. Box plots of additional amino acids and related metabolites in wtIDH1 and mutIDH1^{R132H} LN18 cells. (a) cysteine and methionine metabolism and (b) arginine and proline intermediates. The box plot limits are the 25th and 75th percentile, the middle line is the data median. The whiskers are the minimum and maximum measured values. * = p-value < 0.05 and ** = p-value < 0.01, *** = p-value < 0.001 and **** = p-value < 0.0001, calculated with a Tukey's test. For *N*-acetylmethionine N = 20 for mutIDH1^{R132H} and N = 19 for wtIDH1. For putrescine, 4-hydroxyproline, cysteine and methionine N = 18 for mutIDH1^{R132H} and N = 20 for wtIDH1. N = biological replicates.

Lipid related metabolites increased in wtIDH1 cells

It has been reported in the literature that mutIDH1 glioma cells, mouse models and patient-derived samples have altered phospholipid metabolism (reviewed in [1]), potentially due to higher mitochondrial density to compensate for the decrease in wtIDH1 activity [230]. The harvest and analysis methods in this experiment were not optimised for phospholipid analysis and changes in phospholipid metabolism may not be fully revealed. However, two metabolites related to lipid metabolism were detected and both were appreciably and significantly more abundant in wtIDH1 than mutIDH1^{R132H} LN18 cells: glycerate (FC = 1.28, p-value < 0.01) and isopentenyl pyrophosphate (IPP) (FC = 1.29, p-value < 0.01), FC = WT/MUT and p-values from Tukey's test). The lipid related metabolites are summarised in **Figure 3.4.5**.

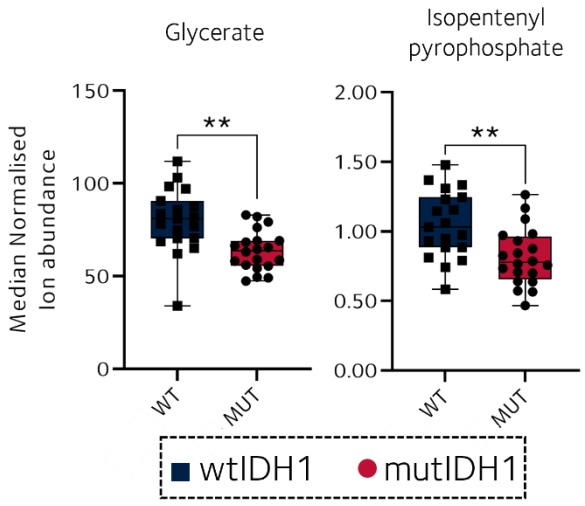

Figure 3.4.5. Box plots of lipid metabolism related metabolites in wtIDH1 and mutIDH1^{R132H} LN18 cells. glycerate and IPP. The box plot limits are the 25th and 75th percentile, the middle line is the data median. The whiskers are the minimum and maximum measured values. * = p-value < 0.05 and ** = p-value < 0.01, *** = p-value < 0.001 and **** = p-value < 0.0001, calculated with a Tukey's test. N = 20 for mutIDH1^{R132H} and N = 19 for wtIDH1 for all metabolites shown. N = biological replicates.

Glycerate can be phosphorylated and enter glycolysis, or metabolised further to the *O*-phosphoserine precursor 3-phosphatehydroxypyruvate. *O*-phosphoserine can be dephosphorylated to serine, which can be further metabolised to cysteine and glutathione (as described above). If there is a difference in glutathione metabolism between wtIDH1 and mutIDH1^{R132H} cells, the effect of that may be observed as far back as glycerate and *O*-phosphoserine. However, this would have to be confirmed with enzyme expression levels and potentially also ^{13}C tracer studies using different labelled metabolites to probe the contribution of different pathways.

IPP is an intermediate of the mevalonate pathway [reviewed in 359]. Previously, U87 and U251 glioblastoma cells expressing mutIDH1^{R132H} were reported to have increased expression of *de novo* cholesterol synthesis enzymes and were more sensitive than their wtIDH1 counterparts to inhibition of HMG CoA reductase [232], the rate limiting step of the mevalonate pathway. The decreased level of IPP in mutIDH1^{R132H} LN18 cells could indicate increased consumption for cholesterol biosynthesis; this would have to be confirmed with *e.g.,* measurement of expression levels of pathway related enzymes and ^{13}C flux analysis.

Other metabolites

The metabolites NAAG and B-CG are closely related as they are biosynthesised by homologous enzymes [360] and catabolised by structural homologues [361-363]. NAAG is a neurotransmitter [364], while B-CG is found in developing brain tissue [365, 366] and testes [367]. Neither biosynthesis nor breakdown of either metabolites are thought to require 2-OG or NADPH, but glutamate is required for biosynthesis in both cases. The metabolite abundances were appreciably and significantly higher in wtIDH1 than mutIDH1^{R132H} cells (FC_{NAAG} = 1.92 and $FC_{B\text{-}CG}$ = 1.77 (WT/MUT) and p-value < 0.0001, Tukey's test), see **Figure 3.4.6**. A final metabolite without a clear connection to either 2-OG or $NADP^+$/NADPH was methylisocitrate, which was also significantly decreased in mutIDH1^{R132H} LN18 cells (FC = 1.84 (WT/MUT) and p-value < 0.0001, Tukey's test), see **Figure 3.4.6**. Methylisocitrate exists in all living species, but its role in human metabolism is not well understood.

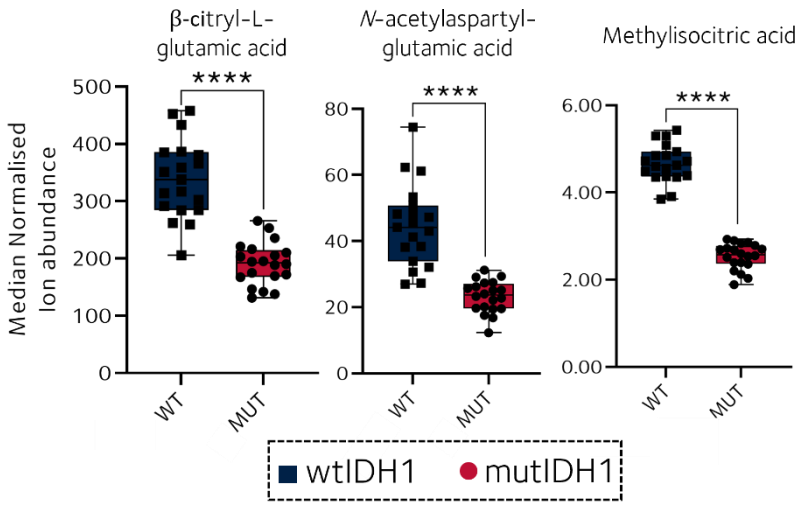

Figure 3.4.6. Box plots of other metabolites in wtIDH1 and mutIDH1^{R132H} LN18 cells. NAAG, B-CG and methylisocitrate. The box plot limits are the 25th and 75th percentile, the middle line is the data median. The whiskers are the minimum and maximum measured values. * = p-value < 0.05 and ** = p-value < 0.01, *** = p-value < 0.001 and **** = p-value < 0.0001, calculated with a Tukey's test. N = 19 for mutIDH1^{R132H} and N = 18 for wtIDH1 for all metabolites shown. N = biological replicates.

In summary, in addition to 2-HG, a number of metabolites related to a variety of metabolic pathways were identified as significantly altered in abundance. Notably, nucleotides and related intermediates appear to generally be elevated in mutIDH1^{R132H} rather than wtIDH1 LN18 cells. Amino acid intermediates requiring 2-OG for direct synthesis had lower abundance in mutIDH1^{R132H} LN18 cells, while other amino acids and intermediates with less direct link to 2-OG were increased in abundance in mutIDH1^{R132H} LN18 cells. Two metabolites considered a part of lipid metabolism, glycerate and IPP, were decreased in mutIDH1^{R132H} LN18 cells. Finally, NAAG, B-CG and methylisocitrate were also decreased in mutIDH1^{R132H} LN18 cells, but none of the metabolites have clear links to 2-OG or NADP^{+}/NADPH and the reason for their decreased abundance remains unclear.

3.5. Untargeted metabolic pathway analysis reveals changes in amino acid, short chain fatty acid and vitamin C and B1 metabolism in mutIDH1^{R132H} LN18 cells

Individual metabolite changes associated with *IDH1* mutations were reported in the previous section and also in the literature [reviewed in 1]. However, there has not always been agreement in the literature over which metabolites are significantly altered, as described in **Chapter 1**. The differences in reported metabolite abundance changes are likely due to a variety of factors, including sample type (patient sample, mouse model or cultured cells), sample preparation and suitability of the analysis methods used. A more functional approach to investigate altered metabolism beyond accumulation of 2-HG is to perform pathways analysis. The aim of UPA is to provide a biological interpretation of LC-MS metabolomics data. The UPA methodology highlights pathways of interest without relying on prior metabolite identification, as described in **chapter 1**.

Data processing and analysis

Untargeted metabolic pathway analysis using the functional analysis [313] methodology provided by the MetaboAnalystR [325] package was performed using the IC-MS data. The derivatised RPLC-MS data was not used because of the added complexity of the additional mass of the derivatising agent (The mass could be subtracted from each feature, but compounds containing more than one amine group can be derivatised more than once. The double derivatised compound would result in a different retention time and *m/z* value than the single derivatised version of the same compound. It is not possible to readily tell whether a specific LC-MS feature is from a single or double derivatised compound, or in fact if it has been derivatised at all. Sorting out these ambiguities was beyond the scope and time available for this project).

The *m/z* and retention times peak-picked by Progenesis QI in the IC-MS data were used and the data was otherwise processed as previously described for univariate analysis (IQR filtration and median normalisation). The p-values and t-scores were calculated without MCTe. Features were ranked by p-value and the cut-off for including a feature as significant was set to p-value ≤ 0.05. The mummichog algorithm and the human MFN organism library were used [313, 318]. R code was written with the packages MetaboAnalystR [325] and

rstatix [328] to enable efficient analysis and data output. Calculation of p-values and t-scores was included in the code. Further detailed description of the parameters is provided in **Section 2.8.3** in **Chapter 2** and the code is provided in **Appendix X**.

Results

The analysis output provided a list of metabolic pathways, the overall significance of a pathway, and the number of significant empirical compound (EC) hits within that pathway. In the analysis, a total of 66 pathways were found, of which 10 had significant EASE score adjusted p-value (< 0.05). That suggested there were a number of metabolic pathways that were significantly altered due to the presence of mutIDH1^{R132H} in the LN18 cells. In **Figure 3.5.1**, a plot of pathway -log(p) versus enrichment factor is shown, and the top 10 pathways ranked by EASE score adjusted p-value are labelled. The enrichment factor (x-axis) is a ratio between the number of significant EC hits within a pathway to the total number of metabolites in the pathway. The top 10 pathways are also listed in **Table 3.5.1** and all pathways are provided in **Table A.II.4**.

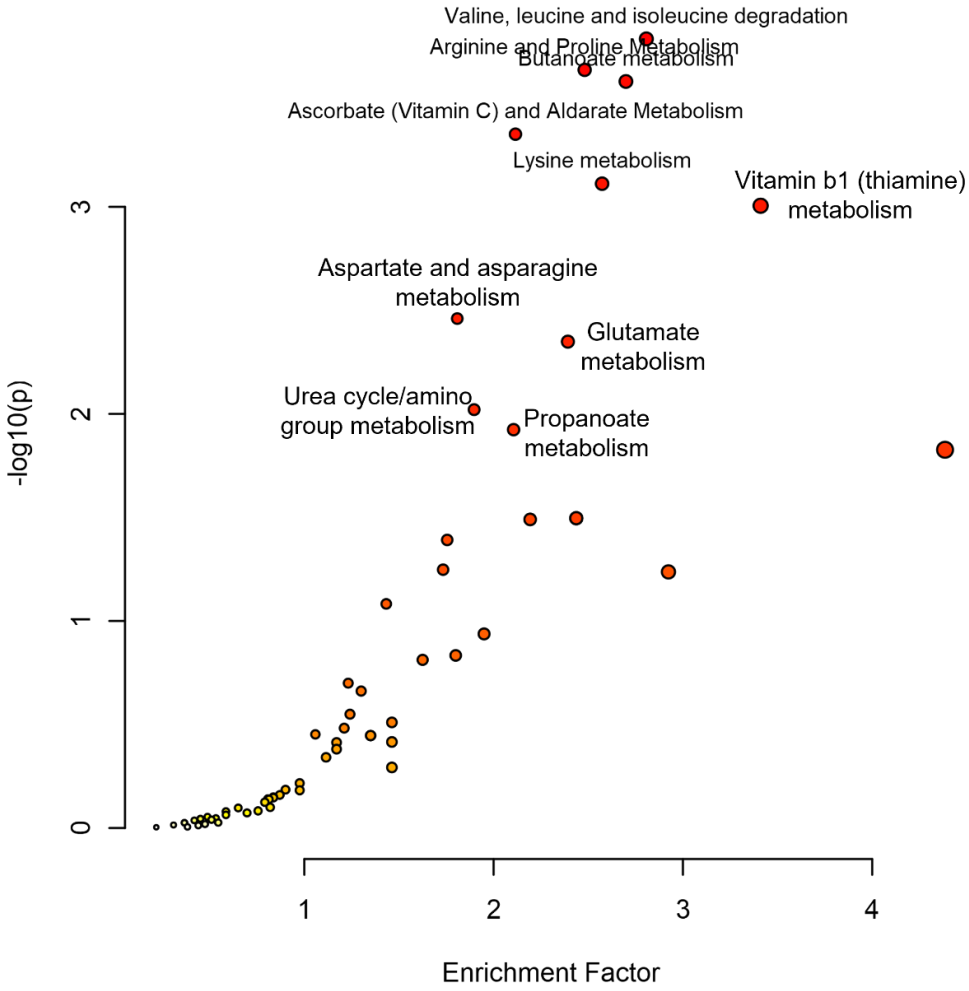

Figure 3.5.1. Plot of enrichment factor versus -log(p) for pathway hits in the UPA of IC-MS data of wtIDH1 and mutIDH1^{R132H} LN18 cells. The UPA was carried out using the mummichog algorithm and the human MFN organism library.

Table 3.5.1. Overview of metabolic pathways with significant (< 0.05) EASE score adjusted p-values found in the UPA of IC-MS data of wtIDH1 and mutIDH1^{R132H} LN18 cells. The pathway name, total number of metabolites in the pathway, number of hits for each pathway and number of significant hits are included. All output provided by the UPA can be found in Table A.II.4.

Pathway name	Pathway total	Hits total	Hits significant	EASE score adjusted p-value
Amino acid related metabolism				
Valine, leucine and isoleucine degradation	25	25	12	0.0007
Arginine and Proline Metabolism	33	33	14	0.0008
Lysine metabolism	25	25	11	0.0030
Aspartate and asparagine metabolism	55	55	17	0.0081
Glutamate metabolism	22	22	9	0.0156
Urea cycle/amino group metabolism	37	37	12	0.0239
Fatty acid related metabolism				
Butanoate metabolism	26	26	12	0.0011
Propanoate metabolism	25	25	9	0.0346
Vitamin related metabolism				
Ascorbate (Vitamin C) and Aldarate Metabolism	47	47	17	0.0013
Vitamin B1 (thiamine) metabolism	12	12	7	0.0062

Only ECs were listed in the pathway output, not KEGG metabolites codes. The analysis did provide a list of matches between ECs and KEGG metabolite codes. R code was therefore written to match significant ECs for a given pathway to KEGG metabolite codes, as well as retain the *m/z* values and retention times (see **Appendix X** for the codes). Based on the EC to KEGG matches, the top 10 pathways consisted mostly of putative annotations of various carboxylic acids, which the anion-exchange column used in the IC-MS method is capable of separating [148]. Certain pathways had amino acids suggested that were unlikely to be measured, but they did not comprise a majority of the empirical compounds in the pathways. However, in five pathways, ECs with the same retention time as 2-HG (9.901 minutes) were included, but the annotation was not 2-HG. Considering the high significance of 2-HG changes (p-values < 9.0E-16)), often also reflected in adducts and fragments, it was important to assess whether the features at 9.901 minutes were disproportionately favouring specific pathways. The analysis was therefore repeated after removing all *m/z* values with retention time 9.901 minutes. The same top 10 pathways as in **Table 3.5.1** still had EASE score adjusted p-values < 0.05 and no additional significant pathways were found. Therefore, finding an occasional metabolite that, from experience is either a different metabolite or known as unsuitable for separation and/or detection by IC-MS, did not compromise the overall predictive capability of the UPA. That supported the justification of the mummichog algorithmic approach, which relies on putative identifications, but only reports significance at a pathways level [313].

A drawback with UPA in its current iteration was that it did not provide the opportunity to include known metabolic alterations such as the *IDH1* mutation. The functional analysis output therefore did not incorporate 2-HG as a putative identification or within the proper pathway and context. As demonstrated above, removing 2-HG and adducts from the dataset still led to the same significant pathways, yet it was not known how that may have changed if a pathway with the *IDH1* mutation accounted for was present as well. Caution was therefore exercised during the interpretation of the significant pathways. In general, the output from functional analysis should be examined for accuracy in putative identifications, robustness in loss of significant features and placed within the context of complementary data.

With that in mind, the functional analysis performed here identified multiple pathways linked to amino acid metabolism, metabolites of which also appeared in the univariate analysis or have been reported in the literature. The valine, leucine and isoleucine degradation pathway was significant in the UPA, while isoleucine and transaminase product 3M2OV acid were observed in univariate analysis. The pathway lysine degradation was found by UPA and the degradation intermediates oxoadipate, 2-aminoadipate and pipecolate were observed in univariate analysis. Decreased 2-aminoadipate had also previously been reported in HOG cells expressing mutIDH1^{R132H} compared to empty vector cells [175], but lysine degradation as a pathway has received little attention. Glutamate, arginine & histidine, aspartate & asparagine pathways were also significant in the pathway analysis and several intermediates were observed in the univariate analysis (4-hydroxyproline, putrescine, asparagine and 2-OG). Glutamate is an important anaplerotic substrate for mutIDH1^{R132H} cells and supplies the majority of carbon for 2-HG biosynthesis (see **section 3.6**) [147, 208]. Arginine & proline metabolism had previously been reported as a pathway distinguishing wtIDH1 from mutIDH1 glioma based on abundances of identified metabolites from analysis of plasma samples [368]. The urea cycle pathway was significant, but the two identified intermediates, citrulline and arginine, were not significantly different between wtIDH1 and mutIDH1^{R132H} LN18 cells in the univariate analysis (FC < 1.10 and p-value > 0.05, Tukey's test).

Butanoate and propanoate metabolism included several different carboxylic acids, one of which was also found in the univariate analysis (methylisocitrate). The pathways have not previously been reported in the literature, but will be discussed further in **section 3.8**. The vitamin B1 pathway did not include thiamine phosphates in the list of potential identifications, but instead had oxoadipate, pyruvate, malonic semialdehyde and 2-OG. The suggested metabolite annotations for vitamin C metabolism included intermediates shown in the KEGG pathway, and also included a compound observed in the univariate analysis (methylisocitrate). Metabolites from vitamin C metabolism have been reported as correlated with onset of GBM in a prospective serum study [369], but otherwise there are few reports on either vitamin B1 or vitamin C and mutIDH1 glioma in the literature.

In summary, 'functional analysis' from the MetaboAnalystR package is a data analysis tool used to perform UPA. Despite the current iteration not being able to take the IDH1 *mutation*

into account, it suggested several pathways that were supported by univariate statistical analysis and previous reports in the literature. The features that were known as 2-HG or adducts and fragments were used in the UPA, yet removing them did not change which pathways were considered significantly altered. The output was therefore validated, both experimentally and by previously known metabolic differences between wtIDH1 and mutIDH1 glioma.

3.6. The major carbon source for 2-HG in both wtIDH1 and mutIDH1^{R132H} LN18 cells is glutamine not glucose

In both univariate and functional analysis, metabolites and pathways closely related to 2-OG and glutamate were altered. Previous studies have reported that glutamine, rather than glucose, is the major carbon source for 2-HG (a patient-derived mutIDH1^{R132H} glioma cell line (TS603) [208], a GBM cell line expressing mutIDH1^{R132H} via lentiviral vector (U251) [147], chondrosarcoma cell lines (JJ02 and CS1) [165] and human myeloma cell lines (RPMI-8226 and MM1S) [370]). In this section a ^{13}C experiment was performed to assess whether that was the case in LN18 cells as well. The ^{13}C tracer experiment used [1,2-$^{13}C_2$]-glucose and [U-$^{13}C_5$]-glutamine to confirm whether the current LN18 cell model preferentially utilised glutamine or glucose in 2-HG biosynthesis.

Data processing and analysis

The ^{13}C labelling experiments are described in detail in **section 2.5.3**-**2.5.4**, and harvested and processed as described in **sections 2.5.5** and **2.6.1**. In short, the cells were incubated with either unlabelled glucose and glutamine, [1,2-$^{13}C_2$]-glucose and unlabelled glutamine, or unlabelled glucose and [U-$^{13}C_5$]-glutamine. The cells were incubated with labelled or fresh non-labelled media for 24 hours. The glucose and glutamine concentrations matched that of standard supplemented LG DMEM, *i.e.,* 1.0 g/L glucose and 2 mM glutamine. The DNA concentrations used to normalise the samples prior to analysis with IC-MS are provided in **Table A.III.6** in **appendix III**. The isotope distributions were measured by manual integration, as described in **section 2.8.1**.

Results

The total 2-HG abundance was significantly and substantially higher in mutIDH1^{R132H} than wtIDH1 LN18 cells for each comparison of cells cultured in non-labelled, [1,2-^{13}C]-glucose or [U-^{13}C]-glutamine labelled media (FC > 100 (MUT/WT) and p-value < 0.0001, one-way ANOVA with Šidák MCT). Thus, the labelling did not affect the difference in 2-HG levels between wtIDH1 and mutIDH1^{R132H} LN18 cells. The 2-HG abundance was not significantly different for cells of the same mutational status grown in media with labelled or non-labelled glucose and glutamine (p-value > 0.05, one-way ANOVA with Šidák MCT), *i.e.,* the labelling did not cause more or less biosynthesis of 2-HG.

In the wtIDH1 and mutIDH1^{R132H} LN18 cells cultured with non-labelled media, the isotope distribution of 2-HG was not significantly different between wtIDH1 and mutIDH1^{R132H} cells for any of the five isotopes (p-value > 0.05, two-tailed t-test). The [M+0] isotopologue was 94.7 ± 0.4% of the total 2-HG pool and the [M+1] isotopologue was 5.3 ± 0.4%. The other isotopologues ([M+3], [M+4] and [M+5]) were not detected. The wtIDH1 and mutIDH1^{R132H} LN18 cells cultured with [1,2-$^{13}C_2$]-glucose also did not have significantly different labelling of 2-HG (p-value > 0.05, two-tailed t-test). However, the [M+0] isotopologue was now only 89 ± 2% of the total 2-HG pool, and the [M+1] and [M+2] isotopologues were 5 ± 2% and 5.2 ± 0.4%, respectively. The other three isotopologues were the combined 0.5% of the remaining 2-HG pool. In the mutIDH1^{R132H} LN18 cells that were cultured with [U-$^{13}C_5$]-glutamine, the [M+0] and [M+5] isotopologues of 2-HG were 13.1 ± 0.2% and 72 ± 1% of the total 2-HG pool, respectively. While in the wtIDH1 LN18 cells that were cultured with [U-$^{13}C_5$]-glutamine, the [M+0] and the [M+5] isotopologues of 2-HG were 26 ± 2% and 58 ± 3% of the total 2-HG pool, respectively. The [M+0] 2-HG isotopologue was a significantly larger part of the total 2-HG pool in the wtIDH1 LN18 cells (p-value > 0.0001, one-way ANOVA with Šidák MCT). Unsurprisingly, the [M+5] 2-HG isotopologue was significantly larger part of the total 2-HG pool in the mutIDH1^{R132H} LN18 cells (p-value > 0.0001, one-way ANOVA with Šidák MCTe). The [M+1], [M+2] and [M+3] isotopologues were not significantly different between wtIDH1 and mutIDH1 LN18 cells (p-value > 0.05, one-way ANOVA with Šidák MCTe). The isotope distributions of 2-HG in the non-labelled, [1,2-$^{13}C_2$]-glucose and [U-$^{13}C_5$]-glutamine media are summarised in **Figure 3.6.1**.

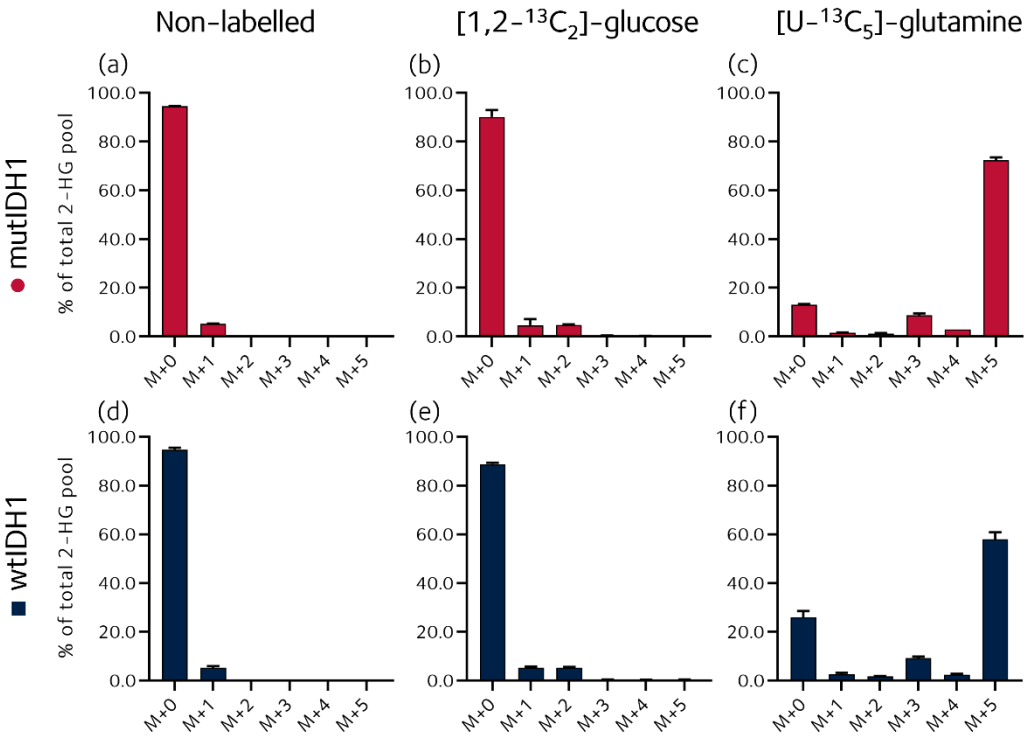

Figure 3.6.1. ^{13}C labelling of 2-HG in mutIDH1^{R132H} and wtIDH1 LN18 cells cultured with non-labelled, [1,2-$^{13}C_2$]-glucose or [U-$^{13}C_5$]-glutamine media. The 2-HG pool was quantified by measuring the peak area of the $[M-H]^-$ EICs of the up to six 2-HG isotopes present ([M+0], [M+1], [M+2], [M+3], [M+4] and [M+5]). The isotope distribution of 2-HG in mutIDH1^{R132H} LN18 cells cultured with (a) non-labelled, (b) [1,2-$^{13}C_2$]-glucose and (c) [U-$^{13}C_5$]-glutamine media. The isotope distribution of 2-HG in wtIDH1 LN18 cells cultured with (d) non-labelled, (e) [1,2-$^{13}C_2$]-glucose and (f) [U-$^{13}C_5$]-glutamine media. The number of biological replicates was N = 3 for cells grown in non-labelled media and N = 5 for cells grown in labelled media. Each bar is the percentage of the total 2-HG pool and the error bar was one standard deviation.

The data presented above confirmed that glutamine, rather than glucose, was the main carbon source for 2-HG in both wtIDH1 and mutIDH1^{R132H} LN18 cells. It was somewhat surprising that there was a significant difference in isotope distribution for labelled glutamine only. If there was a difference in carbon source then glucose would be considered the most likely source, yet the labelling from glucose was the same. Potentially other carbon sources, *e.g.,* amino acids from the FBS in the media, contributed to the pool of 2-OG to a greater extent in wtIDH1 than mutIDH1^{R132H} LN18 cells. However, the pool of 2-HG in mutIDH1^{R132H} LN18 cells was also significantly larger than in wtIDH1 cells. Thus, if the amount of carbon from other amino acids was the same it would have a far smaller relative contribution to the total 2-HG pool in mutIDH1^{R132H} LN18 cells.

In summary, glutamine was the major carbon source for 2-HG in both wtIDH1 and mutIDH1^{R132H} LN18 cells, in accordance with previous reports in the literature. The isotope distribution of 2-HG was the same for wtIDH1 and mutIDH1^{R132H} LN18 cells cultured with

non-labelled and [1,2-$^{13}C_2$]-glucose. The percentage of the total 2-HG pool that was labelled from [U-$^{13}C_5$]-glutamine was significantly higher in mutIDH1^{R132H} than wtIDH1 LN18 cells. That was potentially due to the contribution of non-labelled amino acids from FBS being, relatively speaking, smaller for 2-HG in mutIDH1^{R132H} cells than wtIDH1 cells because the total 2-HG pool was significantly larger for the former.

3.7. Measuring redox metabolites NAD$^+$, NADH, NADP$^+$ and NADPH with HILIC-MS

The main focus thus far has been on the 2-OG to 2-HG axis of mutIDH1^{R132H}, but upon mutation, IDH1 changes from predominantly producing NADPH by oxidative decarboxylation of isocitrate, to consuming NAPDH for the reduction of 2-OG to 2-HG. This has potentially profound effects on cellular redox homeostasis as it presumably places a greater demand on other NADPH-producing pathways. Changes in redox homeostasis have been reported for glioma and other cell lines expressing mutIDH1^{R132H} via lentiviral vectors [220-222]. Therefore, it was of interest to measure NADP$^+$ and NADPH concentrations in cellular samples. The redox metabolites NAD$^+$, NADH, NADP$^+$ and NADPH can be measured with NMR [371], colorimetric assays [372, 373], genetically encoded fluorescent probes [374-377], or LC-MS methods such as ion-paired RPLC-MS or HILIC-MS [310, 322, 378]. HILIC-MS was chosen as the preferred approach in this project and an LC-MS method was developed and optimised for this. This is described below, followed by the measurement of cellular levels of the redox metabolites.

Prior to measurement of the redox metabolites, they had to be extracted from the cell samples. The four redox metabolites (NAD$^+$, NADH, NADP$^+$ and NADPH) are all sensitive to degradation and interconversion [322, reviewed in 379, 380] so sample preparation and storage were important factors to consider. The sample preparation was done following the recommendations by Lu *et al*. [322]. They developed a protocol to quench metabolic activity and decrease interconversion between the reduced and oxidised forms of the metabolites. The recommended method was an extraction solution of 40:40:20 acetonitrile:methanol:water with 0.1M formic acid. After cell scraping and transfer to a sample tube, 15% (w/v) ammonium bicarbonate in water was added to neutralise the sample (8.7 µL neutralising solvent per 100 µL extraction solvent). Samples were stored at

-80 °C, but due to column and instrument issues, the samples were stored for several months prior to analysis.

3.7.1. HILIC-MS method development

Three different stationary phase column chemistries were evaluated during method development: amide (BEH Amide, 21. × 100 mm, 1.7 µm particle size), ZIC with phosphorylcholine (SeQuant® cHILIC, 2.1 × 150 mm, 3 µm particle size) and ZIC with sulfobetaine (BEH Z-HILIC, 2.1 × 100 mm, 1.7 µm particle size). The former two were tested based on previous publications [310, 322], while the lattermost was chosen based on recommendation from the manufacturer (Waters Ltd.). Columns were assessed with standards of NAD^+, NADH, $NADP^+$ and NADPH (3.0 µM) dissolved in the extraction and neutralising solutions described for redox harvest of cells, see **section 2.3.4** for preparation details.

The amide column was tested under the chromatographic conditions and MS parameters described by Lu *et al.* [322], which is detailed in **section 2.7.4**. In brief, the two mobile phases were 95:5 water:acetonitrile with 20 mM ammonium acetate and 20 mM ammonium hydroxide (pH 9.5) (mobile phase A) and pure acetonitrile (mobile phase B). The total chromatographic method length was 20 minutes, with an 11.5-minute gradient starting at 90% and ending at 0% mobile phase B, with flow rate of 0.200 mL/min. The most abundant adduct for all four redox metabolites was $[M-H]^-$. Only NAD^+ and NADH achieved acceptable peak shape (base peak width < 1 min). $NADP^+$ and NADPH had broad peaks (base peak width > 5 min) and poor sensitivity. EICs for all four metabolites are shown in **Figure 3.7.1.(a)**. Peak shape was not improved with changing flow rate or gradient length.

The ZIC phosphorylcholine column was used with a method adapted from Smith *et al*. [310], which is detailed in **section 2.7.4**. Mobile phase A was 20 mM ammonium acetate (pH 6) and mobile phase B was pure acetonitrile. Total method length was 19 minutes, with a 14-minute gradient starting at 70% and ending at 40% mobile phase B, with a flow rate of 0.300 mL/min. Similar to the amide column, NAD^+ and NADH had acceptable sensitivity and peak shape (base peak width < 0.5 min). $NADP^+$ had a broad peak and a tenth of the peak hight achieved by NAD^+ and NADH. NADPH had even poorer sensitivity. The EICs are summarised in **Figure 3.7.1.(b)**. Efforts to improve sensitivity by adjusting MS parameters

and increasing the pH of mobile phase A to pH 9 were not successful. Furthermore, the column had issues with high back pressure after less than 100 sample injections. The same back pressure issues occurred again with a new column and it was decided to no longer pursue this specific column for the measurement of redox metabolites.

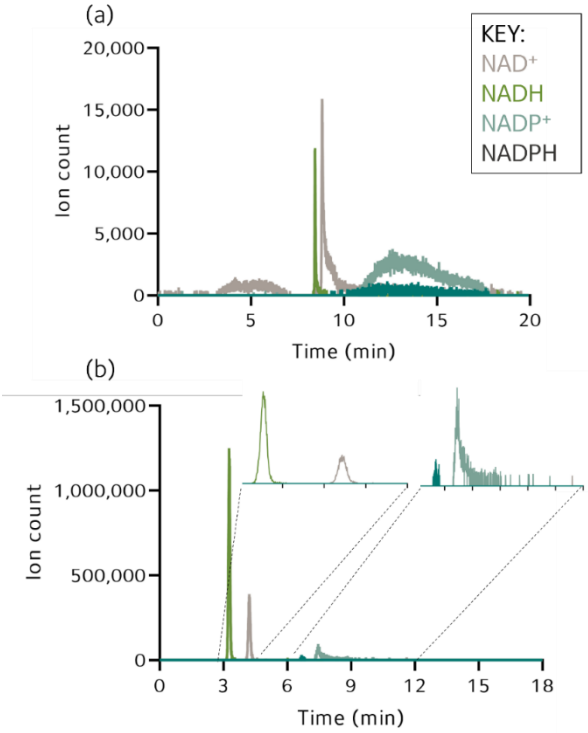

Figure 3.7.1. Extracted ion chromatograms of NAD^+, NADH, $NADP^+$ and NADPH from analysis with (a) the HILIC amide column and (b) the ZIC phosphorylcholine column. The mobile phases for the amide column was acetonitrile and 95:5 water:acetonitrile with 20 mM ammonium acetate plus 20 mM ammonium hydroxide (pH 9). Mobile phases for the ZIC phosphoryl column were acetonitrile and 20 mM ammonium acetate (pH 6). Both columns were tested on the Ultimate-3000 pump plus Exploris 240™ MS. EICs are from a single injection of a mixed standard (3 µM) of NAD^+, NADH, $NADP^+$ and NADPH, all EICs are of the $[M-H]^-$ adduct.

The final column tested, a ZIC column with sulfobetaine stationary phase, was more robust than the previous ZIC column with regards to stable back pressure during use. It was first tested with the Vion MS system and accompanying Acquity pump. Mobile phase A was 20 mM ammonium acetate (pH 6) and mobile phase B was acetonitrile. The initial gradient was based on Smith *et al*. [310]. Flow rate was 0.400 mL/min and column temperature were 40 °C. Similar to the two previous columns, NAD^+ and NADH had acceptable peak shape and ten-fold higher peak height relative to $NADP^+$ and NADPH, as shown in **Figure 3.7.2.(a)**.

A number of parameters were adjusted to improve peak shape of $NADP^+$ and NADPH, including increasing the pH of mobile phase A from 6 to 9, increasing column temperature (from 40 °C to 50 °C), increasing flow rate (from 0.400 mL/min to 0.500 mL/min) and increasing or decreasing the length and steepness of the gradient. Major challenges remained with the sensitivity of measuring $NADP^+$ and NADPH, which were found to be due to issues with the detector in the MS, rather than chromatographic settings. Cleaning instrument components (cone, ion step wave) and adjusting parameters such as cone voltage and temperature did not help.

However, based on NAD^+ and NADH, the chromatographic method was at least optimised to start at a higher amount of acetonitrile as this increased retention time of NAD^+ and NADH (from 2 to 6 minutes). Higher column temperature (50 °C) improved back pressure, without having much of an effect on peak shape. Higher flow rate did not improve peak shape. EICs of NAD^+, NADH, $NADP^+$ and NADPH from the final chromatographic method are shown in **Figure 3.7.2.(b)**. The final chromatographic method had the following gradient, where mobile phase A was 20 mM ammonium acetate (pH 9) and mobile phase B was acetonitrile: 0.0 min, 95% B; 1.0 min 95% B; 9.0 min, 50% B; 13.0 min, 50% B; 13.5 min, 95% B; 18.0 min, 95% B.

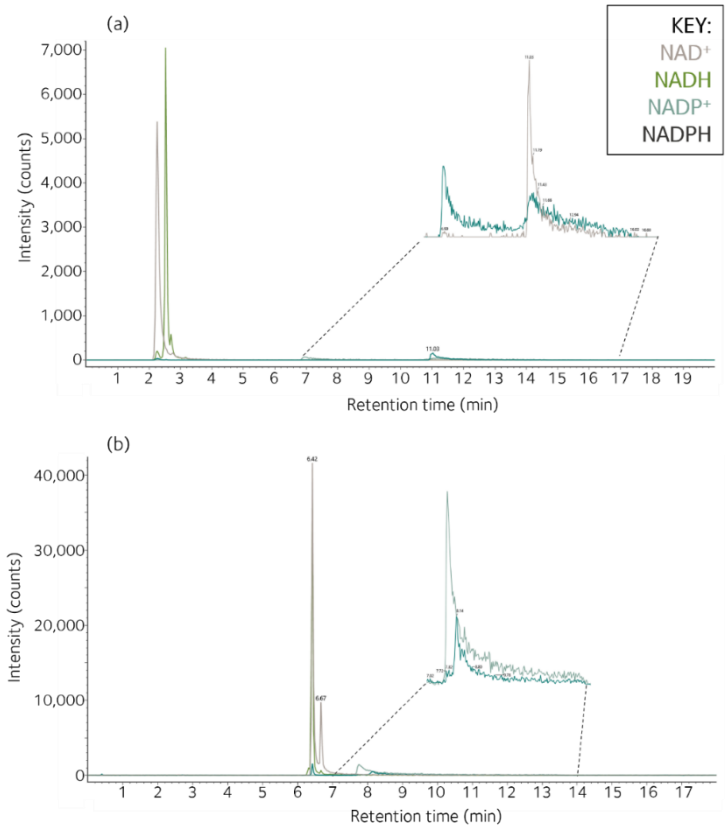

Figure 3.7.2. Extracted ion chromatograms of NAD^+, NADH, $NADP^+$ and NADPH from analysis with the ZIC sulfobetaine column. (a) First chromatographic method with 20 mM ammonium acetate (pH 6). (b) Final chromatographic method with 20 mM ammonium acetate (pH 9) and highest percent starting acetonitrile (95%). EICs are from a single injection of a mixed standard (3 µM) of NAD^+, NADH, $NADP^+$ and NADPH, all EICs are of the $[M-H]^-$ adduct.

The ZIC sulfobetaine column was then tested on the Ultimate-3000 pump and Exploris 240™ MS system, with improved sensitivity of $NADP^+$ and NADPH. A variety of buffers were tested to assess their effect on the peak shape of $NADP^+$ and NADPH: 5 mM ammonium formate (pH 6), 20 mM ammonium formate (pH 3, 6 and pH 9), and 20 mM ammonium acetate (pH 9). When the 20 mM ammonium acetate (pH 3) was used, the MS was operated in positive mode due protonated species being more likely than de-protonated species when the mobile phase was acidic. Only NADH was detected in positive mode and the EIC is not shown.

The main effect the different buffers had was on retention time and not peak shape, although 20 mM ammonium formate (pH 9) led to somewhat narrower peaks and was therefore chosen for analysis of cellular samples. Extracted ion chromatograms of NAD^+, NADH, $NADP^+$ and NADPH analysed with 20 mM ammonium acetate at pH 6 or 9, 5 mM ammonium formate at pH 6, and ammonium formate at pH 6 and 9 are provided in **Figure 3.7.3.(a)-(e)**.

Finally, the ion transfer tube and vaporiser temperature were assessed to find the settings that provided the highest sensitivity (largest EIC peak area). Per recommendations from the manufacturer (Thermo Fisher), temperatures in the range of 200-300 °C were tested. A low, medium and high temperature were chosen: 200 °C, 250 °C and 300 °C. Nine different combinations of the three different temperatures for the ion transfer tube and vaporiser were carried out. Higher peak area of $NADP^+$ and NADPH was prioritised over NAD^+ and NADH. Medium (250 °C) ion transfer tube and high (300 °C) vaporiser temperature led to the highest peak area for NAD^+, $NADP^+$, NADPH and second-highest for NADH and was therefore used for future analyses. The peak areas of the EICs of each redox metabolite at each temperature combination is provided in **Figure 3.7.4**.

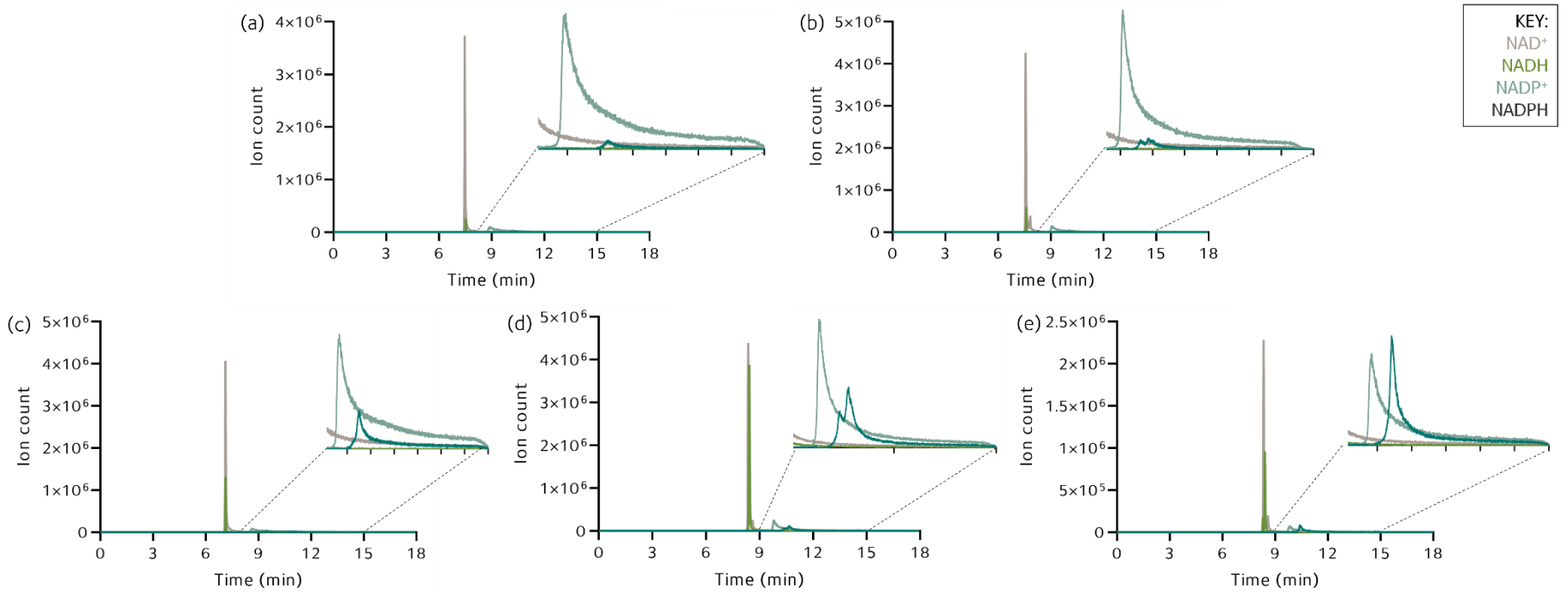

Figure 3.7.3. Extracted ion chromatograms of NAD^+, NADH, $NADP^+$ and NADPH from analysis with the ZIC sulfobetaine column with the ULTIMATE-3000 pump and Exploris 240™ MS. (a) Mobile phase A = 20 mM ammonium acetate (pH 6). (b) Mobile phase A = 20 mM ammonium acetate (pH 9). (c) Mobile phase A = 5 mM ammonium formate (pH 6). (d) 20 mM ammonium formate (pH 6). (e) Mobile phase A = 20 mM ammonium formate (pH 9). Mobile phase B = acetonitrile. The same chromatographic and MS parameters were used for all analyses. EICs are from a single injection of a mixed standard (3 µM) of NAD^+, NADH, $NADP^+$ and NADPH, all EICs are of the $[M-H]^-$ adduct.

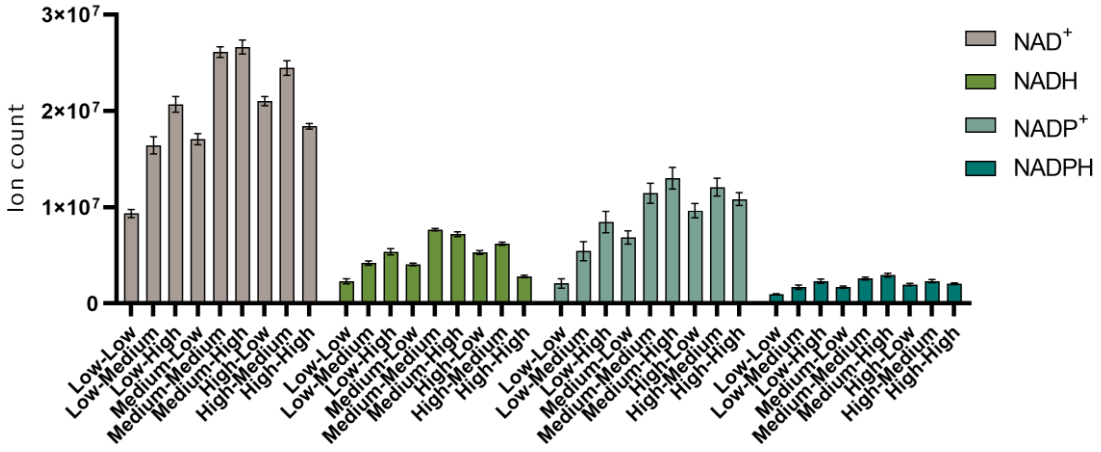

Figure 3.7.4. Peak area of extracted ion chromatograms NAD^+, NADH, $NADP^+$ and NADPH from analysis with the ZIC sulfobetaine column under different ion transfer tube and vaporiser temperatures. Low = 200 °C, medium = 250 °C and high = 300 °C. The first temperature is for the ion transfer tube and the second temperature is for vaporisation. N = 4, which was repeat injections of the same standard. The standard was made as one large solution, split into 9 vials. All EIC are of the $[M-H]^-$ adduct.

3.7.2. NADPH/$NADP^+$ ratio not significantly altered between wtIDH1 and mutIDH1^{R132H} LN18 cells

LN18 wtIDH1 and mutIDH1^{R132H} cells were grown as described previously in **Section 2.5.3**, but harvested with the method from Lu *et al.* optimised for decreasing the interconversion between the reduced and oxidised form of the redox metabolites [322], see **Section 2.5.6**. See **Table A.III.2** for DNA measurements used for normalisation of the samples. The samples were analysed using the Z-HILIC LC-MS method as described in **Section 2.7.4**, with 20 mM ammonium formate (pH 9) as mobile phase A and pure acetonitrile as mobile phase B. The vaporiser and ion transfer tube temperature set to 250 °C and 300 °C, respectively. $NADP^+$ and NADPH were quantified using an external calibration curve. The calibration standard solutions were made as described in **section 2.3.4** with the extraction and neutralising solutions used for redox harvest. The most abundant adduct for $NADP^+$ and NADPH was $[M-H]^-$ for both standards and cell samples. Extracted ion chromatograms of $NADP^+$ and NADPH in cell samples are provided in **Figure 3.7.5**.

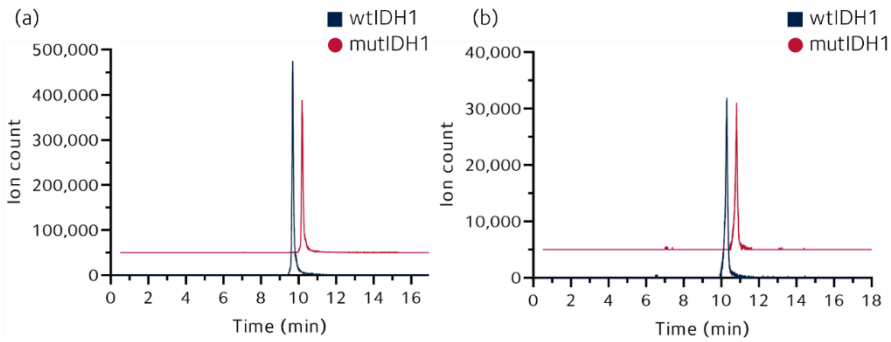

Figure 3.7.5. Extracted ion chromatograms of $NADP^+$ and NADPH in LN18 cell samples. All EIC are of the $[M-H]^-$ adduct for $NADP^+$ and NADPH. (a) EIC of $NADP^+$ in wtIDH1 (blue) and mutIDH1^{R132H} (red) LN18 cells. (b) EIC of NADPH in wtIDH1 (blue) and mutIDH1^{R132H} (red) LN18 cells. All chromatograms are of a single injection.

There was no significant difference in NADPH concentration between wtIDH1 (0.13 ± 0.04 µM) and mutIDH1^{R132H} (0.13 ± 0.04 µM) LN18 cells (p-value > 0.9999, unpaired two-sided t-test). $NADP^+$ trended toward significantly different between wtIDH1 (1.1 ± 0.2 µM) and mutIDH1^{R132H} (0.8 ± 0.3 µM) LN18 cells (p-value = 0.0731, unpaired two-sided t-test). A ratio of NADPH/$NADP^+$ was calculated for each sample (N = 10 biological replicates per experimental group) and the ratios were averaged. The ratio of NADPH/$NADP^+$ was not significantly different between wtIDH1 (0.17 ± 0.06) and mutIDH1^{R132H} (0.2 ± 0.1) LN18 cells either (p-value = 0.1155, unpaired two-sided t-test). Box plots of ratios and individual measurements are provided in **Figure 3.7.6**, as well as the calibration curves.

NAD^+ and NADH were also measured. There was no significant difference between wtIDH1 and mutIDH1^{R132H} LN18 cells for the peak areas of the extracted ion chromatograms of NAD^+, using the $[M-H]^-$ adduct (p-value = 0.5657). The peak area of the extracted ion chromatograms of NADH ($[M-H]^-$) in the cell samples were too variable to perform meaningful statistical tests (up to 98.8% CV). The large degree of variability was seen in biological samples only, not standards. All four redox metabolites had variable peak areas in the biological samples: 9-15% CV for NAD^+, 19-40% CV for $NADP^+$ and 40% CV for NADPH. The harvesting method and storage time (at -80 °C) will need to be assessed further to determine whether the variability is due to experimental or biological variation. The variability is likely not just analytical, as the standards generally had a CV of 2.1-14.7% (analytical N = 3-5).

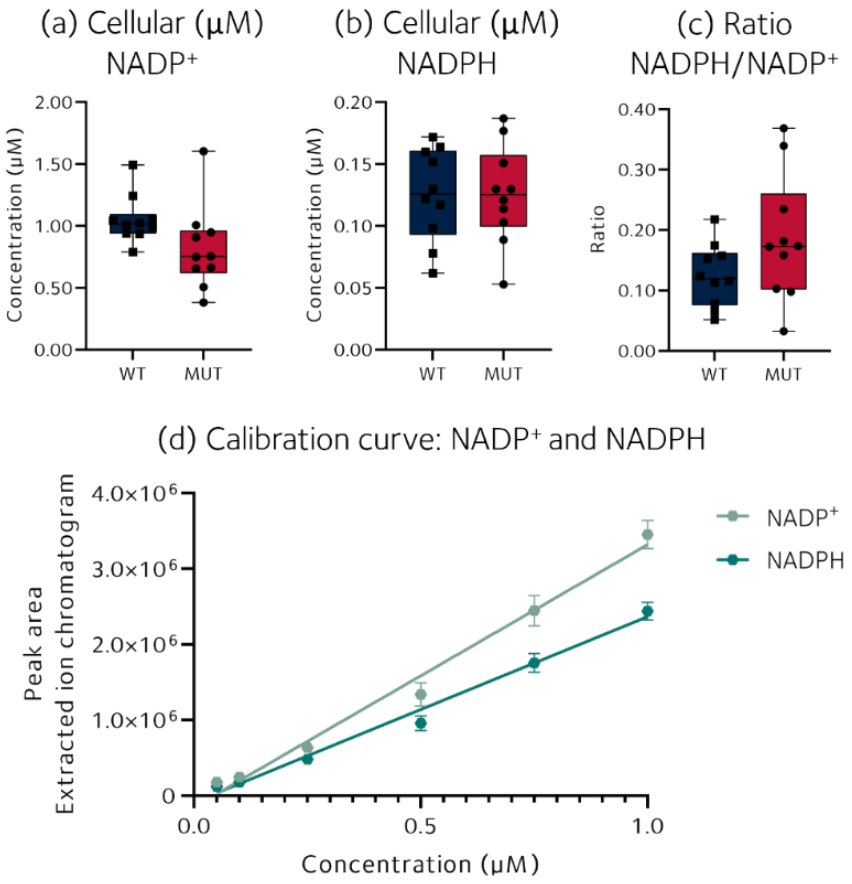

Figure 3.7.6. Measurement of NADP$^+$ and NADPH in wtIDH1 and mutIDH1^{R132H} LN18 cells. (a) Total cellular concentration (µM) of NADP$^+$ (b) Total cellular concentration (µM) of NADPH. (c) Ratio of NADPH/NADH. The number of biological replicates (N) was 10 for wtIDH1 and mutIDH1^{R132} LN18 cell samples. The box plot limits are the 25th and 75th percentile, the middle line is the data median. The whiskers are the minimum and maximum measured values. (d) Calibration curve of NADP$^+$ and NADPH. Simple linear regression, slopes were significantly non-zero (p-value < 0.0001). R^2 for the NADP$^+$ = 0.978; R^2 for the NADPH = 0.984. N = 4 (analytical replicate, *i.e.,* repeat injection of standards: 0.05, 0.10, 0.25, 0.50, 0.75 and 1.00 µM). Each data point is the mean and the error bars are one standard deviation.

In summary, a HILIC-MS method for measuring and quantifying the four redox metabolites NAD$^+$, NADH, NADP$^+$ and NADPH was developed. The method had issues with peak shape of NADP$^+$ and NADPH and efforts to improve the peak shape had marginal impact. Sample stability was poor for all metabolites, but total cellular NAD$^+$, NADP$^+$ and NADPH could be measured. There was no significant difference in NAD$^+$ levels, NADP$^+$ or NADPH concentrations, nor in the ratio of NADPH/NADP$^+$, between wtIDH1 and mutIDH1^{R132H} LN18 cells. Cellular NADH levels were too variable to perform statistical tests upon. Sample collection, preparation and analysis requires further consideration to obtain a workable quantitative method.

3.8. Discussion

3.8.1. 2-HG is substantially increased in mutIDH1 cells while 2-OG is decreased to a lesser extent

In studies of mutIDH1 glioma cell lines, mouse models and patient tissue biopsies, 2-HG was significantly increased in the mutIDH1 samples compared to the wtIDH1 samples [76, 143, 144, 147, 148, 157, 158, 173-175]. There are few reports in the literature of FC values of 2-HG in mutIDH1 versus wtIDH1 gliomas patient samples (reviewed in [1]), but one publication notes that mutIDH1^{R132H} patient samples had a 100-fold higher 2-HG levels than wtIDH1 samples [76]. The LN18 mutIDH1^{R132H} cells used here had significantly and substantially higher 2-HG levels than the wtIDH1 LN18 cells (FC = 52.9 (MUT/WT), Tukey's test p-value < 0.0001). The FC was lower than what was found in a first generation LN18 with mutIDH1^{R132H} expressed via lentiviral vector, which was over 100-fold higher than wtIDH1 LN18 cells [148]. The two generations of LN18 were prepared separately and with different lentiviral vectors (first generation: pCC.sin.36.MCS.PPTWpre.CMV.tTA-S2tet [148, 320] and second generation: pUltra-Chilli [312]). The difference in FC of 2-HG was therefore likely due to different expression levels of the mutIDH1^{R132H} enzymes in the two cell lines. However, since both generations of mutIDH1^{R132H} LN18 cell lines led to high levels of 2-HG a difference in FC was acceptable because the cell lines did not need to match in expression levels to each provide a useful model for the research questions outlined previously. All later direct comparisons of experiments, *e.g.,* where mutIDH1 inhibitors were compared, were carried out with the second-generation cell line to ensure different enzyme expression levels would not bias the analysis.

The level of 2-OG in mutIDH1^{R132H} glioma cells is slightly lower than in wtIDH1 glioma cells (FC = 1.30 (WT/MUT), Tukey's test p-value < 0.01), but nowhere near the change in 2-HG levels (FC = 52.9 (MUT/WT)). Published papers using glioma cell lines expressing mutIDH1^{R132H} via lentiviral vector report either a significant decrease in 2-OG in mutIDH1^{R132H} relative to wtIDH1 glioma cells [148, 175] or find no significant difference [174, 221]. As discussed in the introduction, reported metabolite levels vary between different research papers. 2-OG is a central metabolite [reviewed in 349] and it is unsurprising that it is not equally lowered in mutIDH1^{R132H} cells as 2-HG is elevated. There

are multiple enzymes that produce 2-OG [reviewed in 349], and its utilisation by mutIDH1^{R132H} is likely compensated for by these enzymes, at least when the cells are not placed under further metabolic duress.

3.8.2. Altered amino acid metabolism is indicated by changes in amino acid abundance and UPA in mutIDH1^{R132H} LN18 cells

Amino acid metabolism in cancer cells facilitates continued cell proliferation, even under limited nutrient availability [reviewed in 381, 382, 383]. In mutIDH1 glioma, the focus has up-to-date been on the key role of glutamate mutIDH1 glioma in *e.g.,* TCA cycle anaplerosis and the decreased expression levels and activity of BCAT1. All 20 proteogenic amino acids and several related intermediates of amino acid metabolism have been measured in wtIDH1 and mutIDH1 glioma cell lines [reviewed in 1]. However, there was little consensus in reported amino acid abundance differences between wtIDH1 and mutIDH1 glioma cell lines and additional insights into amino acid metabolism remains limited [reviewed in 1].

Glutamate and 2-OG are closely linked in amino acid metabolism. The first step of catabolising most other amino acids is to transfer an amine group to 2-OG and form glutamate. Glutamate can also be oxidised 'back' to 2-OG by GLUD [reviewed in 384]. GLUD is expressed at significantly higher levels in mutIDH1^{R132H} than wtIDH1 glioma [183, 192, 193, 201, 202]. The increased expression indicates increased breakdown of glutamate to 2-OG in mutIDH1^{R132H} compared to wtIDH1 glioma cells. The increased utilisation of glutamate to form 2-OG, which can then be reduced to 2-HG, is supported by the dual tracer experiments with ^{13}C labelled glucose and glutamine shown in **section 3.6**. Glutamine carbon atoms were incorporated into 2-HG to a much greater extent than glucose carbon atoms, which has also been reported in the literature previously [165, 208, 370]. Despite its central role in 2-HG production, glutamate was not significantly decreased in mutIDH1^{R132H} compared to wtIDH1 LN18 cells. In the literature, glutamate was reported as significantly lower in mutIDH1 than wtIDH1 glioma cell lines, PDX mouse models and PTBs [142, 144, 158, 174, 175, 181, 183, 184]. However, the pool of available glutamate is relatively large for the LN18 cells, as the media was supplemented with 2 mM GM™ which meant the cells were not restricted in glutamine supply. Thus, despite not having the expected decrease in cellular glutamate levels, the mutIDH1^{R132H} LN18 cell line

biosynthesised 2-HG with the expected carbon source (glutamate via glutamine) and behaved similarly to other glioma models in this regard.

Glutamate is linked to the metabolic pathways of amino acids such as arginine, proline and aspartate. From the UPA, arginine & proline and aspartate & asparagine metabolism, as well as the urea cycle, were predicted to be significantly different between wtIDH1 and mutIDH1^{R132H} LN18 cells. The pathways and their interconnectivity are illustrated in **Figure 3.8.1**. The only significantly and substantially altered identified metabolites from those pathways were putrescine, 4-hydroxyproline and asparagine denoted with * in **Figure 3.8.1**. All three had higher abundance in mutIDH1^{R132H} than wtIDH1 LN18 cells. Putrescine can be further metabolised to either GABA or to spermine, neither of which can be used to replenish glutamate levels, see area II in **Figure 3.8.1**. The increase in putrescine over other intermediates in arginine metabolism may indicate that arginine is not a source for glutamate replenishment. Arginine metabolism and how it may be affected by *IDH1* mutations in glioma or other cancers has not been explored to a great extent in the literature.

Proline can be metabolised to glutamate, but not via 4-hydroxyproline, as shown in area I in **Figure 3.8.1.** Instead, 4-hydroxyproline is produced during post-translational modification of proline in pre-collagen [reviewed in 357]. As noted in the results section, increased production of 4-hydroxyproline would be counterintuitive due the inhibitory effects of 2-HG on collagen maturation [358]. However, the breakdown of 4-hydroxyproline does require 2-OG and it is more likely that catabolism is limited by either limited 2-OG or inhibition by 2-HG (indicated by a red 4-pointed star in **Figure 8.3.1**). The exact metabolic fate of 4-hydroxyproline has not been studied in detail in the context of mutIDH1 glioma. Yet it originates from matured collagen and collagen maturation is likely affected by high 2-HG levels, indicating that the LN18 model is potentially capturing that effect to some extent.

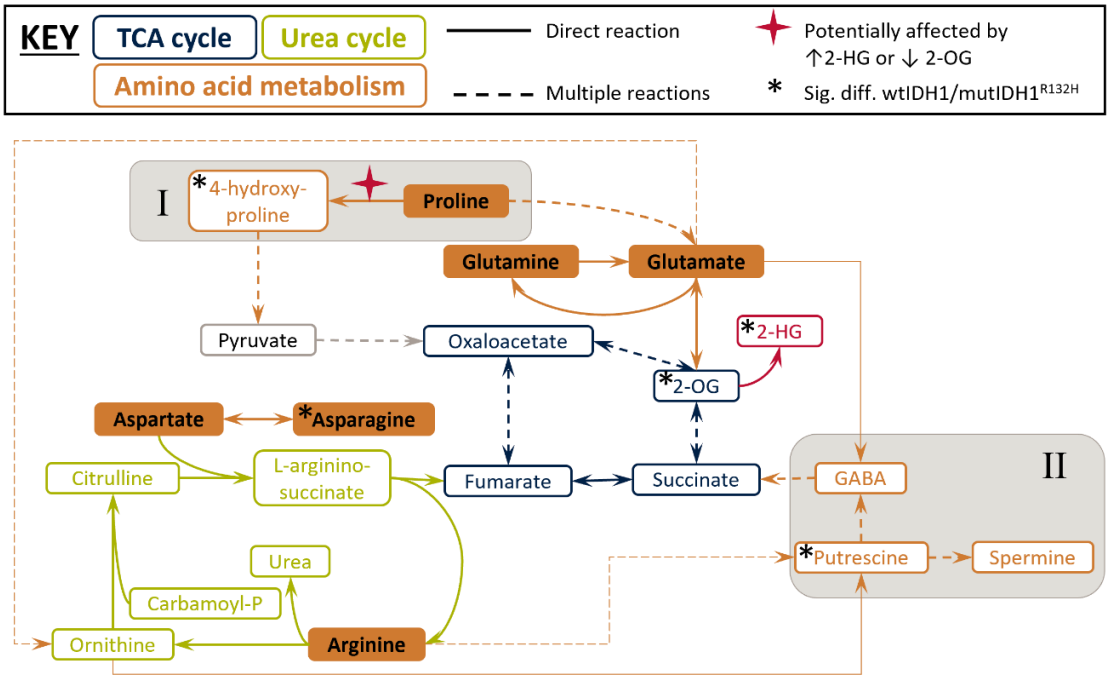

Figure 3.8.1. Metabolic pathways of aspartate, asparagine, arginine, proline and glutamate and the urea cycle in *H. sapiens.* Adapted from KEGG [385]. The amino acids are in orange filled boxes. Colour coding: orange = amino acid metabolism, red = TCA cycle and green = urea cycle. Grey regions I and II were placed to highlight that 4-hdyroxyproline and putrescine are not metabolic intermediates to glutamate from proline and arginine, respectively. The * denoted metabolites that were significantly and appreciable different between wtIDH1 and mutIDH1^{R132H} LN18 cells (p-value < 0.05, Tukey's test and FC > 1.20). Reactions with a red 4-pointed star denoted reactions speculated to be inhibited by 2-HG or affected by decreased 2-OG abundance. Abbreviations: 2-HG = 2-hydroxyglutarate, 2-OG = 2-oxoglutarate; GABA = γ-aminobutyric acid; sig. diff = significant difference.

BCAAs (valine, leucine and isoleucine) and their catabolism has been discussed in the literature previously in relation to metabolic effects in mutIDH1 cells. It has been shown by others that expression of BCAT1, which catalyses the first step of BCAA catabolism (transamination), was significantly lower in mutIDH1^{R132H} glioma PTB and PDX, compared to wtIDH1 glioma samples [183, 192, 204]. It has been found that 2-HG is able to directly inhibit BCAT1 at millimolar concentrations [173], although there are contradicting reports [204]. BCAA transamination would be counterproductive to replenishing 2-OG via glutamate. Thus, the accumulation of isoleucine in mutIDH1^{R132H} LN18 cells and decrease in the resulting ketoacid, 3M2OV, is sensible and in agreement with previous reports in the literature.

Three metabolites in the lysine degradation pathway were significantly depleted in abundance in mutIDH1^{R132H} cells: 2-aminoadipate, oxoadipate and pipecolate. The lysine degradation pathway was significantly different between wild type and mutant cells in the

UPA. The degradation pathway for lysine relies on 2-OG for the first step of transamination of lysine to saccharopine and for a second transamination of 2-aminoadipate to oxoadipate. The pathway is summarised in **Figure 3.8.2**, with 2-OG included where the reactions require it as a substrate. There have been few reports on lysine degradation in the literature, but 2-aminoadipate was also found as significantly depleted in mutIDH1^{R132H} expressing HOG cells compared to HOG cells with empty vector [175].

Potentially, the lower levels of 2-aminoadipate and oxoadipate are due to lower levels of 2-OG, or because 2-HG is inhibiting the enzymes reliant on 2-OG. Other 2-OG dependent enzymes can be inhibited by 2-HG when present at high enough concentrations (mM), which can be achieved in mutIDH1 expressing cells [84, 386]. The relevant reactions where this was speculated to take place are denoted with a 4-pointed red star in **Figure 3.8.2**. The decrease in pipecolate abundance is more unclear. The loss of the α-amine in lysine is via oxidation rather than transamination, thus formation of pipecolate is not dependent on 2-OG. Further experiments examining the expression levels of the enzymes or the biochemical properties of the enzymes is warranted. Specifically, which branch of the lysine degradation is most active in the LN18 cells and are the activities of any of the enzymes affected by 2-HG?

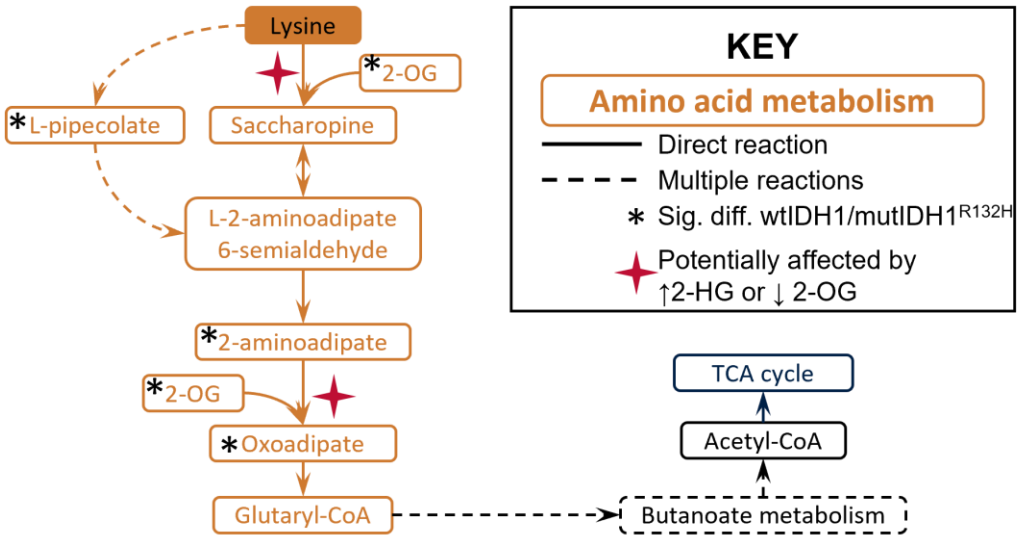

Figure 3.8.2. Lysine degradation pathway in *H. sapiens.* Adapted from KEGG [385]. Amino acids and related metabolites are shown in orange. Black denoted butanoate metabolism, which is how glutaryl-CoA is further metabolised to acetyl-CoA before entering the TCA cycle (blue). The * denoted metabolites that were significantly and appreciable different between wtIDH1 and mutIDH1^{R132H} LN18 cells (p-value < 0.05, Tukey's test and FC > 1.20). Reactions with a red 4-pointed star were speculated to be inhibited by 2-HG or affected by decreased 2-OG abundance. Abbreviations: 2-HG = 2-hydroxyglutarate, 2-OG = 2-oxoglutarate; sig. diff = significant difference.

Methionine and NAM were slightly, but significantly, elevated in mutIDH1^{R132H} cells, but the cysteine and methionine pathways did not quite reach significant in the UPA (EASE score adjusted p-value = 0.0929). The relevant portion of the pathway is illustrated in **Figure 3.8.3**. Methionine was reported as unchanged in PTBs [142], significantly increased in mutIDH1^{R132H} HOG cells, while NAM was reported as depleted in the same HOG cell line [175]. A connection between NAM and mutIDH1 glioma has not been reported on in the literature. However, methionine is needed for the biosynthesis of L-homocysteine, which combines with serine to form cystathionine. Serine was also significantly, but only slightly, elevated in mutIDH1^{R132H} LN18 cells (FC = 1.17, p-value < 0.05, Tukey's test). Cysteine is used for glutathione synthesis and can be sourced from cystathionine, shown in **Figure 3.8.3**. MutIDH1 astrocytoma cells show critical reliance on the CSE enzyme [141].

The accumulation of methionine and serine could be indicative of decreased cystathionine synthesis, but that would not explain the concomitant accumulation of cysteine. Additionally, U251 glioma cells expressing mutIDH1^{R132H} were shown to increase the expression of glutathione synthesis related enzymes [225]. Thus, it would be expected that cysteine levels would decrease in mutIDH1 cells relative to wtIDH1 cells, as the cysteine would be used for increased glutathione biosynthesis. Glutathione was not significantly different between wtIDH1 and mutIDH1^{R132H} LN18 cells. However, reduced and oxidised glutathione cannot be confidently measured with the current sample preparation, as it is not optimised towards maintaining the two pools of metabolites. The LN18 cell line may be an appropriate model to study this section of amino acid and glutathione metabolism, as clearly several different components are significantly altered in the pathway compared to wtIDH1 cells. Further work must be done to ensure more confident measurement of oxidised/reduced glutathione levels and therefore be able to more thoroughly understand the processes occurring in the cells. Measurement of expression levels of relevant enzymes could indicate whether the pathway was significantly upregulated upon introduction of mutIDH1^{R132H} into the cells.

An additional metabolite related to this area of cellular metabolism is *O*-phosphoserine. It was significantly depleted in mutIDH1^{R132H} compared to wtIDH1 LN18 cells (FC = 2.45, p-value < 0.0001, Tukey's test). It can be produced by the reversible transamination of 3PHP using glutamate, see **Figure 3.8.3**. If the transamination of *O*-phosphoserine to 3PHP

was decreased due to either decreased availability of 2-OG or direct inhibition from elevated 2-HG, the expectation would have been an accumulation of *O*-phosphoserine in mutIDH1^{R132H} LN18 cells. However, since *O*-phosphoserine decreased in mutant cells it was more likely that either the dephosphorylation to serine was increased or that transamination of 3HPH was decreased. 3PHP can be biosynthesised from 3-phospho-D-glycerate, which is a glycolysis intermediate. WtIDH1 glioma is considered more glycolytic than mutIDH1 glioma [reviewed in 1]. It may simply be that there was less of the glycolysis intermediate available to utilise for *O*-phosphoserine biosynthesis and that is why the differences were observed. Furthermore, 3-phospho-D-glycerate can also be produced via phosphorylation of glycerate followed by isomerisation. Glycerate abundance was significantly higher in wtIDH1 cells (FC = 1.28 (WT/MUT) and p-value < 0.01, Tukey's test). Potentially mutIDH1^{R132H} cells were utilising glycerate to a greater extent than wtIDH1 cells for biosynthesis of serine via *O*-phosphoserine. Thus, whether the decrease of *O*-phosphoserine abundance in mutIDH1^{R132H} LN18 cells was due to direct inhibition by 2-HG or indirect consequences due to other metabolic differences between wtIDH1 and mutIDH1^{R132H} LN18 cells remains unclear.

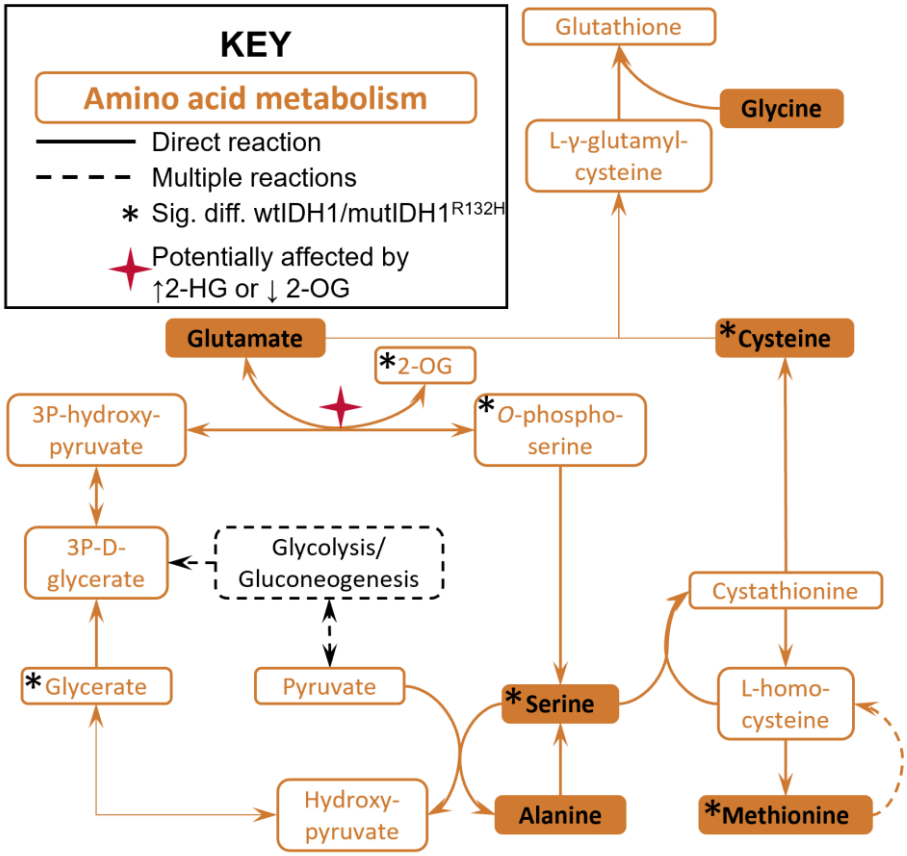

Figure 3.8.3. Interconnectivity of serine, cysteine and methionine metabolism. Adapted from KEGG [385]. The reactions show here are not exhaustive lists of the reactions the metabolites can partake in. Star denotes a transaminase reaction using 2-OG/glutamate. Amino acids and related metabolites are shown in orange. Black denoted glycolysis/gluconeogenesis. The * denoted metabolites that were significantly and appreciable different between wtIDH1 and mutIDH1^{R132H} LN18 cells (p-value < 0.05, Tukey's test and FC > 1.20). Reactions with a red 4-pointed star were speculated to be inhibited by 2-HG or affected by decreased 2-OG abundance. Abbreviations: 2-HG = 2-hydroxyglutarate, 2-OG = 2-oxoglutarate; sig. diff = significant difference.

3.8.3. Significantly altered nucleotide abundances indicated by univariate and multivariate statistical analysis

Nucleotides dADP and UMP, as well as DR5P and pyrimidine related metabolites *N*-carbamoyl-aspartate and B-alanine, were significantly increased in mutIDH1^{R132H} compared wtIDH1 LN18 cells. Other purines and pyrimidines were measured by the IC-MS method, but were not significantly different between mutIDH1^{R132H} and wtIDH1 LN18 cells. Nucleotide metabolism has been an area of interest in both mutIDH1 glioma and wtIDH1 glioblastoma studies. Glioma cell lines expressing mutIDH1 endogenously have been shown to use both *de novo* and salvage pathways for nucleotides, while wtIDH1 glioma cell lines have been shown to rely on *de novo* synthesis to a greater extent [137]. However, a different study, that also used a glioma cell with endogenous mutIDH1^{R132H} expression,

reported that the cells predominantly relied on *de novo* synthesis of pyrimidines and salvage pathways for purines [387]. Furthermore, both patient-derived mutIDH1 glioma cell lines and genetically engineered mutIDH1 glioma mouse models were more sensitive to pyrimidine synthesis inhibition than wtIDH1 glioma [387].

The work in this thesis was limited in scope with regards to a detailed analysis of the implications of increased purine and pyrimidine metabolites in mutIDH1^{R132H} LN18 cells based on the small number of metabolites identified as significantly altered. In addition, isogenic cell lines respond differently to *e.g.* radiation-induced DNA damage than when patient-derived endogenous mutIDH1 glioma cell lines are compared to wtIDH1 glioma cell lines, indicating a model-dependent response [137]. However, the presence of DR5P and the fact that the enzyme DERA is activated by polycarboxylic acids such as citric acid and 2-OG, merits further study.

3.8.4. Changes in lipid metabolism related to isoprenoid precursors synthesis and amino acid degradation

Lipid metabolism involves both the biosynthesis and catabolism of fatty acids, as well as biosynthesising plasma membrane components such as phospholipids, triglycerides, and cholesterol and its derivatives [388]. The LN18 model was not analysed with methods developed for lipid metabolite measurements. It is not possible to comment on how well it recapitulates *e.g.,* changes in phospholipid profiles or detailed analysis of cholesterol metabolism, which have received the most attention to date in mutIDH1 glioma lipid metabolism [reviewed in 1]. However, two metabolites related to lipid metabolism were observed in the univariate analysis, glycerate and IPP. The most likely role glycerate plays is in relation to *O*-phosphoserine metabolism. The isoprenoid precursor IPP is likely related to cholesterol metabolism, as noted in the **section 3.4**. Expression of *de novo* cholesterol metabolism enzymes has been reported as increased in mutIDH1^{R132H} expressing GBM cell lines (U87 and U251). However, as noted, the analysis here is limited due to lack of measurement of other intermediates and cholesterol itself. The LN18 cell lines may be an appropriate model to study the impact of mutIDH1 on lipid metabolism in glioma, but it would require other analytical methods more suited for lipid analysis to determine that suitability.

In addition to the metabolites described above, the butanoate and propanoate pathways involved in the metabolism of short chain fatty acids (SCFAs) acetate, propionate and butyrate were found in the functional analysis. In the human body, SCFAs are usually supplied by the gut microbiome via fermentation of dietary fibres [389]. Glioblastoma patients and mouse models showed changes in the caecal and faecal metabolome, indicating potential effects on the gut-brain axis due to the cancer [390, 391]. The cells used in this experiment were not co-cultured with bacteria, therefore changes in butanoate and propanoate metabolism can only be considered within the context of mutIDH1^{R132H} expression and increased 2-HG levels. The specific metabolites proposed by the untargeted analysis for the two pathways are summarised in **Figure 3.8.4**. Most of the proposed metabolite identities from the two pathways overlap, therefore the pathways are reported together.

Several of the metabolites in the two pathways arise from BCAA and lysine catabolism: propionyl-CoA, crotonoyl-CoA, (*S*)-3-hydroxy-methylglutaryl-CoA, methyl malonate and (S)-3-hydroxy-isobutyric acid. The lysine and BCAA degradation pathways were also found to be significantly altered in the UPA, and individual metabolites in the pathways were significantly decreased in mutIDH1^{R132H} LN18 cells. Additionally, the GABA shunt is considered a part of butanoate metabolism in the KEGG pathway, which has previously been reported as upregulated in mutIDH1^{R132H} glioma tissue [183]. Thus, the appearance of the butanoate and propanoate pathways in the UPA could be due to the inclusion of 'end stage' metabolites emerging from the amino acid degradation pathways. The final steps of the catabolism of these metabolites coincide with what is considered the butanoate and propanoate pathways in human metabolism.

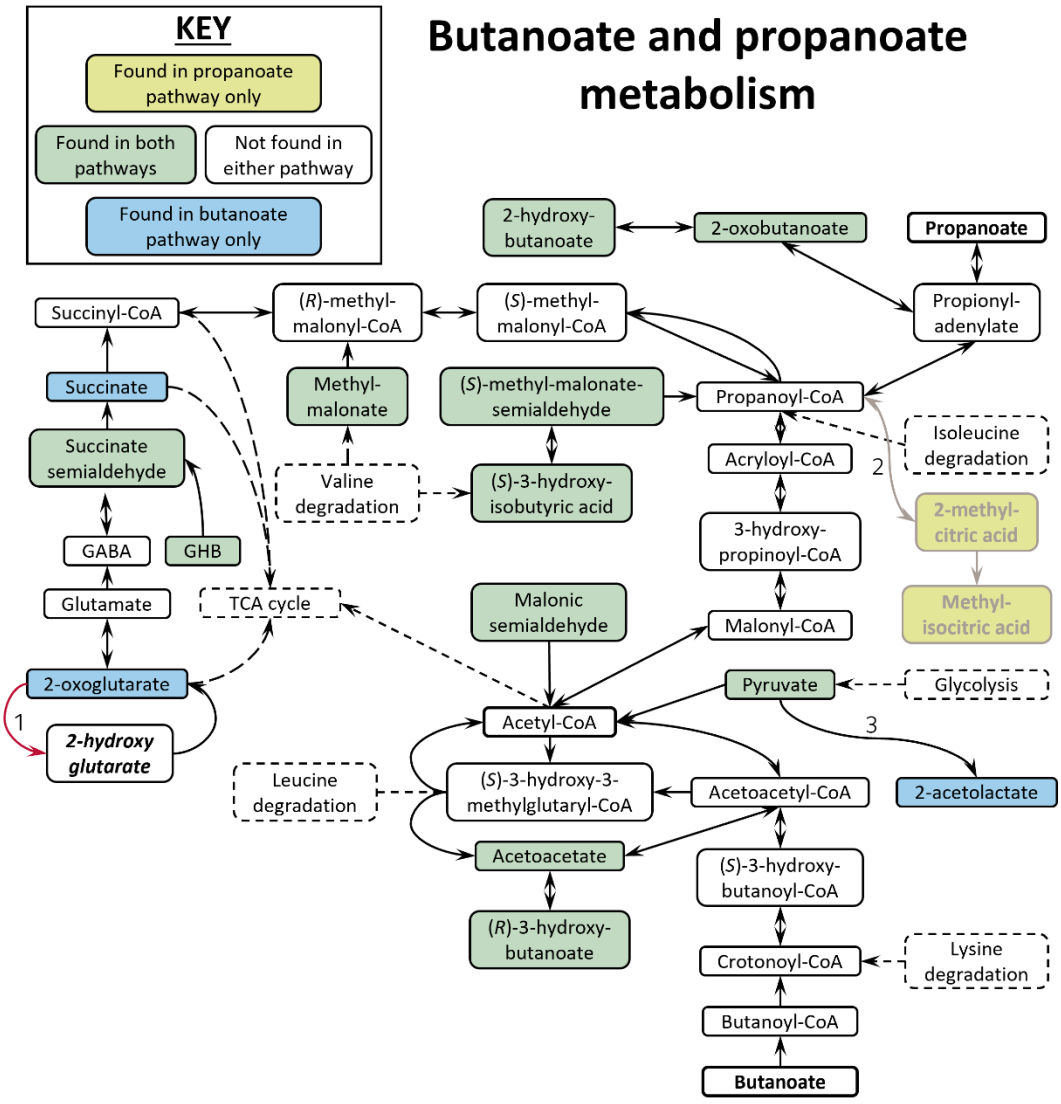

Figure 3.8.4. The butanoate and propanoate pathway in *H. sapiens*. Adapted from KEGG [385]. The metabolites proposed by the UPA are highlighted based on if they only appear in the butanoate pathway analysis results (blue), only in the propanoate pathway analysis result (yellow) or both (green). (1) Only the 2-HG dehydrogenase reaction is included in the KEGG butanoate pathway, but the mutIDH1 reaction is included here for clarity. (2) The synthesis of 2-methylcitric acid from propionyl-CoA, and the conversion of 2-methylcitrate to methylisocitrate, are not catalysed by enzymes expressed in humans according to the KEGG database, but the compounds are found in humans [392, 393]. The reactions are included for clarity. (3) The reaction is not shown as occurring in human cells, but a gene encoding for a protein that is highly similar to bacterial acetolactate synthase is reported as expressed in human tissues, including brain [394].

3.8.5. Vitamin B1 and Vitamin C metabolism

Vitamin B1 is not an endogenous metabolite, but the cells were supplemented with 0.012 mM thiamine hydrochloride in the media. Thiamine pyrophosphate, the active form of vitamin B1, is a co-factor for a number of enzymes including pyruvate dehydrogenase, 2-OG dehydrogenase, transketolases in the pentose phosphate pathway, and branched-chain keto-acid dehydrogenase [395]. However, the UPA did not suggest

thiamine pyrophosphate, nor any other thiamine forms, as potential metabolite annotations. Instead oxoadipate, pyruvic acid, malonic semialdehyde and 2-OG were suggested, indicating that perhaps this pathway was highlighted instead due to role of thiamine pyrophosphate as a co-factor in reactions with these metabolites [395, 396]. The IC-MS method is suited for the analysis of phosphate-containing metabolites and it would be worth pursuing analysis of thiamine and thiamine phosphate standards to expand on the coverage of this pathway.

The ascorbate (vitamin C) and aldarate pathway had a number of potentially identified metabolites that were sensible to expect from IC-MS analysis as they are produced or used by enzymes present in humans and carboxylic acids that the method could detect (*e.g.,* gluconate/gulonate, gluconolactone/gulonolactone and ascorbate). Gluconate, gulonolactone and ascorbate were found in the samples with in-house standards as well, although not significantly altered. Ascorbate has previously been reported as not significantly different between wtIDH1 and mutIDH1^{R132H} glioma PTBs [397]. *Myo*-inositol was also a putatively identified metabolite in the UPA that had been identified with the in-house database. It was not significantly different between wtIDH1 and mutIDH1^{R132H} LN18 cell samples. However, *myo*-inositol was in the top 15 metabolites by VIP score in the PLS-DA. It is a highly abundant metabolite in the human brain and an osmolyte [398], and is considered a part of ascorbate and aldarate metabolism where it is oxygenated to form D-glucuronate. Vitamin B1 and vitamin C metabolism have not been thoroughly investigated within the context of mutIDH1 glioma. Ascorbate is a cofactor for enzymes that are have previously been studied in relation to 2-HG and mutIDH1, *e.g.,* in collagen maturation [358, 399], thus further study is merited.

3.8.6. *N*-acetylaspartylglutamate and B-citryl-L-glutamate

NAAG and B-CG are biosynthesised and catabolised by homologous enzymes [360-363] (see **Figure 3.8.5** for chemical structure and overview of reactions). Both NAAG and B-CG were significantly lower in abundance in mutIDH1^{R132H} than wtIDH1 LN18 cells (FC_{NAAG} = 1.92 and $FC_{B\text{-}CG}$ = 1.77 (WT/MUT), Tukey's test p-value < 0.0001). There has only been one other report of B-CG levels in mutIDH1 glioma to date, in the first generation LN18 wtIDH1 and mutIDH1^{R132H} cell lines. There FC_{NAAG} > 3 and $FC_{B\text{-}CG}$ > 4 ((WT/MUT), both

FDR adjusted p-value < 0.0001) [148]. The higher FC for the first generation compared to the FC reported here might be due to the cells being grown in DMEM with different glucose concentrations (4.5 g/L versus 1.0 g/L). Or, if the degree that NAAG and B-CG suppression in mutIDH1^{R132H} cells was related to 2-HG levels, that could also explain the difference as the first generation LN18 mutIDH1^{R132H} cells had higher 2-HG levels (FC_{1st} > 100 versus FC_{2nd} > 50 (MUT/WT)). The relationship between 2-HG levels and NAAG/B-CG will be explored further in **chapter 4**.

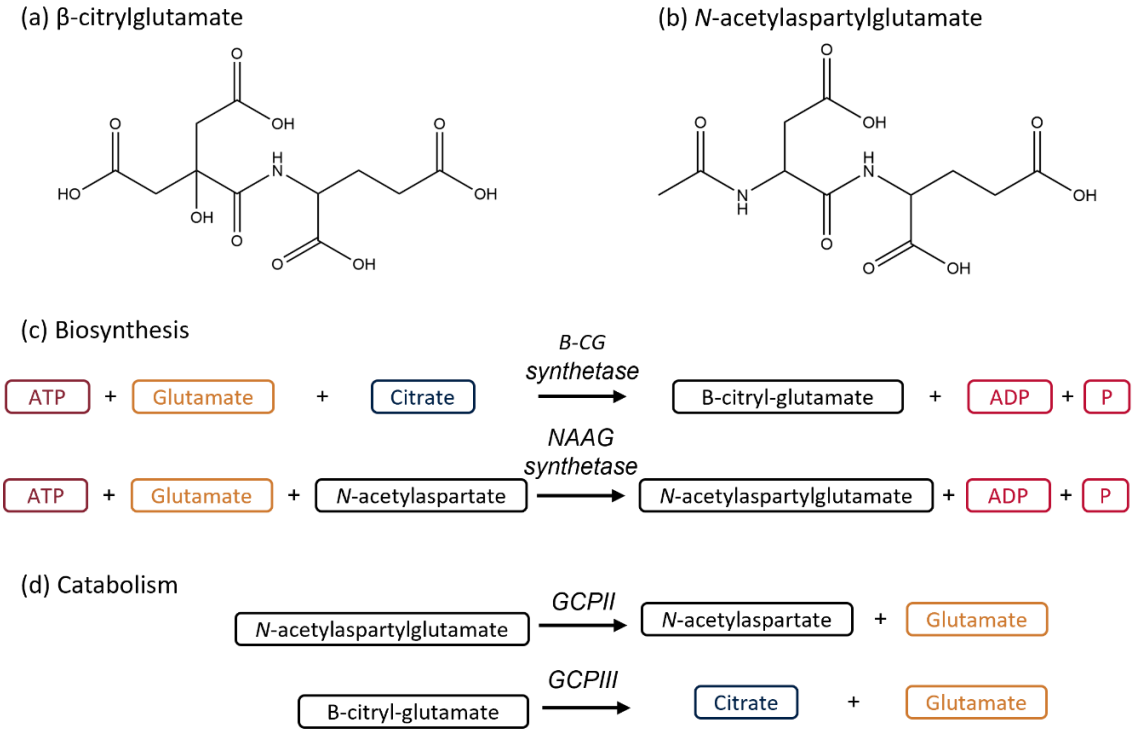

Figure 3.8.5. Overview of B-CG and NAAG metabolism. (a) Chemical structure of B-CG. (b) Chemical structure of NAAG. (c) Biosynthetic reactions of B-CG and NAAG, which are catalysed by homologous enzymes [360]. (d) Catabolic reactions of B-CG and NAAG, which are catalysed by homologous glutamate carboxy peptidase (GCP) II and III [361-363]. Structures in (a-b) made with ChemDraw 20.1.

NAAG has also been reported as significantly and substantially lower (FC = 50 (WT/MUT)) in HOG cells expressing mutIDH1^{R132H} than non-transduced cells [175], but there was no significant difference when comparing wtIDH1 to mutIDH1 PDX mouse models [158]. NAAG has also been suggested as a glutamate reservoir in cancer cells [400] and it would be sensible for mutIDH1^{R132H} cells to utilise it as a source of glutamate either for 2-HG biosynthesis or to compensate for biosynthesis. The functional role(s) of B-CG remain unclear, but it may act as a glutamate reservoir similar to NAAG. B-CG has also been shown to chelate with Fe(II), Fe(III), Cu(II) and Zn(II) [401] and it activates aconitase when in a

[Fe(II)(B-CG)] complex [402]. The [Cu(II)(B-CG)] complex is capable of inhibiting xanthine oxidase (XO) activity, similar to glutathione [403]. XO takes part in purine catabolism by breaking down hypoxanthine to xanthine and then uric acid [388], in which the electrons are transferred to molecular oxygen and hydrogen peroxide is formed [404]. Thus B-CG, when in complex with Cu(II), could have a redox protective role in cells by decreasing XO activity and the production of hydrogen peroxide. The decrease in B-CG levels in mutIDH1^{R132H} might thus result in cells that are more vulnerable to redox mediated damage.

3.8.7. Measuring redox metabolites NAD$^+$, NADH, NADP$^+$ and NADPH

The importance of measuring redox metabolites led to significant effort being put into method development for the measurement of the four redox metabolites NAD, NADH, NADP$^+$ and NADPH. The use of HILIC-MS was based on the possibility of expanding the method to include other redox related metabolites in the future, *e.g.,* oxidised and reduced glutathione. Additionally, sample preparation was similar to the standard metabolomics method, allowing for confident normalisation of samples. Colorimetric assays require simple instrumentation, but often involve several preparation steps and generally do not have robust sample normalisation included in protocols. In addition, to measure the redox metabolites independently and not just as ratios, one assay per metabolite commonly has to be performed. Finally, it would not be possible to as easily expand upon the number of analytes as in *e.g.,* LC-MS or NMR based applications. NMR was a potential option, but due to the lack of temperature control available on the highest field NMR instrument, it was considered less appropriate due to the sensitivity toward interconversion and degradation of the compounds. Finally, ion-pairing RPLC-MS has been used for measuring redox metabolites [310, 322], and would also allow for the measurement of other compounds. However, the ion-pairing agents typically used are known for causing high background signals on MS instruments. Thus, HILIC-MS balanced practical (*i.e.,* temperature, instrument availability) and technical (*i.e.,* sample preparation, expanding the method) considerations.

Three different HILIC columns were tested and NAD$^+$ and NADH were possible to measure on all with desirable peak shapes (peak width at base < 2.0 min and without substantial

asymmetry). $NADP^+$ and NADPH proved considerably more challenging, with substantial tailing and resulting low peak height. Efforts to minimise tailing and improve sensitivity involved testing different column chemistries and adjusting the buffer salt, buffer concentration and pH. The tailing remained for $NADP^+$ and NADPH, but did not prohibit quantification of the two metabolites in cellular samples.

Phosphate groups are known for interacting with metal components in LC-MS systems, which can contribute to peak broadening [405, 406]. Similarly, silica-based ZIC HILIC has been reported as a challenging system to analyse phosphorylated metabolites (*e.g.* nucleotides) [407]. Several different strategies can be employed to improve peak shape, including increasing mobile phase pH [406], lining metal surfaces with a barrier to reduce interactions [405], or swapping to an organic polymer based stationary phase [407]. The first option was tried without success, as demonstrated in **section 3.7**. Peak shape did not change appreciable depending on the mobile phase pH. Lining metal surfaces with a barrier is an option, but care must be taken to not add something that might disrupt other analyses also carried out on the same systems. Finally, for future work, an organic polymer based HILIC column appears to be the best option to try first. It was not carried out in this project due to time constraints.

The final method used provided acceptable linearity ($R^2 > 0.97$) for $NADP^+$ and NADPH standards in the tested concentration range (0.05-1.00 µM). Broader concentration ranges should be tested in future work, as the cellular concentration of $NADP^+$ was at the limit of the calibration curve. The limit of detection was 0.05 µM, but lower standards should be tested as well. However, considering the low peak height and tailing observed for $NADP^+$ and NADPH, it is unlikely that the limit of detection can be much lower without the peak shape improving. Finally, the reproducibility of the method was poor for NADH, $NADP^+$ and NADPH with regards to biological samples with peak areas varying 19-99%. The poor reproducibility is considered mostly due to the biological samples, as the standards had lower peak area variability (2-15%). Overall, the redox metabolites remained a challenge to measure with confidence and further work assessing sample stability must be carried out to improve method repeatability. Without reproducible methods the confidence in the quantification of the redox metabolites would remain low, limiting in-depth investigation of redox metabolism.

3.8.8. $NADP^+$, NADPH and $NADPH/NADP^+$ were not significantly different between wtIDH1 and $mutIDH1^{R132H}$ LN18 cells

After the method development had been carried out, the ZIC sulfobetaine column with the optimised chromatographic and MS settings was used to analyse the abundance of the four redox metabolites in wtIDH1 and $mutIDH1^{R132H}$ LN18 cell samples. No significant difference in $NADP^+$ or NADPH concentrations between wtIDH1 and $mutIDH1^{R132H}$ cells were identified (p-value = (p-value = 0.0731 and 0.954, respectively. Unpaired parametric t-test), nor in the $NADPH/NADP^+$ ratios (p-value = 0.1105, unpaired parametric t-test). Previously, the $NADPH/NADP^+$ ratio has been reported as significantly decreased in astrocytes and colorectal cancer cells (HCT116) expressing $mutIDH1^{R132H}$ via lentiviral vector when compared to wtIDH cells with a colorimetric assay [221]. Similarly, NADPH levels and the $NADPH/(NADP^+ + NADPH)$ ratios were lower in glioblastoma and astrocyte cells expressing $mutIDH1^{R132H}$ via lentiviral vector compared to wtIDH1 cells (empty vector), also measured by colorimetric assay [220].

The cells in the referenced articles were grown in a variety of media (Basal Minimum Eagle, DMEM, minimum essential media (alpha modification) [220], McCoy 5A modified media and astrocyte media [221]) with different glucose concentrations. A major contributor to cellular NADPH is the oxPPP [213, 214] and high levels of available glucose would allow for more flux through the oxPPP. Potentially the glucose levels can affect the extent of differences in redox homeostasis between wtIDH1 and mutIDH1 expressing cells, although the assumption would be that lower glucose levels would exacerbate any difference and not decrease it. The more likely explanation for the lack of difference in the concentrations and ratios reported here is due to experimental variability. The measurements reported in this thesis were quite variable and that could be masking small, but significant differences in redox metabolism between the wtIDH1 and $mutIDH1^{R132H}$ LN18 cells. A major issue, in addition to peak shape, was peak area stability. Even with the most optimised LC-MS method and repeat analysis of the same standard sample, peak area variability was 2.1-14.7% CV. The variability was even more severe for cell samples (18.1-43.1% CV for $NADP^+$ and NADPH, up to 98.8% for NADH). It is likely that both analytical variability and harvesting, processing and sample storage all had a role in the overall outcome.

3.9. Summary and conclusions

The mutIDH1^{R132H} LN18 cell line had substantial and significant accumulation of 2-HG and a significant decrease in 2-OG abundance when compared to wtIDH1 LN18 cells. Glutamine, rather than glucose, was the major carbon source for 2-HG. The presence and activity of the mutIDH1^{R132H} enzyme in LN18 cells led to a number metabolic differences compared to the otherwise isogenic wtIDH1 LN18 cells. In amino acid metabolism, there were a number of individually altered metabolites, and differences on the pathway level, between wtIDH1 and mutIDH1^{R132H} LN18 cells. That included lysine degradation, BCAA degradation, aspartate & asparagine and arginine & proline metabolism, as well as cysteine, serine, methionine and related metabolites. The different pathways and metabolites were closely linked to 2-OG because it is the most common acceptor of an amine group during transamination reactions, which are ubiquitous in amino acid metabolism. Decreased transamination due to either decreased availability of 2-OG or direct inhibition by 2-HG were considered likely explanations for the differences observed between wtIDH1 and mutIDH1^{R132H} LN18 cells. Further work will be carried out to investigate a potential correlation to 2-OG and/or 2-HG for the aforementioned metabolites and pathways.

The metabolites NAAG and B-CG, related by biosynthesis and degradation by homologous enzymes, were both significantly decreased in mutIDH1^{R132H} LN18 cells. The metabolites were not directly associated to 2-OG or NADP+/NADPH, thus their role in mutIDH1^{R132H} LN18 metabolism remained poorly understood. It was only possible to speculate on why the metabolites were decreased in mutIDH1^{R132H} LN18 cells. A better understanding of the relationship between NAAG and B-CG abundance to 2-HG abundance/mutIDH1^{R132H} activity could help point toward a potential mechanism behind the difference between wtIDH1 and mutIDH1^{R132H} glioma.

Nucleotide metabolism was another major avenue explored with regards to mutIDH1 glioma in the literature, and the LN18 model pointed toward an effect being present there too. However, because the model is isogenic and previous work had shown that there are differences between endogenous and isogenic cell lines, care should be taken during interpretation of changes in nucleotide metabolism. Nucleotide metabolism would be an ideal therapeutic target, as cancer cells divide rapidly and require nucleotides for growth.

Despite the limitations of the current isogenic cell model, it will be of interest to examine whether nucleotide metabolites are affected by decreased mutIDH1^{R132H} activity and 2-HG abundance.

Chapter 4. The effect of mutIDH1 inhibitors on wtIDH1 and mutIDH1^{R132H} in glioblastoma cells

4.1. Introduction

Mutation of *IDH1* occurs early in the development of cancers with solid tumours [12, 80] and elevated 2-HG is thought to contribute to tumorigenesis [reviewed in 408], *e.g.,* by inhibiting 2-OG dependent enzymes needed for DNA and histone methylation [27, 83, 84, 409] and disrupting DNA repair [410-412]. MutIDH1 activity and elevated 2-HG levels have also been linked to changes in central carbon, amino acid and lipid metabolism, as well as redox homeostasis [reviewed in 1]. However, the significance and role of these metabolic changes in tumorigenesis remains less well understood.

The mutIDH1 enzyme is considered an ideal target in mutIDH1 cancers, due to its presumed role in tumorigenesis and absence in non-cancer cells. Multiple small-molecule allosteric inhibitors of mutIDH1 have been developed and reported in the literature [176, 246, 247, 249, 250, 413-418]. Two of these mutIDH1 inhibitors have been approved by the FDA for AML [419, 420], and one for cholangiocarcinoma [421]. There are no mutIDH1 inhibitors approved for glioma at this time. The inhibitors have been shown to reduce 2-HG abundance in glioma, AML and chondrosarcoma cell lines and xenograft mouse models, as well as glioma and AML and patients [174, 176, 177, 226, 251-259, 261]. However, in cancers with solid tumours, such as glioma and chondrosarcoma, the effect of the inhibitors on cell viability [177, 226] and patient survival has been limited [245, 263, 422, 423]. Furthermore, resistance to mutIDH1 and mutIDH2 inhibitors, through a variety of mechanisms, has been reported in case studies of AML patients [264-266, 424-426] and cholangiocarcinoma patients [265, 427]. Considering the lack of comprehensive understanding of the role of 2-HG in tumorigenesis, in addition to limited effect of the inhibitors and developing resistance to these drugs, new approaches, therapies and drug targets are needed.

Generally, in earlier studies only one inhibitor was tested across multiple cell lines. Only three studies comparing two or more inhibitors can be found in the literature [251, 255, 256] so there is little comparative literature on their efficacy and impact on metabolism.

Furthermore, there is no data in the literature on the effect of mutIDH1 inhibitors in the LN18 GBM cell line studied here. Consequently, it was of interest to compare multiple mutIDH1 inhibitors to assess their relative effectiveness in decreasing 2-HG abundance in LN18 cells expressing mutIDH1^{R132H}. Four inhibitors (AG-120, AG-881, BAY 1436032 and GSK864) were chosen based on reported efficacy in enzymatic and cellular assays, as well as efficacy in mouse models [247, 249, 250, 416]. AG-120 was also included because it, at the time, was the only FDA approved mutIDH1 inhibitor [419]. AG-881 is a pan-mutIDH inhibitor, *i.e.,* capable of inhibiting both mutIDH1 and mutIDH2 [249]. It was included because it was shown to be brain-penetrant in orthotopic mouse models of glioma [416].

MutIDH1 inhibitors AG-120, AG-881 and GSK864 have been shown as capable of inhibiting wtIDH1 in enzymatic assays (IC_{50} 4-467 nM) [246, 250, 416]. However, that effect has not been studied in depth in wtIDH1 GBM or glioma cells. Additionally, the *IDH1* mutation is usually heterozygous [reviewed in 428] and active wtIDH1 may be present in mutIDH1 glioma tumours as well. Therefore, it was also pertinent to investigate the effect of the inhibitors on wtIDH1 activity in addition to mutIDH1 in the cellular context.

This chapter focusses on comparing multiple inhibitors to investigate their effect on LN18 cell viability and the abundance of key metabolites 2-HG, 2-OG and isocitrate. These activities are compared across different treatment concentrations and treatment time-points. The aims of the research presented in this chapter are therefore to:

1. Develop and test a miniaturised cell culture, harvesting and sample preparation protocol to enable larger-scale metabolomics experiments for comparing multiple drug treatments at different time and concentration points.
2. Measure mutIDH1 inhibitors in cell and media samples:
    i. Develop a sample preparation method to enable measurement of mutIDH1 inhibitors in media.
    ii. Assess column chemistry and LC-MS parameters for the analysis of mutIDH1 inhibitors.

3. Measure the effect of four different mutIDH1 inhibitors (AG-120, AG-881[2], BAY 1436032 and GSK864) on cell viability of mutIDH1^{R132H} LN18 GBM cells at different treatment concentrations and treatment time-points.
4. Characterise the ability of the four different mutIDH1 inhibitors to decrease 2-HG abundance and modulate 2-OG and isocitrate levels:
    i. In wtIDH1 and mutIDH1^{R132H} LN18 GBM cells.
    ii. In mutIDH1^{R132H} LN18 GBM cells treated with different concentrations of mutIHD1 inhibitor.
    iii. In mutIDH1^{R132H} LN18 GBM cells treated with mutIDH1 inhibitors for different exposure times.

[2] AG-881 is a pan mutIDH1 and mutIDH2 inhibitor, but will be labelled as a mutIDH1 inhibitor for brevity.

4.2. A more efficient tissue culture approach for higher-throughput metabolomics

Metabolomics experiments are usually performed as a single batch process, where possible, to limit systematic errors that can occur due to multiple factors such as variations in cell media and cell growth, as well as drift in retention time and ion counts during analysis by LC-MS. If this is not possible, careful attention needs to be given to ensure multi-batch normalisation. Common QCs are usually used across multiple batches and such experiments can be more challenging. Based on the routine method used so far (described in **section 2.5.5**), the highest number of 60-mm dishes that could be physically harvested in a single batch was 60. The 60 samples would take approximately 5 hours to harvest. Increasing the number of dishes would require certain cells to be harvested with even greater difference in incubation time, and also increase the risk of random error due to fatigue. A method with smaller sample plates, however, would take less time per plate to harvest and enable larger experiments to be performed as a single experiment. The new method developed here was used for up to 120 samples harvested simultaneously.

An initial pilot experiment was used to measure 2-HG levels in each sample of wtIDH1 and mutIDH1^{R132H} cells, and for future experiments to focus on 2-HG before and after treatment with mutIDH1 inhibitors. It was envisaged that a relatively low ratio of cell number to harvest solvent volume could be tolerated due to the high abundance of 2-HG in mutIDH1^{R132H} cells. The previous plating methods used 60- or 100-mm dishes, where the extraction solvent volume was 180 or 500 µL and final sample volume was 100 or 300 µL, respectively. The lower final volume compared to extraction volume was determined by three main factors: it was not possible to transfer all of the sample volume from plate to a microtube, a small volume of sample remained in the MWCO filter (~15 µL), a small volume of sample was used for measurement of DNA concentration (5-10 µL) and to be set aside for a QC sample (2-5 µL). The downscaled method therefore had to provide enough sample to account for these fixed volumes, as well as provide enough sample to inject 3-4 times for LC-MS analysis (30-40 µL). The minimum sample volume that would be sufficient for an experiment was therefore chosen as 70 µL.

The cell seeding density of a 60-mm dish was 100,000 cells/mL, with a total volume of 3 mL leading to a total of 300,000 cells per dish. The cells would approximately double after 48 hours of incubation, which meant that there were 500,000-600,000 cells per dish when samples were harvested. The ratio of cell number to solvent volume at harvest was 2,778-3,333 cells/µL. LN18 cells were cultured as an adherent monolayer, therefore the surface area of a dish or plate dictated how many cells could be cultured. The growth area of a 60-mm dish was 21 cm^2, while 6-well and 12-well plates were 9.5 and 3.8 cm^2, respectively. The 6-well plate would provide cell extracts with higher cell number to solvent volume ratio, as more cells could fit per well. However, the time saved during harvest was significantly improved for 12-well plates, and these were therefore chosen for the pilot study. If the same seeding density of cells were used for 12-well plates as a 60-mm dish, then the final ratio of cell number to solvent volume was projected to be 1,292-1,551 cells/µL.

The harvesting method required adjustments to be made for 12-well plates. All 12 wells on the plate would have to be harvested at the same time, to avoid issues of *e.g.,* cooling of neighbouring wells or cross contamination. The original pouring on/off of PBS was replaced with pipetting to avoid cross-contamination between samples. PBS was left on cells while other wells had media removed, to avoid drying out and to minimise cellular stress. Liquid nitrogen was deemed too difficult to work with such small sample containers, and the risk of splashing between wells was too great. Instead, it was decided to cool the extraction solvent (80% $MeOH_{(aq)}$) on dry ice and place the plate on dry ice during extraction and scraping.

Sample preparation after harvest remained largely the same as the method used for 60-mm dishes, except for when the DNA concentration was measured. After having processed a set of pilot samples and an additional large sample set (120 replicates), it became clear that extraction volume at harvest was too small for the subsequent sample processing. First, the loss at harvest from not being able to transfer all of the extraction solvent from a well to a sample tube was greater than expected. Second, the amount of sample left after DNA measurement and filtration was sometimes too small to allow for both multiple (3-4) analyses of a sample and to remove a small volume for the QC sample.

To ameliorate the volume challenges, the extraction volume was therefore increased to 100 µL for subsequent experiments.

Additionally, the protocol was modified to utilise the sample left in the filter for DNA measurements instead of discarding it as there was sufficient volume left in the filter (15 µL) for multiple DNA measurements. An experiment was carried out to compare DNA concentrations before and after filtration to what was left in the filter. A cell sample was diluted 1+3, 1+1 and 3+1 (v+v). The DNA concentration was measured in unfiltered and filtered samples, as well as of what was left inside the filter. The DNA concentration of the in-filter samples was significantly higher than the before and after filtered samples (p-value < 0.05, one-way ANOVA and Šídák MCTe), bar graph provided in **Figure 4.2.1.(a)**. However, the ratio of the DNA concentrations of diluted/original samples were the same for unfiltered, filtered and 'in-filter' samples (**Figure 4.2.1.(b)**). Because normalisation of samples was performed based on relative DNA concentrations, the increase in DNA concentration was not an issue. The ratios between the different diluted samples would be maintained. Relative dilution of samples would be correct as long as DNA was measured from the same type of sample.

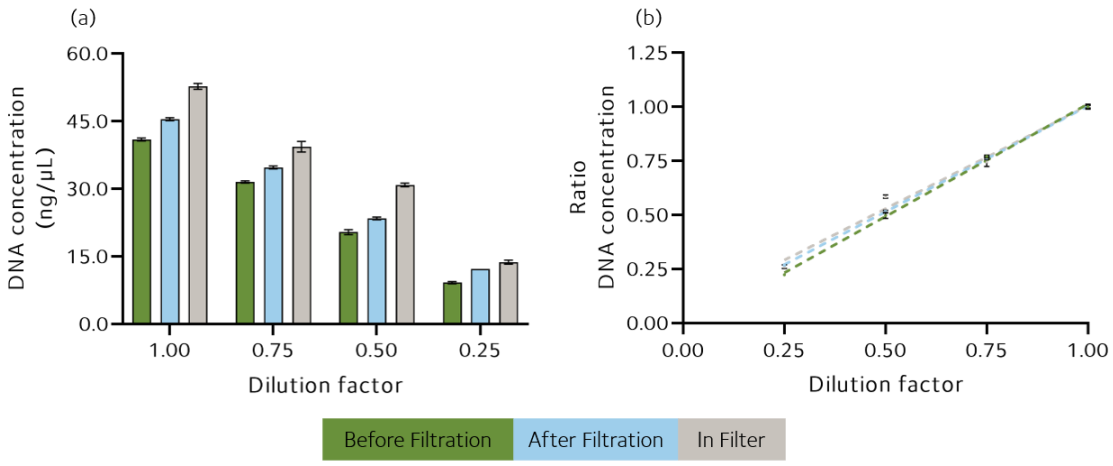

Figure 4.2.1. DNA concentrations of an extracted cell sample before and after filtration and what remained in the MWCO filter. (a) Absolute DNA concentration of the same before and after filtration, and of what remained in the filter. Error bars are one standard deviation (b) Linear regression of the ratio of DNA concentration in samples to the average DNA concentration in the original sample. Each data point was the mean DNA concentration and error bars are one standard deviation. N = 3 repeat measurements. The same cell sample was used to make the dilutions, which were filtered individually.

A pilot study of the new 12-well method was carried out to assess the adjusted plating, harvesting and sample processing methods. First generation LN18 wtIDH1 and mutIDH1^{R132H} cells were transferred to separate plates, 0.7 mL of suspended cells at

200,000 cell/mL in supplemented HG DMEM per well, and incubated for 48 hours. The cells were harvested and processed as described in **section 2.5.5** and **2.6.1**, with the exception being that volume of extraction solvent (80% $MeOH_{(aq)}$) was 70 µL and not 100 µL. Initially three samples from each plate were processed and analysed as a pre-pilot, followed by the nine remaining samples. The data from the nine samples will be presented here, as it provided the best overview of data quality. The DNA concentrations used for sample normalisation are provided in **Table A.IV.1** in **Appendix IV**.

Underivatised samples were analysed by IC-MS (see **section 2.7.1**) and derivatised samples by RPLC-MS (see **section 2.6.2** and **section 2.7.2**). The data was processed with Progenesis QI, as described in **sections 2.8.2,** to assess the total number of features and how many metabolites could be identified. The 12-well pilot was compared to the 60-mm dish experiment described in **chapter 3**, as both had similar experimental conditions. The total number of features were similar in the IC-MS data (> 6,000) and derivatised RPLC-MS data (> 7,000), see **Table 4.2.1** for exact number of features. The number of identified metabolites based on authentic standards was somewhat lower in the 12-well pilot than the 60-mm dish experiment: 127 versus 141 for IC-MS data and 38 versus 53 for derivatised RPLC-MS data. In the IC-MS data, the difference was mainly due to fewer putative identifications (43 versus 55). In the derivatised RPLC-MS data, the 12-well pilot had both fewer confident and putative identifications, see **Table 4.2.1** for details. The identified metabolites and identification criteria for the IC-MS and derivatised RPLC-MS data are listed in **Table A.IV.2** and **Table A.IV.3** in **Appendix IV**, respectively**.** The 12-well pilot showed that far more metabolites than just high abundance 2-HG could be identified. It was therefore of interest to perform univariate and multivariate statistical analyses with the data and compare to the results reported in **chapter 3**.

Table 4.2.1. Summary of total number of features and identified metabolites (confident/putative) from the IC-MS and derivatised RPLC-MS data of the 12-well pilot and 60-mm dish experiment from chapter 3.

Experiment	IC-MS		Derivatised RPLC-MS	
Analysis	12-well pilot	60-mm dish	12-well pilot	60-mm dish
Total features	6,523	6,645	7,205	7,619
Identified metabolites				
Total	127	141	38	53
Confident	84	86	23	34
Putative	43	55	15	19

Prior to univariate and multivariate statistical analysis, further data processing was performed, as described in **section 2.8.3**. The IC-MS and derivatised RPLC-MS data were IQR filtered. The IC-MS data was quantile normalised and auto-scaled, but not transformed. Quantile normalisation and auto-scaling were chosen because together they reduced the small amount of bias found in the heatmap and led to normal or near-normal sample distribution plots. In the derivatised RPLC-MS data, one replicate of mutIDH1^{R132H} LN18 cells was outside of the 95% confidence interval in the PCA scores plot (PC1 × PC2). Closer inspection of the raw data revealed that the abundance of features was elevated in the sample compared to others. That was most likely due to experimental error during sample preparation, *i.e.,* more sample or less buffer was transferred to the sample vial. The data from the sample was removed prior to further data processing. The data was then median normalised as this reduced the small amount of bias found in sample distribution plot. The PCA plot used for identification of outliers is provided in **Figure A.IV.1** and assessment of normalisation is provided in **Figure A.IV.2**, both in **Appendix IV**. Scaling was only applied to multivariate statistical analysis.

In the univariate analysis of the IC-MS and derivatised RPLC-MS data, a total of 44 identified metabolites (34 IC-MS/10 derivatised RPLC-MS) were appreciably (FC ≥ 1.20) and significantly different (p-value < 0.05, Tukey's test). The abundance of 2-HG was significantly and substantially higher in mutIDH1^{R132H} than wtIDH1 cells (FC = 391 (MUT/WT) and p-value < 0.0001, Tukey's test), see **Figure 4.2.2.(a)**. Key metabolites from **Chapter 3** that were also significantly and appreciably different in the 12-well pilot are shown as box plots in **Figure 4.2.2.(b)**. Thus, the 12-well pilot provided univariate analyses that were largely similar to the 60-mm dish experiment.

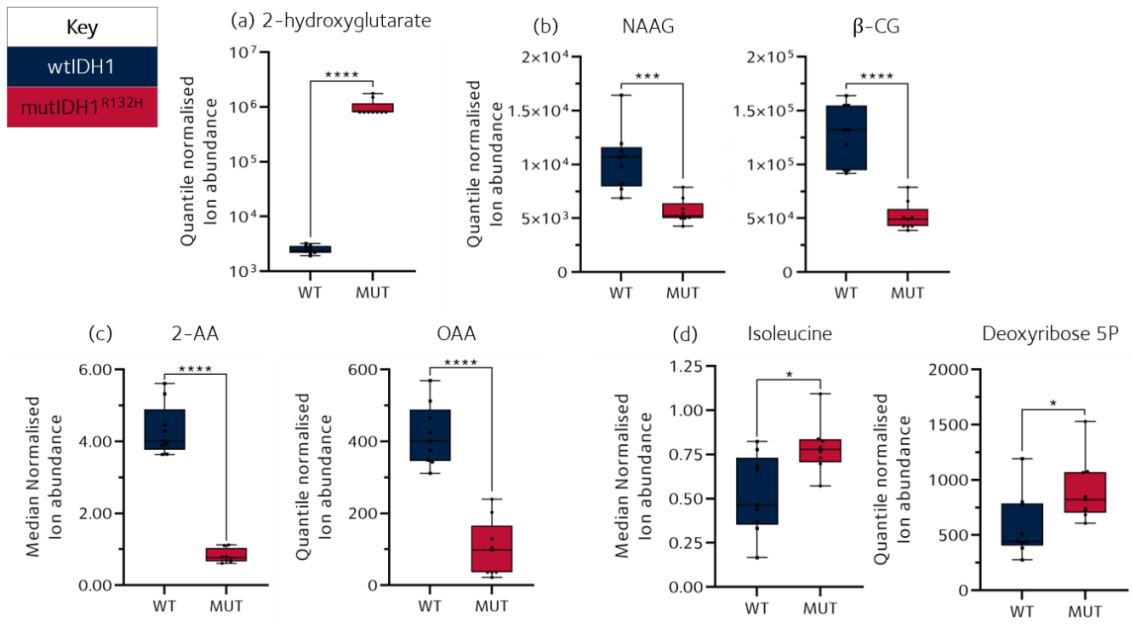

Figure 4.2.2. Summary of univariate statistical analysis 12-well pilot metabolomics data. (a) 2-HG in wtIDH1 and mutIDH1^{R132H} first generation LN18 cells. (b-d) Key metabolites that were significantly and appreciably different in both the univariate analysis carried out in Chapter 3 and in the 12-well pilot. NAAG = *N*-acetylaspartylglutamic acid, β-CG = B-citrylglutamic acid, 2-AA = 2-aminoadipate, OAA = oxoadipate, and P = phosphate. P-values (Tukey's test): * = p-value < 0.05, *** = p-value < 0.001, **** = p-value < 0.0001. The box plot limits are the 25th and 75th percentile, the middle line is the data median. The whiskers are the minimum and maximum measured values. N = 9 biological replicates, except N = 8 for mutIDH1^{R132H} LN18 cell samples for 2-AA and isoleucine

PLS-DA and HCA were performed with the IC-MS data. The two multivariate statistical analysis methods were chosen to assess whether the two experimental groups could be distinguished from each based on the collected data, as was possible for the 60-mm data in **Chapter 3**. As noted in **chapter 3**, the two methods are complementary to each other because one measures similarities between experimental groups by covariance (PLS-DA) and the other by a distance measure (HCA). The analyses were performed as described in **section 2.8.3**, the exception being that all features were included in the HCA.

In the HCA performed with the IC-MS data, wtIDH1 and mutIDH1^{R132H} LN18 cell samples were completely separated with all 2,500 features included, see **Figure 4.2.3.(a)**. The 60-mm dish experiment in **chapter 3** did not have separate clustering of wtIDH1 and mutIDH1^{R132H} with all features included. Thus, the IC-MS data from the 12-well experiment outperformed the previous data set by retaining separation of experimental groups even with all features used during clustering. The PLS-DA performed with the IC-MS data had clear separation of wtIDH1 and mutIDH1^{R132H} cell samples in the first component of the scores plot, see **Figure 4.2.3.(b)**. The LOOCV had R^2 and Q^2 > 0.80 for component 1, as

shown in **Figure 4.2.3.(c)**. The permutation test did not reach significance (p-value = 1; 2,000 permutations and prediction accuracy as test statistic). Neither the 12-well or 60-mm dish data sets had significant permutation tests, but they did have separation in the first component and acceptable cross validation. Additionally, 2-HG and B-CG were among the top 15 VIP scoring features for the PLS-DA model of the 12-well data, similar to the PLS-DA model calculated in **chapter 3**. Overall, the 12-well pilot data retained biological differences between wtIDH1 and mutIDH1^{R132H} cell samples, evident through the ability to distinguish the two experimental groups in both univariate and multivariate data.

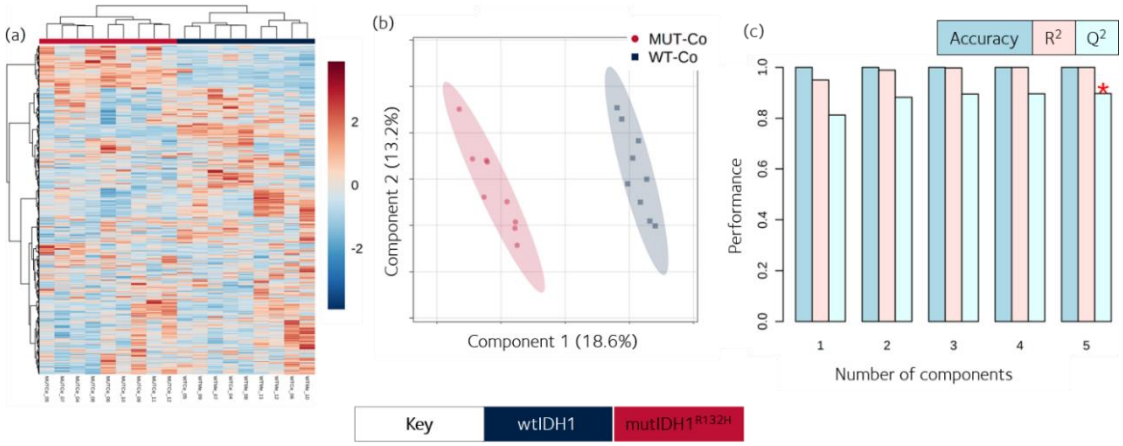

Figure 4.2.3. Summary of multivariate statistical analysis 12-well pilot metabolomics data. (a) HCA heatmap. The Ward clustering method and Euclidian distance measure was used. Both features and samples were clustered. The colour bar indicates relative ion abundance. (b) PLS-DA scores plot (component 1 × component 2) of IC-MS data. (c) LOOCV with 5 components of the PLS-DA. Number of biological replicates: N = 9.

*In summary, a downscaled tissue culture method for metabolomics which provided data with only slightly lower coverage and sensitivity than the standard method with 60-mm dishes was developed. The data from the 12-well pilot led to similar outcomes from univariate and multivariate statistical analysis as that reported in **chapter 3**. Thus, the method could be used to harvest larger numbers of metabolomics samples and still facilitate targeted and untargeted metabolic analysis.*

4.3. Assessing sample preparation and analysis of mutIDH1 inhibitors in cell and media samples

The measurement of the relative abundance of mutIDH1 inhibitors AG-120, AG-881, BAY 1436032 and GSK864 in cell and media samples was performed to support the interpretation of metabolomics data collected with IC-MS and derivatised RPLC-MS. Experiments were carried out to confirm that an appropriate sample analysis method was used and to establish sample preparation protocols. First, all four inhibitors were assessed with regards to retention time and peak shape, as well as ionisation efficiency in positive and negative polarity mode. Sample analysis was carried out with a RPLC-MS method previously developed by Dr John Walsby-Tickle [321]. Second, the potential loss of inhibitor from sample filtration by the MWCO filters used in cell sample preparation was tested. Third, a protocol for the preparation of media samples was developed due to loss of sensitivity after filtration.

Porous silica beads functionalised with C18 alkyl chains are a commonly used stationary phase for LC analysis of pharmaceuticals [reviewed in 429]. It was therefore tested first for analysis of the inhibitors, structures of which are shown in **Figure 4.3.1**. Single standards of each inhibitor (1.00 µM) in 80% $MeOH_{(aq)}$ were analysed in positive ionisation mode with a CORTECS® UPLC® T3 C_{18} column. The four inhibitors had retention time past the system void volume (> 2 min), with symmetric peaks and baseline separation, see **Figure 4.3.2.** C18 was therefore considered the appropriate stationary phase for analysis of the inhibitors and no further optimisation of the LC parameters was needed.

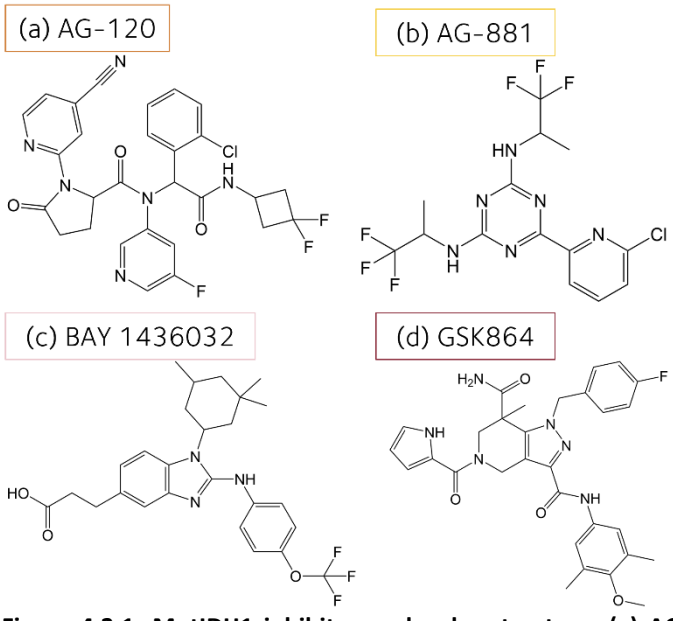

Figure 4.3.1. MutIDH1 inhibitor molecular structure. (a) AG-120. (b) AG-881. (c) BAY 1436032. (d) GSK864. Structures made in ChemDraw 20.1 based on canonical SMILES.

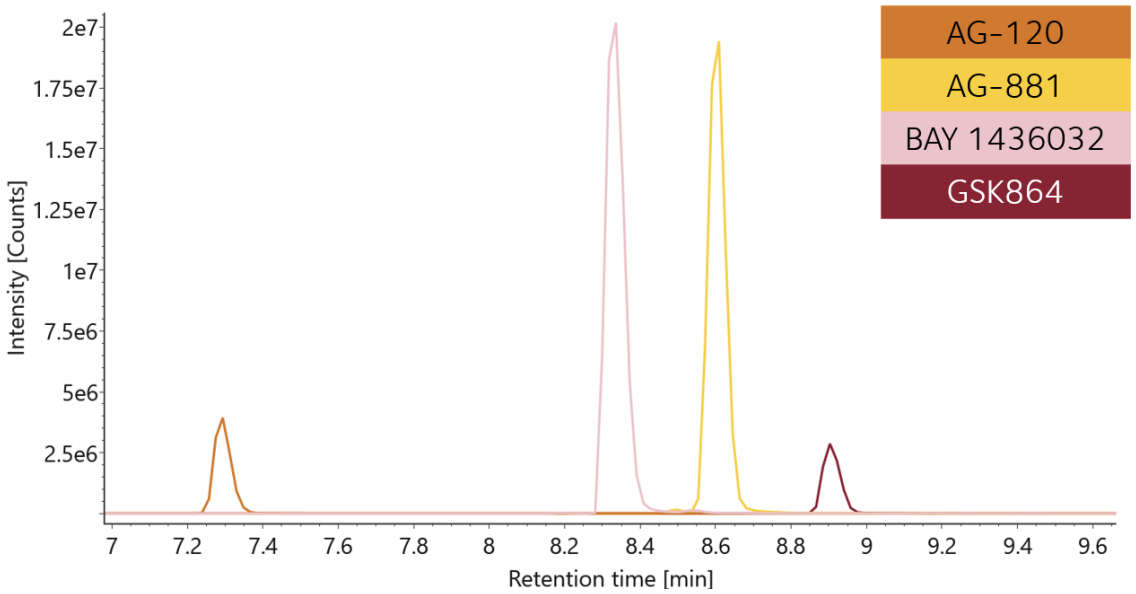

Figure 4.3.2. Extracted ion chromatograms of mutIDH1 inhibitor standards (1.00 µM) with RPLC-MS in positive polarity mode. Single injection (40.6 ppm).

The ionisation efficiency the four inhibitors in positive and negative mode ESI was assessed next. Single standards of each inhibitor (5.00 µM) in 80% $MeOH_{(aq)}$ were analysed with five injections in each polarity mode. All four inhibitors had significantly higher peak area in positive mode ESI than negative mode ESI (p-value < 0.05, unpaired Student's t-test), see **Figure 4.3.3**. ESI with positive polarity was therefore used as the ionisation mode.

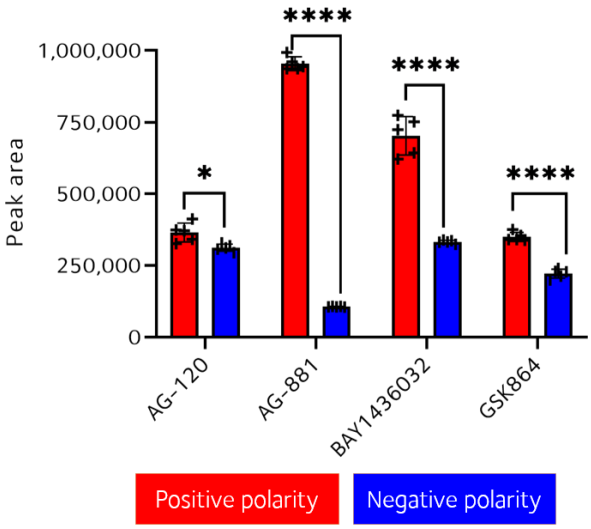

Figure 4.3.3. Peak area of EICs of all four inhibitors in positive and negative mode . N = 5 repeat injections of the same standard. P-values: * = p-value < 0.05 and **** = p-value < 0.0001, unpaired Student's t-test. Error bars are one standard deviation.

After the analysis method had been decided, sample preparation was evaluated next. Cell samples were filtered prior to analysis with MWCO filters (3 or 10 kDa) made of regenerated cellulose. To determine whether there was loss of inhibitor from filtration, 5.00 µM standards in 80% $MeOH_{(aq)}$ were filtered and both the filtered and nonfiltered

standards were analysed with RPLC-MS in positive mode. There was not a significant difference in peak area between filtered and non-filtered standard solutions of any of the four mutIDH1 inhibitors (p-value > 0.05, unpaired t-test). The sample preparation of cell samples therefore did not have to be modified.

Filtered and unfiltered media samples were also compared, but here filtration led to either complete loss of the EIC peak (AG-120, BAY 1436032 and GSK864) or substantial decrease in EIC peak area (1,000 versus 334,000 for AG-881). It was unlikely that the inhibitors were lost by interaction with the filter, as there was no substantial or significant loss of inhibitor in the previous filtration experiment using standard solutions in 80% $MeOH_{(aq)}$. Instead, non-specific binding of the inhibitors to protein in the media was considered a possible explanation. The supplemented media contained 10 % (v/v) FBS, which has a high protein concentration (32-42 mg/mL [430]). In order to explore the possibility of non-specific protein binding of inhibitors, acetonitrile was tested as a protein precipitating agent because it is also an effective protein denaturant [431]. The ratio between sample and precipitating solvent was determined based on a publication on protein precipitation in serum samples, where a 2:1 ratio (or higher) led to > 95% of proteins being precipitated [431]. The pilot experiment was carried out with 3:1 ratio of precipitating solvent to sample, which was decreased to 2:1 for experimental samples to limit sample dilution. Assessment of increasing or decreasing the sample acidity or basicity was included to determine whether it improved the disruption of inhibitor-to-protein binding. Acetonitrile was therefore either acidic (1% (v/v) formic acid), neutral, or basic (1% (v/v) NH_3 in water (~25 %)). After mixing with media, the pH of the samples was 4, 8 and 11, respectively. The pH was measured with pH strips.

LG DMEM containing 10% FBS (v/v) and either 0.50 µM or 5.00 µM of AG-120, AG-881, BAY 1436032 or GSK864 were extracted with either acidic, neutral or basic acetonitrile. The samples were left at -20 °C overnight. Despite acetonitrile being miscible with water, the samples were phase separated with a pink phase at the bottom of the sample tubes, even after 12 hours at -20 °C and when thawed. The pink colour was due to the presence of phenol red in the DMEM. In the acidic extraction, the lower phase was yellow and in the basic extraction it was dark pink, indicating the decreased/increased pH. The phase separation was potentially due to high concentration of salts, lipids and proteins, which

may have decreased the miscibility of water and acetonitrile. There was no visible precipitated protein and no pellet appeared after centrifugation at 14,000 rpm for 10 minutes. The inhibitors were assumed present in the upper phase (acetonitrile), therefore only the upper phase was transferred to a total recovery vial for further analysis.

The peak area of the inhibitors in the extracted samples was within the same order of magnitude as the unfiltered media samples (10^5). The extraction/precipitation of inhibitors from media therefore decreased protein present in the sample without simultaneous loss of signal, as was observed for filtered samples. There was no significant difference in the peak areas of EICs comparing acidic, neutral and basic precipitations/extractions for any of the different inhibitors (p-value > 0.05, one-way ANOVA followed by Šídák MCTe). This applied to both high (5.00 µM) and low (0.50 µM) concentration samples. Since adding formic acid or aqueous ammonia did not significantly improve signal intensity of the inhibitors, the neutral acetonitrile was used for future experiments because it was simpler to prepare.

In summary, the mutIDH inhibitors AG-120, AG-881, BAY1436032 and GSK864 could be analysed with RPLC-MS as the retention time was sufficient (> 2 min). Analysis with positive ECI LC-MS provided significantly higher EIC peak areas than in negative ion mode (p-value < 0.05, unpaired Student's t-test). There was not a loss of inhibitor when filtering standards with 10 kDa MW cut-off filters (p-value > 0.05, unpaired two-sided t-test) but significant loss was observed when filtering inhibitor standards made with media known to contain proteins. The protein in the media samples was denatured/precipitated by acetonitrile. There was no significant difference in peak area of EICs of inhibitors between acidic, neutral or basic acetonitrile precipitation/extraction. Neutral/pure acetonitrile was chosen as the protein precipitation/metabolite extraction solvent for future sample preparations.

4.4. MutIDH1^{R132H} LN18 cell viability not substantially decreased by mutIDH1 inhibitors

Experimental overview

Prior to investigating the impact of mutIDH1 inhibitors on 2-HG, 2-OG and isocitrate abundance, it was of interest to assess the effect of inhibitors on cell viability. If cell viability was significantly decreased by treatment, it could have a confounding effect on the interpretation of alterations of 2-HG, 2-OG and isocitrate. In order to investigate the cell viability under treatment, mutIDH1^{R132H} LN18 cells were cultured with AG-120, AG-881, BAY 1436032 or GSK864 at three concentrations (0.50, 5.00 and 10.0 µM) for 24, 48, 72 or 96 hours. All cells, including control cells, were incubated with 0.2% (v/v) DMSO in the media. Supplemented LG DMEM media was used throughout. Cell viability was assessed with an MTS assay, where the absorbance (*A*) at 490 nm positively correlated to the number of metabolically active (viable) cells in each well [432]. Further experimental details are provided in **sections 2.5.3** (preparation) and **2.7.5** (measurement). The treatment concentrations were chosen based on reports in the literature [246, 247, 250], while the timepoints were chosen based on the length of treatment planned for the metabolomics experiments.

Results

In general, there was no significant difference in cell viability between control and treated samples after 24 hours of incubation, except for cells treated with 0.50 µM AG-120 (p-value < 0.05, one-way ANOVA with Dunnett's test). This significant difference was due to the treated cells having higher absorbance at 490 nm, *i.e.,* there were more viable cells after treatment than for control ($A_{treated}/A_{control}$ = 1.19 ± 0.05). After 48 hours of incubation, cell viability decreased significantly only for cells treated with 10.0 µM AG-881 ($A_{treated}/A_{control}$ = 0.80 ± 0.05) and increased significantly for cells treated with 10.0 µM GSK864 ($A_{treated}/A_{control}$ = 1.2 ± 0.1) (both p-value < 0.05, one-way ANOVA with Dunnett's test). After 72 and 96 hours of incubation, cells treated with 5.00 or 10.0 µM of any mutIDH1 inhibitor had significantly decreased viability compared to control cells ($A_{treated}/A_{control}$ = 0.85 ± 0.04, p value < 0.0001, one-way ANOVA with Dunnett's test). Cells treated with 5.0 µM BAY 1436032 for 96 hours were the exception, they were not significantly different from control cells. The cells treated with 0.50 µM AG-881 had

significantly lower viability than control cells after 72 and 96 hours of incubation ($A_{treated}/A_{control}$ = 0.85 ± 0.03, p-value < 0.0001, one-way ANOVA with Dunnett's test). The absorbance ratio between treated and control for all timepoints and treatment concentrations are summarised in **Figure A.VI.1** in **appendix VI**.

In summary, all four inhibitors were capable of decreasing cell viability when both treatment concentration was high enough (5-10.0 µM) and incubation time with inhibitor present was sufficient (≥ 72 hours). However, the decrease remained small, with only a 15% reduction in cell viability on average across all four inhibitors. Shorter incubation time (24-48 hours) had less of an effect on cell viability, even at 5.00 µM treatment concentration. Thus, decreased cell viability would not be a confounding effect on the study of the metabolism of mutIDH1^{R132H} LN18 cells treated with mutIDH1 inhibitors as long as treatment concentration was not too high or incubation time too long.

4.5. 2-HG decreased and isocitrate increased in wtIDH1 and mutIDH1^{R132H} LN18 cells after treatment with mutIDH1 inhibitors

Experimental overview

The effect on 2-HG, 2-OG and isocitrate after treatment with mutIDH1 inhibitors was compared between wtIDH1 and mutIDH1^{R132H} LN18 cells. The aim was to assess how efficient the different inhibitors were at reducing 2-HG abundance in mutIDH1^{R132H} LN18 cells and whether there was any inhibitory effect on wtIDH1 cells. Both cell lines were treated with AG-120, AG-881, BAY1436032 or GSK864 (5.00 µM) for 24 hours, with a total incubation time of 48 hours. Control samples had 0.1% (v/v) DMSO in their media to match the DMSO concentration of media containing inhibitor. All samples were grown in supplemented LG DMEM. There were 10 replicates of treated and 20 replicates of control each for wtIDH1 and mutIDH1^{R132H} LN18 cells. The cells were plated, treated and harvested as described in **section 2.5.3-2.5.5**. Sample preparation was performed as described in **section 2.6.1** and DNA concentrations were used for sample normalisation (**Table A.II.1** in a**ppendix II**). The samples were analysed by IC-MS (see **section 2.7.1**) and 2-HG, 2-OG and isocitrate were identified using authentic standards (see **section 2.8.2** and **Table A.II.2** for identification criteria).

Results

The control mutIDH1^{R132H} LN18 cells, originally presented in **chapter 3**, had significantly and substantially higher 2-HG levels than the untreated wtIDH1 LN18 cells (FC = 52.9 (MUT/WT), p-value < 0.0001, Tukey's Test). In mutIDH1^{R132H} LN18 cells, all four mutIDH1 inhibitors led to significant and substantially decreased 2-HG abundances (p-value < 0.0001, unpaired t-test with FDR). Cells treated with AG-881 had a smaller decrease in 2-HG levels in mutIDH1^{R132H} LN18 cells than the other inhibitors: FC_{AG881} = 16.7, FC_{AG120} = 40.5, $FC_{BAY\ 1436032}$ = 35.8, and FC_{GSK864} = 45.2 (control/treated). AG-120, AG-881 and GSK864 led to a significant decrease in 2-HG levels in treated wtIDH1 LN18 cells when compared to untreated wtIDH1 LN18 cells (p-value < 0.001, unpaired t-test with FDR). Unlike in the comparison of treated and control mutIDH1^{R132H} LN18 cells, the FCs were small: FC_{AG120} = 1.27, FC_{AG881} = 1.30, and FC_{GSK864} = 1.20 (control/treated). 2-HG abundance in treated and control wtIDH1 and mutIDH1^{R132H} LN18 cells are summarised in **Figure 4.5.1**.

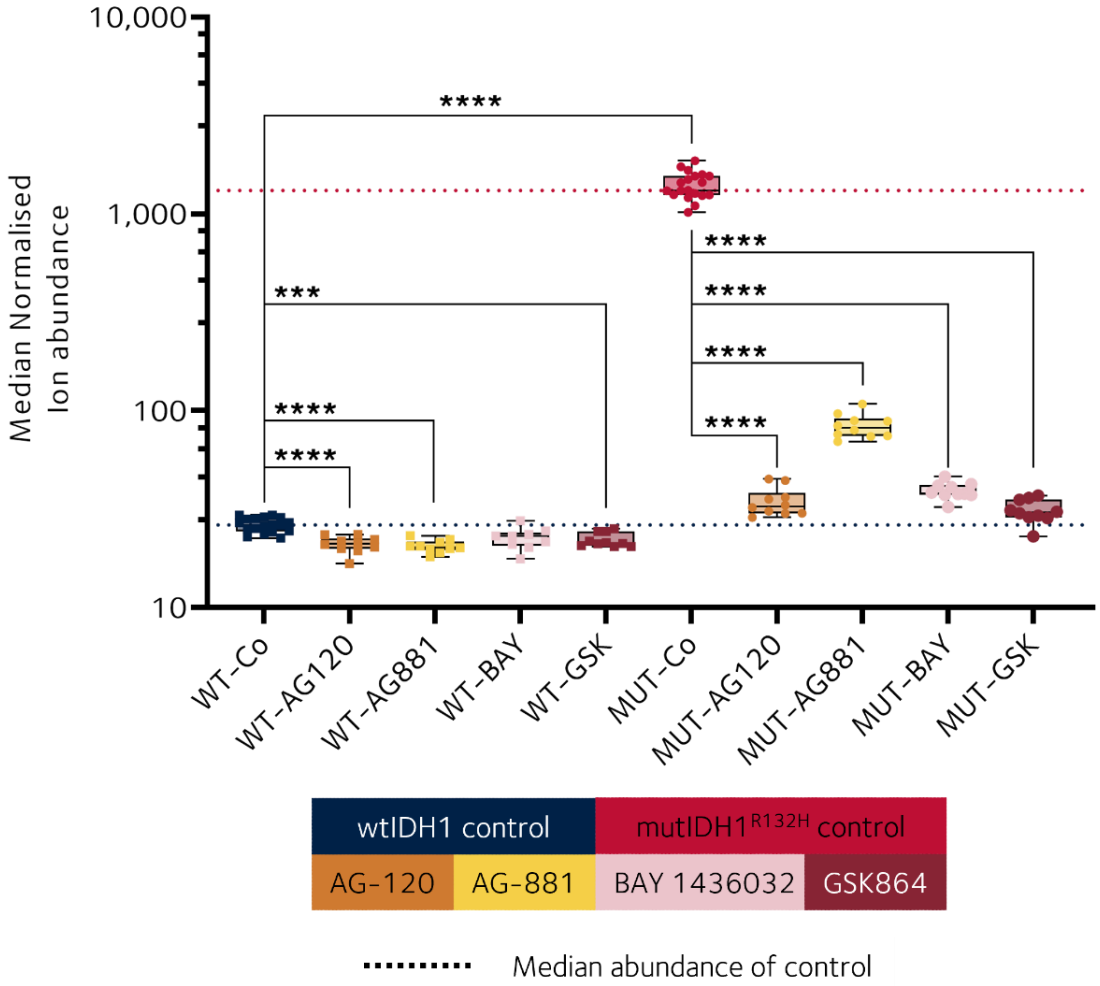

Figure 4.5.1. 2-HG abundance in wtIDH1 and mutIDH1^{R132H} cells treated with mutIDH1 inhibitors AG-120, AG-881, BAY 1436032 and GSK864 (5.00 µM) for 24 hours. Dotted lines indicate median 2-HG abundance in wtIDH1 LN18 cells (blue) and mutIDH1^{R132H} LN18 cells (red). N = 19 for WT-Co, N = 20 for MUT-CO, N = 9 for WT-BAY and N = 10 for the remaining experimental groups. P-value thresholds: *** = p-value < 0.001 and **** = p-value < 0.0001, calculated with Tukey's test for wtIDH1 versus mutIDH1^{R132H} control samples and unpaired t-test with FDR for the treated versus control comparisons. Box plot whiskers are the minimum and maximum ratio calculated for each sample, box plot limits are 25th, 50th and 75th percentile. Abbreviations: WT = wtIDH1, MUT = mutIDH1^{R132H}, Co = control, BAY = BAY 1436032 and GSK = GSK864.

The 2-3 times greater efficiency in 2-HG suppression by AG-120, BAY 1436032 and GSK864 compared to AG-881 was larger than expected, considering that AG-881 had only a slightly higher IC_{50} than the other three inhibitors (30 nM vs 12-15 nM, *in vitro* assays [246, 247, 249, 250]). This experiment only had a single time point and treatment concentration. Potentially AG-881 has improved ability to decrease 2-HG at higher concentrations or if cells were treated for longer. Different concentration ranges and treatment lengths with the four mutIDH1 inhibitors were therefore investigated and the results are presented in **sections 4.6** and **4.7**.

WtIDH1 has previously been shown capable of producing small amounts of 2-HG under normal culturing conditions [113], therefore the decrease of 2-HG in wtIDH1 LN18 cells was likely due to inhibition of wtIDH1 activity. If wtIDH1 activity was inhibited, an accumulation of isocitrate and decrease in 2-OG would be expected, as they are the most common substrate and product of the enzyme. There was no significant decrease in 2-OG abundance in the wtIDH1 cells after treatment with any of the four inhibitors (p-value > 0.05, unpaired t-test with FDR; 1.06 < FC < 1.23 (control/treated)). In mutIDH1^{R132H} LN18 cells, GSK864 led to a significant decrease in 2-OG (FC = 1.39 (control/treated), p-value < 0.01, t-test with FDR). The difference in 2-OG abundance between AG-120, AG-881 and BAY 1436032 treated and control mutIDH1^{R132H} LN18 cells were minimal. Isocitrate, on the other hand, accumulated appreciably and significantly in both wtIDH1 and mutIDH1^{R132H} LN18 cells, when compared to their respective control cells (1.2 < FC < 1.7 (treated/control) and p-value < 0.05, unpaired t-test with FDR). The only exception was wtIDH1 cells treated with BAY 1436032, where the increase was appreciable (FC > 1.22 (treated/control)), but not significant. The abundance of 2-OG and isocitrate found in the different cells is summarised in **Figure 4.5.2.**

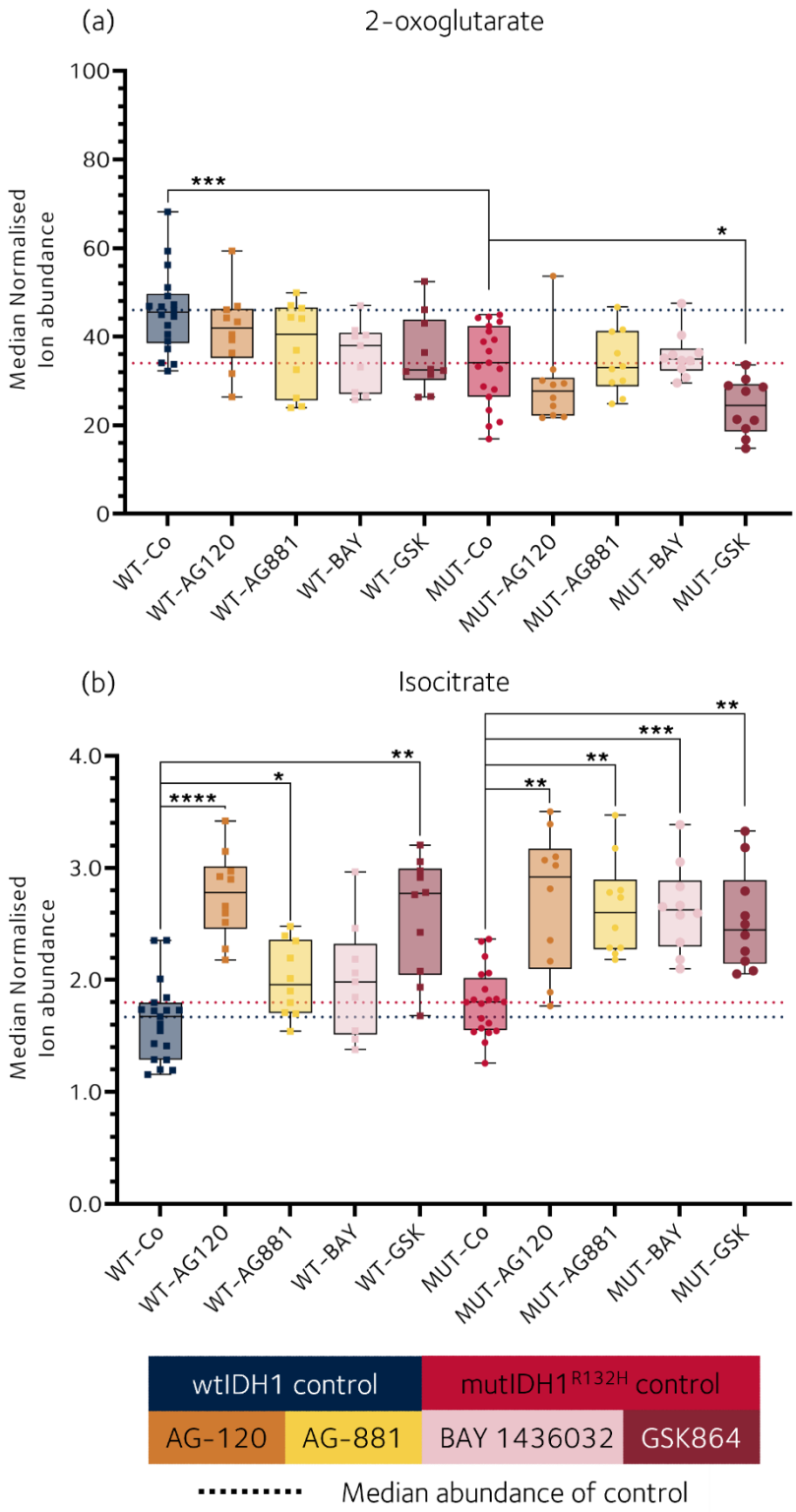

Figure 4.5.2. Abundance (a) 2-OG and (b) isocitrate in wtIDH1 and mutIDH1^{R132H} cells treated with mutIDH1 inhibitors AG-120, AG-881, BAY 1436032 and GSK864 (5.00 µM) for 24 hours. Dotted lines indicate median abundance in wtIDH1 LN18 cells (blue) and mutIDH1^{R132H} LN18 cells (red). N = 19 for WT-Co, N = 20 for MUT-CO, N = 9 for WT-BAY and N = 10 for the remaining experimental groups. P-value thresholds: * = p-value < 0.05, ** = p-value < 0.01 and *** = p-value < 0.001, calculated with Tukey's test for wtIDH1 versus mutIDH1^{R132H} control samples and unpaired t-test with FDR for the treated versus control comparisons. Box plot whiskers are the minimum and maximum ratio calculated for each sample, box plot limits are 25th, 50th and 75th percentile. Abbreviations: WT = wtIDH1, MUT = mutIDH1^{R132H}, Co = control, BAY = BAY 1436032 and GSK = GSK864.

The mutIDH1^{R132H} LN18 cells treated with mutIDH1 inhibitors were no longer accumulating 2-HG and it was hypothesised that the 'relief' from mutIDH1 activity would lead to an increase in 2-OG abundance. It was therefore surprising that 2-OG abundance remained unchanged or even decreased overall in mutIDH1^{R132H} LN18 cells after treatment with the mutIDH1 inhibitors. Cell viability also did not change significantly between treated and control cells at 5.00 µM inhibitor for 24 hours. The consumption-rate of nutrients was therefore judged as similar between control and treated cells. It was speculated that 2-OG previously used for 2-HG biosynthesis was therefore re-directed to other reactions. That re-direction could suggest a major change in 2-OG dependent metabolism in mutIDH1^{R132H} LN18 cells, which will be investigated further in **chapter 5**.

The appreciable increase of isocitrate in both wtIDH1 and mutIDH1^{R132H} LN18 cells indicated that wtIDH1 activity was inhibited in both cell lines. The mutIDH1^{R132H} LN18 cells were still able to express wtIDH1 as the gene had not been knocked down/out. WtIDH1 may be present in patient tumours as well, as the *IDH1* mutation is usually heterozygous [reviewed in 428]. Thus, the presence of active wtIDH1 and subsequent inhibition in the mutIDH1^{R132H} LN18 cell model was not necessarily different from what occurs in tumour cells treated with mutIDH1 inhibitors.

In summary, mutIDH1 inhibitors led to substantial and significant decrease in 2-HG abundance in mutIDH1^{R132H} LN18 cells. The relative suppression of 2-HG in mutIDH1^{R132H} LN18 cells by the different inhibitors were larger than expected based on the low IC_{50} values (in vitro assays) reported in the literature. In wtIDH1 cells, there was a small, but significant decrease in 2-HG abundance. Both cell lines had similar increase in isocitrate abundance after treatment with the mutIDH1 inhibitors, indicating that the wtIDH1 enzyme was inhibited in both cell lines.

4.6. 2-HG, 2-OG and isocitrate abundance in mutIDH1^{R132H} LN18 cells is dependent on mutIDH1 inhibitor type and treatment concentration.

The difference in potential to decrease 2-HG abundance between AG-881 and the other three mutIDH1 inhibitors warranted a concentration range experiment to investigate whether inhibition was improved at higher treatment concentrations. In addition, it was of interest to investigate how the cells responded to a range of inhibitor concentrations, in relation to 2-HG abundance and how that correlated with changes in the abundance of other metabolites.

Data processing and analysis

MutIDH1^{R132H} LN18 cells were cultured with the following concentrations of AG-120, AG-881, BAY 1436032 or GSK864: 0.05, 0.50, 5.00 and 10.0 µM. WtIDH1 LN18 cells were not included because the focus of the experiment was on 2-HG suppression in mutIDH1^{R132H} expressing cells. Incubation with treatment lasted for 24 hours. Each plate had 4 replicates of control samples, with a total of 32 control samples across 8 plates. Each treated experimental group had 4 replicates. Supplemented LG DMEM was used throughout. All samples, treated or control, had 0.2% (v/v) DMSO in the media. Samples were plated, harvested and processed as described in **Section 2.5.3-2.5.5**. Sample preparation was performed as described in **section 2.6.1**. DNA concentrations used for sample normalisation are provided in **Table A.V.1** in **appendix V**. The samples were analysed with IC-MS and 2-HG, 2-OG and isocitrate were identified based on the criteria described in **section 2.8.2** (see **Table A.V.2** for identification criteria).

Results

Cells treated with AG-120 and AG-881 had a substantial and significant decrease in 2-HG abundance at the lowest concentration 0.05 µM inhibitor in media ($FC_{AG\text{-}120}$ = 6.09 and $FC_{AG\text{-}881}$ = 14.8 (control/treated), p-value < 0.0001, one-way ANOVA and Dunnett's MCTe). Treatment with BAY 1436032 and GSK864 (0.05 µM) led to a more modest, but still significant, decrease in 2-HG abundance ($FC_{BAY\ 1436032}$ = 1.94 and FC_{GSK864} = 1.36 (control/treated), p-value < 0.0001, one-way ANOVA and Dunnett's MCTe). Increasing AG-881 treatment concentration to 0.50 µM led to a significant drop in 2-HG levels compared to that achieved with 0.05 µM (p-value < 0.01, unpaired two-sided t-test). No

further significant decrease in 2-HG was achieved by increasing the concentration of AG-881 to either 5.0 or 10.0 µM. Cells treated with AG-120, BAY 1436032 or GSK864 did respond to increased treatment concentration. Cells treated with higher concentration of AG-120, BAY 1436032 or GSK864 had significantly lower 2-HG abundance than cells treated with lower concentration of the inhibitors (p-value < 0.01, t-test with FDR). Moreover, the linear regression of 2-HG abundance to mutIDH1 inhibitor concentration yielded significantly non-zero slopes for AG-120, BAY 1436032 and GSK864 (p-value < 0.05, $R^2 > 0.33$), but not for AG-881. The effect of the different inhibitors at different concentrations on 2-HG levels in mutIDH1^{R132H} LN18 cells is summarised in **Figure 4.6.1**.

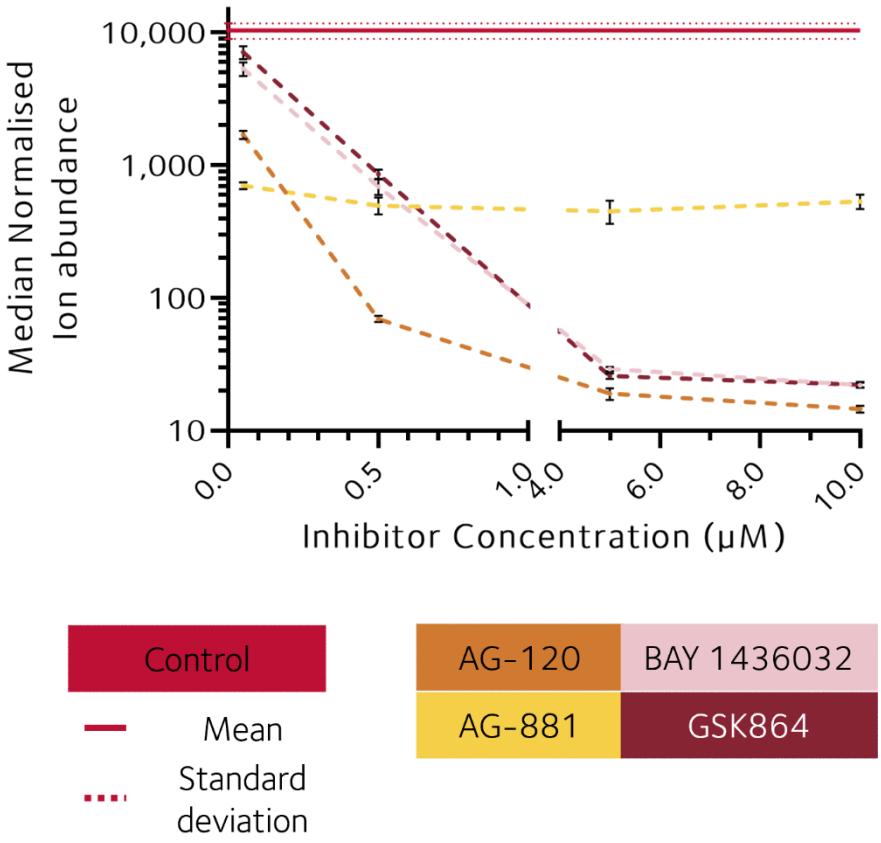

Figure 4.6.1. 2-HG abundance in mutIDH1^{R132H} LN18 cells treated with four different concentrations (0.05, 0.50, 5.0 and 10 µM) of AG-120, AG-881, BAY 1436032 or GSK864. The data points are mean of sum normalised abundance of 2-HG and error bars are one standard deviation. The solid red line indicates the mean abundance of the control samples, the dotted lines are the mean ± one standard deviation. N = 32 for control, N = 4 for all treatment groups except AG881 (5.0 µM) where N = 3.

The depletion in 2-HG abundance after treatment with AG-881 remained modest compared to the other three inhibitors, even at 5.00 µM and 10.0 µM. AG881 reached only

a maximum FC = 23 (control/treated). The other three inhibitors all achieved FC > 350 at the two highest treatment concentrations. All FCs are summarised in **Table 4.6.1**.

Table 4.6.1. FC of 2-HG (control/treatment) achieved at 0.05, 0.50, 5.00 and 10.0 µM treatment concentration with mutIDH1 inhibitors AG-120, AG-881, BAY 1436032 and GSK864 in mutIDH1^{R132H} LN18 cells.

Inhibitor	Fold-change of mean 2-HG in control versus treated mutIDH1R132H LN18 cells			
	0.05 µM	0.50 µM	5.00 µM	10.0 µM
AG-120	6.09	149	545	712
AG-881	14.8	20.8	23.0	19.4
BAY 1436032	1.94	15.0	355	469
GSK864	1.46	12.1	401	467

The lack of correlation between treatment concentration and 2-HG abundance in cells treated with AG-881 was surprising. The mutIDH1 inhibitors were assumed to have a similar mechanism because all bound allosterically to mutIDH1 in the dimer interface [247, 249, 312]. It was therefore expected that 2-HG abundance would decrease with increasing inhibitor concentration. One explanation for the non-correlative behaviour of AG-881 could be that it reached a threshold of 2-HG suppression, *i.e.,* maximum inhibition efficiency, at a far lower concentration than the other inhibitors. AG-120, BAY1436032 and GSK864 only appeared to be approaching a threshold of maximum inhibition efficiency at 10.0 µM treatment concentration. However, it may also be that the cells needed to be treated for longer with AG-881 to achieve a high degree of 2-HG suppression. A time-course experiment was therefore performed and the results are presented in **section 4.7.** In addition, the uptake of AG-881 may have been lower than the other three inhibitors; this was also explored further by comparing the inhibitor levels in both cells and media. The results are presented in **section 4.8**.

2-OG decreased significantly in mutIDH1^{R132H} LN18 cells treated with AG-120 (5.00 µM, 10.0 µM), BAY 1436032 (10.0 µM) and GSK864 (5.00 µM, 10.0 µM) (FC > 1.20 (control/treated), p-value < 0.01, unpaired t-test with FDR). The decrease was linear with increased treatment concentration for AG-120, BAY 1436032 and GSK864 (non-zero slope, p-value < 0.0001, $R^2 > 0.74$), but not for AG-881. The only significant and appreciable increase of isocitrate in treated cells was after treatment with 0.50 µM AG-120 (FC = 1.2 (treated/control)), 5.0 µM AG-881 (FC = 1.33 (treated/control)), 10.0 µM BAY 1436032 (FC = 1.28 (treated/control)) or 10.0 µM GSK864 (FC = 1.50 (treated/control)) (all: p-value < 0.01, t-test with FDR). The increase in isocitrate was only linear with a significantly non-

zero slope for cells treated with GSK864 (p-value = 0.0031, R^2 > 0.48). **Figure 4.6.2** summarises the ion abundance of 2-OG and isocitrate in control cells, as well as the linear regressions of 2-OG and isocitrate versus inhibitor concentration.

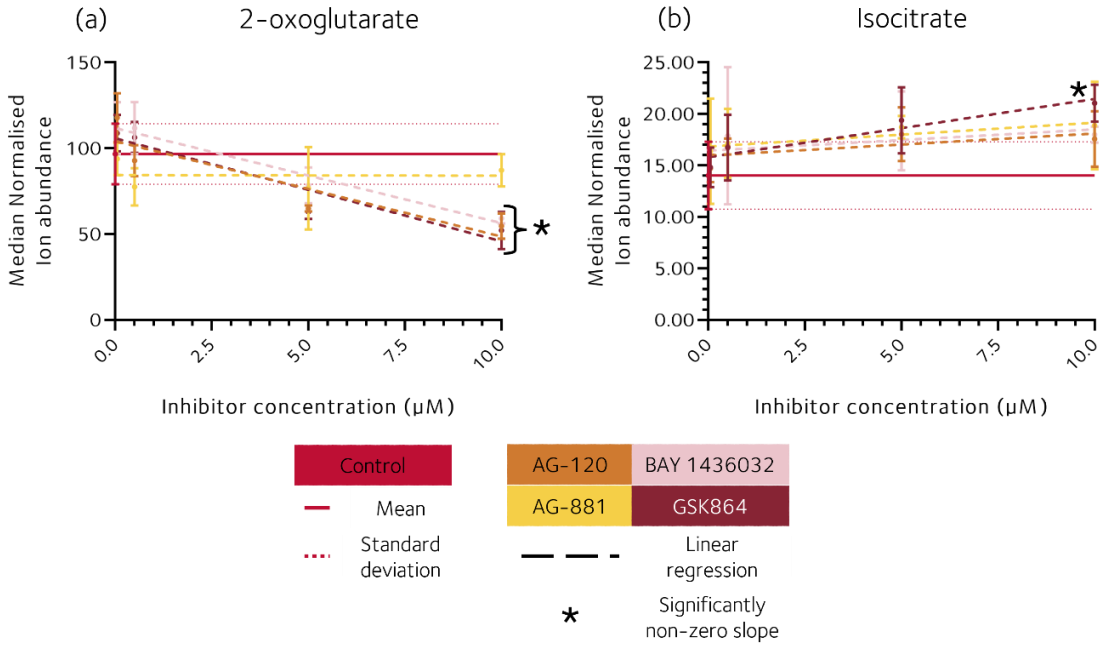

Figure 4.6.2. Abundance and linear regression of (a) 2-OG and (b) isocitrate in mutIDH1^{R132H} LN18 cells treated with four different concentrations (0.05, 0.50, 5.0 and 10 µM) of AG-120, AG-881, BAY 1436032 and GSK864. The data points are mean of median normalised abundance and error bars are one standard deviation. The dashed lines are the linear regressions of ion abundance of 2-OG and isocitrate versus mutIDH1 inhibitor concentration. * = significantly non-zero slope, p-value < 0.01. The solid red line indicates the mean abundance of the control sample, the dotted line mean ± one standard deviation. The lines were added for clarity. Number of biological replicates were N = 32 for control, N = 4 for all treatment groups except AG881 (5.0 µM) where N = 3.

As observed for 2-HG, the decrease in 2-OG abundance was dependent on inhibitor concentration for cells treated with AG-120, BAY 1436032 or GSK864. Isocitrate accumulation appeared to reach a threshold for cells treated with AG-120, AG-881 or BAY 1436032 (5.00 µM), as there was no further increase in abundance at higher concentration (10.0 µM). The accumulation of isocitrate was not as apparent in this experiment compared with the observations in **section 4.5**, but coupled with the decrease in 2-OG, wtIDH1 was still regarded as inhibited at high concentrations of inhibitor.

In summary, both 2-HG and 2-OG abundance decreased in a concentration dependent manner in mutIDH1^{R132H} LN18 cells when treated with AG-120, BAY 1436032 or GSK864. Cells treated with AG-881 had decreased abundances of 2-HG and 2-OG, but not in a concentration dependent manner as there was no linear correlation between metabolite

abundance and treatment concentration. The decrease in 2-HG in cells treated with AG-881 was significantly smaller than for cells treated with the other three inhibitors. Isocitrate increased after treatment with all four of the inhibitors, but only correlated linearly with increasing concentration of GSK864. Thus, both wtIDH1 and mutIDH1^{R132H} were inhibited, but the efficiency in inhibition was drug dependent.

4.7. Length of exposure time to mutIDH1 inhibitor improves 2-HG suppression with maximum reached after 24 hours

Data processing and analysis

In order to assess the ability of the four mutIDH1 inhibitors AG-120, AG-881, BAY 1436032 and GSK864 to decrease 2-HG abundance as well as their effect on 2-OG and isocitrate abundance over time, two different time course experiments were carried out. MutIDH1^{R132H} LN18 cells were separately treated with 5.00 µM of each inhibitor. All media was supplemented LG DMEM with 0.1% (v/v) DMSO, including control sample media. The S-TICO experiment had timepoints of 1, 2, 4, 8, 12, and 24 hours, while the L-TICO experiment had timepoints 24, 48, 72 and 96 hours. The latter three long time points were further split into two groups: group 1 had media replaced every 24 hours and group 2 had media left on for the duration of the time point. Cells were grown in 12-well plates, then harvested and processed as described in **sections 2.5.3-2.5.5**. The number of biological replicates per timepoint was 8 for control and 4 per inhibitor, *i.e.,* 24 samples in total per timepoint. Sample preparation was performed as described in **section 2.6**.1. DNA concentrations used for normalisation are provided in **Table A.VI.1** and **A.VI.2** in **appendix VI** in **Appendix VI**. The samples were analysed with IC-MS and 2-HG, 2-OG and isocitrate were identified based on the criteria described in **section 2.8.2** (see **Table A.VI.3** and **A.VI.4** for identification criteria).

Results

A significant decrease in 2-HG abundance in mutIDH1^{R132H} LN18 cells treated with any of the four inhibitors was first reached at the 2-hour timepoint (FC = 1.64 (control/treated), p-value < 0.0001, one-way ANOVA and Dunnett's MCTe). Up until the 8-hour timepoint the difference in 2-HG abundance between control and treated cells increased due to both a

continued increase of 2-HG abundance in control cells and decrease in treated cells. Between 12 and 24 hours, the difference between control and treated cells was largely due to an increase in 2-HG in control cells and not further decrease in treated cells. All inhibitors were capable of a similar degree of 2-HG suppression up until 4 hours of treatment ($3.7 < FC < 6.2$ (control/treated)), after which AG-881 plateaued ($9.5 < FC < 14.1$ (control/treated)). The remaining three inhibitors continued to decrease 2-HG levels further and by 24 hours all cells treated with AG-120, BAY 1436032 or GSK864 had reached $FC > 100$ (control/treated). All FC calculations are ratios of mean 2-HG abundance between control and treated samples at the same time point. The 2-HG levels measured in the S-TICO experiment are summarised in **Figure 4.6.1.**

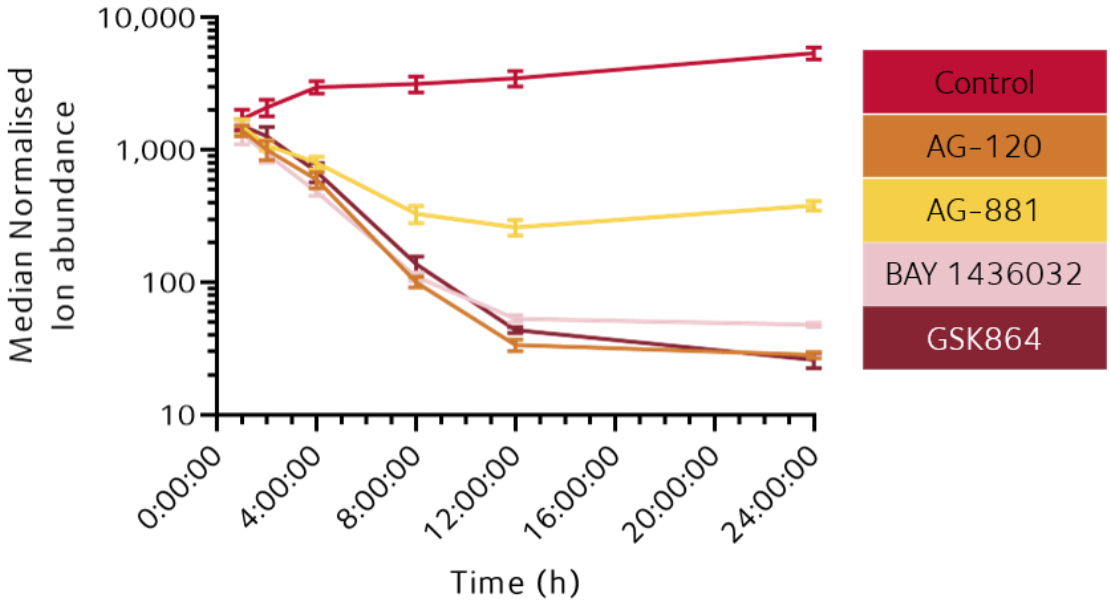

Figure 4.7.1. 2-HG levels in mutIDH1^{R132H} LN18 cells treated with AG-120, AG-881, BAY 1436032 and GSK864 (5.0 µM) for 1, 2, 4, 8, 12 and 24 hours. The number of biological replicates was N = 4 for treated samples and N = 8 for control samples. Data points are mean 2-HG and error bars are one standard deviations.

The difference in 2-HG suppression between AG-881 and the other three inhibitors remained when treatment lasted 48, 72 or 96 hours. The FC of 2-HG was 9.54-24.7 for all timepoints of AG-881 treated cells, while it ranged from 151-349 for AG-120, 69.4-224 for BAY 1436032, and 172-452 for GSK864. FC was calculated as mean 2-HG level in control samples at a specific time point divided by the mean 2-HG level of treated samples at the same time point. All FCs are summarised in **Table 4.7.1.**

Table 4.7.1. FC of mean 2-HG levels between control samples and treated samples at a given timepoint in the L-TICO experiment. Media swaps occurred every 24 hours during incubation. N = 4 for treated samples and N = 8 for control samples. N is separate wells of cells processed and analysed as separate samples.

Media swapped	Timepoint (hours)	FC (control/treated)			
		AG120	AG881	BAY 1436032	GSK864
-	24	210	15.9	110	200
Yes	48	349	16.9	178	281
Yes	72	175	11.9	89.5	172
Yes	96	151	9.54	69.4	176
No	48	243	21.0	213	452
No	72	337	24.7	224	369
No	96	200	20.3	207	362

Changing media every 24 hours did not lead to further decrease in 2-HG abundance in treated cells, as the slope of a linear regression of elapsed time by ion abundance was not significantly different from zero. In cells where media was not swapped during the duration of treatment, 2-HG levels decreased over time (p-value < 0.001, slope of linear regression significantly non-zero). Control samples in both group 1 (swapped media) and group 2 (media not swapped), saw 2-HG levels decrease over time (p-value < 0.0001, slope of linear regression significantly non-zero). Comparing group 1 and 2 cells treated with the same inhibitor revealed that 2-HG abundance was higher in group 1 than group 2 cells (1.17 < FC < 2.94 (group 1/group 2)), except for cells treated with AG-120 at time point 48 hours (FC = 1.29 (group 2/group 1)). The 2-HG abundance for group 1 and 2 are shown in **Figure 4.7.2**.

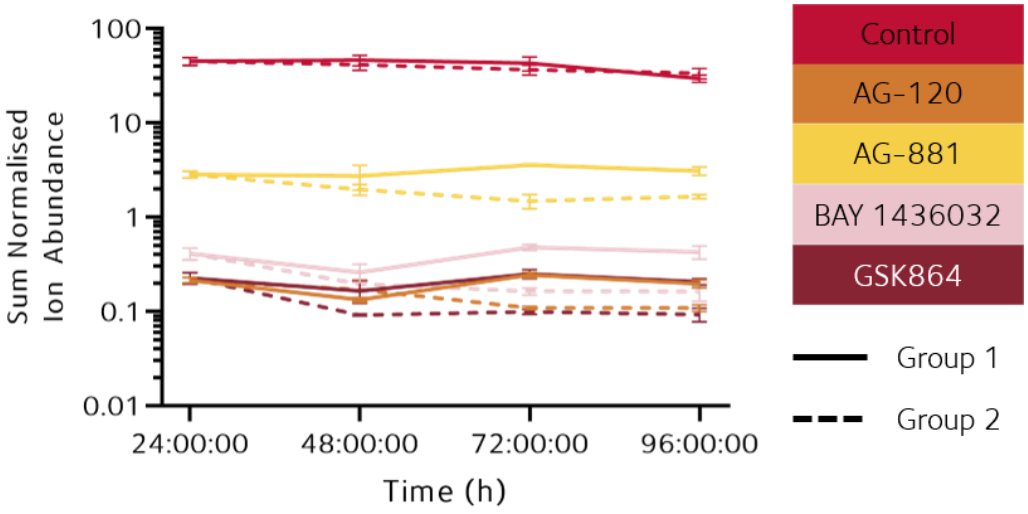

Figure 4.7.2. 2-HG levels in mutIDH1^{R132H} cells treated with AG-120, AG-881, BAY1436032 and GSK864 (5.0 µM) for 24, 48, 72 and 96 hours. Solid lines denote 2-HG abundance in group 1 cell samples and dotted lines denote 2-HG abundance in group 2 cell samples. Timepoint 24 hours was the same set of samples for group 1 and 2. The number of biological replicates was N = 4 for treated samples and N = 8 for control samples. Data points are mean 2-HG and error bars are one standard deviations.

The difference in 2-HG abundance between control and treated cells was far greater than between cells cultured with or without refreshed media. Potential metabolic differences between group 1 and group 2 cells were therefore most likely not due to difference in 2-HG abundance, but rather the effect of replenishing nutrients by renewing media. That was beyond the scope of interest in this chapter, therefore comparisons of group 1 and 2 of metabolites other than 2-HG were not included. Further analysis of L-TICO data was focussed on group 2 because the potential confounding effect of renewing media was not present.

In the S-TICO experiment, there was no significant difference in 2-OG abundance between control and any of the treated samples at any of the timepoints. The abundance of 2-OG increased in all cells from hour 1 to 24, but that was assumed to be due to cell growth, as it was similar for all experimental groups, see **Figure 4.7.3.(a)**. In the L-TICO experiment, cells treated with GSK864 had significantly and appreciably lower 2-OG abundance than control cells at timepoint 48, 72 and 96 hours ($1.52 < FC < 1.74$ (control/treated), p-value < 0.01, unpaired t-test with FDR). The abundance of 2-OG decreased over time in all experimental groups (non-zero slope in linear regression, p-value < 0.001), except cells treated with AG-120, see **Figure 4.7.3.(b)**. In group 1 L-TICO cells, where media was refreshed every 24 hours, 2-OG did not change significantly or appreciably in any of the experimental groups (data not shown). The decrease in group 2 was therefore considered due to limited nutrient availability when cells were incubated for longer than 48 hours total.

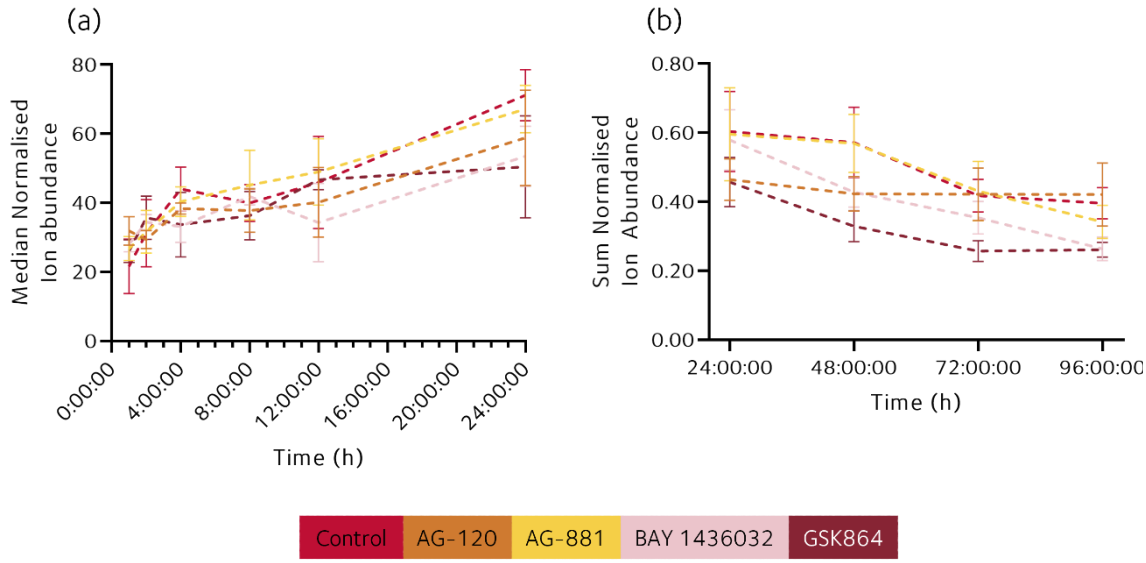

Figure 4.7.3. 2-OG abundance in mutIDH1^{R132H} LN18 cells treated with AG-120, AG-881, BAY 1436032 and GSK864 (5.0 µM) in the S-TICO and L-TICO experiments. (a) S-TICO, timepoints 1, 2, 4, 8, 12 and 24 hours. (b) L-TICO, timepoints 24, 48, 72 and 96 hours. The number of biological replicates was N = 4 for treated samples and N = 8 for control samples. Data points are mean 2-OG and error bars are one standard deviations.

There was no significant difference in isocitrate abundance between the treated and control cells at all timepoints of the S-TICO experiment. Isocitrate increased appreciably and significantly from hour 1 to 24 in control and AG-881 treated cells (FC > 1.4 (hour 24/hour 1) and p-value < 0.05, t-test with FDR), but not in the cells treated with the other inhibitors. Unlike the abundance of 2-OG, which increased throughout, isocitrate levels fell slightly from hour 1 to 4 and did not increase until hour 12 to 24. In the L-TICO experiment, there was an appreciable increase in isocitrate abundance for all treated cells compared to control cells at all timepoints (FC > 1.2 (treated/control). The increase was only statistically significant for the following timepoints and inhibitors: 24 hours, AG-120; 48 hours, AG-881; 72 hours, GSK864; and 96 hours, AG-120, AG-881 and GSK864 (p-value < 0.05, t-test with FDR). Isocitrate abundance decreased in all cells from beginning to end of the time course and experimental groups had linear regressions with significantly non-zero slopes (p-value < 0.01). The overall trend was that of accumulation of isocitrate in treated versus control cells. The isocitrate abundance in the S-TICO and L-TICO experiment are shown in **Figure 4.7.4**.

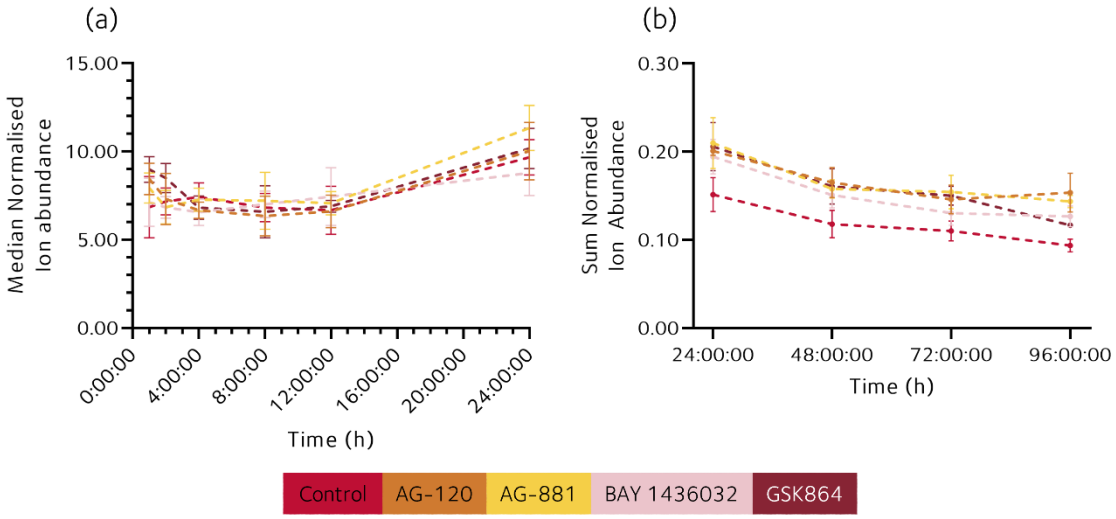

Figure 4.7.4. Isocitrate abundance in mutIDH1^{R132H} LN18 cells treated with AG-120, AG-881, BAY 1436032 and GSK864 (5.0 µM) in the S-TICO and L-TICO experiments. (a) S-TICO, timepoints 1, 2, 4, 8, 12 and 24 hours. (b) L-TICO, timepoints 24, 48, 72 and 96 hours. The number of biological replicates was N = 4 for treated samples and N = 8 for control samples. Data points are mean Isocitrate and error bars are one standard deviations.

Similar to the wtIDH1/mutIDH1 inhibition and concentration range experiments, the decrease in 2-OG and increase in isocitrate in treated cells compared to control cells was small (FC < 2 (control/treated)). The difference in abundance of 2-OG and isocitrate between control and treated cells took 24 hours to establish, compared to 2-HG which became apparent after 2 hours. Of the four inhibitors, GSK864 again was the most effective at decreasing 2-OG abundance, but all inhibitors led to a similar degree of accumulation of isocitrate in treated cells. Potentially the time lag in effect on 2-OG and isocitrate abundance could be due to uptake of inhibitor, *i.e.,* that the concentration was not high enough in the cells to inhibit wtIDH1 until 24 hours of incubation. Or the consequence of limited wtIDH1 activity took longer to become apparent, *i.e.,* the pools of 2-OG and isocitrate took longer to diminish/accumulate due to the metabolites being utilised and supplied by enzymes other than wtIDH1.

In summary, the decrease in 2-HG in treated cells was apparent after 2 hours, but took at least 12 hours for the abundance to equilibrate. In the first 4 hours of exposure, the four inhibitors were similarly capable of decreasing 2-HG abundance. After 4 hours, the difference observed between AG-881 and AG-120, BAY 1436032 and GSK864 was established and remained for the duration of the time course experiments. Refreshing media did not lead to further decrease in 2-HG abundance in treated cells, nor a substantial increase in control cells. There was no significant or appreciable difference between control

and treated cells for the abundance of 2-OG or isocitrate in the first 24 hours of exposure to inhibitor. After 24 hours, 2-OG decreased significantly in cells treated with GSK864 and isocitrate accumulated in all treated cells.

4.8. Cellular uptake and degradation were different for mutIDH1 inhibitors AG-120, AG-881, BAY 1436032 and GSK864

Data processing and analysis

The lack of a correlation between AG-881 concentration and 2-HG abundance, as well as inferior ability to suppress 2-HG over time when compared to the three other inhibitors, was puzzling. In order to rule out that this was not due to lower cell uptake and inhibitor availability in the cells, the cell and media concentration of inhibitor was monitored over a range of concentrations and time. Cell and media samples from the concentration range experiment and the S-TICO and L-TICO experiments were analysed using the underivatised RPLC-MS. Media samples were extracted with acetonitrile to decrease any non-specific protein binding and subsequent loss of small molecules (**section 4.3)**. The sample preparation and analysis are described in **section 2.6.3** and **2.7.3**, respectively.

The four inhibitors had different ionisation efficiencies, therefore to compare the different inhibitors between cell samples or between media samples, a ratio was calculated between the abundance of an inhibitor in biological samples to standard samples. The abundance was measured by peak area of the EIC for each inhibitor, as described in **section 2.8.1**. The cell and media samples were not prepared with the same solvents, therefore different standards were used for each. Cell samples were compared to a solvent-matched (80% $MeOH_{(aq)}$) standard (1.00 µM). The spent media samples were compared to the fresh media samples, which were extracted as described in **section 2.6.3.**

Results: concentration range experiment

In the concentration range experiment, the concentration for all four inhibitors in spent and fresh media increased linearly with significantly non-zero slopes (p-value < 0.0001) and $R^2 > 0.96$, as shown in **Figure 4.8.1.(a)-(d)**. The slope of the linear regression of spent media was noticeably shallower than that of fresh media for AG-120 and GSK864, unlike AG-881 and BAY 1436032 where the gradient was similar. The ratios of inhibitor in spent/fresh media were therefore calculated at each concentration; AG-120 and GSK864 had a ratio of 0.59-0.80, AG-881 a ratio of 0.92-1.03 and BAY 1436032 a ratio of 0.90-1.27. The ratio of AG-120 and GSK864 was significantly lower than the ratios of AG-881 and BAY 1436032 (p-value < 0.05, one-way ANOVA with Tukey's MCT). The difference indicated that there was less AG-120 and GSK864 in media after incubation than for AG-881 and BAY 1436032, which suggested higher uptake into cells or greater rate of degradation. The different ratios are illustrated as box plots in **Figure 4.8.1.(e)-(h).**

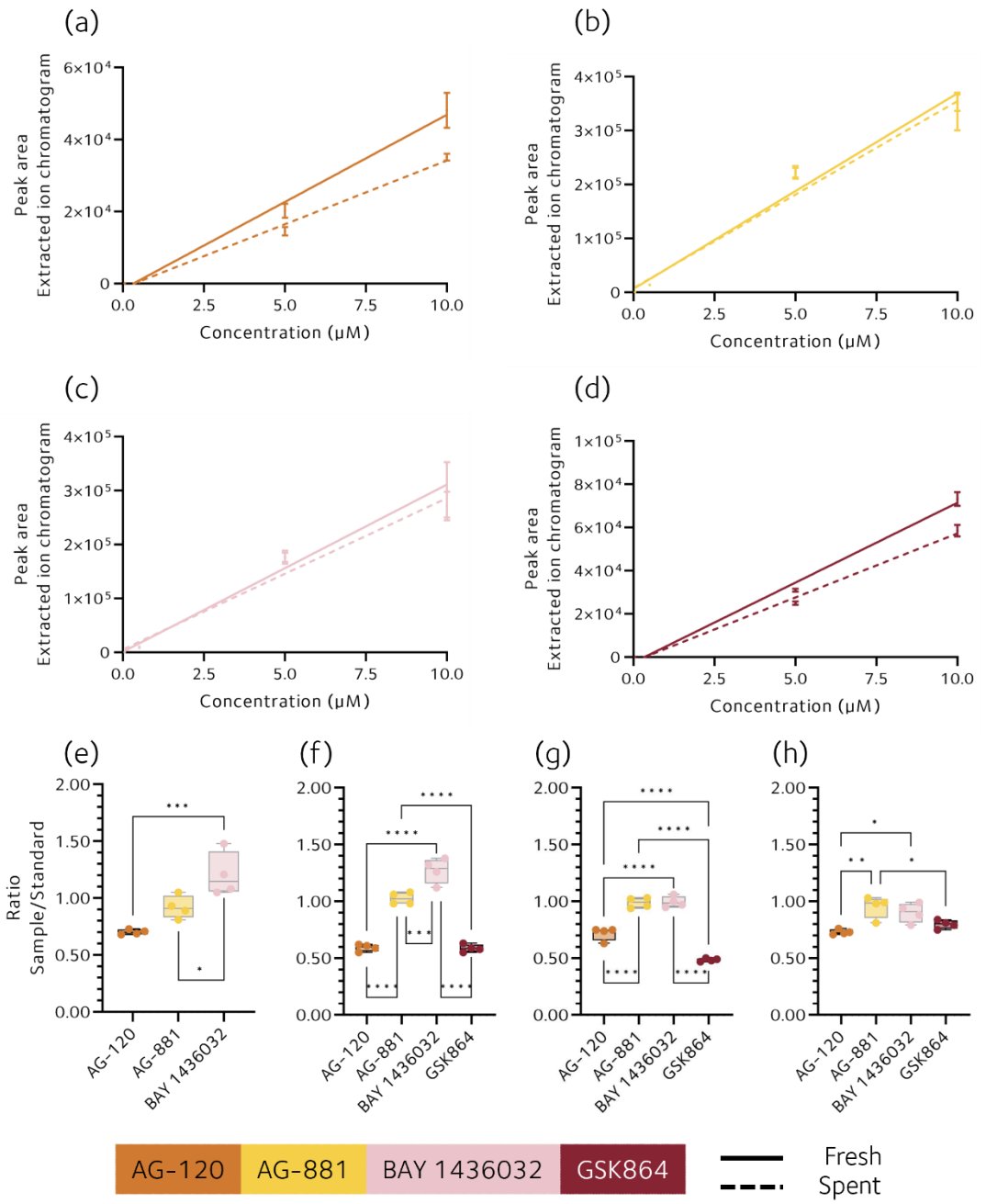

Figure 4.8.1. MutIDH1 inhibitor levels in spent and fresh media in the concentration range experiment. The individual inhibitors and the linear regression of their average EIC peak area are plotted for (a) AG-120, (b) AG-881, (c) BAY 1436032 and (d) GSK864. N = 4 biological replicates for spent media, N = 3 repeat injections of the same extracted sample for fresh media. Each data point is the mean peak area of the inhibitor EIC and the error bar is one standard deviation. Ratio of inhibitor in spent/fresh media are plotted as box plots for (e) 0.05 μM, (f) 0.50 μM, (g) 5.00 μM and (h) 10.0 μM. N = 4 biological replicates for spent media and N = 3 for repeat injections of the same extracted sample for fresh media. Box plot whiskers are the minimum and maximum ratio calculated for each sample, box plot limits are 25th, 50th and 75th percentile. P-values calculated between ratios within a single concentration group with one-way ANOVA and Tukey's MCTe. * = p-value < 0.05, ** = p-value < 0.01, *** = p-value < 0.001 and **** = p-value < 0.0001.

To determine whether cellular uptake was higher for AG-120 and GSK864 than AG-881 and BAY 1436032, the inhibitors were measured in the cell samples. The inhibitors were compared as ratios to their respective standards, as described above. AG-120 had the lowest ratio to standard of all four inhibitors. It was significantly lower than the ratio measured for AG-881, BAY 1436032 and GSK864 at all four treatment concentrations (p-value < 0.05, one-way ANOVA followed by Tukey's MCTe), except to BAY 1436032 at 0.50 µM. AG-881 also had a significantly lower ratio to BAY 1436032 and GSK864 at all concentrations (p-value < 0.05, one-way ANOVA followed by Tukey's MCTe), except for BAY 1436032 at 0.05 µM. Finally, GSK864 had the highest ratio between sample and standard of all the inhibitors, which was significantly higher than all other inhibitors at all treatment concentrations (p-value < 0.001, one-way ANOVA followed by Tukey's MCTe). Despite the difference in cell abundance, all four inhibitors increased linearly in the cells with a significantly non-zero slope (p-value < 0.0001, $R^2 > 0.88$). See **Figure 4.8.2.(a-d)** for the ratios of each inhibitor at the different treatment concentrations.

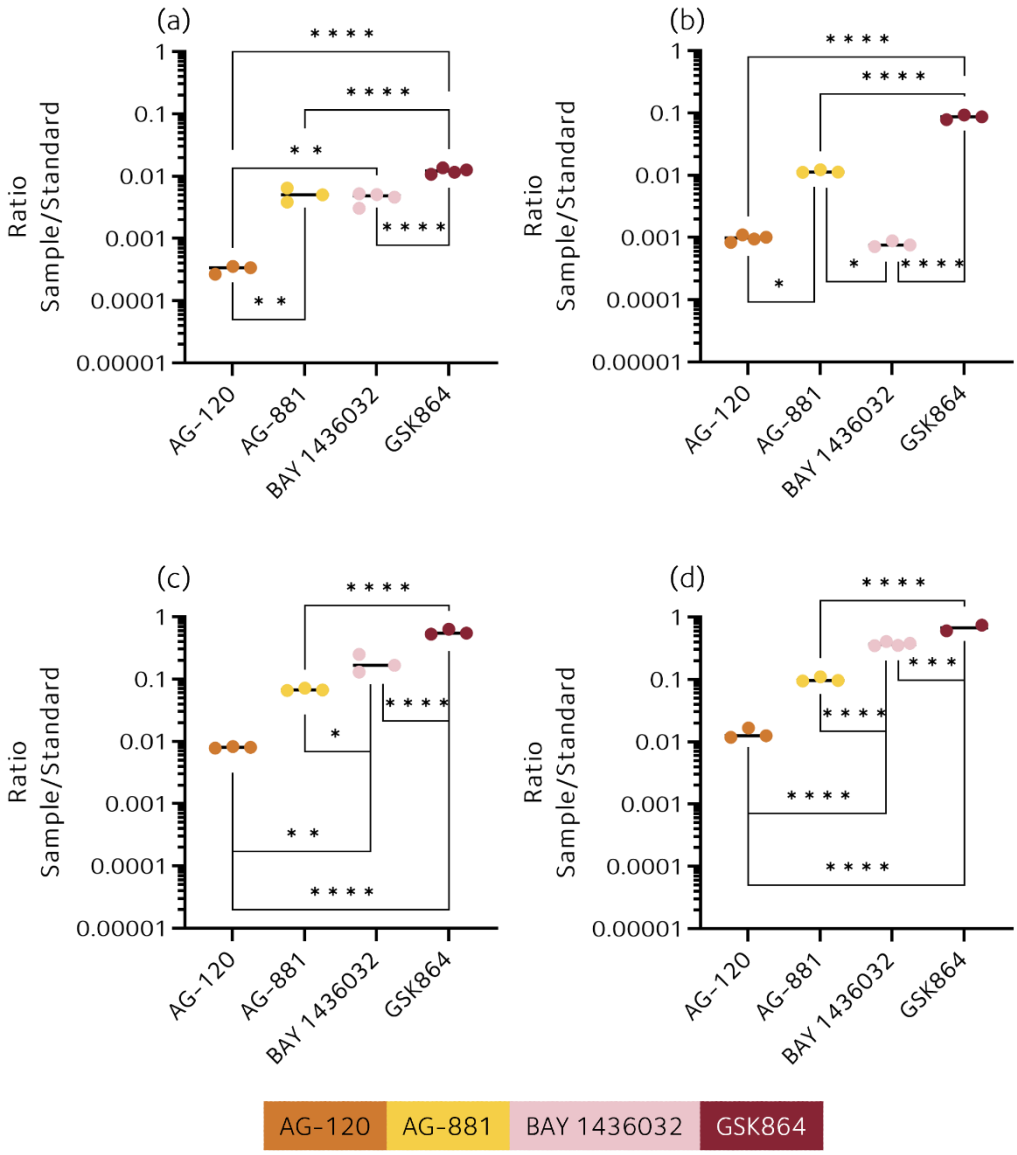

Figure 4.8.2. MutIDH1 inhibitor abundance in the concentration range experiment cell samples as a ratio to a standard (1.00 µM). (a-d) Ratio of inhibitors in cell samples to standard (1.0 µM) for cells treated with the following inhibitor concentrations present in the media: (a) 0.05 µM, (b) 0.50 µM, (c) 5.00 µM and (d) 10.0 µM. Each data point is a singular measurement of inhibitor in cell divided by the mean of the peak are of the inhibitor in the standard. N = 2-4 biological replicates for cell samples and N = 3 repeat injections of the standard (1.00 µM in 80% $MeOH_{(aq)}$). P-values calculated between ratios within a single concentration group with one-way ANOVA and Tukey's MCTe. * = p-value < 0.05, ** = p-value < 0.01, *** = p-value < 0.001 and **** = p-value < 0.0001.

The media samples suggested that AG-120 and GSK864 were either taken up by the cells to a greater extent or degraded more rapidly than AG-881 and BAY 1436032. In the cell samples there was a higher relative abundance of GSK864 than for the other three inhibitors, which indicated that the greater decrease of GSK864 in spent media was due to higher cellular uptake. On the other hand, AG-120 had the lowest relative abundance in cells and that instead implied a greater degree of either active enzymatic degradation or poorer compound stability. AG-881 and BAY 1436032 had similar relative abundance in

cells, between that of AG-120 and GSK864. However, both were present at higher relative abundance in the media samples than AG-120 and GSK864. It was therefore considered unlikely that AG-881 and BAY 1436032 were degrading in the media, and instead the lower cellular abundance relative to GSK864 was either due to poorer uptake or greater enzymatic degradation within the cells.

Finally, the inferior ability of AG-881 in reducing 2-HG levels in treated cells could not be explained by lack of uptake into cells. AG-881 was present in the treated cells at similar relative abundance to BAY 1436032. Furthermore, the inhibitor increased linearly in both media and cell samples. Thus, the lack of concentration dependent relationship between 2-HG and AG-881 was not due to the inhibitor reaching a maximum cellular uptake rate. Instead, it was more likely that there was a difference in how AG-881 interacted with mutIDH1^{R132H} compared to AG-120, BAY 1436032 and GSK864. That difference had to not previously been as apparent in enzyme assays, where IC_{50} values were similar (12-30 nM [246, 247, 250, 416]).

In conclusion, all four inhibitors were present in media and cell samples. The abundance of inhibitor in cell correlated linearly with abundance of inhibitor in media, i.e., exposing the cells to more inhibitor meant that more was taken up by the cells. It was speculated that GSK864 had the highest cellular uptake, while AG-120 degraded to a greater extent than the other inhibitors. AG-881 and BAY 1436032 were not particularly decreased in media samples, therefore their lower cellular abundance than GSK864 was concluded to be due to either lower cellular uptake or greater enzymatic degradation within the cells.

Results: time-course experiments

The inhibitor uptake over time was considered next by investigating the abundance of mutIDH1 inhibitors in the S-TICO and L-TICO experiments. At all timepoints (1-96 hours), AG-120 and GSK864 had lower spent-to-fresh ratio for media samples than AG-881 and BAY 1436032 (see **Figure 4.8.3)**. That was the same trend as observed in the concentration range experiment. In the L-TICO experiment, the level of AG-120, AG-881 and BAY 1436032 did not change significantly over time in either group 1 nor group 2 media (p-value > 0.05, non-zero slope). However, GSK864 levels rose in media over time, in both group 1 and 2 (p-value < 0.05, non-zero slope, R^2 = 0.42 and 0.30), see **Figure 4.8.3(b)**.

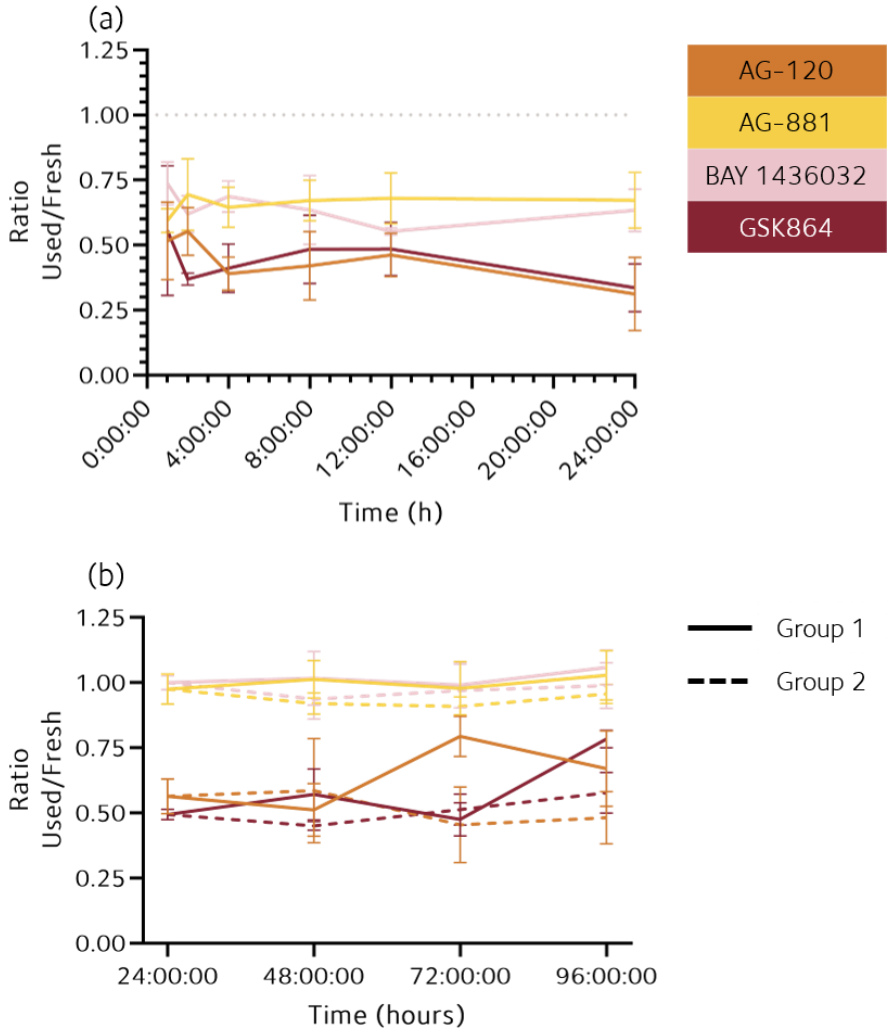

Figure 4.8.3. Ratio between spent and fresh media of mutIDH1 inhibitors in the (a) S-TICO and (b) L-TICO experiment. In (b) solid line is inhibitor level in group 1 (media swapped) and dashed line is inhibitor level in group 2 (media not swapped). MutIDH1 inhibitor concentration in the fresh media was 5.00 µM. N = 4 biological replicates for spent media and N = 3 for repeat injections of the same extracted sample for fresh media. Each data point is the mean of the ratio between spent and fresh media and the error bars are one standard deviation.

The similar ratios between group 1 and 2 showed that refreshing media did not lead to higher or lower levels of inhibitor compared to media placed on cells for the duration of the timepoint. The exception was for AG-120 at timepoint 72 hours, where the ratio of spent-to-fresh media was higher in group 1 than group 2 media. However, the difference at this specific timepoint was likely due to a new fresh media being used, which could potentially have had a slightly different concentration of inhibitor compared to the media

used for timepoints 24 and 48 hours for group 1. The difference between group 1 and 2 for AG-120 was otherwise minimal at timepoints 24, 48 and 96 hours.

In cell extracts, all four inhibitors were detected in samples from the one-hour timepoint onward. The abundance decreased slightly in cell samples incubated for 2 hours, but then increased after 4 hours of incubation and plateaued for the remaining timepoints (8, 12 and 24 hours). The order of lowest to highest ratio to standard (1.00 µM) was AG-120 (0.009 ± 0.002), AG-881 (0.07 ± 0.02), BAY 1436032 (0.11 ± 0.04) and GSK864 (0.21 ± 0.09), see **Figure 4.8.4.** The order was maintained at all timepoints and was the same as in the concentration range experiment.

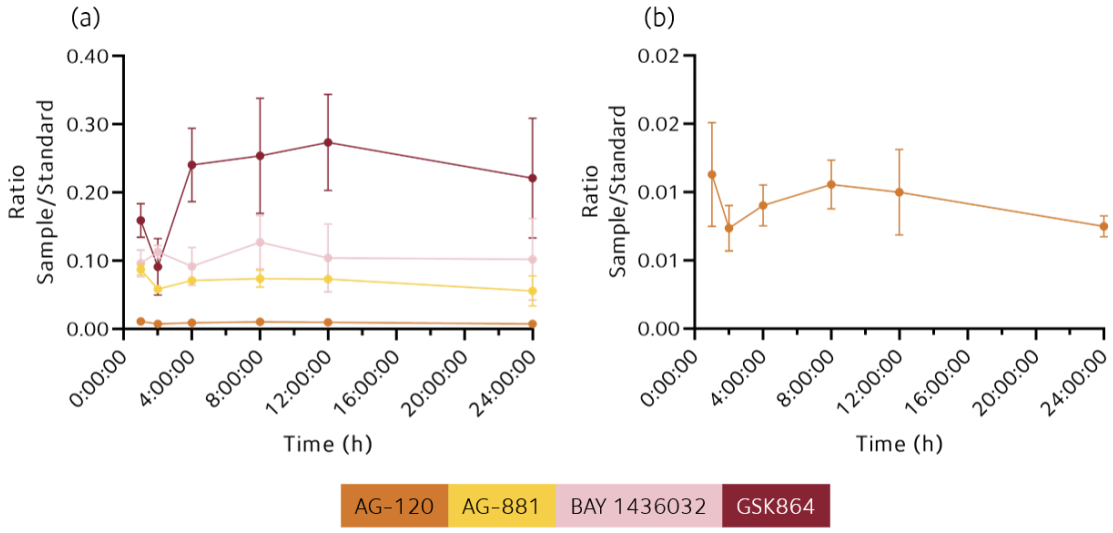

Figure 4.8.4. MutIDH1 inhibitor levels in the S-TICO experiment cell samples as a ratio to a standard (1.00 µM). (a) All four mutIDH1 inhibitors and (b) AG-120 only. The samples and standards were measured with underivatized RPLC-MS. N = 2-4 biological replicates for cell samples and N = 3 repeat injections of the standard (1.00 µM in 80% $MeOH_{(aq)}$). The data points are mean of the ratio of EIC peak area of inhibitor in a cell sample divided by mean EIC peak area of inhibitor in the standard. Error bars are one standard deviation.

The cell and media samples in the S-TICO experiment showed that a maximum abundance of inhibitor was reached after 4 hours of incubation. Subsequently a difference in 2-HG abundance between cells treated with AG-881 and the other three inhibitors was observed. It appeared that the inhibitor abundance in cells had to equilibrate prior to being able to observe a difference in inhibition efficiency. In the L-TICO experiment the lack of substantial change in inhibitor abundance in media, as well as 2-HG abundance in cells, indicated that the abundance of inhibitor remained stable in the cells after 24 hours. The lack of difference

in inhibitor abundance between group 1 and 2 in media samples was expected considering 2-HG abundance was similar in cell samples from both experimental groups.

However, it is of interest that supplying the cells with fresh media did not lead to higher abundance of inhibitor in the cells. It was originally hypothesised that by replacing the media every 24 hours, degraded or metabolised inhibitor would be replaced and inhibition of mutIDH1 would be either maintained or increased. The cells were capable of taking up more inhibitor, because in the concentration range experiment there was a clear correlation between increased inhibitor in media leading to increased inhibitor in cells. Potentially an equilibrium between cells and media was present, whereby refreshing the media with the near-same concentration was not enough to push the cells to take up more inhibitor.

In summary, the four inhibitors differed in abundance present in spent media and in cells. The difference was established after just 1 hour of incubation and remained at 96 hours of incubation. Refreshing media with the same concentration of inhibitor was not enough to push the apparent equilibrium between cells and media. The inferior ability of AG-881 to decrease 2-HG abundance could not be explained by a lack of uptake of inhibitor into cells, as it had similar uptake to BAY 1436032 (a superior inhibitor) across different concentrations and over time (1-96 hours).

4.9. MutIDH1 variant resistant to AG-120 successfully inhibited by allosteric mutIDH1 inhibitor FT2102

The mutIDH1 inhibitor AG-120 was approved by the FDA for treatment of relapsed or refractory AML in 2018 [419]. However, the same year a case study was published where a second site mutation of *IDH1* that conferred resistance to AG-120 was identified [264]. Five additional cases of resistance arising in AML after treatment with AG-120 have since been reported [266, 424]. The mutation leads to a double mutant enzyme (mutIDH1$^{R132H+S280F}$) where the binding affinity of AG-120 to the dimer interface of the enzyme is reduced and the conversion of 2-OG to 2-HG is increased [312]. Resistance has not yet been reported for glioma, but because mutIDH1 inhibitors are being pursued as a therapy for glioma it

was of interest to investigate whether the double mutation could be treated effectively with new inhibitors. Biochemical assays performed by Dr Raphael Reinbold identified three allosteric inhibitors (FT2102, Ds1001b and IDH224) that could overcome the resistance of the double mutant enzyme [312].

Data processing and analysis

The inhibitor FT2102 was compared to AG-120 using three different LN18 cell lines: wtIDH1, single mutIDH1 (R132H) and double mutIDH1 (R132H+S280F), kindly provided by Dr Bardella. The cells were plated in 12-well plates, then treated and harvested as described in **section 2.5.3-2.5.5.** The cells were treated with 5.00 µM AG-120 or FT2102 for 24 hours, control cells were cultured with 0.1% (v/v) DMSO. Supplemented LG DMEM was used throughout. Sample processing was performed as described in **section 2.6.1**. DNA concentrations used for normalisation are provided in **Table A.VII.1** in **appendix VII**. The samples were analysed by IC-MS as described in **section 2.7.1**. The IC-MS data was processed in Progenesis QI (**section 2.8.2**) and 2-HG was identified by comparing retention time (-0.87 min), *m/z* (-0.49 ppm), isotopic similarity (99.8%), and fragmentation pattern (45/100 similarity score) to a known standard, as described in **section 2.8.2**. Ion abundance was measured by integration of the identified peak in Progenesis QI.

Results

AG-120 and FT2102 led to significant and substantial decrease in the abundance of 2-HG in the AG-120-sensitive mutIDH1^{R132H} LN18 cells ($FC_{AG\text{-}120} < 92$, $FC_{FT2102} < 103$, p-value < 0.0001, one-way ANOVA with Šídák MCT). The abundance of 2-HG was significantly decreased by both inhibitors in the AG-120-resistant mutIDH1$^{R132H+S280F}$ LN18 cells (p-value < 0.001, one-way ANOVA with Šídák MCT). The response to AG-120 was far more limited in the resistant cell line, with only a $FC_{AG\text{-}120} < 1.27$ (control/treated). The FC was small enough compared with the effect of AG-120 in mutIDH1^{R132H} LN18 cells that the mutIDH1$^{R132H+S280F}$ LN18 cells was still considered resistant to the inhibitor. The AG-120-resistant cell line responded to FT2102 similarly as the non-resistant cell line: $FC_{FT2102} < 152$ (control/treated). The abundance of 2-HG did not change significantly in the wtIDH1 cells. 2-HG abundance in the three cell lines is summarised in **Figure 4.9.1**.

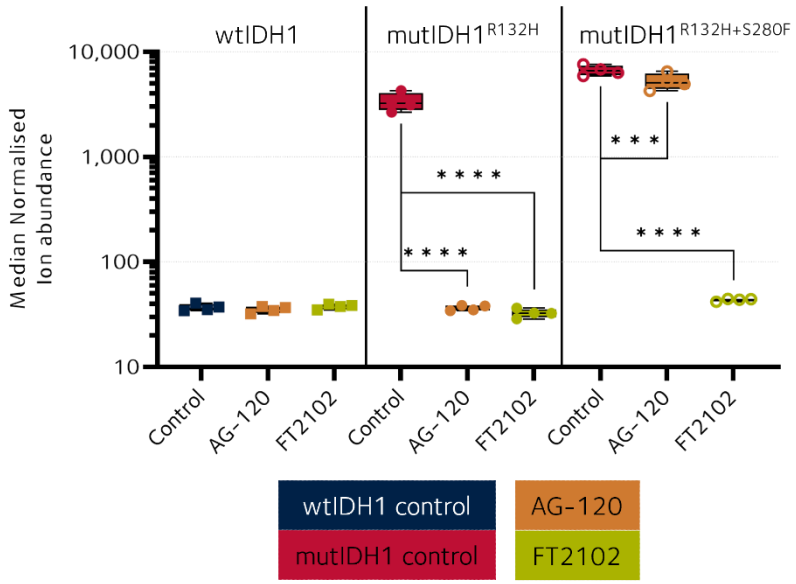

Figure 4.9.1. 2-HG abundance in wtIDH1, mutIDH1^{R132H} and mutIDH1$^{R132H+S280F}$ LN18 cells treated with mutIDH1 inhibitors AG-120 and FT2102. Cells were treated with 5.0 µM AG-120 or FT2102 for 24 hours. Number of biological replicates N = 4 for all experimental groups. Box plot whiskers are the minimum and maximum ratio calculated for each sample, box plot limits are 25th, 50th and 75th percentile. P-values calculated between control and treated within each cell line with one-way ANOVA and Dunnett's MCT. *** = p-value < 0.001 and **** = p-value < 0.0001.

In summary, it was shown that resistance could be overcome by using updated allosteric inhibitors such as FT2102.

4.10. Discussion

Surgery, radiotherapy and adjuvant chemotherapy (usually using alkylating and antineoplastic agents) remain the standard treatment regimen for mutIDH1 glioma [reviewed in 433]. Therapies targeted more specifically to the tumour tissue, to improve survival and decrease side-effects, are needed. The specificity of mutIDH1 to cancer tissue and its apparent role in tumorigenesis, makes it an ideal target for therapeutic intervention. In the past 10 years, several small-molecule mutIDH1 inhibitors have been developed [176, 246, 247, 249, 250, 254, 413-418]. The early clinical trials of the drugs performed in glioma so far have shown that the inhibitors are generally well tolerated, but that improvement in patient survival has been limited [245, 263, 422, 423]. The trials were conducted with patients that had advanced disease, which may have biased the outcome. It remains to be seen how mutIDH1 inhibitors can benefit patients with less advanced disease. At the same time, resistance to the inhibitors has emerged from case studies of AML patients [264-266,

424-426] and cholangiocarcinoma patients [265, 427]. It likely remains only a matter of time before similar reports emerge from the clinical trials of mutIDH1 inhibitors in glioma.

A diverse array of resistance mechanisms have been identified for AML, including second site mutations [264, 266, 424], isoform switching [265], co-occurring mutations [425] or combinations thereof [266]. Second site mutations, where affinity for inhibitor binding is diminished, can be overcome by use of other inhibitors [312], also demonstrated above for FT2102 in the variant of LN18 expressing the AG-120-resistant mutIDh1$^{R132H+S280F}$ enzyme. The diversity of resistance mechanisms, as well as the likelihood of new mutations arising that render cells resistant to *e.g.*, FT2102, means that the search for tractable and effective therapy continues.

To improve upon therapies, a better understanding of the disease at hand and the current therapies available is been needed. The four inhibitors that were investigated in this chapter included an FDA approved drug for treatment of AML and cholangiocarcinoma (AG-120) [419, 421]. Three of the inhibitors were being assessed in phase I/II clinical trials for glioma at the time of selecting inhibitors to pursue (AG-120, AG-881 and BAY 1436032) [238, 263, 422]. None have yet been approved for treatment of glioma. GSK864 was included because of high efficacy in enzymatic and cellular assays, but it appears there are no clinical trials underway. Despite the wide array of inhibitors available for research, the main focus to date in the publications on mutIDH1 inhibitors has been to develop and characterise a specific inhibitor and compare it across different cell lines [246, 247, 250, 415-418]. Alternatively, a single inhibitor was investigated for its ability to decrease 2-HG and cell viability [177, 226]. There have been few studies comparing the various available inhibitors to each other with regards to inhibition efficacy [251, 255, 256], and none that simultaneously compared all four used here.

This study was therefore carried out to gain a better understanding of the relative efficacy of the inhibitors in a cellular environment over a range of concentrations and exposure time. On paper, all four had promising ability to inhibit mutIDH1^{R132H} (IC_{50} 12-30 nM) and were allosteric inhibitors binding in the enzyme dimer interface [246, 247, 250, 416]. AG-120, BAY 1436032 and GSK864 were similar in their ability to decrease 2-HG in mutIDH1^{R132H} LN18 cells, although AG-120 was more effective at the lowest concentrations

of inhibitor (0.05 µM). The reduction in 2-HG abundance in mutIDH1^{R132H} LN18 cells was comparable to that reported for AG-120 in primary mutIDH1 AML cells (99.8% versus 99.7% reduction of 2-HG compared to control, 5.00 µM treatment concentration) [246]. BAY 1436032 performed better in the mutIDH1^{R132H} LN18 cells than in mutIDH1 HEK293 cells (93% versus 70% reduction of 2-HG compared to control, 0.50 µM treatment concentration) [247]. AG-881, however, proved an inferior inhibitor in this study. It was consistently unable to attain similar reductions in 2-HG levels as the other three inhibitors, across concentration ranges and exposure time. It could not be blamed on lack of uptake, as the inhibitor was found in the cells at similar relative abundance as BAY 1436032.

Surprisingly, a comparison of AG-881 to AG-120 and BAY 1436032 in the literature showed that it performed similarly or better than the other two inhibitors. There were two different studies and both used an orthotopic mouse model of U87 with lentiviral mutIDH1^{R132H} expression [255, 256]. AG-881 and AG-120 were similarly capable in reducing 2-HG abundance compared to control samples (reduced 88 and 98%, respectively) [255]. BAY 1436032 was found to be inferior to AG-881 in the second study, only decreasing 2-HG abundance relative to control by 25% versus 58% [256]. The difference in efficacy between AG-881 and BAY 1436032 was also maintained in two patient-derived glioma cell lines [256]. The immediate assumption was that the higher efficacy of AG-881 was due to more of it being taken up by the tumour cells. However, the results presented here showed that increasing the cellular concentration of AG-881 did not necessarily lead to further decrease in the abundance of 2-HG, except an increase from the lowest concentration tested. Potentially the uptake of AG-120 and BAY 1436032 was so poor in comparison to AG-881 that it made up for its lower inhibition efficacy by simply entering the tumour cells more easily.

A time course experiment using multiple inhibitors has not previously been performed. The experiment (spanning 1-96 hours) revealed new information with regards to the efficacy of the inhibitors over time. All four inhibitors had comparable efficacy in reducing 2-HG levels up until the first 4 hours of exposure. That could indicate that it took a similar amount of time for the level of inhibitor to stabilise within the cells. The analysis of cellular uptake of inhibitors supported that hypothesis, as the maximum level of inhibitor in cells was reached at 4 hours. Once the inhibitor concentration had equilibrated in the cells, 2-HG abundance

did not decrease further. The level of inhibitor and abundance of 2-HG could not be easily altered by *e.g.,* refreshing the media. Cells receiving fresh media only had a minor increase in 2-HG abundance compared to cells left in the same media for the duration of their timepoint. It should also be noted that the control cells receiving fresh media did not produce significantly more 2-HG either, despite a continuous supply of nutrients. The resilience to change in 2-HG abundance in the control cells implied that mutIDH1^{R132H} activity was not readily affected by nutrient levels. That could indicate that treatments based on nutrient restriction alone may not be effective, if the goal is to decrease 2-HG by limiting more enzymes than just mutIDH1.

The effect of mutIDH1 inhibitors on 2-OG and isocitrate in wtIDH1 and mutIDH1^{R132H} cells has not previously been reported on in the detail presented here. It was hypothesised that the 'relief' from biosynthesising and accumulating high levels of 2-HG would lead to an increase in 2-OG. Therefore, the lack of increase in 2-OG abundance in mutIDH1 inhibitor treated mutIDH1^{R132H} LN18 cells was surprising. Together with the lack of change in cell viability, it was concluded that 2-OG was re-directed to other reactions. The accumulation of isocitrate was not as consistent as the decrease in 2-HG abundance in mutIDH1^{R132H}. Yet it was present in wtIDH1 cells as well, which indicated that there was enough inhibitor present in the cells at to at least partially inhibit wtIDH1 activity.

4.11. Summary and conclusions

The cellular response to the four allosteric mutIDH1 inhibitors AG-120, AG-881, BAY 1436032 and GSK864 was characterised and the inhibitors were compared to each other. In mutIDH1^{R132H} LN18 cells, all four inhibitors led to a significant and substantial decrease in 2-HG abundance. AG-120, BAY 1436032 and GSK864 demonstrated a clear correlation between increased inhibitor concentration and decreased 2-HG abundance. The inhibition efficacy of AG-881 against mutIDH1^{R132H} was not improved by exposing the cells to higher concentrations, nor incubating them in the presence of inhibitor for longer. The inferior efficacy was not due to lack of cellular uptake, as AG-881 and BAY 1436032 had similar relative abundance in cells. Thus, these experiments revealed that AG-881, within the context of cultured cells, was less effective of an inhibitor compared to AG-120, BAY 1436032 or GSK864. The difference between the inhibitors was greater than enzyme

assays in the literature had indicated. The results presented here therefore demonstrates the importance of comparing inhibitors in multiple model systems for a specific disease.

The time course experiments showed that the inhibitors decreased 2-HG abundance to a similar degree for the first four hours of exposure. It took 4 hours for these inhibitors to reach an equilibrium when measured in cells. 2-HG abundances were considered fully stabilised only after 24 hours of treatment in treated and control mutIDH1^{R132H} LN18 cells. Once stable, 2-HG abundance was not easily altered by refreshing media, not even in control cells. Only increased inhibitor concentration could reduce the intracellular concentration of 2-HG. This indicated that an equilibrium of inhibitor level between cells and media was established. Additionally, the lack of difference in 2-HG abundance between the control cells provided with fresh media and those that were not showed that 2-HG abundance was stable despite the cells facing nutritionally different environments. That could suggest a robustness towards therapies aimed at 'starving' mutIDH1 cancer cells of necessary substrates to biosynthesise 2-HG.

The relatively consistent accumulation of isocitrate in treated cells indicated that the wtIDH1 enzyme was likely inhibited, at least to some extent, by the mutIDH1 inhibitors in both wtIDH1 and mutIDH1^{R132H} LN18 cells. The effect was not as easy to measure as for the inhibition of mutIDH1^{R132H} and warrants further work to fully appreciate whether a concentration dependent effect is also present in wtIDH1 cells. The concomitant inhibition of wtIDH1 and mutIDH1^{R132H} in mutant *IDH1* expressing cells has previously not received much attention, but it will be an important consideration when interpreting changes in wider metabolism after treatment with mutIDH1 inhibitors.

Chapter 5. Exploring the metabolic effects of mutIDH1 inhibitors in wtIDH1 and mutIDH1^{R132H} glioblastoma cells

5.1. Introduction

MutIDH1 glioma metabolism has mainly been studied by comparing wtIDH1 and mutIDH1^{R132H}-expressing primary and immortalised cell lines, PDX mouse models or PTBs [reviewed in 1]. Several different areas of metabolism have been identified as altered in mutIDH1 glioma in previous reports, including aspects of central carbon, amino acid and lipid metabolism, as well as redox homeostasis [reviewed in 1]. The presence of high levels of 2-HG has been directly ascribed as the cause of altered metabolism for *e.g.*, lipids [434, 435], BCAT1 activity [173], and up- or down-regulation of certain metabolites [175]. However, the mechanisms behind many of these metabolic changes remain unclear. Some of these metabolites require 2-OG or NADPH for biosynthesis and are likely affected by either direct inhibition by 2-HG or decreased availability of 2-OG or NADPH. For other metabolites that are altered, but are not thought to require 2-OG or NADPH, the link to mutIDH1 activity and 2-HG abundance remains unclear. Overall, how metabolites and pathways are altered in mutIDH1 glioma models remains poorly understood. To what extent do direct effects (*e.g.*, enzymatic inhibition or lack of substrate) or more indirect effects (*e.g.*, altered gene transcription) initiate the metabolic alterations? Refining the understanding of the influence and role of mutIDH1 in solid cancer metabolism has the potential to provide insight into the tumorigenic activity of the mutation. Furthermore, it could help uncover new therapeutic targets.

Most studies of mutIDH1 inhibitors to date have focussed on the effect on 2-HG abundance and cell viability [165, 176, 177, 246, 247, 250, 252, 253, 416, 436] and specific areas of metabolism [221, 226]. The few metabolic studies on cells treated with mutIDH1 inhibitors have had a narrow scope with regards to metabolite coverage and number of inhibitors compared [174, 255-257]. Comparison of the metabolic changes following treatment with a variety of inhibitors has not been studied in-depth across treatment concentrations or treatment times. Whether the inhibitors lead to similar metabolic changes in treated mutIDH1 cells is therefore not comprehensively understood. Similar and dissimilar

downstream metabolic changes after treatment with different inhibitors would therefore be of interest to study. Similarities between inhibitors would indicate a metabolic change specific to mutIDH1-activity, since all four inhibitors led to a substantial decrease in 2-HG. Secondly, dissimilarities would reduce the number of spurious metabolic changes pursued and potentially help identify 'off-target' effects that could have therapeutic consequences.

WtIDH1 cells have not routinely been included to aid in identifying off-target metabolic changes from those genuinely linked to the activity of the mutant enzyme. The mutIDH1 inhibitors AG-120, AG-881 and GSK864 are capable of inhibiting wtIDH1 activity. A rigorous metabolomics study in which multiple mutIDH1 inhibitors are given to both wtIDH1 and mutIDH1^{R132H} glioma cells would provide a better idea of genuine metabolic responses to mutIDH1 inhibition over other effects by the drugs. True responses to mutIDH1 inhibition could be identified and separated from responses to the inhibition of both wtIDH1 and mutIDH1^{R132H}.

The research aims for this chapter were therefore to:

1. Perform targeted and semi-targeted metabolomics experiments on wtIDH1 and mutIDH1^{R132H} LN18 GBM cells treated with four different mutIDH1 inhibitors (AG-120, AG-881[3], BAY 1436032 and GSK864).
2. Investigate metabolic changes associated with inhibitor treatment in wtIDH1 and mutIDH1^{R132H} LN18 cells.
    a. Identify metabolic changes correlated with 2-HG abundance in mutIDH1^{R132H} LN18 GBM cells.
    b. Identify metabolites that are affected by inhibition of both mutIDH1^{R132H} and wtIDH1.
    c. Explore off-target effects of inhibitor treatment.

[3] AG-881 is a pan mutIDH1 and mutIDH2 inhibitor but will be labelled as a mutIDH1 inhibitor for brevity.

5.2. Multivariate statistical analysis

The metabolic differences between wtIDH1 and mutIDH1 glioma have largely been considered the result of mutIDH1^{R132H} activity and accumulation of 2-HG [reviewed in 1]. The relationship has not been comprehensively interrogated by use of multiple mutIDH1 inhibitors. This section aims to initiate the investigation of that relationship by use of multivariate statistical analyses (PCA, PLS-DA and HCA). The analyses are used to provide a broad and unbiased overview of the data and to help narrow the scope for detailed univariate analysis later on. The following six questions will guide the investigation of the relationship between mutIDH1 activity and wider metabolism:

1) Was mutIDH1^{R132H} cell metabolism brought closer to wtIDH1 cell metabolism after treatment with mutIDH1 inhibitors?
2) Were there metabolites that were only altered in mutIDH1^{R132H} cells after treatment, or in both wtIDH1 and mutIDH1^{R132H} cells?
3) Were there metabolites whose abundance correlated with increased inhibitor concentration/decreased 2-HG abundance?
4) Did the four inhibitors elicit similar concentration dependent metabolic responses in the treated cells?
5) Did metabolite abundance change over time in positive or negative correlation with 2-HG abundance after treatment with mutIDH1 inhibitors?
6) If there was a correlation between 2-HG abundance and other metabolites over time, at what timepoint did it emerge?

The PCA, PLS-DA and HCAs were performed as described in **section 2.8.3**. These multivariate statistical methods were used to examine the degree of similarity between experimental groups and select metabolites of interest. PCA and PLS-DA both reduce data dimensionality and provide a simpler visualisation of the potential relationships between experimental groups and variables (metabolite levels). PCA is unsupervised, i.e., the experimental classifier does not contribute to the model. It can be used when the number of replicates is small (< 10) and was therefore performed for the concentration range and time course experiments. At higher numbers of replicates, the supervised PLS-DA can be used because the risk of overfitting the model is lower. In a supervised analysis, the

experimental classifier is included to e.g., build classifying models or find which features discriminate between experimental groups [437].

It was therefore used for the experiment where wtIDH1 and mutIDH1^{R132H} LN18 cells were treated with mutIDH1 inhibitors. HCA is also an unsupervised method and separates samples based on distance, rather than covariance. HCA was therefore used to complement the PCAs and PLS-DAs in examining similarities and differences between experimental groups. It was also used to identify metabolites with altered abundance between experimental groups that could inform on mutIDH1 metabolism. In all analyses, unidentified features were to ensure a broad and unbiased analysis and to assess whether the metabolic changes occurred beyond the narrower scope of identified metabolites.

5.2.1. MutIDH1^{R132H} LN18 cell metabolism closer to wtIDH1 LN18 cell metabolism after treatment with mutIDH1 inhibitors

Question 1 and 2 stated in the introduction of this section will be considered here. The goal was to inform on which metabolic changes were related to 2-HG only and which were an intersection of mutIDH1 and wtIDH1 activity. The first question was whether the metabolic phenotype of mutIDH1^{R132H} LN18 cells was brought closer to wtIDH1 cells after treatment. If that was the case, then a broad range of metabolic differences were likely diminished by inhibited mutIDH1 activity. The second question was to identify which metabolites only responded to treatment in mutIDH1^{R132H} LN18 cells and which responded in both wtIDH1 and mutIDH1^{R132H} LN18 cells. The former would indicate a relationship to 2-HG only. The latter would indicate a more complex relationship, where metabolite abundance was affected by the interplay of 2-HG, 2-OG and potentially NADPH. The experiment where wtIDH1 and mutIDH1^{R132H} LN18 cells were treated with 5.00 µM mutIDH1 inhibitors (AG-120, AG-881, BAY 1436032 or GSK864) for 24 hours was used to investigate.

Data processing and analysis

The IC-MS data was used for the semi-targeted analysis because it covered a broad range of relevant metabolic pathways, as shown in **Chapter 3**. Data processing and metabolite identification were performed as described in **section 2.8.2**. The IC-MS data yielded 6,645 compound-features (Progenesis QI) and 141 metabolites identifications were made

(86 confident/55 putative). Identified metabolites and identification criteria are outlined in **Table A.II.2** in **appendix II**. One wtIDH1 control sample was not analysed with IC-MS due to an injection error, as mentioned in **section 3.2.** The analysis was not repeated due to limited instrument availability. Filtration, normalisation, transformation and scaling parameters were assessed after outliers were removed, as described in **section 2.8.3**. One further sample was removed prior to data analysis, a wtIDH1 LN18 cell sample treated with BAY 1436032. It was outside the 95% confidence interval in the PCA scores plot (PC1 × PC2), as shown in **Figure A.II.1.(a)** in **appendix II**. This sample had visibly lower abundance across the range of detected features when compared to other biological replicates in the heatmap, it was concluded that an error during DNA normalisation had occurred. The IC-MS data was median normalised and pareto scaled. The normalisation and scaling parameters reduced the small amount of systematic bias observed in the heatmap and led to normal or near-normal feature and sample distribution plots, shown in **Figure A.II.2** in **appendix II**. The number of replicates was high enough (9-20) that PLS-DA could be performed. The PLS-DA and HCA were performed as described in **section 2.8.3**.

Results: PLS-DA

To examine whether there was a difference in the response to treatment between wtIDH1 and mutIDH1^{R132H} treated and control samples, individual PLS-DA models of treated versus control wtIDH1 and mutIDH1^{R132H} LN18 cells for each inhibitor were performed. In all individual PLS-DA models the outcome was similar: separation along component 1 between treated and control. The LOOCV led to R^2 or Q^2 > 0.80 (LOOCV, 5 components) by component 2 for all mutIDH1^{R132H} models, but not the wtIDH1 models. The permutation tests were not significant (p-value > 0.05) for either wtIDH1 or mutIDH1^{R132H} models. Due to the high degree of similarity between the different models, a PLS-DA model where the treated samples were considered a singular group, but still divided by mutational status, was performed instead.

In the scores plot of this 'combined' PLS-DA model (component 1 × component 2), the mutIDH1^{R132H} LN18 control samples were separate from the other three experimental groups along component 1. There was substantial overlap of control wtIDH1, treated wtIDH1 and treated mutIDH1^{R132H} samples, see **Figure 5.2.1.(a)**. The overlap indicated that

the three experimental groups were quite similar metabolically. The permutation test of the resulting PLS-DA model reached significance (p-value < 0.05, 2,000 permutations and prediction accuracy as test statistic), see **Figure 5.2.2.(b)**. However, the cross validation of this model did not reach R^2 or $Q^2 > 0.80$ (LOOCV, 5 components), see **Figure 5.2.2.(c)**. The poor cross validation may be due to the model being unable to distinguish wtIDH1 control, wtIDH1 treated and mutIDH1^{R132H} treated from each other.

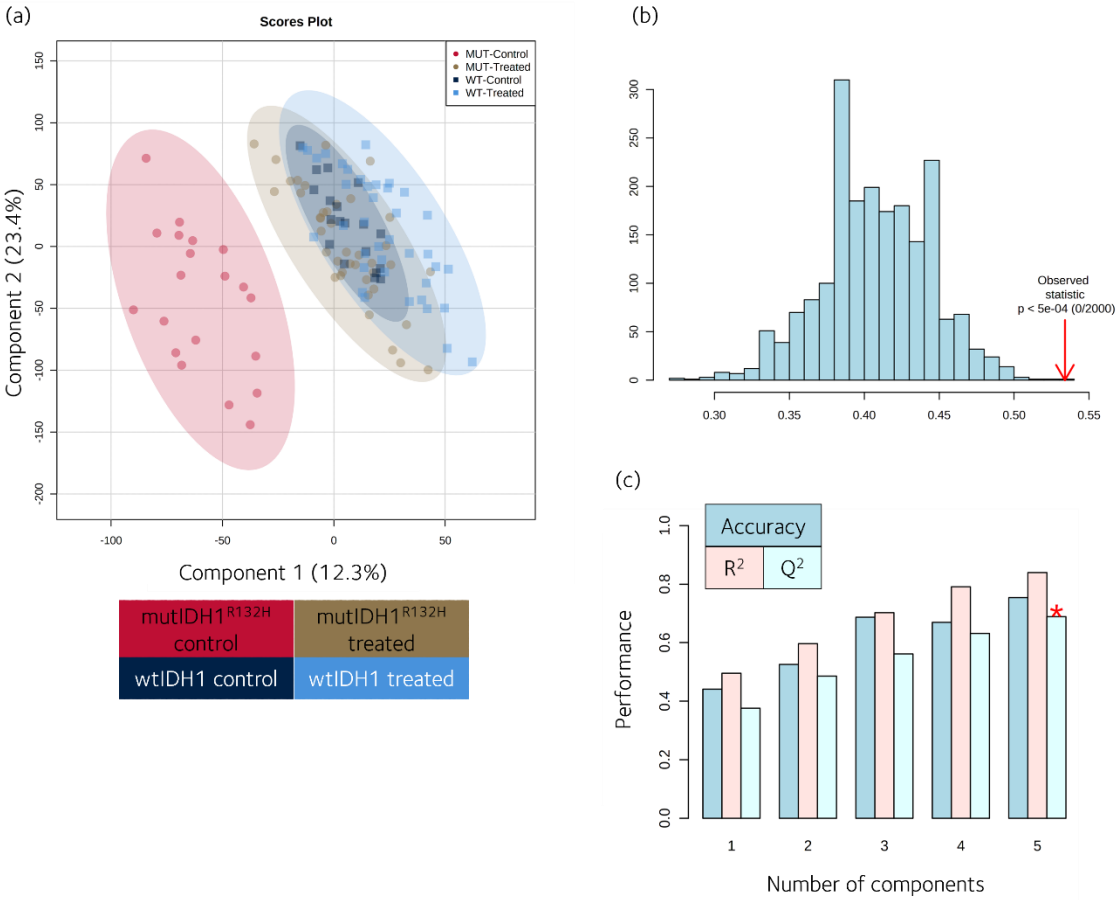

Figure 5.2.1. PLS-DA model of wtIDH1 and mutIDH1^{R132H} LN18 cells treated with mutIDH1 inhibitors versus control cells. (a) PLS-DA scores plot (component 1 × component 2). The number of biological replicates were N = 10 for treated cells, except N = 9 for cells treated with BAY 1436032, N = 19 for control wtIDH1 cells and N = 20 for control mutIDH1^{R132H} cells. (b) Permutation test with prediction accuracy as test statistic and 2,000 permutations. (c) Cross validation and permutation test summary. The cross validation was LOOCV and done for 5 components.

VIP scores were used to assess which identified metabolites contributed the most to the PLS-DA model. Unsurprisingly, 2-HG was the main distinguishing feature in the 'combined' PLS-DA model, with a VIP score nearly three times that of the second highest ranked feature (33.5 versus 11.7), see **Figure 5.2.2.** In the individual PLS-DA models of treated versus control mutIDH1^{R132H} cells, the same difference in VIP score between 2-HG and the second

highest ranked feature was observed. Meanwhile, in the individual PLS-DA models of treated versus control wtIDH1 cells, 2-HG did not have a high VIP score (< 0.20). Therefore, the contribution of 2-HG to the combined model was in separating mutIDH1^{R132H} control from the other three experimental groups.

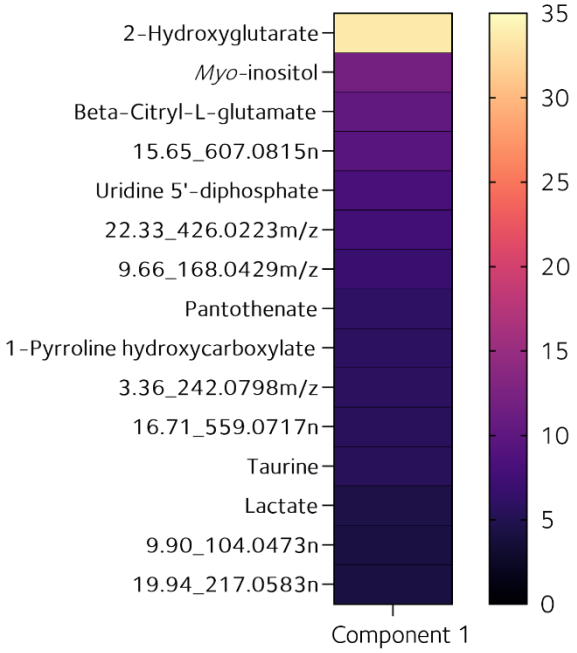

Figure 5.2.2. VIP scores from the PLS-DA model of wtIDH1 and mutIDH1^{R132H} LN18 cells treated with mutIDH1 inhibitors versus control cells. The number of biological replicates were N = 10 for treated cells, except N = 9 for cells treated with BAY 1436032, N = 19 for control wtIDH1 cells and N = 20 for control mutIDH1^{R132H} cells.

In addition to 2-HG, seven identified metabolites had high VIP scores, *i.e.*, were in the top 15 features ranked by VIP score: *myo*-inositol, UDP, B-CG, pantothenate, 1-pyrroline hydroxy-carboxylate, taurine and lactate. Revisiting the individual models, five of these seven metabolites had high VIP scores (> 1.0) in both the wtIDH1 and mutIDH1^{R132H} PLS-DAs. The exceptions were B-CG and pantothenate. Since 2-HG did not contribute significantly to the individual models, it can be inferred that the other metabolites were affected by treatment in general rather the decrease in 2-HG abundance. B-CG was highly ranked by VIP score in all of the individual mutIDH1^{R132H} treated versus control PLS-DA models, but only in the AG-881 treated versus control wtIDH1 model. Thus, B-CG may be more closely correlated to 2-HG abundance rather than the general treatment because 2-HG abundance mainly decreased in the treated mutIDH1^{R132H} LN18 cells.

Pantothenate only had a high VIP score (> 1.0) in the 'combined' model and in a PLS-DA model of treated wtIDH1 versus treated mutIDH1^{R132H}. It did not have a high VIP score (> 1.0) when treated versus control or control versus control were compared in either a mutIDH1 or wtIDH1 model. Its importance in the PLS-DA models of treated cells therefore indicated there was a difference in response to treatment with mutIDH1 inhibitors in

wtIDH1 and mutIDH1^{R132H} LN18 cells. This importance could not be attributed to a difference in 2-HG abundance between the two experimental groups, as it was low in both. Instead, the contribution of pantothenate to the PLS-DA models indicated that there were additional differences between wtIDH1 and mutIDH1^{R132H} LN18 cells in their response to treatment with a mutIDH1 inhibitor.

Results: HCA

The PLS-DA models revealed that after treatment mutIDH1^{R132H} LN18 cells were more similar to wtIDH1 (treated and control) cells and a number of metabolites were altered in both wtIDH1 and mutIDH1^{R132H} cells after treatment. Only B-CG appeared to be closely correlated to 2-HG abundance changes. The IC-MS data was investigated with HCA, maintaining the grouping of samples as treated and control (separated by mutational status), to compare to the 'combined' PLS-DA model. The sample clustering was assessed first; the two major clusters of samples were treated versus control (cluster I versus cluster II), as shown in **Figure 5.2.3**. Within the cluster of control samples (II), mutIDH1^{R132H} samples were entirely separate from wtIDH1 samples, while within the cluster (I) of treated samples, wtIDH1 and mutIDH1^{R132H} samples were mixed. Four of the treated wtIDH1 samples joined in the wtIDH1 control sub-cluster. None of the treated mutIDH1^{R132H} samples clustered with their respective control samples.

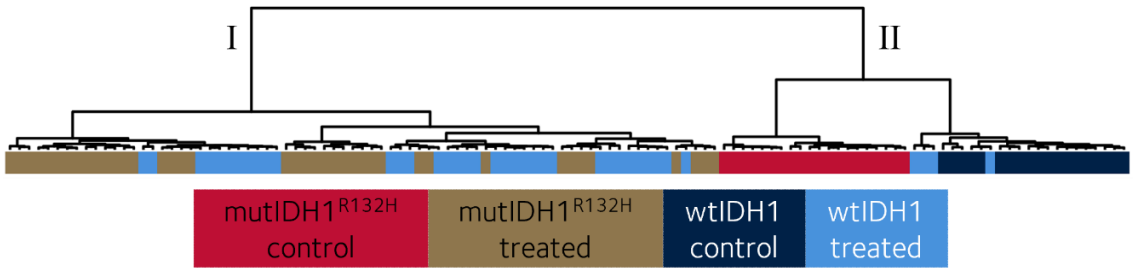

Figure 5.2.3. Hierarchical clustering of treated and control wtIDH1 and mutIDH1^{R132H} LN18 cell sample. Top 50 features ranked by on-way ANOVA with FDR were used and rhe cluster analysis was with Euclidian distance and Ward's linkage method. The data was IQR filtered, median normalised and pareto scaled prior to analysis. Biological replicates were: N = 10 for treated and N = 20 for control samples. Treatment concentration was 5.00 µM and treatment length was 24 hours.

The HCA sample clustering was similar to the separation observed in the PLS-DA, where treated mutIDH1^{R132H} LN18 cells were metabolically closer to treated wtIDH1 LN18 cells than mutIDH1^{R132H} LN18 control cells. Both analyses also showed that there was less of a difference between control and treated wtIDH1 LN18 cells than control and treated mutIDH1^{R132H} LN18 cells. The greater separation of treated and control mutIDH1^{R132H}

samples was likely largely due to the substantial decrease in 2-HG abundance after treatment.

The clustering of the features was assessed without concomitant sample clustering to improve visualisation of difference in abundance of features between the different experimental groups. The two major feature clusters contained either features with either elevated (I) or decreased (II) abundance in mutIDH1^{R132H} control samples, see **Figure 5.2.4**. Within the major cluster with elevated abundance in mutIDH1^{R132H} control samples, two further sub-clusters formed. The first sub-cluster (I.i) included 2-HG and features with the same retention time (9.90 min), all of which had substantially lower abundance in the other three experimental groups. The second sub-cluster (I.ii) included features with elevated abundance in the control cells and decreased abundance in the treated cells, regardless of mutational status. Adenine was the only identified metabolite in this

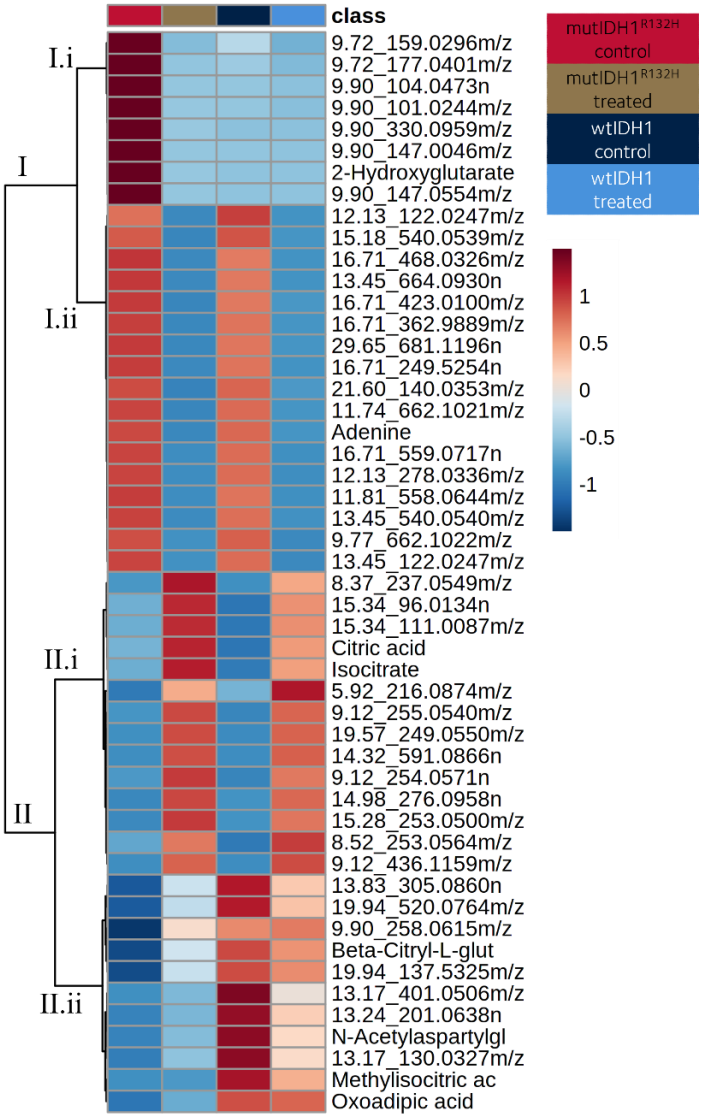

Figure 5.2.4. Hierarchical cluster analysis of top 50 features and identified metabolites from the IC-MS data of control and mutIDH1 inhibitor treated wtIDH1 and mutIDH1^{R132H} LN18 cells. The relative metabolite abundances were averaged for each experimental group. The features and identified metabolites were ranked by p-values from one-way ANOVA. The cluster analysis was with Euclidian distance and Ward's linkage method. The colour bar indicates relative ion abundance. Biological replicates were: N = 39 for treated wtIDH1 samples, N = 40 for treated mutIDH1^{R132H} samples, N = 19 for wtIDH1 control samples and N = 20 for control mutIDH1^{R132H} samples. Treatment concentration was 5.00 µM and treatment length was 24 hours.

sub-cluster, indicating either a wtIDH1 inhibition related effect or an off-target effect by the mutIDH1 inhibitors.

The other major cluster (II) had similar sub-clusters, *i.e.,* where wtIDH1 and mutIDH1^{R132H} control were either similar abundance (II.i) or opposite (II.ii) abundance. In the former, features had increased abundance in both treated wtIDH1 and mutIDH1^{R132H} cells compared to their respective control samples. The sub-cluster included isocitrate and citrate as the only identified metabolites. Accumulation of isocitrate in both wtIDH1 and mutIDH1^{R132H} cells was likely due to inhibition of the wtIDH1 enzyme, as shown in **chapter 4**.

In the latter sub-cluster (II.ii), features had low abundance in control mutIDH1^{R132H} cells and high in wtIDH1 cells. It contained the following identified metabolites: B-CG, NAAG, methylisocitrate and oxoadipate. After treatment with mutIDH1 inhibitors the abundance of the features increased somewhat in mutIDH1^{R132H} cells and decreased somewhat in the wtIDH1 cells. The final sub-cluster (II.ii) therefore contained metabolites which were assumed to be affected by the activity of mutIDH1^{R132H} and/or presence of 2-HG because their abundance was higher in the wtIDH1 than mutIDH1^{R132H} control cells. Additionally, treatment had the opposite effect on the wtIDH1 and mutIDH1^{R132H} cells with regards to change in feature abundance. It indicated that the inhibition of mutIDH1^{R132H} led to an increase in the abundance of the other metabolites. Yet, since decreased abundance was also observed in treated wtIDH1 cells, potentially the inhibition of wtIDH1 played a role in the response as well.

The opposite effect of mutIDH1 inhibition treatment in wtIDH1 and mutIDH1^{R132H} LN18 cells could be explained by 2-HG inhibiting pathways where 2-OG was needed, *i.e.,* upon decreased 2-HG abundance the inhibition relented. WtIDH1 inhibition, on the other hand, would potentially lead to diminished 2-OG availability and decreased metabolic activity of a 2-OG dependent pathway. This explanation would be most sensible for *e.g.,* oxoadipic acid, which is an intermediate in the lysine degradation pathway, where 2-OG is a required substrate. However, neither NAAG, B-CG nor methylisocitrate have a known relationship to 2-OG within their respective metabolic pathways, as discussed in **chapter 3**. Further

evaluation of the metabolites was needed to understand potential correlation to 2-HG abundance and wtIDH1 activity, and this was done by univariate analysis in **section 5.3**.

In summary, mutIDH1 inhibitors brought the metabolic profile of mutIDH1^{R132H} LN18 cells closer to wtIDH1 LN18 cells in both the PLS-DA and HCA. The two analyses also revealed metabolites affected by treatment regardless of mutational status (e.g., adenine, isocitrate and citrate) and metabolites likely affected by the presence of 2-HG in cells (B-CG, NAAG, methylisocitrate, and oxoadipate). Only 2-HG and B-CG were present in both the PLS-DA and the HCA; B-CG was the metabolite with the clearest correlative relationship to 2-HG abundance thus far.

5.2.2. MutIDH1 inhibitor concentration correlated with degree of separation between control and treated samples in PCA and HCA

There are metabolic changes related to 2-HG only and to both mutIDH1 and wtIDH1 activity. To understand them better it was necessary to also assess their correlation to inhibitor concentration and 2-HG abundance. A clear correlative relationship would increase the confidence of the relationship of a metabolite to 2-HG or mutIDH1/wtIDH1 activity. In this section the two following lines of questioning will be considered. First, were there metabolites whose abundance correlated with inhibitor concentration/decreased 2-HG abundance? Second, if a concentration dependent response was present, was it consistent across the four inhibitors or a drug-specific effect? The IC-MS data from the concentration range experiment was used to investigate the two questions. In the concentration range experiment, mutIDH1^{R132H} LN18 cells were treated with 0.05, 0.50, 5.00 or 10.0 µM of AG-120, AG-881, BAY 1436032 or GSK864 for 24 hours.

Data processing and analysis

Data processing and metabolite identification were performed as described in **section 2.8.2.** The IC-MS data had 4,621 features, of which 135 were identified (78 confident/57 putative). The identified metabolites and identification criteria are listed in **A.V.2** in **appendix V**. Data filtration, normalisation, transformation and scaling was carried out as described in **section 2.8.3**. No outliers were identified, and the data was median normalised and autoscaled for multivariate analysis. The normalisation and scaling diminished any small amounts of systematic bias present in the heatmaps and led to

normal or near-normal feature and sample distribution. Heatmaps and distribution plots are provided in **Figure A.V.1** in **appendix V**.

PCA and HCA were performed as described in **section 2.8.3**. PCA was used instead of PLS-DA due to the small number of replicates per treated group (3-4). To compare the different inhibitors, the treated samples were compared to the same set of control samples. Therefore, four different PCAs and HCA were carried out, each with the treated samples of all concentrations of a specific inhibitor and all the control samples.

Results: PCA

In the PCA scores plots (PC1 × PC2), there was separation along PC2 of control and treated samples for all treatment concentrations of AG-881 and high treatment concentrations (5.00 and 10.0 μM) of AG-120, BAY 1436032 and GSK864. The samples treated with lower concentrations (0.05 or 0.50 μM) of AG-120, BAY 1436032 or GSK864 overlapped with control samples. The PCA scores plots are summarised in **Figure 5.2.5**.

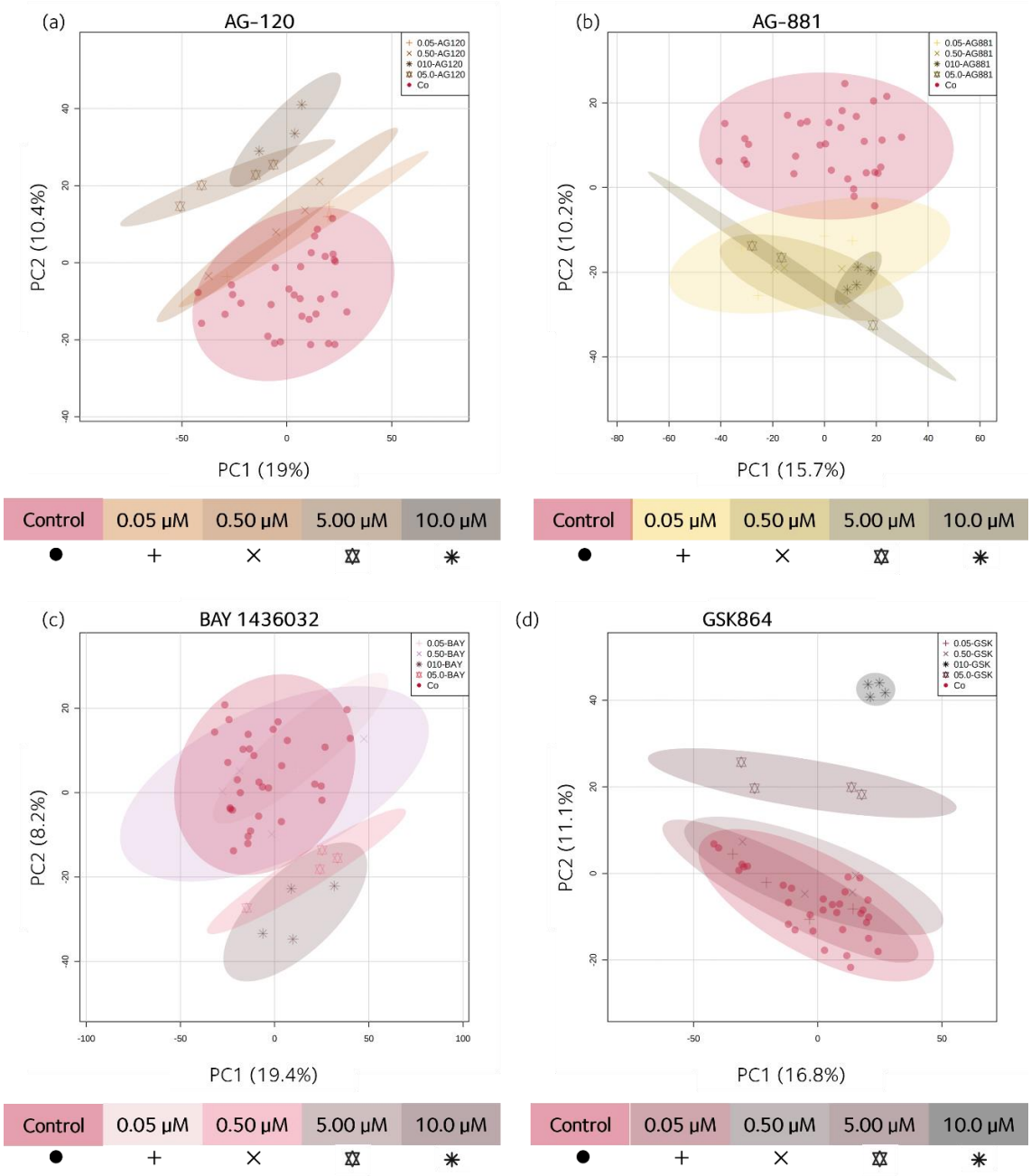

Figure 5.2.5. PCA scores plots (PC1 × PC2) of IC-MS data of mutIDH1^{R132H} LN18 cells treated with a range of concentrations of mutIDH1 inhibitors. All PCA scores plots are made with the same control samples (N = 32 biological replicates). The inhibitor concentrations were 0.05, 0.50, 5.00 and 10.0 µM. The PCA scores plots are carried out for each inhibitor individually: (a) AG-120, (b) AG-881, (c) BAY 1436032 and (d) GSK864. N = 4 for all treated experimental groups, except N = 3 for cells treated with 5.00 µM AG-881.

The PCA scores plots closely followed the trend in 2-HG abundance observed in **section 4.6**. Cells treated with AG-881 had a similar decrease in 2-HG across all treatment concentrations, conversely all treated samples were similarly distanced from the control in the scores plot. The other three inhibitors had a mutIDH1 inhibitor concentration dependent relationship to 2-HG abundance. Subsequently, the distance between control

and treated samples increased with increasing treatment concentration in the scores plot. However, the degree of separation in the scores plots was not only due to 2-HG. The PC2 loadings revealed several additional metabolites with loading scores of similar absolute values to 2-HG. Loading scores indicate the contribution of a feature to the separation of experimental groups. The sign of the loading score for a metabolite showed whether the correlation to the PC was the same or opposite to 2-HG. Metabolites with the same sign and similar magnitude as 2-HG, observed in the PCAs for two or more inhibitors, were *N*-acetyl-L-methionine, DR5P, cytidine, gluconate, and thymidine monophosphate (TMP). Metabolites with similar magnitude, but opposite sign as 2-HG, included B-CG, NAAG, malonate, ethylmalonate, and ophthalmate. By having the same absolute loading score the identified metabolites contributed comparably to the second component as 2-HG. Thus, 2-HG was not the largest or sole contributor to the separation of treated from control samples in the PCAs. The different inhibitors appeared to elicit similar metabolic responses, since several of the metabolites with high absolute loading scores were found in two or more of the PCAs.

Results: HCA

The PCAs were then compared to samples HCAs. In the sample HCAs of AG-120, BAY 1436032 and GSK864, samples treated with 0.05 or 0.50 µM of inhibitor joined the control samples in one of the two major clusters. However, the treated samples did not cluster among the control samples, as shown in **Figure 5.2.6.(a, c, d)**. Samples treated with 5.00 or 10.0 µM inhibitor formed their own major cluster from the first branching point of the HCAs. Only samples treated with AG-881 clustered separately from control samples from the first branching point onward, see **Figure 5.2.6.(b)**.

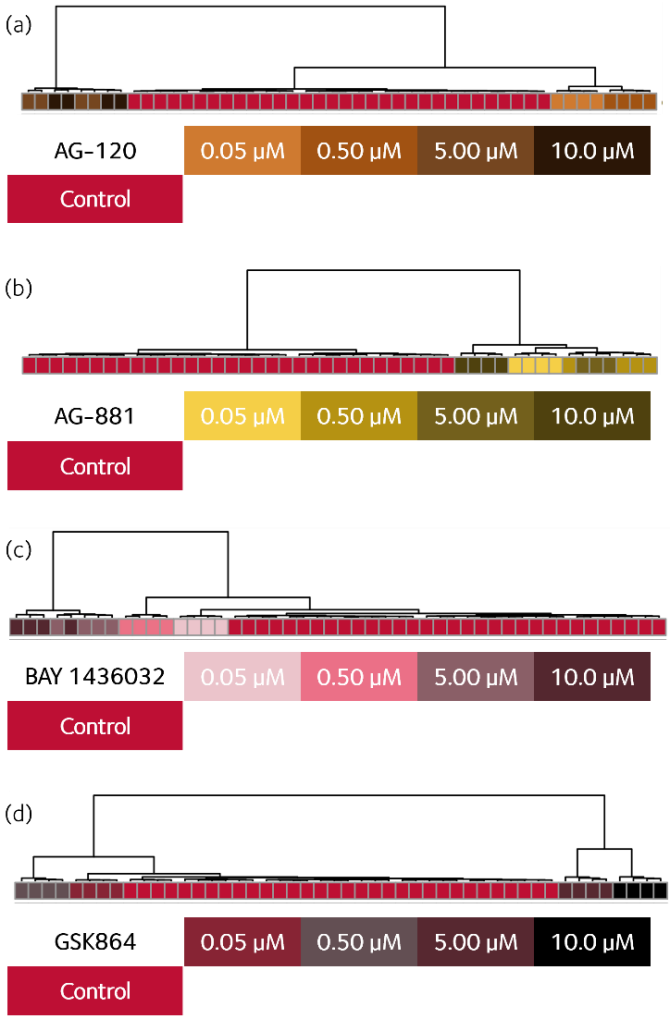

Figure 5.2.6. Hierarchical clustering of mutIDH1^{R132H} LN18 cell samples treated with a range of concentrations of mutIDH1 inhibitors. (a) Samples treated with AG-120, (b) AG-881, (c) BAY1436032 and (d) GSK864. The concentration range for all inhibitors was 0.05, 0.50, 5.00 and 10.0 µM. The top 50 features ranked by One-way ANOVA were used during the cluster analysis, as well as Euclidian distance and Ward's linkage method. Biological replicates were: N = 4 for treated and N = 32 for control samples.

The sample clustering in the HCAs mirrored to some extent the separation observed in the PCAs. All the samples treated with AG-881 at any of the four concentrations did not overlap with control samples in the PCA. In the HCA, the treated samples were separated from control samples at the first branching point. The other three inhibitors only achieved complete separation from control samples in the PCA and HCA for the samples treated with the highest concentrations of inhibitor (5.00 or 10.0 µM). The samples treated with lower concentrations of inhibitor (0.05 or 0.50 µM) overlapped with controls in the PCA but did not fall within the sub-cluster of the control samples. Potentially a metabolic difference was induced already at low concentrations of mutIDH1 inhibitor, which was not as clearly observed in the PCA.

The evidence for metabolic response at low inhibitor concentrations was examined with a feature HCA. The clustering of features was examined without concomitant clustering of samples to make any abundance changes across treatment concentrations easier to observe. The two major clusters were separated based on the metabolite abundance in the control samples. The major cluster with higher abundance in control samples (I) included 2-HG. The abundance of 2-HG decreased in a concentration dependent manner for samples treated with AG-120, BAY 1436032 and GSK864, while samples treated with AG-881 had similar abundance to each other (see **Figure 5.2.7.**).

In the major cluster where metabolite abundance in control samples was low, four distinct sub-clusters formed (II-IV). In cluster II, abundance increased only in samples treated with 5.00 or 10.0 µM of AG-120, BAY 1436032 or GSK864. In **chapter 4**, 2-HG abundance was shown as substantially decreased in those samples (FC > 350 (control/treated)). Taken together, it indicated that the metabolites in cluster II responded to high 2-HG abundance changes only. The response could not be due to wtIDH1 inhibition, as AG-881 was also capable of inhibition at high concentrations (≥ 5.00 µM) (see **chapter 4**). Ethylmalonate, which was present in cluster II, appeared to be more sensitive to 2-HG abundance changes than the other features. It increased in abundance in the treated samples with a $FC_{2\text{-}HG} \geq 12$. Again, wtIDH1 was not the likely explanation because ethylmalate was already increased compared to control cells at 0.05 µM AG-881 and AG-120 which was too low of a concentration to lead to inhibition of wtIDH1, as shown in **chapter 4**.

In cluster III, feature abundance increased most in samples treated with 5.00 or 10.0 µM AG-120 and to some extent in samples treated with 5.00 and 10.0 µM BAY 1436032. The lack of increase in abundance for all inhibitors indicated that the response was not related to $mutIDH1^{R132H}$ or wtIDH1 activity in general, but the specific inhibitors instead. In cluster IV, the abundance increase was the inverse of the decrease observed for 2-HG in cluster I. This indicated a close relationship with 2-HG abundance. B-CG was the only identified metabolite present in this cluster. It has now been likely correlated to 2-HG abundance in two independent experiments.

In cluster V, the feature abundance appeared to correlate with increasing inhibitor concentration in samples treated with AG-120 and AG-881, and to some extent

BAY1436032. Samples treated with GSK864 had an increase in abundance at 5.00 µM inhibitor and then a marked drop in abundance at 10.0 µM. If the metabolic changes in cluster V were due to wtIDH1 inhibition, the lower IC_{50} for wtIDH1 for AG-120 and AG-881 than BAY 1436032 would explain the difference in response to the inhibitors (4-190 nM versus 20 µM [246, 247, 416]). However, the IC_{50} reported for GSK864 in the literature (467 nM [250]) was closer to AG-120 and AG-881 than BAY 1436032. Yet GSK864 did not have a similar trajectory for inhibitor concentration dependent increase in metabolite abundance. Likely there was an off-target effect the other three inhibitors did not exhibit. This effect dominated the changes in feature abundance in cluster V, rather than wtIDH1 inhibition. One exception to the general trend in cluster V was the feature 9.46_140.0119m/z. The abundance increase appeared to correlate with AG-881 and GSK864 concentration. However, the effect could not be considered due to wtIDH1 inhibition, as no concentration dependent response could be observed for AG-120.

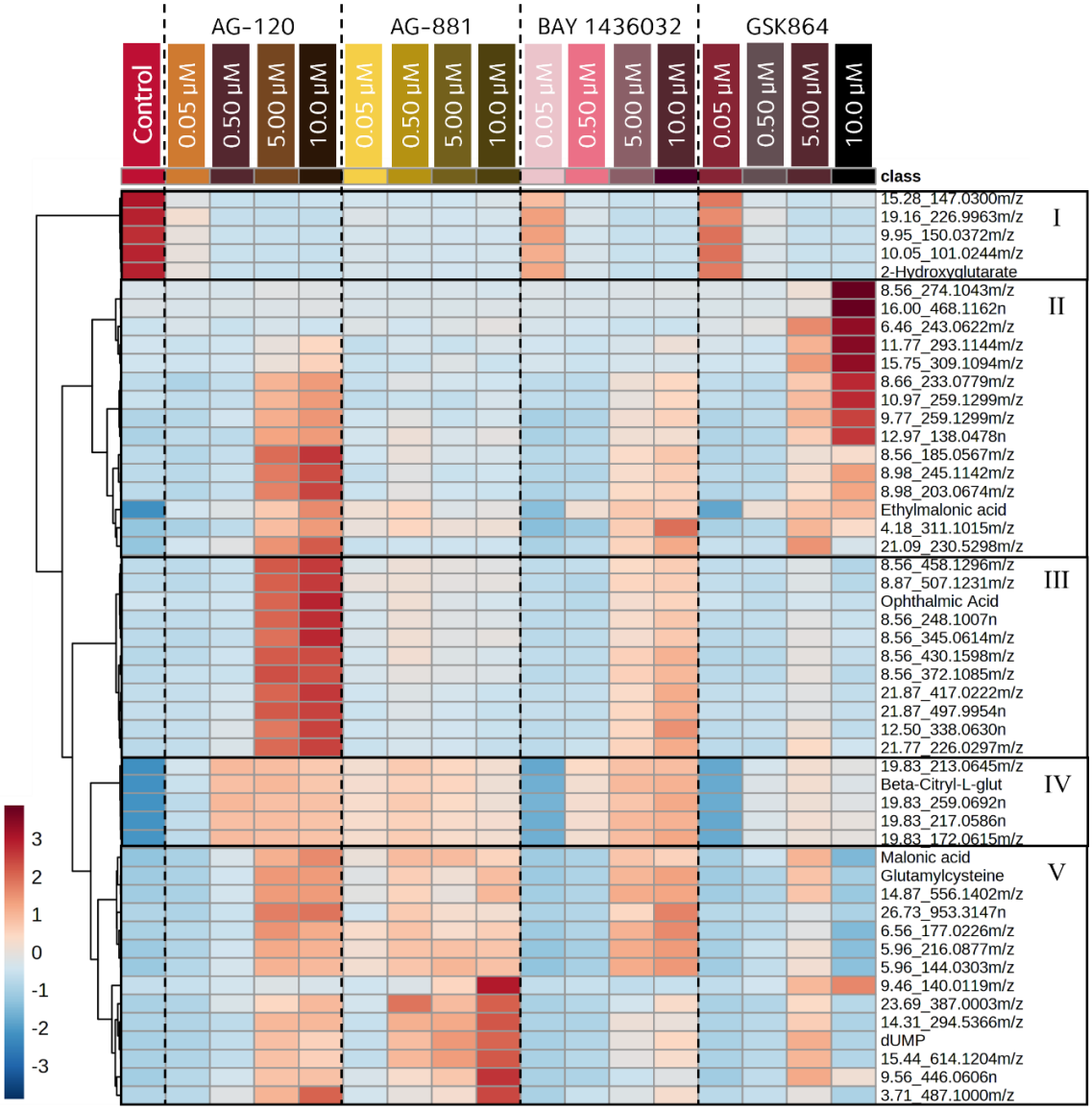

Figure 5.2.7. Hierarchical cluster analysis of top 50 features from IC-MS data of mutIDH1^{R132H} LN18 cells treated with a range of concentrations of AG-120, AG-881, BAY 1436032 and GSK864. I-V denote different sub-clusters of features. Treatment concentration was 0.05, 0.50, 5.00 and 10.0 µM. The features were ranked by One-way ANOVA. The cluster analysis was with Euclidian distance and Ward's linkage method. The colour bar indicates relative ion abundance. N = 32 for control and N = 4 for treated samples, all biological replicates.

The feature HCA revealed that the four different inhibitors elicited both similar and dissimilar responses in wider metabolism. To assess whether there was an overall concentration dependent change in mutIDH1^{R132H} cells upon treatment, the different inhibitors were grouped together into one treated group, now split by inhibitor concentration. A new feature HCA was performed, also as described in **section 2.8.3**. In the first of two major clusters, features and metabolites with high abundance in control

samples were found, labelled I and II in **Figure 5.2.8**. The second major cluster had features and metabolites with the low abundance in control samples (labelled III and IV).

Cluster I contained features that decreased substantially in abundance between control samples and samples treated with 0.05 µM inhibitor. 2-HG was present in this cluster. Cluster II also had an observable difference in abundance between control samples and samples treated with 0.05 µM inhibitor, however the overall decrease in abundance was smaller. To further illustrate the inhibitor concentration dependent decrease, a box plot of DR5P was included in **Figure 5.2.8**. DR5P decreased significantly compared to the control samples even at the lowest concentration of inhibitor (p-value < 0.05, one-way ANOVA with Dunnett MCTe). The relatively sensitive response to low inhibitor concentration indicated a 2-HG dependent effect.

In cluster III, metabolite abundance increased compared to control samples at the lowest inhibitor concentration. Ethylmalonate, B-CG, NAAG and glucuronate were included in this cluster. Investigating B-CG specifically, the abundance was increased significantly compared to control in cells treated with only 0.05 µM inhibitor (p-value < 0.0001 one-way ANOVA with Dunnett MCTe, see **Figure 2.5.8**). The sensitive response indicated a 2-HG dependent effect, as similarly speculated for DR5P. Finally, in cluster IV, abundance increased the most relative to control samples in samples treated with 5.00-10.0 µM inhibitor. Malonate, glutamylcysteine and pyroglutamate were present in cluster IV. The apparent lack of response until higher inhibitor concentration was confirmed for glutamylcysteine. There was no significant difference between control and treated samples at the lowest concentration of inhibitor, but there was a significant increase in glutamylcysteine after treatment with 0.50 µM inhibitor (p-value < 0.001, one-way ANOVA with Dunnett MCT, see **Figure 2.5.8**). Given the response was only significant at higher concentrations of inhibitor, this could indicate that decreased wtIDH1 activity contributed to the altered metabolite abundances. In general, certain features and identified metabolites were dependent on 2-HG abundance (cluster II and IV in **Figure 5.2.7** and cluster II and III in **Figure 5.2.8**) and certain features and metabolites were potentially affected by wtIDH1 inhibited by mutIDH1 inhibitors (cluster V in **Figure 5.2.7** and cluster IV in **Figure 5.2.8**).

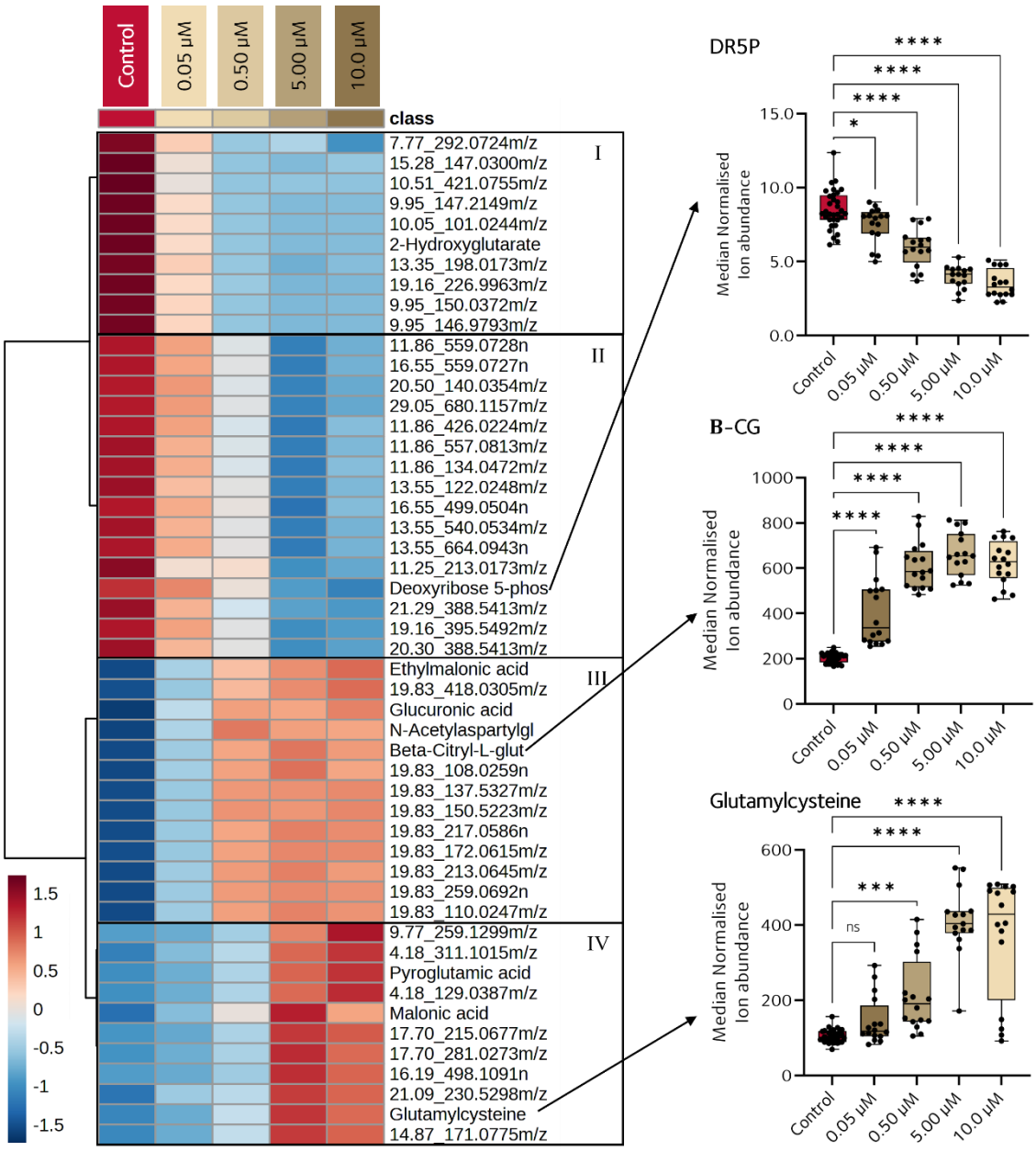

Figure 5.2.8. Hierarchical cluster analysis of top 50 features from IC-MS data of mutIDH1^{R132H} LN18 cells treated with a range of concentrations of mutIDH1 inhibitors (grouped). The relative metabolite abundances were averaged for each experimental group. I-V denote different sub-clusters of features. Treatment concentration was 0.05, 0.50, 5.00 and 10.0 µM. The features were ranked by One-way ANOVA. The cluster analysis was with Euclidian distance and Ward's linkage method. N = 32 for control and N = 16 for treated samples, all biological replicates. The box plots were of specific metabolites from cluster II (DR5P), III (B-CG) and IV (glutamylcysteine). Box plot whiskers are the minimum and maximum ratio calculated for each sample, box plot limits are 25th, 50th and 75th percentile. Significance was calculated with a one-way ANOVA with Dunnett MCT, comparing control to all treatment concentrations. Ns = not significant, * = p-value < 0.05, ** = p-value < 0.01, ** = p-value < 0.001, and **** = p-value < 0.0001.

In summary, the multivariate analyses revealed that the four inhibitors led to some similar and some dissimilar metabolic changes. Samples treated with AG-881 were distinguished from samples treated with the remaining three inhibitors in the PCA and sample HCA. The difference between AG-881 and the other three inhibitors was likely due to the poorer ability of AG-881 to decrease 2-HG and potentially a smaller subsequent effect on wider metabolism. AG-120 and GSK864 led to changes in metabolite abundance which were regarded as off-target effects. Thus, both mutIDH1 activity related and drug-specific related effects were present and care had to be taken in the interpretation of the data. Several metabolites in addition to 2-HG were affected in a concentration dependent manner after treatment with mutIDH1 inhibitors. Ethylmalonate, DR5P, B-CG, NAAG and glucuronate showed the clearest correlation with decreased 2-HG abundance, rather than wtIDH1 inhibition or potentially other off-target effects. Malonate, glutamylcysteine, pyroglutamate and dUMP were potentially affected by wtIDH1 inhibition and not only 2-HG abundance/mutIDH1^{R132H} activity.

5.2.3. Incubation length and exposure time to mutIDH1 inhibitors both inform on cellular metabolic phenotype in the S-TICO and L-TICO experiments

It was now clear that several metabolites had a correlative relationship to 2-HG or had an intersected relationship to both wtIDH1 and mutIDH1 activity. However, it remained unknown when the correlative relationship may have emerged as the previous experiments were just one timepoint (24 hours). When the metabolic change after treatment emerged could inform on the nature of the relationship. Substantial decrease in 2-HG abundance in the S-TICO experiment was first detected after 2 or more hours (see **chapter** 4). Therefore, altered metabolite levels within 1-4 hours of exposure to inhibitor could indicate a direct relationship to 2-HG. If it took 4 ≥ hours to for alterations in metabolites levels to establish, then more distant effects such as changes in transcription levels were more likely. Differentiating the two changes would aid in interpreting the metabolic changes identified thus far. It would also inform on how to best pursue specific metabolites in future work. The IC-MS data from the S-TICO and L-TICO experiments were used. In the experiments, mutIDH1^{R132H} LN18 cells were cultured with 5.00 µM AG-120, AG-881, BAY 1436032 or GSK864 for 1, 2, 4, 8, 12, or 24 hours (S-TICO) or 24, 48, 72 or 96 hours (L-TICO).

Data processing and analysis

Data processing and metabolite identification were performed as described in **section 2.8.2.** The total number of features detected in the IC-MS data was 4,425 and 6,941 for S-TICO and L-TICO, respectively. A total of 137 (79 confident/58 putative) and 143 (89 confident/54 putative) features were identified as metabolites for S-TICO and L-TICO, respectively. Identified metabolites and selection criteria are outlined in **Table A.VI.3-A.VI.4** in **appendix VI**. Data filtration, normalisation, transformation and scaling was carried out as described in **section 2.8.3**. One sample was removed from the S-TICO IC-MS data, a control sample at timepoint 1 hour, because it had lower overall abundance. The sample was known to potentially be an outlier due to being the first sample injected after the analysis sequence was paused because of an instrument error. The S-TICO IC-MS data was median normalised, log transformed and pareto scaled, while the L-TICO IC-MS data was sum normalised and pareto scaled. The normalisation, scaling and transformation parameters were selected as they removed any small amount of systematic bias present in the heatmaps and ensured normal or near-normal sample and feature distribution plot. Heatmaps and sample and feature distribution plots of S-TICO are shown in **Figure A.II.2**, while L-TICO are shown in **Figure A.VI.4**, both in **appendix VI**.

PCA and HCA were performed as described in **section 2.8.3**. The S-TICO and L-TICO IC-MS data had been collected as separate batches; the statistical analyses were therefore performed on each data set individually. The number of replicates per experimental group were low (4-8), and PCA was performed instead of PLS-DA.

Results: PCA

PCAs of the S-TICO and L-TICO IC-MS data were first performed keeping samples treated with different inhibitors as distinct experimental groups. In the scores plots (PC1 × PC2) of the S-TICO and L-TICO data, the different experimental groups of treated samples were significantly overlapped. The overlap remained in PCAs of single timepoints as well. To facilitate the analysis of treated versus control samples, further PCAs of the S-TICO and L-TICO experiments were instead performed with a single 'treated' group per timepoint. In the scores plot (PC1 × PC2) of the 'combined' S-TICO experiment, the treated and control groups overlapped at each timepoint. The only separation of experimental groups was along PC2 of samples from timepoint 24 hours and the rest, see **Figure 5.2.9.(a)**. By

comparison, the treated and control samples had better separation in the scores plot of the L-TICO experiment, see **Figure 5.2.9.(b)**. However, there was still overlap in the 95% confidence regions of treated and control samples. Thus, based on the PCA scores plot (PC1 × PC2) alone, it appeared that incubation length was the major driving force of metabolic difference between experimental groups in the S-TICO experiment. In the L-TICO experiment, a difference between treated and control had become more apparent.

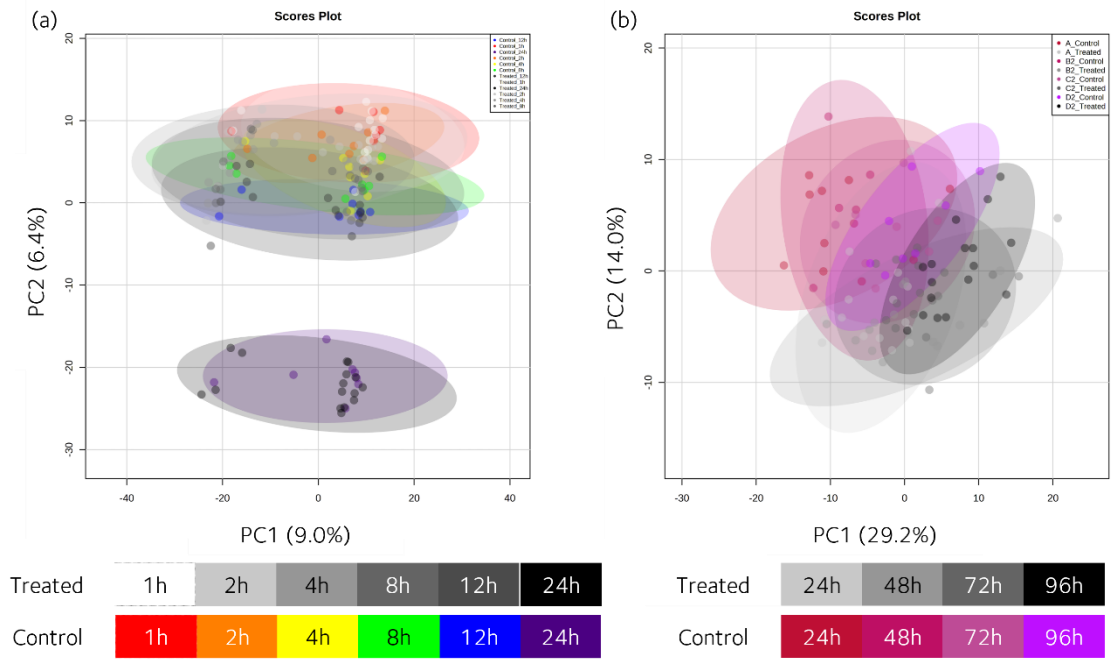

Figure 5.2.9. PCA scores plot of mutIDH1 inhibitor treated and control LN18 mutIDH1^{R132H} LN18 cells in the S-TICO and L-TICO experiments. (a) PCA scores plot of S-TICO experiment, time points 1, 2, 4, 8 ,12 and 24 hours. (b) PCA scores plot of L-TICO experiment, with timepoints 24, 48, 72 and 96 hours. Treatment was with 5.00 µM of either AG-120, AG-881, BAY 1436032 or GSK864. All samples, including control, had 0.1% (v/v) DMSO present in media. Number of biological replicates was N = 4 for treated cells and N = 8 for control cells at each timepoint.

In the concentration range experiment, 2-HG was one of the features contributing substantially to the loadings of PC2, *i.e.,* the component along which treated and control samples were separated. This was not the case for the PCA of the S-TICO experiment. Instead, 2-HG had one-tenth to one-fifth the loading score of the highest-ranking features in PC1 or PC2. None of the other previously identified metabolites of interest (*e.g.,* B-CG, NAAG, UDP or malonate) had high absolute PC1 or PC2 loading scores either. In the L-TICO PCA, 2-HG did contribute substantially to the PC1 and PC2 loading (-0.28 and 0.52, respectively) and was among the top five features based on absolute value of the loading score. Additional metabolites that had high PC loading scores in the L-TICO PC1 and PC2 were glutathione, UDP, B-CG and citrate.

The lower PC loading score of 2-HG in the S-TICO experiment versus the L-TICO experiment was not surprising. It was only after 24 hours that the 2-HG abundance in the treated cells had reached an equilibrium, which was largely maintained in the treated cells in the L-TICO experiment (as shown in **section 4.7** in **chapter 4)**. It is likely that the wider metabolic changes occurring due to mutIDH1^{R132H} inhibition also took time to become established, as those metabolites only contributed to the PC loadings in experiments with a minimum of 24 hours of treatment.

Results: HCA

The HCAs were also performed with all treated samples per timepoint combined into one experimental group. In the sample HCA of the S-TICO data, the major clusters were split based on incubation time. Cluster (I) contained the treated and control samples from the 24-hour timepoint and cluster (II) the other timepoints (1-12h), see **Figure 5.2.10.(a)**. The major clusters reflected the spread of the experimental groups observed in the PCA scores plot in **Figure 5.2.9.(a)**. Within the major clusters, treated samples were separate from control samples from timepoint 4 hours and onward. This indicated there was a metabolic difference emerging between treated and control cells already after 4 hours, something the PCA did not show.

The L-TICO HCA had one major subcluster with the treated and control samples from the 24-hour time point (I), as well as certain replicates from treated samples from later timepoints, see **Figure 5.2.10.(b)**. The other major cluster (II) contained the remaining experimental groups. Within each major cluster, the control groups formed separate clusters from the treated groups. The separation of treated and control mirrored the separation observed in the PCA in **Figure 5.2.9.(b)**. The clear difference between the 24-hour timepoint and the 48-, 72- and 96-hour timepoint indicated that treatment and incubation length also had an effect on metabolic activity.

The decrease in metabolic activity over time could be assessed by re-examining the cell viability assay first described in **section 4.4**. Control and mutIDH1 inhibitor treated mutIDH1^{R132H} LN18 cells were incubated for 24, 48, 72 or 96 hours (experimental details described **section 2.5.3** and **2.7.5**). In the MTS assay, absorbance (*A*) at 490 nm is positively correlated with cell viability [432]. The absorbance of cells incubated for 48, 72 or 96 hours

was 68%, 48% and 46%, respectively, of the absorbance of cells incubated for 24 hours (p-value < 0.001, one-way ANOVA with Dunnett's MCTe). The cells were examined microscopically prior to performing the assay and cell confluency was similar at each endpoint, *i.e.*, a similar number of cells were present when each time-point was measured. DNA concentrations were not measured; thus, the comparison of confluency was qualitative rather than quantitative. The substantial decrease in absorbance over time coupled with similar cell numbers at each time-point indicated metabolic activity in the cells had decreased, which was reflected in the sample HCA as well.

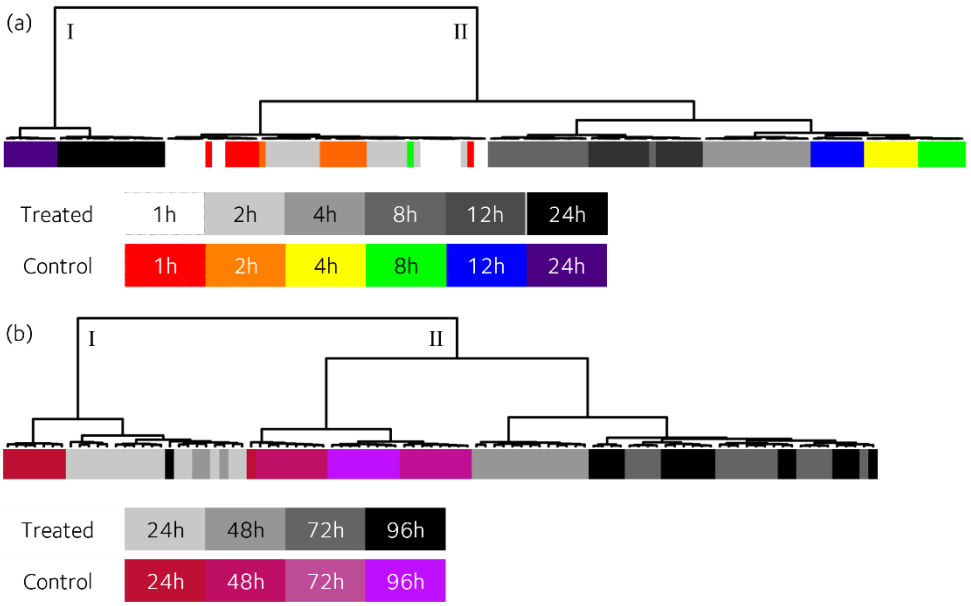

Figure 5.2.10. Hierarchical clustering of mutIDH1 inhibitor treated and control LN18 mutIDH1^{R132H} LN18 cells in the S-TICO and L-TICO experiments. (a) Sample HCA of S-TICO experiment, time points 1, 2, 4, 8 ,12 and 24 hours. (b) Sample HCA of L-TICO experiment, with timepoints 24, 48, 72 and 96 hours. Treatment was with 5.00 µM of either AG-120, AG-881, BAY 1436032 or GSK864 and the treated samples were considered one experimental group with N = 16 biological replicates per timepoint. All samples, including control, had 0.1% (v/v) DMSO present in media. Number of biological replicates for control at each timepoint was N = 8. The top 50 features ranked by One-way ANOVA were used during the cluster analysis, as well as Euclidian distance and Ward's linkage method.

In the feature HCA of S-TICO IC-MS data, the major clusters were metabolites with low abundance from hour 1-12 and then increased substantially by hour 24 (cluster I), or the opposite (cluster II), see **Figure 5.2.11.(a)**. The trend was nearly identical for all features in both treated and control groups, with only a few exceptions. First and foremost, 2-HG started out as elevated in all experimental groups at hour 1 and then continued to increase in control samples for the entire duration of the experiment, including hour 24 (II.i). In the treated samples, the decrease in 2-HG abundance was apparent at earlier timepoints than for other metabolites. In cluster I, B-CG, N-acetylglutamate (NAG), glutamate, and

4-hydroxyproline increased in abundance at an earlier timepoint in treated than control samples. The metabolites also appeared to have a higher 'final' abundance at 24 hours. The difference between the four metabolites in treated and control samples over time indicated a 2-HG-dependent response was occurring in the cells over time.

The first major cluster (I) in the L-TICO HCA included 2-HG and other features where the abundance was high in control samples and low in treated samples at all timepoints, see **Figure 5.2.11.(b)**. The second major cluster (II) had two distinct subclusters. The first (II.i) contained B-CG; the abundance was low in control samples and high in treated samples at all timepoints. The second sub-cluster (II.ii) had features with similar abundance at all timepoints for both control and treated samples; the features started with high abundance at the 24-hour timepoint and then decreased until to the 96-hour timepoint. Isocitrate, citrate, TTP and pantothenate started at a lower abundance in control samples compared to treated samples, and also fell to a lower overall abundance by 96 hours of incubation. The opposite was observed for phosphocreatine, *N*-acetyl-L-methionine and DR5P, *i.e.,* the decrease in abundance from 24 to 96 hours was more apparent for treated than control samples.

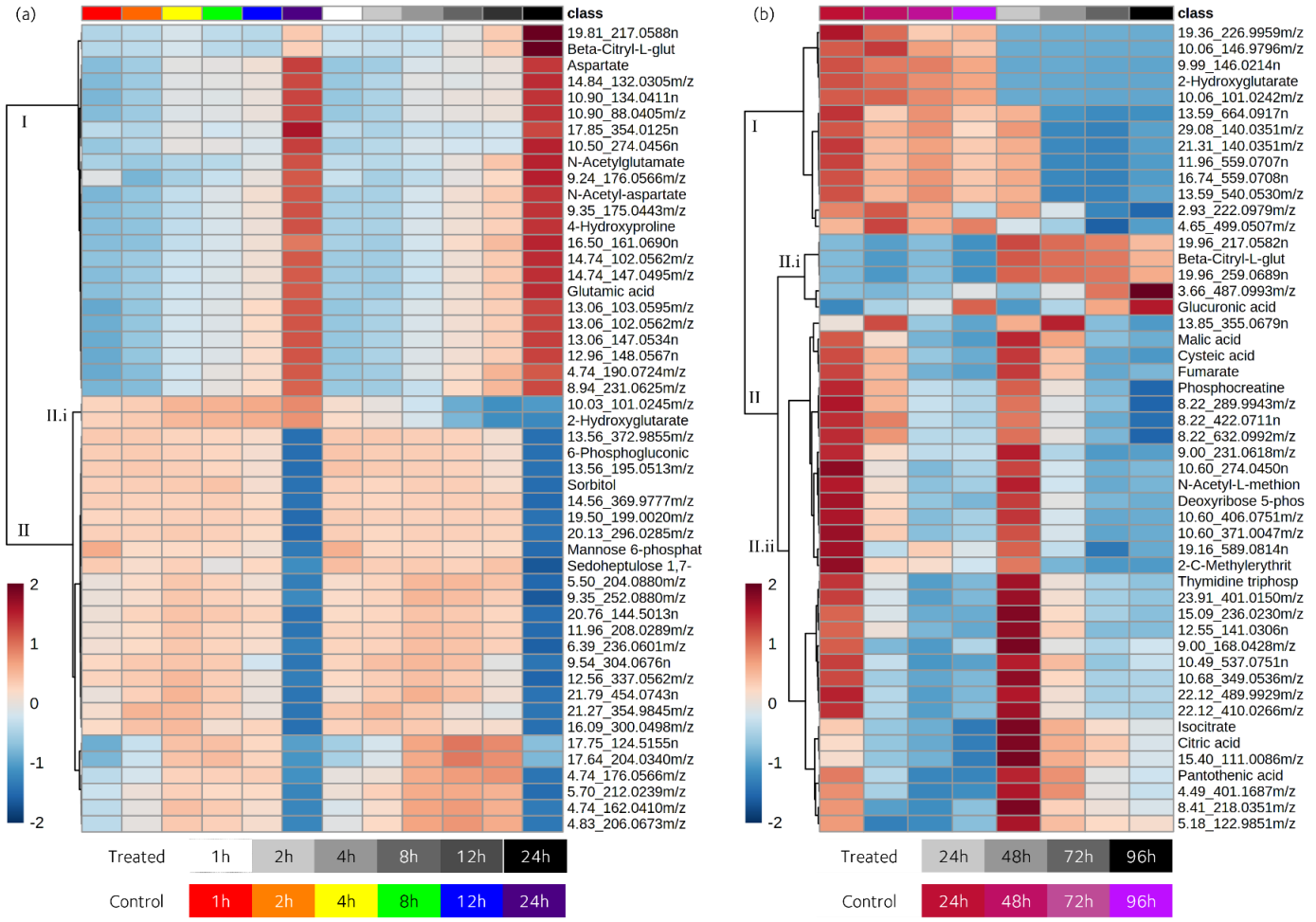

Figure 5.2.11. Hierarchical cluster analysis of top 50 features from IC-MS data of the S-TICO and L-TICO experiments. MutIDH1^{R132H} LN18 cells were treated with 5.00 µM AG-120, AG-881, BAY 1436032 or GSK864 for 1, 2, 4, 8, 12 or 24 hours in (a) and 24, 48, 72 or 96 hours in (b). The treated cells were considered one experimental group per timepoint, with N = 16 biological replicates. The relative metabolite abundances were averaged for each experimental group. Control samples were cells cultured with 0.1% (v/v) DMSO in the media and had N = 8 biological replicates per time point. The features were ranked by one-way ANOVA. The cluster analysis was with Euclidian distance and Ward's linkage method. The colour bars indicates relative ion abundance.

Most metabolite abundances were influenced by incubation time and less so by treatment with inhibitors. It was most apparent in the S-TICO experiment, but the effect of incubation time was also present in the L-TICO experiment. However, the abundance profile of B-CG in both the S-TICO and L-TICO experiment HCAs further underscored the correlative relationship between it and 2-HG that has emerged across all data sets considered in this section. The metabolites glutamate, 4-hydroxyproline, isocitrate, citrate, pantothenate, NAG and TTP also had dissimilar changes in abundance in treated versus control samples, *i.e.*, indicating a correlative relationship to 2-HG and/or inhibitor concentration.

In summary, the multivariate analyses of the S-TICO and L-TICO experiments revealed that incubation time had a substantial impact on the wider metabolism in both control and mutIDH1 inhibitor treated mutIDH1^{R132H} LN18 cells. The effect was most clearly observed in the S-TICO experiment, as it was apparent in both the PCA, sample HCA and feature HCA. In the L-TICO experiment, the effect of incubation and treated versus control was not as easily observed in the PCA, but was apparent in the sample and feature HCAs. Between the PCA and feature HCA, the metabolites B-CG, NAG, NAAG, glutamate, 4-hydroxyproline, TTP, UDP, pantothenate, glutathione, citrate and isocitrate contributed to distinguishing treated from control samples in the S-TICO and L-TICO experiments.

5.3. Univariate statistical analysis of wtIDH1 and mutIDH1^{R132H} LN18 cells treated with mutIDH1 inhibitors

Treatment with mutIDH1 inhibitors led to concentration- and time-dependent wider metabolic changes in mutIDH1^{R132H} LN18 cells. However, several of the same metabolic changes were observed in both wtIDH1 and mutIDH1^{R132H} cell lines after treatment, *i.e.,* certain metabolic changes were not specific to treated mutIDH1^{R132H} LN18 cells. The mutIDH1 inhibitors were present at high enough concentration to likely inhibit wtIDH1 as well as mutIDH1^{R132H}. Therefore, a metabolic response, other than decreased 2-HG abundance, could not exclusively be attributed to inhibition of mutIDH1 activity. The complexities related to inhibition of both wtIDH1 and mutIDH1^{R132H} had to be resolved to be able to reach the aim of a more nuanced understanding of mutDIH1 glioma metabolism. In order to more confidently assign metabolic changes to mutIDH1 activity/2-HG abundance, the ambiguity of wtIDH1 inhibition was reviewed. All identified metabolites from the IC-MS and derivatised RPLC-MS data were surveyed for significant difference between treated and control samples of both wtIDH1 and mutIDH1^{R132H} LN18 cells.

Data processing and analysis

The samples of the three metabolomics experiments described in **section 5.2** were derivatised and analysed by RPLC-MS as described in **section 2.6.2** and **2.7.2**, respectively. Metabolite identification and criteria for confident versus putative identification are described in **Section 2.8.2**. From the derivatised RPLC-MS data, the following number of identifications were made for each experiment: 53 (34 confident/19 putative) for the treated wtIDH1/mutIDH1 experiment; 37 (18 confident/19 putative) for the concentration range experiment; 35 (23 confident/12 putative) for the S-TICO experiment; and 35 (23 confident/12 putative) for the L-TICO experiment. A full list of identified metabolites and identification criteria are provided in **Table A.II.3, A.V.3, A.VI.5** and **A.VI.6**, respectively. The identified metabolites in the IC-MS data set described in **section 5.2** were used. All data sets were median normalised, except the IC-MS data of the L-TICO experiment, which was sum normalised. The normalisation parameter was chosen based on what led to a normal or near-normal sample distribution (see **Figure A.II.3, A.V.2 and A.VI.5**). No scaling or transformation was applied for univariate analysis.

The treated wtIDH1/mutIDH1 experiment was used to identify different metabolites that were significantly and appreciably altered after treatment with a mutIDH1 inhibitor. The treated samples were kept in experimental groups by mutIDH1 inhibitor. It was of interest to determine whether metabolic changes were consistent across the different inhibitors. Two-sided, unpaired t-tests were calculated for all identified metabolites between control samples and each inhibitor in turn, separated by mutational status. FDR was applied to account for multiple comparisons. If the abundance was significantly different (p-value < 0.05, FDR adjusted t-test) between control and treated for a single inhibitor for either the wtIDH1 or mutIDH1 comparison, the FC was calculated. All FCs were calculated as ratios between treated/control, thus an FC below 1.0 would indicate a decrease in metabolite abundance after treatment and a FC above 1.0 would indicate an increase after treatment. FCs between 0.833 and 1.20 were considered too small of a change in abundance to be of interest. Therefore, if the abundance of a metabolite was significantly different between treated and control, but all of the FCs of that comparison fell between 0.833-1.20, it would not be counted as 'significantly and appreciably' different. In addition, the FCs of the treated/control samples were compared to that of wtIDH1 control/mutIDH1 control. The comparison was to assess whether treatment with mutIDH1 inhibitors brought the metabolite abundance in mutIDH1^{R132H} LN18 cells closer to that of the wtIDH1 LN18 cells, *i.e.,* whether the metabolite abundance was 'normalised', after treatment.

CA was used to assess correlation between 2-HG, 2-OG and isocitrate to the other identified metabolites in the concentration range experiment. The analysis was performed as described in **section 2.8.3**. Each CA was calculated per inhibitor across the full treatment concentration range (0.05, 0.50, 5.00 and 10.0 µM) and included the control samples. FC and two-sided, unpaired t-tests with FDR adjustment were performed for the TICO experiments, also as described in **section 2.8.3.** The FC, t-tests calculations for the TICO experiment and the CA of the concentration range experiment were performed to supplement the univariate analysis of the treated wtIDH1/mutIDH1 experiment and will be discussed when relevant.

5.3.1. MutIDH1 inhibitor metabolomics experiment suggests a combination of mechanisms involved in mutIDH1 glioma metabolism

In **chapter 3**, wtIDH1 and mutIDH1^{R132H} LNB18 metabolism was compared and 25 identified metabolites fulfilled the significance and FC criteria outlined above. After treatment, 22 of those metabolites had significantly and appreciably altered abundance for at least one of the inhibitors in either wtIDH1 or mutIDH1^{R132H} LN18 cells. Of the 22 metabolites, six were significantly and appreciably altered exclusively in treated mutIDH1^{R132H} LN18 cells, three exclusively in treated wtIDH1 LN18 cells and 13 in both treated cell types.

The six metabolites that fulfilled the criteria of both being significantly and appreciably different between wtIDH1 and mutIDH1^{R132H} control cells and in one or more treated mutIDH1^{R12H} cells were: 2-OG, dADP, DR5P, oxoadipate, 3M2OV and *N*-carbamoyl-aspartate. The abundance of all of the metabolites, except 2-OG, were 'normalised' upon treatment. Only DR5P and *N*-carbamoyl-aspartate were significantly and appreciably decreased after treatment for more than one of the inhibitors. All three metabolites that were significantly and appreciably different from control in wtIDH1 cells only (glycerate, methionine, isoleucine) were so for a single inhibitor (GSK864 or AG-881). However, isoleucine was appreciably increased for two additional inhibitors (AG-120, BAY 1436032), but the increase did not reach significance (p-value > 0.05, FDR adjusted t-test). Of the 13 metabolites that showed a response to treatment in both wtIDH1 and mutIDH1^{R132H} cells, five were decreased for all responding wtIDH1 and mutIDH1^{R132H} cells: 2-HG, methylisocitrate, IPP, 2-aminoadipate and pipecolate. The remaining eight metabolites had a mixed response, either between wtIDH1 and mutIDH1^{R132H} cells (B-CG, NAAG and B-alanine) or between the inhibitors within the same mutational status (aspartate, cysteine, *N*-acetyl-methionine, *O*-phosphoserine and putrescine). The metabolites, their FC and whether they were significantly different from control cells is summarised in **Figure 5.3.1**.

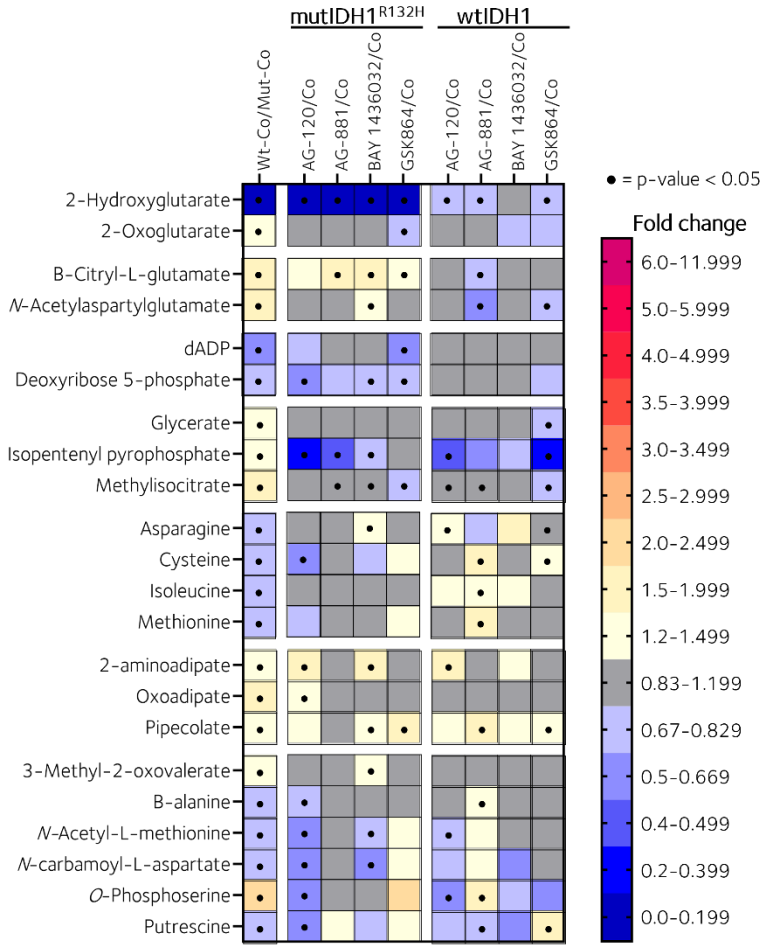

Figure 5.3.1. Metabolites that were significantly different between control wtIDH1 and mutIDH1^{R132H} LN18 cells and also after treatment with one of the mutIDH1 inhibitors (AG-120, AG-881, BAY 1436032 or GSK864). The dot denotes a comparison that had a p-value < 0.05 in a t-test with FDR adjustment. The fold change was calculated between the mean normalised abundances for each comparison. Fold change for control samples was between wtIDH1/mutIDH1 samples and for treated samples it was between treated/control for a specific mutational status.

The changes to metabolite abundance described above had the following three interpretations. First, a metabolite could be considered mainly affected by mutIDH1^{R132H} activity if the abundance of the metabolite was brought closer to that of the wtIDH1 cells in treated mutIDH1^{R132H} cells exclusively. Second, if a metabolite was only affected in wtIDH1 cells after treatment, the inhibition of wtIDH1 potentially had a greater influence than the combined inhibition of mutIDH1^{R132H} and wtIDH1. Or the response to the inhibitor was not apparent at the specific concentration (5.00 µM) used in the experiment the data in **Figure 5.3.1** was from. Third, a metabolite was considered affected by both mutIDH1^{R132H} and wtIDH1 activity if the abundance of the metabolite was decreased or increased in both wtIDH1 and mutIDH1^{R132H} cells after treatment. That was because if a metabolite relied on wtIDH1 activity, either directly for 2-OG or NADPH or indirectly by responding to downstream

outcomes from decreased activity, the same metabolite was likely affected by mutIDH1 activity. MutIDH1 consumes 2-OG and NADPH, and 2-HG has previously been indicated to inhibit 2-OG dependent enzymes [84, 173]. Inhibiting mutIDH1 activity would therefore provide the cells with 'relief' from the use of 2-OG and NADPH, but the concomitant inhibition of wtIDH1 could obscure the decreased utilisation.

DR5P and *N*-carbamoyl-aspartate were 'normalised' in abundance by multiple inhibitors and were therefore considered mainly affected by mutIDH1^{R132H} activity. However, could a response be considered attributable to mutIDH1^{R132H} activity if only one inhibitor led to a response in treated mutIDH1^{R132H} cells, as for *e.g.,* dADP, 3M2OV and oxoadipate? Afterall, all four inhibitors led to a substantial decrease in 2-HG abundance. Similarly, could a metabolic change be attributed to wtIDH1 inhibition if the response was only present for one or two of the inhibitors capable of inhibiting wtIDH1 at the concentrations used in the experiment (AG-120, AG-881, GSK864), as for *e.g.,* glycerate, isoleucine and 2-aminoadipate? Furthermore, there were several metabolites with a mixed response to the mutIDH1 inhibitors in the wtIDH1 and mutIDH1^{R132H} cells, *e.g., O*-phosphoserine, putrescine, B-CG and NAAG. Could the mixed response be attributed to 'relief' from mutIDH1^{R132H} activity, or was it a combined effect of inhibition of wtIDH1 and mutIDH1^{R132H}?

To better understand the effect of the inhibitors, the correlation to 2-HG and 2-OG in the concentration range experiment was quantified by CA [438, 439]. 2-HG and 2-OG had to be used as proxies for mutIDH1 and wtIDH1 activity, respectively, as the experiment had only been performed with mutIDH1^{R132H} LN18 cells due to limited time. The metabolites were appropriate as proxies because 2-HG decreased in abundance at lower concentrations of inhibitor than 2-OG (0.05 and 0.50 µM versus 5.00 and 10.0 µM). Therefore, a considerably higher correlation to 2-HG than 2-OG would indicate a response in metabolites at lower inhibitor concentration, which was inferred as a stronger relationship to mutIDH1^{R132H} activity. Conversely, a similar correlation to 2-HG and 2-OG would indicate activity of both wtIDH1 and mutIDH1 was affected. *N*-carbamoyl-aspartate, IPP, methionine and pipecolate were not identified in the concentration range experiment and therefore only 16 of 20 metabolites could be analysed.

Because 2-HG and 2-OG both decreased in the treated compared to the control cells, a metabolite with positive correlation to either 2-HG or 2-OG would also have decreased abundance, while a negative correlation indicated an increase in abundance after treatment. DR5P, cysteine, NAM and *O*-phosphoserine had positive and significant correlation (FDR adjusted p-value < 0.01) to both 2-HG and 2-OG for two or more inhibitors. The correlation score (CoS) was similar (cysteine, NAM) or slightly higher (DR5P, *O*-phosphoserine) to 2-HG than 2-OG for all inhibitors. B-alanine was positively correlated to both 2-HG and 2-OG, but the effect was only significant in cells treated with GSK864 (FDR adjusted p-value < 0.05). Similarly, isoleucine had a positive correlation to both 2-HG and 2-OG, but it was only significant for 2-HG in cells treated with AG-120 (FDR adjusted p-value < 0.05). There were six metabolites significantly correlated to 2-HG with far less or no correlation to 2-OG: B-CG, NAAG, glycerate, oxoadipate, methylisocitrate and putrescine. The CoS was high (> |0.5|) and significant between two to four inhibitors for B-CG, NAAG, glycerate, oxoadipate and putrescine; methylisocitrate had CS > |0.4|. Finally, 2-aminoadipate, 3M2OV, dADP and asparagine were not significantly correlated to either 2-HG or 2-OG. The correlation scores and whether the relationship was significant are summarised in **Figure 5.3.2** and the exact correlation scores and p-values are provided in **Table A.VIII.1** in **appendix VIII**.

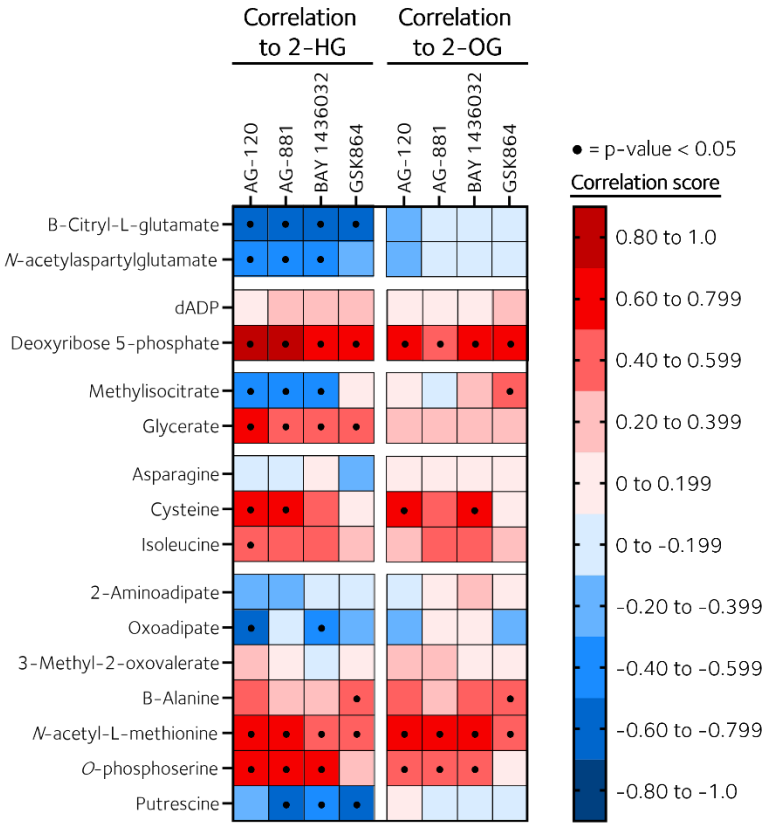

Figure 5.3.2. Heatmap of correlation scores to 2-HG and 2-OG from a selection of metabolites from the concentration range experiment. In the concentration range experiment, mutIDH1^{R132H} LN18 cells were treated with 0.05, 0.50, 5.00 or 10.0 µM of mutIDH1 inhibitors AG-120, AG-881, BAY 1436032 or GSK864. The metabolites were selected because they were significantly different between wtIDH1 and mutIDH1^{R132H} control cells and responded to treatment with one or more of the mutIDH1 inhibitors. The CoSs were separately calculated for each inhibitor and control samples were included. The CA was carried out using Spearman rank correlation as the distance measure. The p-values were FDR adjusted.

Of the metabolites assumed to be affected by mutIDH1^{R132H} activity, but that responded to just one inhibitor in treated mutIDH1^{R132H} cells, only oxoadipate had significant correlation to 2-HG for more than one inhibitor. 3M2OV and dADP had no correlation to either 2-HG nor 2-OG. Therefore, a response from only one inhibitor in a single concentration experiment was an indicator for a lack of a strong response to mutIDH1 inhibition, except for oxoadipate. Glycerate and isoleucine, which had appeared nearly unaffected by mutIDH1 inhibitors, were significantly correlated 2-HG. The exceptions of oxoadipate, glycerate and isoleucine demonstrated the importance of assessing the metabolic response of different inhibitors across a range of inhibitor concentrations.

Further underlining the importance of performing metabolomics across a range of inhibitor concentrations was the fact that DR5P had high correlation scores to both 2-HG ($0.73 < CS < 0.87$) and 2-OG ($0.57 < CS < 0.67$), despite earlier experiments indicating a strong

relationship to decreased 2-HG/mutIDH1^{R132H} activity only. It should be noted that the abundance of both 2-HG and 2-OG decreased and potentially the high CoS for both was simply a consequence of that. However, this was not the case for other metabolites with similarly high CoS, *e.g.,* B-CG and NAAG. The difference in CS between 2-HG and 2-OG for B-CG and NAAG was 0.3-0.5 rather than 0.05-0.3 as for DR5P. Therefore, the correlation analysis refined the understanding of the relationship between DR5P, B-CG and NAAG and mutIDH1^{R132H} activity. DR5P was influenced by the abundance of both 2-HG and 2-OG, while B-CG and NAAG were mostly influenced by the abundance of 2-HG.

The metabolites that responded to treatment in both wtIDH1 and mutIDH1 had a mixed outcome from the CA. Putrescine, B-CG and NAAG demonstrated a clear correlation to 2-HG over 2-OG, while *O*-phosphoserine, NAM and cysteine correlated similarly to both. The mixed results in both the wtIDH1/mutIDH1 treatment and concentration range experiments indicated that the role of *O*-phosphoserine, NAM and cysteine in mutIDH1 glioma metabolism was not straightforward to interpret. Potentially, altered redox homeostasis in the cells contributed to the responses observed, but redox metabolism in treated wtIDH1 and mutIDH1^{R132H} LN18 cells was not measured. It was originally the aim to perform semi-quantitative analysis of the redox metabolites NAD^+, NADH, $NADP^+$ and NADPH. However, this was not possible due to issues with establishing a suitable analysis method (see **chapter 3**).

Another potential explanation for the mixed response to different inhibitors was that instead of direct or one-reaction-removed inhibition of enzyme activity, the expression levels of key enzymes were affected by wtIDH1 and/or mutIDH1^{R132H} inhibition. The time course experiments could yield clues as to which metabolites that would concern, as a delay of at least a couple of hours from treatment to onset of change in expression levels would be expected [440]. Most of the metabolites discussed in this section were not significantly or appreciably different in abundance between treated and control samples in the TICO experiments. Nor were most metabolites discernibly different when abundance was plotted against treatment length. Some metabolites were discernibly, but not necessarily significantly or appreciably, different between treated and control after 48-72 hours of incubation with inhibitor. However, after 72 to 96 hours of incubation cell viability decreased, as shown in **section 4.3**. Changes in metabolite abundance at that stage of the L-TICO experiment could

simply be a response to diminishing cell health rather than a delayed response to treatment with mutIDH1 inhibitors.

The only metabolites, of those presented so far, with a sustained significant and appreciable difference between treated and control mutIDH1^{R132H} cells in the S-TICO and L-TICO experiments were B-CG and NAAG. The difference was apparent from 12 hours onward. The lysine degradation intermediates 2-aminoadipate, oxoadipate and pipecolate had a discernible, but not always significant or appreciable, difference in abundance between control and treated mutIDH1^{R132H} cells from 1-8 hours onwards. The delay of clear and sustained abundance difference of B-CG and NAAG between treated and control cells indicated enzyme expression as an explanation for the metabolic difference to wtIDH1 cells observed for mutIDH1^{R132H} LN18 cells. For the lysine degradation intermediates, both direct or one-reaction-removed inhibition was not unexpected, as 2-OG is a required substrate. However, the delay in discernible difference in abundance of pipecolate between treated and control did not rule out that enzyme expression levels also played a role in the metabolic variations occurring in mutIDH1^{R132H} LN18 cells. Line plots of the abundance of B-CG in the S-TICO and L-TICO experiments and 2-aminoadipate, oxoadipate and pipecolate in the S-TICO experiment are provided in **Figure 5.3.3.**

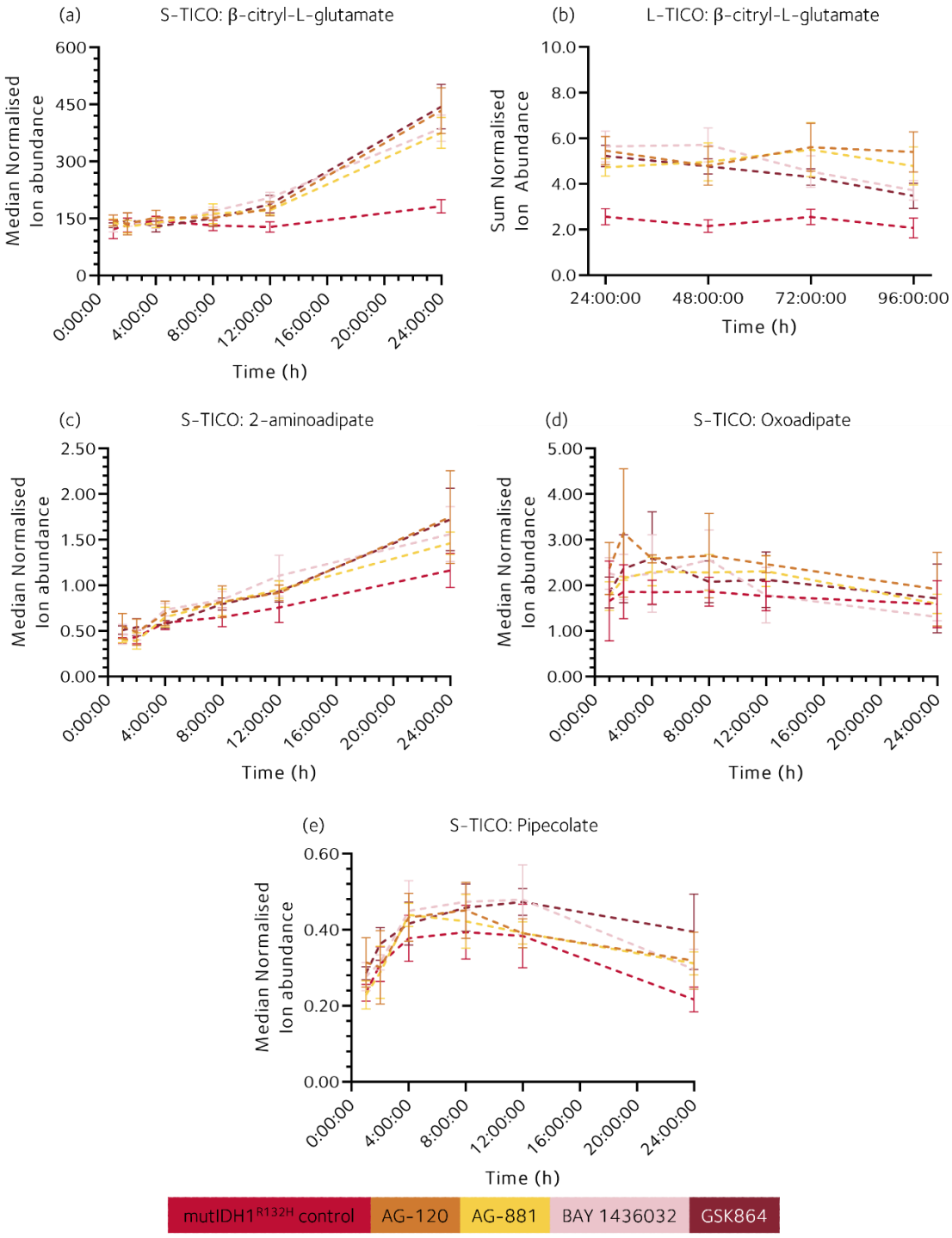

Figure 5.3.3. Line plots of the abundance of B-CG, 2-aminoadipate, oxoadipate and oxoadipate in the TICO experiments. (a) Abundance of B-CG in the S-TICO experiment, (b) abundance B-CG in the L-TICO experiment, and abundance of (c) 2-aminoadipate, (d) oxoadipate and (e) pipecolate in the S-TICO experiment. The mutIDH1^{R132H} LN18 cells were treated with 5.00 µM of AG-120, AG-881, BAY 1436032 or GSK864 for 1, 2, 4, 8, 12 and 24 hours in the S-TICO experiment and for 24, 48, 72 and 96 hours in the L-TICO experiment. Control cells were cultured with 0.1% (v/v) DMSO. Number of biological replicates at each timepoint were N = 4 for treated and N = 8 for control. The data points are mean normalised abundance and the error bars are standard deviation.

In summary, it was not possible to confidently assign the mechanism of action that led to increased or decreased metabolite abundance with the experiments performed thus far. The mutIDH1 inhibitors capable of inhibiting wtIDH1 activity complicated the analysis because mutIDH1 activity could not be independently manipulated. However, the experiments did provide a list of metabolites that are of interest to pursue further, due to their interplay with mutIDH1^{R132H} and wtIDH1 activity. Furthermore, clues as to what had more influence, e.g., 2-HG abundance or decreased wtIDH1 activity in addition to decreased mutIDH1 activity, were found for a number of metabolites. To improve understanding of the role of 2-HG in mutIDH1^{R132H} metabolism, a metabolomics experiment where 2-HG or 2-OG, not both, were decreased without wtIDH1 and mutIDH1^{R132H} activity concomitantly affected is needed. The experiment would then allow for one aspect of mutIDH1 metabolism (2-HG or 2-OG abundance) to be probed. That experiment was performed and can be found in ***Chapter 6****. Future work should also include measuring redox metabolites and determining whether redox homeostasis was altered by treatment with mutIDH1 inhibitors. This could provide further clues as to how and why specific metabolites are affected by the* IDH1 *mutation. Furthermore, expression levels of relevant metabolic enzymes may be increased or decreased after treatment. Measuring expression levels of enzymes could lead to improved understanding of which mechanisms underlying mutIDH1^{R132H} glioma metabolism and tumorigenesis.*

5.3.2. Certain similarities in metabolic response to decreased wtIDH1 activity between wtIDH1 and mutIDH1 glioma cells

There were 25 metabolites that were not significantly different between control wtIDH1 and mutIDH1^{R132} LN18 cells, but that were significantly and appreciably increased and/or decreased in both wtIDH1 and mutIDH1^{R132H} LN18 cells after treatment with mutIDH1 inhibitors. Of those 25 metabolites, 22 either decreased or increased in both wtIDH1 and mutIDH1^{R132H} cells after treatment. A small majority of the metabolites (13/22) were only affected by one or two inhibitors each in treated cells (dTDP-D-glucose, gluconate, glutaconate, butyrate, *myo*-inositol, glutamate, glycine, proline, acetylglycine, 3-hydroxymethylglutarate, *o*-acetylserine, 4-hydroxybenzoate and sorbitol 6-phosphate). The remaining metabolites (9/22) were affected by three of four inhibitors (dUMP, galacturonate, isocitrate, citrate, 2-C-methylerythritol 4-phosphate, 1-pyrroline hydroxycarboxylate, GABA and glutathione). There were no metabolites with a mixed response to treatment when

comparing wtIDH1 to mutIDH1^{R132H} cells. Only three metabolites, ATP, CMP-*N*-acetylneuraminate and sedoheptulose 1-phosphate, had a mixed response to different inhibitors within a cell line. The FC and outcome of the FDR adjusted t-test are provided in **Figure 5.3.4**.

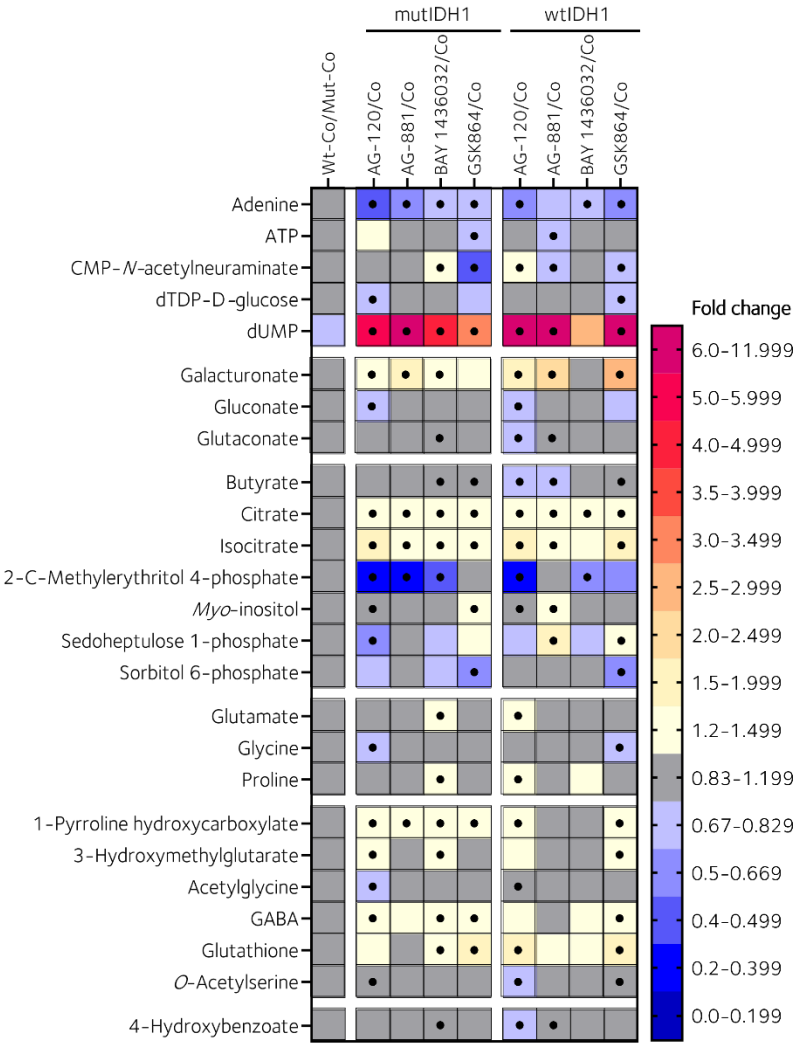

Figure 5.3.4. Metabolites that were not significantly different between control and treated wtIDH1 and mutIDH1^{R132H} cells, but were after treatment with one of the mutIDH1 inhibitors (AG-120, AG-881, BAY 1436032 or GSK864). The dot denotes a comparison that had a p-value < 0.05 in a t-test with FDR adjustment. The fold change was calculated between the mean normalised abundances for each comparison. Fold change for control samples was between wtIDH1/mutIDH1 samples and for treated samples it was between treated/control for a specific mutational status.

Metabolites that were not significantly or appreciably different between wtIDH1 and mutIDH1^{R132H} control cells were not considered particularly related to the specifics of mutIDH1 metabolism. A response to treatment by mutIDH1 inhibitors by previously unaffected metabolites therefore led to different interpretations than for the metabolites discussed above. The metabolites that were increased or decreased in both wtIDH1 and

mutIDH1^{R132H} cells were likely mainly affected by wtIDH1 inhibition. There was a striking number of metabolites that consistently either decreased or increased in both wtIDH1 and mutIDH1^{R132H} cells after treatment with mutIDH1 inhibitors (22/25 = 88%). In the previous sub-section that was the case for only 38.5% (5/13) of the metabolites (see **Figure 5.3.1**). Furthermore, none of the metabolites in **Figure 5.3.4** had a mixed response between treated wtIDH1 and mutIDH1^{R132H} cells, which occurred for 23% (3/13) metabolites in **Figure 5.3.1**. Finally, a mixed response to the different inhibitors within the two cell lines occurred for 38.5% (5/13) of metabolites in **Figure 5.3.1**, but only 12% (3/25) here. Based on the consistency of the change in metabolite abundance between wtIDH1 and mutIDH1^{R132H} cells in this experiment alone, decreased mutIDH1 activity could not be considered to have an effect on these specific metabolites.

In the previous sub-section, the nuance provided by CA of the concentration range experiment was demonstrated. It was of interest to see whether the metabolites listed in **Figure 5.3.4** correlated to 2-HG, 2-OG or isocitrate. The assumption was that the majority would correlate with isocitrate and/or 2-OG, as they are the substrate and product of wtIDH1. Adenine, ATP, dTDP-D-glucose, glutaconate, butyrate and 4-hydroxybenzoate were not identified in the concentration range experiment and were therefore not included. Isocitrate accumulated in the treated mutIDH1^{R132H} LN18 cells with increasing treatment concentration, while 2-HG and 2-OG both decreased. Hence, a metabolite with positive correlation to isocitrate would indicate an abundance increase, while a metabolite with positive correlation to 2-OG or 2-HG would indicate an abundance decrease. 2-HG was again regarded as a proxy for mutIDH1 activity and 2-OG/isocitrate were proxies for wtIDH1 activity.

Isocitrate and was not significantly correlated to either 2-HG or 2-OG. The only metabolite that correlated significantly and exclusively to 2-HG was dUMP. Surprisingly, there were no metabolites that correlated to 2-OG alone, but citrate and gluconate were significantly and positively correlated exclusively to isocitrate. Two metabolites correlated to 2-OG and 2-HG (gluconate and 2-C-methylerythritol 4-phosphate), only one correlated to 2-OG and isocitrate (1-pyrroline hydroxycarboxylate) and none to 2-HG and isocitrate. Finally, a number of metabolites correlated either positively or negatively to all three (CMP-*N*-neuraminate, sorbitol 6-phosphate, 3-hydroxymethylglutarate and *o*-acetylserine). Upon closer inspection, the metabolites all correlating negatively or positively to 2-HG, 2-OG and isocitrate did not

have appreciable abundance increases or decreases at the different inhibitor concentrations (0.833 < FC < 1.20 (treated/control)). Therefore, the metabolites correlating to all three were not of particular interest as the response in the concentration range experiment was minimal. The CA is summarised in **Figure 5.3.5** and the exact correlation and significance test scores are provided in **Table A.VIII.2** in **appendix VIII**.

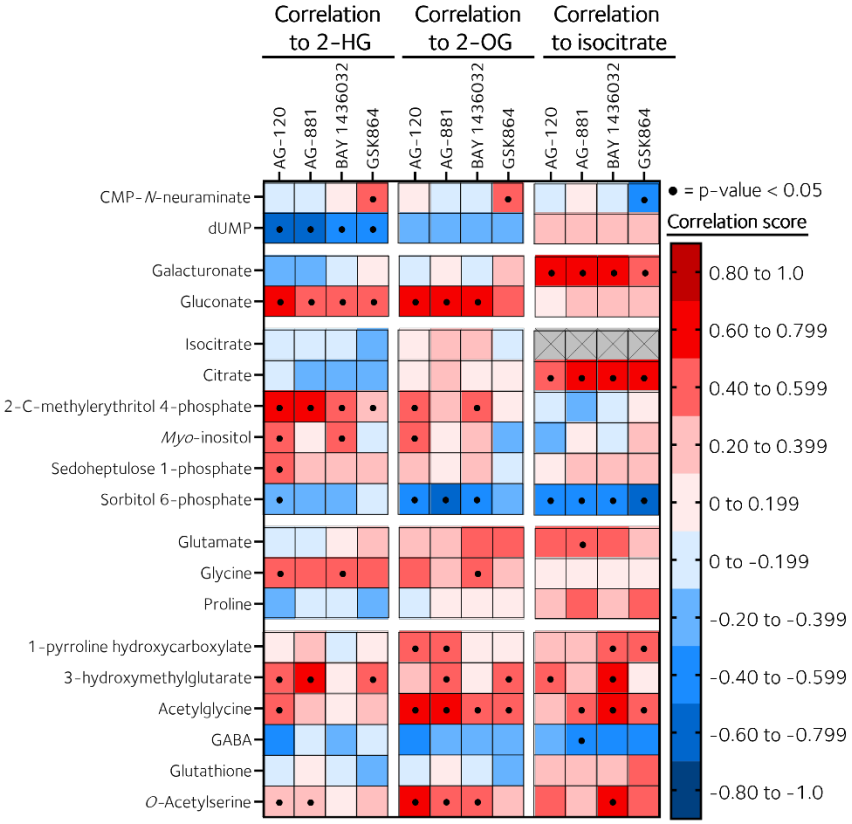

Figure 5.3.5. Heatmap of correlation scores to 2-HG, 2-OG and isocitrate from a selection of metabolites from the concentration range experiment. In the concentration range experiment, mutIDH1^{R132H} LN18 cells were treated with 0.05, 0.50, 5.00 or 10.0 µM of mutIDH1 inhibitors AG-120, AG-881, BAY 1436032 or GSK864. The metabolites were selected because they were significantly different between treated and control wtIDH1 and mutIDH1^{R132H} cells, but not between wtIDH1 and mutIDH1^{R132H} control cells. The CoSs were separately calculated for each inhibitor and control samples were included. The CA was carried out using Spearman rank correlation as the distance measure. The p-values were FDR adjusted.

The CA showed a surprising lack of correlation to 2-OG and isocitrate. There was therefore little evidence for direct metabolic relation to isocitrate and 2-OG for the affected metabolites. Potentially the response to wtIDH1 inhibition was due to reduced availability of NADPH, but that would have to be confirmed with measurements of the relevant redox metabolites. Otherwise, expression levels of key enzymes may have been affected by the decreased wtIDH1 activity in the cells. The S-TICO and L-TICO experiment were again examined for the onset of metabolic response to the mutIDH1 inhibitors. None of the

metabolites had a significant and appreciable difference between treated and control cells in the S-TICO experiment. However, the following metabolites maintained a significant difference between treated and control cells for one or more inhibitors in the L-TICO experiment: 2-C-methylerythritol 4-phosphate, citrate, isocitrate, and dUMP.

In summary, the metabolites that were significantly and appreciably increased in both wtIDH1 and mutIDH1^{R132H} LN18 cells treated with mutIDH1 inhibitors were due to a response to wtIDH1 inhibition. Few of the metabolites correlated strongly with either 2-OG or isocitrate abundance, which was unlike the previous sub-section where a majority of the metabolites correlated to 2-HG or 2-HG/2-OG (10/16). A direct enzymatic effect on wider metabolism due to e.g., accumulated isocitrate was therefore unlikely. More likely the metabolites were the outcome of a response to either altered redox homeostasis and/or expression levels of enzymes. Neither effect was measured due to time constraints, but remains as a promising avenue for future work.

5.3.3. WtIDH1 and mutIDH1^{R132H} LN18 cells treated with mutIDH1 inhibitors produce 'off-target' metabolic changes

The final metabolites considered were not significantly different between control wtIDH1 and mutIDH1^{R132H} LN18 cells, and were only significantly and appreciably altered in one of the two cell lines after treatment. A total of 30 metabolites were significantly and appreciably increased or decreased exclusively in one or the other cell line: nine in treated mutIDH1^{R132H} LN18 cells and 21 in treated wtIDH1 LN18 cells. Of the 21 metabolites that were significantly and appreciably altered exclusively in wtIDH1 cells, 17 were included due to AG-881 leading to an increase (15) or decrease (2) after treatment. The majority of the metabolites affected by AG-881 were either amino acids (9) or related to amino acid metabolism (6). A further three metabolites were included due to a significant and appreciable difference after treatment with AG-120 (CTP) or GSK864 (TMP and glycerol-3-phosphate). The only metabolite affected by more than one inhibitor (AG-120, AG-881) was kojic acid. Treatment with BAY 1436032 did not lead to significantly and appreciably altered abundance of any of the identified metabolites in wtIDH1 cells only. An overview of the metabolites is provided in **Figure 5.3.6.**

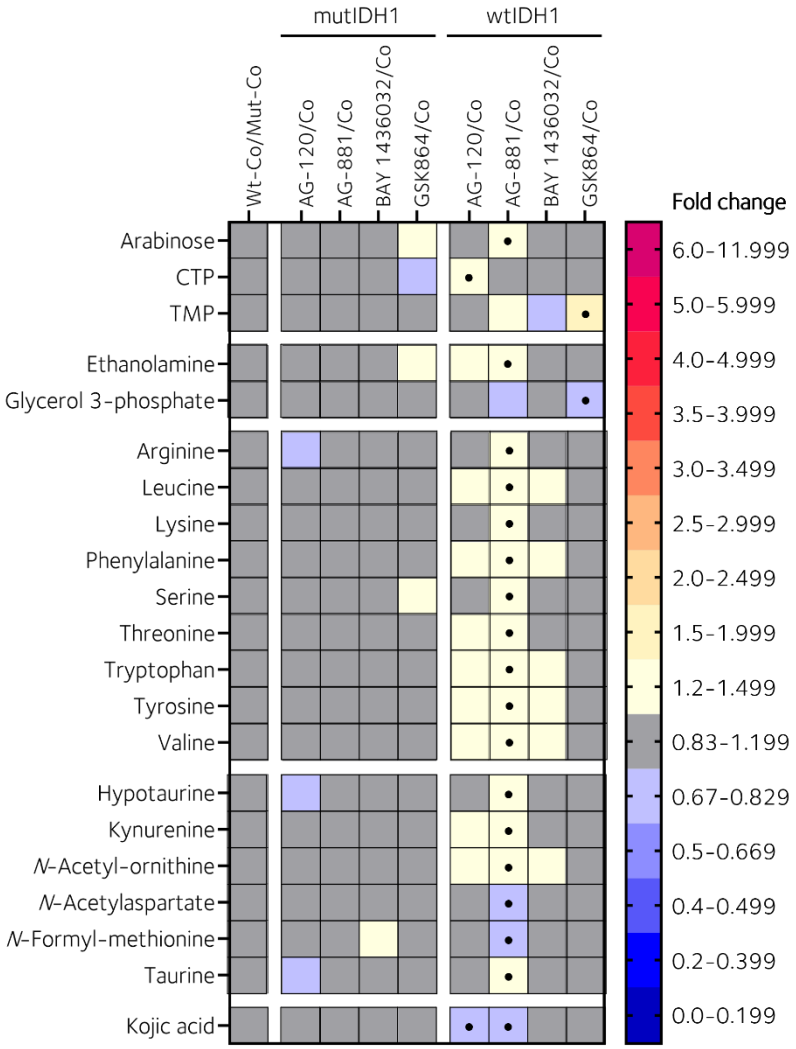

Figure 5.3.6. Metabolites that were only significantly different between control and treated wtIDH1 cells after treatment with one of the mutIDH1 inhibitors (AG-120, AG-881, BAY 1436032 or GSK864). The dot denotes a comparison that had a p-value < 0.05 in a t-test with FDR adjustment. The fold change was calculated between the mean normalised abundances for each comparison. Fold change for control samples was between wtIDH1/mutIDH1 samples and for treated samples it was between treated/control for a specific mutational status.

Since the majority of the metabolites were only altered by a single inhibitor (AG-881), either the inhibitor had an off-target effect or it was a far more efficient wtIDH1 inhibitor than the others. The reported IC_{50} for wtIDH1 inhibition was quite similar for AG-120 and AG-881 (24-71 nM and 4-190 nM respectively [246, 416]). AG-120 would be expected to lead to a similar outcome if the metabolic response was largely due to wtIDH1 inhibition. However, AG-881 is a dual mutIDH1 and mutIDH2 inhibitor and it also has a reported IC_{50} for wtIDH2 of 31-372 nM [416]. The observed 'off-target' effect may have been due to the inhibition of wtIDH2. The other three mutIDH1 specific inhibitors were all poor mutIDH2 and wtIDH2 inhibitors [246, 250]. The mutIDH1^{R132H} LN18 cells were expected to still have active wtIDH2

present and it was therefore not clear why a response to wtIDH2 inhibition would only be present in wtIDH1 cells. The main effect of the wtIDH2 inhibition, if present, was accumulation of amino acids and related metabolites. Potentially the inhibition of wtIDH2 activity decreased 2-OG availability in the wtIDH1 cells to the point where amino acid catabolism was slowed and amino acids accumulated. The mutIDH1^{R132H} LN18 cells may already have altered metabolism to cope with decreased 2-OG availability from mutIDH1^{R132H} activity and were more robust to the inhibition of wtIDH2.

Despite far fewer metabolites significantly and appreciably increasing or decreasing exclusively in mutIDH1^{R132H} LN18 cells (nine), seven were again due to just a single inhibitor. Perhaps surprisingly, treatment with AG-881 was only responsible for one of the eight metabolites (nonate). Significantly and appreciably altered metabolites after treatment with AG-120 were arabitol and *N*-acetyl-alanine, after BAY 1436032 was citrulline, and after GSK864 was ADP, CDP, and TDP. The only metabolite to respond to multiple inhibitors was 5-hydroxyhexanoate (AG-120, AG-881, BAY 1436032). The metabolites are summarised in **Figure 5.3.7**.

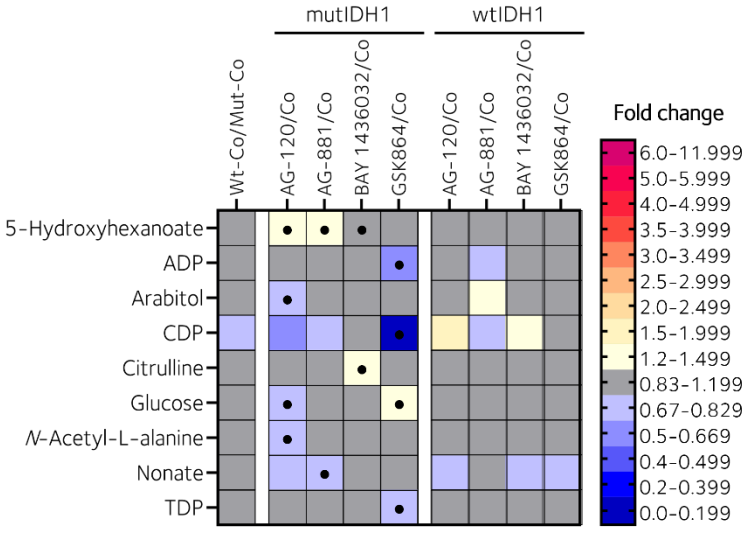

Figure 5.3.7. Metabolites that were only significantly different between control and treated muttIDH1^{R132H} cells after treatment with one of the mutIDH1 inhibitors (AG-120, AG-881, BAY 1436032 or GSK864). The dot denotes a comparison that had a p-value < 0.05 in a t-test with FDR adjustment. The fold change was calculated between the mean normalised abundances for each comparison. Fold change for control samples was between wtIDH1/mutIDH1 samples and for treated samples it was between treated/control for a specific mutational status.

It would be easiest to simply consider the metabolites listed above as off-target effects; most were responding to only one inhibitor and nearly all without a particularly substantial fold

change. Nevertheless, as previously demonstrated, a metabolite could correlate significantly to 2-HG or 2-OG in the concentration range experiment despite having a limited response in the wtIDH1/mutIDH^{R132H} treatment experiment. Therefore, the outcome of a CA of the metabolites in **Figure 5.3.7** were examined. The following metabolites were not included because they were not identified in the concentration range experiment: 5-hydroxyhexanoate, arabitol, CDP and citrulline.

Only TDP significantly correlated to 2-HG and 2-OG for all inhibitors. *N*-acetylalanine correlated to both as well, but the relationship was likely stronger with 2-OG than 2-HG as the correlation was significant for three inhibitors for the former and only one inhibitor for the latter. The remaining metabolites, ADP, glucose and nonate, did not correlate significantly to either 2-HG or 2-OG. The CA is summarised in **Figure 5.3.8** and the exact correlation and significance test scores are provided in **Table A.VIII.3** in **appendix VIII**.

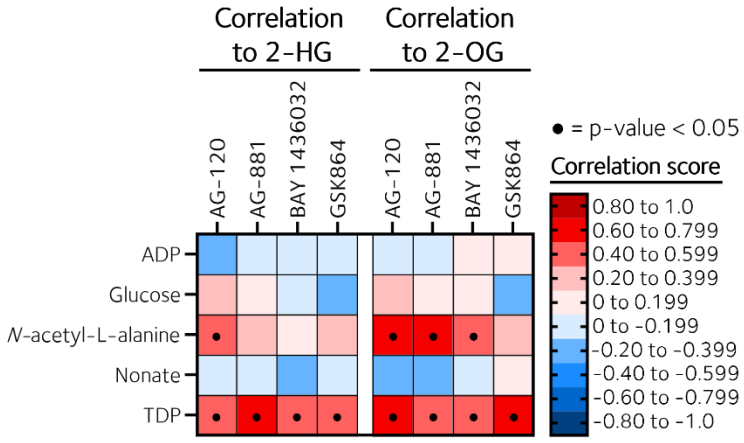

Figure 5.3.8. Heatmap of correlation scores to 2-HG and 2-OG from a selection of metabolites from the concentration range experiment. In the concentration range experiment, mutIDH1^{R132H} LN18 cells were treated with 0.05, 0.50, 5.00 or 10.0 µM of mutIDH1 inhibitors AG-120, AG-881, BAY 1436032 or GSK864. The metabolites were selected because they were significantly different between treated and control mutIDH1^{R132H} cells, but not between wtIDH1 and mutIDH1^{R132H} control cells. The CoSs were separately calculated for each inhibitor and control samples were included. The CA was carried out using Spearman rank correlation as the distance measure. The p-values were FDR adjusted.

TDP and *N*-acetylalanine were the only metabolites with a concentration dependent relationship to 2-HG and 2-OG. It was speculated TDP and *N*-acetylalanine were altered due to 'relief' from mutIDH1^{R132H} activity in the cells. The metabolites without significant correlation to 2-OG or 2-HG could have responded to mutIDH1 inhibition in the mutIDH1^{R132H} cells due to either altered redox homeostasis or changes in expression levels of related enzymes. However, off-target effects were not ruled out for the metabolites with low CoS, as

the responses reported in **Figure 5.3.7** were to one inhibitor only. The time course experiments revealed that none of the metabolites had an early or sustained separation between treated and control samples, as present for *e.g.,* B-CG, NAAG and lysine degradation intermediates. A firm conclusion with regards to the mechanisms behind the response to mutIDH1 inhibitors for 5-hydroxyhexanoate, ADP, CDP, citrulline, glucose and nonate could therefore not be made based on the available data alone.

In summary, the metabolites that were significantly and appreciably increased or decreased exclusively in wtIDH1 LN18 cells after treatment with mutIDH1 inhibitors were speculated to be due to wtIDH2 inhibition by AG-881. A small number of metabolites were significantly and appreciably increased or decreased exclusively in mutIDH1^{R132H} LN18 cells. Only two were correlated to 2-HG and 2-OG abundance in the concentration range experiment. None of the metabolites were significantly and appreciably increased or decreased between treated and control samples in the time course experiments, which made it difficult to assess whether enzyme expression levels were behind the response to the mutIDH1 inhibitors. Based on the low number of metabolites and their relatively small abundance changes across the different experiments, it was characterised as an 'off-target' effect by the inhibitor eliciting a response in the abundances of these metabolites.

5.4. Discussion

The understanding of mutIDH1 glioma metabolism has to date mainly been shaped by studies comparing wtIDH1 and mutIDH1^{R132H} glioma or GBM cell lines, mouse models and PTBs [reviewed in 1]. A small number of studies have expanded upon those findings by directly relating elevated 2-HG abundance to aspects of lipid metabolism [434, 435], BCAT1 activity [173], and up- or down-regulation of certain metabolites [175]. However, the mechanisms behind many of these metabolic changes remains poorly understood. Which aspects of metabolism are affected by 2-HG directly, *e.g.,* enzymatic inhibition, or indirectly, *e.g.,* transcriptional regulation? Characterising the nuances of the metabolic changes would provide guidance for more targeted studies of tumorigenic processes and therapeutic targets. In this chapter, mutIDH1 inhibitors were used as a tool to interrogate the metabolic differences between wtIDH1 and mutIDH1^{R132H} LN18 cells.

The use of multiple mutIDH1 inhibitors for simultaneous investigation of mutIDH1^{R132H} GBM cell metabolism has not previously been described to the extent shown in this chapter. A small number of studies have been published where the metabolic effects of mutIDH1 inhibitors in GBM cells or PTBs were explored [174, 255-257]. Two of the studies compared AG-881 to AG-120 [255] and BAY 1436032 [256], but the number of metabolites covered was far smaller than the work presented here (12-17 versus > 170) [255, 256]. The broader coverage allowed for a more detailed assessment of the metabolic response to the four mutIDH1 inhibitors in treated wtIDH1 and mutIDH1^{R132H} LN18 cells.

Three of the studies focussed on measuring metabolism before and after treatment in mutIDH1 samples only [255-257]. A single study reported on the effect of mutIDH1 inhibitors in both wtIDH1 and mutIDH1^{R132H} samples. U87 GBM cells, with the mutant expressed via lentiviral vector, were treated with mutIDH1 inhibitor AGI5198 [174]. Similar to the wtIDH1 and mutIDH1^{R132H} LN18 cells, the distance between treated mutIDH1^{R132H} U87 cells and control wtIDH1 U87 cells was decreased along component 1 in a PLS-DA. There was also a small shift of treated wtIDH1 U87 cells away from control wtIDH1 U87 cells along component 1 [174]. The response to treatment with mutIDH1 inhibitor in wtIDH1 and mutIDH1^{R132H} variants of U87 and LN18 GBM cells was quite similar.

One study reported on metabolic changes during treatment [256]. The time-course was over a matter of days, rather than hours, because the aim was to measure predictors of survival in orthotopic mouse models [256]. Here, the measurement of metabolic change over a matter of hours presented a dataset (S-TICO) that could be used to search for when trends in altered metabolite levels emerged. The L-TICO experiment provided insight into whether metabolic changes were sustained. Care had to be taken in interpreting the data from both experiments, as cell growth and viability had a substantial impact on the metabolic behaviour. With that in mind, the S-TICO data still revealed that the difference between treated and control cells did not necessarily arise within the first few hours of treatment, with a few exceptions (B-CG, NAAG, lysine degradation intermediates). Furthermore, the L-TICO dataset showed that the difference in abundance between control and treated samples for several metabolites was maintained once established (isocitrate, citrate, B-CG, NAAG, 2-C-methylerythritol 4-phosphate, dUMP). To minimise the effect of cell growth on the data, future S-TICO type experiments should reverse the order of the timepoints, *i.e.,* adding treatment 24-12-8-4-2-1 hours before harvest. Then the shortest exposure times are close to time of harvest and the cells are in a more similar metabolic state as those at the end of the longer time points.

B-CG emerged as the metabolite with the most consistent correlative relationship to 2-HG. It was one of few metabolites that was found in both the treated wtIDH1/mutIDH1 experiment that also had a consistent and sensitive correlation to 2-HG in the concentration range experiment. Moreover, the steady and growing difference between control and treated cells in the S-TICO experiment was only observed for B-CG and NAAG. It was surprising that B-CG, rather than the number of other metabolites that had previously been linked to other mutIDH1 glioma models, had such a strong relationship to 2-HG. B-CG has previously only been detected in the first generation wtIDH1 and mutIDH1^{R132H} LN18 cell line by Dr Walsby-Tickle [148]. The metabolite has four carboxylic acid functional groups, which means IC-MS was a fitting analytical technique for measuring it. Potentially it has been missed in previous studies simply by not being detected. It is unlikely that the metabolite is just a quirk of the LN18 cell line, as the metabolite has been identified in new born rat brain [365] and primary neurons from chick and rat brain [366].

Because of the limited knowledge of the role of B-CG in human metabolism, it is challenging to pinpoint a potential tumorigenic role. However, as previously noted, B-CG in complex with

Cu(II) had a redox protective effect through inhibition of XO activity [403]. Based on the delayed response to 2-HG inhibition in the S-TICO experiment, it was speculated that the transcription of B-CG synthase was decreased in cells with high 2-HG levels. The decreased transcription and subsequent low B-CG levels would deprive the mutIDH1^{R132H} cells of redox protection. Initially, that was judged as counterintuitive because the cells already are considered vulnerable to oxidative species due to the increased consumption of NADPH [161, 215, 220-222, 224]. However, heightened levels of ROS can promote tumorigenesis through activating proliferative responses and inducing genomic instability [reviewed in 441]. Decreased B-CG could be contributing to a cellular environment where tumorigenesis is promoted by ROS-mediated effects. If B-CG metabolism were to be pursued as a therapeutic target, better understanding of its metabolic function is needed first. Currently it is not clear if restoring B-CG or further decreasing it would be the most beneficial. Restoring could mean rendering the cells less sensitive to ROS, but decreasing it further could also further drive its speculated tumorigenic role.

In mutIDH1 glioma, the concentration of 2-HG is high enough (mM) [76] for it to act as a competitive inhibitor of a number of 2-OG dependent enzymes [84, 173, 386]. Some of the metabolites altered in mutIDH1^{R132H} cells were biosynthesised with 2-OG as a substrate, or were up/down-stream of a reaction that required 2-OG. It was therefore speculated that these metabolites could be affected because of potential direct inhibition by 2-HG. The challenge was that wtIDH1 activity was likely impaired by the mutIDH1 inhibitors in the mutIDH1^{R132H} LN18 cells and the response to 2-HG specifically could not be studied. Inhibiting wtIDH1 could potentially decrease 2-OG and NADPH availability, therefore mimicking the effect of mutIDH1 activity. Yet, a metabolite responding in treated wtIDH1 cells as well only strengthened the idea that the metabolite was affected by mutIDH1^{R132H} activity because it was likely dependent on 2-OG and/or NADPH. In conclusion, the data from the experiments performed in this chapter could not be used to fully disentangle the relationship of mutIDH1 activity for these specific metabolites. An experiment that could decrease 2-HG or 2-OG independently of each other, or decrease 2-HG abundance without concomitant inhibition of wtIDH1 activity, was needed. That will be pursued in **chapter 6**.

The numerous metabolic changes that occurred in both wtIDH1 and mutIDH1^{R132H} LN18 cells after treatment with mutIDH1 inhibitors highlighted the importance of including proper

controls. If the aim was to find biomarkers for therapeutic response, then the wtIDH1 controls would not have been necessary. However, the aim of this chapter was to provide nuance in the understanding of mutIDH1 glioma metabolism and point toward tumorigenic processes and potential therapeutic targets. Inclusion of wtIDH1 cells therefore provided two benefits. First, the comparison of wtIDH1 and mutIDH1^{R132H} cells before treatment narrowed the scope of metabolites that were different between cellular environments with and without mutant *IDH1* present. This provided a pre-defined list of metabolites that were of particular interest to assess the response of after treatment with mutIDH1 inhibitors. Second, the treatment of wtIDH1 LN18 cells revealed a number of metabolites that were not on the pre-defined list, but had a consistent response to three or four inhibitors in both cell lines. Without the comparison to wtIDH1 control cells and without the treatment of wtIDH1 cells, all of those metabolites could have been mistakenly considered important to the metabolic phenotype of mutIDH1^{R132H} LN18 cells. Instead, those metabolites are more appropriately considered as biomarkers of general response to mutIDH1 inhibitors.

5.5. Summary and conclusions

The metabolic response to mutIDH1 inhibitors in wtIDH1 and mutIDH1^{R132H} LN18 cells was investigated with multivariate statistical analysis of semi-targeted metabolomics data. PLS-DA and HCA revealed that mutIDH1^{R132H} LN18 cells were metabolically more similar to wtIDH1 cells than control mutIDH1^{R132H} LN18 cells after treatment. The treated wtIDH1 cells were also affected by the mutIDH1 inhibitors, likely due to inhibition of wtIDH1 activity. Multiple metabolites were similarly affected in both treated wtIDH1 and mutIDH1^{R132H} cells. B-CG appeared to specifically respond in a 2-HG dependent manner in mutIDH1^{R132H} LN18 cells after treatment. A concentration dependent response to treatment was apparent in the PCAs and HCAs of semi-targeted metabolomics data from the concentration range experiment. Several metabolites, including B-CG, appeared to be correlated to 2-HG abundance in cells. The metabolic response to inhibitors was not uniform, likely due to the difference in inhibition efficacy and potential off-target effects. AG-120 and GSK864 were the two inhibitors with the most apparent off-target effects in the concentration range experiment. Multivariate analysis of the TICO experiments revealed that cell growth was a major contributor to the data trends observed, but the metabolic response to mutIDH1 inhibitors could be observed as well.

The response to mutIDH1 inhibitors in wtIDH1 and mutIDH1^{R132H} LN18 cells was investigated further with univariate statistical analysis in an attempt to characterize how metabolites were related to mutIDH1^{R132H} activity. It proved challenging as the concomitant inhibition of wtIDH1 and mutIDH1^{R132H} activity in the mutIDH1^{R132H} LN18 cells obscured the effect of 2-HG alone for metabolites that could be affected by both enzymes. The metabolites will have to be studied further in an experiment where wtIDH1 and mutIDH1^{R132H} activity are not simultaneously affected. However, despite the challenges it is clear that a number of metabolites are correlated to 2-HG and mutIDH1^{R132H} activity.

B-CG was the metabolite with the clearest correlative relationship to 2-HG that was identified in this chapter. Its role in normal metabolism is not well known, but it may have a tumorigenic effect in mutIDH1 glioma based on its suggested role as a redox protective compound. Its suitability as a therapeutic target will be better known once its potential role in tumorigenesis is better understood.

Chapter 6. Exploring the metabolic effects of restricting glutamine utilisation in wtIDH1 and mutIDH1^{R132H} glioblastoma cells

6.1. Introduction

The mutIDH1 inhibitor experiments presented in **chapter 4** demonstrated that cell viability was not substantially decreased in the mutIDH1^{R132H} GBM cell line. With resistance to mutIDH1 inhibitors emerging [264-266, 424-427] and therapeutic benefit of these inhibitors in clinical settings currently limited [263, 422, 423], additional strategies for treating mutIDH1 glioma are needed. Furthermore, in **chapter 5**, the role of 2-HG in mutIDH1 glioma metabolism was investigated by decreasing 2-HG abundance with mutIDH1 inhibitors. However, the concomitant inhibition of wtIDH1 and mutIDH1^{R132H} activity in the mutIDH1^{R132H} LN18 cells complicated the understanding of how certain metabolites were affected by mutIDH1 and 2-HG. An experiment where intracellular 2-HG concentration was decreased without wtIDH1 activity also being affected would advance the understanding of mutIDH1 glioma metabolism.

Biosynthesis of 2-HG occurs primarily from glutamate-derived 2-OG (as shown with ^{13}C tracer experiments in **chapter 3** and also reported the literature [147, 165, 370]). Limiting the availability of the main carbon source of 2-HG has previously been suggested as a therapeutic option for mutIDH1 glioma [208, 442]. In this chapter, the aim was to explore the effects on cell viability, proliferation and metabolism when the main carbon source of 2-HG was restricted.

In order to limit glutamine utilisation, cells were treated with the GLS inhibitor CB-839 [443]. GLS catalyses the de-amination of glutamine to glutamate. Ideally, a GLUD inhibitor would have been used to decrease the oxidation of glutamate to 2-OG. However, no specific GLUD inhibitors were available at the time this work was carried out. Chloroquine has been reported to inhibit nerve-specific GLUD [276], but is also an antimalarial agent [274] and autophagy inhibitor [reviewed in 275]. The potential for off-target effects confusing the metabolic interpretation were considered and CB-839 was used instead because it was developed for GLS inhibition specifically [443].

The aims of the research in this chapter are to:

1. Assess the effect of limiting glutamine utilisation on:
    i. Cell viability.
    ii. The abundance of glutamine and glutamate in wtIDH1 and mutIDH1^{R132H} cells.
    iii. The abundance 2-HG and 2-OG in wtIDH1 and mutIDH1^{R132H} cells.
    iv. Wider metabolic changes, with a focus on metabolites that were significantly altered in abundance between wtIDH1 and mutIDH1^{R132H} cells (reported in chapter 3 and further affected by mutIDH1 inhibition in chapter 5).

6.2. Proliferation decreases in cells treated with GLS inhibitor

GLS inhibition by CB-839 has previously been reported to have a mixed ability to decrease cell viability of patient-derived mutIDH1 glioma cells [208]. There were no previous reports on the effect of CB-839 in LN18 cells. It was therefore of interest to measure the effect of CB-839 on wtIDH1 and mutIDH1^{R132H} LN18 cell viability, to determine the sensitivity of this specific cell line and whether IDH1 mutant and wild-type cells responded differently.

Data processing and analysis

Cell viability was measured with an MTS assay. WtIDH1 and mutIDH1^{R132H} LN18 cells were treated for 24 hours with a range of CB-839 concentrations (0.05-5.00 µM) chosen based on the assay performed by Ruiz-Rodado *et al.* [208]. Plating and treatment were completed as described in **section 2.5.3** and **2.5.4**; number of biological replicates per experimental groups was N = 6. The cells were incubated with MTS assay dye for 45 minutes prior to measuring absorbance (*A*) at 490 nm, see **section 2.7.5** for further details. Each plate was measured four times at 15-minute intervals. The absorbance ratios between treated and control samples per measurement timepoint was calculated. The average from each timepoint was used for plotting the data and statistical tests (one-way ANOVA with Dunnett's or Šídák MCTe).

Results

After treatment with ≥ 0.10 µM CB-839, wtIDH1 and mutIDH1^{R132H} LN18 cells had significantly lower absorbance than control cells (p-value < 0.05, Dunnett's MCTe). The smallest ratio in absorbance between treated and control for mutIDH1^{R132H} LN18 cells was 0.74 ± 0.04, *i.e.,* a 26% decrease in cell viability. For wtIDH1 LN18 cells, the smallest ratio between treated and control cells was 0.61 ± 0.06, *i.e.,* a 39% decrease in cell viability. The significance of the difference in response between treated wtIDH1 and mutIDH1^{R132H} LN18 cells was calculated, as wtIDH1 cells were more sensitive to treatment with CB-839. WtIDH1 cells treated with 1.00, 3.00 or 5.00 µM CB-839 had a significantly lower treated-to-control absorbance ratio than mutIDH1^{R132H} cells at the same CB-839 concentrations (p-value < 0.01, one-way ANOVA with Šídák MCTe). The absorbance ratios from the MTS assay are shown in **Figure 6.2.1.**

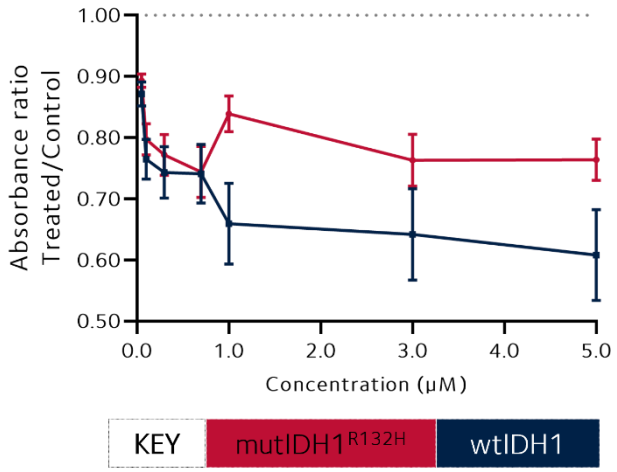

Figure 6.2.1. Cell viability assay of wtIDH1 and mutIDH1^{R132H} LN18 cells treated with CB-839. The data points are ratio of mean absorbance of treated samples to mean absorbance of control samples. The dotted line indicates ratio of 1.0, *i.e.,* no difference between control and treated. N = 6 biological replicates and error bars are one standard deviation.

In **chapter 4,** a similar assay was performed with mutIDH1 inhibitors and treatment with 5.00 μM mutIDH1 inhibitors for 24 hours did not lead to a significant difference in cell viability ($A_{treated}/A_{control}$ = 0.98 ± 0.10). The decrease in cell viability was significantly larger for mutIDH1^{R132H} LN18 cells treated with CB-839 than mutIDH1 inhibitors (p-value < 0.001, two-sided unpaired t-test (N = 6)). As a single therapy, CB-839 was therefore more efficient in reducing cell viability than mutIDH1 inhibitors. However, this comparison was only carried out for a single cell line and as previously noted, the efficacy of CB-839 is cell line dependent [208]. CB-839 as a therapeutic agent would likely benefit from patient stratification *e.g.,* by testing the inhibitor on patient-derived cell lines [444, 445].

WtIDH1 LN18 cells were significantly more sensitive to CB-839 than mutIDH1^{R132H} LN18 cells. That was surprising as the mutIDH1^{R132H} LN18 cells were thought to be under more metabolic stress than the wtIDH1 cells, since mutIDH1 enzyme activity was not otherwise restricted. Three hypotheses were considered. First, wtIDH1 cells were more reliant on GLS activity than mutIDH1^{R132H} LN18 cells to metabolise glutamine to glutamate. Second, if GLS inhibition led to decreased 2-HG abundance, *i.e.,* the mutant cells were using less NADPH to reduce 2-OG to 2-HG, perhaps the treatment provided some form of metabolic relief. Or third, the decrease in glutamate was not drastic enough to provide a particularly substantial decrease in 2-HG. It was therefore of interest to measure glutamine, glutamate, 2-HG and 2-OG abundance in the wtIDH1 and mutIDH1^{R132H} LN18 cells to inform on which metabolic changes had occurred.

In summary, both wtIDH1 and mutIDH1^{R132H} cells cultured with ≥ 0.10 μM CB-839 had significantly lower proliferation than vehicle controls. WtIDH1 LN18 cells were more sensitive to CB-839 than mutIDH1^{R132H} LN18 cells. It was speculated that either the wtIDH1 cells were

more dependent on GLS activity; that the mutIDH1 cells in sum were being relieved of metabolic stress by producing less 2-HG; or that the inhibitor was not decreasing glutamate abundance enough to have an impact on 2-HG biosynthesis. To test the hypotheses, cellular abundance of 2-HG and related metabolites (2-OG, glutamate and glutamine) were measured next.

6.3. 2-HG resilient to decreased 2-OG and glutamate in cells

The cell viability assay of wtIDH1 and mutIDH1^{R132H} LN18 cells treated with CB-839 revealed that the wtIDH1 cells were significantly more sensitive than the mutIDH1^{R132H} LN18 cells to the drug. Previously it has been shown that glutamate-derived 2-OG was the main carbon source for 2-HG in LN18 cells (**chapter 3**). It was therefore hypothesised that the impact of CB-839 was smaller in mutIDH1^{R132H} LN18 cells because the overall effect of limited glutamate was actually relief from the metabolic strain. The relief would occur if limited glutamate led to decreased 2-HG biosynthesis, because that would also decrease utilisation of NADPH by the mutIDH1 enzyme. The alternative hypothesis was that the wtIDH1 cells were more reliant on GLS than the mutIDH1^{R132H} cells. The abundance of 2-HG, 2-OG, glutamate and glutamine were therefore analysed to test the hypotheses.

Data processing and analysis

WtIDH1 and mutIDH1^{R132H} LN18 cells were cultured in 12-well plates with supplemented LG DMEM. The cells were treated with a range of concentrations of CB-839 (0.05-5.00 µM) and all cells, including control, had 0.1% (v/v) DMSO present in the media. Treatment lasted 24 hours with a total incubation time of 48 hours. Number of biological replicates was N = 4 for treated cells and N = 8 for control cells. Sample plating, treatment, harvest and preparation used the procedures as described in **section 2.5.3-2.5.5** and **section 2.6.1-2.6.2**. The measured DNA concentration (ng/µL) is listed in **Table A.IX.1** in **appendix IX** and was used for sample normalisation.

The samples were analysed using both IC-MS and derivatised RPLC-MS methods, as described in **section 2.7.1** and **2.7.2**, respectively. Metabolite identification was performed as described in **section 2.8.2**; the IC-MS data yielded 145 (72 confident/73 putative) metabolite identifications and the RPLC-MS data yielded 40 (23 confident/17 putative) metabolite identifications. Identified metabolites and identification criteria are outlined in **Table A.IX.2**

and **A.IX.3** in **appendix IX**, respectively. The data was filtered and normalised per the processes described in **section 2.8.3**; The IC-MS data was median normalised and the derivatised RPLC-MS data was quantile normalised. The normalisation parameters were chosen because they minimised small amounts of systematic bias present in the data sets, as well as establishing normal, or near normal, sample distribution plots (see **Figure A.IX.1**). The heatmaps and sample distribution plots for IC-MS and derivatised RPLC-MS data is provided in **Figure A.IX.1** and **A.IX.2**, respectively**.**

Results

Glutamate decreased significantly and appreciably in wtIDH1 and mutIDH1^{R132H} LN18 cells treated with ≥ 0.10 µM CB-839 (FC_{MUT} > 2.21 (control/treated), p-value < 0.001 (t-test with FDR); FC_{WT} > 1.72, p-value < 0.05 (t-test with FDR)). Glutamine accumulated significantly and appreciably in wtIDH1 LN18 cells treated with 0.10, 0.30, 1.00 and 3.00 µM CB-839 (FC > 2.39 (treated/control), p-value < 0.05, t-test with FDR). Glutamine also accumulated appreciably in mutIDH1^{R132H} LN18 cells (FC > 1.44 (treated/control)), but was not significant. The concurrent decrease in glutamate abundance and increase in glutamine abundance confirmed that the inhibitor limited glutamine utilisation, as expected. Glutamine and glutamate abundance in wtIDH1 and mutIDH1^{R132H} LN18 cells are provided in **Figure 6.3.1.(a-b)**.

The abundance of 2-OG was appreciably lower in treated wtIDH1 and mutIDH1^{R132H} cells compared to respective control cells (FC > 1.50 (control/treated)). The difference between treated and control groups was significant for all treated mutIDH1^{R132H} cells (p-value < 0.05, t-test with FDR), except those treated with 0.30 µM CB-839. It was only significant for wtIDH1 cells treated with 0.10, 1.00 or 5.00 µM CB-839 (p-value < 0.001, t-test with FDR). The abundance of 2-OG in treated and control cells is shown in **Figure 6.3.1.(c)**. Surprisingly, 2-HG was not significantly nor appreciably altered in either mutIDH1^{R132H} or wtIDH1 LN18 cells, see **Figure 6.3.1.(d)**.

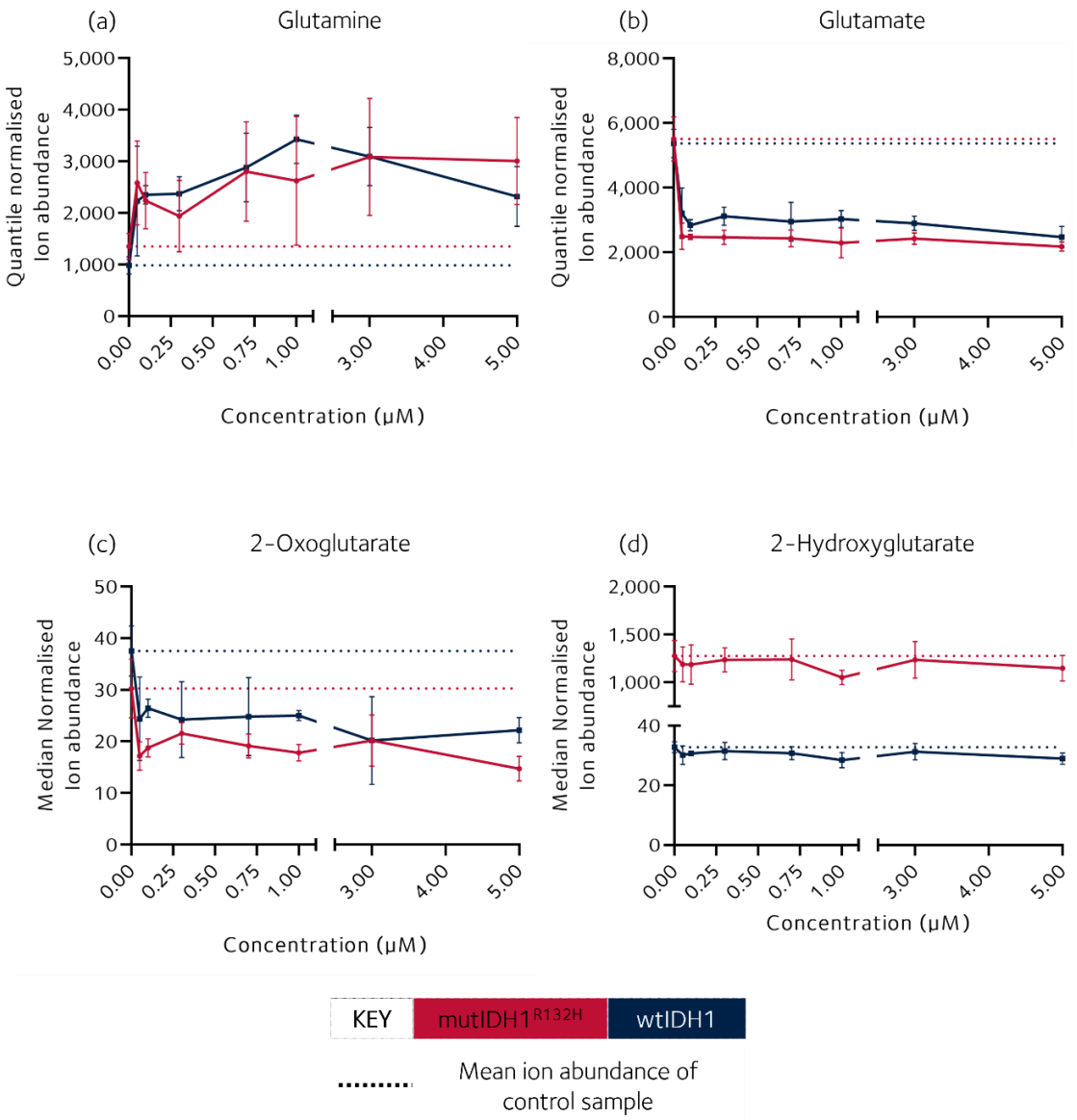

Figure 6.3.1. Glutamine, glutamate, 2-OG and 2-HG abundance in wtIDH1 and mutIDH1^{R132H} LN18 cells that were treated with GLS inhibitor CB-839. The data points are mean abundance and the error bars are one standard deviation. The number of biological replicates per cell line for treated groups was N = 4 and for control group was N = 8.

In mutIDH1^{R132H} LN18 cells, glutamate abundance was twice as high in control versus treated samples (FC > 2.2 (control/treated)), while glutamine abundance was halved after treatment (FC > 1.44 (treated/control). The decrease in glutamate abundance in treated versus control wtIDH1 cells was smaller (FC > 1.67 (control/treated), but the accumulation of glutamine was greater (FC > 2.27 (treated/control). In other words, the wtIDH1 cells accumulated more glutamine, but had glutamate levels closer to that of their respective control samples than mutIDH1^{R132H} cells. The evidence was consistent with wtIDH1 LN18 cells predominantly metabolising glutamine through GLS, while mutIDH1^{R132H} LN18 cells metabolised glutamine

via alternative reactions as well. Glutamate, on the other hand, appeared to be utilised to a greater extent in mutIDH1^{R132H} compared to wtIDH1 LN18 cells, likely for 2-HG biosynthesis. It therefore remained puzzling that the mutIDH1^{R132H} LN18 cells were less sensitive to CB-839 than wtIDH1 cells. Potentially the cells also increased consumption of glucose to make up for the loss of glutamate. The additional glucose could either be directed towards 2-HG biosynthesis or towards other reactions that were restricted by the lack of glutamate-derived 2-OG. Glucose consumption was therefore investigated next.

In summary, the accumulation of glutamine and decrease of glutamate demonstrated that CB-839 limited glutamine utilisation. WtIDH1 LN18 cells were more dependent on GLS for the utilisation of glutamine than mutIDH1^{R132H} LN18 cells. However, mutIDH1^{R132H} LN18 cells consumed more glutamate than the wtIDH1 LN18 cells, likely for 2-HG biosynthesis. There was a significant decrease in 2-OG abundance in treated wtIDH1 and mutIDH1^{R132H} LN18 cells. Yet, 2-HG abundance was not significantly altered between control and treated mutIDH1^{R132H} LN18 cells. That was surprising due to the significant decrease in 2-OG abundance. It was speculated glucose consumption was also increased to support 2-HG biosynthesis.

6.4. Glucose consumption was not increased in wtIDH1 and mutIDH1^{R132H} LN18 cells treated with CB-839

The maintained level of 2-HG in mutIDH1^{R132H} LN18 cells treated with CB-839, despite decreased glutamate abundance, raised the question of whether glucose consumption was increased in response. To assess whether that was the case, the glucose concentration in the media of wtIDH1 and mutIDH1^{R132H} LN18 cells treated with CB-839 was measured.

Data processing and analysis

The wtIDH1 and mutIDH1^{R132H} LN18 cells were plated in 96-well plates and incubated for 24 hours with CB-839 (0.05-5.00 µM) present in the media; control cells with vehicle (0.1% (v/v) DMSO in media) were also included. Plating and treatment were otherwise performed as described in **section 2.5.3** and **2.5.4**. After incubation, aliquots of media were saved and the samples prepared for analysis as described in **section 2.6.4**. Measurement of glucose concentration was by colorimetric assay, as detailed in **section 2.7.5**. Quantification

was performed by constructing an external calibration curve (R^2 > 0.99), shown in **Figure A.IX.2**.

Results

There was no appreciable or significant difference in glucose media concentration between control and CB-839 treated mutIDH1^{R132H} samples (**Figure 6.4.1**). Therefore, the hypothesis suggested in **section 6.3**, where 2-HG biosynthesis was supported by additional glucose consumption in CB-839-treated cells, was contradicted. Instead, glutamine was likely metabolised to glutamate by other enzymes than GLS and (or) glutamate utilisation in other reactions was decreased. There was a significant decrease in glucose media concentration in wtIDH1 samples where the cells had been treated with 0.05, 3.00 or 5.00 µM CB-839 (p-value < 0.01, one-way ANOVA with Dunnett's MCTe) (**Figure 6.4.1)**. It was puzzling that glucose consumption was increased only for cells treated with 0.05, 3.00 and 5.00 µM CB-839. All concentrations of inhibitor led to accumulation of glutamine and decreased glutamate, therefore a compensatory mechanism for limited glutamine utilisation would have been expected at all treatment concentrations. Potentially the exposure length (24 hour) was too short for the differences in glucose consumption to develop fully.

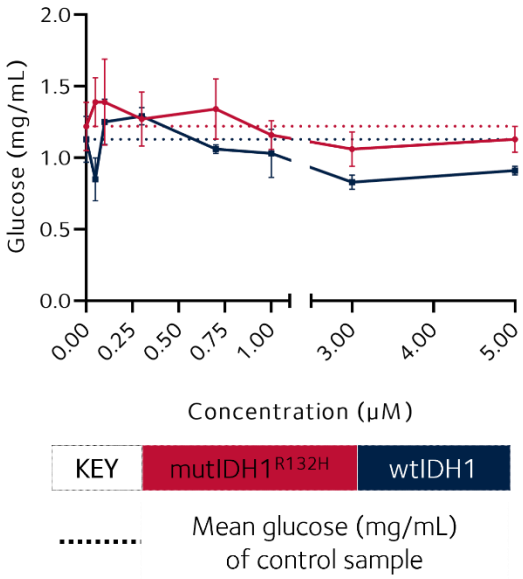

Figure 6.4.1. Glucose concentration (mg/mL) in media of wtIDH1 and mutIDH1^{R132H} LN18 cells treated with CB-839. Dotted lines indicate the mean glucose concentration (mg/mL) in the control samples. The number of biological replicates were N = 6 (treated cells) and N = 18 (control cells). Data points are mean abundance and error bars are one standard deviation.

In summary, there was no consistent significant increase in glucose consumption observed for either wtIDH1 or mutIDH1^{R132H} cells to compensate for decreased glutamate availability.

6.5. Limiting glutamate availability highlighted dependence of other metabolite abundances on 2-OG and 2-HG in mutIDH1^{R132H}

In **chapter 5**, mutIDH1 inhibitors were used to investigate the metabolic differences between wtIDH1 and mutIDH1^{R132H} LN18 cells. The analysis was hindered by the concomitant inhibition of wtIDH1 and mutIDH1^{R132H} enzyme activity in mutIDH1^{R132H} LN18 cells. It was not possible to confidently determine whether specific metabolites were affected by 2-HG/mutIDH1 activity when the inhibition of wtIDH1 could also alter metabolite abundance. An experiment where either 2-HG or 2-OG were altered without concurrent inhibition of wtIDH1 and mutIDH1^{R132H} activity was therefore needed. The CB-839 metabolomics experiment described in **section 6.3** demonstrated that 2-HG abundance was maintained while 2-OG was significantly decreased in all experimental groups. Thus, the metabolites that were significantly different between control wtIDH1 and mutIDH1^{R132H} LN18 cells (**chapter 3**) and also altered by mutIDH1 inhibitor (**chapter 5**) could be investigated.

Data processing and analysis

To quantify whether a metabolite maintained an abundance difference between wtIDH1 and mutIDH1^{R132H} cells after treatment with CB-839, the abundances were 'normalised' by calculating their relative ratio to the abundance in wtIDH1 control cells:

Equation 6.1 $$FC_W = \bar{b}_{WT-Co}/\bar{b}_{WT-Tr}$$

Equation 6.2 $$FC_M = \bar{b}_{WT-Co}/\bar{b}_{MUT-Tr}$$

where $\bar{b}$ was average metabolite abundance, WT = wtIDH1, MUT = mutIDH1^{R132H}, Tr = treated and Co = control. Then the difference (FC_{Diff}) between the two normalised abundances was calculated:

Equation 6.3 $$FC_{Diff} = FC_W - FC_M$$

The FC_{Diff} for all treatment concentrations of CB-839 were used, as the decrease in 2-OG abundance was similar for all. An FC_{Diff} near zero meant that the difference between wtIDH1 and mutIDH1^{R132H} LN18 cells was diminished after treatment with CB-839. Metabolites with

a positive FC_{Diff} had higher abundance in mutIDH1^{R132H} than wtIDH1 LN18 cells and metabolites with negative FC_{Diff} had higher abundance in wtIDH1 than mutIDH1^{R132H} LN18 cells. As an example, the difference in 2-HG abundance remained the same between wtIDH1 and mutIDH1^{R132H} LN18 cells at all CB-839 concentrations (**Figure 6.3.1**) and FC_{Diff} was positive (1.06). However, FC_{Diff} could not be used to distinguish whether the metabolite increased or decreased in wtIDH1 or mutIDH1^{R132H} cells after treatment with CB-839, only its relative abundance. The average FC between treated and control for each cell line was therefore used to determine which metabolites were altered after treatment with CB-839. Significance between treated and control was only reported when it was present for two or more treated groups. FC and significance were calculated as described in **section 2.8.3**. The following metabolites were not detected in the CB-839 experiment and were therefore not included in the results below: cysteine, dADP, glycerate, IPP, and methionine.

Results

Pipecolate and putrescine were the only metabolites with an FC_{Diff} near zero. All of the other metabolites maintained either a negative FC_{Diff} (abundance higher in wtIDH1 cells) or positive FC_{Diff} (abundance higher in mutIDH1^{R132H} cells), see **Figure 6.5.1**. The interpretation of a near zero FC_{Diff} was that decreased 2-OG minimised the metabolic difference previously observed between wtIDH1 and mutIDH1^{R132H} LN18 cells. Maintained FC_{Diff} was interpreted as 2-HG contributing to the difference in metabolite abundance observed between wtIDH1 and mutIDH1^{R132H} LN18 cells.

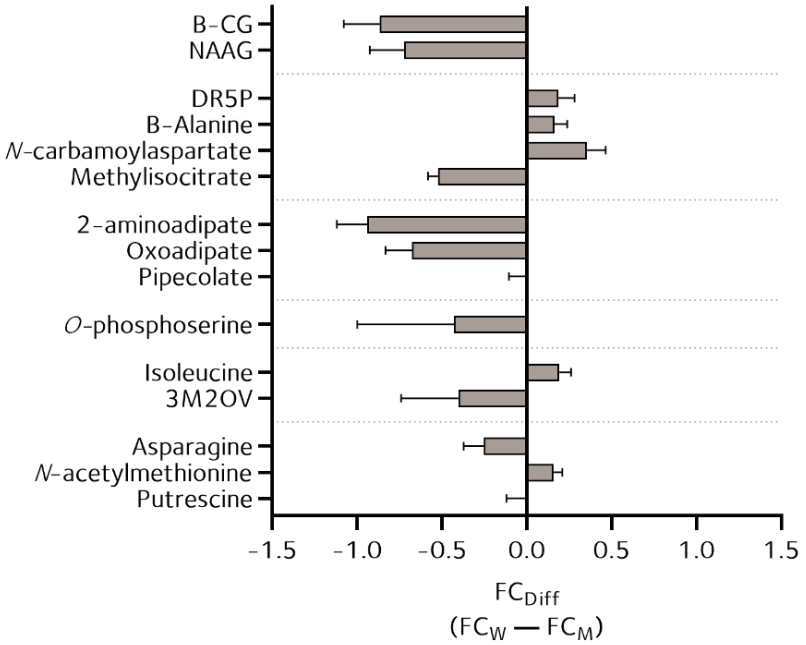

Figure 6.5.1. The FC difference (FC_{Diff}) between FC_W and FC_M. FC_W = control wtIDH1/treated wtIDH1 and FCM = control wtIDH1/treated mutIDH1; both were the average FC for all treatment concentrations. The error bars are one standard deviation. The number of biological replicates per cell line for treated group was N = 28 and for control groups was N = 8.

Next, the average FC (control/treated) of the metabolites in wtIDH1 and mutIDH1^{R132H} LN18 cells were examined to determine which metabolites were altered in abundance after treatment with CB-839. *O*-phosphoserine, methylisocitrate and 2-aminoadipate had significantly higher abundances in control than treated cells for both cell lines (p-value < 0.05, t-test with FDR adjustment). Pipecolate and putrescine had significantly lower abundances in control than treated cells for both cell lines (p-value < 0.05, t-test with FDR adjustment). Oxoadipate had significantly higher abundance in control versus treated wtIDH1 cells only, while 3M2OV had significantly higher abundance in control versus treated mutIDH1^{R132H} cells (p-value < 0.05, t-test with FDR adjustment). FCs are summarised in **Figure 6.5.2**.

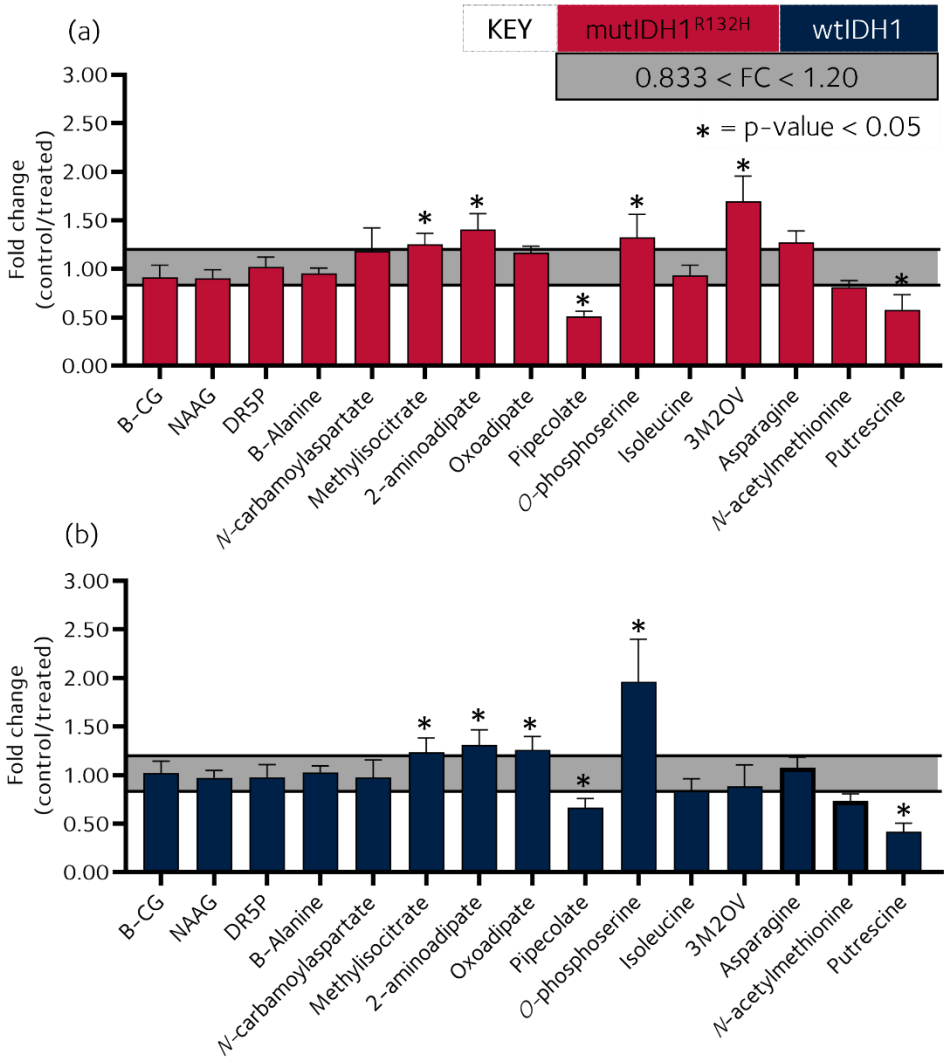

Figure 6.5.2. Average FC between treated/control wtIDH1 and mutIDH1^{R132H} LN18 cells in the CB-839 metabolomics experiment. (a) FC averages for control/treated mutIDH1^{R132H} LN18 cells. (b) FC averages for control/treated mutIDH1^{R132H} LN18 cells. Starred (*) columns had at least two treated groups that were significantly different from control (p-value < 0.05, FDR adjusted t-test). The error bars were one standard deviation. The grey area showed where 0.83 < FC < 1.20, *i.e.,* changes in metabolite abundance that were considered too small to be appreciable. The number of biological replicates per cell line for treated group was N = 28 and for control group was N = 8.

The metabolites that maintained a positive or negative FC_{Diff} and were also not significantly altered after treatment with CB-839 were: B-CG, NAAG, DR5P, B-alanine, *N*-carbamoylaspartate, isoleucine and asparagine. Since the metabolites were not sensitive to decreased 2-OG abundance, the difference between mutIDH1^{R132H} and wtIDH1 LN18 cells was due to elevated 2-HG. B-CG and NAAG were already suggested (in **chapter 5**) to be correlated to 2-HG abundance, but now DR5P, B-alanine, *N*-carbamoylaspartate, isoleucine and asparagine were postulated as well. It was surprising that DR5P was unaffected by the decreased 2-OG in the CB-839 experiment, when in **chapter 5** it appeared to correlate with

both 2-HG and 2-OG abundance in the CA. Potentially it was responding to altered NADPH in the mutIDH1 inhibitors experiment, and it only correlated to 2-OG because it was the proxy for wtIDH1 activity. 2-aminoadipate, *O*-phosphoserine and methylisocitrate maintained a positive or negative FC_{Diff}, but were also significantly altered after treatment with CB-839 in both cell lines. They were therefore sensitive to decreased 2-OG abundance, but as the difference was maintained between wtIDH1 and mutIDH1^{R132H} LN18 cells, these metabolites were also affected by the presence of high levels of 2-HG.

Oxoadipate and 3M2OV maintained a negative FC_{Diff}, however the response to CB-839 was not the same in the wtIDH1 and mutIDH1^{R132H} LN18 cells. Oxoadipate had a significantly higher abundance in control versus treated wtIDH1^{R132H} LN18 cells, but the apparent increase in mutIDH1^{R132H} LN18 cells was not significant. Collectively, 2-HG contributed to the difference in oxoadipate abundance observed between the two cell lines, but the sensitivity to decreased 2-OG concentration was higher in wtIDH1 cells. Oxoadipate is formed during an aminotransferase reaction between 2-aminoadipate and 2-OG. If that reaction was already competitively inhibited by 2-HG, the decreased 2-OG abundance would have less of an impact compared to wtIDH1 cells (where the reaction was not inhibited). However, the same would have been assumed to be the case for 3M2OV, which is the product of the transamination of 2-OG with isoleucine. Yet 3M2OV was more sensitive to decreased 2-OG abundance in mutIDH1^{R132H} than wtIDH1 LN18 cells. Potentially there was a difference in the inhibition kinetics of 2-HG and 2-aminoadipate transaminase and BCAT1 (the enzymes that catalyse biosynthesis of oxoadipate and 3M2OV, respectively). That would be best studied by *in vitro* enzyme assays, but is beyond the scope of this thesis. The difference in sensitivity to variation in 2-OG abundance, when in the presence of high levels of 2-HG, suggested that the impact of 2-HG on similar metabolic processes (*i.e.,* transamination) was more dependent on specific enzymes than perhaps previously appreciated.

The FC_{Diff} of pipecolate and putrescine was near zero, *i.e.,* the decreased 2-OG abundance diminished the differences between wtIDH1 and mutIDH1^{R132H} LN18 cells. The metabolites had significantly lower abundance in control than treated cells for both cell lines, *i.e.,* decreased 2-OG led to accumulation of the metabolites in the cells. Pipecolate is formed by oxidation of the lysine α-amine [353]. The transamination of 2-OG with 2-aminoadipate is downstream of pipecolate in the lysine degradation pathway. Accumulation of pipecolate in

CB-839 treated cells indicated that decreased 2-OG abundance was limiting further catabolism. The impact was greater in mutIDH1^{R132H} than wtIDH1 cells, which was speculated to be due to 2-HG further inhibiting the downstream transaminase reaction. However, it was puzzling that 2-aminoadipate, oxoadipate and pipecolate had such different responses to limited 2-OG availability. That would suggest that the impact of 2-HG was not uniform across the lysine degradation pathway.

Putrescine is biosynthesised in proliferating cells [reviewed in 446, 447]; the cells with limited glutamate and 2-OG exhibited decreased proliferation. Proliferation of glioma cells can be reduced by inhibition of the main enzyme that produces putrescine, ornithine decarboxylase (ODC) and then rescued by supplementation of putrescine [448]. However, high intracellular concentrations of putrescine can induce apoptosis [449]. To understand whether the increased putrescine abundance was due to imminent proliferation or apoptosis, a time course cell proliferation assay is suggested. The proliferation assay could reveal whether cells with limited glutamine utilisation had a lower growth rate than control cells. The accumulation of putrescine at 24 hours would then imply rapid cell proliferation was about to begin. However, if the cells grown with limited glutamine utilisation died off, then it could indicate that putrescine was accumulating to toxic levels.

Putrescine abundance was higher in mutIDH1^{R132H} than wtIDH1 LN18 cells, which could indicate that the presence of the mutation had an effect on polyamine metabolism. The polyamines cadaverine, spermine and spermidine had previously been analysed as standards with the derivatised RPLC-MS method, but they were not detected in the samples. How 2-HG levels and mutIDH1^{R132H} activity factored into these metabolic processes remained unknown. But the difference in response to putrescine levels, between wtIDH1 and mutIDH1^{R132H} cells, and its role in cell proliferation warrants further study.

In summary, the CB-839 metabolomics experiment confirmed that B-CG and NAAG abundance was correlated to 2-HG abundance and not affected by decreased 2-OG. The experiment also revealed that abundances of DR5P, B-alanine, N-carbamoylaspartate, isoleucine and asparagine also were affected by 2-HG exclusively. Elevated 2-HG was also responsible for the observed abundance of 2-aminoadipate, O-phosphoserine and methylisocitrate between wtIDH1 and mutIDH1^{R132H} LN18 cells for, but the three metabolites were also equally affected

by decreased 2-OG in both cell lines. Oxoadipate and 3M2OV were affected by 2-HG, but the CB-839 experiment revealed that the response to decreased 2-OG was different between wtIDH1 and mutIDH1^{R132H} LN18 cells. It was suggested that this was due to differences in how the relevant 2-OG dependent enzymes responded to speculated competitive inhibition by 2-HG, as well as decreased 2-OG abundance. Similarly, pipecolate was considered affected by 2-HG, but decreased 2-OG also limited catabolism, which was most apparent in mutIDH1^{R132H} cells. Finally, putrescine was elevated similarly after treatment in both cell lines and it was suggested that it was due to a cell proliferative response to limited glutamine utilisation.

6.6. Discussion

Directly inhibiting mutIDH1 has received considerable attention in the development of therapies targeted toward mutIDH1 glioma metabolism [reviewed in 1]. Presently, mutIDH1 inhibitors face two challenges: limited impact on disease [263, 422, 423] and the emergence of resistance [264-266, 424-427]. Expanding treatment options by developing alternative therapies would increase the likelihood of successfully treating mutIDH1 glioma. Glutaminase inhibition is currently being pursued as a therapy in glioma [442] and other cancers [273] in phase I trials. It was therefore of interest to investigate the response of the LN18 cell lines to CB-839 and compare this with mutIDH1 inhibitors. As a monotherapy, CB-839 had a significantly greater impact on cell viability than the mutIDH1 inhibitors (p-value < 0.001, two-sided unpaired t-test). The wtIDH1 LN18 cells were significantly more sensitive than the mutIDH1^{R132H} LN18 cells (p-value < 0.01, one-way ANOVA with Šídák MCTe), which prompted further metabolic analysis to better understand the difference.

GLS catalyses the deamination of glutamine to glutamate (see **Figure 6.6.1**). In mutIDH1 glioma, glutamate-derived 2-OG is the main source of carbon for 2-HG (**chapter 3**) [147]. Treatment with CB-839 was expected to lead to an accumulation of glutamine and decreased glutamate abundance. The limited glutamate was hypothesised to consequently deplete 2-HG, however this was not the case. Treated cells had a higher abundance of glutamine and lower abundance of glutamate, in agreement with previous reports of GBM cell lines treated with GLS inhibitors [207, 208, 450]. Furthermore, 2-OG was significantly decreased treated wtIDH1 and mutIDH1^{R132H} LN18 cells, but 2-HG was not affected. Only one previous study

found a small, but significant decrease in 2-HG abundance in a mutIDH1^{R132H} GBM cells (D54) treated with GLS inhibitor BPTES [207]. The maintained 2-HG abundance despite restricted glutamate prompted the question of whether the cells were metabolising additional glucose to compensate. MutIDH1^{R132H} LN18 cells did not have significantly increased glucose consumption after treatment with CB-839. The lack of increase in glucose consumption could have been due to the relatively short exposure time to CB-839 (24 hours) or because the cells were compensating for decreased GLS activity using alternative enzymes.

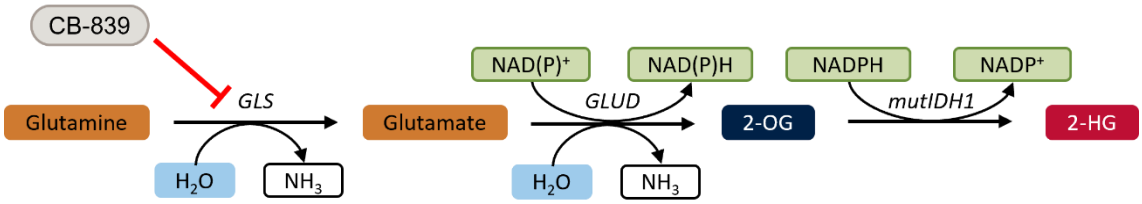

Figure 6.6.1. Overview of reactions catabolised by GLS, GLUD and mutIDH1. Glutamine is hydrolysed to glutamate by GLS and glutamate can be further oxidised to 2-OG by GLUD. MutIDH1 catalyses the reduction of 2-OG to 2-HG. Abbreviations: GLS = glutaminase, GLUD = glutamate dehydrogenase, mutIDH1 = mutant isocitrate dehydrogenase 1, 2-OG = 2-oxoglutarate and 2-HG = 2-hydroxyglutarate.

In a study where patient-derived glioma cell lines that endogenously expressed mutIDH1^{R132H} were treated with CB-839, asparagine synthetase (ASNS) and glutamate oxaloacetate transaminase (GOT) were upregulated in treated cells [208]. ASNS transfers an amine from glutamine to aspartate, producing asparagine and glutamate, whereas GOT transfers the amine from aspartate to 2-OG, producing oxaloacetate and glutamate. Both enzymes allow the cells to 'bypass' GLS inhibition. Potentially, the mutIDH1^{R132H} LN18 cells had increased expression of ASNS and GOT, allowing them to utilise glutamine and maintain 2-HG abundance. It would be of interest to determine whether the expression was already elevated in mutIDH1^{R132H} cells prior to treatment, as a way to increase glutamate availability for 2-HG biosynthesis, or if the increase occurred after treatment with CB-839. Ultimately, the therapeutic benefit of CB-839 depends on whether the cells are able to circumvent the consequence of GLS inhibition or not. If mutIDH1 cells are already primed to access glutamate via other enzymes, CB-839 may not be an effective treatment. The drug would likely benefit from patient stratification, and may perhaps be best used in combination with other treatments and chemotherapies as an adjuvant, rather than a monotherapy.

Treatment with CB-839 offered an opportunity to re-examine metabolic differences between wtIDH1 and mutIDH1^{R132H} LN18 cells. Perhaps surprisingly, B-CG and NAAG, metabolites that

require glutamate for synthesis, remained largely unchanged by limited glutamate levels. NAAG has previously been suggested as a reservoir of glutamate for cancer cells [400]. However, considering the abundance was maintained, despite the limited glutamate supply, the data presented here does not support this hypothesis. The exact role(s) of B-CG in human metabolism remain unknown, but it is also unlikely that it acts as a glutamate pool. A previous study found that it could act in a redox protective manner when complexed with Cu(II) [403]. Yet, glutathione is a redox protective molecule, and it has previously been shown to be decreased in mutIDH1^{R132H}-expressing HOG and NHA cells with decreased glutamate after treatment with CB-839 [173]. If B-CG has a redox protective role in cells, it would be expected to be similarly affected by decreased glutamate as glutathione. A better understanding of the metabolic role of B-CG in glioma is needed before this can be answered, but it is intriguing that its abundance was unaffected by depleted glutamate.

The other metabolites with unclear correlation to 2-HG and mutIDH1^{R132H} activity in **chapter 5** were categorized. All but pipecolate and putrescine were clearly dependent on 2-HG, considering the maintained difference between wtIDH1 and mutIDH1^{R132H} cells after treatment with CB-839. Pipecolate also is suggested to still be affected by the presence of high levels of 2-HG, as it accumulated in both cell lines, but to a greater extent in mutIDH1^{R132H} cells. This was potentially due the downstream transamination of 2-OG with 2-aminoadipate as a result of decreased 2-OG availability and speculated competitive inhibition by 2-HG. The mechanism by which 2-HG is affecting the metabolic pathways has only been explored for BCAAs, where decreased expression of BCAT1 and direct inhibition of BCAT1 have been reported [173, 192, 204]. Potentially a similar mechanism is occurring for lysine degradation, although the different responses of oxoadipate and 3M2OV to treatment with CB-839, indicated that it is not necessarily the same. As both enzymes produce glutamate after transamination of 2-OG, they could potentially be used as therapeutic targets, if the therapeutic objective was to further limit glutamate availability.

Lysine degradation and a number of other amino acids and intermediates have been highlighted throughout **chapter 3-6** as significantly different between mutIDH1^{R132H} and wtIDH1 LN18 cells, associated with decreased 2-HG abundance. The abundance of amino acids and related metabolites have also previously been reported as altered in mutIDH1 glioma, although only BCAT1 has been thoroughly studied [reviewed in 1]. Collectively, these

studies suggest that the *IDH1* mutation leads to altered amino acid metabolism, which could point toward an additional tumorigenic role of the *IDH1* mutation in glioma. Amino acid metabolism provides cells with *e.g.,* anaplerotic sources for the TCA cycle, methyl groups for one-carbon metabolism and building-blocks for glutathione biosynthesis; metabolic reprogramming to facilitate growth and survival has been found in a variety of cancers [reviewed in 381]. Establishing the specifics of mutIDH1 glioma amino acid metabolism may lead to better understanding of the disease and guide development of therapeutic strategies. To achieve deeper insight and to potentially disentangle confounding effects, combining multiple 'omics' data sets to allow for metabolic modelling should be considered. Transcriptomics provides information on changes in gene expression levels, which in turn could aid in identifying which metabolic enzymes or pathways were responding to e.g., mutIDH1 or GLS inhibition.

6.7. Summary and conclusions

The GLS inhibitor CB-839 led to significant decrease in cell viability in both wtIDH1 and mutIDH1^{R132H} LN18 cells. It was more effective at decreasing cell viability than the mutIDH1 inhibitors examined in **chapter 5** after 24 hours of treatment. The greater reliance on GLS for glutamine catabolism was suggested as an explanation for the higher sensitivity toward CB-839 exhibited by the wtIDH1 LN18 cells. In mutIDH1^{R132H} LN18 cells, 2-HG abundance remained high despite significant decrease in 2-OG abundance. 2-HG abundance was not maintained by increased consumption of glucose. It was therefore hypothesised that the cells were compensating for decreased GLS activity with enzymes such as ASNS and GOT, as found in other mutIDH1 glioma cell lines treated with CB-839. For the inhibitor to succeed as a therapeutic agent, it would be beneficial to screen biopsies for increased expression of enzymes that could circumvent GLS inhibition. Most likely though, CB-839 will have to be used in combination with other treatments to address these challenges.

Decreased abundance of 2-OG, without concurrent changes in 2-HG, allowed the study of the relationship between other metabolites and 2-HG to be considered. B-CG and NAAG were yet again confirmed to be affected by 2-HG abundance alone, although this observation was surprising since both require glutamate for biosynthesis. It was not clear why their abundance was maintained when glutamate was depleted, especially as the metabolic role of B-CG

remains unknown. However, the consistent correlation with 2-HG abundance should prompt more research into the metabolic functions of B-CG and whether it contributes to tumorigenesis. Lysine degradation was affected by both 2-HG and 2-OG abundance, similarly to the BCAT1 product 3M2OV, which showed that other transamination enzymes are likely competitively inhibited by 2-HG at high concentration. In general, amino acid metabolism is altered in the mutIDH1^{R132H} LN18 cells and its potential role in tumorigenesis, and opportunities for therapeutic targets, should be further explored.

Chapter 7. Conclusions and further work

7.1. Conclusions

In this thesis, mutIDH1 glioma metabolism was studied by comparing it to a matched wild type *IDH1* cell line and by treating it with inhibitors that either directly affected the mutIDH1^{R132H} enzyme or indirectly limited substrate availability. The aim was to advance the understanding of mutIDH1 glioma metabolism and how 2-HG abundance related to other altered metabolites. With that knowledge, further insight into the tumorigenic capabilities of mutIDH1 glioma metabolism can be established and new therapeutic targets uncovered.

The abundance of 2-HG in mutIDH1 glioma is significantly elevated and that has been linked to altered BCAA and lipid metabolism, as well as changes in abundance of specific metabolites [reviewed in 1]. The glioblastoma cell line LN18 with mutant *IDH1* expressed via lentiviral vector was used as the mutIDH1 glioma model in this thesis and it had significantly higher 2-HG levels than the wtIDH1 LN18 cells. Additional metabolites and pathways that were significantly different between the two cell lines were found with statistical analyses. The cell model covered aspects of metabolism previously reported on (*e.g.,* BCAA catabolism), but metabolites and pathways that have otherwise received limited attention were also found (*e.g.*, B-CG and lysine degradation). Several of the metabolites were either directly dependent on 2-OG as a substrate for biosynthesis or were part of a pathway where one or more reactions required 2-OG as a substrate. Decreased substrate availability or direct competitive inhibition by 2-HG were suggested explanations for their modulation in mutIDH1^{R132H} LN18 cells. Indirect effects, *e.g.*, changes in transcription levels of enzymes, could also lead to altered metabolite abundances. Metabolites that were not thought to require 2-OG or $NADP^+$/NADPH for biosynthesis or catabolism were considered more likely to be affected indirectly than directly by 2-HG. Comparing wtIDH1 and mutIDH1^{R132H} LN18 cells therefore provided metabolites of interest to study further in cells treated with metabolic inhibitors. The need to separate direct from indirect effects of 2-HG informed the design and choice of subsequent experiments.

The four mutIDH1 inhibitors AG-120, AG-881, BAY 1436032 and GSK864 were capable of significantly and substantially decreasing 2-HG abundance in treated mutIDH1^{R132H} LN18 cells.

However, mutIDH1^{R1342H} LN18 cell viability was not substantially decreased. AG-120, AG-881 and GSK864 had IC_{50} for wtIDH1 in the low nM-μM range [246, 250, 416] and were capable of inhibiting wtIDH1 activity in both cell lines (≥ 5.00 μM); isocitrate accumulated significantly in treated cells. AG-120, BAY 1436032 and GSK864 were similar in their ability to decrease 2-HG abundance over a range of concentrations and exposure times. AG-881 was an inferior inhibitor to the other three, despite having similar cellular levels as BAY 1436032. It was unable to reach the same substantial decrease in 2-HG abundance, even when cells were exposed to inhibitor for longer. The limited effect on cell viability had previously been reported [reviewed in 1], but the comparison of the four inhibitors over a range of concentrations and treatment timepoints had not. The differences in when and to what extent 2-HG abundance was decreased by the inhibitors supported the interpretation of altered mutIDH1 metabolism. Establishing that wtIDH1 was inhibited at high enough concentrations of AG-120, AG-881 and GSK864 also influenced the understanding of how other metabolites responded to treatment.

MutIDH1 inhibitors were yet to be used to interrogate mutIDH1 glioma metabolism with the metabolic coverage and range of experiments described here. Treatment with mutIDH1 inhibitors brought the mutIDH1^{R132H} LN18 cells closer to wtIDH1 cells metabolically. The modulation of metabolites appeared to correlate with 2-HG abundance in the multivariate analyses. However, several metabolites responded similarly to mutIDH1 inhibitors in wtIDH1 and mutIDH1^{R132H} cells. It prompted the question of whether a response was due to inhibited mutIDH1^{R132H}, wtIDH1 or both. Univariate analyses were performed in an attempt to discern what was the main driver behind metabolite modulation. Metabolites altered from inhibition of both enzymes did not necessarily exclude them from being regarded as affected by 2-HG abundance, but it was difficult to estimate the degree of influence. Despite the challenging data interpretation resulting from concurrent wtIDH1 and mutIDH1^{R132H} inhibition, the work further supported the hypothesis that mutIDH1 metabolism was affected by 2-HG abundance through direct and indirect effects. Furthermore, the altered metabolite abundances correlated to 2-HG abundance and both direct and indirect effects were suggested to be responsible. The correlative relationship to 2-HG suggested a role in tumorigenesis that also may offer new therapeutic targets.

GLS inhibition was explored as an alternative therapeutic strategy. MutIDH1 inhibitors did not decrease mutIDH1^{R132H} LN18 cells viability substantially, but treatment with GLS inhibitor CB-839 did. WtIDH1 and mutIDH1^{R132H} LN18 cells were not similarly sensitive to CB-839; it was suggested that the wtIDH1 cells were less able to bypass GLS inhibition than the mutIDH1^{R132H} LN18 cells. Furthermore, treatment with inhibitor led to decreased glutamate and 2-OG abundance, but it did not lead to the expected decreased abundance in 2-HG. The cells did not compensate by increasing glucose consumption, and the hypothesis that mutIDH1^{R132H} cells were better able to compensate for decreased GLS activity was strengthened. The maintained 2-HG abundance coupled with decreased 2-OG abundance was suited to probe the effect of 2-HG and 2-OG abundance on different metabolites. It was possible to distinguish metabolites that were only affected by 2-HG abundance, affected by maintained 2-HG and decreased 2-OG, and affected by maintained 2-HG but with a dissimilar response to decreased 2-OG abundance. Collectively, the metabolomics experiments presented in this thesis advanced the knowledge of which metabolites were correlated with 2-HG abundance, whether 2-HG was likely to have a direct, indirect or combined effect and which areas of metabolism to focus future work.

The pitfalls of adaptation and resistance to metabolic inhibition are evident. Treatment based on metabolic targets will likely have to be based on combinations of therapies. It also remains to be determined what the focus should be; is it most beneficial to decrease 2-HG abundance or rather to challenge the cells to maintain 2-HG abundance under substrate deprivation? Which treatment strategy is most efficient, or perhaps when it is most suitably applied, depends on whether sustaining high 2-HG abundance contributes to tumorigenesis in mutIDH1 glioma. The correlation of 2-HG with a number of metabolites points toward a benefit of altering pathway activities. The potential benefits provided by the mutIDH1 specific alterations of amino acid metabolism for tumour development are not well understood. Similarly, the function of B-CG in the cellular environment remains to be determined. Only once the potential role and impact on tumorigenesis is appreciated can the merit of amino acid metabolism and B-CG as targets for therapy be evaluated.

7.2. Limitations and further work

The work presented in this thesis had certain limitations. The cell-based experiments were carried out with a single immortalised cell GBM cell line. Certain metabolic changes may have been specific to this cell line and therefore cannot be applied to glioma more broadly. Furthermore, the cells were cultured under conditions that did not necessarily match physiological levels of specific metabolites, which can affect cellular metabolism significantly [451]. However, the consistency of certain metabolic changes and the biological reasoning behind those changes have identified areas to focus future work. The inability to measure and quantify NAD^+/NADH and $NADP^+$/NADPH in cell samples limited the interpretation of modulated metabolism to a degree, because changes in redox homeostasis could not be quantified. Finally, the IC-MS and derivatised RPLC-MS methods did not provide full coverage of the metabolome and metabolic changes linked to 2-HG abundance may have been missed. For example, phospholipid metabolism has previously been reported as consistently altered in mutIDH1 glioma [reviewed in 1], but was not covered by the methods used here. The effects of 2-HG abundance and mutIDH1^{R132H} activity on phospholipid metabolism merits further work, as it may inform on whether the modulations are pro-tumorigenic.

The findings in this thesis showed that metabolism was altered upon introduction of mutant *IDH1* in a GBM cell line, and that those metabolic alterations correlated with 2-HG abundance. The modulation of metabolism after treatment with mutIDH1 and GLS inhibitors should be studied in additional glioma cell lines to corroborate these findings. Preferably the cell lines would have an endogenous *IDH1* mutation and be cultured in media customised for glial cells to more closely match *in vivo* conditions. Furthermore, $NADP^+$ and NADPH needs to be measured in cells treated with mutIDH1 inhibitors to support the analysis of mutIDH1 glioma metabolism. Preferably, a LC-MS method capable of repeatably analysing and quantifying NAD^+, NADH, $NADP^+$ and NADPH would be developed. There are cellular assays available, but they do not provide the same flexibility as LC-MS does or the option of expanding the analysis to include other redox related metabolites (*e.g.*, glutathione, flavine adenine dinucleotide). Method development should focus on improving sample stability and chromatographic performance, which will both contribute to improving repeatability and sensitivity.

Chapter 8. References

1. Hvinden, I.C., et al., *Metabolic adaptations in cancers expressing isocitrate dehydrogenase mutations.* Cell Reports Medicine, 2021. **2**(12): p. 100469.
2. Fouad, Y.A. and C. Aanei, *Revisiting the hallmarks of cancer.* American journal of cancer research, 2017. **7**(5): p. 1016-1036.
3. DeBerardinis, R.J. and N.S. Chandel, *Fundamentals of cancer metabolism.* Science Advances, 2016. **2**(5): p. e1600200.
4. Balss, J., et al., *Analysis of the IDH1 codon 132 mutation in brain tumors.* Acta Neuropathologica, 2008. **116**(6): p. 597-602.
5. Parsons, D.W., et al., *An Integrated Genomic Analysis of Human Glioblastoma Multiforme.* Science, 2008. **321**(5897): p. 1807-1812.
6. Mardis, E.R., et al., *Recurring Mutations Found by Sequencing an Acute Myeloid Leukemia Genome.* New England Journal of Medicine, 2009. **361**(11): p. 1058-1066.
7. Gross, S., et al., *Cancer-associated metabolite 2-hydroxyglutarate accumulates in acute myelogenous leukemia with isocitrate dehydrogenase 1 and 2 mutations.* The Journal of Experimental Medicine, 2010. **207**(2): p. 339-334.
8. Ward, P.S., et al., *The Common Feature of Leukemia-Associated IDH1 and IDH2 Mutations Is a Neomorphic Enzyme Activity Converting α-Ketoglutarate to 2-Hydroxyglutarate.* Cancer Cell, 2010. **17**(3): p. 225-234.
9. Yan, H., et al., *IDH1 and IDH2 Mutations in Gliomas.* New England Journal of Medicine, 2009. **360**(8): p. 765-773.
10. Hartmann, C., et al., *Type and frequency of IDH1 and IDH2 mutations are related to astrocytic and oligodendroglial differentiation and age: a study of 1,010 diffuse gliomas.* Acta Neuropathologica, 2009. **118**(4): p. 469-474.
11. Ichimura, K., et al., *IDH1 mutations are present in the majority of common adult gliomas but rare in primary glioblastomas.* Neuro-Oncology, 2009. **11**(4): p. 341-347.
12. Watanabe, T., et al., *IDH1 Mutations Are Early Events in the Development of Astrocytomas and Oligodendrogliomas.* The American Journal of Pathology, 2009. **174**(4): p. 1149-1153.
13. Wang, H.-Y., et al., *The comparison of clinical and biological characteristics between IDH1 and IDH2 mutations in gliomas.* Journal of Experimental & Clinical Cancer Research, 2016. **35**(1): p. 86.
14. Amary, M.F., et al., *IDH1 and IDH2 mutations are frequent events in central chondrosarcoma and central and periosteal chondromas but not in other mesenchymal tumours.* The Journal of Pathology, 2011. **224**(3): p. 334-343.
15. Arai, M., et al., *Frequent IDH1/2 mutations in intracranial chondrosarcoma: a possible diagnostic clue for its differentiation from chordoma.* Brain Tumor Pathology, 2012. **29**(4): p. 201-206.
16. Lu, C., et al., *Induction of sarcomas by mutant IDH2.* Genes & Development, 2013. **27**(18): p. 1986-1998.
17. Kato Kaneko, M., et al., *Isocitrate dehydrogenase mutation is frequently observed in giant cell tumor of bone.* Cancer Science, 2014. **105**(6): p. 744-748.
18. Jin, Y., et al., *Mutant IDH1 Dysregulates the Differentiation of Mesenchymal Stem Cells in Association with Gene-Specific Histone Modifications to Cartilage- and Bone-Related Genes.* PLOS ONE, 2015. **10**(7): p. e0131998.
19. Lugowska, I., et al., *IDH1/2 mutations to predict shorter survival in chondrosarcoma.* Journal of Clinical Oncology, 2016. **34**(15): p. 11024-11024.
20. Cleven, A.H.G., et al., *IDH1 or -2 mutations do not predict outcome and do not cause loss of 5-hydroxymethylcytosine or altered histone modifications in central chondrosarcomas.* Clinical Sarcoma Research, 2017. **7**: p. 1-10.
21. Tallegas, M., et al., *IDH mutation status in a series of 88 head and neck chondrosarcomas: different profile between tumors of the skull base and tumors involving the facial skeleton and the laryngotracheal tract.* Human Pathology, 2019. **84**: p. 183-191.
22. Abbas, S., et al., *Acquired mutations in the genes encoding IDH1 and IDH2 both are recurrent aberrations in acute myeloid leukemia: prevalence and prognostic value.* Blood, 2010. **116**(12): p. 2122-2126.

23. Marcucci, G., et al., *IDH1 and IDH2 gene mutations identify novel molecular subsets within de novo cytogenetically normal acute myeloid leukemia: a Cancer and Leukemia Group B study.* Journal of clinical oncology : official journal of the American Society of Clinical Oncology, 2010. **28**(14): p. 2348-2355.
24. Schnittger, S., et al., *IDH1 mutations are detected in 6.6% of 1414 AML patients and are associated with intermediate risk karyotype and unfavorable prognosis in adults younger than 60 years and unmutated NPM1 status.* Blood, 2010. **116**(25): p. 5486-5496.
25. Wagner, K., et al., *Impact of IDH1 R132 Mutations and an IDH1 Single Nucleotide Polymorphism in Cytogenetically Normal Acute Myeloid Leukemia: SNP rs11554137 Is an Adverse Prognostic Factor.* Journal of Clinical Oncology, 2010. **28**(14): p. 2356-2364.
26. Molenaar, R.J., et al., *Clinical and biological implications of ancestral and non-ancestral IDH1 and IDH2 mutations in myeloid neoplasms.* Leukemia, 2015. **29**: p. 2134-2142.
27. Figueroa, M.E., et al., *Leukemic IDH1 and IDH2 Mutations Result in a Hypermethylation Phenotype, Disrupt TET2 Function, and Impair Hematopoietic Differentiation.* Cancer Cell, 2010. **18**(6): p. 553-567.
28. Paschka, P., et al., *IDH1 and IDH2 Mutations Are Frequent Genetic Alterations in Acute Myeloid Leukemia and Confer Adverse Prognosis in Cytogenetically Normal Acute Myeloid Leukemia With NPM1 Mutation Without FLT3 Internal Tandem Duplication.* Journal of Clinical Oncology, 2010. **28**(22): p. 3636-3643.
29. Borger, D.R., et al., *Frequent Mutation of Isocitrate Dehydrogenase (IDH)1 and IDH2 in Cholangiocarcinoma Identified Through Broad-Based Tumor Genotyping.* The Oncologist, 2012. **17**(1): p. 72-79.
30. Kipp, B.R., et al., *Isocitrate dehydrogenase 1 and 2 mutations in cholangiocarcinoma.* Human Pathology, 2012. **43**(10): p. 1552-1558.
31. Wang, P., et al., *Mutations in isocitrate dehydrogenase 1 and 2 occur frequently in intrahepatic cholangiocarcinomas and share hypermethylation targets with glioblastomas.* Oncogene, 2012. **32**: p. 3091-3100.
32. Jiao, Y., et al., *Exome sequencing identifies frequent inactivating mutations in BAP1, ARID1A and PBRM1 in intrahepatic cholangiocarcinomas.* Nature Genetics, 2013. **45**: p. 1470-1473.
33. Ross, J.S., et al., *New routes to targeted therapy of intrahepatic cholangiocarcinomas revealed by next-generation sequencing.* The oncologist, 2014. **19**(3): p. 235-242.
34. Farshidfar, F., et al., *Integrative Genomic Analysis of Cholangiocarcinoma Identifies Distinct IDH-Mutant Molecular Profiles.* Cell Reports, 2017. **18**(11): p. 2780-2794.
35. Lee, J.H., et al., *IDH1 R132C mutation is detected in clear cell hepatocellular carcinoma by pyrosequencing.* World Journal of Surgical Oncology, 2017. **15**: p. 1-8.
36. Nepal, C., et al., *Genomic perturbations reveal distinct regulatory networks in intrahepatic cholangiocarcinoma.* Hepatology, 2018. **68**(3): p. 949-963.
37. Wang, J., et al., *IDH1 mutation correlates with a beneficial prognosis and suppresses tumor growth in IHCC.* Journal of Surgical Research, 2018. **231**: p. 116-125.
38. Cairns, R.A., et al., *IDH2 mutations are frequent in angioimmunoblastic T-cell lymphoma.* Blood, 2012. **119**(8): p. 1901-1903.
39. Odejide, O., et al., *A targeted mutational landscape of angioimmunoblastic T-cell lymphoma.* Blood, 2014. **123**(9): p. 1293-1296.
40. Sakata-Yanagimoto, M., et al., *Somatic RHOA mutation in angioimmunoblastic T cell lymphoma.* Nature Genetics, 2014. **46**: p. 171-175.
41. Wang, C., et al., *IDH2^{R172} mutations define a unique subgroup of patients with angioimmunoblastic T-cell lymphoma.* Blood, 2015. **126**(15): p. 1741-1752.
42. Dogan, S., et al., *Frequent IDH2 R172 mutations in undifferentiated and poorly-differentiated sinonasal carcinomas.* J Pathol, 2017. **242**(4): p. 400-408.
43. Jo, V.Y., et al., *Recurrent IDH2 R172X mutations in sinonasal undifferentiated carcinoma.* Modern Pathology, 2017. **30**: p. 650-659.
44. Riobello, C., et al., *IDH2 Mutation Analysis in Undifferentiated and Poorly Differentiated Sinonasal Carcinomas for Diagnosis and Clinical Management.* American Journal of Surgical Pathology, 2020. **44**(3): p. 396-405.
45. Chiang, S., et al., *IDH2 Mutations Define a Unique Subtype of Breast Cancer with Altered Nuclear Polarity.* Cancer Research, 2016. **76**(24): p. 7118-7129.

46. Lozada, J.R., et al., *Solid papillary breast carcinomas resembling the tall cell variant of papillary thyroid neoplasms (solid papillary carcinomas with reverse polarity) harbour recurrent mutations affecting IDH2 and PIK3CA: a validation cohort.* Histopathology, 2018. **73**(2): p. 339-344.
47. Pusch, S., et al., *Scientific correspondence: Glioma IDH1 mutation patterns off the beaten track.* Neuropathology and Applied Neurobiology, 2011. **37**(4): p. 428-430.
48. Gupta, R., et al., *Expanding the spectrum of IDH1 mutations in gliomas.* Modern Pathology, 2013. **26**: p. 619-625.
49. Balss, J., et al., *Enzymatic assay for quantitative analysis of (d)-2-hydroxyglutarate.* Acta Neuropathologica, 2012. **124**(6): p. 883-891.
50. Kang, M.R., et al., *Mutational analysis of IDH1 codon 132 in glioblastomas and other common cancers.* International Journal of Cancer, 2009. **125**(2): p. 353-355.
51. Thol, F., et al., *IDH1 mutations in patients with myelodysplastic syndromes are associated with an unfavorable prognosis.* Haematologica, 2010. **95**(10): p. 1668-1674.
52. Pardanani, A., et al., *IDH1 and IDH2 mutation analysis in chronic- and blast-phase myeloproliferative neoplasms.* Leukemia, 2010. **24**: p. 1146-1151.
53. Tefferi, A., et al., *IDH1 and IDH2 mutation studies in 1473 patients with chronic-, fibrotic- or blast-phase essential thrombocythemia, polycythemia vera or myelofibrosis.* Leukemia, 2010. **24**(7): p. 1302-1309.
54. Oki, K., et al., *IDH1 and IDH2 mutations are rare in pediatric myeloid malignancies.* Leukemia, 2011. **25**: p. 382-384.
55. Andersson, A.K., et al., *IDH1 and IDH2 mutations in pediatric acute leukemia.* Leukemia, 2011. **25**: p. 1570-1577.
56. Ally, A., et al., *Comprehensive and Integrative Genomic Characterization of Hepatocellular Carcinoma.* Cell, 2017. **169**(7): p. 1327-1341.e23.
57. Zhu, G.G., et al., *Genomic Profiling Identifies Association of IDH1/IDH2 Mutation with Longer Relapse-Free and Metastasis-Free Survival in High-Grade Chondrosarcoma.* Clinical Cancer Research, 2020. **26**(2): p. 419-427.
58. Liu, X., et al., *Isocitrate dehydrogenase 2 mutation is a frequent event in osteosarcoma detected by a multi-specific monoclonal antibody MsMab-1.* Cancer Medicine, 2013. **2**(6): p. 803-814.
59. Na, K.Y., et al., *IDH Mutation Analysis in Ewing Sarcoma Family Tumors.* Journal of pathology and translational medicine, 2015. **49**(3): p. 257-261.
60. Pansuriya, T.C., et al., *Somatic mosaic IDH1 and IDH2 mutations are associated with enchondroma and spindle cell hemangioma in Ollier disease and Maffucci syndrome.* Nature Genetics, 2011. **43**: p. 1256-1261.
61. Amary, M.F., et al., *Ollier disease and Maffucci syndrome are caused by somatic mosaic mutations of IDH1 and IDH2.* Nature Genetics, 2011. **43**: p. 1262-1265.
62. Fathi, A.T., et al., *Isocitrate Dehydrogenase 1 (IDH1) Mutation in Breast Adenocarcinoma Is Associated With Elevated Levels of Serum and Urine 2-Hydroxyglutarate.* Oncologist, 2014. **19**(6): p. 602-607.
63. Li-Chang, H.H., et al., *Retrospective review using targeted deep sequencing reveals mutational differences between gastroesophageal junction and gastric carcinomas.* BMC Cancer, 2015. **15**(1): p. 32.
64. Hartman, D.J., et al., *Isocitrate dehydrogenase-1 is mutated in inflammatory bowel disease-associated intestinal adenocarcinoma with low-grade tubuloglandular histology but not in sporadic intestinal adenocarcinoma.* Am J Surg Pathol, 2014. **38**(8): p. 1147-56.
65. Lopez, G.Y., et al., *IDH1R132 mutation identified in one human melanoma metastasis, but not correlated with metastases to the brain.* Biochemical and Biophysical Research Communications, 2010. **398**(3): p. 585-587.
66. Toth, L.N., F.B. de Abreu and L.J. Tafe, *Non–small cell lung cancers with isocitrate dehydrogenase 1 or 2 (IDH1/2) mutations.* Human Pathology, 2018. **78**: p. 138-143.
67. Gaal, J., et al., *Isocitrate Dehydrogenase Mutations Are Rare in Pheochromocytomas and Paragangliomas.* The Journal of Clinical Endocrinology & Metabolism, 2010. **95**(3): p. 1274-1278.
68. Hinsch, A., et al., *Immunohistochemically detected IDH1R132H mutation is rare and mostly heterogeneous in prostate cancer.* World Journal of Urology, 2018. **36**(6): p. 877-882.
69. Kurek, K.C., et al., *R132C IDH1 Mutations Are Found in Spindle Cell Hemangiomas and Not in Other Vascular Tumors or Malformations.* The American Journal of Pathology, 2013. **182**(5): p. 1494-1500.

70. Murugan, A.K., E. Bojdani and M. Xing, *Identification and functional characterization of isocitrate dehydrogenase 1 (IDH1) mutations in thyroid cancer.* Biochemical and Biophysical Research Communications, 2010. **393**(3): p. 555-559.
71. Hemerly, J.P., A.U. Bastos and J.M. Cerutti, *Identification of several novel non-p.R132 IDH1 variants in thyroid carcinomas.* European Journal of Endocrinology, 2010. **163**(5): p. 747-755.
72. Rakheja, D., et al., *Isocitrate dehydrogenase 1/2 mutational analyses and 2-hydroxyglutarate measurements in Wilms tumors.* Pediatric Blood & Cancer, 2011. **56**(3): p. 379-383.
73. Louis, D.N., et al., *The 2016 World Health Organization Classification of Tumors of the Central Nervous System: a summary.* Acta Neuropathologica, 2016. **131**(6): p. 803-820.
74. Louis, D.N., et al., *The 2021 WHO Classification of Tumors of the Central Nervous System: a summary.* Neuro-Oncology, 2021. **23**(8): p. 1231-1251.
75. Zhao, S., et al., *Glioma-Derived Mutations in IDH1 Dominantly Inhibit IDH1 Catalytic Activity and Induce HIF-1α.* Science, 2009. **324**(5924): p. 261-265.
76. Dang, L., et al., *Cancer-associated IDH1 mutations produce 2-hydroxyglutarate.* Nature, 2009. **462**: p. 739-746.
77. Gregersen, N., J. Ingerslev and K. Rasmussen, *Low Molecular Weight Organic Acids In The Urine Of The Newborn.* Acta Paediatrica, 1977. **66**(1): p. 85-89.
78. Hoffmann, G., et al., *Quantitative analysis for organic acids in biological samples: batch isolation followed by gas chromatographic-mass spectrometric analysis.* Clinical Chemistry, 1989. **35**(4): p. 587-595.
79. Janin, M., et al., *Serum 2-hydroxyglutarate production in IDH1-and IDH2-mutated de novo acute myeloid leukemia: a study by the Acute Leukemia French Association group.* Journal of clinical oncology, 2014. **32**(4): p. 297-305.
80. Suzuki, H., et al., *Mutational landscape and clonal architecture in grade II and III gliomas.* Nature Genetics, 2015. **47**(5): p. 458-468.
81. Abdel-Wahab, O., et al., *Genetic Analysis of Transforming Events That Convert Chronic Myeloproliferative Neoplasms to Leukemias.* Cancer Research, 2010. **70**(2): p. 447-452.
82. Xie, M., et al., *Age-related mutations associated with clonal hematopoietic expansion and malignancies.* Nature Medicine, 2014. **20**(12): p. 1472-1478.
83. Chowdhury, R., et al., *The oncometabolite 2-hydroxyglutarate inhibits histone lysine demethylases.* EMBO reports, 2011. **12**(5): p. 463-469.
84. Xu, W., et al., *Oncometabolite 2-Hydroxyglutarate Is a Competitive Inhibitor of α-Ketoglutarate-Dependent Dioxygenases.* Cancer Cell, 2011. **19**(1): p. 17-30.
85. Ye, D., K.-L. Guan and Y. Xiong, *Metabolism, Activity, and Targeting of D- and L-2-Hydroxyglutarates.* Trends in Cancer, 2018. **4**(2): p. 151-165.
86. Johannessen, T.-C.A., et al., *Rapid Conversion of Mutant IDH1 from Driver to Passenger in a Model of Human Gliomagenesis.* Molecular Cancer Research, 2016. **14**(10): p. 976-983.
87. Walker, O.S., et al., *Photoactivation of Mutant Isocitrate Dehydrogenase 2 Reveals Rapid Cancer-Associated Metabolic and Epigenetic Changes.* Journal of the American Chemical Society, 2016. **138**(3): p. 718-721.
88. Cairns, R.A. and T.W. Mak, *Oncogenic Isocitrate Dehydrogenase Mutations: Mechanisms, Models, and Clinical Opportunities.* Cancer Discovery, 2013. **3**(7): p. 730-741.
89. D'Adamo, A.F. and D.E. Haft, *An alternate pathway of α-ketoglutarate catabolism in the isolated, perfused rat liver I. Studies with DL-glutamate-2-and-5-14C.* Journal of Biological Chemistry, 1965. **240**(2): p. 613-617.
90. Dalziel, K. and J.C. Londesborough, *The mechanisms of reductive carboxylation reactions. Carbon dioxide or bicarbonate as substrate of nicotinamide-adenine dinucleotide phosphate-linked isocitrate dehydrogenase and 'malic' enzyme.* Biochemical Journal, 1968. **110**(2): p. 223-230.
91. Gabriel, J.L., P.R. Zervos and G.W.E. Plaut, *Activity of purified NAD-specific isocitrate dehydrogenase at modulator and substrate concentrations approximating conditions in mitochondria.* Metabolism, 1986. **35**(7): p. 661-667.
92. Lowenstein, J.M. and S.R. Smith, *Intra- and extramitochondrial isocitrate dehydrogenases.* Biochimica et Biophysica Acta, 1962. **56**: p. 385-387.
93. Geisbrecht, B.V. and S.J. Gould, *The Human PICD Gene Encodes a Cytoplasmic and Peroxisomal NADP+-dependent Isocitrate Dehydrogenase.* Journal of Biological Chemistry, 1999. **274**(43): p. 30527-30533.

94. Chen, R.F. and G.W.E. Plaut, *Activation and Inhibition of DPN-linked Isocitrate Dehydrogenase of Heart by Certain Nucleotides*.* Biochemistry, 1963. **2**(5): p. 1023-1032.
95. Plaut, G.W. and T. Aogaichi, *Purification and properties of diphosphopyridine nuleotide-linked isocitrate dehydrogenase of mammalian liver.* The Journal of biological chemistry, 1968. **243**(21): p. 5572-5583.
96. Koh, H.-J., et al., *Cytosolic NADP+-dependent Isocitrate Dehydrogenase Plays a Key Role in Lipid Metabolism.* Journal of Biological Chemistry, 2004. **279**(38): p. 39968-39974.
97. Jo, S.-H., et al., *Cellular Defense against UVB-Induced Phototoxicity by Cytosolic NADP+-Dependent Isocitrate Dehydrogenase.* Biochemical and Biophysical Research Communications, 2002. **292**(2): p. 542-549.
98. Kim, S.Y., et al., *Regulation of singlet oxygen-induced apoptosis by cytosolic NADP+-dependent isocitrate dehydrogenase.* Molecular and Cellular Biochemistry, 2007. **302**(1): p. 27-34.
99. Metallo, C.M., et al., *Reductive glutamine metabolism by IDH1 mediates lipogenesis under hypoxia.* Nature, 2011. **481**: p. 380-384.
100. Mullen, A.R., et al., *Reductive carboxylation supports growth in tumour cells with defective mitochondria.* Nature, 2011. **481**: p. 385-388.
101. Jo, S.-H., et al., *Control of Mitochondrial Redox Balance and Cellular Defense against Oxidative Damage by Mitochondrial NADP+-dependent Isocitrate Dehydrogenase.* Journal of Biological Chemistry, 2001. **276**(19): p. 16168-16176.
102. Lee, J.H., et al., *Regulation of Ionizing Radiation-induced Apoptosis by Mitochondrial NADP+-dependent Isocitrate Dehydrogenase.* Journal of Biological Chemistry, 2007. **282**(18): p. 13385-13394.
103. Wise, D.R., et al., *Hypoxia promotes isocitrate dehydrogenase-dependent carboxylation of α-ketoglutarate to citrate to support cell growth and viability.* Proceedings of the National Academy of Sciences, 2011. **108**(49): p. 19611-19616.
104. Hoffmann, G.F., et al., *Quantitative organic acid analysis in cerebrospinal fluid and plasma: reference values in a pediatric population.* Journal of Chromatography B: Biomedical Sciences and Applications, 1993. **617**(1): p. 1-10.
105. Janin, M., et al., *Serum 2-hydroxyglutarate production in IDH1-and IDH2-mutated de novo acute myeloid leukemia: a study by the Acute Leukemia French Association group.* J Clin Oncol, 2014. **32**(4): p. 297-305.
106. Lindahl, G., G. Lindstedt and S. Lindstedt, *Metabolism of 2-amino-5-hydroxyadipic acid in the rat.* Archives of Biochemistry and Biophysics, 1967. **119**: p. 347-352.
107. Kaufman, E.E., et al., *Isolation and characterization of a hydroxyacid-oxoacid transhydrogenase from rat kidney mitochondria.* Journal of Biological Chemistry, 1988. **263**(32): p. 16872-16879.
108. Struys, E.A., et al., *Kinetic characterization of human hydroxyacid–oxoacid transhydrogenase: Relevance toD-2-hydroxyglutaric and γ-hydroxybutyric acidurias.* Journal of Inherited Metabolic Disease, 2005. **28**(6): p. 921-930.
109. Rzem, R., et al., *l-2-Hydroxyglutaric aciduria, a defect of metabolite repair.* Journal of Inherited Metabolic Disease, 2007. **30**(5): p. 681-689.
110. Fan, J., et al., *Human Phosphoglycerate Dehydrogenase Produces the Oncometabolite d-2-Hydroxyglutarate.* ACS Chemical Biology, 2015. **10**(2): p. 510-516.
111. Intlekofer, Andrew M., et al., *Hypoxia Induces Production of L-2-Hydroxyglutarate.* Cell Metabolism, 2015. **22**(2): p. 304-311.
112. Oldham, William M., et al., *Hypoxia-Mediated Increases in l-2-hydroxyglutarate Coordinate the Metabolic Response to Reductive Stress.* Cell Metabolism, 2015. **22**(2): p. 291-303.
113. Intlekofer, A.M., et al., *L-2-Hydroxyglutarate production arises from noncanonical enzyme function at acidic pH.* Nature Chemical Biology, 2017. **13**: p. 494-500.
114. Nadtochiy, S.M., et al., *Acidic pH Is a Metabolic Switch for 2-Hydroxyglutarate Generation and Signaling *.* Journal of Biological Chemistry, 2016. **291**(38): p. 20188-20197.
115. Kranendijk, M., et al., *IDH2 Mutations in Patients with D-2-Hydroxyglutaric Aciduria.* Science, 2010. **330**(6002): p. 336.
116. Achouri, Y., et al., *Identification of a dehydrogenase acting on D-2-hydroxyglutarate.* Biochemical Journal, 2004. **381**(1): p. 35-42.
117. Rzem, R., et al., *A gene encoding a putative FAD-dependent L-2-hydroxyglutarate dehydrogenase is mutated in L-2-hydroxyglutaric aciduria.* Proceedings of the National Academy of Sciences of the United States of America, 2004. **101**(48): p. 16849-16854.

118. Steenweg, M.E., et al., *An overview of L-2-hydroxyglutarate dehydrogenase gene (L2HGDH) variants: a genotype–phenotype study.* Human Mutation, 2010. **31**(4): p. 380-390.
119. Struys, E.A., et al., *Mutations in the d-2-Hydroxyglutarate Dehydrogenase Gene Cause d-2-Hydroxyglutaric Aciduria.* The American Journal of Human Genetics, 2005. **76**(2): p. 358-360.
120. Topçu, M., et al., *l-2-Hydroxyglutaric aciduria: identification of a mutant gene C14orf160, localized on chromosome 14q22.1.* Human Molecular Genetics, 2004. **13**(22): p. 2803-2811.
121. Kranendijk, M., et al., *Evidence for genetic heterogeneity in D-2-hydroxyglutaric aciduria.* Human Mutation, 2010. **31**(3): p. 279-283.
122. Kranendijk, M., et al., *Progress in understanding 2-hydroxyglutaric acidurias.* Journal of Inherited Metabolic Disease, 2012. **35**(4): p. 571-587.
123. London, F. and A. Jeanjean, *Gliomatosis cerebri in L-2-hydroxyglutaric aciduria.* Acta Neurologica Belgica, 2015. **115**(4): p. 749-751.
124. Patay, Z., et al., *Cerebral Neoplasms in L-2 Hydroxyglutaric Aciduria: 3 New Cases and Meta-Analysis of Literature Data.* American Journal of Neuroradiology, 2012. **33**(5): p. 940-943.
125. Fourati, H., et al., *MRI features in 17 patients with L2 hydroxyglutaric aciduria.* European Journal of Radiology Open, 2016. **3**: p. 245-250.
126. Pietrak, B., et al., *A Tale of Two Subunits: How the Neomorphic R132H IDH1 Mutation Enhances Production of αHG.* Biochemistry, 2011. **50**(21): p. 4804-4812.
127. Liu, S., et al., *Roles of metal ions in the selective inhibition of oncogenic variants of isocitrate dehydrogenase 1.* Communications Biology, 2021. **4**(1): p. 1243.
128. Deng, G., et al., *Selective inhibition of mutant isocitrate dehydrogenase 1 (IDH1) via disruption of a metal binding network by an allosteric small molecule.* J Biol Chem, 2015. **290**(2): p. 762-74.
129. Ward, P.S., et al., *The Potential for Isocitrate Dehydrogenase Mutations to Produce 2-Hydroxyglutarate Depends on Allele Specificity and Subcellular Compartmentalization.* Journal of Biological Chemistry, 2013. **288**(6): p. 3804-3815.
130. Moure, C.J., et al., *CRISPR Editing of Mutant IDH1 R132H Induces a CpG Methylation-Low State in Patient-Derived Glioma Models of G-CIMP.* Molecular Cancer Research, 2019. **17**(10): p. 2042-2050.
131. Dexter, J.P., et al., *Lack of evidence for substrate channeling or flux between wildtype and mutant isocitrate dehydrogenase to produce the oncometabolite 2-hydroxyglutarate.* J Biol Chem, 2018. **293**(52): p. 20051-20061.
132. Jin, G., et al., *2-Hydroxyglutarate Production, but Not Dominant Negative Function, Is Conferred by Glioma-Derived NADP+-Dependent Isocitrate Dehydrogenase Mutations.* PLOS ONE, 2011. **6**(2): p. e16812.
133. Pusch, S., et al., *D-2-Hydroxyglutarate producing neo-enzymatic activity inversely correlates with frequency of the type of isocitrate dehydrogenase 1 mutations found in glioma.* Acta Neuropathologica Communications, 2014. **2**(1): p. 19.
134. Sahm, F., et al., *Detection of 2-Hydroxyglutarate in Formalin-Fixed Paraffin-Embedded Glioma Specimens by Gas Chromatography/Mass Spectrometry.* Brain Pathology, 2012. **22**(1): p. 26-31.
135. Shen, X., et al., *A Noninvasive Comparison Study between Human Gliomas with IDH1 and IDH2 Mutations by MR Spectroscopy.* Metabolites, 2019. **9**(2): p. 11.
136. Piaskowski, S., et al., *Glioma cells showing IDH1 mutation cannot be propagated in standard cell culture conditions.* British Journal Of Cancer, 2011. **104**: p. 968-970.
137. Garrett, M., et al., *Metabolic characterization of isocitrate dehydrogenase (IDH) mutant and IDH wildtype gliomaspheres uncovers cell type-specific vulnerabilities.* Cancer & Metabolism, 2018. **6**(1): p. 1-15.
138. Mazor, T., et al., *Clonal expansion and epigenetic reprogramming following deletion or amplification of mutant IDH1.* Proceedings of the National Academy of Sciences, 2017. **114**(40): p. 10743-10748.
139. Luchman, H.A., et al., *An in vivo patient-derived model of endogenous IDH1-mutant glioma.* Neuro-oncology, 2012. **14**(2): p. 184-191.
140. Luchman, H.A., et al., *Spontaneous loss of heterozygosity leading to homozygous R132H in a patient-derived IDH1 mutant cell line.* Neuro-Oncology, 2013. **15**(8): p. 979-980.
141. Cano-Galiano, A., et al., *Cystathionine-γ-lyase drives antioxidant defense in cysteine-restricted IDH1-mutant astrocytomas.* Neuro-Oncology Advances, 2021. **3**(1): p. 1-12.
142. Ohka, F., et al., *Quantitative metabolome analysis profiles activation of glutaminolysis in glioma with IDH1 mutation.* Tumor Biology, 2014. **35**(6): p. 5911-5920.
143. Izquierdo-Garcia, J.L., et al., *Glioma Cells with the IDH1 Mutation Modulate Metabolic Fractional Flux through Pyruvate Carboxylase.* PLOS ONE, 2014. **9**(9): p. e108289.

144. Izquierdo-Garcia, J.L., et al., *Metabolic Reprogramming in Mutant IDH1 Glioma Cells.* PLOS ONE, 2015. **10**(2): p. e0118781.
145. Zhang, J., et al., *Glutamate dehydrogenase (GDH) regulates bioenergetics and redox homeostasis in human glioma.* Oncotarget, 2016. **295**(10): p. 799-800.
146. Viswanath, P., et al., *2-Hydroxyglutarate-Mediated Autophagy of the Endoplasmic Reticulum Leads to an Unusual Downregulation of Phospholipid Biosynthesis in Mutant IDH1 Gliomas.* Cancer Research, 2018. **78**(9): p. 2290-2304.
147. Hujber, Z., et al., *GABA, glutamine, glutamate oxidation and succinic semialdehyde dehydrogenase expression in human gliomas.* Journal of Experimental & Clinical Cancer Research, 2018. **37**(1): p. 271.
148. Walsby-Tickle, J., et al., *Anion-exchange chromatography mass spectrometry provides extensive coverage of primary metabolic pathways revealing altered metabolism in IDH1 mutant cells.* Communications Biology, 2020. **3**(1): p. 247.
149. Eckel-Passow, J.E., et al., *Glioma Groups Based on 1p/19q, IDH, and TERT Promoter Mutations in Tumors.* New England Journal of Medicine, 2015. **372**(26): p. 2499-2508.
150. Lenting, K., et al., *Glioma: experimental models and reality.* Acta Neuropathologica, 2017. **133**(2): p. 263-282.
151. Carbonneau, M., et al., *The oncometabolite 2-hydroxyglutarate activates the mTOR signalling pathway.* Nature Communications, 2016. **7**: p. 1-12.
152. Verheul, C., et al., *Generation, characterization, and drug sensitivities of 12 patient-derived IDH1-mutant glioma cell cultures.* Neuro-Oncology Advances, 2021. **3**(1): p. vdab103.
153. Kelly, J.J.P., et al., *Oligodendroglioma cell lines containing t(1;19)(q10;p10).* Neuro-Oncology, 2010. **12**(7): p. 745-755.
154. Dao Trong, P., et al., *Identification of a Prognostic Hypoxia-Associated Gene Set in IDH-Mutant Glioma.* Int J Mol Sci, 2018. **19**(10): p. 2903.
155. Trong, P.D., et al., *Large-Scale Drug Screening in Patient-Derived IDH(mut)Glioma Stem Cells Identifies Several Efficient Drugs among FDA-Approved Antineoplastic Agents.* Cells, 2020. **9**(6): p. 1389.
156. Klink, B., et al., *A Novel, Diffusely Infiltrative Xenograft Model of Human Anaplastic Oligodendroglioma with Mutations in FUBP1, CIC, and IDH1.* PLOS ONE, 2013. **8**(3): p. e59773.
157. Navis, A.C., et al., *Increased mitochondrial activity in a novel IDH1-R132H mutant human oligodendroglioma xenograft model: in situ detection of 2-HG and α-KG.* Acta Neuropathologica Communications, 2013. **1**(1): p. 18.
158. Fack, F., et al., *Altered metabolic landscape in IDH-mutant gliomasaffects phospholipid, energy, and oxidative stress pathways.* Embo Molecular Medicine, 2017. **9**(12): p. 1681-1695.
159. Golebiewska, A., et al., *Patient-derived organoids and orthotopic xenografts of primary and recurrent gliomas represent relevant patient avatars for precision oncology.* Acta neuropathologica, 2020. **140**(6): p. 919-949.
160. Addie, R.D., et al., *Exploration of the chondrosarcoma metabolome; the mTOR pathway as an important pro-survival pathway.* Journal of Bone Oncology, 2019. **15**: p. 100222.
161. Badur, M.G., et al., *Oncogenic R132 IDH1 mutations limit NADPH for de novo lipogenesis through (D) 2-Hydroxyglutarate production in fibrosarcoma cells.* Cell reports, 2018. **25**(6): p. 1018-1026.
162. Ma, S., et al., *D-2-hydroxyglutarate is essential for maintaining oncogenic property of mutant IDH-containing cancer cells but dispensable for cell growth.* Oncotarget, 2015. **6**(11): p. 8606-8620.
163. Peterse, E.F.P., et al., *Targeting glutaminolysis in chondrosarcoma in context of the IDH1/2 mutation.* British journal of cancer, 2018. **118**(8): p. 1074-1083.
164. Peterse, E.F.P., et al., *NAD Synthesis Pathway Interference Is a Viable Therapeutic Strategy for Chondrosarcoma.* Molecular Cancer Research, 2017. **15**(12): p. 1714-1721.
165. Salamanca-Cardona, L., et al., *In Vivo Imaging of Glutamine Metabolism to the Oncometabolite 2-Hydroxyglutarate in IDH1/2 Mutant Tumors.* Cell Metabolism, 2017. **26**(6): p. 830-841.e3.
166. van Oosterwijk, J.G., et al., *Three new chondrosarcoma cell lines: one grade III conventional central chondrosarcoma and two dedifferentiated chondrosarcomas of bone.* BMC cancer, 2012. **12**: p. 375-375.
167. Carrabba, M.G., et al., *Integrating a prospective pilot trial and patient-derived xenografts to trace metabolic changes associated with acute myeloid leukemia.* Journal of Hematology & Oncology, 2016. **9**(1): p. 1-5.

168. Boutzen, H., et al., *Isocitrate dehydrogenase 1 mutations prime the all-trans retinoic acid myeloid differentiation pathway in acute myeloid leukemia.* The Journal of Experimental Medicine, 2016. **213**(4): p. 483-497.
169. Emadi, A., et al., *Inhibition of glutaminase selectively suppresses the growth of primary acute myeloid leukemia cells with IDH mutations.* Experimental Hematology, 2014. **42**(4): p. 247-251.
170. Stuani, L., et al., *Stable Isotope Labeling Highlights Enhanced Fatty Acid and Lipid Metabolism in Human Acute Myeloid Leukemia.* International Journal of Molecular Sciences, 2018. **19**(11): p. 3325.
171. Fujiwara, H., et al., *Mutant IDH1 confers resistance to energy stress in normal biliary cells through PFKP-induced aerobic glycolysis and AMPK activation.* Scientific Reports, 2019. **9**: p. 1-14.
172. Saha, S.K., et al., *Mutant IDH inhibits HNF-4α to block hepatocyte differentiation and promote biliary cancer.* Nature, 2014. **513**: p. 110-114.
173. McBrayer, S.K., et al., *Transaminase Inhibition by 2-Hydroxyglutarate Impairs Glutamate Biosynthesis and Redox Homeostasis in Glioma.* Cell, 2018. **175**(1): p. 101-116.e25.
174. Wen, H., et al., *Metabolomic comparison between cells over-expressing isocitrate dehydrogenase 1 and 2 mutants and the effects of an inhibitor on the metabolism.* Journal of Neurochemistry, 2015. **132**(2): p. 183-193.
175. Reitman, Z.J., et al., *Profiling the effects of isocitrate dehydrogenase 1 and 2 mutations on the cellular metabolome.* Proceedings of the National Academy of Sciences, 2011. **108**(8): p. 3270-3275.
176. Nakagawa, M., et al., *Selective inhibition of mutant IDH1 by DS-1001b ameliorates aberrant histone modifications and impairs tumor activity in chondrosarcoma.* Oncogene, 2019. **38**: p. 6835–6849.
177. Suijker, J., et al., *Inhibition of mutant IDH1 decreases D-2-HG levels without affecting tumorigenic properties of chondrosarcoma cell lines.* Oncotarget, 2015. **6**(14): p. 12505-12519.
178. Emir, U.E., et al., *Noninvasive Quantification of 2-Hydroxyglutarate in Human Gliomas with IDH1 and IDH2 Mutations.* Cancer Research, 2016. **76**(1): p. 43-49.
179. Lo Presti, C., et al., *The metabolic reprogramming in acute myeloid leukemia patients depends on their genotype and is a prognostic marker.* Blood Advances, 2021. **5**(1): p. 156-166.
180. Mohammad, N., et al., *Characterisation of isocitrate dehydrogenase 1/isocitrate dehydrogenase 2 gene mutation and the d-2-hydroxyglutarate oncometabolite level in dedifferentiated chondrosarcoma.* Histopathology, 2019. **76**(5): p. 722-730.
181. Zhou, L., et al., *Integrated Metabolomics and Lipidomics Analyses Reveal Metabolic Reprogramming in Human Glioma with IDH1 Mutation.* Journal of Proteome Research, 2019. **18**(3): p. 960-969.
182. Winter, H., et al., *Identification of Circulating Genomic and Metabolic Biomarkers in Intrahepatic Cholangiocarcinoma.* Cancers, 2019. **11**(12): p. 1895.
183. Lenting, K., et al., *Isocitrate dehydrogenase 1–mutated human gliomas depend on lactate and glutamate to alleviate metabolic stress.* The FASEB Journal, 2018. **33**(1): p. 557-571.
184. Jalbert, L.E., et al., *Metabolic Profiling of IDH Mutation and Malignant Progression in Infiltrating Glioma.* Scientific Reports, 2017. **7**: p. 1-10.
185. Choi, C., et al., *2-hydroxyglutarate detection by magnetic resonance spectroscopy in IDH-mutated patients with gliomas.* Nature Medicine, 2012. **18**: p. 624-629.
186. An, Z.X., et al., *Detection of 2-hydroxyglutarate in brain tumors by triple-refocusing MR spectroscopy at 3T in vivo.* Magnetic Resonance in Medicine, 2017. **78**(1): p. 40-48.
187. Grassian, A.R., et al., *IDH1 mutations alter citric acid cycle metabolism and increase dependence on oxidative mitochondrial metabolism.* Cancer Research, 2014. **74**(12): p. 3317-3331.
188. Li, S., et al., *Overexpression of isocitrate dehydrogenase mutant proteins renders glioma cells more sensitive to radiation.* Neuro-Oncology, 2012. **15**(1): p. 57-68.
189. Su, L., et al., *Mutation of Isocitrate Dehydrogenase 1 in Cholangiocarcinoma Impairs Tumor Progression by Inhibiting Isocitrate Metabolism.* Frontiers in Endocrinology, 2020. **11**(189): p. 189.
190. Wei, S., et al., *Heterozygous IDH1R132H/WT created by "single base editing" inhibits human astroglial cell growth by downregulating YAP.* Oncogene, 2018. **37**(38): p. 5160-5174.
191. Su, R., et al., *R-2HG Exhibits Anti-tumor Activity by Targeting FTO/m6A/MYC/CEBPA Signaling.* Cell, 2018. **172**(1): p. 90-105.e23.
192. Khurshed, M., et al., *In silico gene expression analysis reveals glycolysis and acetate anaplerosis in IDH1 wild-type glioma and lactate and glutamate anaplerosis in IDH1-mutated glioma.* Oncotarget, 2017. **8**(30): p. 49165-49177.
193. Dekker, L.J.M., et al., *Metabolic changes related to the IDH1 mutation in gliomas preserve TCA-cycle activity: An investigation at the protein level.* Faseb Journal, 2020. **34**(3): p. 3646– 3657.

194. Tanaka, K., et al., *Compensatory glutamine metabolism promotes glioblastoma resistance to mTOR inhibitor treatment.* The Journal of clinical investigation, 2015. **125**(4): p. 1591-1602.
195. Mashimo, T., et al., *Acetate Is a Bioenergetic Substrate for Human Glioblastoma and Brain Metastases.* Cell, 2014. **159**(7): p. 1603-1614.
196. Viswanath, P., et al., *Mutant IDH1 expression is associated with down-regulation of monocarboxylate transporters.* Oncotarget, 2016. **7**(23): p. 34942-34955.
197. Chaumeil, M.M., et al., *Hyperpolarized C-13 MR imaging detects no lactate production in mutant IDH1 gliomas: Implications for diagnosis and response monitoring.* Neuroimage-Clinical, 2016. **12**: p. 180-189.
198. Chesnelong, C., et al., *Lactate dehydrogenase A silencing in IDH mutant gliomas.* Neuro-Oncology, 2014. **16**(5): p. 686-695.
199. Izquierdo-Garcia, J.L., et al., *IDH1 Mutation Induces Reprogramming of Pyruvate Metabolism.* Cancer Research, 2015. **75**(15): p. 2999-3009.
200. Turcan, S., et al., *IDH1 mutation is sufficient to establish the glioma hypermethylator phenotype.* Nature, 2012. **483**: p. 479-483.
201. Waitkus, M.S., et al., *Adaptive Evolution of the GDH2 Allosteric Domain Promotes Gliomagenesis by Resolving IDH1^{R132H}-Induced Metabolic Liabilities.* Cancer Research, 2018. **78**(1): p. 36-50.
202. Chen, R., et al., *Hominoid-specific enzyme GLUD2 promotes growth of IDH1^{R132H} glioma.* Proceedings of the National Academy of Sciences, 2014. **111**(39): p. 14217-14222.
203. García-Espinosa, M.A., et al., *Widespread neuronal expression of branched-chain aminotransferase in the CNS: implications for leucine/glutamate metabolism and for signaling by amino acids.* Journal of Neurochemistry, 2007. **100**(6): p. 1458-1468.
204. Tönjes, M., et al., *BCAT1 promotes cell proliferation through amino acid catabolism in gliomas carrying wild-type IDH1.* Nature Medicine, 2013. **19**: p. 901-908.
205. ICHIHARA, A. and E. KOYAMA, *Transaminase of branched chain amino acids.* The Journal of Biochemistry, 1966. **59**(2): p. 160-169.
206. Yang, L., S. Venneti and D. Nagrath, *Glutaminolysis: A Hallmark of Cancer Metabolism.* Annual Review of Biomedical Engineering, 2017. **19**(1): p. 163-194.
207. Seltzer, M.J., et al., *Inhibition of Glutaminase Preferentially Slows Growth of Glioma Cells with Mutant IDH1.* Cancer Research, 2010. **70**(22): p. 8981-8987.
208. Ruiz-Rodado, V., et al., *Metabolic plasticity of IDH1-mutant glioma cell lines is responsible for low sensitivity to glutaminase inhibition.* Cancer & Metabolism, 2020. **8**(1): p. 23.
209. Muir, A., et al., *Environmental cystine drives glutamine anaplerosis and sensitizes cancer cells to glutaminase inhibition.* Elife, 2017. **6**: p. e27713.
210. Karlstaedt, A., et al., *Oncometabolite D-2-hydroxyglutarate impairs α-ketoglutarate dehydrogenase and contractile function in rodent heart.* Proceedings of the National Academy of Sciences, 2016. **113**(37): p. 10436-10441.
211. Moloney, J.N. and T.G. Cotter, *ROS signalling in the biology of cancer.* Seminars in Cell & Developmental Biology, 2018. **80**: p. 50-64.
212. Griffith, O.W., *Biologic and pharmacologic regulation of mammalian glutathione synthesis.* Free Radical Biology and Medicine, 1999. **27**(9): p. 922-935.
213. Chen, L., et al., *NADPH production by the oxidative pentose-phosphate pathway supports folate metabolism.* Nature metabolism, 2019. **1**: p. 404-415.
214. Charitou, P., et al., *FOXOs support the metabolic requirements of normal and tumor cells by promoting IDH1 expression.* EMBO reports, 2015. **16**(4): p. 456-466.
215. Bleeker, F.E., et al., *The prognostic IDH1R132mutation is associated with reduced NADP+-dependent IDH activity in glioblastoma.* Acta Neuropathologica, 2010. **119**(4): p. 487-494.
216. Han, S.J., et al., *IDH2 deficiency increases the liver susceptibility to ischemia-reperfusion injury via increased mitochondrial oxidative injury.* Redox Biology, 2018. **14**: p. 142-153.
217. Han, S.J., et al., *Mitochondrial NADP$^+$-Dependent Isocitrate Dehydrogenase Deficiency Exacerbates Mitochondrial and Cell Damage after Kidney Ischemia-Reperfusion Injury.* Journal of the American Society of Nephrology, 2017. **28**(4): p. 1200-1215.
218. Ku, H.J., et al., *IDH2 deficiency promotes mitochondrial dysfunction and cardiac hypertrophy in mice.* Free Radical Biology and Medicine, 2015. **80**: p. 84-92.
219. Park, J.H., et al., *Idh2 Deficiency Exacerbates Acrolein-Induced Lung Injury through Mitochondrial Redox Environment Deterioration.* Oxidative Medicine and Cellular Longevity, 2017. **2017**: p. 1595103.

220. Biedermann, J., et al., *Mutant IDH1 Differently Affects Redox State and Metabolism in Glial Cells of Normal and Tumor Origin.* Cancers, 2019. **11**(12): p. 2028.
221. Gelman, S.J., et al., *Consumption of NADPH for 2-HG synthesis increases pentose phosphate pathway flux and sensitizes cells to oxidative stress.* Cell reports, 2018. **22**(2): p. 512-522.
222. Shi, J., et al., *An IDH1 mutation inhibits growth of glioma cells via GSH depletion and ROS generation.* Neurological Sciences, 2014. **35**(6): p. 839-845.
223. Mugoni, V., et al., *Vulnerabilities in mIDH2 AML confer sensitivity to APL-like targeted combination therapy.* Cell Research, 2019. **29**(6): p. 446-459.
224. Tiburcio, P.D.B., et al., *Extracellular glutamate and IDH1(R132H) inhibitor promote glioma growth by boosting redox potential.* Journal of Neuro-Oncology, 2020. **146**(3): p. 427-437.
225. Tang, X.Y., et al., *Blockade of Glutathione Metabolism in IDH1-Mutated Glioma.* Molecular Cancer Therapeutics, 2020. **19**(1): p. 221-230.
226. Tateishi, K., et al., *Extreme Vulnerability of IDH1 Mutant Cancers to NAD+ Depletion.* Cancer Cell, 2015. **28**(6): p. 773-784.
227. Calvert, A.E., et al., *Cancer-Associated IDH1 Promotes Growth and Resistance to Targeted Therapies in the Absence of Mutation.* Cell Reports, 2017. **19**(9): p. 1858-1873.
228. Wahl, D.R., et al., *Glioblastoma Therapy Can Be Augmented by Targeting IDH1-Mediated NADPH Biosynthesis.* Cancer Research, 2017. **77**(4): p. 960-970.
229. Leonardi, R., et al., *Cancer-associated Isocitrate Dehydrogenase Mutations Inactivate NADPH-dependent Reductive Carboxylation.* Journal of Biological Chemistry, 2012. **287**(18): p. 14615-14620.
230. Esmaeili, M., et al., *IDH1 R132H mutation generates a distinct phospholipid metabolite profile in gliomas.* Cancer Research, 2014. **74**(17): p. 4898-4907.
231. Wenger, K.J., et al., *In vivo Metabolic Profiles as Determined by P-31 and short TE H-1 MR-Spectroscopy: No Difference Between Patients with IDH Wildtype and IDH Mutant Gliomas.* Clinical Neuroradiology, 2019. **29**(1): p. 27-36.
232. Yang, R., et al., *Isocitrate dehydrogenase 1 mutation enhances 24(S)-hydroxycholesterol production and alters cholesterol homeostasis in glioma.* Oncogene, 2020. **39**(40): p. 6340-6353.
233. *NCT03564821: IDH1 Inhibition Using Ivosidenib as Maintenance Therapy for IDH1-mutant Myeloid Neoplasms Following Allogeneic Stem Cell Transplantation*. [cited 2019 August 01]; Available from: https://ClinicalTrials.gov/show/NCT03564821.
234. *NCT03515512: IDH2 Inhibition Using Enasidenib as Maintenance Therapy for IDH2-mutant Myeloid Neoplasms Following Allogeneic Stem Cell Transplantation*. [cited 2019 August 01]; Available from: https://ClinicalTrials.gov/show/NCT03515512.
235. *NCT03471260: Ivosidenib and Venetoclax With or Without Azacitidine in Treating Participants With IDH1 Mutated Hematologic Malignancies*. [cited 2019 August 01]; Available from: https://ClinicalTrials.gov/show/NCT03471260.
236. *NCT03383575: Azacitidine and Enasidenib in Treating Patients With IDH2-Mutant Myelodysplastic Syndrome*. Available from: https://ClinicalTrials.gov/show/NCT03383575.
237. *NCT03343197: Study of AG-120 and AG-881 in Subjects With Low Grade Glioma*. [cited 2019 August 01]; Available from: https://ClinicalTrials.gov/show/NCT03343197.
238. *NCT02746081: Phase I Study of BAY1436032 in IDH1-mutant Advanced Solid Tumors*. [cited 2019 August 01]; Available from: https://ClinicalTrials.gov/show/NCT02746081.
239. *NCT02073994: Study of Orally Administered AG-120 in Subjects With Advanced Solid Tumors, Including Glioma, With an IDH1 Mutation*. [cited 2019 August 01]; Available from: https://ClinicalTrials.gov/show/NCT02073994.
240. *A Study of FT 2102 in Participants With Advanced Solid Tumors and Gliomas With an IDH1 Mutation*. [cited 2019 August 01]; Available from: https://ClinicalTrials.gov/show/NCT03684811.
241. *NCT03683433: Enasidenib and Azacitidine in Treating Patients With Recurrent or Refractory Acute Myeloid Leukemia and IDH2 Gene Mutation*. [cited 2019 August 01]; Available from: https://ClinicalTrials.gov/show/NCT03683433.
242. *NCT03127735: BAY1436032 in Patients With Mutant IDH1(mIDH1) Advanced Acute Myeloid Leukemia (AML)*. [cited 2019 August 01]; Available from: https://ClinicalTrials.gov/show/NCT03127735.
243. *NCT02977689: Trial of IDH305 in IDH1 Mutant Grade II or III Glioma*. [cited 2019 August 01]; Available from: https://ClinicalTrials.gov/show/NCT02977689.

244. *NCT02677922: A Safety and Efficacy Study of Oral AG-120 Plus Subcutaneous Azacitidine and Oral AG-221 Plus Subcutaneous Azacitidine in Subjects With Newly Diagnosed Acute Myeloid Leukemia (AML).* [cited 2019 August 01]; Available from: https://ClinicalTrials.gov/show/NCT02677922.
245. Abou-Alfa, G.K., et al., *Ivosidenib in IDH1-mutant, chemotherapy-refractory cholangiocarcinoma (ClarIDHy): a multicentre, randomised, double-blind, placebo-controlled, phase 3 study.* The Lancet. Oncology, 2020. **21**(6): p. 796-807.
246. Popovici-Muller, J., et al., *Discovery of AG-120 (Ivosidenib): A First-in-Class Mutant IDH1 Inhibitor for the Treatment of IDH1 Mutant Cancers.* ACS Medicinal Chemistry Letters, 2018. **9**(4): p. 300-305.
247. Pusch, S., et al., *Pan-mutant IDH1 inhibitor BAY 1436032 for effective treatment of IDH1 mutant astrocytoma in vivo.* Acta Neuropathologica, 2017. **133**(4): p. 629-644.
248. Yen, K., et al., *AG-221, a First-in-Class Therapy Targeting Acute Myeloid Leukemia Harboring Oncogenic IDH2 Mutations.* Cancer Discovery, 2017. **7**(5): p. 478-493.
249. Ma, R. and C.-H. Yun, *Crystal structures of pan-IDH inhibitor AG-881 in complex with mutant human IDH1 and IDH2.* Biochemical and Biophysical Research Communications, 2018. **503**(4): p. 2912-2917.
250. Okoye-Okafor, U.C., et al., *New IDH1 mutant inhibitors for treatment of acute myeloid leukemia.* Nature Chemical Biology, 2015. **11**(11): p. 878-886.
251. Urban, D.J., et al., *Assessing inhibitors of mutant isocitrate dehydrogenase using a suite of pre-clinical discovery assays.* Scientific Reports, 2017. **7**(1): p. 12758.
252. Li, L.Y., et al., *Treatment with a Small Molecule Mutant IDH1 Inhibitor Suppresses Tumorigenic Activity and Decreases Production of the Oncometabolite 2-Hydroxyglutarate in Human Chondrosarcoma Cells.* Plos One, 2015. **10**(9): p. e0133813.
253. Chaturvedi, A., et al., *Pan-mutant-IDH1 inhibitor BAY1436032 is highly effective against human IDH1 mutant acute myeloid leukemia in vivo.* Leukemia, 2017. **31**(10): p. 2020-2028.
254. Rohle, D., et al., *An Inhibitor of Mutant IDH1 Delays Growth and Promotes Differentiation of Glioma Cells.* Science, 2013. **340**(6132): p. 626-630.
255. Molloy, A.R., et al., *MR-detectable metabolic biomarkers of response to mutant IDH inhibition in low-grade glioma.* Theranostics, 2020. **10**(19): p. 8757-8770.
256. Radoul, M., et al., *Early Noninvasive Metabolic Biomarkers of Mutant IDH Inhibition in Glioma.* Metabolites, 2021. **11**(2): p. 109.
257. Andronesi, O.C., et al., *Pharmacodynamics of mutant-IDH1 inhibitors in glioma patients probed by in vivo 3D MRS imaging of 2-hydroxyglutarate.* Nature Communications, 2018. **9**: p. 9.
258. Amatangelo, M.D., et al., *Enasidenib induces acute myeloid leukemia cell differentiation to promote clinical response.* Blood, 2017. **130**(6): p. 732-741.
259. DiNardo, C.D., et al., *Durable Remissions with Ivosidenib in IDH1-Mutated Relapsed or Refractory AML.* N Engl J Med, 2018. **378**(25): p. 2386-2398.
260. Roboz, G.J., et al., *Ivosidenib induces deep durable remissions in patients with newly diagnosed IDH1-mutant acute myeloid leukemia.* Blood, 2020. **135**(7): p. 463-471.
261. Stein, E.M., et al., *Molecular remission and response patterns in patients with mutant-IDH2 acute myeloid leukemia treated with enasidenib.* Blood, 2019. **133**(7): p. 676-687.
262. Jin, X., X. Jin and H. Kim, *Cancer stem cells and differentiation therapy.* Tumor Biology, 2017. **39**(10): p. 1010428317729933.
263. Mellinghoff, I.K., et al., *Ivosidenib in Isocitrate Dehydrogenase 1–Mutated Advanced Glioma.* Journal of Clinical Oncology, 2020. **38**(29): p. 3398-3406.
264. Intlekofer, A.M., et al., *Acquired resistance to IDH inhibition through trans or cis dimer-interface mutations.* Nature, 2018. **559**(7712): p. 125-129.
265. Harding, J.J., et al., *Isoform Switching as a Mechanism of Acquired Resistance to Mutant Isocitrate Dehydrogenase Inhibition.* Cancer Discovery, 2018. **8**(12): p. 1540-1547.
266. Choe, S., et al., *Molecular mechanisms mediating relapse following ivosidenib monotherapy in IDH1-mutant relapsed or refractory AML.* Blood Advances, 2020. **4**(9): p. 1894-1905.
267. Molenaar, R.J., et al., *Study protocol of a phase IB/II clinical trial of metformin and chloroquine in patients with IDH1 or IDH2-mutated solid tumours.* BMJ Open, 2017. **7**(6): p. e014961.
268. Elhammali, A., et al., *A High-Throughput Fluorimetric Assay for 2-Hydroxyglutarate Identifies Zaprinast as a Glutaminase Inhibitor.* Cancer Discovery, 2014. **4**(7): p. 828-839.
269. Cuyàs, E., et al., *Oncometabolic mutation IDH1 R132H confers a metformin-hypersensitive phenotype.* Oncotarget, 2015. **6**(14): p. 12279-12296.

270. *NCT03528642: CB-839 With Radiation Therapy and Temozolomide in Treating Participants With IDH-Mutated Diffuse Astrocytoma or Anaplastic Astrocytoma*. April 24 2020 [cited 2020 24 April]; Available from: https://clinicaltrials.gov/ct2/show/NCT03528642.
271. Mukhopadhyay, S., et al., *Undermining Glutaminolysis Bolsters Chemotherapy While NRF2 Promotes Chemoresistance in KRAS-Driven Pancreatic Cancers.* Cancer Research, 2020. **80**(8): p. 1630-1643.
272. Romero, R., et al., *Keap1 loss promotes Kras-driven lung cancer and results in dependence on glutaminolysis.* Nature medicine, 2017. **23**(11): p. 1362-1368.
273. Harding, J.J., et al., *A Phase I Dose-Escalation and Expansion Study of Telaglenastat in Patients with Advanced or Metastatic Solid Tumors.* Clinical Cancer Research, 2021. **27**(18): p. 4994-5003.
274. Loeb, F., et al., *ACTIVITY OF A NEW ANTIMALARIAL AGENT, CHLOROQUINE (SN 7618): Statement Approved by the Board for Coordination of Malarial Studies.* Journal of the American Medical Association, 1946. **130**(16): p. 1069-1070.
275. Pascolo, S., *Time to use a dose of Chloroquine as an adjuvant to anti-cancer chemotherapies.* European Journal of Pharmacology, 2016. **771**: p. 139-144.
276. Choi, M.-M., et al., *Inhibitory properties of nerve-specific human glutamate dehydrogenase isozyme by chloroquine.* BMB Reports, 2007. **40**(6): p. 1077-1082.
277. Firat, E., et al., *Chloroquine or Chloroquine-PI3K/Akt Pathway Inhibitor Combinations Strongly Promote γ-Irradiation-Induced Cell Death in Primary Stem-Like Glioma Cells.* PLOS ONE, 2012. **7**(10): p. e47357.
278. Lampman, G.M.P., Donald L.; George, S. Kriz; Vyvyan, James R. , *Spectroscopy International Edition*. 4th ed. 2010, Canada: Mary Finch.
279. Claridge, T.D.W., *High-resolution NMR techniques in organic chemistry*. Third ed. 2016, Amsterdam

London: Elsevier.
280. Stump, M.J., et al., *MATRIX-ASSISTED LASER DESORPTION MASS SPECTROMETRY.* Applied Spectroscopy Reviews, 2002. **37**(3): p. 275-303.
281. Agüi-Gonzalez, P., S. Jähne and N.T.N. Phan, *SIMS imaging in neurobiology and cell biology.* Journal of Analytical Atomic Spectrometry, 2019. **34**(7): p. 1355-1368.
282. Zaima, N., et al., *Matrix-Assisted Laser Desorption/Ionization Imaging Mass Spectrometry.* International Journal of Molecular Sciences, 2010. **11**(12): p. 5040-5055.
283. Bedair, M. and L.W. Sumner, *Current and emerging mass-spectrometry technologies for metabolomics.* TrAC Trends in Analytical Chemistry, 2008. **27**(3): p. 238-250.
284. Lei, Z., D.V. Huhman and L.W. Sumner, *Mass Spectrometry Strategies in Metabolomics.* Journal of Biological Chemistry, 2011. **286**(29): p. 25435-25442.
285. Rohner, T.C., N. Lion and H.H. Girault, *Electrochemical and theoretical aspects of electrospray ionisation.* Physical chemistry chemical physics, 2004. **6**(12): p. 3056-3068.
286. Wilm, M., *Principles of electrospray ionization.* Molecular & cellular proteomics : MCP, 2011. **10**(7): p. M111.009407-M111.009407.
287. Fiehn Lab. *Mass Resolution and Resolving Power*. 2016 [cited 2022 12.01.2023]; Available from: https://fiehnlab.ucdavis.edu/projects/seven-golden-rules/mass-resolution.
288. Glish, G.L. and R.W. Vachet, *The basics of mass spectrometry in the twenty-first century.* Nature reviews drug discovery, 2003. **2**(2): p. 140-150.
289. Makarov, A., et al., *Performance Evaluation of a Hybrid Linear Ion Trap/Orbitrap Mass Spectrometer.* Analytical Chemistry, 2006. **78**(7): p. 2113-2120.
290. Hu, Q., et al., *The Orbitrap: a new mass spectrometer.* Journal of Mass Spectrometry, 2005. **40**(4): p. 430-443.
291. Makarov, A., *Electrostatic Axially Harmonic Orbital Trapping: A High-Performance Technique of Mass Analysis.* Analytical Chemistry, 2000. **72**(6): p. 1156-1162.
292. Perry, R.H., R.G. Cooks and R.J. Noll, *Orbitrap mass spectrometry: Instrumentation, ion motion and applications.* Mass Spectrometry Reviews, 2008. **27**(6): p. 661-699.
293. Koppenaal, D.W., et al., *MS detectors*. 2005, ACS Publications.
294. Boudah, S., et al., *Annotation of the human serum metabolome by coupling three liquid chromatography methods to high-resolution mass spectrometry.* Journal of Chromatography B, 2014. **966**: p. 34-47.
295. Tang, D.-Q., et al., *HILIC-MS for metabolomics: An attractive and complementary approach to RPLC-MS.* Mass Spectrometry Reviews, 2016. **35**(5): p. 574-600.

296. Nordström, A., et al., *Derivatization for LC-Electrospray Ionization-MS: A Tool for Improving Reversed-Phase Separation and ESI Responses of Bases, Ribosides, and Intact Nucleotides.* Analytical Chemistry, 2004. **76**(10): p. 2869-2877.
297. Sánchez-López, E., A.L. Crego and M.L. Marina, *Design of strategies to study the metabolic profile of highly polar compounds in plasma by reversed-phase liquid chromatography–high resolution mass spectrometry.* Journal of Chromatography A, 2017. **1490**: p. 156-165.
298. Guo, Y. and S. Gaiki, *Retention and selectivity of stationary phases for hydrophilic interaction chromatography.* Journal of Chromatography A, 2011. **1218**(35): p. 5920-5938.
299. Hemström, P. and K. Irgum, *Hydrophilic interaction chromatography.* Journal of Separation Science, 2006. **29**(12): p. 1784-1821.
300. Inc., T.F.S., *Product Manual for the DRS 600 Suppressor*. 2021, Thermo Fisher Scientific Inc: Waltham, MA, USA.
301. Hu, S., et al., *Targeted Metabolomic Analysis of Head and Neck Cancer Cells Using High Performance Ion Chromatography Coupled with a Q Exactive HF Mass Spectrometer.* Analytical Chemistry, 2015. **87**(12): p. 6371-6379.
302. Wang, J., et al., *Metabolomic Profiling of Anionic Metabolites in Head and Neck Cancer Cells by Capillary Ion Chromatography with Orbitrap Mass Spectrometry.* Analytical Chemistry, 2014. **86**(10): p. 5116-5124.
303. Petucci, C., et al., *Use of Ion Chromatography/Mass Spectrometry for Targeted Metabolite Profiling of Polar Organic Acids.* Analytical Chemistry, 2016. **88**(23): p. 11799-11803.
304. Schwaiger, M., et al., *Anion-Exchange Chromatography Coupled to High-Resolution Mass Spectrometry: A Powerful Tool for Merging Targeted and Non-targeted Metabolomics.* Analytical Chemistry, 2017. **89**(14): p. 7667-7674.
305. Sun, P., et al., *The recent development of fluorescent probes for the detection of NADH and NADPH in living cells and in vivo.* Spectrochimica Acta Part A: Molecular and Biomolecular Spectroscopy, 2021. **245**: p. 118919.
306. Crump, N.T., et al., *Chromatin accessibility governs the differential response of cancer and T cells to arginine starvation.* Cell Reports, 2021. **35**(6): p. 109101.
307. Green, C.J., et al., *Metformin maintains intrahepatic triglyceride content through increased hepatic de novo lipogenesis.* European Journal of Endocrinology, 2022. **186**(3): p. 367-377.
308. Haythorne, E., et al., *Altered glycolysis triggers impaired mitochondrial metabolism and mTORC1 activation in diabetic β-cells.* Nature Communications, 2022. **13**(1): p. 6754.
309. Ling, Q., et al., *The chloroplast-associated protein degradation pathway controls chromoplast development and fruit ripening in tomato.* Nature Plants, 2021. **7**(5): p. 655-666.
310. Smith, E.N., et al., *Limitations of Deuterium-Labelled Substrates for Quantifying NADPH Metabolism in Heterotrophic Arabidopsis Cell Cultures.* Metabolites, 2019. **9**(10): p. 205.
311. Vaughan-Jackson, A., et al. *Density dependent regulation of inflammatory responses in macrophages*. Frontiers in immunology, 2022. **13**, 895488 DOI: 10.3389/fimmu.2022.895488.
312. Reinbold, R., et al., *Resistance to the isocitrate dehydrogenase 1 mutant inhibitor ivosidenib can be overcome by alternative dimer-interface binding inhibitors.* Nature Communications, 2022. **13**(1): p. 4785.
313. Li, S., et al., *Predicting Network Activity from High Throughput Metabolomics.* PLOS Computational Biology, 2013. **9**(7): p. e1003123.
314. Pang, Z., et al., *MetaboAnalyst 5.0: narrowing the gap between raw spectra and functional insights.* Nucleic Acids Research, 2021. **49**(W1): p. W388-W396.
315. Kanehisa, M., et al., *From genomics to chemical genomics: new developments in KEGG.* Nucleic acids research, 2006. **34**(1): p. D354-D357.
316. Duarte, N.C., et al., *Global reconstruction of the human metabolic network based on genomic and bibliomic data.* Proceedings of the National Academy of Sciences, 2007. **104**(6): p. 1777-1782.
317. Ma, H., et al., *The Edinburgh human metabolic network reconstruction and its functional analysis.* Molecular Systems Biology, 2007. **3**(1): p. 135.
318. Li, S., et al., *Constructing a fish metabolic network model.* Genome Biology, 2010. **11**(11): p. R115.
319. Hosack, D.A., et al., *Identifying biological themes within lists of genes with EASE.* Genome Biology, 2003. **4**(10): p. R70.
320. Bardella, C., et al., *Expression of Idh1R132H in the murine subventricular zone stem cell niche recapitulates features of early gliomagenesis.* Cancer cell, 2016. **30**(4): p. 578-594.

321. Walsby-Tickle, J., *Investigating isocitrate dehydrogenase mutations in cancer using new metabolomics methods*, J. McCullagh, Editor. 2020.
322. Lu, W., et al., *Extraction and Quantitation of Nicotinamide Adenine Dinucleotide Redox Cofactors.* Antioxidants & Redox Signaling, 2017. **28**(3): p. 167-179.
323. Horai, H., M. Arita and T. Nishioka. *Comparison of ESI-MS Spectra in MassBank Database*. in *2008 International Conference on BioMedical Engineering and Informatics*. 2008.
324. R Core Team, *R: A Language and Environment for Statistical Computing*. 2021, Vienna, Austria: R Foundation for Statistical Computing.
325. Chong, J. and J. Xia, *MetaboAnalystR: an R package for flexible and reproducible analysis of metabolomics data.* Bioinformatics, 2018. **34**(24): p. 4313-4314.
326. Wickham, H., et al., *Welcome to the Tidyverse.* Journal of open source software, 2019. **4**(43): p. 1686.
327. Wickham, H., *ggplot2: Elegant Graphics for Data Analysis*. 2016: Springer-Verlag New York.
328. Kassambara, A. *rstatix: Pipe-Friendly Framework for Basic Statistical Tests. R package version 0.7.0.* . 2021; Available from: https://CRAN.R-project.org/package=rstatix.
329. Urbanek, S., *png: Read and write PNG images*. 2013.
330. Auguie, B., *gridExtra: Miscellaneous Functions for "Grid" Graphics*. 2017.
331. Wickham, H.H., Jim; Chang, Winston; Müller, Kirill; Cook, Daniel, *memoise: Memoisation of Functions*. 2021.
332. Wickham, H., *The Split-Apply-Combine Strategy for Data Analysis.* Journal of Statistical Software, 2011. **40**(1): p. 1-29.
333. Wickham, H.S., Dana, *scales: Scale Functions for Visualization*. 2020.
334. Spiess, A.-N., *qpcR: Modelling and Analysis of Real-Time PCR Data*. 2018.
335. Hester, J.W., Hadley; Csárdi, Gábor, *fs: Cross-Platform File System Operations Based on 'libuv'*. 2021.
336. Firke, S., *janitor: Simple Tools for Examining and Cleaning Dirty Data.* 2021.
337. van den Berg, R.A., et al., *Centering, scaling, and transformations: improving the biological information content of metabolomics data.* BMC Genomics, 2006. **7**(1): p. 142.
338. Wulff, J.E. and M.W. Mitchell, *A comparison of various normalization methods for LC/MS metabolomics data.* Advances in Bioscience and Biotechnology, 2018. **9**(08): p. 339.
339. Karaman, I., *Preprocessing and Pretreatment of Metabolomics Data for Statistical Analysis*, in *Metabolomics: From Fundamentals to Clinical Applications*, A. Sussulini, Editor. 2017, Springer International Publishing: Cham. p. 145-161.
340. Vijaya, S. Sharma and N. Batra. *Comparative Study of Single Linkage, Complete Linkage, and Ward Method of Agglomerative Clustering*. in *2019 International Conference on Machine Learning, Big Data, Cloud and Parallel Computing (COMITCon)*. 2019.
341. Brereton, R.G. and G.R. Lloyd, *Partial least squares discriminant analysis: taking the magic away.* Journal of Chemometrics, 2014. **28**(4): p. 213-225.
342. Mehmood, T. and B. Ahmed, *The diversity in the applications of partial least squares: an overview.* Journal of Chemometrics, 2016. **30**(1): p. 4-17.
343. Farrés, M., et al., *Comparison of the variable importance in projection (VIP) and of the selectivity ratio (SR) methods for variable selection and interpretation.* Journal of Chemometrics, 2015. **29**(10): p. 528-536.
344. Mehmood, T., et al., *A review of variable selection methods in Partial Least Squares Regression.* Chemometrics and Intelligent Laboratory Systems, 2012. **118**: p. 62-69.
345. Ghiorghi, Y.K., et al., *The c-Myc Target Gene Rcl (C6orf108) Encodes a Novel Enzyme, Deoxynucleoside 5'-monophosphate N-Glycosidase*.* Journal of Biological Chemistry, 2007. **282**(11): p. 8150-8156.
346. Salleron, L., et al., *DERA is the human deoxyribose phosphate aldolase and is involved in stress response.* Biochimica et Biophysica Acta (BBA) - Molecular Cell Research, 2014. **1843**(12): p. 2913-2925.
347. Jedziniak, J.A. and F.J. Lionetti, *Purification and properties of deoxyriboaldolase from human erythrocytes.* Biochimica et Biophysica Acta (BBA) - Enzymology, 1970. **212**(3): p. 478-487.
348. Jiang, N.-S. and D.P. Groth, *Polycarboxylic Acid Activation of Rat Liver Deoxyribose Phosphate Aldolase.* Journal of Biological Chemistry, 1962. **237**(11): p. 3339-3341.
349. Abla, H., et al., *The multifaceted contribution of α-ketoglutarate to tumor progression: An opportunity to exploit?* Seminars in Cell & Developmental Biology, 2020. **98**: p. 26-33.
350. Yelamanchi, S.D., et al., *A pathway map of glutamate metabolism.* Journal of Cell Communication and Signaling, 2016. **10**(1): p. 69-75.

351. Hallen, A., J.F. Jamie and A.J.L. Cooper, *Lysine metabolism in mammalian brain: an update on the importance of recent discoveries.* Amino Acids, 2013. **45**(6): p. 1249-1272.
352. Fjellstedt, T.A. and J.C. Robinson, *Purification and properties of l-lysine-α-ketoglutarate reductase from human placenta.* Archives of Biochemistry and Biophysics, 1975. **168**(2): p. 536-548.
353. Murthy, S.N. and M.K. Janardanasarma, *Identification of L-amino acid/L-lysine α-amino oxidase in mouse brain.* Molecular and Cellular Biochemistry, 1999. **197**(1): p. 13-23.
354. Forman, H.J., H. Zhang and A. Rinna, *Glutathione: Overview of its protective roles, measurement, and biosynthesis.* Molecular Aspects of Medicine, 2009. **30**(1): p. 1-12.
355. Smith, T., M.S. Ghandour and P.L. Wood, *Detection of N-acetyl methionine in human and murine brain and neuronal and glial derived cell lines.* Journal of Neurochemistry, 2011. **118**(2): p. 187-194.
356. Yoon, B.-E. and C.J. Lee, *GABA as a rising gliotransmitter.* Frontiers in Neural Circuits, 2014. **8**.
357. Gorres, K.L. and R.T. Raines, *Prolyl 4-hydroxylase.* Critical Reviews in Biochemistry and Molecular Biology, 2010. **45**(2): p. 106-124.
358. Sasaki, M., et al., *D-2-hydroxyglutarate produced by mutant IDH1 perturbs collagen maturation and basement membrane function.* Genes & Development, 2012.
359. Göbel, A., et al., *Cholesterol and beyond - The role of the mevalonate pathway in cancer biology.* Biochimica et Biophysica Acta (BBA) - Reviews on Cancer, 2020. **1873**(2): p. 188351.
360. Collard, F., et al., *Molecular identification of N-acetylaspartylglutamate synthase and β-citrylglutamate synthase.* Journal of Biological Chemistry, 2010. **285**(39): p. 29826-29833.
361. Hlouchová, K., et al., *Biochemical characterization of human glutamate carboxypeptidase III.* Journal of Neurochemistry, 2007. **101**(3): p. 682-696.
362. Collard, F., et al., *Molecular Identification of β-Citrylglutamate Hydrolase as Glutamate Carboxypeptidase 3.* Journal of Biological Chemistry, 2011. **286**(44): p. 38220-38230.
363. Navrátil, M., et al., *Comparison of human glutamate carboxypeptidases II and III reveals their divergent substrate specificities.* Febs j, 2016. **283**(13): p. 2528-45.
364. Neale, J.H., et al., *Advances in understanding the peptide neurotransmitter NAAG and appearance of a new member of the NAAG neuropeptide family.* Journal of Neurochemistry, 2011. **118**(4): p. 490-498.
365. Miyake, M., Y. Kakimoto and M. Sorimachi, *Isolation and identification of β-citryl-L-glutamic acid from newborn rat brain.* Biochimica et Biophysica Acta (BBA) - General Subjects, 1978. **544**(3): p. 656-666.
366. Narahara, M., et al., *Immunocytochemical Localization of β-Citryl-L-glutamate in Primary Neuronal Cells and in the Differentiation of P19 Mouse Embryonal Carcinoma Cells into Neuronal Cells.* Biological & Pharmaceutical Bulletin, 2000. **23**(11): p. 1287-1292.
367. Miyake, M., S. Kume and Y. Kakimoto, *Correlation of the level of β-citryl-l-glutamic acid with spermatogenesis in rat testes.* Biochimica et Biophysica Acta (BBA) - General Subjects, 1982. **719**(3): p. 495-500.
368. Zhao, H., et al., *Metabolomics profiling in plasma samples from glioma patients correlates with tumor phenotypes.* Oncotarget, 2016. **7**(15): p. 20486-20495.
369. Huang, J., et al., *A prospective study of serum metabolites and glioma risk.* Oncotarget, 2017. **8**(41): p. 70366-70377.
370. Gonsalves, W.I., et al., *Glutamine-derived 2-hydroxyglutarate is associated with disease progression in plasma cell malignancies.* JCI insight, 2018. **3**(1): p. e94543.
371. Nagana Gowda, G.A., et al., *Simultaneous Analysis of Major Coenzymes of Cellular Redox Reactions and Energy Using ex Vivo 1H NMR Spectroscopy.* Analytical Chemistry, 2016. **88**(9): p. 4817-4824.
372. Bernofsky, C. and M. Swan, *An improved cycling assay for nicotinamide adenine dinucleotide.* Analytical Biochemistry, 1973. **53**(2): p. 452-458.
373. Kupfer, D. and T. Munsell, *A colorimetric method for the quantitative determination of reduced pyridine nucleotides (NADPH and NADH).* Analytical Biochemistry, 1968. **25**: p. 10-16.
374. Bilan, D.S., et al., *Genetically encoded fluorescent indicator for imaging NAD+/NADH ratio changes in different cellular compartments.* Biochimica et Biophysica Acta (BBA) - General Subjects, 2014. **1840**(3): p. 951-957.
375. Cameron, W.D., et al., *Apollo-NADP+: a spectrally tunable family of genetically encoded sensors for NADP+.* Nature Methods, 2016. **13**(4): p. 352-358.
376. Zhao, Y., et al., *Genetically encoded fluorescent sensors for intracellular NADH detection.* Cell metabolism, 2011. **14**(4): p. 555-566.

377. Tao, R., et al., *Genetically encoded fluorescent sensors reveal dynamic regulation of NADPH metabolism.* Nature methods, 2017. **14**(7): p. 720-728.
378. Røst, L.M., et al., *Zwitterionic HILIC tandem mass spectrometry with isotope dilution for rapid, sensitive and robust quantification of pyridine nucleotides in biological extracts.* Journal of Chromatography B, 2020. **1144**: p. 122078.
379. Gil, A., et al., *Stability of energy metabolites—An often overlooked issue in metabolomics studies: A review.* ELECTROPHORESIS, 2015. **36**(18): p. 2156-2169.
380. Lerma-Ortiz, C., et al., *'Nothing of chemistry disappears in biology': the Top 30 damage-prone endogenous metabolites.* Biochemical Society Transactions, 2016. **44**(3): p. 961-971.
381. Wei, Z., et al., *Metabolism of Amino Acids in Cancer.* Frontiers in Cell and Developmental Biology, 2021. **8**.
382. Vettore, L., R.L. Westbrook and D.A. Tennant, *New aspects of amino acid metabolism in cancer.* British Journal of Cancer, 2020. **122**(2): p. 150-156.
383. Pan, S., et al., *Serine, glycine and one-carbon metabolism in cancer (Review).* Int J Oncol, 2021. **58**(2): p. 158-170.
384. McKenna, M.C., et al., *Glutamate oxidation in astrocytes: Roles of glutamate dehydrogenase and aminotransferases.* Journal of Neuroscience Research, 2016. **94**(12): p. 1561-1571.
385. Kanehisa, M. and S. Goto, *KEGG: kyoto encyclopedia of genes and genomes.* Nucleic Acids Res, 2000. **28**(1): p. 27-30.
386. Joberty, G., et al., *Interrogating the Druggability of the 2-Oxoglutarate-Dependent Dioxygenase Target Class by Chemical Proteomics.* ACS Chemical Biology, 2016. **11**(7): p. 2002-2010.
387. Shi, D.D., et al., *De novo pyrimidine synthesis is a targetable vulnerability in IDH mutant glioma.* Cancer Cell, 2022.
388. Nelson, D.L., A.L. Lehninger and M.M. Cox, *Lehninger Principles of biochemistry*. 6th ed. Principles of biochemistry. 2013, New York: W.H. Freeman.
389. Morrison, D.J. and T. Preston, *Formation of short chain fatty acids by the gut microbiota and their impact on human metabolism.* Gut Microbes, 2016. **7**(3): p. 189-200.
390. Aglae, H., et al., *Late-Stage Glioma Is Associated with Deleterious Alteration of Gut Bacterial Metabolites in Mice.* Metabolites, 2022. **12**(4).
391. Dono, A., et al., *Glioma induced alterations in fecal short-chain fatty acids and neurotransmitters.* CNS Oncology, 2020. **9**(2): p. CNS57.
392. Amaral, A.U., et al., *2-Methylcitric acid impairs glutamate metabolism and induces permeability transition in brain mitochondria.* Journal of Neurochemistry, 2016. **137**(1): p. 62-75.
393. Wishart, D.S., et al., *HMDB 5.0: the Human Metabolome Database for 2022.* Nucleic Acids Res, 2022. **50**(D1): p. D622-d631.
394. Fagerberg, L., et al., *Analysis of the human tissue-specific expression by genome-wide integration of transcriptomics and antibody-based proteomics.* Mol Cell Proteomics, 2014. **13**(2): p. 397-406.
395. Fattal-Valevski, A., *Thiamine (Vitamin B1).* Journal of Evidence-Based Complementary & Alternative Medicine, 2011. **16**(1): p. 12-20.
396. Nemeria, N.S., et al., *Functional Versatility of the Human 2-Oxoadipate Dehydrogenase in the L-Lysine Degradation Pathway toward Its Non-Cognate Substrate 2-Oxopimelic Acid.* International Journal of Molecular Sciences, 2022. **23**(15).
397. Crake, R.L.I., et al., *Ascorbate content of clinical glioma tissues is related to tumour grade and to global levels of 5-hydroxymethyl cytosine.* Scientific Reports, 2022. **12**(1): p. 14845.
398. Haris, M., et al., *In vivo mapping of brain myo-inositol.* NeuroImage, 2011. **54**(3): p. 2079-2085.
399. Kuiper, C. and M.C.M. Vissers, *Ascorbate as a Co-Factor for Fe- and 2-Oxoglutarate Dependent Dioxygenases: Physiological Activity in Tumor Growth and Progression.* Frontiers in Oncology, 2014. **4**.
400. Nguyen, T., et al., *Uncovering the Role of N-Acetyl-Aspartyl-Glutamate as a Glutamate Reservoir in Cancer.* Cell Reports, 2019. **27**(2): p. 491-501.e6.
401. Hamada-Kanazawa, M., et al., *β-Citryl-L-glutamate Is an Endogenous Iron Chelator That Occurs Naturally in the Developing Brain.* Biological and Pharmaceutical Bulletin, 2010. **33**(5): p. 729-737.
402. Hamada-Kanazawa, M., et al., *β-Citryl-L-glutamate Acts as an Iron Carrier to Activate Aconitase Activity.* Biological and Pharmaceutical Bulletin, 2011. **34**(9): p. 1455-1464.
403. Narahara, M., et al., *Superoxide Scavenging and Xanthine Oxidase Inhibiting Activities of Copper–β-Citryl-<small>L</small>-glutamate Complex.* Biological and Pharmaceutical Bulletin, 2010. **33**(12): p. 1938-1943.

404. Garattini, E., et al., *Mammalian molybdo-flavoenzymes, an expanding family of proteins: structure, genetics, regulation, function and pathophysiology.* Biochemical Journal, 2003. **372**(1): p. 15-32.
405. Tanna, N., et al., *Improving LC/MS/MS-based bioanalytical method performance and sensitivity via a hybrid surface barrier to mitigate analyte – Metal surface interactions.* Journal of Chromatography B, 2021. **1179**: p. 122825.
406. Heaton, J.C. and D.V. McCalley, *Some factors that can lead to poor peak shape in hydrophilic interaction chromatography, and possibilities for their remediation.* Journal of Chromatography A, 2016. **1427**: p. 37-44.
407. Johnsen, E., et al., *Hydrophilic interaction chromatography of nucleoside triphosphates with temperature as a separation parameter.* Journal of Chromatography A, 2011. **1218**(35): p. 5981-5986.
408. Liu, S., T. Cadoux-Hudson and C.J. Schofield, *Isocitrate dehydrogenase variants in cancer — Cellular consequences and therapeutic opportunities.* Current Opinion in Chemical Biology, 2020. **57**: p. 122-134.
409. Lu, C., et al., *IDH mutation impairs histone demethylation and results in a block to cell differentiation.* Nature, 2012. **483**: p. 474.
410. Chen, F., et al., *Oncometabolites d-and l-2-hydroxyglutarate inhibit the AlkB family DNA repair enzymes under physiological conditions.* Chemical research in toxicology, 2017. **30**(4): p. 1102-1110.
411. Sulkowski, P.L., et al., *Oncometabolites suppress DNA repair by disrupting local chromatin signalling.* Nature, 2020. **582**(7813): p. 586-591.
412. Wang, P., et al., *Oncometabolite D-2-Hydroxyglutarate Inhibits ALKBH DNA Repair Enzymes and Sensitizes IDH Mutant Cells to Alkylating Agents.* Cell Reports, 2015. **13**(11): p. 2353-2361.
413. Caravella, J.A., et al., *Structure-Based Design and Identification of FT-2102 (Olutasidenib), a Potent Mutant-Selective IDH1 Inhibitor.* Journal of Medicinal Chemistry, 2020. **63**(4): p. 1612-1623.
414. Gao, M., et al., *Pharmacological characterization of TQ05310, a potent inhibitor of isocitrate dehydrogenase 2 R140Q and R172K mutants.* Cancer science, 2019. **110**(10): p. 3306-3314.
415. Jia, P., et al., *I-8, a novel inhibitor of mutant IDH1, inhibits cancer progression in vitro and in vivo.* European Journal of Pharmaceutical Sciences, 2019. **140**: p. 105072.
416. Konteatis, Z., et al., *Vorasidenib (AG-881): A First-in-Class, Brain-Penetrant Dual Inhibitor of Mutant IDH1 and 2 for Treatment of Glioma.* Acs Medicinal Chemistry Letters, 2020. **11**(2): p. 101-107.
417. Machida, Y., et al., *A Potent Blood-Brain Barrier-Permeable Mutant IDH1 Inhibitor Suppresses the Growth of Glioblastoma with IDH1 Mutation in a Patient-Derived Orthotopic Xenograft Model.* Molecular Cancer Therapeutics, 2020. **19**(2): p. 375-383.
418. Popovici-Muller, J., et al., *Discovery of the First Potent Inhibitors of Mutant IDH1 That Lower Tumor 2-HG in Vivo.* ACS Medicinal Chemistry Letters, 2012. **3**(10): p. 850-855.
419. Norsworthy, K.J., et al., *FDA Approval Summary: Ivosidenib for Relapsed or Refractory Acute Myeloid Leukemia with an Isocitrate Dehydrogenase-1 Mutation.* Clinical Cancer Research, 2019. **25**(11): p. 3205-3209.
420. website, U.S.F.a.D.A. *FDA approves olutasidenib for relapsed or refractory acute myeloid leukemia with a susceptible IDH1 mutation*. 2022 01/12/2022 [cited 2023 January 5]; Available from: https://www.fda.gov/drugs/resources-information-approved-drugs/fda-approves-olutasidenib-relapsed-or-refractory-acute-myeloid-leukemia-susceptible-idh1-mutation.
421. Casak, S.J., et al., *FDA Approval Summary: Ivosidenib for the Treatment of Patients with Advanced Unresectable or Metastatic, Chemotherapy Refractory Cholangiocarcinoma with an IDH1 Mutation.* Clinical Cancer Research, 2022. **28**(13): p. 2733-2737.
422. Mellinghoff, I.K., et al., *Vorasidenib, a Dual Inhibitor of Mutant IDH1/2, in Recurrent or Progressive Glioma; Results of a First-in-Human Phase I Trial.* Clinical Cancer Research, 2021. **27**(16): p. 4491-4499.
423. de la Fuente, M.I., et al., *Olutasidenib (FT-2102) in patients with relapsed or refractory IDH1-mutant glioma: A multicenter, open-label, phase Ib/II trial.* Neuro-Oncology, 2022. **25**(1): p. 146-156.
424. Oltvai, Z.N., et al., *Assessing acquired resistance to IDH1 inhibitor therapy by full-exon IDH1 sequencing and structural modeling.* Molecular Case Studies, 2021. **7**(2): p. a006007.
425. Wang, F., et al., *Leukemia stemness and co-occurring mutations drive resistance to IDH inhibitors in acute myeloid leukemia.* Nature Communications, 2021. **12**(1): p. 2607.
426. Lyu, J., et al., *Disabling Uncompetitive Inhibition of Oncogenic IDH Mutations Drives Acquired Resistance.* Cancer discovery, 2022: p. CD-21-1661.

427. Cleary, J.M., et al., *Secondary IDH1 resistance mutations and oncogenic IDH2 mutations cause acquired resistance to ivosidenib in cholangiocarcinoma.* npj Precision Oncology, 2022. **6**(1): p. 61.
428. Dang, L., S. Jin and S.M. Su, *IDH mutations in glioma and acute myeloid leukemia.* Trends in Molecular Medicine, 2010. **16**(9): p. 387-397.
429. Yabré, M., et al., *Greening Reversed-Phase Liquid Chromatography Methods Using Alternative Solvents for Pharmaceutical Analysis.* Molecules, 2018. **23**(5): p. 1065.
430. Zheng, X., et al., *Proteomic Analysis for the Assessment of Different Lots of Fetal Bovine Serum as a Raw Material for Cell Culture. Part IV. Application of Proteomics to the Manufacture of Biological Drugs.* Biotechnology Progress, 2006. **22**(5): p. 1294-1300.
431. Polson, C., et al., *Optimization of protein precipitation based upon effectiveness of protein removal and ionization effect in liquid chromatography–tandem mass spectrometry.* Journal of Chromatography B, 2003. **785**(2): p. 263-275.
432. Malich, G., B. Markovic and C. Winder, *The sensitivity and specificity of the MTS tetrazolium assay for detecting the in vitro cytotoxicity of 20 chemicals using human cell lines.* Toxicology, 1997. **124**(3): p. 179-192.
433. Weller, M., et al., *EANO guidelines on the diagnosis and treatment of diffuse gliomas of adulthood.* Nature Reviews Clinical Oncology, 2021. **18**(3): p. 170-186.
434. Viswanath, P., et al., *Mutant IDH1 gliomas downregulate phosphocholine and phosphoethanolamine synthesis in a 2-hydroxyglutarate-dependent manner.* Cancer Metabolism, 2018. **6**(1): p. 3.
435. Reitman, Z.J., et al., *Cancer-associated Isocitrate Dehydrogenase 1 (IDH1) R132H Mutation and D-2-hydroxyglutarate Stimulate Glutamine Metabolism under Hypoxia.* Journal of Biological Chemistry, 2014.
436. Chaturvedi, A., et al., *In vivo efficacy of mutant IDH1 inhibitor HMS-101 and structural resolution of distinct binding site.* Leukemia, 2020. **34**(2): p. 416-426.
437. Broadhurst, D.I. and D.B. Kell, *Statistical strategies for avoiding false discoveries in metabolomics and related experiments.* Metabolomics, 2006. **2**(4): p. 171-196.
438. Xia, J., et al., *MetaboAnalyst 2.0—a comprehensive server for metabolomic data analysis.* Nucleic Acids Research, 2012. **40**(W1): p. W127-W133.
439. Pavlidis, P., *Using ANOVA for gene selection from microarray studies of the nervous system.* Methods, 2003. **31**(4): p. 282-289.
440. Chen, H., et al., *Amino Acid Deprivation Induces the Transcription Rate of the Human Asparagine Synthetase Gene through a Timed Program of Expression and Promoter Binding of Nutrient-responsive Basic Region/Leucine Zipper Transcription Factors as Well as Localized Histone Acetylation *.* Journal of Biological Chemistry, 2004. **279**(49): p. 50829-50839.
441. Sabharwal, S.S. and P.T. Schumacker, *Mitochondrial ROS in cancer: initiators, amplifiers or an Achilles' heel?* Nature Reviews Cancer, 2014. **14**(11): p. 709-721.
442. Kizilbash, S.H., et al., *A phase Ib trial of CB-839 (telaglenastat) in combination with radiation therapy and temozolomide in patients with IDH-mutated diffuse astrocytoma and anaplastic astrocytoma (NCT03528642).* Journal of Clinical Oncology, 2019. **37**(15_suppl): p. TPS2075-TPS2075.
443. Gross, M.I., et al., *Antitumor Activity of the Glutaminase Inhibitor CB-839 in Triple-Negative Breast Cancer.* Molecular Cancer Therapeutics, 2014. **13**(4): p. 890-901.
444. Skaga, E., et al., *Feasibility study of using high-throughput drug sensitivity testing to target recurrent glioblastoma stem cells for individualized treatment.* Clinical and Translational Medicine, 2019. **8**(1): p. 33.
445. Skaga, E., et al., *Intertumoral heterogeneity in patient-specific drug sensitivities in treatment-naïve glioblastoma.* BMC Cancer, 2019. **19**(1): p. 628.
446. Luk, G.D. and R.A. Casero, *Polyamines in normal and cancer cells.* Advances in Enzyme Regulation, 1987. **26**: p. 91-105.
447. Heby, O., *Role of Polyamines in the Control of Cell Proliferation and Differentiation.* Differentiation, 1981. **19**(1): p. 1-20.
448. Terzis, A.J.A., et al., *Effects of DFMO on glioma cell proliferation, migration and invasion in vitro.* Journal of Neuro-Oncology, 1998. **36**(2): p. 113-121.
449. Takao, K., et al., *Induction of apoptotic cell death by putrescine.* The International Journal of Biochemistry & Cell Biology, 2006. **38**(4): p. 621-628.
450. Koch, K., et al., *A comparative pharmaco-metabolomic study of glutaminase inhibitors in glioma stem-like cells confirms biological effectiveness but reveals differences in target-specificity.* Cell Death Discovery, 2020. **6**(1): p. 20.

451. Vande Voorde, J., et al., *Improving the metabolic fidelity of cancer models with a physiological cell culture medium.* Science Advances, 2019. **5**(1): p. eaau7314.

Chapter 9. Appendices

9.1. Appendix I

The database for the IC-MS method described in **section 2.7.1** is provided in **Table A.I.1** and for the derivatised RPLC-MS method described in **section 2.7.2** is provided in **Table A.I.2**. The database contained the following information: compound ID, description, neutral mass (NM), adduct, retention time (RT (min)) and formula). They were used within the program Progenesis QI to aid metabolite identification. The databases were established by members of the McCullagh group.

Table A.I.1. Data base of metabolites measured by IC-MS. Abbreviations: RT = retention time.

Compound ID	Description	Neutral mass	RT (min)	Formula
HMDB0013674	1,2,3-Trihydroxybenzene/Pyrogallol	126.0322	23.21	C6H6O3
HMDB0000957	1,2-Dihydroxybenzene	110.0368	25.92	C6H6O2
HMDB0013593	1,4 dihydrotheritol	154.0122	14.86	C4H10O2S2
HMDB0001213	1-Deoxy-D-xylulose 5-phosphate	214.0242	10.32	C5H11O7P
NA	1-Hydroxy-2-methyl-2-butenyl 4-pyrophosphate	262.0007	16.68	C5H12O8P2
NA	1-Methyl indole	131.0740	28.33	C9H9N
HMDB0000001	1-Methylhistidine	169.0851	12.89	C7H11N3O2
HMDB0001369	1-Pyrroline hydroxycarboxylic acid	129.0426	4.48	C5H7NO3
HMDB0001301	1-Pyrroline-5-carboxylic acid	113.0477	9.37	C5H7NO2
HMDB0002006	2,3-Diaminopropionic acid	104.0591	11.75	C3H8N2O2
HMDB0001294	2,3-Diphosphoglyceric acid	265.9593	22.21	C3H8O10P2
HMDB0000152	2,5-Dihydroxybenzoic acid	154.0266	32.16	C7H6O4
HMDB0000370	2-Amino-3-phosphonopropionic acid	169.0146	14.56	C3H8NO5P
NA	2-amino-5-hydroxybenzoic acid	153.0431	33.19	C7H7NO3
HMDB0001123	2-Aminobenzoic acid/Anthranilic acid	137.0477	25.09	C7H7NO2
HMDB0001906	2-Aminoisobutyric acid	103.0633	9.92	C4H9NO2
HMDB0032059	2-Bromophenol	171.9529	9.03	C6H5BrO
NA	2-butyl-3-ureido-succinate	232.1059	11.98	C9H16N2O5
NA	2-C-Methyl-D-erythritol-2,4-cyclopyrophosphate	277.9962	15.28	C5H12O9P2
NA	2-C-Methylerythritol 4-phosphate	214.0242	9.88	C5H13O7P
NA	2-Hydroxy-4-phenylbutanoic acid	180.0792	14.39	C10H12O3
HMDB0000008	2-Hydroxybutyric acid	104.0473	5.41	C4H8O3
HMDB0059655	2-Hydroxyglutarate	148.0372	10.90	C5H8O5
HMDB0001624	2-Hydroxyhexanoic acid	132.0792	7.98	C6H12O3
HMDB0000402	2-Isopropylmalic acid	176.0685	12.32	C7H12O5
HMDB0000005	2-Ketobutyric acid	102.0317	7.86	C4H6O3
HMDB0000379	2-Methylcitric acid	206.0432	16.09	C7H10O7
HMDB0000208	2-Oxoglutaric acid	146.0215	12.85	C5H6O5
HMDB0000362	2-Phosphoglyceric acid	185.9929	16.34	C3H7O7P
HMDB0000397	2-Pyrocatechuic acid	154.0266	33.01	C7H6O4
HMDB0002039	2-Pyrrolidinone	85.0533	13.37	C4H7NO
HMDB0002441	3,3 Dimethyl glutarate	160.0736	11.41	C7H12O4
HMDB0012153	3,4,Dihydroxybenzylamine	139.0639	13.52	C7H9NO2
HMDB0001336	3,4-dihydroxyphenyl acetic acid	168.0423	22.60	C8H8O4
HMDB0003911	3-Aminoisobutanoic acid	103.0633	10.32	C4H9NO2
HMDB0003540	3'-AMP	347.0625	13.43	C10H14N5O7P
HMDB0012710	3-Dehydroquinate	190.0477	5.51	C7H10O6
HMDB0001376	3-deoxy-2-keto-6-phosphogluconic acid	258.0141	15.93	C6H11O9P

HMDB0001476	3-Hydroxyanthranilic acid	153.0431	26.46	C7H7NO3
HMDB0002466	3-Hydroxybenzoic acid	138.0322	22.66	C7H6O3
HMDB0000357	3-Hydroxybutyric acid	104.0473	5.36	C4H8O3
HMDB0000023	3-Hydroxyisobutyric acid	104.0473	5.04	C4H8O3
HMDB0000754	3-Hydroxyisovaleric acid	118.0635	5.34	C5H10O3
HMDB0000355	3-Hydroxymethylglutarate	162.0528	10.76	C6H10O5
HMDB0013188	3-Hydroxypicolinic acid	139.0269	18.07	C6H5NO3
HMDB0005784	3-Hydroxytyrosol	154.0630	15.76	C8H10O3
HMDB0059969	3-methoxyphenylacetic acid	166.0630	10.04	C9H10O3
HMDB0000491	3-Methyl-2-oxovaleric acid	130.0630	10.67	C6H10O3
HMDB0001904	3-Nitrotyrosine	226.0590	8.77	C9H10N2O5
HMDB0000807	3-Phosphoglyceric acid	185.9929	15.84	C3H7O7P
HMDB0061881	4-Acetylbutyrate	130.0635	5.09	C6H10O3
HMDB0000291	4-Hydroxy-3-methoxymandelic acid	198.0528	15.77	C9H10O5
HMDB0000500	4-Hydroxybenzoic acid	138.0317	18.86	C7H6O3
HMDB0000710	4-Hydroxybutyric acid	104.0473	10.65	C4H8O3
NA	4-hydroxyphenyl glycine	167.0582	18.59	C8H9NO3
NA	4-Hydroxyphenylbutyric acid	179.0714	17.51	C10H12O3
HMDB0000707	4-Hydroxyphenylpyruvic acid	180.0423	27.88	C9H8O4
HMDB0000725	4-Hydroxyproline	131.0582	9.68	C5H9NO3
NA	4-Hydroxypyrrolidinone	101.0477	2.94	C4H7NO2
NA	4-Methyl-2-ureido-pentanoic acid	174.1010	6.36	C7H14N2O3
HMDB0000873	4-Methylcatechol	124.0530	29.91	C7H8O2
HMDB0036619	5,7-Dihydroxyflavone (Chrysin)	254.0585	4.33	C15H10O4
HMDB0001149	5-Aminolevulinic acid	131.0588	3.89	C5H9NO3
NA	5-Formyl-dCTP	494.9851	20.45	C10H16N3O14P3
HMDB0000525	5-Hydroxyhexanoic acid	132.0792	6.83	C6H12O3
HMDB0000763	5-Hydroxyindoleacetic acid	191.0582	26.83	C10H9NO3
NA	5-Hydroxymethyl-2'-deoxyuridine	258.0850	6.48	C10H14N2O6
NA	5-Hydroxy-methyl-dCTP	497.0002	19.40	C10H18N3O14P3
HMDB0004096	5-Methoxyindoleacetate	205.0739	29.66	C11H11NO3
NA	5-Methyl-dCTP	481.0052	18.96	C10H18N3O13P3
HMDB0038804	6-hydroxy-2,5,7,8-tetramethylchromane-2-carboxylic acid	250.1205	29.39	C14H18O4
HMDB0001316	6-Phosphogluconic acid	276.0246	15.18	C6H13O10P
HMDB0001127	6-phosphonoglucono-lactone	258.0146	11.52	C6H11O9P
HMDB0003333	8-Hydroxy-deoxyguanosine	283.0917	19.83	C10H13N5O5
HMDB0011615	8-Oxo-dGTP	522.9901	19.78	C10H16N5O14P3
HMDB0036093	Abscisic acid	264.1362	13.64	C15H20O4
HMDB0000042	Acetic acid	60.0211	3.85	C2H4O2
HMDB0000060	Acetoacetate	102.0317	5.14	C4H6O3
HMDB0001484	Acetoacetyl-CoA	851.1363	33.10	C25H40N7O18P3S
HMDB0001206	Acetyl-CoA	809.1258	7.59	C23H38N7O17P3S
HMDB0001890	Acetylcysteine	163.0303	11.56	C5H9NO3S
HMDB0000532	Acetylglycine	117.0426	4.07	C4H7NO3
HMDB0001494	Acetylphosphate	139.9880	12.66	C2H5O5P
HMDB0000034	Adenine	135.0545	15.32	C5H5N5
HMDB0011616	Adenosine 2',3'-cyclic phosphate	329.0520	9.41	C10H12N5O6P
HMDB0001341	Adenosine diphosphate	427.0294	19.79	C10H15N5O10P2
HMDB0000045	Adenosine monophosphate	347.0631	13.84	C10H14N5O7P
HMDB0000538	Adenosine triphosphate	506.9957	24.53	C10H16N5O13P3
HMDB0001332	Adenylsuccinate	463.0740	23.15	C14H18N5O11P
HMDB0012882	Adipate semialdehyde	130.0630	11.34	C6H10O3
HMDB0000508	Adonitol (ribitol)	152.0685	2.86	C5H12O5
HMDB0006557	ADP Glucose	589.0822	14.30	C16H25N5O15P2
HMDB0000462	Allantoin	158.0445	5.95	C4H6N4O3
HMDB0001151	Allose	180.0634	3.04	C6H12O6
HMDB0000650	Alpha-aminobutyrate	103.0633	10.32	C4H9NO2
HMDB0002166	Alpha-aminoisobutyrate	103.0633	10.06	C4H9NO2
HMDB0000539	Arabinonic acid	166.0477	4.9	C5H10O6

HMDB0000646	Arabinose	150.0528	3.06	C5H10O5
HMDB0029942	Arabinose	150.0528	3.06	C5H10O5
HMDB0000568	Arabitol	152.0685	2.71	C5H12O5
HMDB0000044	Ascorbate	176.0321	12.36	C6H8O6
HMDB0000191	Aspartate	133.0375	11.78	C4H7NO4
NA	Benzoyl-L-citrulline methyl ester	293.1381	11.17	C14H19N3O4
HMDB0000056	Beta-Alanine	89.0477	4.73	C3H7NO2
HMDB0013220	Beta-Citryl-L-glutamic acid	321.0696	20.62	C11H15NO10
NA	Butyl ureidosuccinic acid	232.1065	10.61	C9H16N2O5
HMDB0000039	Butyric acid	88.0524	6.32	C4H8O2
HMDB0000535	Caproic acid	116.0843	8.58	C6H12O2
HMDB0001096	Carbamoyl phosphate	140.9827	15.06	CH4NO5P
HMDB0000033	Carnosine	225.0993	3.93	C9H14N4O3
HMDB0011621	Cinnamoylglycine	205.0733	20.81	C11H11NO3
HMDB0000072	cis-Aconitic acid	174.0164	18.12	C6H6O6
HMDB0000634	Citraconic acid	130.0266	11.96	C5H6O4
HMDB0000426	Citramalic acid	148.0372	10.75	C5H8O5
HMDB0000094	Citric acid	192.0270	16.91	C6H8O7
HMDB0000904	Citrulline	175.0957	4.12	C6H13N3O3
HMDB0015020	Clomifene	405.1859	16.22	C26H28ClNO
HMDB0001423	Coenzyme A	767.1152	25.32	C21H36N7O16P3S
HMDB0000058	Cyclic AMP	329.0525	15.10	C10H12N5O6P
HMDB0001314	Cyclic GMP	345.0474	24.09	C10H12N5O7P
HMDB0060150	Cysteamine	77.0299	9.87	C2H7NS
HMDB0002757	Cysteic acid	169.0045	12.19	C3H7NO5S
HMDB0000574	Cysteine	121.0197	15.66	C3H7NO2S
HMDB0000089	Cytidine	243.0861	8.48	C9H13N3O5
HMDB0001546	Cytidine diphosphate	403.0176	16.34	C9H15N3O11P2
HMDB0000095	Cytidine monophosphate	323.0519	11.78	C9H14N3O8P
HMDB0001176	Cytidine monophosphate N-acetylneuraminic acid	614.1473	9.79	C20H31N4O16P
HMDB0000082	Cytidine triphosphate	482.9845	21.06	C9H16N3O14P3
HMDB0000630	Cytosine	111.0433	5.52	C4H5N3O
HMDB0001508	dADP	411.0345	18.27	C10H15N5O9P2
HMDB0000905	dAMP	331.0682	12.88	C10H14N5O6P
HMDB0001245	dCDP	387.0233	30.12	C9H15N3O10P2
HMDB0001202	dCMP	307.0569	10.06	C9H14N3O7P
HMDB0000998	dCTP	466.9896	19.55	C9H16N3O13P3
HMDB0000101	Deoxyadenosine	251.1018	12.14	C10H13N5O3
HMDB0001532	Deoxyadenosine triphosphate	491.0008	24.33	C10H16N5O12P3
HMDB0000014	Deoxycytidine	227.0912	4.69	C9H13N3O4
HMDB0000085	deoxyguanosine	283.0922	4.08	C10H13N5O4
HMDB0001031	Deoxyribose 5-phosphate	214.0242	11.06	C5H11O7P
NA	Deoxythymidine	225.0881	7.67	C10H14N2O4
HMDB0000012	Deoxyuridine	228.0746	7.62	C9H12N2O5
HMDB0000960	dGDP	427.0294	24.67	C10H15N5O10P2
HMDB0001044	dGMP	347.0631	20.57	C10H14N5O7P
HMDB0001440	dGTP	506.9952	29.43	C10H16N5O13P3
NA	Diaminocyclohexane-N,N,N',N'-tetraacetic acid	345.1303	8.92	C14H22N2O8
HMDB0014724	Diclofenac	295.0161	1.22	C14H11Cl2NO2
HMDB0003349	Dihydroorotic acid	158.0328	11.63	C5H6N2O4
HMDB0000076	Dihydrouracil	114.0424	13.43	C4H6N2O2
HMDB0001882	Dihydroxyacetone	90.0317	4.74	C3H6O3
HMDB0001473	Dihydroxyacetone phosphate	169.9980	11.19	C3H7O6P
HMDB0000181	Dihydroxyphenylalanine	197.0688	32.44	C9H11NO4
HMDB0031257	Dimethyl fumarate	144.0423	13.16	C6H8O4
HMDB0001120	Dimethylallyl pyrophosphate	246.0058	18.73	C5H12O7P2
HMDB0000092	Dimethylglycine	103.0633	10.15	C4H9NO2
HMDB0006555	dIMP	332.0522	18.99	C10H13N4O7P
NA	DL-Threo-beta-Hydroxyaspartic acid	148.0251	10.43	C4H7NO5

HMDB0000073	Dopamine	153.0790	19.68	C8H11NO2
HMDB0001328	dTDP-D-glucose	564.0758	17.06	C16H26N2O16P2
HMDB0001000	dUDP	388.0073	19.60	C9H14N2O11P2
HMDB0001409	dUMP	308.0410	17.10	C9H13N2O8P
HMDB0001191	dUTP	467.9736	25.45	C9H15N2O14P3
HMDB0015109	EDTA	292.0907	10.83	C10H16N2O8
HMDB0000900	Ergocalciferol	396.3387	4.21	C28H44O
HMDB0000878	Ergosterol	396.3387	1.13	C28H44O
HMDB0001321	Erythrose 4-phosphate	200.0086	12.91	C4H9O7P
Ethionine	Ethionine	163.0672	33.54	C6H13NO2S
HMDB0000622	Ethylmalonic acid	132.0423	11.62	C5H8O4
HMDB0001248	FAD	785.1571	28.12	C27H33N9O15P2
HMDB0000954	Ferulic acid	194.0579	27.02	C10H10O4
HMDB0014684	Fluorouracil	130.0179	13.57	C4H3FN2O2
HMDB0014615	Fluoxetine	309.1346	21.52	C17H18F3NO
HMDB0000660	Fructose	180.0634	3.06	C6H12O6
HMDB0001058	Fructose 1,6-bisphosphate	339.9960	20.44	C6H14O12P2
HMDB0001047	Fructose 2,6 diphosphate	339.9960	17.52	C6H14O12P2
HMDB0000124	Fructose 6-phosphate	260.0297	11.88	C6H13O9P
HMDB0000134	Fumarate	116.0110	13.63	C4H4O4
HMDB0000639	Galactaric acid	210.0376	10.94	C6H10O8
HMDB0000143	Galactose	180.0634	3.02	C6H12O6
HMDB0000645	Galactose 1-phosphate	260.0297	9.39	C6H13O9P
NA	Galactose-6-phosphate	260.0292	11.77	C6H13O9P
HMDB0002545	Galacturonic acid	194.0427	7.52	C6H10O7
HMDB0013233	Gamma-delta-Dioxovaleric acid	130.0266	10.65	C5H6O4
HMDB0003559	Gibberellin A3	346.1416	12.68	C19H22O6
HMDB0000625	Gluconate	196.0583	4.67	C6H12O7
HMDB0000150	Gluconolactone	178.0477	4.71	C6H10O6
HMDB0001514	Glucosamine	179.0794	11.58	C6H13NO5
HMDB0001254	Glucosamine 6-phosphate	259.0457	13.18	C6H14NO8P
HMDB0000122	Glucose	180.0634	3.43	C6H12O6
HMDB0001586	Glucose 1-phosphate	260.0297	9.66	C6H13O9P
HMDB0001401	Glucose 6-phosphate	260.0297	12.38	C6H13O9P
HMDB0000127	Glucuronic acid	194.0427	8.27	C6H10O7
HMDB0000620	Glutaconic acid	130.0266	12.69	C5H6O4
HMDB0000148	Glutamic acid	147.0532	14.79	C5H9NO4
HMDB0000641	Glutamine	146.0691	11.67	C5H10N2O3
HMDB0001049	Glutamylcysteine	250.0629	16.61	C8H14N2O5S
HMDB0000661	Glutaric acid	132.0423	10.87	C5H8O4
HMDB0001339	Glutaryl CoA	881.1469	19.81	C26H42N7O19P3S
HMDB0000125	Glutathione (GSH)	307.0838	15.16	C10H17N3O6S
HMDB0001112	Glyceraldehyde 3-phosphate	169.9980	11.73	C3H7O6P
HMDB0000139	Glyceric acid	106.0266	5.23	C3H6O4
HMDB0000131	Glycerol	92.0473	2.86	C3H8O3
HMDB0000126	Glycerol 3-phosphate	172.0137	9.79	C3H9O6P
HMDB0003344	Glycoaldehyde	60.0211	7.52	C2H4O2
HMDB0000115	Glycolic acid	76.0160	5.24	C2H4O3
HMDB0000119	Glyoxylic acid	74.0004	8.05	C2H2O3
HMDB0000133	Guanosine	283.0917	22.22	C10H13N5O5
HMDB0001201	Guanosine diphosphate	443.0238	27.56	C10H15N5O11P2
HMDB0001397	Guanosine monophosphate	363.0580	22.22	C10H14N5O8P
HMDB0001273	Guanosine triphosphate	522.9907	30.62	C10H16N5O14P3
HMDB0012326	Gulose	180.0634	3.05	C6H12O6
HMDB0005782	Hesperitin	302.0785	28.50	C16H14O6
HMDB0000714	Hippuric acid	179.0582	11.63	C9H9NO3
HMDB0000870	Histamine	111.0802	7.08	C5H9N3
NA	Homarine	137.0477	11.66	C7H7NO2
HMDB0000130	Homogentisic acid	168.0423	17.49	C8H8O4

HMDB0000118	Homovanillic acid	182.0579	17.21	C9H10O4
HMDB0001212	Hydantoin-5-propionic acid	172.0479	11.40	C6H8N2O4
HMDB0000764	Hydrocinnamic acid	150.0686	15.63	C9H10O2
HMDB0000528	Hydroorotic acid	158.0328	10.36	C5H6N2O4
HMDB0001855	Hydroxy-indole acetic acid	177.0790	26.62	C10H11NO2
HMDB0062640	Hydroxy-isobutyric acid	103.0401	4.46	C4H7O3
HMDB0126088	Hydroxy-isobutyric acid	104.0473	4.46	C4H8O3
HMDB0002207	Hydroxyisoheptanoic acid	146.0948	9.74	C7H14O3
HMDB0000732	Hydroxykynurenine	224.0803	13.91	C10H12N2O4
NA	Hydroxy-methyl-dUTP	497.9842	20.48	C10H17N2O15P3
HMDB0000711	Hydroxyoctanoic acid	160.1105	7.52	C8H16O3
HMDB0000700	Hydroxypropionic acid	90.0322	4.88	C3H6O3
HMDB0001352	Hydroxypyruvic acid	104.0110	11.64	C3H4O4
HMDB0000965	Hypotaurine	109.0197	14.89	C2H7NO2S
HMDB0000157	Hypoxanthine	136.0385	21.34	C5H4N4O
HMDB0011140	Hypusine	233.1745	9.42	C10H23N3O3
HMDB0003335	IDP	428.0134	26.55	C10H14N4O11P2
HMDB0001190	Indole-3-acetaldehyde	159.0684	27.44	C10H9NO
HMDB0000671	Indole-3-lactic acid	205.0739	27.23	C11H11NO3
HMDB0000197	Indoleacetic acid	175.0633	28.43	C10H9NO2
HMDB0000195	Inosine	268.0808	5.60	C10H12N4O5
HMDB0000175	Inosine monophosphate	348.0471	21.97	C10H13N4O8P
HMDB0000189	Inosine triphosphate	507.9798	30.13	C10H15N4O14P3
HMDB0001143	Inositol 1,3,4-trisphosphate	419.9624	25.85	C6H15O15P3
HMDB0000193	Isocitrate	192.0270	17.55	C6H8O7
HMDB0001347	Isopentenyl pyrophosphate	246.0058	18.45	C5H12O7P2
HMDB0000718	Isovaleric Acid	102.0686	9.43	C5H10O2
HMDB0000678	Isovalerylglycine	159.0895	6.07	C7H13NO3
HMDB0002092	Itaconic acid	130.0266	12.13	C5H6O4
HMDB0032797	Jasmonic acid	210.1256	12.22	C12H18O3
HMDB0032923	Kojic acid	142.0266	8.81	C6H6O4
HMDB0000715	Kynurenic acid	189.0426	27.57	C10H7NO3
HMDB0000684	Kynurenine	208.0848	8.81	C10H12N2O3
HMDB0000190	Lactic acid	90.0317	5.05	C3H6O3
HMDB0000186	Lactose	342.1168	3.04	C12H22O11
HMDB0062180	Lactoyl-isoleucine	203.1163	7.02	C9H17NO4
Lanthionine	Lanthionine	208.0523	33.00	C6H12N2O4S
HMDB0004823	Lanthionine ketimine	189.0101	30.82	C6H7NO4S
HMDB0000624	Leucic acid	132.0792	7.51	C6H12O3
HMDB0000176	Maleic acid	116.0110	12.43	C4H4O4
HMDB0000744	Malic acid	134.0215	11.14	C4H6O5
HMDB0002928	Malitol	344.1319	3.08	C12H24O11
HMDB0006112	Malondialdehyde	72.0211	8.86	C3H4O2
HMDB0000691	Malonic acid	104.0110	12.01	C3H4O4
HMDB0060486	Manelonitrile	133.0528	29.49	C8H7NO
HMDB0000765	Mannitol	182.0790	2.76	C6H14O6
HMDB0000169	Mannose	180.0634	3.14	C6H12O6
HMDB0001078	Mannose 6-phosphate	260.0297	12.73	C6H13O9P
HMDB0001892	Menadione	172.0530	11.43	C11H8O2
HMDB0000749	Mesaconic acid	130.0266	12.51	C5H6O4
HMDB0029965	Methyl beta-D-glucopyranoside	194.0790	2.74	C7H14O6
HMDB0001167	Methyl glyoxal	72.0217	4.89	C3H4O2
HMDB0032617	Methyl phenylacetate	150.0686	14.11	C9H10O2
NA	Methyl-3-hydroxybenzoic acid	152.0479	28.57	C8H8O3
HMDB0004815	Methyl-4-hydroxybenzoic acid	152.0479	32.63	C8H8O3
HMDB0000752	Methylglutaric acid	146.0579	10.73	C6H10O4
HMDB0006471	Methylisocitric acid	206.0427	15.82	C7H10O7
HMDB0032572	Methylparaben	152.0473	17.77	C8H8O3
HMDB0000227	Mevalonic acid	148.0736	15.14	C6H12O4

HMDB0001343	Mevalonic acid-5P	228.0399	14.84	C6H13O7P
Mildronate	Mildronate	146.1050	1.20	C6H4N2O2
HMDB0000211	Myoinositol	180.0634	2.81	C6H12O6
HMDB0003502	Myo-inositol hexakisphosphate	659.8619	24.31	C6H18O24P6
HMDB0039002	Mytilin A	332.1225	3.67	C13H20N2O8
HMDB0033442	Mytilin B	346.1382	3.50	C14H22N2O8
HMDB0033816	Mytilitol	194.0796	2.58	C7H14O6
NA	N-Acetyl cytosine	153.0544	8.13	C6H7N3O2
HMDB0003357	N-Acetyl ornithine	174.1004	8.73	C7H14N2O3
HMDB0094701	N-Acetyl proline	157.0744	4.42	C7H11NO3
HMDB0000812	N-Acetyl-aspartate	175.0481	10.03	C6H9NO5
HMDB0001067	N-Acetylaspartylglutamic acid	304.0907	14.40	C11H16N2O8
HMDB0000215	N-Acetyl-D-glucosamine	221.0899	3.02	C8H15NO6
HMDB0001062	N-Acetyl-D-Glucosamine 6-Phosphate	301.0563	12.41	C8H16NO9P
HMDB0001121	N-Acetyl-D-mannosamine 6-phosphate	301.0563	12.11	C8H16NO9P
HMDB0001367	N-acetyl-glucosamine-1-phosphate	301.0563	11.66	C8H16NO9P
HMDB0001138	N-Acetylglutamate	189.0643	9.84	C7H11NO5
HMDB0000766	N-Acetyl-L-alanine	131.0582	4.23	C5H9NO3
HMDB0006488	N-Acetyl-L-glutamate 5-semialdehyde	173.0688	13.97	C7H11NO4
HMDB0011745	N-Acetyl-L-methionine	191.0616	5.91	C7H13NO3S
HMDB0000512	N-Acetyl-L-phenylalanine	207.0895	8.89	C11H13NO3
HMDB0001129	N-Acetylmannosamine	221.0899	5.39	C8H15NO6
HMDB0006268	N-Acetylneuraminate 9-phosphate	389.0723	13.98	C11H20NO12P
HMDB0000230	N-Acetylneuraminic acid	309.1060	4.83	C11H19NO9
HMDB0013713	N-Acetyltryptophan	246.1004	18.41	C13H14N2O3
HMDB0011757	N-Acetylvaline	159.0895	4.83	C7H13NO3
HMDB0000902	NAD+	664.1169	9.94	C21H28N7O14P2
HMDB0001487	NADH	665.1248	17.00	C21H29N7O14P2
HMDB0000217	NADP+	744.0833	16.43	C21H29N7O17P3
HMDB0000221	NADPH	745.0911	21.37	C21H30N7O17P3
HMDB0000828	N-carbamoyl-L-aspartic acid	176.0433	10.86	C5H8N2O5
HMDB0013287	Ne,Ne dimethyllysine	174.1368	3.79	C8H18N2O2
NA	N-Formyl-DL-ethionine	191.0622	7.53	C7H13NO3S
HMDB0001200	N-Formylkynurenine	236.0803	22.44	C11H12N2O4
HMDB0001015	N-Formyl-methionine	177.0460	6.73	C6H11NO3S
HMDB0001406	Nicotinamide	122.0480	24.05	C6H6N2O
NA	Nicotinic Acid N-Oxide	139.0269	5.94	C6H5NO3
HMDB0002393	N-Methyl-D-aspartic acid	147.0532	10.06	C5H9NO4
HMDB0011717	Nonate	188.1054	13.85	C9H16O4
HMDB0013716	Norvaline	117.0795	33.46	C5H11NO2
NA	N-Oxalylglycine	147.0168	12.59	C4H5NO5
HMDB0003011	O-Acetylserine	147.0532	4.36	C5H9NO4
HMDB0000482	Octanoic acid	144.1150	19.95	C8H16O2
HMDB0001721	O-Phosphoserine	185.0089	14.86	C3H8NO6P
HMDB0005765	Ophthalmic Acid	289.1279	8.51	C11H19N3O6
HMDB0000226	Orotic acid	156.0171	16.58	C5H4N2O4
HMDB0000788	Orotidine	288.0588	16.11	C10H12N2O8
HMDB0000218	Orotidylic acid	368.0262	9.67	C10H13N2O11P
HMDB0000223	Oxalacetic acid	132.0059	10.30	C4H4O5
HMDB0002329	Oxalic acid	89.9953	13.40	C2H2O4
HMDB0062802	Oxalylyurea	114.0060	8.17	C3H2N2O3
HMDB0000225	Oxoadipic acid	160.0372	13.08	C6H8O5
HMDB0001865	Oxovaleric Acid	116.0479	7.56	C5H8O3
HMDB0014733	Oxytetracylcine	460.1482	29.58	C22H24N2O9
HMDB0000210	Pantothenic acid	219.1107	5.00	C9H17NO5
HMDB0002035	p-Coumaric acid	164.0473	29.16	C9H8O3
HMDB0015050	Phenformin	241.1100	14.07	C10H16ClN5
HMDB0040733	Phenylacetic Acid	136.0530	13.28	C8H8O2
HMDB0000821	Phenylacetylglycine	193.0744	9.23	C10H11NO3

HMDB0000205	Phenylpyruvic acid	164.0473	30.55	C9H8O3
HMDB0001511	Phosphocreatine	211.0364	8.56	C4H10N3O5P
HMDB0000263	Phosphoenolpyruvic acid	167.9824	17.96	C3H5O6P
HMDB0000816	Phosphoglycolic acid	155.9824	16.32	C2H5O6P
HMDB0000280	Phosphoribosyl pyrophosphate	389.9518	22.27	C5H13O14P3
HMDB0000020	p-Hydroxyphenylacetic acid	152.0479	16.97	C8H8O3
HMDB0000774	Pregnenolone sulfate	396.1976	21.87	C21H32O5S
HMDB0012283	Prephenic Acid	226.0477	11.47	C10H10O6
HMDB0015169	Procainamide	235.1685	21.97	C13H21N3O
HMDB0000237	Propionic acid	74.0373	5.69	C3H6O2
HMDB0001275	Propionyl-CoA	823.1420	10.52	C24H40N7O17P3S
HMDB0000783	Propionyl-glycine	131.0582	4.27	$C_5H_9NO_3$
HMDB0001856	Protocatechuic acid	154.0266	25.29	C7H6O4
HMDB0001491	Pyridoxal 5'-phosphate	247.0246	21.74	C8H10NO6P
HMDB0001431	Pyridoxamine	168.0899	6.71	C8H12N2O2
HMDB0000267	Pyroglutamic acid	129.0431	4.49	C5H7NO3
HMDB0000243	Pyruvic acid	88.0160	6.80	C3H4O3
HMDB0005794	Quercetin	302.0421	28.65	C15H10O7
HMDB0003072	Quinic acid	192.0634	4.74	C7H12O6
HMDB0000232	Quinolinic acid	167.0219	13.74	C7H5NO4
NA	Quisqualic acid	189.0391	14.33	C5H7N3O5
HMDB0003213	Raffinose	504.1690	2.80	C18H32O16
HMDB0001852	Retinoic acid	300.2095	8.39	C20H28O2
HMDB0000244	Riboflavin	376.1383	24.51	C17H20N4O6
HMDB0000283	Ribose	150.0528	3.17	C5H10O5
HMDB0001548	Ribose 5-phosphate	230.0192	13.19	C5H11O8P
HMDB0000621	Ribulose	150.0528	3.51	C5H10O5
NA	Ribulose 1,5,diphosphate	309.9860	19.79	C5H12O11P2
HMDB0000618	Ribulose 5-phosphate	230.0192	9.67	C5H11O8P
HMDB0000663	Saccharic acid	210.0376	12.05	C6H10O8
HMDB0000279	Saccharopine	276.1321	13.56	C11H20N2O6
HMDB0001185	S-adenosyl methionine	399.1451	8.71	C15H23N6O5S
HMDB0001895	Salicylic acid	138.0322	32.17	C7H6O3
HMDB0006088	Scyllitol	180.0634	2.67	C6H12O6
HMDB0000792	Sebacic acid	202.1205	18.30	C10H18O4
HMDB0060274	Sedoheptulose 1,7-bisphosphate	370.0066	19.08	C7H16O13P2
HMDB0060509	Sedoheptulose 1-phosphate	290.0403	10.74	C7H15O10P
HMDB0001068	Sedoheptulose 7-phosphate	290.0403	13.21	C7H15O10P
HMDB0000187	Serine	105.0426	14.89	C3H7NO3
HMDB0003070	Shikimic acid	174.0528	5.13	C7H10O5
HMDB0032616	Sinapic acid	224.0685	25.12	C11H12O5
HMDB0000247	Sorbitol	182.0790	2.77	C6H14O6
HMDB0005831	Sorbitol-6-phosphate	262.0454	9.23	C6H15O9P
HMDB0001266	Sorbose	180.0634	3.06	C6H12O6
HMDB0006797	Sorbose 1-phosphate	260.0292	11.96	C6H13O9P
HMDB0000254	Succinic acid	118.0266	11.11	C4H6O4
HMDB0001259	Succinic acid semialdehyde	102.0317	12.69	C4H6O3
NA	Succinyl-Homoserine	219.0740	9.41	C8H13NO6
HMDB0002085	Syringic acid	198.0528	17.50	C9H10O5
Compound ID	Description	NM	RT (min)	Formula
HMDB0029416	Targinine	188.1279	33.55	C7H16N4O2
HMDB0000251	Taurine	125.0147	5.14	C2H7NO3S
HMDB0000234	Testosterone	288.2095	27.34	C19H28O2
HMDB0003193	Testosterone glucuronide	464.2405	8.06	C25H36O8
HMDB0002833	Testosterone sulfate	368.1663	18.09	C19H28O5S
HMDB0014897	Tetracycline	444.1527	20.98	C22H24N2O8
HMDB0002825	Theobromine	180.0642	17.74	C7H8N4O2
HMDB0029178	Thialysine	164.0625	33.42	C5H12N2O2S
HMDB0001372	Thiamine pyrophosphate	425.0450	25.64	C12H19N4O7P2S

HMDB0004136	Threitol	122.0579	2.78	C4H10O4
HMDB0001227	Thymidine 5'-phosphate	322.0566	16.77	C10H15N2O8P
HMDB0001274	Thymidine diphosphate	402.0229	21.72	C10H16N2O11P2
HMDB0001342	Thymidine triphosphate	481.9893	25.42	C10H17N2O14P3
HMDB0000262	Thymine	126.0429	9.90	C5H6N2O2
HMDB0015256	Tolbutamide	270.1044	15.08	C12H18N2O3S
HMDB0062562	Trans-urocanate	137.0357	18.19	C6H5N2O2
HMDB0004284	Tyrosol	138.0681	17.77	C8H10O2
HMDB0000302	UDP-galactose	566.0550	18.00	C15H24N2O17P2
HMDB0000935	UDP-glucoronate	580.0343	24.31	C15H22N2O18P2
HMDB0000286	UDP-glucose	566.0550	18.40	C15H24N2O17P2
HMDB0000300	Uracil	112.0273	8.92	C4H4N2O2
HMDB0000026	Ureidopropionic acid	132.0540	4.46	C4H8N2O3
HMDB0000289	Uric acid	168.0283	19.45	C5H4N4O3
HMDB0000296	Uridine	244.0695	9.04	C9H12N2O6
HMDB0000295	Uridine 5'-diphosphate	404.0022	23.85	C9H14N2O12P2
HMDB0000288	Uridine 5'-monophosphate	324.0359	18.60	C9H13N2O9P
HMDB0000290	Uridine diphosphate-N-acetylglucosamine	607.0816	17.77	C17H27N3O17P2
HMDB0000285	Uridine triphosphate	483.9685	27.32	C9H15N2O15P3
HMDB0000892	Valeric Acid	102.0686	9.65	C5H10O2
HMDB0001554	Xanthylic acid	364.0426	20.70	C10H13N4O9P
HMDB0002917	Xylitol	152.0685	2.79	C5H12O5
HMDB0001644	Xylulose	150.0528	3.64	C5H10O5
HMDB0000868	Xylulose 5-phosphate	230.0192	13.16	C5H11O8P
HMDB0015464	Yohimbine	354.1949	26.07	C21H26N2O3

Table A.I.2. Data base of metabolites measured by derivatised RPLC-MS. Abbreviations: NM = neutral mass, RT = retention time and UD = underivatised.

Compound ID	Description	NM	RT (min)	Formula	UD formula	UD mass
HMDB0002166	(S)-b-aminoisobutyric acid	273.1108	5.46	C14H15N3O3	C4H9NO2	103.0628
HMDB0002166	(S)-b-aminoisobutyric acid	273.1108	5.53	C14H15N3O3	C4H9NO2	103.0628
HMDB0000002	1,3-Diaminopropane	244.1319	1.61	C13H16N4O	C3H10N2	74.0838
HMDB0000002	1,3-Diaminopropane	414.1793	6.31	C23H22N6O2	C3H10N2	74.0838
HMDB0029737	1H-Indole-3-carboxaldehyde	315.1002	6.79	C19H13N3O2	C9H7NO	145.0522
HMDB0000001	1-Methylhistidine	339.1326	2.80	C17H17N5O3	C7H11N3O2	169.0846
HMDB0000699	1-Methylnicotinamide	307.1190	8.41	C17H15N4O2	C7H9N2O	137.0709
HMDB0002362	2,4-Diaminobutyric acid (2xD)	458.1692	5.78	C24H22N6O4	C4H10N2O2	118.0737
HMDB0000510	2-Aminoadipic acid	331.1163	5.24	C16H17N3O5	C6H11NO4	161.0683
HMDB0061680	2-Aminonicotinic acid	308.0904	5.37	C16H12N4O3	C6H6N2O2	138.0424
NA	2-Methyl-1-pyrroline	253.1210	8.17	C15H15N3O	C5H9N	83.0730
HMDB0002039	2-Pyrrolidinone	255.1002	5.40	C14H13N3O2	C4H7NO	85.0522
NA	2-Pyrrolidinone, 1-(hydroxymethyl)-	285.1108	8.52	C15H15N3O3	C5H9NO2	115.0628
NA	3,4-Dehydro-L-proline	283.0951	5.35	C15H13N3O3	C5H7NO2	113.0471
HMDB0031654	3-Aminobutanoic acid	273.1108	6.22	C14H15N3O3	C4H9NO2	103.0628
HMDB0001476	3-Hydroxyanthranilic acid	323.0901	7.05	C17H13N3O4	C7H7NO3	153.0420
HMDB0006524	3-Indoleacetonitrile	326.1162	8.41	C20H14N4O	C10H8N2	156.0682
HMDB0002096	3-Indolebutyric acid	373.1421	6.88	C22H19N3O3	C12H13NO2	203.0941
HMDB0060374	3-Methoxyanthranilate	337.1057	6.75	C18H15N3O4	C8H9NO3	167.0577
HMDB0001904	3-Nitrotyrosine	396.1064	7.67	C19H16N4O6	C9H10N2O5	226.0584
HMDB0061877	4-Amino-3-hydroxybutyrate	289.1057	3.83	C14H15N3O4	C4H9NO3	119.0577
HMDB0001392	4-Aminobenzoic acid	307.0951	7.07	C17H13N3O3	C7H7NO2	137.0471
NA	4-amino-crotonic acid	271.0951	4.69	C14H13N3O3	C4H7NO2	101.0471
NA	4-Guanidinobutyric acid	315.1326	6.46	C15H17N5O3	C5H11N3O2	145.0846
HMDB0000725	4-Hydroxyproline	301.1057		C15H15N3O4	C5H9NO3	131.0577
NA	4-Methylthioamphetamine	351.1400	8.27	C20H21N3OS	C10H15NS	181.0920
NA	5-Aminopyridine-2-carboxylic acid	308.0904	5.12	C16H12N4O3	C6H6N2O2	138.0424
NA	5'-Deoxy-5'-methylthioadenosine	467.1370	7.58	C21H21N7O4S	C11H15N5O3S	297.0890
HMDB0000763	5-Hydroxyindoleacetic acid	361.1057	7.43	C20H15N3O4	C10H9NO3	191.0577
HMDB0000450	5-Hydroxylysine	332.1479	5.78	C16H20N4O4	C6H14N2O3	162.0999
HMDB0004096	5-Methoxyindoleacetate	375.1214	8.59	C21H17N3O4	C11H11NO3	205.0733
HMDB0001890	Acetylcysteine	333.0778	8.57	C15H15N3O4S	C5H9NO3S	163.0298
HMDB0000050	Adenosine	437.1442	6.37	C20H19N7O5	C10H13N5O4	267.0962
HMDB0000045	Adenosine monophosphate	517.1105	0.44	C20H20N7O8P	C10H14N5O7P	347.0625
HMDB0000538	Adenosine triphosphate	677.0432	0.43	C20H22N7O14P3	C10H16N5O13P3	506.9952
HMDB0000058	Adenosine3,5-cyclic monophosphate	499.1000	5.10	C20H18N7O7P	C10H12N5O6P	329.0520
HMDB0000068	Adrenaline	353.1370	5.88	C19H19N3O4	C9H13NO3	183.0890
HMDB0001432	Agmatine	300.1693	4.32	C15H20N6O	C5H14N4	130.1213
HMDB0000161	Alanine	259.0951	4.86	C13H13N3O3	C3H7NO2	89.0471
HMDB0000462	Allantoin	328.0915	2.90	C14H12N6O4	C4H6N4O3	158.0434
NA	Amino methoxybenzoic acid	337.1057	6.79	C18H15N3O4	C8H9NO3	167.0577
HMDB0000112	Aminobutyric acid-GABA	273.1108	5.97	C14H15N3O3	C4H9NO2	103.0628
HMDB0000517	Arginine	344.1591	3.10	C16H20N6O3	C6H14N4O2	174.1111
HMDB0000052	Argininosuccinic acid	460.1701	3.50	C20H24N6O7	C10H18N4O6	290.1221
HMDB0000168	Asparagine	302.1010	2.32	C14H14N4O4	C4H8N2O3	132.0529
HMDB0000191	Aspartic acid	303.0850	7.19	C14H13N3O5	C4H7NO4	133.0370
HMDB0000056	beta-Alanine	259.0951	4.26	C13H13N3O3	C3H7NO2	89.0471
HMDB0000043	Betaine	288.1343	1.26	C15H18N3O3	C5H12NO2	118.0863
HMDB0002322	Cadaverine	272.1632	7.70	C15H20N4O	C5H14N2	102.1152
HMDB0002706	Canavanine	346.1384	6.23	C15H18N6O4	C5H12N4O3	176.0904
HMDB0002706	Canavanine (2xD)	516.1859	6.23	C25H24N8O5	C5H12N4O3	176.0904
HMDB0000062	Carnitine	331.1527	1.98	C17H21N3O4	C7H15NO3	161.1046

HMDB0000033	Carnosine	396.1541	3.10	C19H20N6O4	C9H14N4O3	226.1060
HMDB0000904	Citrulline	345.1432	4.08	C16H19N5O4	C6H13N3O3	175.0951
HMDB0000064	Creatine	301.1169	4.60	C14H15N5O3	C4H9N3O2	131.0689
HMDB0000562	Creatinine	283.1064	5.40	C14H13N5O2	C4H7N3O	113.0584
HMDB0014405	Cycloserine	272.0904	4.01	C13H12N4O3	C3H6N2O2	102.0424
HMDB0002991	Cysteamine	247.0774	7.56	C12H13N3OS	C2H7NS	77.0294
HMDB0000574	Cysteine	291.0672	6.46	C13H13N3O3S	C3H7NO2S	121.0192
HMDB0000192	Cystine	410.0713	6.07	C16H18N4O5S2	C6H12N2O4S2	240.0233
HMDB0000089	Cytidine	413.1330	5.95	C19H19N5O6	C9H13N3O5	243.0850
HMDB0000095	Cytidine monophosphate	493.0993	5.45	C19H20N5O9P	C9H14N3O8P	323.0513
HMDB0000630	Cytosine	281.0907	6.05	C14H11N5O2	C4H5N3O	111.0427
HMDB0001370	Diaminopimelic acid	360.1428	8.58	C17H20N4O5	C7H14N2O4	190.0948
HMDB0000181	Dihydroxyphenylalanine	367.1163	6.13	C19H17N3O5	C9H11NO4	197.0683
NA	Dimethyl L-glutamate	345.1319	7.02	C17H19N3O5	C7H13NO4	175.0839
HMDB0000991	DL-2-Aminooctanoic acid	329.1734	8.37	C18H23N3O3	C8H17NO2	159.1254
HMDB0000149	Ethanolamine	231.1002	3.37	C12H13N3O2	C2H7NO	61.0522
HMDB0001514	Glucosamine	349.1268	8.14	C16H19N3O6	C6H13NO5	179.0788
HMDB0000148	Glutamic acid	317.1006	4.05	C15H15N3O5	C5H9NO4	147.0526
HMDB0000641	Glutamine	316.1166	3.10	C15H16N4O4	C5H10N2O3	146.0686
HMDB0000125	Glutathione	477.1313	6.06	C20H23N5O7S	C10H17N3O6S	307.0833
HMDB0000123	Glycine	245.0795	3.19	C12H11N3O3	C2H5NO2	75.0315
HMDB0001842	Guanidine	229.0958	3.05	C11H11N5O	CH5N3	59.0478
HMDB0000128	Guanidineacetic acid	287.1013	2.79	C13H13N5O3	C3H7N3O2	117.0533
HMDB0000132	Guanine	321.0969	5.90	C15H11N7O2	C5H5N5O	151.0489
HMDB0000133	Guanosine	453.1391	6.21	C20H19N7O6	C10H13N5O5	283.0911
HMDB0000714	Hippuric acid	349.1057	7.35	C19H15N3O4	C9H9NO3	179.0577
HMDB0000870	Histamine	281.1271	3.08	C15H15N5O	C5H9N3	111.0791
HMDB0000177	Histidine	495.1644	1.93	C16H15N5O3	C6H9N3O2	155.0689
HMDB0000670	Homo-L-arginine (2xD)	358.1748	6.44	C27H28N8O4	C7H16N4O2	188.1268
HMDB0000719	Homoserine	289.1057	3.31	C14H15N3O4	C4H9NO3	119.0577
HMDB0000732	Hydroxykynurenine	394.1272	6.91	C20H18N4O5	C10H12N2O4	224.0792
HMDB0000965	Hypotaurine	279.0672	2.89	C12H13N3O3S	C2H7NO2S	109.0192
HMDB0000157	Hypoxanthine	306.0860	5.85	C15H10N6O2	C5H4N4O	136.0380
HMDB0005785	Indole-3-carbinol	317.1159	6.41	C19H15N3O2	C9H9NO	147.0679
HMDB0002302	Indole-3-propionic acid	359.1264	7.25	C21H17N3O3	C11H11NO2	189.0784
HMDB0001190	Indoleacetaldehyde	329.1159	4.77	C20H15N3O2	C10H9NO	159.0679
HMDB0000671	Indolelactate	375.1214	6.86	C21H17N3O4	C11H11NO3	205.0733
HMDB0034198	Isobutylamine	243.1366	7.48	C14H17N3O	C4H11N	73.0886
Isobutylamine	Isobutylamine	243.1366	7.53	C14H17N3O	C4H11N	73.0886
HMDB0000172	Isoleucine	301.1421	7.68	C16H19N3O3	C6H13NO2	131.0941
HMDB0000715	Kynurenic acid	359.0901	8.41	C20H13N3O4	C10H7NO3	189.0420
HMDB0000684	Kynurenine	378.1323	7.65	C20H18N4O4	C10H12N2O3	208.0842
HMDB0000557	L-Alloisoleucine	301.1421	7.78	C16H19N3O3	C6H13NO2	131.0941
HMDB0000099	L-Cystathionine	392.1149	6.13	C17H20N4O5S	C7H14N2O4S	222.0669
HMDB0000687	Leucine	301.1421	7.78	C16H19N3O3	C6H13NO2	131.0941
HMDB0034365	L-Theanine	344.1479	5.21	C17H20N4O4	C7H14N2O3	174.0999
HMDB0000182	Lysine	316.1530	6.55	C16H20N4O3	C6H14N2O2	146.1050
HMDB0060486	Mandelonitrile	303.1002	7.82	C18H13N3O2	C8H7NO	133.0522
HMDB0000696	Methionine	319.0985	4.05	C15H17N3O3S	C5H11NO2S	149.0505
HMDB0002005	Methionine sulfoxide	335.0934	3.65	C15H17N3O4S	C5H11NO3S	165.0454
NA	Methyl picolinate	307.0951	8.29	C17H13N3O3	C7H7NO2	137.0471
NA	Methyl serine	289.1057	1.98	C14H15N3O4	C4H9NO3	119.0577
HMDB0032609	Methyl-Anthranilic Acid	321.1108	6.92	C18H15N3O3	C8H9NO2	151.0628
HMDB0002038	Methyl-L-Lysine	330.1686	6.87	C17H22N4O3	C7H16N2O2	160.1206
NA	N-(Phosphonomethyl)glycine	339.0615	5.68	C13H14N3O6P	C3H8NO5P	169.0135
NA	N-Acetyl cytosine	323.1013	8.47	C16H13N5O3	C6H7N3O2	153.0533
NA	N-Acetyl-2-pyrrolidone	297.1108	8.52	C16H15N3O3	C6H9NO2	127.0628
HMDB0000812	N-Acetylaspartate	345.0955	8.31	C16H15N3O6	C6H9NO5	175.0475
HMDB0001138	N-Acetylglutamic acid	359.1112	8.39	C17H17N3O6	C7H11NO5	189.0632

HMDB0000766	N-Acetyl-L-alanine	301.1057	6.24	C15H15N3O4	C5H9NO3	131.0577
HMDB0011745	N-Acetyl-L-methionine	361.1091	8.39	C17H19N3O4S	C7H13NO3S	191.0611
HMDB0000512	N-Acetyl-L-phenylalanine	377.1370	6.34	C21H19N3O4	C11H13NO3	207.0890
NA	N-Acetylornithine	344.1479	5.03	C17H20N4O4	C7H14N2O3	174.0999
HMDB0003357	N-Acetyl-ornithine	344.1479	4.96	C17H20N4O4	C7H14N2O3	174.0999
HMDB0094701	N-Acetylproline	327.1214	6.40	C17H17N3O4	C7H11NO3	157.0733
HMDB0013713	N-acetyltryptophan	416.1479	8.72	C23H20N4O4	C13H14N2O3	246.0999
HMDB0011757	N-Acetylvaline	329.1370	4.76	C17H19N3O4	C7H13NO3	159.0890
HMDB0001488	Nicotinic acid	293.0795	0.59	C16H11N3O3	C6H5NO2	123.0315
NA	Nicotinic acid N-oxide	309.0744	8.59	C16H11N3O4	C6H5NO3	139.0264
NA	N-methyl ornithine	316.1530	8.47	C16H20N4O3	C6H14N2O2	146.1050
NA	N-Methyl-L-glutamic acid	331.1163	6.10	C16H17N3O5	C6H11NO4	161.0683
NA	nordihydroguaiaretic acid	472.1993	6.18	C28H28N2O5	C18H22O4	302.1513
NA	N-Oxalylglycine	317.0642	0.33	C14H11N3O6	C4H5NO5	147.0162
NA	N-Phenylanthranilic acid	383.1264	4.74	C23H17N3O3	C13H11NO2	213.0784
HMDB0003011	O-Acetylserine	317.1006	4.60	C15H15N3O5	C5H9NO4	147.0526
HMDB0000224	O-Phosphoethanolamine	311.0666	2.14	C12H14N3O5P	C2H8NO4P	141.0185
HMDB0005765	Ophthalmic acid	459.1748	5.16	C21H25N5O7	C11H19N3O6	289.1268
HMDB0000214	Ornithine	302.1373	6.06	C15H18N4O3	C5H12N2O2	132.0893
HMDB0000226	Orotic Acid	326.0646	8.58	C15H10N4O5	C5H4N2O4	156.0166
HMDB0003337	Oxidised Glutathione (2xD)	952.2469	6.09	C40H44N10O14S2	C20H32N6O12S2	612.1514
HMDB0000210	Pantothenic acid	389.1581	7.04	C19H23N3O6	C9H17NO5	219.1101
HMDB0000159	Phenylalanine	335.1264	7.88	C19H17N3O3	C9H11NO2	165.0784
HMDB0001511	Phosphocreatine	381.0833	0.42	C14H16N5O6P	C4H10N3O5P	211.0353
HMDB0000272	Phosphoserine	355.0564	1.19	C13H14N3O7P	C3H8NO6P	185.0084
HMDB0000070	Pipecolic acid	299.1264	6.85	C16H17N3O3	C6H11NO2	129.0784
HMDB0000162	Proline	285.1108	5.47	C15H15N3O3	C5H9NO2	115.0628
HMDB0006078	Putreanine	331.1765	6.86	C17H23N4O3	C7H17N2O2	161.1285
HMDB0001414	Putrescine	258.1475	1.74	C14H18N4O	C4H12N2	88.0995
HMDB0001414	Putrescine	258.1475	2.83	C14H18N4O	C4H12N2	88.0995
HMDB0001414	Putrescine (2xD)	428.1950	6.68	C24H24N6O2	C4H12N2	88.0995
HMDB0001491	Pyridoxal 5-phosphate	417.0720	8.26	C18H16N3O7P	C8H10NO6P	247.0240
HMDB0001431	Pyridoxamine	338.1373	5.50	C18H18N4O3	C8H12N2O2	168.0893
NA	Pyroglutamic Acid	299.0901	5.71	C15H13N3O4	C5H7NO3	129.0420
HMDB0000805	Pyrrolidonecarboxylic acid	299.0901	5.61	C15H13N3O4	C5H7NO3	129.0420
HMDB0000232	Quinolinic acid	337.0693	0.33	C17H11N3O5	C7H5NO4	167.0213
HMDB0000939	S-(5-Adenosyl)-L-homocysteine	554.1691	5.79	C24H26N8O6S	C14H20N6O5S	384.1210
HMDB0000279	Saccharopine	446.1796	6.91	C21H26N4O7	C11H20N2O6	276.1316
HMDB0001185	S-Adenosylmethionine	569.1925	6.07	C25H29N8O6S	C15H23N6O5S	399.1445
HMDB0000271	Sarcosine	259.0951	7.80	C13H13N3O3	C3H7NO2	89.0471
HMDB0003966	Selenomethionine	361.0489	7.15	C15H17N3O3Se	C5H11NO2Se	191.0009
HMDB0000187	Serine	275.0901	2.86	C13H13N3O4	C3H7NO3	105.0420
HMDB0000259	Serotonin	346.1424	7.01	C20H18N4O2	C10H12N2O	176.0944
HMDB0001256	Spermine	372.2632	6.47	C20H32N6O	C10H26N4	202.2152
HMDB0001256	Spermine	372.2632	7.56	C20H32N6O	C10H26N4	202.2152
HMDB0003334	Symmetric dimethylarginine	372.1904	4.52	C18H24N6O3	C8H18N4O2	202.1424
HMDB0001372	Thiamine pyrophosphate	595.0924	6.06	C22H25N6O8P2S	C12H19N4O7P2S	425.0444
HMDB0062164	Thioproline	303.0672	5.85	C14H13N3O3S	C4H7NO2S	133.0192
HMDB0000167	Threonine	289.1057	4.46	C14H15N3O4	C4H9NO3	119.0577
HMDB0000262	Thymine	296.0904	6.07	C15H12N4O3	C5H6N2O2	126.0424
HMDB0062562	Trans-urocanate	308.0904	0.43	C16H12N4O3	C6H6N2O2	138.0424
HMDB0000303	Tryptamine	330.1475	8.31	C20H18N4O	C10H12N2	160.0995
HMDB0000929	Tryptophan	374.1373	8.00	C21H18N4O3	C11H12N2O2	204.0893
HMDB0000306	Tyramine	307.1315	7.21	C18H17N3O2	C8H11NO	137.0835
HMDB0000158	Tyrosine	351.1214	6.65	C19H17N3O4	C9H11NO3	181.0733
HMDB0000300	Uracil	282.0747	8.58	C14H10N4O3	C4H4N2O2	112.0267

HMDB0000289	Uric acid	338.0758	4.89	C15H10N6O4	C5H4N4O3	168.0278
HMDB0000301	Urocanic acid	308.0904	0.43	C16H12N4O3	C6H6N2O2	138.0424
HMDB0000883	Valine	287.1264	6.93	C15H17N3O3	C5H11NO2	117.0784
HMDB0000292	Xanthine	322.0809	4.81	C15H10N6O3	C5H4N4O2	152.0329
HMDB0001554	Xanthylic acid	534.0895	6.52	C20H19N6O10P	C10H13N4O9P	364.0415

9.2. Appendix II

The experiment that the data in this appendix is based on was a metabolomics experiment of wtIDH1 and mutIDH1^{R132H} LN18 cells treated with four mutIDH1 inhibitors (AG-120, AG-881, BAY 1436032 and GSK864). The control samples from this experiment were presented in **chapter 3** (**sections 3.2-3.5**). The 2-HG, 2-OG and isocitrate measurements were used in **chapter 4** (**section 4.5**) and the full metabolomics data was used in **chapter 5**. This appendix includes a DNA concentration table (**Table A.II.1**), IC-MS identifications (**Table A.II.2**), derivatised RPLC-MS identifications (**Table A.II.3**), and data processing information (**Figure A.II.1** and **A.II.2**). The full output from the untargeted pathway analysis (**section 3.5**) is provided in **Table A.II.4**.

Table A.II.1. DNA concentration of wtIDH1 and mutIDH1R132H LN18 mutIDH1 inhibitor treated and control cells.

Sample name	DNA 1 (ng/µL)	DNA 2 (ng/µL)	DNA 3 (ng/µL)	Average (ng/µL)	Relative DNA concentration	µL solvent	µL sample
WT-AG120-01	73.4	67.17		70.285	1.078	5.8	74.2
WT-AG120-02	128.63	127.47		128.050	1.965	39.3	40.7
WT-AG120-03	121.72	114.28		118.000	1.810	35.8	44.2
WT-AG120-04	86.94	87.22		87.080	1.336	20.1	59.9
WT-AG120-05	89.9	95.06		92.480	1.419	23.6	56.4
WT-AG120-06	107.03	110.26		108.645	1.667	32.0	48.0
WT-AG120-07	72.6	78.01		75.305	1.155	10.8	69.2
WT-AG120-08	138.22	115.07	101.34	118.210	1.814	35.9	44.1
WT-AG120-09	100.36	112.89		106.625	1.636	31.1	48.9
WT-AG120-10	110.3	110.18		110.240	1.691	32.7	47.3
WT-AG881-01	95.1	114.42		104.760	1.607	30.2	49.8
WT-AG881-02	72.38	76.86		74.620	1.145	10.1	69.9
WT-AG881-03	105.82	103.6		104.710	1.606	30.2	49.8
WT-AG881-04	88.78	100.5	80.31	89.863	1.379	22.0	58.0
WT-AG881-05	113.92	129.52	116.2	119.880	1.839	36.5	43.5
WT-AG881-06	75	69.38		72.190	1.108	7.8	72.2
WT-AG881-07	62.24	76.14	57.16	65.180	1.000	0.0	80.0
WT-AG881-08	86.68	95.34		91.010	1.396	22.7	57.3
WT-AG881-09	88.56	83.78		86.170	1.322	19.5	60.5
WT-AG881-10	102.34	99.73		101.035	1.550	28.4	51.6
WT-BAY-01	96.38	93.82		95.100	1.459	25.2	54.8
WT-BAY-02	126.15	132.76		129.455	1.986	39.7	40.3
WT-BAY-03	123.92	126.2		125.060	1.919	38.3	41.7
WT-BAY-04	143.92	155.34		149.630	2.296	45.2	34.8
WT-BAY-05	200.59	205.95		203.270	3.119	54.3	25.7
WT-BAY-06	98.86	107.5		103.180	1.583	29.5	50.5
WT-BAY-07	175.8	164		169.900	2.607	49.3	30.7
WT-BAY-08	159.66	168.88		164.270	2.520	48.3	31.7
WT-BAY-09	128.82	121.17		124.995	1.918	38.3	41.7
WT-BAY-10	71.86	74.11		72.985	1.120	8.6	71.4
WT-Co1-01	180.83	180.48		180.655	2.772	51.1	28.9
WT-Co1-02	139.2	128.22		133.710	2.051	41.0	39.0
WT-Co1-03	118.66	111.83		115.245	1.768	34.8	45.2
WT-Co1-04	125.46	126.56		126.010	1.933	38.6	41.4
WT-Co1-05	131.62	143.92		137.770	2.114	42.2	37.8
WT-Co1-06	135.79	139.43		137.610	2.111	42.1	37.9
WT-Co1-07	84.95	86.08		85.515	1.312	19.0	61.0
WT-Co1-08	153.84	169.24	124.74	149.273	2.290	45.1	34.9
WT-Co1-09	161.4	169.8		165.600	2.541	48.5	31.5
WT-Co1-10	151.34	153.18		152.260	2.336	45.8	34.2
WT-Co2-01	137.23	132.08		134.655	2.066	41.3	38.7
WT-Co2-02	120.5	116.2		118.350	1.816	35.9	44.1
WT-Co2-03	95.96	100.12		98.040	1.504	26.8	53.2
WT-Co2-04	121.3	125.8		123.550	1.896	37.8	42.2
WT-Co2-05	91.93	140.77	118.36	117.020	1.795	35.4	44.6
WT-Co2-06	134.44	123.96		129.200	1.982	39.6	40.4
WT-Co2-07	136.9	124.31		130.605	2.004	40.1	39.9
WT-Co2-08	126.61	120.52		123.565	1.896	37.8	42.2
WT-Co2-09	110.06	109.82		109.940	1.687	32.6	47.4

Sample name	DNA 1 (ng/µL)	DNA 2 (ng/µL)	DNA 3 (ng/µL)	Average (ng/µL)	Relative DNA concentration	µL solvent	µL sample
WT-Co2-10	90.45	76.43		83.440	1.280	17.5	62.5
WT-GSK-01	114.72	139.13	126.04	126.630	1.943	38.8	41.2
WT-GSK-02	105.68	105.46		105.570	1.620	30.6	49.4
WT-GSK-03	82.92	82.66		82.790	1.270	17.0	63.0
WT-GSK-04	82.94	73.43		78.185	1.200	13.3	66.7
WT-GSK-05	106.81	107.44		107.125	1.644	31.3	48.7
WT-GSK-06	112.09	108.53		110.310	1.692	32.7	47.3
WT-GSK-07	119.38	117.99		118.685	1.821	36.1	43.9
WT-GSK-08	133.22	125.59		129.405	1.985	39.7	40.3
WT-GSK-09	88.98	91.02		90.000	1.381	22.1	57.9
WT-GSK-10	150.6	171.5	161.56	161.220	2.473	47.7	32.3
MUT-AG120-01	152.27	139.26	145.05	145.527	2.233	44.2	35.8
MUT-AG120-02	153.37	156.34		154.855	2.376	46.3	33.7
MUT-AG120-03	110.16	123.03	105.93	113.040	1.734	33.9	46.1
MUT-AG120-04	111.57	122.9		117.235	1.799	35.5	44.5
MUT-AG120-05	126.65	127.16		126.905	1.947	38.9	41.1
MUT-AG120-06	100.38	113.78		107.080	1.643	31.3	48.7
MUT-AG120-07	180.28	193.55		186.915	2.868	52.1	27.9
MUT-AG120-08	131.96	132.77	123.15	129.293	1.984	39.7	40.3
MUT-AG120-09	152.82	162.45		157.635	2.418	46.9	33.1
MUT-AG120-10	91.42	100.88		96.150	1.475	25.8	54.2
MUT-AG881-01	148.8	142.88		145.840	2.237	44.2	35.8
MUT-AG881-02	129.09	111.94	122.93	121.320	1.861	37.0	43.0
MUT-AG881-03	85.11	96.72		90.915	1.395	22.6	57.4
MUT-AG881-04	121.91	123.34		122.625	1.881	37.5	42.5
MUT-AG881-05	124.4	112.14		118.270	1.815	35.9	44.1
MUT-AG881-06	97.88	108.12		103.000	1.580	29.4	50.6
MUT-AG881-07	90.47	90.86		90.665	1.391	22.5	57.5
MUT-AG881-08	111.57	90.52		101.045	1.550	28.4	51.6
MUT-AG881-09	138.17	145.91		142.040	2.179	43.3	36.7
MUT-AG881-10	93.8	103.5		98.650	1.514	27.1	52.9
MUT-BAY-01	114.1	124.78		119.440	1.832	36.3	43.7
MUT-BAY-02	121.42	120.07		120.745	1.852	36.8	43.2
MUT-BAY-03	116.2	114.66		115.430	1.771	34.8	45.2
MUT-BAY-04	108.66	114.22		111.440	1.710	33.2	46.8
MUT-BAY-05	101.86	105.51		103.685	1.591	29.7	50.3
MUT-BAY-06	113.82	105.8		109.810	1.685	32.5	47.5
MUT-BAY-07	158.27	151.59		154.930	2.377	46.3	33.7
MUT-BAY-08	123.76	117.96		120.860	1.854	36.9	43.1
MUT-BAY-09	94.54	107.72	89.02	97.093	1.490	26.3	53.7
MUT-BAY-10	121.24	121.16		121.200	1.859	37.0	43.0
MUT-Co1-01	148.36	132.64		140.500	2.156	42.9	37.1
MUT-Co1-02	120.72	107.86	115.28	114.620	1.759	34.5	45.5
MUT-Co1-03	98.01	115.71		106.860	1.639	31.2	48.8
MUT-Co1-04	107.37	104.06		105.715	1.622	30.7	49.3
MUT-Co1-05	85.12	82.1		83.610	1.283	17.6	62.4
MUT-Co1-06	143.26	135.8		139.530	2.141	42.6	37.4
MUT-Co1-07	139.8	147.04		143.420	2.200	43.6	36.4
MUT-Co1-08	155.18	161.46		158.320	2.429	47.1	32.9
MUT-Co1-09	197.57	201.68		199.625	3.063	53.9	26.1

Sample name	DNA 1 (ng/µL)	DNA 2 (ng/µL)	DNA 3 (ng/µL)	Average (ng/µL)	Relative DNA concentration	µL solvent	µL sample
MUT-Co1-10	148.84	139.16		144.000	2.209	43.8	36.2
MUT-Co2-01	110.94	109.24		110.090	1.689	32.6	47.4
MUT-Co2-02	80.18	80.17		80.175	1.230	15.0	65.0
MUT-Co2-03	101.25	111.8		106.525	1.634	31.0	49.0
MUT-Co2-04	72.06	88.9	96.48	85.813	1.317	19.2	60.8
MUT-Co2-05	84.58	89.74		87.160	1.337	20.2	59.8
MUT-Co2-06	93.95	107.44		100.695	1.545	28.2	51.8
MUT-Co2-07	95.1	93.56		94.330	1.447	24.7	55.3
MUT-Co2-08	114.74	116.6		115.670	1.775	34.9	45.1
MUT-Co2-09	110.3	95.54	126.12	110.653	1.698	32.9	47.1
MUT-Co2-10	117.76	118.34		118.050	1.811	35.8	44.2
MUT-GSK-01	94.47	108		101.235	1.553	28.5	51.5
MUT-GSK-02	82.68	90.69		86.685	1.330	19.8	60.2
MUT-GSK-03	92.3	106.64	97.73	98.890	1.517	27.3	52.7
MUT-GSK-04	102.99	103.98		103.485	1.588	29.6	50.4
MUT-GSK-05	119.3	112.65		115.975	1.779	35.0	45.0
MUT-GSK-06	113.8	98.55		106.175	1.629	30.9	49.1
MUT-GSK-07	88.78	78.53		83.655	1.283	17.7	62.3
MUT-GSK-08	81.5	78.12		79.810	1.224	14.7	65.3
MUT-GSK-09	115.2	122.87		119.035	1.826	36.2	43.8
MUT-GSK-10	61.56	70.96		66.260	1.017	1.3	78.7

Table A.II.2. Annotated metabolites from the IC-MS data of mutIDH1 inhibitor treated and control wtIDH1 and mutIDH1^{R132H} LN18 cells. Includes the parameters used for determining whether it was a putative or confident identification. FS = fragmentation score, ME = mass error, ISS = isotope similarity score, RTE = retention time error, max. abun. = max abundance and min. CV% = minimum coefficient of variance, C = Confident and P = putative. When provided as a comment, the abbreviation indicates what brought the identification from confident to putative (RTE > 1.5 min, ME > 3 ppm, ISS < 90%).

Accepted identification	FS	ME (ppm)	ISS	RTE (min)	Max. Abun.	Min. CV%	C/ P	Comment
1-Pyrroline hydroxycarboxylic acid	0	-0.59	94.0	-0.46	801533	13.5	P	Isomer of pyroglutamic acid
2-Hydroxybutyric acid	41.8	-0.37	97.7	-0.74	7260	10.2	C	
2-Hydroxyglutarate	71.8	-0.72	99.7	-1.00	2589196	6.6	C	
2-Isopropylmalic acid	0	-1.78	93.5	-1.88	116	30.9	P	RTE
2-Oxoglutaric acid	46.4	-1.54	-	-1.30	80366	15.1	C	
2-Phosphoglyceric acid	74.3	0.10	97.8	-1.90	28501	45.6	P	RTE
3,3 Dimethyl glutarate	70.6	-1.31	95.2	-1.09	2147	7.6	C	
3,4-dihydroxy-phenyl acetic acid	0	-0.44	90.9	0.57	372	18.3	C	
3-Dehydroquinate	31.9	-1.35	97.2	-0.16	3720	14.2	C	
3-Hydroxymethyl-glutarate	74	-0.96	98.5	-1.04	21343	11.8	C	
3-Hydroxytyrosol	0	-0.13	93.4	-0.98	3932	3.5	C	
3-methoxyphenyl-acetic acid	0	-1.15	99.4	-1.03	178	34.5	C	
3-Methyl-2-oxovaleric acid	0	-0.73	99.8	-0.83	139291	21.4	C	
3-Phosphoglyceric acid	0	-0.85	97.1	0.54	3027	84.6	P	Isomer of 2-phosphglyceric acid
4-Hydroxy-3-methoxymandelic acid	0	0.02	94.9	-0.93	3486	8.5	C	
4-Hydroxybenzoic acid	0	-0.65	96.1	1.32	38777	6.1	C	
4-Hydroxyproline	89.7	-0.69	99.0	-0.44	14407	9.7	C	
5-Hydroxyhexanoic acid	0	-4.68	99.7	-0.04	6876	9.1	P	ME
5-Hydroxymethyl-2'-deoxyuridine	0	0.24	87.7	-0.32	228	40.7	P	ISS
6-Phosphogluconic acid	0	0.26	97.5	-1.67	70673	21.2	P	RTE
8-Hydroxy-deoxyguanosine	0	0.03	93.1	0.35	4658	59.7	C	
Acetylglycine	37.6	-0.38	98.4	-0.26	2738	10	C	
Adenine	0	-0.19	93.1	1.39	9408	16.2	C	
Adenosine diphosphate	16.4	0.27	97.9	-1.51	1905916	8.6	C	
Adenosine triphosphate	5.56	0.39	92.2	0.51	5126	17	C	

Accepted identification	FS	ME (ppm)	ISS	RTE (min)	Max.	Min.	C/P	Comment
Arabinonic acid	56.5	-1.66	94.6	-0.82	9921	12.4	C	
Arabinose	30	-1.75	95.1	-0.30	1844	17.3	P	Isomer of ribose/xylulose
Arabitol	63.4	-1.12	96.2	-0.01	10513	11.4	P	Isomer of adonotil/xylitol
Ascorbate	8.26	-1.56	99.2	-1.33	40293	10.4	C	
Beta-Alanine	52.9	-0.44	88.1	-0.92	1960	4.2	C	
Beta-Citryl-L-glutamic acid	0	-0.35	98.4	-0.68	654760	15.9	C	
Butyric acid	85.1	-1.00	97.7	-0.46	10122	3.7	C	
Caffeic acid	0	-3.15	90.5		2504	12.5	P	ME, no RT
Citric acid	0	-1.80	96.9	-1.57	8076	10.4	P	RT
Cytidine diphosphate	0	0.78	85.5	-1.11	1434	63.7	P	ISS
Cytidine monophosphate	0	0.23	92.0	-0.09	25836	17.3	C	
Cytidine monophosphate N-acetylneuraminic acid	0	0.09	96.7	-0.88	152883	12.3	C	
Cytidine triphosphate	6.63	-0.10	98.0	-1.74	433497	15.9	P	RTE
dADP	0	-0.05	92.0	-0.74	4193	16.9	C	
dCTP	78	-0.32	92.9	-1.04	6125	28.6	C	
Deoxyribose 5-phosphate	3.59	1.41	96.8	-0.13	4093	13.1	C	
Deoxyuridine	11.6	-1.95	88.9	-0.76	1475	22.5	P	ISS
dGTP	0	1.35	90.0	0.58	418	86.3	C	
Dihydroxyacetone	0	-2.18	98.6	-1.98	199696	5.3	P	RTE
Dimethyl fumarate	0	-0.50	96.4	-1.03	3108	7.6	C	
dTDP-D-glucose	0	0.03	96.6	-1.42	123018	17.4	C	
dUDP	0	0.25	93.0	0.81	5262	43.9	C	
dUMP	0	0.03	97.9	-1.62	129278	35.1	P	RTE
dUTP	0	-0.30	93.7	-1.61	11615	38.7	P	RTE
EDTA	0	-0.85	98.1	-1.99	2076624	23.7	P	RTE
Ferulic acid	0	-0.37	84.9	-0.45	296	25.1	P	ISS
Flavin Mononucleotide	0	-0.26	89.6		13495	12.1	P	No RT
Fructose 2,6 diphosphate	0	-0.37	99.2	-0.16	161016	34.4	C	
Fructose 6-phosphate	82.6	-0.85	95.8	-0.28	34805	21.8	P	Isomer of mannose 6-phosphate
Fumarate	0	-4.62	94.9	1.09	273	13.1	P	ME
Galacturonic acid	67.6	-1.39	97.6	-0.09	8170	14.9	P	Isomer of glucuronic acid
Gluconate	66	-1.22		-0.65	95978	12.5	C	
Gluconolactone	0	-0.81	92.4	0.13	333	18	C	
Glucosamine 6-phosphate	0	-1.21	90.1	1.40	242	30.7	C	
Glucose	0	-0.99	80.4	1.33	2158	12.9	P	Isomers

Accepted identification	FS	ME (ppm)	ISS	RTE (min)	Max.	Min.	C/P	Comment
Glucose 1-phosphate	51.6	-0.90	99.2	-0.89	383812	37.4	P	Isomer of galactose 1-phosphate
Glutaconic acid	0	-0.19	96.3	0.29	6350	8.1	P	Isomers
Glutamine	0	-0.58	94.6	0.96	3732	17.3	C	
Glutaric acid	0	-0.18	96.5	0.16	3432	7	P	Isomer of ethylmalonic acid
Glyceric acid	1.08	-1.00		0.69	143328	9.8	C	
Glycerol	54.9	-0.78	100.0	-0.10	1949346	4.5	C	
Glycerol 3-phosphate	71.2	-0.48		-0.88	20805	16.7	C	
Guanosine diphosphate	96.9	1.15	97.8	0.10	1747597	17.2	C	
Hippuric acid	67.3	-1.28	90.2	-1.31	15607	25.6	C	
Hydroxy-isobutyric acid	42	-0.20	99.2	-1.25	3540	11.8	C	
Hydroxy-isoheptanoic acid	0	-3.72	98.3	0.36	72	49.9	P	ME
Inosine	1.77	-4.75	93.3	-1.73	3934	40.5	P	RTE
Inositol 1,3,4-trisphosphate	0	0.73	98.0	-1.94	10713	94.2	P	RTE
Isocitrate	0	-1.75	96.6	-1.12	4994	14.9	P	Isomer of citric acid
Isopentenyl pyrophosphate	0	-1.44	93.1	-1.30	1882	20.7	P	Isomer of dimethylallyl pyrophosphate
Isovalerylglycine	49.1	-0.68	92.0	-0.38	256	37.5	C	
Kojic acid	92.2	-0.25	97.1	-0.63	6907	7.5	C	
Kynurenic acid	0	0.24	88.8	0.73	299	85.1	P	ISS
Lactic acid	28.2	-0.95	99.7	-0.78	3248049	13	P	Isomer of dihydroacetone
Lactose	84.7	-1.77	89.5	-0.23	499657	16.8	C	
Lactoyl-isoleucine	0	-3.63	96.5	-0.12	5240	15.7	C	
Maleic acid	65.1	-0.58	97.9	-0.30	45233	6.4	C	
Malic acid	82.8	-0.62	99.3	-1.00	376096	7.4	C	
Manelonitrile	0	-0.52	91.1	-0.35	2082	29.7	C	
Mannitol	0	-0.08	96.6	0.78	1325	34.8	P	Isomer of sorbitol
Mannose 6-phosphate	93.6	-0.92	91.6	-1.52	50415	20.3	P	Isomer of fructose 6-phosphate
Methionine sulfoxide	0	-0.57	88.9		968	46.1	P	ISS
Methyl beta-D-glucopyranoside	0	-1.16	97.5	-0.43	1557	81	C	
Methyl phenylacetate	0	-4.05	90.3	-1.84	285	18.5	P	RTE and ME
Methylisocitric acid	0	-0.23	96.9	-1.10	7956	6.4	P	Isomer of 2-methylcitric acid
Myoinositol	94.1	-1.02	97.6	-0.20	2042414	7.8	P	
N-Acetyl ornithine	0	-1.97	91.3	0.11	11238	58.8	C	
N-Acetyl-aspartate	97	-1.51	92.5	-0.79	265901	9.6	C	

Accepted identification	FS	ME (ppm)	ISS	RTE (min)	Max.	Min.	C/P	Comment
N-Acetylaspartyl-glutamic acid	0	-0.09	96.9	-1.23	91866	11.2	C	
N-acetyl-glucosamine-1-phosphate	0	0.02	95.7	-0.52	13651	24.2	C	
N-Acetylglutamate	0	-4.18	75.1	0.87	2907	18.4	P	ME
N-Acetyl-L-alanine	96.9	-0.91	97.6	-0.42	10596	10.7	C	
N-Acetyl-L-methionine	75.8	-0.30	94.2	-0.56	15290	15.9	C	
N-Acetyl-L-phenylalanine	37.7	-0.27	98.1	-0.71	172	20.9	C	
N-Acetylneuraminic acid	88.7	-0.33	94.7	-0.62	61869	9	C	
NADH	95.1	0.21	94.9	-0.91	166918	44.4	C	
NADPH	0	-0.51	91.0	0.76	1414	40.3	C	
N-carbamoyl-L-aspartic acid	0	-0.83	96.0	-1.09	4150	22.3	C	
N-Formyl-methionine	0	-1.38	94.7	-0.73	1608	15.9	C	
Nicotinic Acid N-Oxide	69.4	-0.53	93.0	-1.86	3393	10.4	P	RTE
Nonate	0	-3.63	95.0	-0.48	7757	12.5	P	
O-Acetylserine	0	-0.73	93.5	-0.55	90438	5.1	C	
O-Phosphoserine	72.7	-0.38	99.3	-1.18	73236	17.9	C	
Oxoadipic acid	51.5	-1.02	95.8	-1.65	3313	11.3	P	RTE
Pantothenic acid	62.6	-1.29	98.0	-0.73	589423	10.6	C	
Phenylacetylglycine	0	-3.72	96.7	0.54	1018	23.7	P	ME
Phosphocreatine	5.43	-2.72	97.2	-0.38	57977	59.8	C	
Phosphoribosyl pyrophosphate	0	0.30	96.6	-1.51	5868	76.2	C	
p-Hydroxyphenyl-acetic acid	0	-4.52	95.8	-1.74	8488	7.6	P	RTE
Prephenic Acid	0	0.51	88.4	0.66	2575	13	P	ISS
Pyridoxal 5'-phosphate	0	-1.42	90.0	-0.65	3856	16.4	C	
Quinolinic acid	0	-1.57	91.5	-1.61	560	20.7	P	RTE
Raffinose	0	-0.04	93.1	-0.14	3568	106.2	C	
Ribose 5-phosphate	62.6	1.57	96.7	-1.25	16692	14.9	P	Isomer of xylulose 5-phosphate
Ribulose 1,5,diphosphate	0	-1.46	98.7	-1.51	96318	9.4	C	
Ribulose 5-phosphate	31.3	1.08	96.4	-0.67	30274	16.2	C	
Scyllitol	0	-0.85	98.6	-0.01	146546	6.7	P	Isomer of *e.g.* myo-inositol
Sebacic acid	0	0.09	88.8	-1.87	315	23.5	P	RTE and ISS
Sedoheptulose 1,7-bisphosphate	0	-0.10	89.7	-1.25	1115	112.3	C	
Sedoheptulose 1-phosphate	0	0.77	95.5	-0.72	11748	18.1	C	

Accepted identification	FS	ME (ppm)	ISS	RTE (min)	Max.	Min.	C/P	Comment
Sedoheptulose 7-phosphate	66.3	0.81		-1.08	24674	32.3	C	
Sorbitol	70.7	-1.24	99.2	-0.11	228325	15.4	C	
Sorbitol-6-phosphate	0	-0.18	97.9	0.23	43652	32.4	C	
Succinic acid	91.2	-0.38	98.7	-1.01	103980	7.3	C	
Syringic acid	0	-0.47	97.6	0.93	2738	10.3	C	
Taurine	92.5	-0.89	93.2	-0.66	1534026	6.1	C	
TDP	92.4	-0.12	90.8	-1.31	11426	13.5	C	
Threitol	71	-0.55	98.0	-0.08	18187	9	C	
Thymidine 5'-phosphate	91.3	-0.23	97.3	-1.24	25036	29.9	C	
Thymidine triphosphate	6.1	-0.06	94.1	-1.51	20856	17.3	C	
UDP-galactose	0	-0.17	96.5	-1.13	72092	16.5	P	Isomer of UDP-glucose
Uracil	77.4	-0.81	94.8	-1.35	2063	10.5	C	
Ureidopropionic acid	0	-4.22	94.3	1.10	3570	12.1	P	
Uridine 5'-diphosphate	13.1	-0.31	98.7	0.91	4596118	18.7	C	
Uridine 5'-monophosphate	50.7	-0.13	98.6	-1.79	573322	30.8	P	
Xylitol	0	-0.37	99.7	-0.03	2471	10.2	P	Isomer of arabitol and adonitol

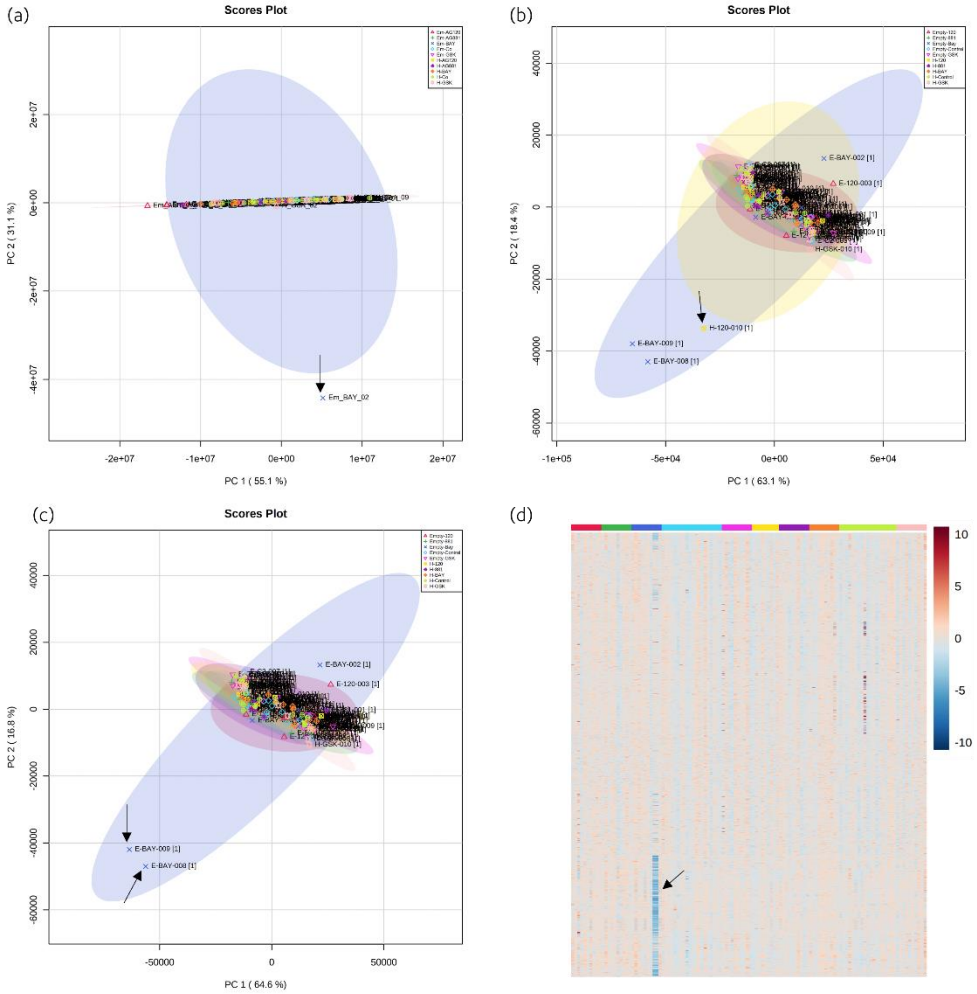

Figure A.II.1. PCA scores plots (PC1 × PC2) and heatmap used for identifications of outliers in IC-MS and derivatised RPLC-MS data from the experiment treating both wtIDH1 and mutIDH1^{R132H} LN18 cells with mutIDH1 inhibitors. Both datasets were IQR filtered, but not normalised, scaled or transformed, prior to plotting. (a) PCA scores plot (PC1 × PC2) of IC-MS data, black arrow indicating outlier that was removed (BAY 1436032 treated wtIDH1 LN18 cell sample). (b) PCA scores plot (PC1 × PC2) of derivatised RPLC-MS data, with black arrow indicating the first outlier that was removed (AG-120 treated mutIDH1^{R132H} LN18 cell sample). (c) PCA scores plot (PC1 × PC2) of derivatised RPLC-MS data, with black arrow indicating two additional outliers that were removed (BAY 1436032 treated wtIDH1 LN18 cell samples). (d) Heatmap of the same data in (c), with black arrow indicating the same two samples as indicated in (c). N = biological replicates and N = 10 for treated samples, unless an outlier was removed, N = 19 for wtIDH1 LN18 cell samples in (a), = 20 for wtIDH1 LN18 cell samples in (b-d) and N = 20 for mutIDH1^{R132H} LN18 cell samples in (a-d).

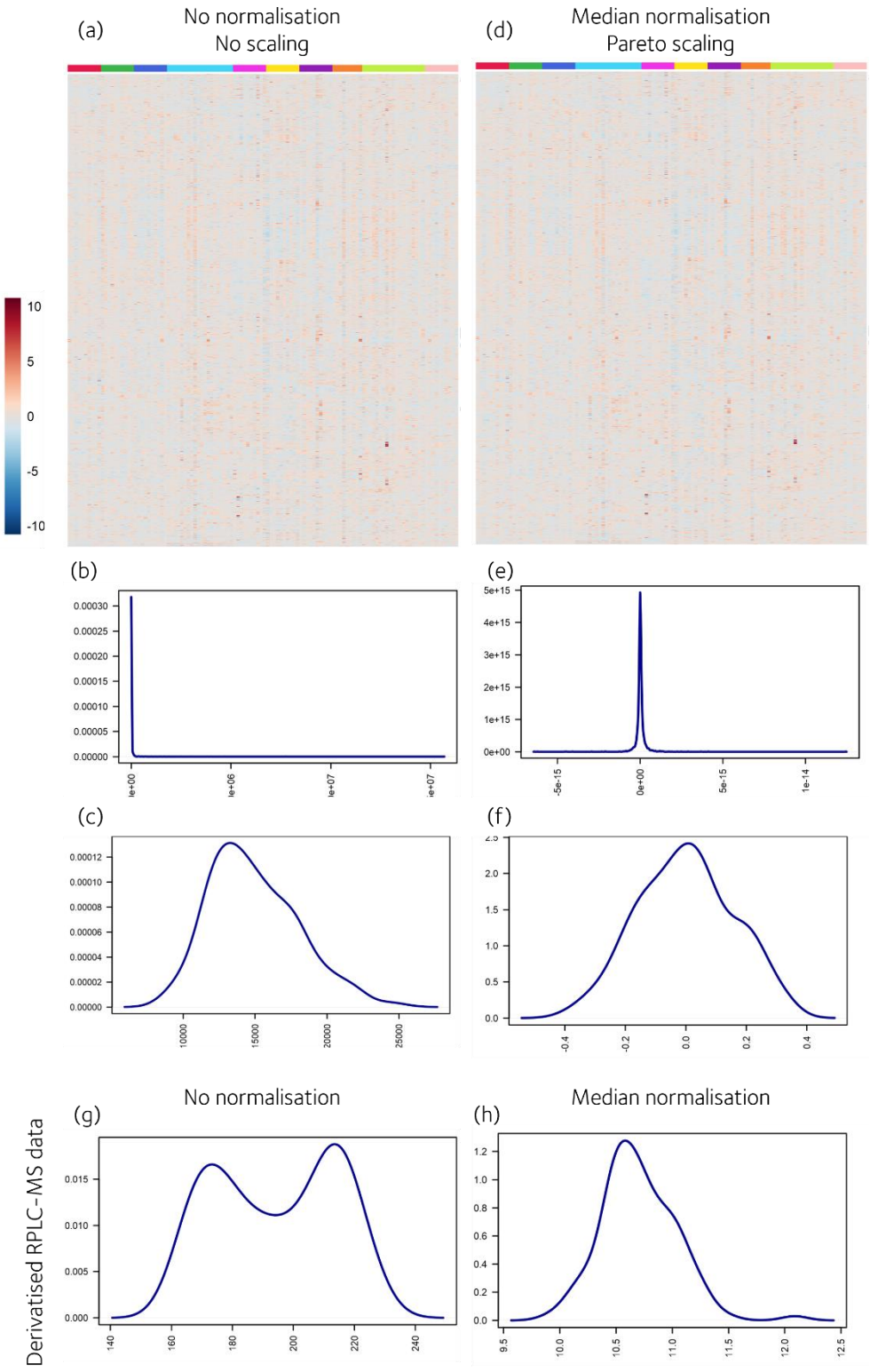

Figure A.II.2. Heatmaps, feature and sample distribution plots before and after normalisation of IC-MS data from the wtIDH1 and mutIDH1^{R132H} LN18 metabolomics experiment. (a) Heatmap, (b) feature distribution and (c) sample distribution plots of IC-MS data before normalisation and scaling. (d) Heatmap, (e) feature distribution and (f) sample distribution plots of IC-MS data after median normalisation and pareto-scaling. Derivatised RPLC-MS data distribution (g) before and (h) after normalisation.

Table A.II.3. Annotated metabolites from the derivatised RPLC-MS data of mutIDH1 inhibitor treated and control wtIDH1 and mutIDH1^{R132H} LN18 cells. with parameters used for determining whether it was a putative or confident identification. ME = mass error, ISS = isotope similarity score, RTE = retention time error, max. abun. = max abundance and min. CV% = minimum coefficient of variance, C = Confident and P = putative. When provided as a comment, the abbreviation indicates what brought the identification from confident to putative (RTE > 0.5 min, ME > 3 ppm, ISS < 90%).

Accepted Description	ME (ppm)	ISS	RTE (min)	Max. abun.	Min. CV%	C/P	Comment
1,3-Diaminopropane	1.88	96.3	0.07	6.426	23.3	C	
2-Aminoadipic acid	0.87	94.0	0.09	507	14.3	C	
4-Hydroxyproline	2.17	94.8		37	22.1	P	No RT
5-Hydroxylysine	0.91	96.1	0.13	0.67	34.2	C	
Alanine	0.75	96.0	0.13	14931	7.8	C	
GABA	0.20	96.4	0.02	39	10.9	C	
Arginine	-0.08	96.5	0.12	424	17.9	C	
Argininosuccinic acid	-0.80	92.9	0.11	1.73	17.8	C	
Asparagine	-0.73	95.7	0.01	165	11	C	
Aspartic acid	3.15	96.8	-0.90	2.52	29.8	P	RTE
beta-Alanine	2.22	97.1	0.13	1089	10.5	C	
Carnosine	-2.23	91.5	0.11	2.69	38.2	C	
Citrulline	-1.27	93.1	0.10	40	16.3	C	
Cysteine	-0.90	94.9	-0.94	336	19.3	P	RTE
Ethanolamine	-1.46	96.9	0.12	13	5.9	C	
Glutamic acid	0.82	95.9	0.13	10010	8.9	C	
Glutamine	0.35	96.1	0.07	3563	30	C	
Glycine	0.03	93.8	0.15	2597	10	C	
Histidine	-0.70	96.8	0.08	417	12.9	C	
Homocysteine	-1.38	91.7	-0.11	7.76	23.1	P	Not compared to standard yet
Homoserine	-0.38	95.6	0.18	10	24.2	C	
Hydroxy-L-tryptophan	0.54	92.7		7.32	20.1	P	Not compared to standard yet
Hypotaurine	1.47	93.4	0.23	181	10.6	C	
Hypoxanthine	-4.70	93.9	-0.27	7.84	13.5	P	ME
Isobutylamine	0.82	95.4	0.15	1.68	21.6	C	
Isoleucine	0.87	94.9	0.20	6638	12.5	P	Isomer of leucine
Kynurenine	-0.21	94.4	0.08	17	18.8	C	
L-Cystathionine	-0.93	85.6	0.08	8	11.6	P	IS
L-Cystine	1.31	91.8		3	39.6	P	No RT
Leucine	1.13	94.5	0.00	6037	13.6	P	Isomer of isoleucine
L-Theanine	1.11	94.6	0.33	0.27	43.4	P	Isomer of N-acetyl-ornithine
Lysine	0.25	93.7	0.09	3991	16.4	C	
Methionine	-4.84	88.3	-1.01	40	11.8	P	RTE and ME
Methyl-L-Lysine	-1.19	96.4	0.09	0.45	52.4	C	
N-Acetyl-ornithine	-0.70	96.0	0.12	22	9.3	P	Isomer of L-Theanine
N-Methyl-L-glutamic acid	-0.76	88.5	-0.29	0.48	73.9	P	IS
Octapine	2.15	95.9		6.46	25.3	P	No RT
Ornithine	-1.64	95.1	0.19	9.38	14.7	C	
Oxidised Glutathione	0.41	92.5	0.06	2760	14.7	C	
Phenylalanine	0.83	92.1	0.11	4565	12.7	C	
Pipecolic acid	-2.58	95.2	0.48	70	13	C	

Accepted Description	ME (ppm)	ISS	RTE (min)	Max. abun.	Min. CV%	C/P	Comment
Proline	-0.36	98.0	0.12	759	10.2	C	
Putrescine	1.44	96.3	0.03	151	21.2	C	
Pyroglutamic Acid	0.39	93.8	-0.97	18	29.7	P	RTE
S-(5-Adenosyl)-L-homocysteine	-1.38	91.7	0.10	4.37	34.2	C	
Serine	-0.36	96.3	0.16	1167	9.1	C	
Serotonin	-1.25	87.1	0.02	7.04	8.1	P	IS
Taurine	-0.55	95.1		1580	9.6	P	No RT
Threonine	0.88	97.4	0.11	5808	10.8	C	
Tryptophan	-0.25	95.1	0.09	640	12.8	C	
Tyrosine	0.43	95.1	0.10	2773	12.1	C	
Urea	-3.57	93.6	0.17	0.49	31.4	P	ME
Valine	0.98	95.9	0.10	5434	13.3	C	

Table A.II.4. All pathways found by the untargeted pathway analysis (functional analysis from the R package MetaboAnalystR). FET = Fisher's Exact Test, EASE = Expression Analysis Systematic Explorer. PW = pathway, tot = total, sig = significant, Exp = expected, EC = empirical compound, p-val = p-value, adj = adjusted, emp = empirical.

Pathway Name	PW tot	Hits	Hits sig.	Exp. #EC	FET p-val	EASE p-val	γ-adj p-val	Emp. hits	Emp. p-val	EC hits
Valine, leucine and isoleucine degradation	25	25	12	4.3	0.0002	0.0007	0.0051	0	0	EC00014, EC00091, EC00092, EC00093, EC000116, EC000117, EC00029, EC00030, EC000355, EC000170, EC000356, EC000591
Arginine and Proline Metabolism	33	33	14	5.6	0.0002	0.0008	0.0051	0	0	EC000129, EC00014, EC00011, EC00012, EC000448, EC000430, EC00059, EC000282, EC000414, EC000252, EC00029, EC00030, EC00036, EC000242
Butanoate metabolism	26	26	12	4.4	0.0002	0.0011	0.0051	0	0	EC00014, EC00011, EC00012, EC00091, EC00092, EC00093, EC000355, EC000356, EC000531, EC00029, EC00030, EC000336
Ascorbate (Vitamin C) and Aldarate Metabolism	47	47	17	8.0	0.0004	0.0013	0.0051	0	0	EC000177, EC000161, EC000163, EC000307, EC000311, EC000157, EC000488, EC00054, EC00058, EC000137, EC000138, EC000325, EC000243, EC000246, EC000247, EC000416, EC000418
Lysine metabolism	25	25	11	4.3	0.0008	0.003	0.0051	2	0.02	EC00014, EC000208, EC000211, EC000212, EC000213, EC000259, EC000260, EC000430, EC000242, EC00029, EC00030
Vitamin B1 (thiamine) metabolism	12	12	7	2.1	0.001	0.0062	0.0051	0	0	EC000208, EC000211, EC000212, EC000213, EC00011, EC00012, EC00014
Aspartate and asparagine metabolism	55	55	17	9.4	0.0035	0.0081	0.0051	2	0.02	EC00014, EC000129, EC000252, EC00091, EC00092, EC00093, EC000578, EC000450, EC000282, EC00036, EC000242, EC000472, EC000355, EC000356, EC000414, EC000365, EC000430
Glutamate metabolism	22	22	9	3.8	0.0045	0.0156	0.0051	1	0.01	EC00014, EC00011, EC00012, EC00029, EC00030, EC000448, EC00091, EC00092, EC00093
Urea cycle/amino group metabolism	37	37	12	6.3	0.0095	0.0239	0.0052	1	0.01	EC000129, EC000448, EC000430, EC000289, EC00059, EC000282, EC00014, EC000252, EC000395, EC00036, EC000242, EC000604
Propanoate metabolism	25	25	9	4.3	0.0119	0.0346	0.0053	4	0.04	EC00091, EC00092, EC00093, EC000307, EC000311, EC000355, EC000356, EC00011, EC00012

Pathway Name	PW tot	Hits	Hits sig.	Exp. #EC	FET p-val	EASE p-val	γ-adj p-val	Emp. hits	Emp. p-val	EC hits
Methionine and cysteine metabolism	30	30	9	5.1	0.0406	0.0929	0.0058	8	0.08	EC00014, EC00011, EC00012, EC00091, EC00092, EC00093, EC00059, EC00052, EC000429
Squalene and cholesterol biosynthesis	16	16	6	2.7	0.0323	0.0989	0.0056	3	0.03	EC000113, EC000249, EC000370, EC00091, EC00092, EC00093
D4&E4-neuroprostanes formation	12	12	5	2.1	0.0319	0.1121	0.0056	2	0.02	EC00054, EC00058, EC000243, EC000246, EC000247
Beta-Alanine metabolism	12	12	5	2.1	0.0319	0.1121	0.0056	4	0.04	EC00014, EC000282, EC00036, EC00011, EC00012
Fatty acid oxidation, peroxisome	4	4	3	0.7	0.0149	0.1241	0.0053	3	0.03	EC00014, EC00029, EC00030
TCA cycle	27	27	8	4.6	0.0565	0.1277	0.0061	3	0.03	EC00014, EC000137, EC000138, EC00029, EC00030, EC000243, EC000246, EC000247
Glycine, serine, alanine and threonine metabolism	49	49	12	8.4	0.0827	0.1471	0.0066	11	0.11	EC00014, EC00011, EC00012, EC000182, EC000358, EC00059, EC000252, EC00052, EC00091, EC00092, EC00093, EC000148
Phytanic acid peroxisomal oxidation	6	6	3	1.0	0.0579	0.2502	0.0061	8	0.08	EC00014, EC00029, EC00030
Pentose phosphate pathway	57	57	12	9.7	0.1998	0.3023	0.0097	27	0.27	EC000108, EC000412, EC000413, EC000177, EC000161, EC000163, EC00066, EC000544, EC000258, EC00016, EC000388, EC000302
Histidine metabolism	12	12	4	2.1	0.1155	0.3032	0.0074	11	0.11	EC00014, EC000256, EC00011, EC00012
Prostaglandin formation from arachidonate	18	18	5	3.1	0.1542	0.328	0.0084	10	0.1	EC000243, EC000246, EC000247, EC00054, EC00058
Selenoamino acid metabolism	13	13	4	2.2	0.1467	0.3514	0.0082	13	0.13	EC00052, EC00091, EC00092, EC00093
Porphyrin metabolism	36	36	8	6.2	0.2182	0.3581	0.0103	21	0.21	EC000252, EC000157, EC00054, EC00058, EC000338, EC000243, EC000246, EC000247
Tryptophan metabolism	33	33	7	5.6	0.2822	0.4467	0.0128	39	0.39	EC00014, EC000208, EC000211, EC000212, EC000213, EC00016, EC000457
Pyrimidine metabolism	94	94	17	16.1	0.3533	0.4507	0.0163	54	0.54	EC000412, EC000413, EC00011, EC00012, EC000234, EC000164, EC000165, EC000255, EC00091, EC00092, EC00093, EC00086, EC00087, EC000115, EC000302, EC00066, EC00036

Pathway Name	PW tot	Hits	Hits sig.	Exp. #EC	FET p-val	EASE p-val	γ-adj p-val	Emp. hits	Emp. p-val	EC hits
Pentose and Glucuronate Interconversions	29	29	6	5.0	0.3296	0.5155	0.0151	32	0.32	EC00086, EC00087, EC000108, EC000157, EC000177, EC000388
Hexose phosphorylation	25	25	5	4.3	0.3866	0.595	0.0184	47	0.47	EC00016, EC00066, EC000115, EC000164, EC000165
Chondroitin sulfate degradation	12	12	3	2.1	0.3092	0.602	0.014	32	0.32	EC00016, EC000157, EC000108
C5-Branched dibasic acid metabolism	13	13	3	2.2	0.3579	0.6476	0.0166	37	0.37	EC00011, EC00012, EC000264
Heparan sulfate degradation	13	13	3	2.2	0.3579	0.6476	0.0166	34	0.34	EC00016, EC000157, EC000108
Alanine and Aspartate Metabolism	20	20	4	3.4	0.4163	0.6523	0.0204	43	0.43	EC00014, EC00011, EC00012, EC00036
Carbon fixation	21	21	4	3.6	0.4561	0.6864	0.0235	34	0.34	EC00066, EC00011, EC00012, EC00036
Lipoate metabolism	8	8	2	1.4	0.3844	0.7576	0.0182	37	0.37	EC000307, EC000311
Purine metabolism	74	74	11	12.7	0.6931	0.7925	0.059	75	0.75	EC000108, EC000115, EC000302, EC000293, EC00011, EC00012, EC00036, EC000164, EC000165, EC00054, EC00058
N-Glycan biosynthesis	42	42	6	7.2	0.7103	0.8394	0.0634	72	0.72	EC00086, EC00087, EC000113, EC000214, EC00016, EC00066
Tyrosine metabolism	100	100	14	17.1	0.7953	0.8619	0.0935	72	0.72	EC00014, EC00011, EC00012, EC000243, EC000246, EC000247, EC00054, EC00058, EC000498, EC000603, EC000226, EC00091, EC00092, EC00093
Fructose and mannose metabolism	36	36	5	6.2	0.7283	0.8625	0.0686	83	0.83	EC000214, EC00066, EC00016, EC000433, EC000585
Starch and Sucrose Metabolism	29	29	4	5.0	0.7252	0.875	0.0677	74	0.74	EC00086, EC00087, EC00066, EC00016
Sialic acid metabolism	37	37	5	6.3	0.7516	0.877	0.0762	79	0.79	EC00016, EC00066, EC00052, EC000161, EC000163
Pyruvate Metabolism	12	12	2	2.1	0.6081	0.8816	0.0417	50	0.5	EC00011, EC00012
Glyoxylate and Dicarboxylate Metabolism	13	13	2	2.2	0.6536	0.9011	0.05	47	0.47	EC000182, EC000108
Glycerophospholipid metabolism	62	62	8	10.6	0.8276	0.9041	0.1099	82	0.82	EC00011, EC00012, EC000413, EC000182, EC00072, EC00052, EC00016, EC00066
Glycolysis and Gluconeogenesis	42	42	5	7.2	0.8464	0.9315	0.1214	85	0.85	EC000336, EC00066, EC00011, EC00012, EC00016
Glutathione Metabolism	20	20	2	3.4	0.8652	0.9722	0.1347	84	0.84	EC000414, EC000450

Pathway Name	PW tot	Hits	Hits sig.	Exp. #EC	FET p-val	EASE p-val	γ-adj p-val	Emp. hits	Emp. p-val	EC hits
Glycosphingolipid biosynthesis - globoseries	22	22	2	3.8	0.8991	0.9807	0.1654	84	0.84	EC000214, EC00016
Galactose metabolism	43	43	4	7.4	0.9427	0.9812	0.2272	97	0.97	EC00016, EC00066, EC000161, EC000163
Glycosphingolipid biosynthesis - ganglioseries	23	23	2	3.9	0.9129	0.984	0.1813	85	0.85	EC00016, EC000214
Linoleate metabolism	23	23	2	3.9	0.9129	0.984	0.1813	87	0.87	EC00054, EC00058
Glycosphingolipid metabolism	37	37	3	6.3	0.9585	0.9897	0.2625	94	0.94	EC00016, EC000214, EC00052
Aminosugars metabolism	40	40	3	6.8	0.9728	0.9937	0.3078	98	0.98	EC00011, EC00012, EC00066
Phosphatidylinositol phosphate metabolism	46	46	3	7.9	0.9888	0.9977	0.3963	99	0.99	EC00016, EC00066, EC000157
Drug metabolism - cytochrome P450	4	4	1	0.7	0.5103	1	0.0287	38	0.38	EC000565
Nitrogen metabolism	6	6	1	1.0	0.658	1	0.0509	74	0.74	EC00036
CoA Catabolism	7	7	1	1.2	0.7143	1	0.0646	62	0.62	EC000331
Vitamin B9 (folate) metabolism	9	9	1	1.5	0.8009	1	0.0961	83	0.83	EC00052
Glycosylphosphatidyl-inositol (GPI)-anchor biosynthesis	10	10	1	1.7	0.8338	1	0.1135	87	0.87	EC00066
N-Glycan Degradation	10	10	1	1.7	0.8338	1	0.1135	87	0.87	EC00016
Keratan sulfate degradation	12	12	1	2.1	0.8844	1	0.1509	97	0.97	EC00016
Hyaluronan Metabolism	13	13	1	2.2	0.9037	1	0.1704	84	0.84	EC000157
Vitamin B5 - CoA biosynthesis from pantothenate	13	13	1	2.2	0.9037	1	0.1704	81	0.81	EC000331
Nucleotide Sugar Metabolism	14	14	1	2.4	0.9197	1	0.1902	91	0.91	EC00066
Glycosphingolipid biosynthesis - lactoseries	16	16	1	2.7	0.9443	1	0.2304	88	0.88	EC000214
Blood Group Biosynthesis	16	16	1	2.7	0.9443	1	0.2304	88	0.88	EC000214
Glycosphingolipid biosynthesis - neolactoseries	16	16	1	2.7	0.9443	1	0.2304	88	0.88	EC000214
C21-steroid hormone biosynthesis and metabolism	19	19	1	3.2	0.9679	1	0.2901	89	0.89	EC000314
Vitamin B3 (nicotinate and nicotinamide) metabolism	27	27	1	4.6	0.9927	1	0.4363	97	0.97	EC00036

9.3. Appendix III

The DNA concentration for the ^{13}C tracer experiment (**section 3.6)** and the measurement of redox metabolites (**section 3.7**) are provided in **Table A.III.1** and **Table A.III.2**, respectively. The samples for the ^{13}C tracer experiments were originally part of a larger experiment, but that data was not included in this thesis. The lowest DNA concentration that the relative DNA concentration was calculated for was 79.1 ng/µL.

Table A.III.1. DNA concentration of wtIDH1 and mutIDH1^{R132H} LN18 cells in the ^{13}C tracer experiments.

Sample name	DNA 1 (ng/µL)	DNA 2 (ng/µL)	DNA 3 (ng/µL)	Average (ng/µL)	Relative DNA concentration	µL solvent	µL sample
MUT-No-^{13}C-24h-01	123.0	126.5		124.75	1.58	29.3	50.7
MUT-No-^{13}C-24h-02	125.4	125.7		125.55	1.59	29.6	50.4
MUT-No-^{13}C-24h-03	134.5	134.9		134.70	1.70	33.0	47.0
MUT-^{13}C-Gln-24h-01	159.7	163.3	163.0	162.00	2.05	40.9	39.1
MUT-^{13}C-Gln-24h-02	158.7	157.0		157.85	2.00	39.9	40.1
MUT-^{13}C-Gln-24h-03	132.4			132.40	1.67	32.2	47.8
MUT-^{13}C-Gln-24h-04	161.5	157.2		159.35	2.01	40.3	39.7
MUT-^{13}C-Gln-24h-05	124.3	123.5		123.90	1.57	28.9	51.1
MUT-^{13}C-Gluc-24h-01	149.8	152.0		150.90	1.91	38.1	41.9
MUT-^{13}C-Gluc-24h-02	146.4	147.0		146.70	1.85	36.9	43.1
MUT-^{13}C-Gluc-24h-03	121.7	123.2		122.45	1.55	28.3	51.7
MUT-^{13}C-Gluc-24h-04	150.1	143.5	147.8	147.13	1.86	37.0	43.0
MUT-^{13}C-Gluc-24h-05	169.0	171.9		170.45	2.15	42.9	37.1
WT-^{13}C-Gln-24h-01	158.5	154.9		156.70	1.98	39.6	40.4
WT-^{13}C-Gln-24h-02	153.3	154.5		153.90	1.95	38.9	41.1
WT-^{13}C-Gln-24h-03	137.4	138.4		137.90	1.74	34.1	45.9
WT-^{13}C-Gln-24h-04	188.5	180.1	185.4	184.67	2.33	45.7	34.3
WT-^{13}C-Gln-24h-05	157.7	159.1		158.40	2.00	40.1	39.9
WT-^{13}C-Gluc-24h-01	127.4	134.0	131.9	131.10	1.66	31.7	48.3
WT-^{13}C-Gluc-24h-02	161.4	159.9		160.65	2.03	40.6	39.4
WT-^{13}C-Gluc-24h-03	141.0	143.5		142.25	1.80	35.5	44.5
WT-^{13}C-Gluc-24h-04	139.7	139.0		139.35	1.76	34.6	45.4
WT-^{13}C-Gluc-24h-05	177.0	175.8		176.40	2.23	44.1	35.9
WT-No-^{13}C-24h-01	108.0	105.4		106.70	1.35	20.7	59.3
WT-No-^{13}C-24h-02	167.3	166.9		167.10	2.11	42.1	37.9
WT-No-^{13}C-24h-03	174.3	175.2		174.75	2.21	43.8	36.2

Table A.III.2. DNA concentration of wtIDH1 and mutIDH1^{R132H} LN18 cells harvested with the redox method and analysed with HILIC LC-MS.

Sample name	DNA 1 (ng/µL)	DNA 2 (ng/µL)	Average (ng/µL)	Relative DNA concentration	µL solvent	µL sample
MUT_01	136.50	132.60	134.55	1.097	6.2	63.8
MUT_02	138.20	139.70	138.95	1.133	8.2	61.8
MUT_03	122.80	122.50	122.65	1.000	0.0	70.0
MUT_04	92.60	93.60	93.10	0.759	0.0	70.0
MUT_05	128.50	127.90	128.20	1.046	3.1	66.9
MUT_06	134.60	131.60	133.10	1.086	5.5	64.5
MUT_07	149.40	148.70	149.05	1.216	12.4	57.6
MUT_08	122.90	124.10	123.50	1.007	0.5	69.5
MUT_09	105.50	104.60	105.05	0.857	0.0	70.0
MUT_10	127.70	127.40	127.55	1.040	2.7	67.3
WT_01	159.40	159.70	159.55	1.301	16.2	53.8
WT_02	142.00	138.40	140.20	1.144	8.8	61.2
WT_03	167.70	167.90	167.80	1.369	18.9	51.1
WT_04	153.90	151.40	152.65	1.245	13.8	56.2
WT_05	141.10	141.50	141.30	1.153	9.3	60.7
WT_06	150.70	150.40	150.55	1.228	13.0	57.0
WT_07	123.70	123.40	123.55	1.008	0.5	69.5
WT_08	143.70	147.05	145.38	1.186	11.0	59.0
WT_09	145.50	146.20	145.85	1.190	11.2	58.8
WT_10	139.30	143.70	141.50	1.154	9.3	60.7

9.4. Appendix IV

Data for the 12-well pilot described in **section 4.2**. The DNA concentrations for normalisation are listed in **Table A.IV.1**, IC-MS metabolite identifications in **Table A.IV.2**, derivatised RPLC-MS metabolite identifications in **Table A.IV.3**, and data processing in **Figure A.IV.1** and **Figure A.IV.2.**

Table A.IV.1. DNA concentration of wtIDH1 mutIDH1R132H LN18 cells from the 12-well pilot experiment. Total sample volume was 50 µL. Rel. DNA conc. = relative DNA concentration.

Sample Name	DNA 1 (ng/µL)	DNA 2 (ng/µL)	DNA 3 (ng/µL)	Average (ng/µL)	Rel. DNA conc.	µL Sample	µL Solvent
MUT_04	49.01	43.32		46.165	1.042	2	48
MUT_05	45.36	50.58	48.31	48.083	1.086	4	46
MUT_06	38.27	53.12	41.48	44.290	1.000	0	50
MUT_07	33.55	28.37		30.960	0.699	0	50
MUT_08	43.39	40.12	54.92	46.143	1.042	2	48
MUT_09	55.04	53.03		54.035	1.220	9	41
MUT_10	51	61.99	58.35	57.113	1.290	11	39
MUT_11	67.15	41.08		54.115	1.222	9	41
MUT_12	64.86	61.76	61.2	62.607	1.414	15	35
WT_04	56.77	50.82	50.79	52.793	1.192	8	42
WT_05	57.21	64.23		60.720	1.371	14	36
WT_06	51.01	59.86	70.13	60.333	1.362	13	37
WT_07	54.5	44.23		49.365	1.115	5	45
WT_08	55.44	53.16	42.77	50.457	1.139	6	44
WT_09	55.04	53.03		54.035	1.220	9	41
WT_10	85.52	73.3		79.410	1.793	22	28
WT_11	50.88	57.69	57.68	55.417	1.251	10	40
WT_12	49.91	49.88	42.82	47.537	1.073	3	47

Table A.IV.2. Annotated metabolites from the IC-MS data of the 12-well pilot experiment. Parameters used for determining whether it was a putative or confident identification. FS = fragmentation score, ME = mass error, ISS = isotope similarity score, RTE = retention time error, max. abun. = max abundance and min. CV% = minimum coefficient of variance, C = Confident and P = putative. When provided as a comment, the abbreviation indicates what brought the identification from confident to putative (isomers, RTE > 1.5 min, ME > 3 ppm, IS < 90%).

Accepted identification	FS	ME (ppm)	ISS	RTE (min)	Max. Abun.	Min. CV%	C/P	Comment
1-Pyrroline hydroxycarboxylic acid	0	-2.56	96.9	-0.62	45054	14.5	C	
2-butyl-3-ureido-succinate	0	-2.81	98.8	1.09	214	17.6	C	
2-Hydroxyglutarate	81	-2.54	99.8	-0.88	1960444	10.3	C	
2-Ketobutyric acid	76.8	-2.35	98.1	-0.73	3422	10.2	C	
2-Oxoglutaric acid	71.5	-2.57		-1.11	452544	8.8	C	
2-Phosphoglyceric acid	77.7	-2.59	98.6	-1.59	14453	23.1	C	
3,3 Dimethyl glutarate	95.3	-2.49	99.5	-1.49	9685	6.5	C	
3-Dehydroquinate	33.7	-2.88	97.9	-0.74	53766	8.9	C	
3-deoxy-2-keto-6-phosphate	0	-2.83	94.9	-0.02	1663	19.1	C	
3-Hydroxymethylglutarate	88.3	-3.01	99.7	-0.92	36806	8.8	C	
3-Hydroxytyrosol	0	-1.82	97.4	-0.63	2534	9.3	C	
3-methoxyphenylacetic acid	0	-1.95	97.1	1.27	11350	11.7	C	
3-Methyl-2-oxovaleric acid	0	-2.14	99.8	-0.58	3544304	13.9	C	
4-Hydroxy-3-methoxymandelic acid	45	-2.83	98.9	-1.36	797	29.7	C	
4-Hydroxybenzoic acid	0	-2.55	98.2	-0.10	2789	15.1	C	
4-Hydroxybutyric acid	0	-2.07	99.2	0.66	2079	9.4	C	
4-Hydroxyproline	81.3	-1.54	98.4	-0.37	4177	8.4	C	
Acetic acid	0	-2.45	97.4	0.18	36448	5.4	C	
Acetoacetate	0	-2.18	97.9	-0.86	406	13.9	C	
Acetylcysteine	67.6	-2.77	92.0	-0.97	12003	12.2	C	
Acetylglycine	92.5	-1.76	97.8	-0.12	941	13.7	C	
Adenine	0	-2.36	93.0	1.66	764	25.8	P	RTE
Adenosine diphosphate	0	3.85	92.7	-1.24	10137	35.5	P	ME
Adenosine monophosphate	0	1.57	86.6	0.15	629	136.3	P	RTE and IS
Adenosine triphosphate	5.86	-3.08	98.0	-1.81	3206978	30.2	P	RTE and ME
Adonitol	0	-1.85	98.5	0.66	1274	26	P	Isomer with xylitol and arabitol
ADP Glucose	17.5	-2.11	96.9	-1.32	2067	60.5	C	
Arabinonic acid	59.7	-2.82	93.6	-0.87	96342	11.6	C	
Ascorbate	30.8	-3.32	99.5	-1.15	1175956	5.7	P	ME
Aspartate	86.7	-2.45	94.6	-0.48	208122	13.5	C	
Beta-Citryl-L-glutamic acid	0	-2.97	98.2	-0.35	244580	12.7	C	
Butyric acid	64.1	-3.03	95.9	-0.86	12319	11.2	C	
cis-Aconitic acid	0	-2.19	97.5	-1.39	576	20.5	C	
Citraconic acid	0	-1.60	93.8	-0.66	2075	8.5	P	Isomer of e.g. itaconic acid
Citric acid	0	-3.24	99.3	0.22	36452	6.2	P	ME and isomer of isocitric acid
Coenzyme A	54.1	-2.01	92.3	-1.87	110738	14	P	RTE
Cysteic acid	94.6	-3.21	91.1	-1.17	3200	9.3	C	

Accepted identification	FS	ME (ppm)	ISS	RTE (min)	Max. Abun.	Min. CV%	C/P	Comment
Cytidine diphosphate	0	-0.63	94.9	-0.90	13061	15.1	C	
Cytidine monophosphate N-acetylneuraminic acid	0	-0.79	95.4	-0.73	15548	20.8	C	
CTP	7.05	-3.21	98.3	-1.37	214109	22.7	P	ME
dCTP	0	-2.56	86.9	-0.69	2846	16.9	P	IS
Deoxyribose 5-phosphate	21.8	-2.00		0.03	1713	29.1	C	
dGDP	0	-2.12	97.9	-1.95	4863829	37.2	P	RTE
Dihydrouracil	0	3.05	94.6	0.46	81	27.4	P	ME
dTDP-D-glucose	0	-1.06	90.5	-1.15	6234	39.5	C	
dUMP	0	-1.77	95.7	-1.40	3437	38.9	C	
Flavin Mononucleotide	0	-1.74	97.0		3011	25.6	P	No RTE
Fructose 1,6-bisphosphate	52.1	-2.52		-1.34	2156	24.4	C	
Fructose 2,6 diphosphate	0	-2.57	94.2	-0.29	15332	12	C	
Fructose 6-phosphate	91.9	-2.86	99.2	-0.19	1345	44.6	P	Isomer of mannose 6P
Fumarate	44.3	-2.00	96.3	1.60	573	9.5	P	RTE
Galactaric acid	59.9	-2.71	99.5	-0.92	29615	8.5	C	
Galacturonic acid	86.3	-3.09	99.3	0.04	20516	5.5	P	Isomer of glucuronic acid
Gluconate	78.7	-3.11		-0.72	729946	5.7	C	
Glucose 1-phosphate	86.1	-3.50	98.9	-0.60	18780	6.6	P	Isomer of galactose 1P
Glutaconic acid	0	-1.57	93.8	0.80	207	18.5	P	Isomer of e.g. mesaconic and isaconic acid
Glutamine	0	-2.27	96.7	-0.73	17864	4.9	C	
Glutamylcysteine	0	-4.80	94.3	-0.61	266	74.8	P	ME
Glutaric acid	0	-1.65	99.0	0.34	23651	9.7	P	Isomer of ethylmalonic acid
Glutathion	0	-2.70	94.2	-0.10	143308	8.4	C	
Glyceric acid	37.8	-2.30		0.70	1342820	5.2	C	
Glycerol	63.5	-2.92	98.9	-0.09	17535	11.5	C	
Glycerol 3-phosphate	42.2	-2.92		-0.82	17399	7.2	C	
Glycolic acid	41.5	-3.20	99.2	-0.96	7386	4.4	C	
Guanosine diphosphate	97.5	-2.17	97.5	0.59	496626	26.6	C	
Guanosine monophosphate	25.8	-2.18	92.8	-1.72	5525	34.1	P	RTE
Hippuric acid	67.1	-3.13	90.6	-1.11	181977	8.2	C	
Homogentisic acid	13.9	-2.90	90.9	1.37	296	47.4	C	
Hydroxy-isobutyric acid	0	-2.41	95.0	0.22	233	17.8	P	Isomer of 2- and 3-hydroxybutyric acid
IDP	25.2	-2.20	97.5	1.22	174	120.2	C	
Indole-3-lactic acid	28.5	-2.49	97.9	-0.73	306	44.7	C	
Inositol 1,3,4-trisphosphate	0	-1.35	97.1	-1.56	1377	45.6	P	RTE
Isopentenyl pyrophosphate	17.5	-2.12	98.1	-1.32	143	51.7	P	Isomer of dimethylallyl pyrophosphate
Itaconic acid	59.2	-2.02	99.7	-0.83	7976	8.8	P	Isomer of e.g. mesaconic and glutaconic acid

Accepted identification	FS	ME (ppm)	ISS	RTE (min)	Max. Abun.	Min. CV%	C/P	Comment
Kojic acid	0	-1.59	92.8	-0.62	909	7.2	C	
Lactose	0	0.75	89.0	-0.27	43261	18	C	
Maleic acid	82.5	-2.20	99.9	-0.42	21435	11.5	C	
Malic acid	89.2	-1.85	99.7	-0.87	562296	5.8	C	
Malitol	53.2	-1.41	94.6	-0.31	1758	77.7	C	
Malondialdehyde	0	-4.41	98.5	1.16	1760	6.4	P	ME
Malonic acid	60.9	-2.09	99.9	-0.99	903	9.5	C	
Mannose 6-phosphate	88.6	-3.43	87.8	-1.79	1297	57.9	P	Isomer of fructuse 6P and IS
Methylglutaric acid	85.8	-2.22	88.4	-0.81	19430	15.8	C	
Methylisocitric acid	0	-2.55	99.4	-0.30	14989	9	C	
Myoinositol	89.2	-3.18	95.6	-0.12	303277	5.3	P	Isomer of scyllitol and other hexoses
N-Acetyl-aspartate	94.7	-2.02	94.3	-0.72	75248	7.8	C	
N-Acetylaspartylglutamic acid	0	-1.75	99.1	-1.00	19647	15.8	C	
N-Acetyl-D-glucosamine	25.7	-2.65	93.8	0.00	262	61.1	C	
N-Acetyl-L-alanine	67.2	-2.63	94.2	-0.28	6651	13.8	C	
N-Acetyl-L-methionine	95.9	-2.82	96.3	-0.64	8658	5.9	C	
N-Acetyl-L-phenylalanine	39.5	-2.40	98.4	-0.53	653	23.9	C	
N-Acetylneuraminic acid	92.6	-1.85	96.8	-0.80	1897237	11.3	C	
N-Acetyltryptophan	95.5	-3.06	97.3	-1.36	1351	13.3	C	
NADPH	75	1.29	96.1	-0.30	722	109	C	
N-Formyl-methionine	0	-3.15	96.6	-0.71	4478	10.6	P	ME
Nicotinic Acid N-Oxide	87.1	-2.32	93.1	-1.27	604	40.2	C	
O-Acetylserine	0	-1.84	93.7	-0.41	5449586	3.2	C	
Octanoic acid	15	-2.57	99.5	-1.73	27775	5.4	P	RTE
O-Phosphoserine	87.3	-2.31	98.7	-0.97	8491	35.4	C	
Orotic acid	35.2	-2.24	93.6	-1.75	2563	10.9	P	RTE
Orotidine	0	-0.14	93.4	-1.89	1070	16	P	RTE
Oxalic acid	70.6	-2.44	99.5	-1.16	27148	6	C	
Oxoadipic acid	86.6	-2.83	99.8	-1.34	2103	26.9	C	
Pantothenic acid	63.9	-2.86	97.9	-0.72	3619929	4.2	C	
Phosphoenolpyruvic acid	47.3	-2.82	99.0	-0.83	3083	14.7	C	
Phosphoribosyl pyrophosphate (PRPP)	0	-2.84	97.6	-1.20	26239	34.4	C	
Pyridoxal 5'-phosphate	46.5	-3.44	95.3	-1.54	2004	9.7	P	RTE and ME
Quinic acid	46.6	-2.57	91.3	-0.79	210	52.3	C	
Ribose 5-phosphate	70.5	-2.65	93.7	-1.09	778	31.6	P	Isomer of xylulose 5P
Scyllitol	0	-2.63	96.5	0.02	7231	10.6	P	Isomer of hexoses
Sedoheptulose 7-phosphate	67.7	-2.00		-0.88	1016	54.1	C	
Sorbitol	85.3	-2.19	97.9	-0.08	28986	11.2	C	
Succinic acid	87.9	-1.83	99.8	-0.84	612106	4.6	C	
Taurine	94.4	-2.54	92.6	-0.61	235194	7.4	C	
TDP	0	-2.72	86.7	-0.98	1092	35.9	P	IS
Threitol	71.1	-2.12	97.5	-0.09	2017	24.2	C	

Accepted identification	FS	ME (ppm)	ISS	RTE (min)	Max. Abun.	Min. CV%	C/P	Comment
Thymidine 5'-monophosphate	95.8	-1.46	98.7	-0.93	6050	33.9	C	
Thymidine triphosphate	6.28	-2.70	95.2	-1.04	15118	21.7	C	
UDP-galactose	0	-2.67	86.3	-0.77	6133	36.5	P	Isomer of UDP/glucose
Uric acid	82.1	-3.84	95.7	-1.90	220256	8.6	P	RTE
Uridine	27.8	-2.75	96.7	0.12	22018	14.5	C	
Uridine 5'-diphosphate	14.2	-2.22	98.6	1.36	1175238	24.4	C	
Uridine 5'-monophosphate	53.7	-1.80	97.4	-1.47	43377	30.7	C	
Uridine diphosphate-N-acetylglucosamine	4.59	-1.99	98.2	-1.86	362028	25.4	P	RTE
Xylitol	47.1	-2.64	99.2	-0.02	852	18.6	P	Isomer of arabitol and adonitol
Xylulose	33.9	-3.05	93.6	0.22	18588	11.5	P	Isomer of other pentoses
Xylulose 5-phosphate	61.9	-2.14	94.3	0.83	1998	18.6	P	Isomer of ribose 5P

Table A.IV.3. Annotated metabolites from the derivatised RPLC-MS data of the 12-well pilot experiment. Parameters used for determining whether it was a putative or confident identification. ME = mass error, ISS = isotope similarity score, RTE = retention time error, max. abun. = max abundance and min. CV% = minimum coefficient of variance, C = Confident and P = putative. When provided as a comment, the abbreviation indicates what brought the identification from confident to putative (isomer, RTE > 0.5 min, ME > 3 ppm, IS < 90%).

Accepted Description	ME (ppm)	ISS	RTE (min)	Max. abun.	Min. CV%	C/P	Comment
2-Aminoadipic acid	-0.09	95.3	0.12	104	18.4	C	
4-Hydroxyproline	0.73	96.8		7.95	14	P	No RT
Alanine	-1.12	97.4	0.16	3679	13.7	C	
GABA	-0.95	96.2	-0.36	0.75	25.3	P	
Arginine	-1.54	96.7	0.15	36	19.4	C	
Asparagine	-2.00	95.6	0.05	31	16.7	C	
β-Alanine	0.19	97.7	-0.18	2.81	11.5	C	
Citrulline	-1.93	95.6	0.13	4.23	20.7	C	
Cysteine	-2.78	93.9	-0.93	47	17.9	P	RTE
Ethanolamine	-3.86	95.0	0.15	1.01	44.4	P	ME
Glucosamine	-1.99	95.1	-1.97	1.12	33.5	P	RTE
Glutamic acid	-1.20	95.6	0.16	2178	9.6	C	
Glutamine	-1.44	95.9	0.11	763	9.6	C	
Glutathione	-1.42	89.0	0.09	524	10.4	P	IS
Glycine	-1.47	97.7	0.2	766	11.1	C	
Histidine	-1.42	96.3	0.13	61	16.2	C	
Homoserine	-2.92	95.0	0.44	0.22	61.7	C	
Hypotaurine	2.19	88.3	0.25	29	10	P	IS
Isobutylamine	0.06	97.9	-0.41	35	15.7	C	
Isoleucine	-0.24	96.5	0.67	20	17.9	P	Isomer of leucine
Kynurenine	-0.95	95.6	0.11	0.57	56.2	C	
Leucine	-0.22	96.5	0.03	1022	13.9	P	Isomer of isoleucine
Lysine	0.06	97.3	0.09	483	17.4	C	
Mandelonitrile	-4.17	92.5	-0.41	40	11.5	C	
N-Acetyl-ornithine	-1.87	94.7	0.02	2.65	19.5	P	Isomer of L-Theanine
N-Acetylproline	2.73	88.6	0.65	2.31	18.9	P	RTE and IS
Nicotinic acid	-4.45	87.6	0.07	0.75	27.1	P	ME
Octapine	-2.66	90.8		255	8.1	P	No RT
Oxidised Glutathione	-1.37	85.7	0.06	51	12.8	P	IS
Phenylalanine	-0.06	96.0	0.12	821	12.8	C	
Pipecolic acid	-2.99	95.3	0.48	7.2	28.6	C	
Proline	-1.71	95.7	0.15	207	17.4	C	
Pyroglutamic Acid	-1.24	92.5	0	0.38	43.7	C	
Serine	-1.81	97.4	0.21	188	9.7	C	
Taurine	-2.57	93.5		286	9.6	P	No RT
Threonine	-0.80	97.2	0.16	1294	12.2	C	
Tryptophan	-0.99	94.9	0.1	130	12.1	C	
Tyrosine	-0.60	95.9	0.11	480	12.9	C	
Valine	-0.58	96.4	0.12	836	11.7	C	

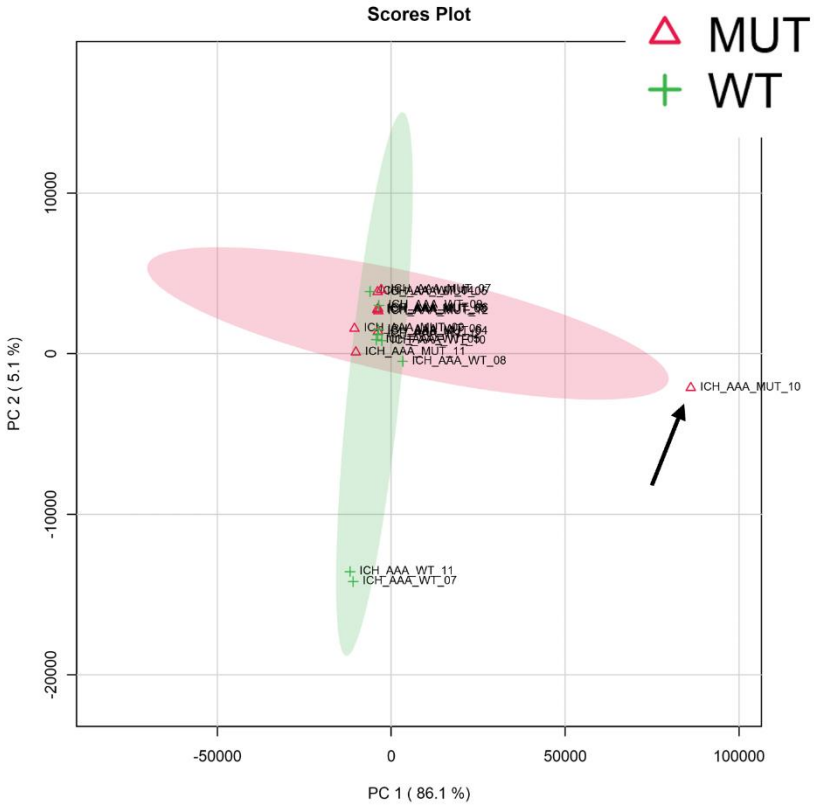

Figure A.IV.1. PCA scores plot (PC1 × PC2) used in the assessment of derivatised RPLC-MS data from analysis of wtIDH1 and mutIDH1R132H LN18 cells grown in and harvested from 12-well plates. PCA scores plot of derivatised RPLC-MS data without normalisation, transformation or scaling applied. Black arrow indicates the outlier sample. N = 9 biological replicates for wtIDH1 and mutIDH1R132H Ln18 cells, except in (c) where N = 8 for wtIDH1 LN18 cells.

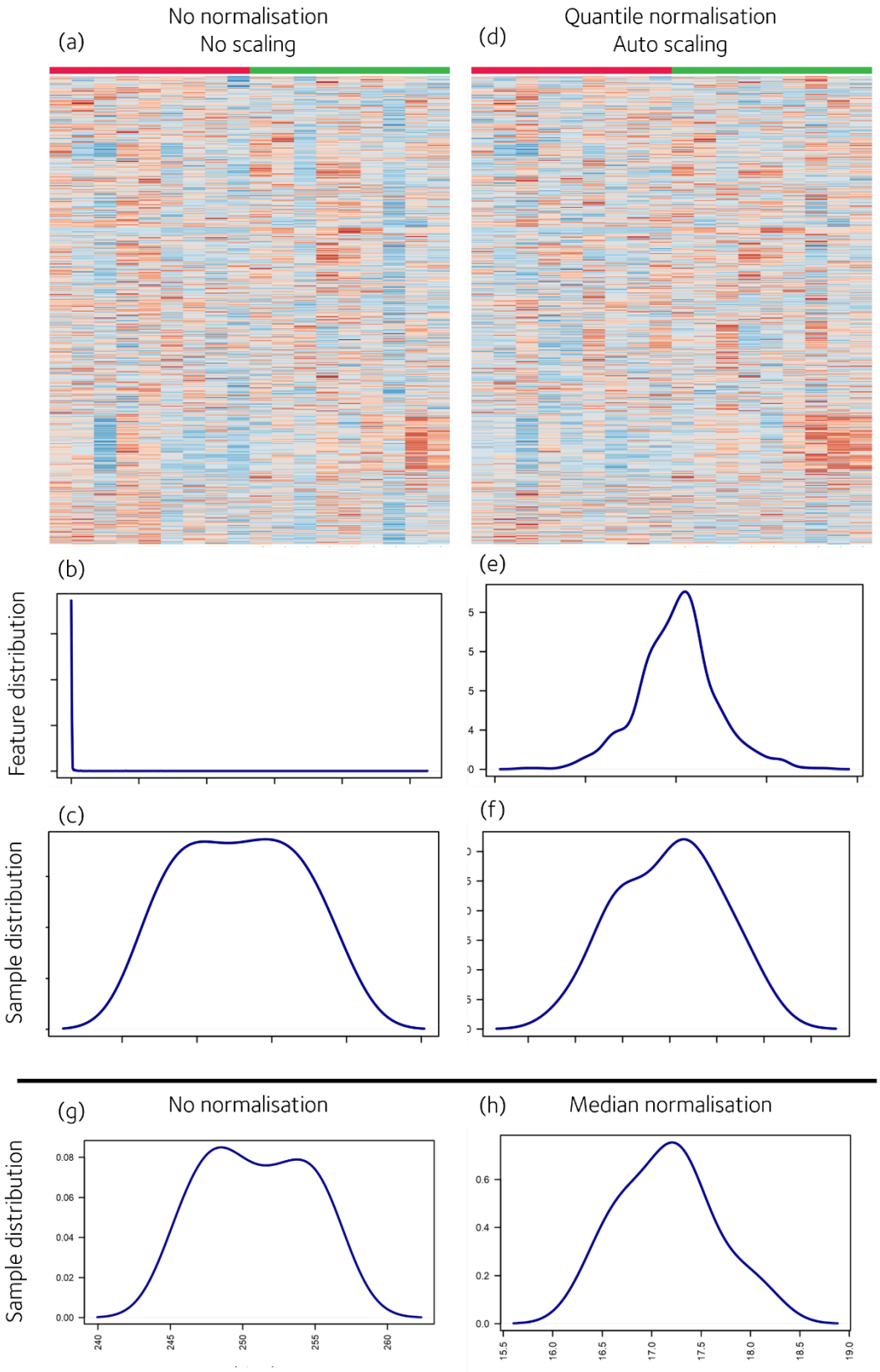

Figure A.IV.2. Heatmaps and feature and sample distribution plots used in the assessment of IC-MS and derivatised RPLC-MS data from analysis of wtIDH1 and mutIDH1R132H LN18 cells grown in and harvested from 12-well plates. Heatmap, feature and sample distribution plots of IC-MS data (a-c) before and (d-f) after quantile normalisation and auto-scaling. Sample distribution plot of derivatised RPLC-MS data (g) before and (h) after median normalisation. N = 9 biological replicates for wtIDH1 and mutIDH1R132H Ln18 cells, except in (c) where N = 8 for wtIDH1 LN18 cells.

9.5. Appendix V

The experiment that the data in this appendix is based on was a metabolomics experiment of mutIDH1^{R132H} LN18 cells treated with a range of concentrations (0.05, 0.50, 5.00 and 10.0 μM) of four mutIDH1 inhibitors (AG-120, AG-881, BAY 1436032 and GSK864). The 2-HG, 2-OG and isocitrate measurements were used in **chapter 4** (**section 4.6**) and the full metabolomics data was used in **chapter 5**. This appendix includes a DNA concentration table (**Table A.V.1**), IC-MS identifications (**Table A.V.2**), derivatised RPLC-MS identifications (**Table A.V.3**), and data processing information (**Figure A.V.1**).

Table A.V.1. DNA concentration of mutIDH1^{R132H} LN18 cells in the mutIDH1 inhibitor concentration range experiment. The maximum possible volume was made up for each sample, usually 50 µL and sometimes less. Rel. DNA conc. = relative DNA concentration. Abbreviations: Co = control, BAY = BAY 1436032 and GSK = GSK864.

Sample Name	DNA 1 (ng/µL)	DNA 2 (ng/µL)	Average (ng/µL)	Rel. DNA conc.	µL Sample	µL Solvent	Total (µL)
0.05-AG881_01	65.2	65.3	65.3	1.431	29.0	12.5	41.5
0.05-AG881_02	72.5	72.7	72.6	1.592	31.4	18.6	50.0
0.05-AG881_03	68.6	70.9	69.8	1.530	32.7	17.3	50.0
0.05-AG881_04	59.7	60.1	59.9	1.314	38.1	11.9	50.0
0.5-AG881_01	71.0	71.5	71.3	1.563	28.8	16.2	45.0
0.5-AG881_02	69.6	70.1	69.9	1.532	32.6	17.4	50.0
0.5-AG881_03	77.1	79.8	78.5	1.720	29.1	20.9	50.0
0.5-AG881_04	79.9	80.1	80.0	1.754	28.5	21.5	50.0
5.0-AG881_01	56.9	57.5	57.2	1.254	39.9	10.1	50.0
5.0-AG881_02	60.0	59.0	59.5	1.305	38.3	11.7	50.0
5.0-AG881_03	56.8	57.5	57.2	1.253	39.9	10.1	50.0
5.0-AG881_04	61.5	61.8	61.7	1.352	37.0	13.0	50.0
10.0-AG881_01	55.6	56.2	55.9	1.226	36.7	8.3	45.0
10.0-AG881_02	55.0	54.7	54.9	1.203	41.6	8.4	50.0
10.0-AG881_03	67.4	66.8	67.1	1.471	34.0	16.0	50.0
10.0-AG881_04	69.2	69.0	69.1	1.515	33.0	17.0	50.0
Co_01	57.9	54.5	56.2	1.232	31.5	7.3	38.8
Co_02	64.9	64.0	64.5	1.413	35.4	14.6	50.0
Co_03	64.7	63.9	64.3	1.410	35.5	14.5	50.0
Co_04	78.2	80.6	79.4	1.741	25.8	19.2	45.0
Co_05	46.2	46.3	46.3	1.014	39.4	0.6	40.0
Co_06	46.9	45.5	46.2	1.013	43.4	0.6	44.0
Co_07	55.3	55.4	55.4	1.214	41.2	8.8	50.0
Co_08	63.8	63.9	63.9	1.400	35.7	14.3	50.0
0.05-AG120_01	62.4	62.2	62.3	1.366	32.9	12.1	45.0
0.05-AG120_02	66.3	66.8	66.6	1.459	34.3	15.7	50.0
0.05-AG120_03	64.7	66.7	65.7	1.441	34.7	15.3	50.0
0.05-AG120_04	67.9	68.4	68.2	1.495	33.5	16.5	50.0
0.5-AG120_01	63.1	64.1	63.6	1.395	32.3	12.7	45.0
0.5-AG120_02	64.9	65.6	65.3	1.431	34.9	15.1	50.0
0.5-AG120_03	71.2	70.8	71.0	1.557	32.1	17.9	50.0
0.5-AG120_04	71.8	73.1	72.5	1.589	31.5	18.5	50.0
5.0-AG120_01	64.5	63.7	64.1	1.406	35.6	14.4	50.0
5.0-AG120_02	68.8	69.0	68.9	1.511	33.1	16.9	50.0
5.0-AG120_03	69.9	70.2	70.1	1.536	32.5	17.5	50.0
5.0-AG120_04	75.5	76.2	75.9	1.663	30.1	19.9	50.0
10.0-AG120_01	65.1	66.5	65.8	1.443	34.7	15.3	50.0
10.0-AG120_02	70.6	70.1	70.4	1.543	32.4	17.6	50.0
10.0-AG120_03	72.2	72.9	72.6	1.591	31.4	18.6	50.0
10.0-AG120_04	79.2	79.0	79.1	1.735	28.8	21.2	50.0
Co_09	46.1	45.9	46.0	1.009	35.0	0.0	35.0
Co_10	60.5	59.7	60.1	1.318	30.3	9.7	40.0
Co_11	63.4	60.3	61.9	1.356	36.9	13.1	50.0
Co_12	64.5	65.6	65.1	1.427	35.0	15.0	50.0
Co_13	53.7	52.7	53.2	1.167	37.6	6.3	43.9
Co_14	61.7	63.3	62.5	1.371	36.5	13.5	50.0
Co_15	62.2	62.4	62.3	1.366	36.6	13.4	50.0

Sample Name	DNA 1 (ng/µL)	DNA 2 (ng/µL)	Average (ng/µL)	Rel. DNA conc.	µL Sample	µL Solvent	Total (µL)
Co_16	64.6	65.7	65.2	1.429	35.0	15.0	50.0
0.05-BAY_01	56.9	57.7	57.3	1.256	33.8	8.7	42.5
0.05-BAY_02	54.3	53.8	54.1	1.185	42.2	7.8	50.0
0.05-BAY_03	56.8	56.3	56.6	1.240	40.3	9.7	50.0
0.05-BAY_04	62.2	63.7	63.0	1.380	36.2	13.8	50.0
0.5-BAY_01	51.4	51.9	51.7	1.133	34.3	4.6	38.9
0.5-BAY_02	53.3	54.4	53.9	1.181	38.1	6.9	45.0
0.5-BAY_03	65.2	65.5	65.4	1.433	34.9	15.1	50.0
0.5-BAY_04	69.2	69.0	69.1	1.515	33.0	17.0	50.0
5.0-BAY_01	60.9	62.3	61.6	1.351	37.0	13.0	50.0
5.0-BAY_02	71.4	70.9	71.2	1.560	32.0	18.0	50.0
5.0-BAY_03	75.8	75.5	75.7	1.659	30.1	19.9	50.0
5.0-BAY_04	71.8	71.3	71.6	1.569	31.9	18.1	50.0
10.0-BAY_01	77.3	77.3	77.3	1.695	29.5	20.5	50.0
10.0-BAY_02	76.3	76.4	76.4	1.674	29.9	20.1	50.0
10.0-BAY_03	77.3	78.9	78.1	1.713	29.2	20.8	50.0
10.0-BAY_04	71.9	73.0	72.5	1.589	31.5	18.5	50.0
Co_17	55.8	55.6	55.7	1.221	36.8	8.2	45.0
Co_18	50.5	50.9	50.7	1.112	40.5	4.5	45.0
Co_19	56.6	56.6	56.6	1.241	40.3	9.7	50.0
Co_20	54.5	53.3	53.9	1.182	32.8	6.0	38.8
Co_21	57.4	57.1	57.3	1.255	30.2	7.7	37.9
Co_22	56.9	55.9	56.4	1.237	40.4	9.6	50.0
Co_23	77.6	78.6	78.1	1.713	29.2	20.8	50.0
Co_24	68.2	66.9	67.6	1.481	33.8	16.2	50.0
0.05-GSK_01	58.1	58.2	58.2	1.275	35.3	9.7	45.0
0.05-GSK_02	60.6	61.2	60.9	1.336	37.4	12.6	50.0
0.05-GSK_03	57.6	59.3	58.5	1.282	39.0	11.0	50.0
0.05-GSK_04	62.1	62.3	62.2	1.364	36.7	13.3	50.0
0.5-GSK_01	59.3	59.4	59.4	1.302	29.5	8.9	38.4
0.5-GSK_02	65.7	65.1	65.4	1.434	34.9	15.1	50.0
0.5-GSK_03	59.4	59.8	59.6	1.307	38.3	11.7	50.0
0.5-GSK_04	69.1	69.4	69.3	1.519	32.9	17.1	50.0
5.0-GSK_01	65.9	65.1	65.5	1.436	34.8	15.2	50.0
5.0-GSK_02	64.9	65.3	65.1	1.428	35.0	15.0	50.0
5.0-GSK_03	74.6	75.7	75.2	1.648	30.3	19.7	50.0
5.0-GSK_04	72.9	71.6	72.3	1.584	31.6	18.4	50.0
10.0-GSK_01	80.7	79.8	80.3	1.760	28.4	21.6	50.0
10.0-GSK_02	82.3	82.6	82.5	1.808	27.7	22.3	50.0
10.0-GSK_03	63.9	63.5	63.7	1.397	35.8	14.2	50.0
10.0-GSK_04	85.4	85.5	85.5	1.874	26.7	23.3	50.0
Co_25	47.0	47.8	47.4	1.039	32.5	0.0	32.5
Co_26	54.6	55.5	55.1	1.207	37.3	7.7	45.0
Co_27	59.1	59.4	59.3	1.299	38.5	11.5	50.0
Co_28	61.6	63.6	62.6	1.373	36.4	13.6	50.0
Co_29	45.2	46.0	45.6	1.000	50.0	0.0	50.0
Co_30	55.4	56.2	55.8	1.224	40.9	9.1	50.0
Co_31	58.0	57.0	57.5	1.261	39.7	10.3	50.0
Co_32	60.3	61.3	60.8	1.333	37.5	12.5	50.0

Table A.V.2. Annotated metabolites from the IC-MS data of the concentration range experiment. Parameters used for determining whether it was a putative or confident identification. FS = fragmentation score, ME = mass error, ISS = isotope similarity score, RTE = retention time error, max. abun. = max abundance and min. CV% = minimum coefficient of variance, C = Confident and P = putative. When provided as a comment, the abbreviation indicates what brought the identification from confident to putative (RTE > 1.5 min, ME > 3 ppm, IS < 90%).

Accepted identification	FS	ME (ppm)	ISS	RTE (min)	Max. Abun.	Min. CV%	C/P	Comment
1-Pyrroline-5-carboxylic acid	0.0	0.37	99.1	0.00	317	2.6	P	Isomer of 4-hydroxyproline
2,3-Diphosphoglyceric acid	0.0	-0.04	97.6	-1.81	2777	22	P	RTE
2-butyl-3-ureido-succinate	0.0	0.56	97.7	0.99	106	8.9	C	
2-Hydroxybutyric acid	0.0	-0.04	97.8	1.35	346	10.2	P	Isomer of 3-hydroxybutyric acid
2-Hydroxyglutarate	83.0	0.22	99.8	-0.85	3815038	2.2	C	
2-Isopropylmalic acid	0.0	-0.29	92.2	-1.81	151	3.1	P	RTE
2-Ketobutyric acid	0.0	-0.14	98.1	0.11	339	3.3	C	
2-Oxoglutaric acid	39.9	0.33		-1.35	43690	4.9	C	
2-Phosphoglyceric acid	72.2	0.20	99.2	-1.88	47230	1.1	P	RTE and isomer of 3-phospho-glyceric acid
3,3 Dimethyl glutarate	58.3	-0.08	95.2	-0.99	692	11.8	C	
3,4-dihydroxyphenyl acetic acid	0.0	-0.07	90.9	-1.22	143	7.6	C	
3'-AMP	0.0	2.49	96.1	-0.36	351	5.2	P	Isomer of AMP
3-Dehydroquinate	0.0	-0.49	91.3	-0.03	173	4.3	C	
3-Hydroxyisovaleric acid	0.0	-4.34	97.7	-0.80	1810	5	P	ME
3-Hydroxymethyl-glutarate	78.6	-0.31	99.5	-0.99	9671	3.1	C	
3-Hydroxytyrosol	0.0	0.46	91.0	-1.21	276	6.1	C	
3-methoxyphenyl-acetic acid	0.0	-0.21	94.8	0.93	464	9.2	C	
3-Methyl-2-oxovaleric acid	0.0	0.59	98.1	-1.30	15156	4	P	Isomer of adipate semialdehyde
3-Phosphoglyceric acid	0.0	-0.12	98.5	0.46	5466	6.3	C	
4-Acetylbutyrate	0.0	4.74	94.8	-1.77	3248	7.5	P	RTE and ME
4-Hydroxybutyric acid	0.0	0.00	99.0	-0.70	57512	2.3	C	
4-hydroxyphenyl glycine	0.0	0.07	90.7	0.85	161	3.3	C	
4-Hydroxy-pyrrolidinone	0.0	-0.06	97.0	0.68	250	5.9	C	
6-Phosphogluconic acid	0.0	-0.41	96.6	-1.63	10041	3.3	P	RTE
Acetic acid	0.0	0.03	99.5	0.33	794	6.1	C	
Acetoacetate	0.0	-0.29	99.1	-0.04	665	2.1	C	
Acetylcysteine	34.8	0.13	94.4	-0.87	2391	4.5	C	
Acetylglycine	84.8	0.21	97.5	-0.07	1749	2.4	C	
Adenosine diphosphate	14.5	0.56	97.4	-1.60	258685	5.7	P	RTE

Accepted identification	FS	ME (ppm)	ISS	RTE (min)	Max. Abun.	Min. CV%	C/P	Comment
Adenosine monophosphate	54.1	0.93	96.0	-1.24	31926	4.5	P	Isomer of 3'-AMP
Adonitol	72.1	0.06	96.7	0.08	1064	2.5	P	Isomer of arabitol and xylitol
Allantoin	0.0	-3.76	95.8	-0.66	838	2.3	P	ME
Arabinonic acid	65.9	-0.27	97.2	-0.62	3508	2.1	C	
Ascorbate	3.6	-0.61	92.4	-1.30	369	1.6	C	
Aspartate	85.4	0.41	94.8	-0.81	469751	1.3	C	
Beta-Alanine	78.1	-0.02	96.8	-0.73	527	2.2	C	
Beta-Citryl-L-glutamic acid	0.0	1.00	98.6	-0.79	268643	4.7	C	
Caproic acid	0.0	-4.53	94.4	0.50	627	7.5	P	ME
Citric acid	87.8	-0.05	99.6	-1.63	1194317	3.7	P	RTE
Cysteic acid	79.3	-0.24	94.5	-1.30	3805	10.3	C	
Cytidine	0.0	4.53	92.3	-0.71	1505	2.1	C	
Cytidine monophosphate	39.8	0.74	92.5	-1.55	3550	5.1	P	RTE
Cytidine monophosphate N-acetylneuraminic acid	0.0	3.41	98.1	-0.71	29513	1.8	C	
Cytidine triphosphate	5.9	0.29	98.3	-1.80	350048	6.9	P	RTE
dADP	0.0	0.79	94.2	-0.77	616	9.5	C	
Deoxyribose 5-phosphate	9.7	0.93	96.2	0.01	3149	3.1	C	
Dihydrouracil	0.0	4.88	98.4	0.20	236	6.1	P	ME
Dihydroxyacetone	73.5	-0.06	99.4	-0.38	182028	5.8	P	Isomer of lactic acid
Dimethyl fumarate	0.0	0.52	95.4	-1.39	84	9.7	C	
dUDP	0.0	0.71	87.6	0.70	695	32.5	C	
dUMP	0.0	0.66	97.4	-1.66	84699	3.2	P	RTE
dUTP	0.0	0.37	91.6	-1.76	1743	15	P	RTE
EDTA	0.0	0.58	94.6	-1.46	369	10.6	C	
Ethylmalonic acid	73.6	0.31	96.1	-1.67	3691	5.3	P	Isomer of glutaric acid
Fructose 1,6-bisphosphate	0.0	0.82		-1.78	555	15.3	P	Isomer of fructose 2,6-bisphosphate
Fructose 2,6 diphosphate	0.0	0.89	98.8	-0.21	15786	4.5	C	
Fructose 6-phosphate	64.4	-0.45	95.9	-0.63	5982	5.2	P	Isomer of mannose 6-phosphate
Galactaric acid	43.8	0.28	91.2	-1.09	5233	3.8	C	
Galactose 1-phosphate	0.0	-0.03	95.7	-1.62	26507	1.9	P	RTE and isomer of glucose 1-phosphate
Galacturonic acid	64.8	-0.14	97.8	-0.05	5070	3.2	P	Isomer of glucuronic acid
Gluconate	56.1	-0.23		-0.49	43192	4.5	C	
Glucose	0.0	-0.16	47.3	1.57	323	6.9	P	Isomers

Accepted identification	FS	ME (ppm)	ISS	RTE (min)	Max. Abun.	Min. CV%	C/P	Comment
Glucose 1-phosphate	44.1	-0.40	98.9	-0.79	24946	3.7	P	Isomer of galactose 1-phosphate
Glucuronic acid	0.0	-0.04	96.3	1.58	391	4.3	P	Isomer of galacturonic acid
Glutamic acid	84.1	0.33	94.3	1.31	1008751	3.6	C	
Glutamylcysteine	0.0	-2.38	95.0	-1.74	183915	5.7	P	RTE
Glutathione (GSH)	43.8	0.62	94.4	-0.52	10194510	2.2	C	
Glyceric acid	2.8	-0.20		-0.95	1509	6	C	
Glycerol	0.0	-0.41	98.4	0.18	4147	3.2	C	
Glycerol 3-phosphate	26.6	0.06		-0.81	9661	1.5	C	
Glycolic acid	53.2	-0.66	98.6	-0.70	8858	2	C	
Guanosine diphosphate (GDP)	97.5	1.97	97.8	-0.24	694088	10.4	C	
Hippuric acid	0.0	-0.27	95.1	-1.30	554	3.9	C	
Homogentisic acid	0.0	-0.04	94.0	1.27	612	10.6	C	
Hydroxy-isobutyric acid	0.0	0.22	98.6	-0.93	467	6.7	P	Isomer of 2- and 3-hydroxybutyric acid
Hydroxyoctanoic acid	0.0	-3.28	96.3	-0.15	141	8.9	C	
Hydroxypyruvic acid	0.0	-0.06	95.9	-1.97	162	4.6	P	Isomer of malonic acid
Isocitrate	0.0	-0.63	97.4	-1.25	7747	5.6	P	Isomer of citric acid
Kojic acid	0.0	0.55	91.1	-0.85	730	2.5	C	
Kynurenic acid	0.0	0.42	88.8	1.09	349	4.8	P	ISS
Lactic acid	0.0	-1.40	97.8	0.14	2579	6.9	P	Isomer of dihydroxyacetone
Lactose	64.0	-0.48	94.4	-0.11	4007	26	C	
Lactoyl-isoleucine	0.0	-2.63	96.7	-0.06	1223	4.2	C	
Maleic acid	67.5	0.23	99.3	-0.30	10628	1.4	P	Isomer of fumarate
Malic acid	36.9	0.36	99.8	-0.91	198555	1.1	C	
Malondialdehyde	0.0	-1.86	99.3	1.37	1227	1.2	C	
Malonic acid	79.2	0.16	98.3	-1.42	2431	2.3	P	Isomer of hydroxypyruvic acid
Mannitol	0.0	0.07	96.6	0.95	537	11.7	P	Isomer of sorbitol
Methylglutaric acid	39.8	1.22	96.2	-0.68	3553	10.1	C	
Methylisocitric acid	0.0	-0.09	95.8	-1.18	2016	2.2	P	Isomer of 2-methylcitric acid
Myoinositol	87.6	-0.18	98.2	0.13	128447	2.6	P	Isomers
N-Acetyl-aspartate	91.5	-0.43	93.0	-0.66	135415	4.2	C	
N-Acetylaspartyl-glutamic acid	0.0	0.59	97.1	-1.15	19062	4.8	C	

Accepted identification	FS	ME (ppm)	ISS	RTE (min)	Max. Abun.	Min. CV%	C/P	Comment
N-acetyl-glucosamine-1-phosphate	0.0	0.45	92.6	-0.16	1881	6.5	P	Isomer of N-acetylmannosamine 6-phosphate and N-acetyl-glucosamine 6-phosphate
N-Acetylglutamate	74.1	-2.96	98.1	-0.66	10239	4.2	C	
N-Acetyl-L-alanine	92.4	-0.14	98.3	-0.23	5888	3.4	C	
N-Acetyl-L-methionine	86.4	0.02	97.3	-0.43	6599	3.2	C	
N-Acetyl-L-phenylalanine	0.0	0.66	95.9	-0.54	105	6.5	C	
N-Acetylneuraminic acid (Sialic acid)	89.1	0.51	94.8	-0.47	5185	3.3	C	
N-Acetylvaline	80.8	0.14	97.8	-0.29	197	8.9	C	
NADH	86.7	1.19	93.7	-0.90	23985	11.9	C	
NADPH	0.0	0.87	95.7	0.70	32123	34.2	C	
N-Formyl-methionine	0.0	-0.49	94.2	-0.67	871	1.9	C	
Nonate	0.0	-2.98	97.9	-0.60	12681	20.6	C	
N-Oxalylglycine	0.0	0.32	94.3	-1.25	32	36.9	C	
O-Acetylserine	0.0	0.19	98.2	-0.36	36592	1.1	C	
O-Phosphoserine	84.2	0.15	98.9	-1.13	22654	7.8	C	
Ophthalmic Acid	0.0	-1.45	92.7	0.15	1958	2.3	C	
Oxalic acid	44.6	0.11	98.0	-1.44	12438	2.1	C	
Oxoadipic acid	64.4	-0.09	95.9	-1.66	829	2.6	P	RTE
Oxovaleric Acid	0.0	-4.54	96.4	0.11	2485	2.8	P	MTE
Pantothenic acid	59.7	-0.19	99.1	-0.55	165518	3.2	C	
Phosphocreatine	17.8	-2.55	98.2	-0.41	218068	3.1	C	
Phosphoribosyl pyrophosphate	0.0	0.79	98.5	-1.58	12476	1.6	P	RTE
Pyroglutamic acid	19.2	-3.91	94.0	-0.31	166415	5.9	P	RTE
Pyruvic acid	60.0	-0.27	98.5	-0.84	12896	5	C	
Quinolinic acid	0.0	0.16	91.5	-1.61	39	7.3	P	RTE
Ribose 5-phosphate	66.6	0.62	88.6	-1.50	1251	3.8	P	Isomer of xylulose 5-phosphate
Ribulose 1,5,diphosphate	0.0	-1.12	98.7	0.90	9809	3.9	P	RTE
Salicylic acid	0.0	-3.54	94.2	0.21	4381	5	P	ME
Sedoheptulose 1-phosphate	0.0	0.15	95.2	-0.32	2846	4.7	C	
Sedoheptulose 7-phosphate	57.6	0.22		-1.08	2052	6.6	P	Isoemr of seduheptulose 1-phosphate
Serine	77.4	0.29	96.0	-1.16	440	3.9	C	
Sorbitol	54.9	-0.29	98.1	0.17	6475	5.8	P	Isomer of mannitol
Sorbitol-6-phosphate	0.0	-0.41	97.3	0.33	1933	6.1	C	
Succinic acid	88.5	0.42	98.6	-0.96	14477	3.5	C	
Taurine	92.1	0.03	93.3	-0.51	255875	2	C	
TDP	96.7	0.88	97.9	1.97	27457	3.2	C	
Threitol	87.6	0.24	97.2	0.26	896	4.4	C	

Accepted identification	FS	ME (ppm)	ISS	RTE (min)	Max. Abun.	Min. CV%	C/P	Comment
Thymidine 5'-phosphate (TMP)	86.3	1.47	94.0	-1.27	4318	2.5	C	
Thymidine triphosphate	5.7	0.20	97.6	-1.73	18812	3.2	P	RTE
UDP-galactose	0.0	1.50	95.0	-1.25	40817	11.2	P	Isomer of UDP-glucose
Ureidopropionic acid	0.0	-3.73	94.3	0.73	161	19.8	P	ME
Uridine 5'-monophosphate	46.5	1.10	97.7	-1.85	150381	2.6	P	RTE
Xylulose	19.9	-0.15	95.7	0.45	631	6.7	P	Isomers

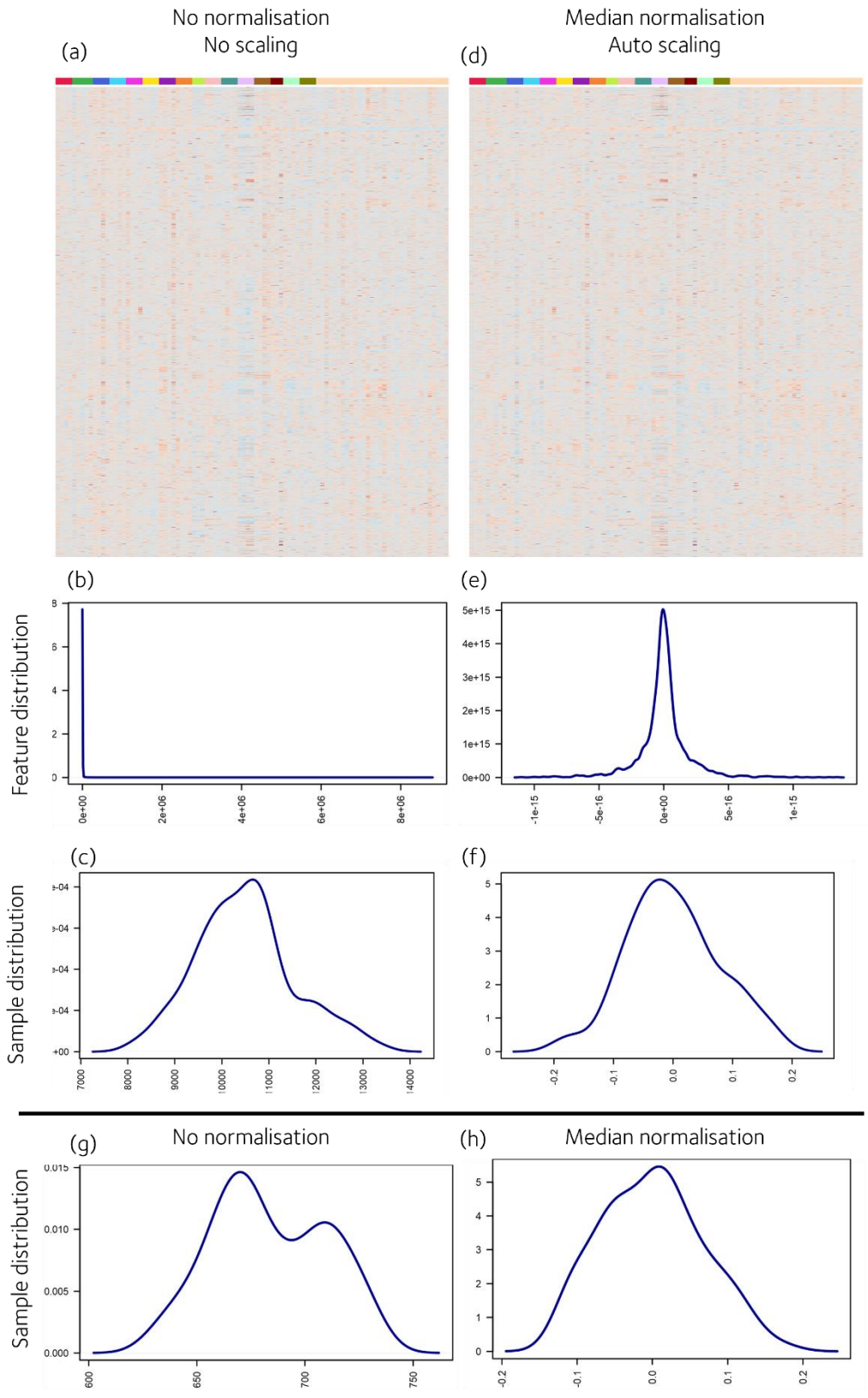

Figure A.V.1. Heatmaps and feature and sample distribution plots used in the assessment of IC-MS and derivatised RPLC-MS data the concetration range experiment. Heatmap, feature and sample distribution plots of IC-MS data (a-c) before and (d-f) after median normalisation and auto-scaling. Sample distribution plot of derivatised RPLC-MS data (g) before and (h) after median normalisation. Number of biological replicates is N = 4 treated group (N = 3 for AG-881 (5.00 µM)) and N = 32 for control.

Table A.V.3. Annotated metabolites from the derivatised RPLC-MS data of the concentration range experiment. Parameters used for determining whether it was a putative or confident identification. ME = mass error, ISS = isotope similarity score, RTE = retention time error, max. abun. = max abundance and min. CV% = minimum coefficient of variance, C = Confident and P = putative. When provided as a comment, the abbreviation indicates what brought the identification from confident to putative (isomer, RTE > 0.5 min, ME > 3 ppm, IS < 90%).

Accepted Description	ME (ppm)	ISS	RTE (min)	Max. abun.	Min. CV%	C/P	Comment
1,3-Diaminopropane	-4.78	93.2	0.12	5.3	15.5	P	ME
2-Aminoadipic acid	-1.27	97.1	0.13	728.6	5.9	C	
4-Hydroxyproline	-2.26	93.5		94.5	3.8	P	No RT
Adrenaline	3.76	92	0.95	31.1	4.2	P	RTE and ME
Alanine	-1.55	94.9	0.18	17420.2	1.9	C	
GABA	-3.45	96.7	0.1	133.6	4.1	P	ME
Arginine	-3.19	94	0.17	235.9	2.1	P	ME
Asparagine	-3.37	93.7	0.05	243.3	4.7	P	ME
beta-Alanine	-0.44	96.7	0.2	2487.5	4.4	C	
Citrulline	-4.54	89.2	0.14	30.4	8.3	P	ME
Cysteine	-2.93	93.5	-0.92	201.4	6.2	P	ME
Glutamic acid	-1.04	94.1	0.17	11722.9	5.5	C	
Glutamine	-2.06	94.7	0.12	5869.5	1.7	C	
Glycine	-2.43	95.6	0.22	5173.9	4.2	C	
Histidine	-3.24	97.5	0.13	607.6	3.9	P	ME
Homoserine	-3.45	96	0.17	106.5	10	P	ME
Hydroxyarginine	4.81	92.8		8.9	7.9	P	No confirmed RT
Hypotaurine	-1.21	95.2	0.22	478.3	4.8	C	
Isobutylamine	-2.95	96.5	-0.35	1758	27.3	C	
Isoleucine	-1.48	93.2	0.23	6431.2	1.4	P	Isomer of leucine
Leucine	-1.59	94.6	0.04	6049.4	3.5	P	Isomer of isoleucine
Lysine	-2.26	94.8	0.12	3860.5	4.4	C	
N-Acetyl-ornithine	-2.83	93.5	0.04	35.1	7.5	P	Isomer of L-Theanine
Octapine	-3.71	92.8		1168.5	5.8	P	No RT
Oxidised Glutathione	-1.67	89	0.05	5382.6	9.9	P	ISS
Phenylalanine	-2.08	96.1	0.13	4418.3	2.2	C	
Proline	-2.81	97.4	0.18	999	1.4	C	
Putrescine	-1.84	96.8	0.06	862.4	6.7	C	
Pyroglutamic Acid	-1.57	95.6	-0.91	75	10.6	P	Isomer of [M+H-H2O] adduct of glutamate
Serine	-3.02	94.7	0.23	1499.2	1.5	C	
Serotonin	-3.15	88.2	0.05	13.4	7.1	P	ISS and isomer of N-acetylproline
Taurine	-2.51	93.3		3075.6	4.6	P	No RT
Thioproline	-1.52	92.1	-0.13	208.3	4.3	C	
Threonine	-1.43	96.4	0.17	7965.3	2	C	
Tryptophan	-3.01	94.5	0.1	832.1	4	C	
Tyrosine	-2.19	93.5	0.12	3287.5	2.3	C	
Valine	-1.65	96.2	0.14	5333.1	2.3	C	

9.6. Appendix VI

The experiment that the data in this appendix is based on was the S-TICO and L-TICO experiments described in **chapter 4** (**section 4.7**) and **chapter 5**. The cell viability assay is provided in **Figure A.VI.**1. This appendix includes a DNA concentration table for the S-TICO experiment (**Table A.VI.1**) and the L-TICO experiment (**Table A.VI.2**), IC-MS identifications (**Table A.VI.3** and **A.VI.4**), derivatised RPLC-MS identifications (**Table A.VI.5** and **Table A.VI.6**), and data processing information (**Figure A.VI.2-4**).

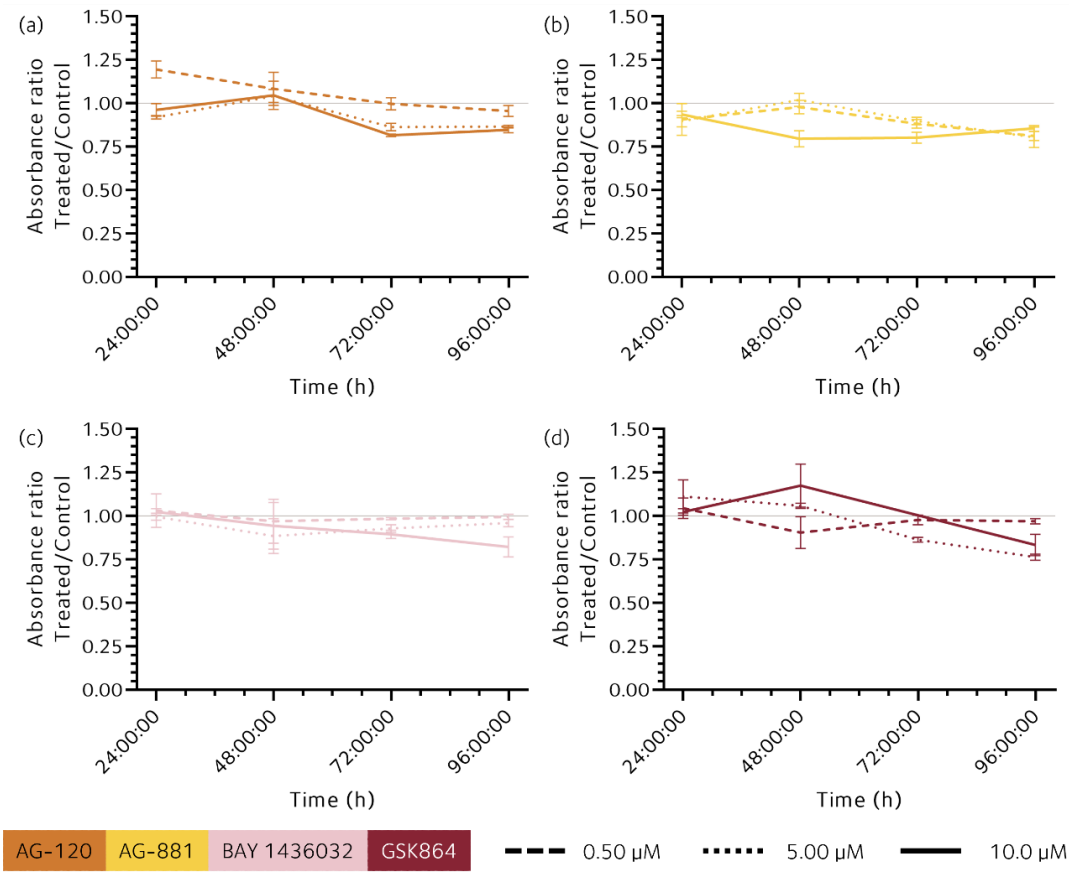

Figure A.VI.1. Ratio of absorbance between treated and control samples in an MTS assay of mutIDH1^{R132H} LN18 cells cultured for 24-96 hours with mutIDH1 inhibitors (a) AG-120, (b) AG-881, (c) BAY 1436032 or (d) GSK864. Cells were treated with 0.50, 5.00 or 10.0 µM inhibitor, which was added after an initial 24 hours of incubation. Each point is the mean ratio of absorbance at 490 nm of treated versus control samples, N = 4 treated samples and N = 12 control samples (biological replicates). Error bars are standard deviation.

Table A.VI.1. DNA concentration of mutIDH1R132H LN18 cells from the short time course (S-TICO) experiment. Harvested with 12-well harvesting method and subsequently analysed with IC-MS, derivatised RPLC-MS and underivatized RPLC-MS. The maximum possible volume was made up for each sample, usually 50 µL and sometimes less. Rel. DNA conc. = relative DNA concentration.

Sample Name	DNA 1 (ng/µL)	DNA 2 (ng/µL)	DNA 3 (ng/µL)	Average (ng/µL)	Rel. DNA conc.	µL Sample	µL Solvent	Total (µL)
1h-AG120_01	26.90	27.20		27.05	1.202	28.0	5.7	33.7
1h-AG120_02	32.40	29.50		30.95	1.376	32.7	12.3	45.0
1h-AG120_03	31.00	29.50		30.25	1.344	29.8	10.2	40.0
1h-AG120_04	33.10	31.90		32.50	1.444	34.6	15.4	50.0
1h-AG881_01	31.50	28.20		29.85	1.327	37.7	12.3	50.0
1h-AG881_02	27.70	26.90		27.30	1.213	41.2	8.8	50.0
1h-AG881_03	25.30	25.40		25.35	1.127	39.9	5.1	45.0
1h-AG881_04	23.10	25.20		24.15	1.073	46.6	3.4	50.0
1h-BAY_01	32.60	30.80		31.70	1.409	31.9	13.1	45.0
1h-BAY_02	29.30	28.10		28.70	1.276	31.4	8.6	40.0
1h-BAY_03	30.90	27.90		29.40	1.307	36.0	11.0	47.0
1h-BAY_04	43.10	46.70		44.90	1.996	25.1	24.9	50.0
1h-Co_01	29.80	30.50		30.15	1.340	37.3	12.7	50.0
1h-Co_02	31.10	27.60		29.35	1.304	38.3	11.7	50.0
1h-Co_03	23.00	22.30		22.65	1.007	44.7	0.5	45.2
1h-Co_04	25.20	25.40		25.30	1.124	44.5	5.5	50.0
1h-Co_05	32.70	34.90		33.80	1.502	33.3	16.7	50.0
1h-Co_06	32.40	34.10		33.25	1.478	29.0	13.9	42.9
1h-Co_07	33.00	31.10		32.05	1.424	35.1	14.9	50.0
1h-Co_08	29.30	29.20		29.25	1.300	25.0	7.5	32.5
1h-GSK_01	27.70	27.70		27.70	1.231	32.5	7.5	40.0
1h-GSK_02	32.00	28.00	25.80	28.60	1.271	38.0	10.3	48.3
1h-GSK_03	25.50	27.00		26.25	1.167	38.6	6.4	45.0
1h-GSK_04	25.40	26.50		25.95	1.153	43.4	6.6	50.0
2h-AG120_01	43.50	41.20	43.90	42.87	1.905	26.2	23.8	50.0
2h-AG120_02	31.00	28.10		29.55	1.313	34.3	10.7	45.0
2h-AG120_03	26.00	26.30		26.15	1.162	34.4	5.6	40.0
2h-AG120_04	24.90	23.90		24.40	1.084	46.1	3.9	50.0
2h-AG881_01	36.10			36.10	1.604	28.0	17.0	45.0
2h-AG881_02	35.40	36.90		36.15	1.607	31.1	18.9	50.0
2h-AG881_03	25.30	25.60		25.45	1.131	35.4	4.6	40.0
2h-AG881_04	36.20	37.50		36.85	1.638	30.5	19.5	50.0
2h-BAY_01	25.50	24.20		24.85	1.104	38.0	4.0	42.0

2h-BAY_02	**25.10**			**25.10**	**1.116**	**39.7**	**4.6**	**44.3**
2h-BAY_03	**25.90**	**25.10**		**25.50**	**1.133**	**39.2**	**5.2**	**44.4**
2h-BAY_04	**25.90**	**25.00**		**25.45**	**1.131**	**35.4**	**4.6**	**40.0**
2h-Co_01	**32.70**	**35.00**		**33.85**	**1.504**	**33.2**	**16.8**	**50.0**
2h-Co_02	**36.80**	**32.70**	**34.10**	**34.53**	**1.535**	**24.0**	**12.8**	**36.8**
2h-Co_03	**33.00**	**31.30**		**32.15**	**1.429**	**31.5**	**13.5**	**45.0**
2h-Co_04	**23.10**	**23.30**		**23.20**	**1.031**	**36.0**	**1.2**	**37.2**
2h-Co_05	**24.30**	**24.20**		**24.25**	**1.078**	**39.5**	**3.1**	**42.6**
2h-Co_06	**25.30**	**21.10**	**21.10**	**22.50**	**1.000**	**38.0**	**0.0**	**38.0**
2h-Co_07	**33.90**	**29.00**		**31.45**	**1.398**	**34.8**	**13.9**	**48.7**
2h-Co_08	**37.00**	**35.20**		**36.10**	**1.604**	**31.2**	**18.8**	**50.0**
2h-GSK_01	**26.50**	**27.60**		**27.05**	**1.202**	**32.0**	**6.5**	**38.5**
2h-GSK_02	**26.30**	**26.70**		**26.50**	**1.178**	**34.0**	**6.0**	**40.0**
2h-GSK_03	**26.60**	**25.70**		**26.15**	**1.162**	**34.4**	**5.6**	**40.0**
2h-GSK_04	**28.50**	**32.70**		**30.60**	**1.360**	**33.1**	**11.9**	**45.0**
4h-AG120_01	**35.40**	**35.70**		**35.55**	**1.580**	**28.5**	**16.5**	**45.0**
4h-AG120_02	**43.20**	**44.30**		**43.75**	**1.944**	**25.7**	**24.3**	**50.0**
4h-AG120_03	**41.10**	**37.10**		**39.10**	**1.738**	**28.8**	**21.2**	**50.0**
4h-AG120_04	**39.80**	**41.20**		**40.50**	**1.800**	**27.8**	**22.2**	**50.0**
4h-AG881_01	**40.20**	**38.60**		**39.40**	**1.751**	**28.6**	**21.4**	**50.0**
4h-AG881_02	**39.30**	**40.40**		**39.85**	**1.771**	**28.2**	**21.8**	**50.0**
4h-AG881_03	**38.70**	**39.80**		**39.25**	**1.744**	**28.7**	**21.3**	**50.0**
4h-AG881_04	**39.50**	**40.60**		**40.05**	**1.780**	**28.1**	**21.9**	**50.0**
4h-BAY_01	**25.20**	**24.20**		**24.70**	**1.098**	**36.4**	**3.6**	**40.0**
4h-BAY_02	**28.30**	**26.00**		**27.15**	**1.207**	**33.1**	**6.9**	**40.0**
4h-BAY_03	**29.20**	**30.10**		**29.65**	**1.318**	**37.9**	**12.1**	**50.0**
4h-BAY_04	**32.10**	**33.80**		**32.95**	**1.464**	**34.1**	**15.9**	**50.0**
4h-Co_01	**31.50**	**28.90**		**30.20**	**1.342**	**33.5**	**11.5**	**45.0**
4h-Co_02	**43.00**	**45.10**		**44.05**	**1.958**	**25.5**	**24.5**	**50.0**
4h-Co_03	**30.70**	**32.40**		**31.55**	**1.402**	**35.7**	**14.3**	**50.0**
4h-Co_04	**40.50**	**41.20**		**40.85**	**1.816**	**27.5**	**22.5**	**50.0**
4h-Co_05	**28.70**	**31.70**		**30.20**	**1.342**	**33.5**	**11.5**	**45.0**
4h-Co_06	**34.50**	**35.30**		**34.90**	**1.551**	**32.2**	**17.8**	**50.0**
4h-Co_07	**39.30**	**39.80**		**39.55**	**1.758**	**28.4**	**21.6**	**50.0**
4h-Co_08	**60.50**	**58.60**		**59.55**	**2.647**	**18.9**	**31.1**	**50.0**
4h-GSK_01	**40.90**	**41.10**		**41.00**	**1.822**	**27.4**	**22.6**	**50.0**
4h-GSK_02	**33.00**	**33.40**		**33.20**	**1.476**	**33.9**	**16.1**	**50.0**
4h-GSK_03	**36.20**	**39.40**		**37.80**	**1.680**	**29.8**	**20.2**	**50.0**
4h-GSK_04	**37.40**	**38.30**		**37.85**	**1.682**	**29.7**	**20.3**	**50.0**
8h-AG120_01	**28.50**	**27.60**		**28.05**	**1.247**	**40.1**	**9.9**	**50.0**
8h-AG120_02	**36.20**	**31.20**	**33.80**	**33.73**	**1.499**	**33.3**	**16.7**	**50.0**
8h-AG120_03	**32.90**	**32.20**		**32.55**	**1.447**	**34.6**	**15.4**	**50.0**

8h-AG120_04	29.40	29.50		29.45	1.309	32.0	9.9	41.9
8h-AG881_01	37.00	36.20		36.60	1.627	30.7	19.3	50.0
8h-AG881_02	38.20	37.90		38.05	1.691	29.6	20.4	50.0
8h-AG881_03	32.60	34.10		33.35	1.482	33.7	16.3	50.0
8h-AG881_04	31.50	29.80		30.65	1.362	36.7	13.3	50.0
8h-BAY_01	25.60	23.70		24.65	1.096	28.0	2.7	30.7
8h-BAY_02	31.10	30.60		30.85	1.371	36.5	13.5	50.0
8h-BAY_03	27.30	27.40		27.35	1.216	41.1	8.9	50.0
8h-BAY_04	29.60	32.50		31.05	1.380	36.2	13.8	50.0
8h-Co_01	31.60	31.40		31.50	1.400	35.7	14.3	50.0
8h-Co_02	48.20	42.30		45.25	2.011	24.9	25.1	50.0
8h-Co_03	33.30	31.60		32.45	1.442	34.7	15.3	50.0
8h-Co_04	25.90	28.70	27.90	27.50	1.222	40.9	9.1	50.0
8h-Co_05	29.90	28.10		29.00	1.289	34.9	10.1	45.0
8h-Co_06	30.60	29.50		30.05	1.336	30.0	10.0	40.0
8h-Co_07	23.20	23.60		23.40	1.040	36.0	1.4	37.4
8h-Co_08	34.10	31.80		32.95	1.464	34.1	15.9	50.0
8h-GSK_01	26.30	25.90		26.10	1.160	43.1	6.9	50.0
8h-GSK_02	37.90	36.60		37.25	1.656	30.2	19.8	50.0
8h-GSK_03	29.30	29.80		29.55	1.313	38.1	11.9	50.0
8h-GSK_04	29.70	30.50		30.10	1.338	37.4	12.6	50.0
12h-AG120_01	37.30	34.30		35.80	1.591	31.4	18.6	50.0
12h-AG120_02	40.00	40.80		40.40	1.796	27.8	22.2	50.0
12h-AG120_03	40.70	39.50		40.10	1.782	28.1	21.9	50.0
12h-AG120_04	40.20	40.50		40.35	1.793	27.9	22.1	50.0
12h-AG881_01	27.60	27.80		27.70	1.231	29.0	6.7	35.7
12h-AG881_02	35.80	37.10		36.45	1.620	30.9	19.1	50.0
12h-AG881_03	29.60	30.90		30.25	1.344	37.2	12.8	50.0
12h-AG881_04	37.30	36.70		37.00	1.644	30.4	19.6	50.0
12h-BAY_01	22.50	24.60		23.55	1.047	38.2	1.8	40.0
12h-BAY_02	33.80	32.20		33.00	1.467	30.7	14.3	45.0
12h-BAY_03	32.50	30.40		31.45	1.398	35.0	13.9	48.9
12h-BAY_04	30.80	31.10		30.95	1.376	36.3	13.7	50.0
12h-Co_01	30.90	32.40		31.65	1.407	27.9	11.4	39.3
12h-Co_02	33.00	34.70		33.85	1.504	33.2	16.8	50.0
12h-Co_03	32.10	34.10		33.10	1.471	34.0	16.0	50.0
12h-Co_04	36.60	36.30		36.45	1.620	30.9	19.1	50.0

12h-Co_05	40.60	39.90		40.25	1.789	28.0	22.0	50.0
12h-Co_06	39.50	36.10		37.80	1.680	29.8	20.2	50.0
12h-Co_07	35.40	35.50		35.45	1.576	31.7	18.3	50.0
12h-Co_08	43.80	42.80		43.30	1.924	26.0	24.0	50.0
12h-GSK_01	34.90	36.80		35.85	1.593	31.4	18.6	50.0
12h-GSK_02	35.20	32.00		33.60	1.493	33.5	16.5	50.0
12h-GSK_03	26.30	25.50		25.90	1.151	43.4	6.6	50.0
12h-GSK_04	31.70	31.70		31.70	1.409	35.5	14.5	50.0
24h-AG120_01	40.80	42.40		41.60	1.849	27.0	23.0	50.0
24h-AG120_02	41.00	39.10		40.05	1.780	28.1	21.9	50.0
24h-AG120_03	43.80	42.80		43.30	1.924	26.0	24.0	50.0
24h-AG120_04	44.70	47.50		46.10	2.049	24.4	25.6	50.0
24h-AG881_01	54.10	54.20		54.15	2.407	20.8	29.2	50.0
24h-AG881_02	46.40	44.00		45.20	2.009	24.9	25.1	50.0
24h-AG881_03	47.10	47.70		47.40	2.107	23.7	26.3	50.0
24h-AG881_04	47.20	49.70		48.45	2.153	23.2	26.8	50.0
24h-BAY_01	30.60	30.60		30.60	1.360	36.8	13.2	50.0
24h-BAY_02	48.10	44.50		46.30	2.058	24.3	25.7	50.0
24h-BAY_03	40.00	41.10		40.55	1.802	27.7	22.3	50.0
24h-BAY_04	41.70	35.90	38.00	38.53	1.713	29.2	20.8	50.0
24h-Co_01	34.60	35.90		35.25	1.567	31.9	18.1	50.0
24h-Co_02	42.70	43.80		43.25	1.922	26.0	24.0	50.0
24h-Co_03	45.60	47.80	47.80	47.07	2.092	23.9	26.1	50.0
24h-Co_04	48.50	51.30		49.90	2.218	22.5	27.5	50.0
24h-Co_05	44.30	43.10		43.70	1.942	25.7	24.3	50.0
24h-Co_06	64.10	60.40		62.25	2.767	18.1	31.9	50.0
24h-Co_07	48.20	49.30		48.75	2.167	23.1	26.9	50.0
24h-Co_08	47.30	47.00		47.15	2.096	23.9	26.1	50.0
24h-GSK_01	41.90	42.10		42.00	1.867	26.8	23.2	50.0
24h-GSK_02	41.70	42.80		42.25	1.878	26.6	23.4	50.0
24h-GSK_03	43.90	42.00		42.95	1.909	26.2	23.8	50.0
24h-GSK_04	50.90	46.30		48.60	2.160	23.1	26.9	50.0

Table A.VI.2. DNA concentration of mutIDH1R132H LN18 cells from the long time course (L-TICO) experiment. Harvested with 12-well harvesting method and subsequently analysed with IC-MS, derivatised RPLC-MS and underivatized RPLC-MS. The maximum possible volume was made up for each sample, usually 50 µL and sometimes less. Rel. DNA conc. = relative DNA concentration. Treatment length: A = 24 hours, B = 48 hours, C = 72 hours and D = 96 hours. Group 1 and group 2 indicated with number after treatment length.

Sample Name	DNA 1 (ng/µL)	DNA 2 (ng/µL)	Average (ng/µL)	Rel. DNA conc.	µL Sample	µL Solvent	Total (µL)
A-AG120_01	58.4	59.5	58.95	2.661	18.8	31.2	50.0
A-AG120_02	58.1	56.6	57.35	2.589	19.3	30.7	50.0
A-AG120_03	58.1	57.4	57.75	2.607	19.2	30.8	50.0
A-AG120_04	51.1	53.4	52.25	2.359	21.2	28.8	50.0
A-AG881_01	47.1	46.8	46.95	2.120	23.6	26.4	50.0
A-AG881_02	58.4	56.4	57.40	2.591	19.3	30.7	50.0
A-AG881_03	55.2	56.1	55.65	2.512	19.9	30.1	50.0
A-AG881_04	53.2	53.6	53.40	2.411	20.7	29.3	50.0
A-BAY_01	43.1	46.5	44.80	2.023	24.7	25.3	50.0
A-BAY_02	54.7	54.8	54.75	2.472	20.2	29.8	50.0
A-BAY_03	62.3	59.8	61.05	2.756	18.1	31.9	50.0
A-BAY_04	35.9	34.0	34.95	1.578	31.7	18.3	50.0
A-Co_01	56.3	56.9	56.60	2.555	19.6	30.4	50.0
A-Co_02	52.2	52.8	52.50	2.370	21.1	28.9	50.0
A-Co_03	56.7	55.0	55.85	2.521	19.8	30.2	50.0
A-Co_04	56.7	55.6	56.15	2.535	19.7	30.3	50.0
A-Co_05	48.5	49.2	48.85	2.205	22.7	27.3	50.0
A-Co_06	52.1	51.1	51.60	2.330	21.5	28.5	50.0
A-Co_07	52.6	50.3	51.45	2.323	21.5	28.5	50.0
A-Co_08	57.7	57.8	57.75	2.607	19.2	30.8	50.0
A-GSK_01	59.0	59.5	59.25	2.675	18.7	31.3	50.0
A-GSK_02	52.8	53.2	53.00	2.393	20.9	29.1	50.0
A-GSK_03	60.7	59.2	59.95	2.707	18.5	31.5	50.0
A-GSK_04	54.3	53.4	53.85	2.431	20.6	29.4	50.0
B1-AG120_01	69.8		69.80	3.151	15.9	34.1	50.0
B1-AG120_02	80.9	82.6	81.75	3.691	13.5	36.5	50.0
B1-AG120_03	77.3	78.2	77.75	3.510	14.2	35.8	50.0
B1-AG120_04	85.9	86.0	85.95	3.880	12.9	37.1	50.0
B1-AG881_01	46.3	46.5	46.40	2.095	23.9	26.1	50.0
B1-AG881_02	52.8	50.2	51.50	2.325	21.5	28.5	50.0
B1-AG881_03	81.2	79.2	80.20	3.621	13.8	36.2	50.0
B1-AG881_04	95.4	97.1	96.25	4.345	11.5	38.5	50.0
B1-BAY_01	60.8	61.6	61.20	2.763	18.1	31.9	50.0
B1-BAY_02	66.5	67.1	66.80	3.016	16.6	33.4	50.0
B1-BAY_03	70.3	68.7	69.50	3.138	15.9	34.1	50.0
B1-BAY_04	61.1	61.2	61.15	2.761	18.1	31.9	50.0
B1-Co_01	39.2	39.7	39.45	1.781	28.1	21.9	50.0
B1-Co_02	51.6	51.2	51.40	2.321	21.5	28.5	50.0
B1-Co_03	49.1	49.3	49.20	2.221	22.5	27.5	50.0
B1-Co_04	50.3	50.0	50.15	2.264	22.1	27.9	50.0
B1-Co_05	46.4	45.8	46.10	2.081	24.0	26.0	50.0
B1-Co_06	60.6	59.5	60.05	2.711	18.4	31.6	50.0
B1-Co_07	62.3	59.4	60.85	2.747	18.2	31.8	50.0
B1-Co_08	67.2	69.2	68.20	3.079	16.2	33.8	50.0
B1-GSK_01	46.4	49.9	48.15	2.174	23.0	27.0	50.0

B1-GSK_02	**57.1**	**57.1**	**57.10**	**2.578**	**19.4**	**30.6**	**50.0**
B1-GSK_03	**65.8**	**64.9**	**65.35**	**2.950**	**16.9**	**33.1**	**50.0**
B1-GSK_04	**61.2**	**59.6**	**60.40**	**2.727**	**18.3**	**31.7**	**50.0**
B2-AG120_01	**35.0**	**33.4**	**34.20**	**1.544**	**32.4**	**17.6**	**50.0**
B2-AG120_02	**36.7**	**35.4**	**36.05**	**1.628**	**30.7**	**19.3**	**50.0**
B2-AG120_03	**39.9**	**41.0**	**40.45**	**1.826**	**27.4**	**22.6**	**50.0**
B2-AG120_04	**45.1**	**46.1**	**45.60**	**2.059**	**24.3**	**25.7**	**50.0**
B2-AG881_01	**37.3**	**36.8**	**37.05**	**1.673**	**29.9**	**20.1**	**50.0**
B2-AG881_02	**42.6**	**41.9**	**42.25**	**1.907**	**26.2**	**23.8**	**50.0**
B2-AG881_03	**43.6**	**43.2**	**43.40**	**1.959**	**25.5**	**24.5**	**50.0**
B2-AG881_04	**51.0**	**51.4**	**51.20**	**2.312**	**21.6**	**28.4**	**50.0**
B2-BAY_01	**34.3**	**34.1**	**34.20**	**1.544**	**32.4**	**17.6**	**50.0**
B2-BAY_02	**42.5**	**41.8**	**42.15**	**1.903**	**26.3**	**23.7**	**50.0**
B2-BAY_03	**44.1**	**45.8**	**44.95**	**2.029**	**24.6**	**25.4**	**50.0**
B2-BAY_04	**52.9**	**50.3**	**51.60**	**2.330**	**21.5**	**28.5**	**50.0**
B2-Co_01	**43.1**	**43.4**	**43.25**	**1.953**	**25.6**	**24.4**	**50.0**
B2-Co_02	**37.4**	**36.7**	**37.05**	**1.673**	**29.9**	**20.1**	**50.0**
B2-Co_03	**48.8**	**49.9**	**49.35**	**2.228**	**22.4**	**27.6**	**50.0**
B2-Co_04	**51.6**	**52.7**	**52.15**	**2.354**	**21.2**	**28.8**	**50.0**
B2-Co_05	**41.8**	**43.4**	**42.60**	**1.923**	**26.0**	**24.0**	**50.0**
B2-Co_06	**49.0**	**49.5**	**49.25**	**2.223**	**22.5**	**27.5**	**50.0**
B2-Co_07	**38.2**	**38.4**	**38.30**	**1.729**	**28.9**	**21.1**	**50.0**
B2-Co_08	**47.4**	**48.1**	**47.75**	**2.156**	**23.2**	**26.8**	**50.0**
B2-GSK_01	**36.3**	**36.0**	**36.15**	**1.632**	**30.6**	**19.4**	**50.0**
B2-GSK_02	**41.9**	**42.3**	**42.10**	**1.901**	**26.3**	**23.7**	**50.0**
B2-GSK_03	**48.2**	**48.3**	**48.25**	**2.178**	**23.0**	**27.0**	**50.0**
B2-GSK_04	**43.6**	**42.8**	**43.20**	**1.950**	**25.6**	**24.4**	**50.0**
C1-AG120_01	**34.5**	**34.2**	**34.35**	**1.551**	**32.2**	**17.8**	**50.0**
C1-AG120_02	**39.7**	**40.2**	**39.95**	**1.804**	**27.7**	**22.3**	**50.0**
C1-AG120_03	**44.9**	**43.8**	**44.35**	**2.002**	**25.0**	**25.0**	**50.0**
C1-AG120_04	**47.4**	**48.4**	**47.90**	**2.163**	**23.1**	**26.9**	**50.0**
C1-AG881_01	**46.1**	**45.5**	**45.80**	**2.068**	**24.2**	**25.8**	**50.0**
C1-AG881_02	**46.3**	**46.1**	**46.20**	**2.086**	**24.0**	**26.0**	**50.0**
C1-AG881_03	**55.3**	**55.9**	**55.60**	**2.510**	**19.9**	**30.1**	**50.0**
C1-AG881_04	**31.1**	**30.4**	**30.75**	**1.388**	**36.0**	**14.0**	**50.0**
C1-BAY_01	**43.4**	**43.7**	**43.55**	**1.966**	**25.4**	**24.6**	**50.0**
C1-BAY_02	**40.1**	**40.6**	**40.35**	**1.822**	**27.4**	**22.6**	**50.0**
C1-BAY_03	**51.4**	**51.3**	**51.35**	**2.318**	**21.6**	**28.4**	**50.0**
C1-BAY_04	**43.2**	**41.7**	**42.45**	**1.916**	**26.1**	**23.9**	**50.0**
C1-Co_01	**40.5**	**40.3**	**40.40**	**1.824**	**27.4**	**22.6**	**50.0**
C1-Co_02	**28.9**	**28.6**	**28.75**	**1.298**	**38.5**	**11.5**	**50.0**
C1-Co_03	**50.1**	**51.1**	**50.60**	**2.284**	**21.9**	**28.1**	**50.0**
C1-Co_04	**48.1**	**48.4**	**48.25**	**2.178**	**23.0**	**27.0**	**50.0**
C1-Co_05	**43.7**	**44.2**	**43.95**	**1.984**	**25.2**	**24.8**	**50.0**
C1-Co_06	**48.4**	**48.5**	**48.45**	**2.187**	**22.9**	**27.1**	**50.0**
C1-Co_07	**50.3**	**50.0**	**50.15**	**2.264**	**22.1**	**27.9**	**50.0**
C1-Co_08	**48.6**	**47.7**	**48.15**	**2.174**	**23.0**	**27.0**	**50.0**
C1-GSK_01	**41.6**	**40.1**	**40.85**	**1.844**	**27.1**	**22.9**	**50.0**
C1-GSK_02	**47.3**	**46.7**	**47.00**	**2.122**	**23.6**	**26.4**	**50.0**
C1-GSK_03	**49.6**	**50.8**	**50.20**	**2.266**	**22.1**	**27.9**	**50.0**
C1-GSK_04	**44.5**	**45.7**	**45.10**	**2.036**	**24.6**	**25.4**	**50.0**
C2-AG120_01	**33.8**	**35.3**	**34.55**	**1.560**	**32.1**	**17.9**	**50.0**

C2-AG120_02	40.2	40.9	40.55	1.831	27.3	22.7	50.0
C2-AG120_03	33.8	35.2	34.50	1.558	32.1	17.9	50.0
C2-AG120_04	36.3	39.1	37.70	1.702	29.4	20.6	50.0
C2-AG881_01	39.8	38.6	39.20	1.770	28.3	21.7	50.0
C2-AG881_02	47.2	45.8	46.50	2.099	23.8	26.2	50.0
C2-AG881_03	44.3	44.4	44.35	2.002	25.0	25.0	50.0
C2-AG881_04	41.9	45.5	43.70	1.973	25.3	24.7	50.0
C2-BAY_01	37.0	40.2	38.60	1.743	28.7	21.3	50.0
C2-BAY_02	41.0	40.5	40.75	1.840	27.2	22.8	50.0
C2-BAY_03	39.1	40.6	39.85	1.799	27.8	22.2	50.0
C2-BAY_04	33.3	34.2	33.75	1.524	32.8	17.2	50.0
C2-Co_01	41.1	38.6	39.85	1.799	27.8	22.2	50.0
C2-Co_02	45.5	44.5	45.00	2.032	24.6	25.4	50.0
C2-Co_03	45.1	45.3	45.20	2.041	24.5	25.5	50.0
C2-Co_04	41.1	40.4	40.75	1.840	27.2	22.8	50.0
C2-Co_05	43.3	43.0	43.15	1.948	25.7	24.3	50.0
C2-Co_06	48.1	48.4	48.25	2.178	23.0	27.0	50.0
C2-Co_07	41.4	40.9	41.15	1.858	26.9	23.1	50.0
C2-Co_08	40.7	40.4	40.55	1.831	27.3	22.7	50.0
C2-GSK_01	34.5	33.6	34.05	1.537	32.5	17.5	50.0
C2-GSK_02	39.4	40.4	39.90	1.801	27.8	22.2	50.0
C2-GSK_03	36.9	37.4	37.15	1.677	29.8	20.2	50.0
C2-GSK_04	34.7	34.9	34.80	1.571	31.8	18.2	50.0
D1-AG120_01	32.5	32.0	32.25	1.456	34.3	15.7	50.0
D1-AG120_02	31.8	31.7	31.75	1.433	34.9	15.1	50.0
D1-AG120_03	32.0	35.0	33.50	1.512	33.1	16.9	50.0
D1-AG120_04	38.1	39.2	38.65	1.745	28.7	21.3	50.0
D1-AG881_01	33.3	32.9	33.10	1.494	33.5	16.5	50.0
D1-AG881_02	40.8	40.8	40.80	1.842	27.1	22.9	50.0
D1-AG881_03	41.6	41.1	41.35	1.867	26.8	23.2	50.0
D1-AG881_04	41.9	42.5	42.20	1.905	26.2	23.8	50.0
D1-BAY_01	41.7	41.6	41.65	1.880	26.6	23.4	50.0
D1-BAY_02	37.8	36.3	37.05	1.673	29.9	20.1	50.0
D1-BAY_03	34.7	34.0	34.35	1.551	32.2	17.8	50.0
D1-BAY_04	36.1	36.2	36.15	1.632	30.6	19.4	50.0
D1-Co_01	36.1	35.9	36.00	1.625	30.8	19.2	50.0
D1-Co_02	41.2	42.1	41.65	1.880	26.6	23.4	50.0
D1-Co_03	39.8	40.3	40.05	1.808	27.7	22.3	50.0
D1-Co_04	37.8	40.6	39.20	1.770	28.3	21.7	50.0
D1-Co_05	35.3	35.2	35.25	1.591	31.4	18.6	50.0
D1-Co_06	41.1	41.4	41.25	1.862	26.8	23.2	50.0
D1-Co_07	38.7	39.3	39.00	1.761	28.4	21.6	50.0
D1-Co_08	36.6	37.7	37.15	1.677	29.8	20.2	50.0
D1-GSK_01	32.9	33.6	33.25	1.501	33.3	16.7	50.0
D1-GSK_02	38.7	39.0	38.85	1.754	28.5	21.5	50.0
D1-GSK_03	35.2	34.1	34.65	1.564	32.0	18.0	50.0
D1-GSK_04	30.5	30.8	30.65	1.384	36.1	13.9	50.0
D2-AG120_01	28.6	30.5	29.55	1.334	29.0	9.0	38.0
D2-AG120_02	34.1	34.8	34.45	1.555	32.1	17.9	50.0
D2-AG120_03	32.2	32.4	32.30	1.458	34.3	15.7	50.0
D2-AG120_04	26.4	26.4	26.40	1.192	42.0	8.0	50.0
D2-AG881_01	31.6	31.5	31.55	1.424	28.1	11.9	40.0

D2-AG881_02	**32.9**	**33.3**	**33.10**	**1.494**	**33.5**	**16.5**	**50.0**
D2-AG881_03	**33.2**	**33.3**	**33.25**	**1.501**	**30.0**	**15.0**	**45.0**
D2-AG881_04	**25.8**	**27.7**	**26.75**	**1.208**	**33.1**	**6.9**	**40.0**
D2-BAY_01	**22.3**	**22.3**	**22.30**	**1.007**	**35.0**	**0.0**	**35.0**
D2-BAY_02	**35.8**	**33.0**	**34.40**	**1.553**	**32.2**	**17.8**	**50.0**
D2-BAY_03	**30.5**	**29.6**	**30.05**	**1.357**	**29.5**	**10.5**	**40.0**
D2-BAY_04	**23.2**	**23.4**	**23.30**	**1.052**	**38.0**	**2.0**	**40.0**
D2-Co_01	**27.8**	**31.1**	**29.45**	**1.330**	**30.1**	**9.9**	**40.0**
D2-Co_02	**42.0**	**43.8**	**42.90**	**1.937**	**25.8**	**24.2**	**50.0**
D2-Co_03	**33.6**	**34.0**	**33.80**	**1.526**	**32.8**	**17.2**	**50.0**
D2-Co_04	**34.5**	**34.6**	**34.55**	**1.560**	**32.1**	**17.9**	**50.0**
D2-Co_05	**27.7**	**30.1**	**28.90**	**1.305**	**34.5**	**10.5**	**45.0**
D2-Co_06	**33.0**	**32.5**	**32.75**	**1.479**	**33.8**	**16.2**	**50.0**
D2-Co_07	**33.2**	**33.2**	**33.20**	**1.499**	**33.4**	**16.6**	**50.0**
D2-Co_08	**34.0**	**33.7**	**33.85**	**1.528**	**32.7**	**17.3**	**50.0**
D2-GSK_01	**25.6**	**25.0**	**25.30**	**1.142**	**30.6**	**4.4**	**35.0**
D2-GSK_02	**31.3**	**31.3**	**31.30**	**1.413**	**35.4**	**14.6**	**50.0**
D2-GSK_03	**28.2**	**28.0**	**28.10**	**1.269**	**31.5**	**8.5**	**40.0**
D2-GSK_04	**21.7**	**22.6**	**22.15**	**1.000**	**35.0**	**0.0**	**35.0**

Table A.VI.3. Annotated metabolites from the IC-MS data of S-TICO experiment. Parameters used for determining whether it was a putative or confident identification. FS = fragmentation score, ME = mass error, ISS = isotope similarity score, RTE = retention time error, max. abun. = max abundance and min. CV% = minimum coefficient of variance, C = Confident and P = putative. When provided as a comment, the abbreviation indicates what brought the identification from confident to putative (RTE > 1.5 min, ME > 3 ppm, IS < 90%).

Accepted identification	FS	ME (ppm)	ISS	RTE (min)	Max. Abun.	Min. CV%	C/P	Comment
1,2,3-Trihydroxybenzene	0	-3.53	96.8	-0.56	64	3.3	P	ME
2,3-Diphosphoglyceric acid	0	1.02	99.3	-1.77	25508	6.2	P	RTE
2-C-Methylerythritol 4-phosphate	0	3.09	85.7	-0.64	328	4.1	P	ME and ISS
2-Hydroxybutyric acid	0	1.08	98.0	1.39	470	6.4	P	Isomer of 3-hydroxybutyric acid
2-Hydroxyglutarate	82.3	1.60	99.8	-0.87	1169802	3	C	
2-Ketobutyric acid	0	1.31	97.9	0.24	306	2.6	C	
2-Oxoglutaric acid	38.7	1.76		-1.29	15454	3	C	
2-Phosphoglyceric acid	70.3	1.86	99.1	-1.88	40697	6.4	P	RTE and isomer of 3-phosphoglyceric acid
3,3 Dimethyl glutarate	77.8	1.24	95.4	-0.91	594	2.8	C	
3'-AMP	0	3.78	86.6	-0.37	146	7	P	ME, ISS and isomer of AMP
3-Dehydroquinate	0	1.38	91.3	-0.21	586	10.6	C	
3-Hydroxyisovaleric acid	0	-2.98	96.6	-0.79	902	6.4	C	
3-Hydroxymethyl-glutarate	67.6	1.16	97.6	-0.90	2715	1.8	C	
3-methoxyphenyl-acetic acid	0	0.78	94.4	0.96	470	5.7	C	
3-Methyl-2-oxovaleric acid	0	1.91	98.6	-0.81	6737	1.6	P	Isomer of adipate semialdehyde
3-Nitrotyrosine	0	3.48	88.9	-0.67	744	74	P	ISS
4-Hydroxy-3-methoxymandelic acid	0	1.12	89.6	-0.65	188	6.8	C	
4-Hydroxybutyric acid	0	1.46	98.6	-0.62	18323	0.9	C	
4-Hydroxyproline	80.2	1.55	98.1	-0.33	2528	4.7	C	
4-Hydroxypyrrolidinone	0	1.09	90.8	0.66	94	3.3	C	
5-Aminolevulinic acid	0	-3.68	93.7	-0.86	635	69.6	P	ME and isomer of N-acetyl-L-alanine
6-Phosphogluconic acid	0	1.02	99.2	-1.62	106206	3.5	P	RTE
Acetoacetate	0	1.12	98.7	-0.03	447	2.8	C	
Acetylcysteine	40.2	1.24	95.8	-0.86	4184	6.2	C	
Acetylglycine	40.6	1.65	96.2	-0.08	840	3.5	C	
Adenine	0	1.77	93.1	1.29	544	2.8	C	

Accepted identification	FS	ME (ppm)	ISS	RTE (min)	Max. Abun.	Min. CV%	C/P	Comment
Adenosine monophosphate	52.6	2.12	95.0	-1.18	15352	4.7	P	Isomer of 3'-AMP
Adenylsuccinate	0	1.55	93.3	-1.98	1056	5.4	P	RTE
Adonitol (ribitol)	73.5	1.48	96.6	0.08	1025	1.7	P	Isomer of arabitol and xylitol
Allantoin	0	-2.37	96.0	-0.65	1343	1.2	C	
Arabinonic acid	56.7	1.01	96.1	-0.62	2036	5.2	C	
Ascorbate	3.41	0.80	95.3	-1.26	674	4.1	C	
Aspartate	82.5	1.76	94.7	-0.88	148474	2.4	C	
Beta-Alanine	72.1	1.78	86.1	-0.27	500	1.9	C	
Beta-Citryl-L-glutamic acid	0	2.28	98.2	-0.81	97405	4.8	C	
Caproic acid	0	-3.23	96.7	0.56	1186	6.1	P	ME
Citric acid	87.4	1.17	99.6	-1.60	372107	6.1	P	RTE
Cytidine monophosphate	0	2.08	92.0	-1.47	1421	2.4	C	
Cytidine monophosphate N-acetylneuraminic acid	0	4.77	97.2	-0.75	10312	3.3	P	ME
Cytidine triphosphate	5.99	1.49	98.2	-1.76	124904	5.2	P	RTE
dCTP	86.8	1.77	94.9	-1.08	1815	3.8	C	
Deoxyribose 5-phosphate	6.42	2.71	95.0	-0.01	1041	3.5	C	
Dihydroxyacetone	76.3	1.25	99.7	-0.38	212454	3.4	P	Isomer of lactic acid
Dimethyl fumarate	0	0.54	97.7	-1.40	253	5.4	C	
dTDP-D-glucose	0	3.13	92.6	-1.47	5455	4.7	P	ME
EDTA	0	1.70	94.6	-1.38	1919	3.4	C	
Ethylmalonic acid	74.9	1.46	96.4	-1.68	1535	3	P	RTE and isomer of glutaric acid
Ethylmalonic acid	58.8	1.71	93.8	1.75	2002	4.6	P	RTE
Ferulic acid	0	1.26	93.1	1.16	381	4.7	C	
Flavin Mononucleotide	0	2.01	90.2		676	3.3	P	No RT
Fructose 1,6-bisphosphate	45.5	2.26		-1.75	30330	9.9	P	RTE and isomer of fructose 2,6-bisphosphate
Fructose 2,6 diphosphate	0	2.30	98.5	-0.19	22340	2.9	C	
Galactose 1-phosphate	0	1.08	96.9	-1.67	53784	1.3	P	RTE and isomer of glucose 1-phosphate
Galacturonic acid	37.7	1.33	96.5	-0.11	1490	2.8	P	Isomer of glucuronic acid
Gluconate	66.4	1.16		-0.48	27075	6.2	C	
Glucose 1-phosphate	53.8	0.81	98.5	-0.73	25445	3.8	P	Isomer of galactose 1-phosphate

Accepted identification	FS	ME (ppm)	ISS	RTE (min)	Max. Abun.	Min. CV%	C/P	Comment
Glucuronic acid	0	1.09	95.9	0.14	307	5.1	P	Isomer of galacturonic acid
Glutamic acid	86.4	1.69	94.0	-0.05	333755	6.4	C	
Glutamylcysteine	0	-0.93	92.2	-1.49	7413	2.2	C	
Glutathione (GSH)	44	1.89	95.5	-0.70	2398121	4.3	C	
Glyceric acid	2.54	1.15		-0.95	3215	1.6	C	
Glycerol	56.2	1.07	99.7	0.17	126710	3.7	C	
Glycerol 3-phosphate	0	1.44		-0.14	449	2.6	C	
Glycolic acid	55.1	0.70	98.6	-0.69	8129	1.5	C	
Guanosine diphosphate	96.9	3.28	97.8	-0.20	296111	6.1	C	
Hippuric acid	31.4	1.20	95.7	-1.32	951	9.5	C	
Homogentisic acid	0	-0.10	94.9	1.51	1576	7.7	C	
Hydroorotic acid	0	0.94	98.1	0.04	87	9.1	P	Isomer of ureidosuccinic acid
Hydroxy-isobutyric acid	0	1.53	98.2	-0.95	472	14.8	P	Isomer of 2- and 3-hydroxyisobutyric acid
Hydroxyisoheptanoic acid	0	-2.47	92.0	-0.29	57	13.4	C	
Hypotaurine	0	1.83	92.1	-1.53	307	4.1	C	
Inosine	0	-4.02	93.1	-0.69	381	4.4	P	ISS
Inositol 1,3,4-trisphosphate	0	2.81	90.3	-1.27	507	41.4	C	
Isocitrate	0	0.88	97.2	-1.26	2421	3.7	P	Isomer of citric acid
Isopentenyl pyrophosphate	0	1.13	98.3	-1.54	435	4.4	P	RTE and isomer of dimethylallyl pyrophosphate
Lactic acid	0	-0.24	98.6	-1.92	4228	1.7	P	RTE and isomer of dihydroxyacetone
Lactose	64.9	0.98	97.0	-0.10	10080	17.5	C	
Lactoyl-isoleucine	0	-1.44	95.6	-0.02	617	4.6	C	
Maleic acid	72	1.47	99.4	-0.28	7265	4.2	P	Isomer of fumarate
Malic acid	51.5	1.63	99.8	-0.93	128079	2.9	C	
Malondialdehyde	0	-0.46	98.0	1.35	496	2.3	C	
Malonic acid	74.6	1.41	97.6	-1.41	916	4.3	C	
Mannitol	0	1.37	96.2	1.04	827	9.1	P	Isomer of sorbitol
Mannose 6-phosphate	84.1	0.81	97.2	-1.94	13813	2.7	P	Isomer of fructoe 6-phosphate
Methyl beta-D-glucopyranoside	0	1.28	95.2	0.20	296	32.8	P	Isomer of mytilitol

Accepted identification	FS	ME (ppm)	ISS	RTE (min)	Max. Abun.	Min. CV%	C/P	Comment
Methylglutaric acid	40	2.64	96.0	-0.70	4540	7.7	C	
Methylisocitric acid	0	1.17	95.1	-0.69	390	3.3	P	Isomer of 2-methylcitric acid
Myoinositol	70.7	1.15	98.4	0.13	79313	5.1	P	Isomers
Myo-inositol hexakisphosphate	0	1.20	96.4	-1.76	584	24.5	P	RTE
Mytilitol	0	-2.60	91.3	1.22	156	13.3	P	Isomer of methyl beta-D-glucopyranoside
N-Acetyl-aspartate	90	0.85	96.5	-0.68	58200	2.2	C	
N-Acetylaspartyl-glutamic acid	0	1.91	96.5	-1.14	7344	4	C	
N-acetyl-glucosamine-1-phosphate	0	1.79	87.9	-0.19	1794	7.2	P	Isomer of N-acetyl-D-glucosamine 6-phosphate and N-acetyl-D-mannosamine 6-phosphate
N-Acetylglutamate	70.9	-1.73	98.4	-0.60	4643	1.8	C	
N-Acetyl-L-alanine	89.5	1.30	97.6	-0.24	2712	0.9	C	
N-Acetyl-L-methionine	77.5	1.43	94.5	-0.50	4096	3	C	
N-Acetyl-L-phenylalanine	25.1	0.94	96.6	-0.59	226	14.7	C	
N-Acetylneuraminate 9-phosphate	0	1.63	90.9	-0.82	83	10.4	C	
N-Acetylneuraminic acid	93.3	2.14	95.0	-0.47	4549	1.4	C	
N-Acetylvaline	71	0.30	95.5	-0.28	116	12	C	
NADH	93.9	3.63	95.5	-0.91	21156	10.2	C	
NADPH	0	2.23	88.9	-1.35	364	41.5	P	ISS
N-Formyl-methionine	0	1.28	91.7	-0.64	264	4.9	C	
Nonate	0	-1.68	97.1	-0.59	3098	7.7	C	
O-Phosphoserine	89	1.53	95.9	-1.11	11570	4.6	C	
Oxalic acid	71.3	1.42	97.7	-1.44	9985	3	C	
Oxoadipic acid	57.8	1.16	96.0	-1.61	829	2.5	P	RTE
Oxovaleric Acid	0	-3.15	97.8	0.16	1364	0.6	P	ME
Pantothenic acid	59.6	1.11	98.8	-0.54	80573	3.5	C	
Phenylacetylglycine	0	-2.30	98.0	-1.40	971	5.1	C	
Phosphocreatine	10.5	-1.27	99.1	-0.36	118507	3.7	C	
Phosphoenolpyruvic acid	0.054	1.39	97.7	-1.67	2052	8.7	P	RTE and isomer of 2- and 3-phosphoglyceric acid
Phosphoribosyl pyrophosphate	0	2.18	98.5	-1.51	9484	3.4	C	

Accepted identification	FS	ME (ppm)	ISS	RTE (min)	Max. Abun.	Min. CV%	C/P	Comment
Pyroglutamic acid	16.2	-2.42	93.9	-0.30	31434	3.9	P	Isomer of [M-H2O-H] of glutamate
Pyruvic acid	71.9	0.99	98.7	-0.81	15467	6.7	C	
Quinic acid	15.2	1.28	95.1	-0.75	310	11.6	C	
Quinolinic acid	0	1.07	91.5	-1.59	89	20.3	P	RTE
Ribose 5-phosphate	70.4	1.82	97.9	-1.14	2687	8.2	P	Isomer of xylulose 5-phosphate
Ribulose 1,5,diphosphate	0	-0.17	96.9	-1.63	3313	2.5	P	RTE
Salicylic acid	0	-2.25	94.4	0.26	6309	1.1	C	
Sedoheptulose 1,7-bisphosphate	0	2.26	94.9	-1.33	1598	4.8	C	
Sedoheptulose 1-phosphate	0	1.26	95.3	-0.63	1622	4.6	C	
Sedoheptulose 7-phosphate	62.9	1.44		-1.06	1972	4	C	
Serine	75	1.69	96.3	-1.14	311	1.5	C	
Sorbitol	72.3	1.16	98.9	0.17	17673	1.9	P	Isomer of mannitol
Sorbitol-6-phosphate	0	0.77	97.4	0.31	2195	6.2	C	
Succinic acid semialdehyde	0	1.05	98.8	-1.14	2349	4.3	C	
Taurine	92.6	1.43	93.2	-0.49	135108	2.5	C	
TDP	88.2	2.31	97.8	1.97	11577	2.9	P	RTE
Threitol	90.5	1.76	97.4	0.16	1250	6.6	C	
Thymidine 5'-phosphate	0	2.13	96.5	-1.27	822	5.2	C	
Thymidine triphosphate	5.78	1.65	97.0	-1.73	7136	1.3	P	RTE
UDP-galactose	0	3.28	97.7	-1.19	45634	8.1	P	Isomer of UDP-glucose
UDP-N-acetyl-D-mannosamine	0	2.23	98.9		477818	3.5	P	Isomer of UDP-N_acetyl-glucosamine
Uracil	0	1.36	94.6	-1.20	99	6.2	C	
Uridine 5'-diphosphate	11.7	1.90	95.5	-1.76	6393	4.2	P	RTE
Uridine 5'-monophosphate	45.5	2.19	99.2	-1.90	129502	1.4	P	RTE
Valeric Acid	0	-4.28	94.7	0.38	326	9.3	C	
Xylulose	17.4	0.95	95.8	0.45	467	3.6	P	Isomer of ribulose, ribose and arabinose
Xylulose 5-phosphate	19.6	2.01	94.5	0.40	733	5.6	P	Isomer of ribose 5-phosphate

Table A.VI.4. Annotated metabolites from the IC-MS data of L-TICO experiment. Parameters used for determining whether it was a putative or confident identification. FS = fragmentation score, ME = mass error, ISS = isotope similarity score, RTE = retention time error, max. abun. = max abundance and min. CV% = minimum coefficient of variance, C = Confident and P = putative. When provided as a comment, the abbreviation indicates what brought the identification from confident to putative (RTE > 1.5 min, ME > 3 ppm, IS < 90%).

Accepted identification	FS	ME (ppm)	ISS	RTE (min)	Max. Abun.	Min. CV%	C/P	Comment
1-Pyrroline hydroxycarboxylic acid	0	-0.96	96.6	-0.16	940	11.7	C	
2,3-Diphosphoglyceric acid	0	-1.15	99.2	-1.63	7747	34	P	RTE
2,5-Dihydroxybenzoic acid	87.1	-0.99	97.8	0.94	696	8.6	C	
2-butyl-3-ureido-succinate	0	-1.68	97.4	0.57	721	1.9	C	
2-Hydroxyglutarate	77	-1.40	99.8	-0.84	1733427	3.9	C	
2-Ketobutyric acid	0	0.15	96.6	1.95	163	37.8	P	RTE
2-Oxoglutaric acid	32.8	-1.19		-1.24	23281	5.7	C	
2-Phosphoglyceric acid	87.1	-0.69	98.8	-1.80	25460	2.9	P	RTE
3-(2,5-Dioxoimidazolidin-4-yl)propanoic acid	0	3.23	98.6		1620	5.9	P	No RT
3,3 Dimethyl glutarate	98.6	-1.22	99.6	-1.42	846	8.4	C	
3-Dehydroquinate	27	-0.06	98.8	-0.61	208	6.3	C	
3-deoxy-2-keto-6-phosphogluconic acid	89.8	-0.07	99.4	-1.31	348	21.3	C	
3-Hydroxymethylglutarate	76.9	-1.76	99.4	-0.86	7749	5.7	C	
3-methoxyphenylacetic acid	0	-1.34	97.6	-0.60	1313	6.7	C	
3-Methyl-2-oxovaleric acid	0	-1.02	98.6	-1.06	16216	2.4	C	
4-Acetylbutyrate	0	-4.85	93.0	-0.60	112	16.3	P	ME
4-Hydroxybenzoic acid	0	-1.21	97.7	-1.67	3846	10.1	P	RTE
4-Hydroxyproline	78.9	-1.53	98.2	-0.32	5812	2.4	C	
4-Hydroxypyrrolidinone	0	-0.67	98.0	0.81	244	8.7	C	
4-Methyl-2-ureido-pentanoic acid	0	-4.81	95.2	-0.73	706	43.5	P	ME
6-Phosphogluconic acid	0	-1.44	97.9	-1.59	23727	10.9	P	RTE
6-phosphonoglucono-lactone	0	-0.73	97.2	-0.59	76	6.1	C	
Abscisic acid	16.8	4.22	96.6	-1.25	436	6.7	P	ME
Acetic acid	0	-1.45	99.5	0.31	1454	7	C	
Acetoacetate	0	-1.41	96.8	-1.98	1036	2	P	RTE
Acetylcysteine	56.8	-1.09	91.2	-0.88	4103	5	C	
Acetylglycine	77.5	-1.00	97.5	0.09	1201	4.5	C	
Adenosine diphosphate	0	-1.53	92.8	-1.44	3014	1.8	C	
Adenosine monophosphate (AMP)	36.7	-1.37	96.6	-1.11	45631	7.9	C	
Adenosine triphosphate	4.64	-2.24	98.0	0.45	385	18.8	C	
Adenylsuccinate	0	-1.60	93.1	-1.84	3834	2	P	RTE

Adonitol	**78.7**	**-1.42**	**98.4**	**0.07**	**2185**	**2.6**	**P**	**Isomer of aravitol and xylitol**
ADP Glucose	**14.9**	**-0.04**	**98.7**	**-1.24**	**1090**	**50.3**	**C**	
Arabinonic acid	**53.1**	**-1.97**	**95.2**	**-0.66**	**2531**	**3.4**	**C**	
Arabinose	**0**	**-0.78**	**98.4**	**-0.31**	**391**	**4.6**	**P**	**Isomer of other pentoses**
Arabitol	**0**	**-1.15**	**99.4**	**-0.53**	**99**	**20**	**P**	**Isomer of adonitol and xylitol**
Ascorbate	**4.76**	**-1.22**	**95.1**	**-1.17**	**495**	**10.3**	**C**	
Aspartate	**85.5**	**-1.38**	**94.7**	**-0.85**	**281840**	**1.4**	**C**	
Beta-Alanine	**77.7**	**-0.78**	**98.2**	**-0.57**	**724**	**4.7**	**C**	
β-Citryl-L-glutamic acid	**0**	**-1.40**	**98.5**	**-0.66**	**243308**	**2.3**	**C**	
Citric acid	**83.8**	**-1.57**	**99.6**	**-1.51**	**673923**	**3.4**	**C**	
Cyclic AMP	**77.9**	**-0.37**	**95.8**	**-1.61**	**273**	**12.5**	**P**	**RTE**
Cysteic acid	**90.5**	**-1.99**	**93.3**	**-1.16**	**1828**	**6.6**	**C**	
Cytidine monophosphate	**45.7**	**-1.40**	**93.7**	**-1.46**	**4966**	**1.3**	**C**	
Cytidine monophosphate N-acetylneuraminic acid	**0**	**-1.89**	**97.4**	**-0.70**	**33316**	**3.8**	**C**	
Cytidine triphosphate	**5.99**	**-1.38**	**98.1**	**-1.63**	**227845**	**2.9**	**P**	**RTE**
dCTP	**85**	**-1.86**	**93.3**	**-0.94**	**2409**	**6.5**	**C**	
Deoxyribose 5-phosphate	**6.58**	**0.32**		**0.00**	**2329**	**2.8**	**C**	
Dihydroorotic acid	**86.1**	**-1.76**	**91.9**	**-0.27**	**619**	**8**	**P**	**Isomer of hydroorotic acid**
Dihydroxyacetone	**0**	**-2.44**	**98.0**	**-1.81**	**6109**	**2.5**	**P**	**RTE**
Dihydroxyphenylalanine	**0**	**-0.28**	**89.5**	**-0.80**	**452**	**37.2**	**P**	**IS**
Dimethyl fumarate	**0**	**-0.88**	**99.1**	**1.62**	**197**	**23.7**	**P**	**RTE**
dTDP-D-glucose	**0**	**-1.62**	**90.2**	**-1.30**	**7540**	**8.6**	**C**	
dUMP	**0**	**-1.14**	**96.7**	**-1.57**	**29391**	**7.2**	**P**	**RTE**
EDTA	**0**	**-1.00**	**95.0**	**-1.22**	**4010**	**22.4**	**C**	
Ethylmalonic acid	**72.9**	**-1.01**	**98.7**	**-1.38**	**2630**	**2.9**	**P**	**Isomer of glutaric acid**
Flavin Mononucleotide	**0**	**-1.20**	**91.6**		**1339**	**4.9**	**P**	**No RT**
Fructose 1,6-bisphosphate	**44.9**	**-1.25**		**-1.65**	**5665**	**10.9**	**C**	
Fructose 2,6 diphosphate	**0**	**-1.72**	**97.9**	**-0.09**	**24234**	**3.2**	**C**	
Fructose 6-phosphate	**81.5**	**-1.52**	**99.3**	**-0.95**	**11120**	**6.5**	**P**	**Isomer of mannose 6P**
Fumarate	**62**	**-1.36**	**99.1**	**-1.43**	**8850**	**7.6**	**P**	**Isomer of maleic acid**
Galactose	**0**	**-1.41**	**96.9**	**-0.09**	**7071**	**1.9**	**P**	**Isomer of other hexoses**
Galacturonic acid	**79.7**	**-1.55**	**98.9**	**0.06**	**2873**	**3.1**	**P**	**Isomer of glucuronic acid**
Gluconate	**78.9**	**-1.62**		**-1.92**	**2461**	**11.8**	**P**	**RTE**
Gluconolactone	**0**	**-0.85**	**99.4**	**-1.63**	**540**	**12.9**	**P**	**RTE**

Glucose 1-phosphate	**65.4**	**-1.95**	**99.1**	**-0.77**	**25707**	**2.9**	**P**	**Isomer of galactose 1P**
Glucuronic acid	**83**	**-1.86**	**99.0**	**-1.91**	**2215**	**5.5**	**P**	**RTE and isomer of galacturonic acid**
Glutamic acid	**93.2**	**-1.36**	**93.5**	**-0.01**	**187951**	**2.6**	**C**	
Glutathione (GSH)	**43.8**	**-1.17**	**95.9**	**-0.69**	**6822029**	**1**	**C**	
Glyceric acid	**0**	**-1.34**		**0.04**	**24557**	**2.1**	**C**	
Glycerol	**48.5**	**-1.57**	**99.3**	**0.16**	**123198**	**1**	**C**	
Glycerol 3-phosphate	**39.5**	**-1.09**		**-0.70**	**5104**	**1**	**C**	
Guanosine diphosphate	**98.3**	**-0.07**	**97.6**	**-0.02**	**377178**	**5.4**	**C**	
Hippuric acid	**64**	**-1.51**	**89.9**	**-1.14**	**666**	**6.4**	**C**	
Hydroorotic acid	**0**	**-1.61**	**97.7**	**0.05**	**291**	**13.5**	**P**	**Isomer of dihydroorotic acid**
Hydroxy-isobutyric acid	**41.3**	**-0.76**	**99.3**	**-1.53**	**1396**	**2.6**	**P**	**RTE**
Hydroxyoctanoic acid	**0**	**-4.71**	**95.4**	**0.06**	**239**	**9.4**	**C**	
IDP	**20.2**	**-2.15**	**97.7**	**-1.03**	**1540**	**23.3**	**C**	
Indole-3-lactic acid	**19.8**	**3.07**	**98.4**	**-0.14**	**183**	**42.4**	**P**	**ME**
Inositol 1,3,4-trisphosphate	**0**	**-0.41**	**99.8**	**-1.94**	**691**	**4.5**	**P**	**RTE**
Isocitrate	**0**	**-1.81**	**99.0**	**-1.17**	**8259**	**3.5**	**P**	**Isomer of citric acid**
Isopentenyl pyrophosphate	**0**	**-1.04**	**95.8**	**-1.18**	**414**	**9**	**P**	**Isomer of dimethylallyl pyrophosphate**
Kojic acid	**72.2**	**-0.36**	**97.4**	**-0.01**	**247**	**10.5**	**C**	
Kynurenic acid	**0**	**-0.88**	**99.2**	**-1.12**	**1082**	**5.4**	**C**	
Lactic acid	**32.7**	**-1.26**	**99.4**	**-0.64**	**378450**	**7.8**	**P**	**Isomer of dihydroxyacetone**
Lactose	**70.2**	**-2.13**	**83.9**	**-1.42**	**594**	**31.5**	**P**	**IS**
Lactoyl-isoleucine	**0**	**-4.27**	**95.4**	**0.08**	**1493**	**3.8**	**C**	
Maleic acid	**52.5**	**-1.38**	**99.5**	**-1.50**	**2698**	**3.6**	**C**	
Malic acid	**66.1**	**-1.20**	**99.8**	**-0.90**	**171652**	**3.5**	**C**	
Malitol	**49.3**	**-1.47**	**92.5**	**-1.75**	**612**	**59**	**P**	**RTE**
Malondialdehyde	**0**	**-1.31**	**95.8**	**0.40**	**408**	**4.5**	**C**	
Malonic acid	**73**	**-0.63**	**99.9**	**-0.05**	**2749**	**4**	**C**	
Mannose 6-phosphate	**74.8**	**-0.96**	**91.6**	**1.02**	**63**	**72.2**	**P**	**Isomer of fructose 6-phosphate**
Methyl-3-hydroxybenzoic acid	**0**	**-4.72**	**98.3**	**-1.11**	**2127**	**5.1**	**C**	
Methylglutaric acid	**83.3**	**-0.98**	**98.8**	**-0.67**	**13940**	**17**	**C**	
Methylisocitric acid	**0**	**-1.30**	**99.4**	**-0.65**	**1880**	**9.2**	**P**	**Isomer of 2-methylcitric acid**
Myoinositol	**89.6**	**-1.73**	**99.0**	**0.12**	**120348**	**2.6**	**P**	**Isomer of scyllitol**
N-Acetyl-aspartate	**93.6**	**-2.08**	**92.8**	**-0.59**	**144405**	**4.6**	**C**	

N-Acetylaspartylglutamic acid	0	-0.60	96.0	-0.99	3556	6.2	C	
N-Acetyl-D-glucosamine	60.5	-0.92	94.1	0.22	191	42.9	C	
N-acetyl-glucosamine-1-phosphate	0	-1.56	95.1	-0.12	3071	6.5	P	Isomer of N-acetyl-glucosamine 6P
N-Acetylglutamate	72.4	-4.18	98.9	-0.48	13717	3.3	C	
N-Acetyl-L-alanine	96	-1.21	94.1	-0.07	5164	8.3	C	
N-Acetyl-L-methionine	96.7	-0.92	96.6	-0.19	6462	6.4	C	
N-Acetyl-L-phenylalanine	36.1	-1.05	97.6	-0.48	118	9.7	C	
N-Acetylneuraminic acid	91.5	-0.59	97.9	-0.34	10143	3.6	C	
N-Acetyltryptophan	96.4	-1.61	96.8	-1.86	458	32.8	P	RTE
N-Acetylvaline	98.5	-1.21	92.9	-0.18	92	6.1	C	
NADH	88.8	-0.97	92.8	-0.71	20411	8.4	C	
NADPH	90	-1.08	97.9	-1.41	1009	33.1	C	
N-Formyl-methionine	0	-1.58	96.9	-0.46	443	4.9	C	
Nonate	0	-4.65	96.6	-0.44	9519	10.4	C	
O-Acetylserine	0	-0.87	93.7	-0.20	115666	7.2	C	
Octanoic acid	5.4	-1.58	97.5	-1.16	5807	2.3	C	
O-Phosphoserine	88.1	-0.78	97.6	-1.11	14428	6.1	C	
Ophthalmic Acid	0	-3.08	93.4	0.11	6415	4.8	C	
Oxalic acid	65.2	-1.02	99.0	-1.37	11631	3.4	C	
Oxoadipic acid	0	-0.32	97.7	-1.20	177	4.4	C	
Pantothenic acid	58.8	-1.88	98.6	-0.51	150827	3.7	C	
Parabanic Acid	0	4.01	97.0	-0.14	951	7.9	C	
Phosphocreatine	18.8	-4.29	98.3	-0.34	71575	3.4	C	
Phosphoenolpyruvic acid	40.1	-1.41	98.8	-1.58	3182	5.3	P	RTE
Phosphoribosyl pyrophosphate	0	-1.13	97.7	-1.42	22111	3.5	C	
Protocatechuic acid	24.7	-0.65	96.2	1.70	882	7.2	P	RTE
Ribulose 1,5,diphosphate	0	-2.76	97.9	1.06	14700	7.5	C	
Saccharic acid	87.2	-1.42	99.5	-1.99	5476	3.7	P	RTE
Sebacic acid	36.5	-1.12	94.8	-1.92	842	8.3	P	RTE
Sedoheptulose 1,7-bisphosphate	0	-1.73	93.6	-1.26	1939	6.4	C	
Sedoheptulose 1-phosphate	0	-0.83	98.8	0.19	3500	7.5	C	
Sedoheptulose 7-phosphate	0	-0.03		-0.39	232	5	C	
Sorbitol	0	-1.10	96.1	0.98	1292	42.4	P	Isomer of mannitol
Sorbitol-6-phosphate	0	-2.01	97.5	0.38	4289	15.5	C	
Succinic acid	90.2	-0.94	99.1	-0.87	32901	0.9	C	
Syringic acid	0	-0.73	99.2	0.49	73	12	C	
Taurine	92.4	-1.76	93.2	-0.49	218232	3.7	C	
Threitol	85.9	-1.40	97.3	0.30	2653	2.8	C	
Thymidine 5'-phosphate	93.7	-0.89	98.6	-1.17	2964	13.8	C	
Thymidine triphosphate	5.61	-1.42	95.6	-1.51	11302	4.3	P	RTE

UDP-galactose	**0**	**-1.55**	**97.1**	**-1.07**	**55355**	**6.3**	**C**	
Uridine 5'-diphosphate	**10.9**	**-1.35**	**98.6**	**0.87**	**1067865**	**3.4**	**C**	
Uridine 5'-monophosphate	**45.4**	**-1.25**	**99.0**	**-1.78**	**185915**	**6.3**	**P**	**RTE**
Vanillin	**0**	**-4.41**	**98.4**		**1054**	**3.3**	**P**	**No RT**
Xanthylic acid	**0**	**-2.42**	**94.2**	**-1.64**	**211**	**16.3**	**P**	**RTE**

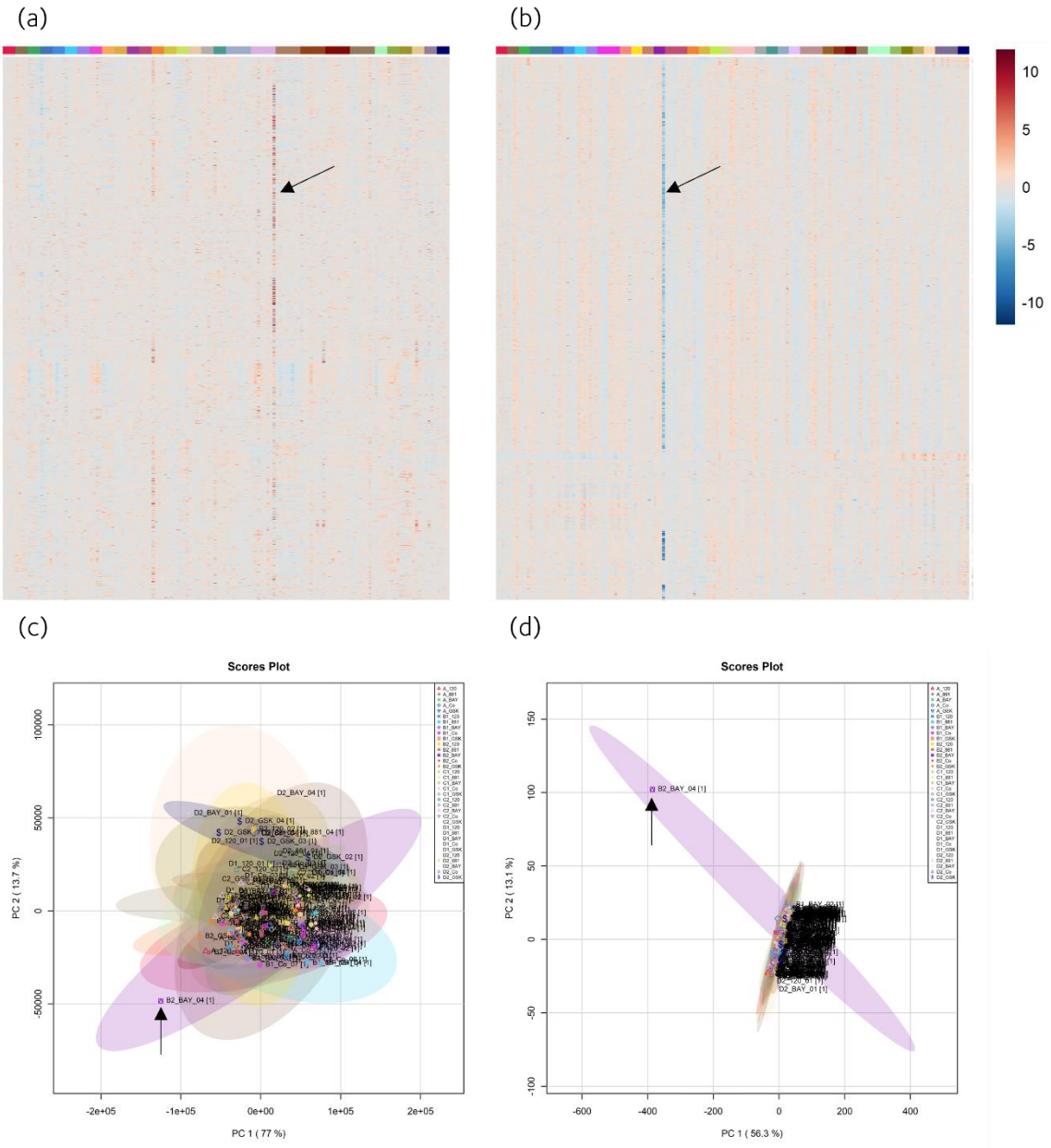

Figure A.VI.2. Heatmaps and PCA scores plots (PC1 × PC2) used to identify outliers in S-TICO IC-MS data and L-TICO derivatised RPLC-MS data. Heatmap of IQR filtered but not normalised, scaled or transformed (a) S-TICO IC-MS data and (b) derivatised RPLC-MS L-TICO data. The black arrow indicates the outlier samples that were removed. PCA scores plot (PC1 × PC2) of derivatised RPLC-MS L-TICO data (a) before normalisation, scaling or transformation and (d) after median normalisation and pareto scaling. The black arrow indicates the outlier sample that was removed.

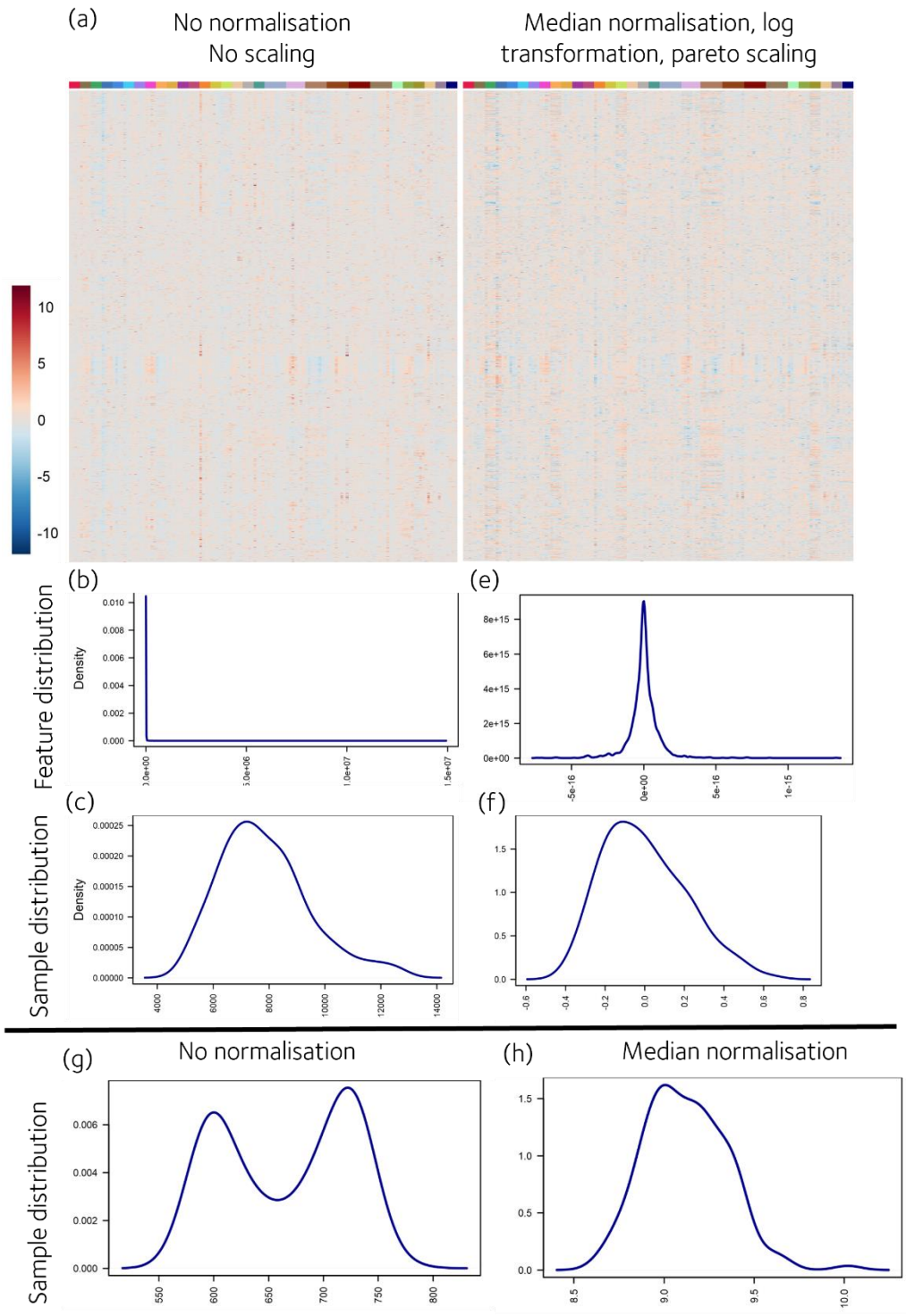

Figure A.VI.3. Heatmaps and feature and sample distribution plots used in the assessment of IC-MS and derivatised RPLC-MS data the S-TICO experiment. Heatmap, feature and sample distribution plots of IC-MS data (a-c) before and (d-f) after median normalisation and pareto-scaling. Sample distribution plot of derivatised RPLC-MS data (g) before and (h) after median normalisation. Number of biological replicates is N = 4 treated group and N = 8 for control per timepoint.

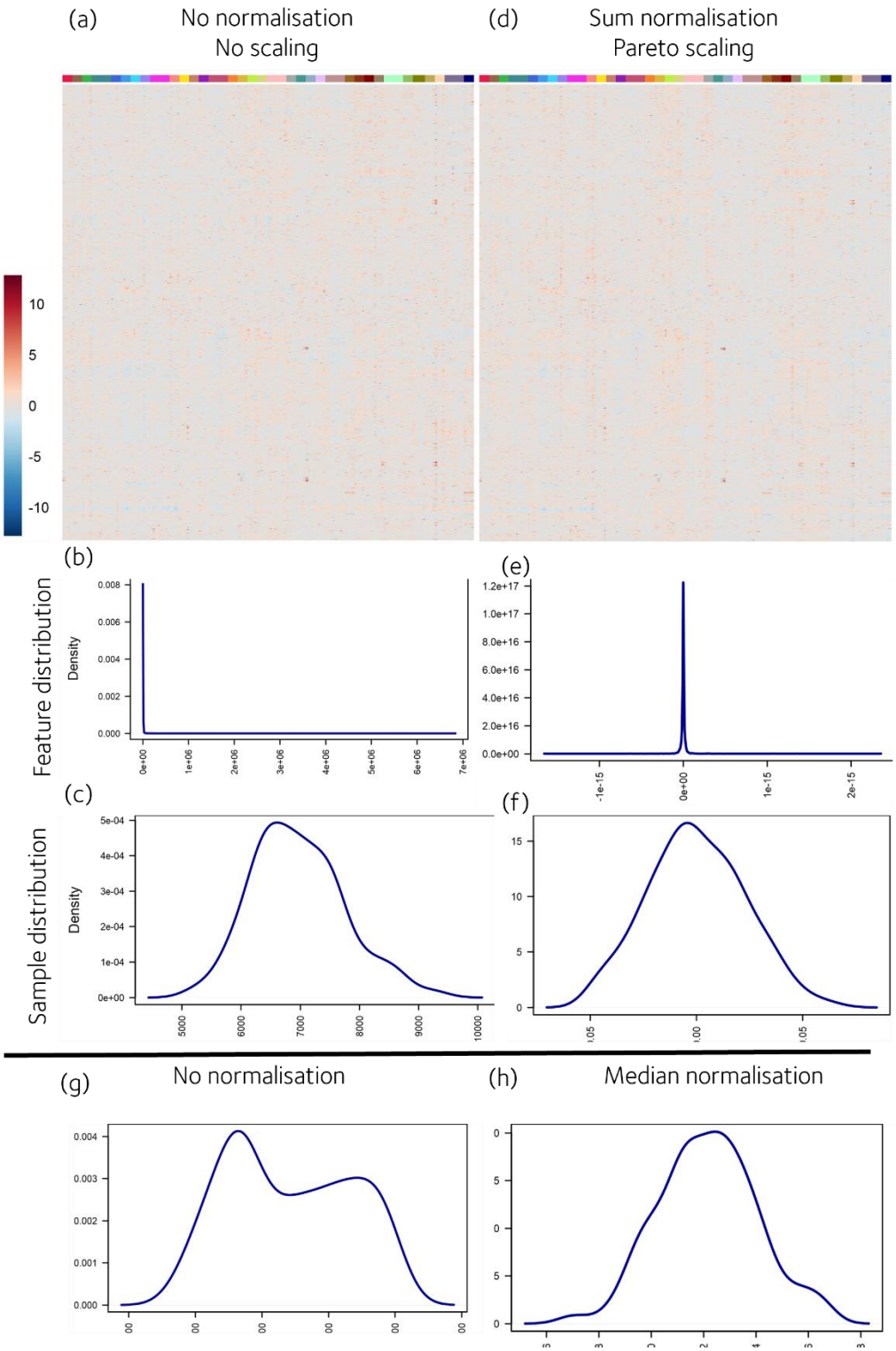

Figure A.VI.4. Heatmaps and feature and sample distribution plots used in the assessment of IC-MS and derivatised RPLC-MS data the L-TICO experiment. Heatmap, feature and sample distribution plots of IC-MS data (a-c) before and (d-f) after sum normalisation and pareto-scaling. Sample distribution plot of derivatised RPLC-MS data (g) before and (h) after median normalisation. Number of biological replicates is N = 4 treated group and N = 8 for control per timepoint.

Table A.VI.5. Annotated metabolites from the derivatised RPLC-MS data of the S-TICO experiment. Parameters used for determining whether it was a putative or confident identification. ME = mass error, ISS = isotope similarity score, RTE = retention time error, max. abun. = max abundance and min. CV% = minimum coefficient of variance, C = Confident and P = putative. When provided as a comment, the abbreviation indicates what brought the identification from confident to putative (isomer, RTE > 0.5 min, ME > 3 ppm, IS < 90%).

Accepted Description	ME (ppm)	ISS	RTE (min)	Max. abun.	Min. CV%	C/ P	Comment
2-Aminoadipic acid	1.29	94.2	0.14	229	4.2	C	
4-Hydroxyproline	-1.21	89.5		40	10.6	P	No RT
Alanine	-0.74	96.0	0.2	11641	3.5	C	
Arginine	-0.55	93.4	0.21	172	7.5	C	
Asparagine	-3.26	89.5	0.07	74	5.8	C	
β-Alanine	0.37	96.3	0.22	1066	4.5	C	
Citrulline	-2.89	88.4	0.18	20	10.4	P	IS
Cysteine	-1.21	90.3	-0.91	107	9.1	P	RTE
Ethanolamine	-3.06	93.6	0.21	50	13.6	P	ME
GABA	-1.68	95.5	0.1	154	12.3	C	
Glutamic acid	-0.38	94.7	0.21	6937	2.5	C	
Glutamine	-1.03	95.0	0.16	3203	4.4	C	
Glycine	-1.61	95.9	0.25	3355	5.3	C	
Histidine	-1.04	93.5	0.17	401	4.9	C	
Homoserine	-2.92	88.9	0.21	25	20.3	P	IS
Hypotaurine	1.92	89.6	0.28	201	1.3	C	
Isobutylamine	-1.85	96.5	-0.36	1103	4.1	C	
Isoleucine	-0.60	94.8	0.22	4036	4.2	P	Isomer of leucine
Leucine	-0.74	93.7	0.04	3718	4.6	P	Isomer of isoleucine
Lysine	0.81	93.8	0.11	2622	6.2	C	
N-Acetyl-ornithine	-2.90	86.8	0.06	14	8.8	P	IS and isomer of L/theanine
Octapine	-2.20	88.2		128	6.3	P	IS and no RT
Oxidised Glutathione	-1.46	92.2	0.06	3985	9.6	C	
Phenylalanine	-0.68	94.6	0.13	2751	4.4	C	
Pipecolic acid	-3.67	92.8	0.52	62	5.9	P	RTE and ME
Proline	-1.32	97.1	0.19	300	3.7	C	
Putrescine	1.17	95.8	0.06	1664	8.6	C	
Serine	-1.60	95.6	0.26	1658	4.3	C	
Serotonin	-3.32	87.0	0.05	11	5.9	P	IS and ME
Taurine	-1.50	95.2		1318	2.2	P	No RT
Thioproline	0.42	92.4	-0.11	146	9.2	C	
Threonine	-0.74	97.2	0.21	5116	2.6	C	
Tryptophan	-0.33	97.2	0.1	500	1.3	C	
Tyrosine	-0.68	93.7	0.12	2178	5.2	C	
Valine	-0.97	98.7	0.15	3342	4.7	C	

Table A.VI.6. Annotated metabolites from the derivatised RPLC-MS data of the L-TICO experiment. Parameters used for determining whether it was a putative or confident identification. ME = mass error, ISS = isotope similarity score, RTE = retention time error, max. abun. = max abundance and min. CV% = minimum coefficient of variance, C = Confident and P = putative. When provided as a comment, the abbreviation indicates what brought the identification from confident to putative (isomer, RTE > 0.5 min, ME > 3 ppm, IS < 90%).

Accepted Description	ME (ppm)	ISS	RTE (min)	Max. abun.	Min. CV%	C/ P	Comment
2-Aminoadipic acid	0.87	96.4	0.14	618	3.2	C	
4-Hydroxyproline	-0.97	89.7		71	5	P	No RT
Alanine	-0.16	95.5	0.2	20996	2	C	
GABA	-3.30	91.3	0.26	48	5.4	C	
Arginine	-0.67	90.7	0.21	319	4	C	
Asparagine	-2.26	92.1	0.09	194	4.1	C	
β-Alanine	0.69	97.0	0.21	1642	3	C	
Citrulline	-1.78	87.8	0.17	37	8.4	P	IS
Ethanolamine	-4.66	95.9	0.2	61	13.9	P	ME
Glutamic acid	-0.06	95.5	0.19	11994	3.2	C	
Glutamine	-0.75	95.6	0.15	4439	3.9	C	
Glycine	-1.18	95.9	0.23	5815	2	C	
Histidine	-1.02	95.2	0.18	605	3.1	C	
Homoserine	-1.99	92.1	0.16	107	5.6	C	
Hypotaurine	2.10	90.4	0.27	302	5.8	C	
Isobutylamine	-1.25	99.2	-0.36	3446	10.1	C	
Isoleucine	-0.66	95.8	0.22	6412	4	P	Isomer of leucine
Leucine	-0.72	98.7	0.04	5950	5.1	P	Isomer of isoleucine
Lysine	0.85	96.1	0.11	3882	2.2	C	
N-Acetyl-ornithine	-2.23	88.7	0.06	17	10.9	P	IS and isomer of L-Theanine
Octapine	-1.62	89.4		149	5.3	P	No RTE
Oxidised Glutathione	-1.30	95.4	0.06	8035	1.6	C	
Phenylalanine	-0.48	94.1	0.14	4477	3	C	
Pipecolic acid	-4.08	94.7	0.52	119	2.5	P	ME and RTE
Proline	-1.27	96.9	0.18	967	3.3	C	
Putrescine	1.05	91.8	0.06	319	8.2	C	
Pyroglutamic Acid	-1.85	89.6	0.03	31	19.8	P	IS
Serine	-1.60	96.2	0.26	1699	2.7	C	
Serotonin	-0.85	87.8	0.05	5	19.7	P	IS
Taurine	-1.50	94.8		2061	2.5	P	No RT
Thioproline	-0.30	87.9	-0.11	144	6.9	P	IS
Threonine	-0.56	96.8	0.19	7416	1.1	C	
Tryptophan	-0.33	96.8	0.11	800	6.3	C	
Tyrosine	-0.31	93.4	0.12	3336	4.3	C	
Valine	-0.92	97.0	0.13	5195	3	C	

9.7. Appendix VII

DNA concentration (ng/µL) of control and treated (AG-120 or FT2102) wtIDH1, mutIDH1^{R132H} and mutIDH1$^{R132H+S280F}$ cells is provided in **Table A.VII.1**. The samples were part of a larger experiment where the lowest DNA concentration was 20.65 ng/µL.

Table A.VII.1. DNA concentration of wtIDH1 mutIDH1^{R132H} LN18 cells from the mutIDH1 resistance experiment. Total sample volume was 50 µL. Rel. DNA conc. = relative DNA concentration.

Sample Name	DNA 1 (ng/µL)	DNA 2 (ng/µL)	DNA 3 (ng/µL)	Average (ng/µL)	Rel. DNA conc.	µL Sample	µL Solvent
R132H+S280F-AG_01	31.10	31.20		31.15	1.508	33.1	16.9
R132H+S280F-AG_02	35.90	35.60		35.75	1.731	28.9	21.1
R132H+S280F-AG_03	34.20	33.10		33.65	1.630	30.7	19.3
R132H+S280F-AG_04	37.80	38.20		38.00	1.840	27.2	22.8
R132H+S280F-Co_01	28.60	28.90		28.75	1.392	35.9	14.1
R132H+S280F-Co_02	33.50	33.90		33.70	1.632	30.6	19.4
R132H+S280F-Co_03	29.00	29.50		29.25	1.416	35.3	14.7
R132H+S280F-Co_04	34.80	35.20		35.00	1.695	29.5	20.5
R132H+S280F-FT_01	29.80	30.10		29.95	1.450	34.5	15.5
R132H+S280F-FT_02	43.60	43.90		43.75	2.119	23.6	26.4
R132H+S280F-FT_03	39.20	39.60		39.40	1.908	26.2	23.8
R132H+S280F-FT_04	44.30	44.10		44.20	2.140	23.4	26.6
R132H-AG_01	26.30	26.20		26.25	1.271	39.3	10.7
R132H-AG_02	33.30	32.70		33.00	1.598	31.3	18.7
R132H-AG_03	38.00	38.10		38.05	1.843	27.1	22.9
R132H-AG_04	32.90	33.20		33.05	1.600	31.2	18.8
R132H-Co_01	12.30	12.50		12.40	0.600	83.3	-33.3
R132H-Co_02	28.10	29.10		28.60	1.385	36.1	13.9
R132H-Co_03	28.50	27.90		28.20	1.366	36.6	13.4
R132H-Co_04	20.80	20.50		20.65	1.000	50.0	0.0
R132H-FT_01	26.30	26.70		26.50	1.283	39.0	11.0
R132H-FT_02	38.70	38.80		38.75	1.877	26.6	23.4
R132H-FT_03	41.30	42.20		41.75	2.022	24.7	25.3
R132H-FT_04	29.70	30.10		29.90	1.448	34.5	15.5
WT-AG_01	35.10	35.10		35.10	1.700	29.4	20.6
WT-AG_02	37.20	37.20		37.20	1.801	27.8	22.2
WT-AG_03	44.10	44.30		44.20	2.140	23.4	26.6
WT-AG_04	40.70	40.80		40.75	1.973	25.3	24.7
WT-Co_01	39.80	40.10		39.95	1.935	25.8	24.2
WT-Co_02	48.80	50.10	49.50	49.47	2.395	20.9	29.1
WT-Co_03	53.20	54.20		53.70	2.600	19.2	30.8
WT-Co_04	49.70	50.00		49.85	2.414	20.7	29.3
WT-FT_01	36.80	37.30		37.05	1.794	27.9	22.1
WT-FT_02	45.40	45.50		45.45	2.201	22.7	27.3
WT-FT_03	46.60	46.30		46.45	2.249	22.2	27.8
WT-FT_04	50.90	50.00		50.45	2.443	20.5	29.5

9.8. Appendix VIII

The CAs described in **section 5.3** are listed below with exact correlation score, p-value and FDR adjusted p-value between specific metabolites and 2-HG, 2-OG and isocitrate. **Table A.VIII.1** and **A.VIII.2** list metabolites whose abundances were significantly altered after treatment with mutIDH1 inhibitors, but where there was or was not a significant difference between control wtIDH1 and mutIDH1^{R132H} LN18 cells, respectively. **Table A.VIII.3** lists metabolites that were not significantly different between control wtIDH1 and mutIDH1^{R132H} LN18 cells and whose abundance was significantly altered in mutant cells only after treatment.

Table A.VIII.1. Template match correlation analysis to 2-HG and 2-OG of metabolites that were significantly different between wtIDH1 and mutIDH1^{R132H} LN18 control cells and responded to treatment with mutIDH1 inhibitors (AG-120, AG-881, BAY 1436032 and GSK864). The CSs were separately calculated for each inhibitor and control samples were included. The template match analysis was carried out using Spearman rank correlation as the distance measure. FDR = FDR adjusted p-value.

		2-hydroxyglutarate			2-oxoglutarate		
Inhibitor	Metabolite	Correlation	p-value	FDR	Correlation	p-value	FDR
AG-120	2-Aminoadipate	-0.38732	0.0068688	0.23793	-0.086735	0.55663	0.99464
AG-881		-0.21797	0.14079	0.98724	0.15368	0.30135	0.9959
BAY 1436032		-0.088797	0.54725	0.77947	0.27323	0.06053	0.54835
GSK864		-0.047981	0.7454	0.98933	0.17792	0.22559	0.94929
AG-120	3-Methyl-2-oxovalerate	0.2411	0.098798	0.2464	0.33771	0.019347	0.099074
AG-881		0.090079	0.54592	0.78826	0.23693	0.10877	0.35918
BAY 1436032		-0.079462	0.5903	0.74957	0.15697	0.28569	0.53519
GSK864		0.039839	0.78753	0.91329	0.027898	0.85041	0.93109
AG-120	Asparagine	-0.025836	0.86138	1	0.1256	0.39381	0.99464
AG-881		-0.020698	0.89003	0.98724	0.17276	0.24471	0.9959
BAY 1436032		0.050261	0.73373	0.87371	0.057968	0.69472	0.96227
GSK864		-0.2069	0.15786	0.9308	0.0034737	0.98152	0.99704
AG-120	B-Alanine	0.40621	0.0044497	0.16815	0.45278	0.0013757	0.11039
AG-881		0.3173	0.030218	0.76903	0.392	0.0067711	0.26451
BAY 1436032		0.37864	0.0083226	0.20551	0.50239	0.00032883	0.044783
GSK864		0.51889	0.00019503	0.037417	0.53832	0.00010206	0.02314
AG-120	B-Citryl-L-glutamate	-0.65936	7.79E-07	1.93E-05	-0.21342	0.14497	0.36119
AG-881		-0.62685	4.18E-06	7.25E-05	-0.093432	0.53102	0.7861
BAY 1436032		-0.67195	4.42E-07	2.76E-05	-0.089991	0.54186	0.75522
GSK864		-0.65968	7.67E-07	3.62E-05	-0.15208	0.3011	0.56447
AG-120	Cysteine	0.66337	6.50E-07	0.00054053	0.64405	1.54E-06	0.0012823
AG-881		0.68918	2.73E-07	0.00022687	0.51145	0.00028958	0.10317
BAY 1436032		0.50239	0.00032883	0.064799	0.61224	6.11E-06	0.0076189
GSK864		0.13754	0.3501	0.96378	0.12603	0.39216	0.98824
AG-120	dADP	0.14221	0.33386	0.54318	0.13428	0.36171	0.60126
AG-881		0.21924	0.13844	0.38715	0.054579	0.71482	0.87437
BAY 1436032		0.20929	0.15304	0.3062	0.19855	0.17563	0.41523
GSK864		0.26205	0.072187	0.27332	0.30004	0.038681	0.17639

		2-Hydroxyglutarate			2-Oxoglutarate		
Inhibitor	Metabolite	Correlation	p-value	FDR	Correlation	p-value	FDR
AG-120	Deoxyribose 5-phosphate	0.80601	0	0	0.63667	2.14E-06	0.00016689
AG-881		0.83407	0	0	0.57447	3.39E-05	0.002645
BAY 1436032		0.72699	3.31E-08	5.81E-06	0.63102	2.74E-06	0.00022055
GSK864		0.74381	9.38E-09	1.38E-06	0.66522	5.99E-07	7.48E-05
AG-120	Glycerate	0.65252	1.06E-06	2.42E-05	0.25065	0.085847	0.26355
AG-881		0.52162	0.00021011	0.0021969	0.26168	0.075797	0.28874
BAY 1436032		0.57903	2.32E-05	0.00062469	0.27833	0.055741	0.2163
GSK864		0.47286	0.00078945	0.0096236	0.37082	0.009853	0.074841
AG-120	Isoleucine	0.5064	0.00029022	0.042577	0.38808	0.0067529	0.28036
AG-881		0.47583	0.00082967	0.089965	0.47329	0.0008909	0.13574
BAY 1436032		0.47036	0.00084734	0.10094	0.44941	0.0015053	0.085325
GSK864		0.26596	0.067924	0.83699	0.20354	0.16485	0.90195
AG-120	Methylisocitrate	-0.42032	0.0031681	0.0182	0.11518	0.43446	0.65867
AG-881		-0.49352	0.0004984	0.0046648	-0.040241	0.78775	0.91504
BAY 1436032		-0.41858	0.0033058	0.022695	0.23795	0.10338	0.31392
GSK864		0.11952	0.41724	0.69374	0.59933	1.04E-05	0.0006703
AG-120	N-Acetyl-aspartyl-glutamate	-0.56828	3.49E-05	0.00041774	-0.22384	0.12599	0.33496
AG-881		-0.52024	0.00021962	0.0022868	-0.079672	0.59342	0.81976
BAY 1436032		-0.50402	0.00031264	0.0041044	-0.0698	0.63638	0.8133
GSK864		-0.36854	0.010343	0.068743	-0.069257	0.63901	0.83345
AG-120	N-Acetyl-L-methionine	0.74783	5.59E-09	3.32E-07	0.66153	7.06E-07	8.02E-05
AG-881		0.71219	9.96E-08	3.70E-06	0.64443	1.96E-06	0.00054313
BAY 1436032		0.54418	8.33E-05	0.00164	0.7221	4.34E-08	1.55E-05
GSK864		0.46353	0.001026	0.011925	0.55851	5.01E-05	0.0019858
AG-120	O-Phosphoserine	0.69746	1.41E-07	4.96E-06	0.51107	0.00025055	0.0042452
AG-881		0.6657	7.66E-07	1.88E-05	0.51087	0.00029483	0.009096
BAY 1436032		0.60258	9.12E-06	0.00028486	0.5508	6.60E-05	0.0017368
GSK864		0.22905	0.11724	0.36762	0.078919	0.59285	0.80517
AG-120	Oxoadipate	-0.65176	1.09E-06	2.42E-05	-0.21418	0.14352	0.35972
AG-881		-0.16478	0.26744	0.56996	0.090888	0.54231	0.79299
BAY 1436032		-0.50923	0.0002656	0.0035878	0.033652	0.81997	0.91315
GSK864		-0.3401	0.018467	0.10441	-0.2196	0.13346	0.35405

		2-Hydroxyglutarate			2-Oxoglutarate		
Inhibitor	**Metabolite**	**Correlation**	**p-value**	**FDR**	**Correlation**	**p-value**	**FDR**
AG-120	**Putrescine**	**-0.32121**	**0.026456**	**0.56849**	**0.15458**	**0.29316**	**0.99464**
AG-881		**-0.62037**	**5.49E-06**	**0.0022815**	**-0.1213**	**0.41546**	**0.9959**
BAY 1436032		**-0.57154**	**3.09E-05**	**0.019279**	**-0.043856**	**0.76666**	**0.96537**
GSK864		**-0.63417**	**2.38E-06**	**0.0029734**	**-0.11832**	**0.42194**	**0.99373**

Table A.VIII.2. Template match correlation analysis to 2-HG and 2-OG of metabolites that were *not* significantly different between wtIDH1 and mutIDH1^{R132H} LN18 control cells, but responded to treatment with mutIDH1 inhibitors (AG-120, AG-881, BAY 1436032 and GSK864). The CSs were separately calculated for each inhibitor and control samples were included. The template match analysis was carried out using Spearman rank correlation as the distance measure. FDR = FDR adjusted p-value.

		2-Hydroxyglutarate			2-Oxoglutarate			Isocitrate		
Inhibitor	Metabolite	Correlation	p-value	FDR	Correlation	p-value	FDR	Correlation	p-value	FDR
AG-120	CMP-N-neuraminate	-0.01845	0.90083	0.94468	0.017369	0.90665	0.95987	-0.0774	0.60001	0.87322
AG-881		-0.16397	0.26983	0.57046	-0.04949	0.74045	0.89117	0.038737	0.79552	0.92621
BAY 1436032		0.11018	0.45475	0.64423	-0.05493	0.71002	0.85386	-0.03463	0.81483	0.93153
GSK864		0.42271	0.002987	0.027145	0.44073	0.001892	0.022838	-0.44985	0.001488	0.021073
AG-120	dUMP	-0.71852	5.22E-08	2.29E-06	-0.33337	0.021039	0.1037	0.21667	0.13882	0.51701
AG-881		-0.6886	2.80E-07	7.86E-06	-0.22549	0.12735	0.38762	0.28272	0.054497	0.22851
BAY 1436032		-0.56568	3.85E-05	0.000952	-0.29548	0.041849	0.18188	0.21798	0.13642	0.44447
GSK864		-0.58218	2.06E-05	0.000499	-0.2487	0.088381	0.28462	0.26672	0.067119	0.28238
AG-120	Galacturonate	-0.24522	0.093031	0.23785	-0.19985	0.17277	0.3994	0.66077	7.31E-07	0.000225
AG-881		-0.37165	0.010509	0.060095	0.12465	0.4026	0.6924	0.71404	9.17E-08	3.02E-05
BAY 1436032		-0.13374	0.36367	0.55789	-0.0761	0.60618	0.79228	0.68139	2.90E-07	3.15E-05
GSK864		0.18009	0.21991	0.51408	0.33315	0.021126	0.11972	0.41544	0.003569	0.040356
AG-120	Gluconate	0.64525	1.46E-06	3.05E-05	0.70202	1.15E-07	4.09E-05	0.18508	0.20722	0.61212
AG-881		0.58441	2.33E-05	0.000311	0.608	9.16E-06	0.001346	0.34968	0.016431	0.10686
BAY 1436032		0.43281	0.002319	0.017448	0.70517	9.91E-08	3.10E-05	0.28105	0.053322	0.25095
GSK864		0.49034	0.000474	0.006407	0.54125	9.23E-05	0.003141	0.26813	0.065645	0.27757
AG-120	Isocitrate	-0.08294	0.5741	0.73536	0.099001	0.50201	0.70877	1	0	0
AG-881		-0.16975	0.25312	0.55389	0.31973	0.028925	0.16171	1	0	0
BAY 1436032		-0.13059	0.37515	0.56681	0.22286	0.12769	0.3495	1	0	0
GSK864		-0.24631	0.091558	0.31911	-0.00836	0.95515	0.97785	1	0	0
AG-120	Citrate	-0.1726	0.23994	0.45084	0.001303	0.99325	0.99722	0.59585	1.20E-05	0.001259
AG-881		-0.23057	0.11881	0.35516	0.22086	0.1355	0.39978	0.69241	2.37E-07	4.34E-05
BAY 1436032		-0.21809	0.13622	0.27812	0.13645	0.35394	0.59967	0.65328	1.02E-06	9.46E-05
GSK864		-0.24381	0.094974	0.32247	0.053951	0.71496	0.87884	0.69106	1.88E-07	2.24E-05
AG-120	Myo-inositol	0.51238	0.00024	0.002093	0.42727	0.002667	0.022439	-0.20376	0.16439	0.55069
AG-881		0.035731	0.81111	0.92539	0.18259	0.21858	0.51531	0.10476	0.4822	0.74047
BAY 1436032		0.55688	5.31E-05	0.001252	0.27964	0.054569	0.21341	-0.15914	0.27902	0.64028
GSK864		-0.09368	0.52535	0.76711	-0.28561	0.049451	0.20094	0.26086	0.073531	0.29686

		2-Hydroxyglutarate			2-Oxoglutarate			Isocitrate		
Inhibitor	Metabolite	Correlation	p-value	FDR	Correlation	p-value	FDR	Correlation	p-value	FDR
AG-120	Sedoheptulose 1P	0.50901	0.000267	0.002265	0.29418	0.042793	0.16894	0.1104	0.45386	0.81652
AG-881		0.35812	0.013884	0.074615	0.14049	0.34509	0.6407	0.233	0.1149	0.36577
BAY 1436032		0.29885	0.039491	0.11847	0.26064	0.073777	0.25607	0.20593	0.15987	0.47571
GSK864		0.30417	0.035988	0.1713	-0.0406	0.78357	0.91611	0.20582	0.16009	0.44207
AG-120	Sorbitol 6P	-0.39991	0.005156	0.027414	-0.51498	0.000221	0.003921	-0.49924	0.000362	0.012751
AG-881		-0.33279	0.022737	0.10906	-0.64038	2.33E-06	0.000583	-0.50243	0.000382	0.007574
BAY 1436032		-0.23024	0.11531	0.24671	-0.51845	0.000198	0.00366	-0.58619	1.76E-05	0.000758
GSK864		-0.07479	0.61237	0.82011	-0.28517	0.04981	0.20174	-0.64231	1.67E-06	0.000107
AG-120	Glutamate	-0.03789	0.79774	1	0.22699	0.12065	0.99464	0.45973	0.001139	0.21736
AG-881		-0.07956	0.59395	0.98724	0.2315	0.11731	0.9959	0.56244	5.26E-05	0.015066
BAY 1436032		0.088906	0.54676	0.77947	0.41869	0.003297	0.12459	0.44507	0.001689	0.19206
GSK864		0.20158	0.16901	0.9308	0.40056	0.005079	0.30156	0.28984	0.046066	0.32738
AG-120	Glycine	0.56274	4.29E-05	0.013371	0.50879	0.000269	0.051657	0.12104	0.41131	0.71166
AG-881		0.47826	0.000775	0.089965	0.38714	0.007537	0.28057	0.19681	0.18432	0.57774
BAY 1436032		0.54038	9.51E-05	0.040568	0.5203	0.000186	0.034866	0.15632	0.28772	0.91056
GSK864		0.41413	0.003683	0.19544	0.36257	0.011728	0.40992	0.16403	0.26438	0.52475
AG-120	Proline	-0.29244	0.044078	0.76875	-0.06198	0.6747	0.99464	0.39731	0.005476	0.45749
AG-881		-0.17727	0.23247	0.98724	0.16859	0.2564	0.9959	0.43975	0.002176	0.12623
BAY 1436032		-0.00195	0.98974	0.99613	0.020083	0.8921	0.98665	0.32707	0.023713	0.57676
GSK864		-0.22178	0.12959	0.92625	0.055905	0.70509	0.99373	0.44084	0.001886	0.12721
AG-120	1-pyrroline hydroxycarboxylate	0.15827	0.28167	0.49293	0.40187	0.004927	0.03538	0.38211	0.007712	0.09539
AG-881		0.32678	0.025429	0.11746	0.47895	0.00076	0.015664	0.30296	0.038877	0.184
BAY 1436032		-0.09043	0.5399	0.71271	0.080439	0.58572	0.77786	0.59086	1.46E-05	0.000717
GSK864		0.087603	0.55267	0.78607	0.067521	0.64746	0.83965	0.50782	0.000278	0.005831
AG-120	3-hydroxy-Methyl-glutarate	0.4238	0.002908	0.0169	0.24414	0.094523	0.27987	0.44627	0.001636	0.035871
AG-881		0.62199	5.13E-06	8.66E-05	0.57366	3.49E-05	0.002645	0.30631	0.036687	0.17802
BAY 1436032		0.051889	0.72543	0.84618	0.12429	0.39876	0.64002	0.70908	8.26E-08	1.72E-05
GSK864		0.59477	1.25E-05	0.000329	0.51096	0.000251	0.005984	0.1485	0.31273	0.60302
AG-120	Acetylglycine	0.43736	0.002064	0.012641	0.6827	2.73E-07	5.69E-05	0.387	0.006919	0.089996
AG-881		0.3639	0.012342	0.067638	0.60187	1.17E-05	0.001396	0.45294	0.001547	0.020735
BAY 1436032		0.13797	0.34857	0.54138	0.46874	0.000887	0.011085	0.6498	1.19E-06	0.000103
GSK864		0.31405	0.030166	0.15047	0.44865	0.001536	0.019889	0.41424	0.003673	0.04135

		2-Hydroxyglutarate			2-Oxoglutarate			Isocitrate		
Inhibitor	**Metabolite**	**Correlation**	**p-value**	**FDR**	**Correlation**	**p-value**	**FDR**	**Correlation**	**p-value**	**FDR**
AG-120	**GABA**	**-0.44637**	**0.001632**	**0.10174**	**-0.51042**	**0.000256**	**0.051657**	**-0.25608**	**0.079108**	**0.59717**
AG-881		**-0.19484**	**0.18881**	**0.98724**	**-0.3617**	**0.01291**	**0.39265**	**-0.52995**	**0.00016**	**0.024183**
BAY 1436032		**-0.24577**	**0.092292**	**0.40235**	**-0.3794**	**0.008186**	**0.21046**	**-0.41088**	**0.003983**	**0.28391**
GSK864		**-0.12245**	**0.40584**	**0.96424**	**-0.3008**	**0.038173**	**0.68002**	**-0.47916**	**0.000659**	**0.082205**
AG-120	**Glutathione**	**-0.02551**	**0.86311**	**1**	**-0.12386**	**0.40042**	**0.99464**	**0.22981**	**0.11601**	**0.60008**
AG-881		**0.001041**	**0.99475**	**0.99798**	**0.056545**	**0.705**	**0.9959**	**0.29672**	**0.043242**	**0.40639**
BAY 1436032		**-0.0076**	**0.95925**	**0.98775**	**-0.03322**	**0.82226**	**0.98051**	**0.3097**	**0.03262**	**0.65762**
GSK864		**-0.28441**	**0.050442**	**0.79121**	**-0.23241**	**0.11185**	**0.87283**	**0.4746**	**0.000751**	**0.083089**
AG-120	**O-acetylserine**	**0.39188**	**0.006198**	**0.031484**	**0.67434**	**3.97E-07**	**6.79E-05**	**0.40686**	**0.004382**	**0.065569**
AG-881		**0.39674**	**0.00609**	**0.038723**	**0.58372**	**2.39E-05**	**0.00221**	**0.3861**	**0.007711**	**0.064232**
BAY 1436032		**0.13591**	**0.35588**	**0.54991**	**0.45028**	**0.001471**	**0.01641**	**0.60617**	**7.87E-06**	**0.000468**
GSK864		**0.31177**	**0.031435**	**0.15555**	**0.39069**	**0.006368**	**0.053764**	**0.40187**	**0.004927**	**0.050254**
AG-120	**2-C-methylerythritol 4P**	**0.76053**	**0**	**0**	**0.40328**	**0.004767**	**0.03463**	**-0.16175**	**0.27114**	**0.6893**
AG-881		**0.74919**	**1.18E-08**	**6.02E-07**	**0.36644**	**0.011712**	**0.093509**	**-0.25856**	**0.079455**	**0.28818**
BAY 1436032		**0.57371**	**2.85E-05**	**0.000726**	**0.47547**	**0.000733**	**0.009489**	**-0.10508**	**0.47601**	**0.77593**
GSK864		**0.38797**	**0.006769**	**0.050197**	**0.19507**	**0.18343**	**0.42897**	**0.044941**	**0.76105**	**0.90675**

Table A.VIII.3. Template match correlation analysis to 2-HG and 2-OG of metabolites that were *not* significantly different between wtIDH1 and mutIDH1^{R132H} LN18 control cells, and where only mutIDH1^{R132H} LN18 cells responded to treatment with mutIDH1 inhibitors (AG-120, AG-881, BAY 1436032 and GSK864). The CSs were separately calculated for each inhibitor and control samples were included. The template match analysis was carried out using Spearman rank correlation as the distance measure. FDR = FDR adjusted p-value.

		2-Hydroxyglutarate			2-Oxoglutarate		
Inhibitor	**Metabolite**	**correlation**	**p-value**	**FDR**	**correlation**	**p-value**	**FDR**
AG-120	ADP	-0.26943	0.064307	0.18578	-0.10204	0.48892	0.70098
AG-881		-0.18548	0.21128	0.49716	-0.17438	0.24027	0.5385
BAY 1436032		-0.02399	0.87121	0.93905	0.004234	0.97742	0.98877
GSK864		-0.05743	0.69744	0.87059	0.10074	0.49451	0.73602
AG-120	Glucose	0.33869	0.018983	0.076513	0.30656	0.034501	0.1505
AG-881		0.12939	0.38483	0.67017	0.12234	0.41144	0.69614
BAY 1436032		-0.03181	0.82971	0.91269	0.19127	0.19224	0.43435
GSK864		-0.31991	0.027101	0.13848	-0.23155	0.11322	0.32862
AG-120	N-acetyl-alanine	0.43758	0.002052	0.012633	0.68606	2.35E-07	5.47E-05
AG-881		0.35835	0.013819	0.074428	0.60442	1.06E-05	0.001393
BAY 1436032		0.093465	0.52632	0.70297	0.40556	0.004519	0.037766
GSK864		0.23328	0.11049	0.35398	0.32251	0.025824	0.13558
AG-120	Nonate	-0.17282	0.23934	0.45062	-0.24056	0.099578	0.29071
AG-881		-0.1028	0.49049	0.74786	-0.25173	0.087936	0.31357
BAY 1436032		-0.31828	0.027925	0.092306	-0.16229	0.26952	0.5197
GSK864		-0.02855	0.84695	0.9328	0.12972	0.37836	0.64103
AG-120	TDP	0.47264	0.000794	0.005754	0.60671	7.69E-06	0.000401
AG-881		0.69496	2.12E-07	6.31E-06	0.47722	0.000798	0.016211
BAY 1436032		0.55384	5.92E-05	0.00131	0.54983	6.84E-05	0.001779
GSK864		0.49598	0.0004	0.005586	0.62766	3.17E-06	0.000293

9.9. Appendix IX

The experiment that the data in this appendix is based on was a metabolomics experiment of mutIDH1^{R132H} LN18 cells treated with a range of concentrations (0.05, 0.50, 5.00 and 10.0 μM) of CB-839 in **chapter 6**. This appendix includes a DNA concentration table (**Table A.IX.1**), IC-MS identifications (**Table A.IX.2**), derivatised RPLC-MS identifications (**Table A.IX.3**), and data processing information (**Figure A.IX.1**). The calibration curve used for quantifying glucose in media samples is shown in **Figure A.IX.2**, with the absorbance and calculated concentrations for the samples in **Table A.IX.4** (wtIDH1 samples) and **A.IX.5** (mutIDH1^{R132H} samples).

Table A.IX.1. DNA concentration of wtIDH1 (WT) and mutIDH1^{R132H} (MUT) LN18 cells from the CB-839 concentration range experiment. Harvested with 12-well harvesting method and subsequently analysed with IC-MS, derivatised RPLC-MS and underivatized RPLC-MS. The maximum possible volume was made up for each sample, usually 50 µL and sometimes less. Rel. DNA conc. = relative DNA concentration.

Sample Name	DNA 1 (ng/µL)	DNA 2 (ng/µL)	DNA 3 (ng/µL)	Average (ng/µL)	Rel. DNA conc.	µL Sample	µL Solvent
MUT-0.05_01	31.90	31.80		31.85	1.093	4.2	45.8
MUT-0.05_02	35.10	35.10		35.10	1.204	8.5	41.5
MUT-0.05_03	39.20	38.50		38.85	1.333	12.5	37.5
MUT-0.05_04	50.80	51.60		51.20	1.756	21.5	28.5
MUT-0.10_01	39.30	40.70		40.00	1.372	13.6	36.4
MUT-0.10_02	37.00	37.10		37.05	1.271	10.7	39.3
MUT-0.10_03	41.10	42.10		41.60	1.427	15.0	35.0
MUT-0.10_04	33.40	33.50		33.45	1.148	6.4	43.6
MUT-0.30_01	36.00	35.20		35.60	1.221	9.1	40.9
MUT-0.30_02	42.50	42.60		42.55	1.460	15.7	34.3
MUT-0.30_03	38.70	39.00		38.85	1.333	12.5	37.5
MUT-0.30_04	44.80	45.70		45.25	1.552	17.8	32.2
MUT-0.70_01	33.70	32.70		33.20	1.139	6.1	43.9
MUT-0.70_02	36.70	37.00		36.85	1.264	10.4	39.6
MUT-0.70_03	39.30	39.10		39.20	1.345	12.8	37.2
MUT-0.70_04	38.80	39.10		38.95	1.336	12.6	37.4
MUT-1.0_01	18.90	19.30		19.10	-	0.00	50.00
MUT-1.0_02	35.30	34.90		35.10	1.204	8.5	41.5
MUT-1.0_03	35.90	36.10		36.00	1.235	9.5	40.5
MUT-1.0_04	32.40	33.30		32.85	1.127	5.6	44.4
MUT-3.0_01	38.30	39.60		38.95	1.336	12.6	37.4
MUT-3.0_02	35.90	34.80		35.35	1.213	8.8	41.2
MUT-3.0_03	37.20	37.70		37.45	1.285	11.1	38.9
MUT-3.0_04	35.80	35.80		35.80	1.228	9.3	40.7
MUT-5.0_01	32.20	32.70		32.45	1.113	5.1	44.9
MUT-5.0_02	37.00	38.20		37.60	1.290	11.2	38.8
MUT-5.0_03	34.20	34.20		34.20	1.173	7.4	42.6
MUT-5.0_04	34.50	35.20		34.85	1.196	8.2	41.8
MUT-Co_01	37.80	37.80		37.80	1.297	11.4	38.6
MUT-Co_02	41.30	46.70		44.00	1.509	16.9	33.1
MUT-Co_03	70.50	70.40		70.45	2.417	29.3	20.7
MUT-Co_04	53.20	54.70		53.95	1.851	23.0	27.0
MUT-Co_05	39.20	39.80		39.50	1.355	13.1	36.9
MUT-Co_06	41.30	43.00		42.15	1.446	15.4	34.6
MUT-Co_07	52.90	52.90		52.90	1.815	22.4	27.6
MUT-Co_08	52.60	54.00		53.30	1.828	22.7	27.3
WT-0.05_01	37.50	37.00		37.25	1.278	10.9	39.1
WT-0.05_02	36.10	35.20		35.65	1.223	9.1	40.9
WT-0.05_03	52.30	53.20		52.75	1.810	22.4	27.6
WT-0.05_04	64.00	60.50	63.10	62.53	2.145	26.7	23.3
WT-0.10_01	39.70	44.20	43.90	42.60	1.461	15.8	34.2
WT-0.10_02	40.40	40.40		40.40	1.386	13.9	36.1
WT-0.10_03	46.80	45.20		46.00	1.578	18.3	31.7
WT-0.10_04	63.10	60.30		61.70	2.117	26.4	23.6
WT-0.30_01	41.10	41.60		41.35	1.419	14.8	35.2
WT-0.30_02	48.30	47.10		47.70	1.636	19.4	30.6
WT-0.30_03	43.30	43.30		43.30	1.485	16.3	33.7
WT-0.30_04	39.80	40.60		40.20	1.379	13.7	36.3
WT-0.70_01	39.00	39.00		39.00	1.338	12.6	37.4

Sample Name	DNA 1 (ng/µL)	DNA 2 (ng/µL)	DNA 3 (ng/µL)	Average (ng/µL)	Rel. DNA conc.	µL Sample	µL Solvent
WT-0.70_02	42.30	43.70		43.00	1.475	16.1	33.9
WT-0.70_03	42.70	44.40		43.55	1.494	16.5	33.5
WT-0.70_04	45.50	45.80		45.65	1.566	18.1	31.9
WT-1.0_01	38.20	38.30		38.25	1.312	11.9	38.1
WT-1.0_02	30.20	32.90	31.70	31.60	1.084	3.9	46.1
WT-1.0_03	30.40	30.20		30.30	1.039	1.9	48.1
WT-1.0_04	40.40	41.10		40.75	1.398	14.2	35.8
WT-3.0_01	39.00	39.50		39.25	1.346	12.9	37.1
WT-3.0_02	42.20	43.00		42.60	1.461	15.8	34.2
WT-3.0_03	44.20	43.60		43.90	1.506	16.8	33.2
WT-3.0_04	50.70	49.50		50.10	1.719	20.9	29.1
WT-5.0_01	29.00	29.30		29.15	1.000	0.0	50.0
WT-5.0_02	40.50	40.70		40.60	1.393	14.1	35.9
WT-5.0_03	40.00	40.50		40.25	1.381	13.8	36.2
WT-5.0_04	43.20	44.30		43.75	1.501	16.7	33.3
WT-Co_01	47.90	49.10		48.50	1.664	19.9	30.1
WT-Co_02	53.20	54.00		53.60	1.839	22.8	27.2
WT-Co_03	57.50	59.30		58.40	2.003	25.0	25.0
WT-Co_04	65.10	67.00		66.05	2.266	27.9	22.1
WT-Co_05	45.90	45.60		45.75	1.569	18.1	31.9
WT-Co_06	52.40	52.30		52.35	1.796	22.2	27.8
WT-Co_07	52.20	53.10		52.65	1.806	22.3	27.7
WT-Co_08	58.70	59.10		58.90	2.021	25.3	24.7

Table A.IX.2. Annotated metabolites from the IC-MS data of CB-839 concentration range experiment. Parameters used for determining whether it was a putative or confident identification. FS = fragmentation score, ME = mass error, ISS = isotope similarity score, RTE = retention time error, max. abun. = max abundance and min. CV% = minimum coefficient of variance, C = Confident and P = putative. When provided as a comment, the abbreviation indicates what brought the identification from confident to putative (RTE > 1.5 min, ME > 3 ppm, IS < 90%).

Accepted identification	FS	ME (ppm)	ISS	RTE (min)	Max. Abun.	Min. CV%	C/P	Comment
1,2,3-Trihydroxybenzene	0	-4.71	93.0	-1.18	117	17.8	P	ME
1-Pyrroline hydroxycarboxylic acid	0	-1.22	96.0	-0.57	489	15.2	C	
2-butyl-3-ureido-succinate	0	-2.95	97.3	-1.65	127	35.6	P	RTE
2-Hydroxybutyric acid	47.9	0.05	96.6	-0.88	5506	4.1	P	Isomer of 3-hydroxybutyric acid
2-Hydroxyglutarate	77.1	-1.39	99.8	-1.14	1667393	3.6	C	
2-Isopropylmalic acid	5.77	-2.72	94.1	-1.17	815	12.9	C	
2-Ketobutyric acid	42.3	-0.03	96.7	-0.96	4953	2.5	C	
2-Oxoglutaric acid	48.3	-1.81		-1.45	47878	5.2	C	
3-(2,5-Dioxoimidazolidin-4-yl) propanoic acid	0	2.55	98.5		4221	8.7	P	No RT
3,3 Dimethyl glutarate	93.8	-1.92	99.0	-1.71	5105	4.1	P	RTE
3,4-dihydroxyphenyl acetic acid	0	-1.38	94.4	-1.7	657	8.8	P	RTE
3-Dehydroquinate	58.8	-1.68	97.9	-0.31	3220	2.5	C	
3-deoxy-2-keto-6-phosphogluconic acid	74.8	3.08	97.7	-1.61	698	7.6	P	RTE
3-Hydroxyisovaleric acid	0	-4.94	97.8	0.11	521	3.7	P	ME
3-Hydroxymethyl-glutarate	80.2	-1.91	98.5	-1.16	17414	9	C	
3-methoxyphenyl-acetic acid	0	-2.42	97.0	0.96	4121	2.6	C	
3-Methyl-2-oxovaleric acid	0	-0.68	99.8	-0.91	33011	5.5	C	
3-Phosphoglyceric acid	25.9	-1.58	98.5	-1.59	30275	14.6	P	RTE
4-Hydroxy-3-methoxymandelic acid	0	-0.7	90.8	-1.11	7971	4.3	C	
4-Hydroxybenzoic acid	0	-1.43	94.4	-1.72	10158	3.3	P	RTE
4-Hydroxyproline	91	-1.24	98.4	-0.6	13261	8.6	C	
4-Hydroxy-pyrrolidinone	0	-1.26	99.2	0.43	425	25.5	C	
5-Hydroxyhexanoic acid	0	-4.79	93.0	-0.88	346	6.3	P	ME

Accepted identification	FS	ME (ppm)	ISS	RTE (min)	Max. Abun.	Min. CV%	C/P	Comment
6-Phosphogluconic acid	0	-0.49	96.9	-1.97	2451	4.8	P	RTE
Abscisic acid	18.5	-1.23	96.7	-1.75	314	22	P	RTE
Acetic acid	0	-0.91	99.5	-1.06	1235	10.8	C	
Acetoacetate	0	-1.04	92.8	-1.17	1957	4.7	C	
Acetylcysteine	42.6	-1.72	94.5	-1.13	6596	2.9	C	
Acetylglycine	78.3	-0.95	95.9	-0.31	2341	4.8	C	
Adenosine diphosphate	17.7	-1.42	96.9	-1.71	997880	3	P	RTE
Adenosine monophosphate	43.5	-1.89	95.0	-0.7	155825	6.3	C	
Adenosine triphosphate	0	-1.88	85.3	1.36	1292	18.1	P	IS
Adonitol	80.1	-1.53	99.5	-0.24	6799	1.9	P	Isomer of arabitol and xylitol
ADP Glucose	16.7	-0.3	99.3	-1.65	1422	20	P	RTE
Arabinonic acid	64.9	-2.53	94.9	-1.45	3609	2.6	C	
Arabinose	28.4	-1.86	96.7	-0.19	823	6.8	P	Isomer of pentoses
Arabitol	0	-1.29	99.2	-0.48	5794	6.4	P	Isomer of adonitol and xylitol
Ascorbate	6.59	-2.33	99.2	-1.48	3878	4.7	C	
Beta-Alanine	59.5	-0.97	74.7	-0.97	1469	5.5	C	
Beta-Citryl-L-glutamic acid	0	-1.43	98.4	-0.84	549545	10.4	C	
Butyric acid	85.5	-1.43	91.9	-1.67	3097	2.3	P	RTE
Caffeic acid	0	-3.99	96.7		4688	3.4	P	No RT and ME
Citraconic acid	0	-0.17	98.9	-1.02	3171	3	P	Isomer of e.g. itaconic and mesaconic acid
Citric acid	0	-2.77	98.7	-0.71	6781	3.6	P	Isomer of isocitric acid
Cytidine monophosphate	0	-1.66	87.9	-1.25	9937	6.7	P	IS
Cytidine monophosphate N-acetylneuraminic acid	0	-1.78	97.1	-0.99	99993	2.5	C	
Cytidine triphosphate	7.2	-1.79	97.9	-1.85	297888	4.5	P	RTE
dCTP	0	-2.48	95.3	-1.15	2658	4.9	C	
Deoxyribose 5-phosphate	13.1	-1.08		-0.22	3431	4.2	C	
Dihydroxyacetone	75.7	-0.92	99.9	-0.65	1291053	4.1	P	Isomer of lactic acid
Dihydroxyacetone phosphate	0	-1.77	99.1	-1.55	445	7.6	P	RTE
Dimethyl fumarate	0	-0.87	96.8	-0.77	12480	2.7	C	
dTDP-D-glucose	0	-1.89	95.8	-1.61	81734	2.5	P	RTE
dUMP	0	-1.74	94.8	-1.81	17534	8.9	P	RTE

Accepted identification	FS	ME (ppm)	ISS	RTE (min)	Max. Abun.	Min. CV%	C/P	Comment
Ferulic acid	0	-1.75	89.6	-0.38	2772	4.8	P	IS
Flavin Mononucleotide	0	-1.98	91.5		15806	4.7	P	No RT
Fructose 1,6-bisphosphate	50.1	-1.38		-1.88	649	30	C	
Fructose 2,6 diphosphate	0	-2.02	98.4	-0.31	65185	2.4	C	
Fructose 6-phosphate	67.1	-2.3	99.2	-1.21	5291	1.7	P	Isomer of mannose 6P
Fumarate	0	-0.68	94.9	-0.64	320	7	C	
Galactaric acid	35.4	-1.46	97.0	-1.18	5569	7.9	C	
Galacturonic acid	78.1	-2.25	99.6	-0.18	2538	6	P	Isomer of glucuronic acid
Gluconate	72.8	-2.19		-0.76	54864	6.7	C	
Gluconolactone	0	-2.1	92.4	1.51	902	8.2	P	RTE
Glucose	0	-1.63	89.2	1.1	1560	2.7	P	Isomer of hexoses
Glucose 1-phosphate	87.1	-2.4	98.7	-1	74703	11.9	P	Isomer of galactose 1P
Glucuronic acid	0	-1.81	95.1	1.33	307	16.9	C	
Glutaconic acid	0	-0.4	99.0	0.3	3651	4.6	P	Isomer of e.g. mesaconic and itaconic acid
Glutamylcysteine	0	-4.22	93.1	-0.27	32759	4.3	P	ME
Glutaric acid	73.7	-1.41	96.5	-1.17	11823	1	P	Isomer of ethylmalonic acid
Glutathione (GSH)	0	-1.59	88.5	1.18	1112	12.3	P	IS
Glycerol	58.6	-1.02	100.0	-0.19	3386295	2.9	C	
Glycerol 3-phosphate	0	1.59		-0.29	415	9.2	C	
Guanosine diphosphate	97.4	-0.51	97.7	-0.14	2171922	7.2	C	
Hippuric acid	67.7	-1.88	90.3	-1.37	2943	10.6	C	
Homogentisic acid	0	-1.6	90.9	0.04	609	7.5	C	
Hydroxy-isobutyric acid	0	-2.01	98.7	-1.25	1294	43.3	P	Isomer of 3-hydroxybutyric acid
Hydroxyiso-heptanoic acid	0	-4.62	98.5	1.01	99	17.8	P	ME
Isocitrate	0	-3.11	97.9	-0.09	3892	3.8	P	IS and isomer of citric acid
Kojic acid	93.7	-1.24	97.5	-0.15	4019	2.3	C	
Kynurenic acid	0	-1.64	88.8	-1.75	707	50.3	P	RTE
Lactic acid	0	-1.52	96.1	0.23	814	10.5	P	Isoemr of dihydroxyacetone
Lactose	80.4	-3.35	89.6	-0.37	770275	13.6	P	ME and IS
Lactoyl-isoleucine	0	-4.67	96.7	-0.21	3338	5.2	C	
Maleic acid	0	-4.98	94.9	1.82	630	3.6	C	
Malic acid	72.7	-0.92	99.1	-1.13	189122	4.6	C	
Malitol	0	-2.69	93.9	-0.55	8291	4.6	C	

Accepted identification	FS	ME (ppm)	ISS	RTE (min)	Max. Abun.	Min. CV%	C/P	Comment
Methionine sulfoxide	0	-0.7	88.9		223	30.1	P	No RT and IS
Methylglutaric acid	23.1	-0.92	95.4	-0.89	8075	7.8	C	
Methylisocitric acid	0	-1.16	98.9	-0.91	5693	3.7	P	Isomer of 2-methylcitric acid
Myoinositol	94.5	-2.06	97.3	-0.23	3530570	5	P	Isomer of e.g. scyllitol
N-Acetyl-aspartate	0	-1.93	98.7	-0.95	314574	6.5	C	
N-Acetylaspartyl-glutamic acid	0	-0.83	99.4	-1.41	72005	3.4	C	
N-Acetyl-D-glucosamine	52.2	-1.11	95.2	-0.15	404	69.3	C	
N-acetyl-glucosamine-1-phosphate	0	-1.96	97.4	-0.66	3289	7	C	
N-Acetylglutamate	70.4	-4.85	91.4	-0.84	26639	6.5	P	ME
N-Acetyl-L-alanine	83.8	-1.52	94.9	-0.47	8087	3.5	C	
N-Acetyl-L-methionine	97.3	-1.55	95.3	-0.46	8599	9.4	C	
N-Acetyl-L-phenylalanine	38.6	-1.96	98.5	-0.84	287	14.1	C	
N-Acetylneuraminic acid	90.1	-1.31	94.9	-0.78	269933	15.4	C	
N-Acetylvaline	68.8	-2.24	92.0	-0.56	715	14.7	C	
NADH	0	-1.51	94.1	-1.63	776	11.1	P	RTE
NADPH	0	-1.96	91.7	0.66	11128	23	C	
N-carbamoyl-L-aspartic acid	0	-1.71	97.2	-1.22	3622	4.8	C	
N-Formyl-methionine	0	-2.42	95.3	-0.86	1154	7.8	C	
Nonate	0	-4.79	95.4	-0.64	9444	8.5	C	
O-Acetylserine	0	-0.63	93.7	-0.6	311820	3.9	C	
O-Phosphoserine	77.4	-1.4	97.2	-1.38	43696	6.7	C	
Oxoadipic acid	50.2	-2.67	96.2	-1.82	3941	5	P	ME
Pantothenic acid	61.8	-2.06	97.8	-0.8	418670	7.5	C	
Phenylacetic Acid	0	-4.62	91.3	1.31	4975	2.3	P	ME
Phenylacetylglycine	0	-4.17	97.1	0.47	178	32.1	P	ME
Phosphocreatine	47.1	-4.13	98.4	-0.63	99087	9.7	P	ME
Phosphoenolpyruvic acid	26.9	-2.09	99.5	-1.76	6347	10.3	P	RTE
Phosphoglycolic acid	78	-1.22	99.7	-1.59	148	34.5	P	RTE
Phosphoribosyl pyrophosphate	0	-1.74	95.4	-1.66	9282	7.9	P	RTE
Protocatechuic acid	0	-2.96	90.0	-1.23	684	10.9	C	
Pyridoxal 5'-phosphate	0	-2.82	90.0	-1.71	1564	5.1	P	RTE
Pyruvic acid	73.4	-1.01	99.8	-1.01	61794	2.5	C	
Quercetin	0	4.92	83.6	-0.63	755	9.4	P	ME
Quinic acid	34.5	-1.98	94.6	-1.04	1093	16.4	C	
Quinolinic acid	0	3.93	91.5	-0.03	1375	8.3	C	
Raffinose	0	-0.98	89.2	-0.01	1646	68.5	P	IS

Accepted identification	FS	ME (ppm)	ISS	RTE (min)	Max. Abun.	Min. CV%	C/P	Comment
Ribose 5-phosphate	66.8	1.53	97.0	-1.37	85858	1	P	Isomer of xylulose 5P
Ribulose 5-phosphate	16.8	1.18	94.4	-0.75	8117	5.3	C	
Scyllitol	0	-1.57	98.6	-0.09	126789	3.7	P	Isomer of myo-inositol
Sebacic acid	0	-0.18	88.8	-1.81	440	2.8	P	RTE and IS
Sedoheptulose 1-phosphate	0	-0.17	92.1	-0.56	3057	5.9	C	
Sedoheptulose 7-phosphate	67.8	-0.73		-1.24	2834	3.1	C	
Sorbitol	76.9	-2.31	99.4	-0.19	118229	8.2	P	Isomer of mannitol
Sorbitol-6-phosphate	0	-1.03	97.8	0.1	22226	10.2	C	
Succinic acid	0	0.1	97.1	-1.2	14989	1.7	C	
Succinic acid semialdehyde	0	-0.56	98.8	-1.3	11125	4.5	C	
Taurine	92.9	-1.29	93.2	-0.81	1033558	4.5	C	
TDP	0	-2.19	86.7	-1.51	3317	5.9	P	RTE and IS
Threitol	87.7	-0.74	98.3	-0.16	22079	7	C	
Thymidine triphosphate	6.71	-1.93	92.3	-1.69	12287	4.5	P	RTE
Tyrosol	0	-0.6	85.4	1.24	237	4.8	P	IS
UDP-galactose	0	-1.73	96.5	-1.34	22771	8.6	P	Isomer of UDP/glucose
Uracil	76.7	0.08	94.9	-1.49	362	10.6	C	
Ureidopropionic acid	0	-4.1	94.4	1.76	249	8.8	P	RTE
Uridine 5'-diphosphate	13.7	-1.9	98.7	0.71	3173857	4.6	C	
Uridine 5'-monophosphate	53.3	-1.98	97.8	-1.99	149042	2.7	P	RTE
Xanthylic acid	0	-3.24	95.8	0.2	186	50.2	P	ME
Xylitol	0	-0.6	99.6	0.72	161	21.3	P	Isomer of arabitol and adonitol

Table A.IX.3. Annotated metabolites from the derivatised RPLC-MS data of the CB-839 concentration range experiment. Parameters used for determining whether it was a putative or confident identification. ME = mass error, ISS = isotope similarity score, RTE = retention time error, max. abun. = max abundance and min. CV% = minimum coefficient of variance, C = Confident and P = putative. When provided as a comment, the abbreviation indicates what brought the identification from confident to putative (isomer, RTE > 0.5 min, ME > 3 ppm, IS < 90%).

Accepted Description	ME (ppm)	ISS	RTE (min)	Max. abun.	Min. CV%	C/ P	Comment
2-Aminoadipic acid	-0.04	97.7	0.21	301	7.7	C	
4-Hydroxyproline	-0.53	96.3		30	6.7	P	No RT
Alanine	-0.68	97.3	0.24	9343	3	C	
Amino methoxybenzoic acid	-3.47	92.9	-0.29	6	14.2	P	ME
GABA	-2.91	81	0.33	35	1.7	P	Isomer of 3-amino-2-methylpropanoic acid
Arginine	-0.89	97.4	0.28	102	4.5	C	
Asparagine	-2.09	95	0.18	91	4.6	C	
B-alanine	-0.11	91.9	0.25	581	2.5	C	
Citrulline	-1.87	96.6	0.21	26	7.7	C	
Cysteine	-3.36	88.7	-0.85	34	5.7	P	IS
Glutamic acid	-0.43	95.8	0.23	5110	3.5	C	
Glutamine	-0.61	96.1	0.21	3200	9.7	C	
Glycine	-1.18	97.4	0.31	2251	1.9	C	
Gly-Gly	-0.32	88		8	7.3	P	No RT and IS
Histidine	-1.31	96	0.29	236	11.4	C	
Homocysteine	-2.03	93.7	0	5	8.6	C	
Homoserine	-3.05	96	0.2	7	8.9	C	
Hypotaurine	0.46	93.5	0.3	109	2.1	C	
Hypoxanthine	-4.93	95.2	-0.13	4	16.1	P	ME
Isoleucine	-0.59	97.2	0.27	3741	2	P	Isomer of leucine
Kynurenine	-2.91	88.3	0.17	2	34.4	P	IS
L-Cystathionine	-1.40	84.7	0.15	2	18.2	P	IS
L-Cystine	-0.42	93		3	20.1	P	No RT
Leucine	-0.56	95	0.09	2890	4.8	P	Isomer of isoleucine
Lysine	0.12	96.7	0.14	2023	4.1	C	
N-Acetyl-ornithine	-1.88	97.6	0.11	16	3.1	P	Isomer of L-theanine
Ornithine	-3.77	94.8	0.29	23	5.4	P	ME
Oxidised Glutathione	-0.15	92	0.1	1688	6.5	C	
Phenylalanine	-0.68	95.9	0.18	2484	4.4	C	
Pipecolic acid	-4.38	95.7	0.54	33	7.9	P	ME
Proline	-1.53	98.5	0.25	470	3.7	C	
Putrescine	-0.73	95.8	0.09	199	5.1	C	
Pyroglutamic Acid	-0.88	90.5	-0.89	12	3.7	P	RTE
Serine	-1.62	97.7	0.33	736	2.3	C	
Serotonin	1.02	85	0.05	19	4.7	P	IS
Taurine	-2.09	95.6		881	4.2	P	No RT
Threonine	-0.62	96.2	0.26	3521	1	C	
Tryptophan	-1.19	93.2	0.16	438	2.4	C	
Tyrosine	-0.57	95.8	0.17	1761	3.1	C	
Valine	-0.69	97.2	0.19	2735	1.1	C	

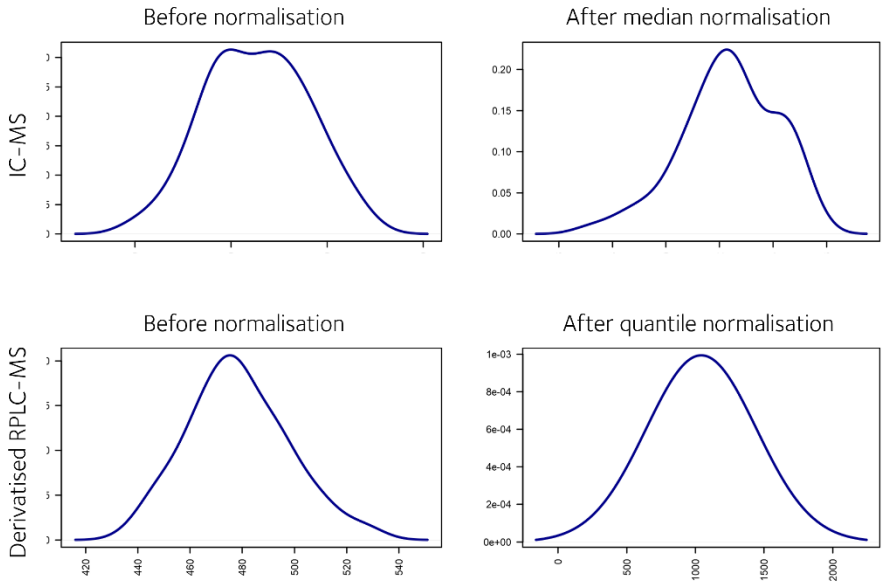

Figure A.IX.1. Sample distribution plots of IC-MS and derivatised RPLC-MS data from the CB-839 concentration range experiment before and after normalisation.

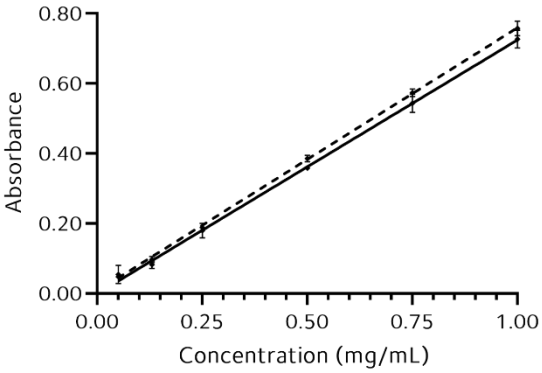

Plate	Line	Formula	R^2
WT	———	Y = 0.7236 + 0.0006	0.9994
MUT	– – – .	y = 0.7508x + 0.0083	0.9996

Figure A.IX.2. Calibration curves for quantifying glucose in media (mg/mL). The samples were measured on two plates and calibration curves were prepared for each plate.

Table A.IX.4. Absorbance and calculated concentration of glucose concentration (mg/mL) in the wtIDH1 media samples of the CB-839 concentration range experiment. The concentration was calculated with the formula given for WT in Figure A.IX.2**.**

Concentration CB-839 (µM)	Absorbance		Glucose concentration (mg/mL)	
	Average	Standard deviation	Average	Standard deviation
0	0.82	0.09	1.1	0.2
0.05	0.62	0.12	0.8	0.2
0.10	0.91	0.04	1.3	0.2
0.30	0.94	0.02	1.29	0.06
0.70	0.77	0.02	1.06	0.03
1.00	0.74	0.07	1.0	0.2
3.00	0.60	0.12	0.83	0.05
5.00	0.66	0.04	0.91	0.03

Table A.IX.5. Absorbance and calculated concentration of glucose concentration (mg/mL) in the mutIDH1^{R132H} media samples of the CB-839 concentration range experiment. The concentration was calculated with the formula given for MUTT in Figure A.IX.2**.**

Concentration CB-839 (µM)	Absorbance		Glucose concentration (mg/mL)	
	Average	Standard deviation	Average	Standard deviation
0	0.87	0.34	1.2	0.2
0.05	1.01	0.21	1.3	0.2
0.10	1.01	0.13	1.3	0.3
0.30	0.92	0.15	1.2	0.2
0.70	0.97	0.12	1.3	0.2
1.00	0.84	0.13	1.1	0.1
3.00	0.77	0.07	1.0	0.1
5.00	0.82	0.09	1.08	0.09

9.10. Appendix X

R code used for data analysis is presented below.

CHECKING DATA NORMALISATION, SCALING AND TRANSFORMATION

```
##### SECTION 1: SET VARIABLES #####
# Fill in the path to the correct folder and NB! You need FORWARD slashes, not backward slashes
wd = "…/Folder"

# File name, needs to include .csv at the end! And be in the folder set in wd.
filnm = " example.csv "

# Filtration parameters
# filt options: rsd, nrsd, mean, sd, mad, iqr or none
filt = "iqr"

#########################################################################
##### SECTION 2 #####

### SET WORKING DIRECTORY ###
# Working directory is also where generated files will be saved
setwd(wd)

### INSTALL AND LOAD PACKAGES ####
pacman::p_load(pacman, rio, tidyverse, tibble)
library(png);library(grid);library(gridExtra); library(ggplot2); library(MetaboAnalystR)

# Missing library needed to do CVs: library(mvrVal)

### READING THE DATAFILE ###
# Make the object the data goes into
mSet<-InitDataObjects("pktable", "stat", FALSE)

# Upload file
# Add the correct file name in here -- make sure it is in the correct folder!
# Check the Read.TextData() on how to correctly specify data format and label types.
mSet<-Read.TextData(mSet, filnm, "colu", "disc")

### DATA INTEGRITY CHECK AND REPLACE MISSING VALUES ###
# Check the data
mSet$msgSet$read.msg
mSet<-SanityCheckData(mSet)
mSet<-ContainMissing(mSet)

# Replace missing data with a minimum value
mSet<-ReplaceMin(mSet)
mSet<-SanityCheckData(mSet)
mSet<-ContainMissing(mSet)

### FILTRATION ###
mSet<-FilterVariable(mSet, filt, "F", 25)

### NORMALISATION, SCALING AND TRANSFORMATION ###
#  Prepare for normalization
mSet<-PreparePrenormData(mSet)
```

```
# Vectors with the different normalization, transformation and scaling parameters
Norm<-c("NULL", "SumNorm", "MedianNorm", "QuantileNorm")
Trans<-c("NULL", "LogNorm")
Scal<-c("NULL", "AutoNorm", "ParetoNorm")

# Looping through different normaliZation, transformation and scaling methods
# mSet2 is the mSet object used within the loop, while the original non-normalised mSet is retained outside of the loop.
for (i in Norm){
 for (j in Trans){
  for(k in Scal){
   # Do normalization/transformation/scaling
   mSet2<-Normalization(mSet, rowNorm = i, transNorm = j, scaleNorm = k, ratio=FALSE, ratioNum=20)

   # Make a title indicating what normalization etc has been done
   title = paste(i, j, k)

   # Make the Sample and feature normalization plots
   mSet2<-PlotNormSummary(mSet2, paste("FEATURES", title, sep = " "), "png", 300, width=NA)
   mSet2<-PlotSampleNormSummary(mSet2, paste("SAMPLES", title, sep = " "), "png", 300, width=NA)

   # Do PCA and make scatter plots of PC1 versus PC2
   mSet2<-PCA.Anal(mSet2)
   mSet2<-PlotPCA2DScore(mSet2, paste("PCA", title, sep = " "), "png", 300, width=NA, 1, 2)

   # Plot HEATMAP
   mSet2<-PlotHeatMap(mSet2, paste("HEATMAP", title, sep = " "), "png", 300, width=NA, "norm", "row",
              "euclidean", "ward.D","bwm", "overview", F, F, NULL, T, F)

   # Save each .png with title etc
   title1<-paste("FEATURES ", title, "dpi300", ".png", sep="")
   plot1<-readPNG(title1, native = FALSE, info = FALSE)

   title2<-paste("SAMPLES ", title, "dpi300", ".png", sep="")
   plot2<-readPNG(title2, native = FALSE, info = FALSE)

   title3<-paste("PCA ", title, "dpi300", ".png", sep="")
   plot3<-readPNG(title3, native = FALSE, info = FALSE)

   title4<-paste("HEATMAP ", title, "dpi300", ".png", sep="")
   plot4<-readPNG(title4, native = FALSE, info = FALSE)

   # Combine the .pngs into a group image
   ggsave(paste("GROUP", title, ".png"), arrangeGrob(rasterGrob(plot1), rasterGrob(plot2), rasterGrob(plot3), rasterGrob(plot4), nrow=1, top=title), height=12.0, units="cm", dpi=300)

  }}}
```

OUTPUT NORMALISED DATA FILE AND CALCULATE MEAN AND STANDARD DEVIATION

```
##### SECTION 1: SET VARIABLES #####
#Fill in the path to the correct folder and NB! You need FORWARD slashes, not backward slashes
wd = "…/folder"

# Filename, needs to include .csv at the end! And be in the folder set in wd.
filnm = "example.csv "

# File name for mean and SD calculations
filn_ms = "example_tidy.csv "

# Filtration parameters
# filt options: rsd, nrsd, mean, sd, mad, iqr or none
filt = "iqr"

# Set normalisation, transformation and scaling parameters
# norm options: NULL, SumNorm, MedianNorm, QuantileNorm
# tran options: NULL, LogNorm, CrNorm
# scal options: NULL, MeanCenter, AutoNorm, ParetoNorm, RangeNorm
norm = "MedianNorm"
tran = "LogNorm"
scal = "NULL"

# SET WORKING DIRECTORY #
#Working directory is also where generated files will be saved
setwd(wd)

# INSTALL AND LOAD PACKAGES #
# Pacman for various plotting stuff -- tidyverse for piping (%>%)
pacman::p_load(pacman, rio, tidyverse, tibble)

# Load various libraries that will/might be useful
library(MetaboAnalystR);library(png);library(grid);library(gridExtra); library(ggplot2);
library(plyr); library(dplyr); library(memoise); library(readr)

# READING THE DATAFILE #
#Make the object the data goes into
mSet<-InitDataObjects("pktable", "stat", FALSE)

# Upload file
# Check the Read.TextData() on how to correctly specify data format and label types.
mSet<-Read.TextData(mSet, filnm, "colu", "disc")

# DATA INTEGRITY CHECK AND REPLACE MISSING VALUES #
# Check the data
mSet$msgSet$read.msg
mSet<-SanityCheckData(mSet)
mSet<-ContainMissing(mSet)

# Replace missing data with a minimum value
mSet<-ReplaceMin(mSet)
mSet<-SanityCheckData(mSet)
mSet<-ContainMissing(mSet)

# FILTRATION #
# No data filtration, check FilterVariable() if you want to filter data
mSet<-FilterVariable(mSet, filt, "F", 25)
```

```
# NORMALISATION, SCALING AND TRANSFORMATION #
# Prepare for normalization
mSet<-PreparePrenormData(mSet)

# Normalise, scale and transform det data
mSet<-Normalization(mSet, rowNorm=norm, transNorm=tran, scaleNorm=scal, ratio=FALSE, ratioNum=20)

# Save the processed data as a .csv file, returns 'data_original', 'data_processed', 'data_normalized'
mSet<-SaveTransformedData(mSet)

# READ THE NORMALISED DATA FILE AND TRANSPOSE IF NECESSARY #
# Read the new .csv file -- it should just be in the working directory, so no need to specify location
# dp = processed data
dp<-as.data.frame(read.csv(filsb))
# Change the name of the first column to 'Sample'
colnames(dp)[colnames(dp) == "X"] <- "Sample"

# Now we must check if this file requires transposing or not. File must have data in columns and samples in rows for later sub-setting to work
nm = as.data.frame(names(dp))

if (nm[2,] != "Label"){
  # First, save the compound ion/metabolite names and check that it's correct
  metabo_names<-dp[,1]
  metabo_names<-metabo_names[-c(1)]
  # Second save the sample names
  Sample<-as.data.frame(colnames(dp))
  Sample<-Sample[-c(1),]

  # To avoid row-name issues after transposing, we will add a row of numbers to the top
  # First, make the numbers. Go from 1 to n, n = ncol(dp)
  nrcol <- ncol(dp)
  rf <- as.data.frame(matrix(ncol=nrcol, nrow=1))
  for(i in 1:nrcol) {rf[1,i] = as.character(i)}
  # Rename the columns after the rows, i.e. numbers as characters
  names(rf)<-rf
  # Then we change the column names of dp to match rf, so that they can merge without R throwing a fit
  names(dp) <- names(rf)
  # Finally, save the first row as a data frame, so this can be added back as a column later
  Label<-as.data.frame(t(dp[1,]))
  Label<-Label[-c(1),]

  # Then transpose the data frame, except for the first column
  dp_transpose<- as.data.frame(t((dp[,-1])))
  # Then transform the data to numeric values
  dp_transpose<-data.frame(lapply(dp_transpose[,-1], as.numeric))
  # Add back the correct compound ion/metabolite names and then check to see that the file looks correct
  colnames(dp_transpose)<-metabo_names
  # Add back the column containing "sample" information
  dp_transpose<-cbind(Sample, Label, dp_transpose)

} else {
  # Re-load dp, but such that it doesn't mess up the column names
  dp_transpose<-as.data.frame(read.csv("data_normalized.csv", check.names=FALSE))
  # Change the name of the first column to 'Sample'
```

```
  names(dp_transpose)[1]<-"Sample"
}

# First save how many unique groups there are in the data set
dp_uniq <- unique(dp_transpose$Label)
cnt <- length(dp_uniq)
print(paste("Number of experimental groups is", cnt))

### Output mean and standard deviation for all compounds ###
# Tidy column names of dp_transpose
names(dp_transpose)<- gsub("/", "_", names(dp_transpose))
names(dp_transpose)<- gsub(" ", "_", names(dp_transpose))
names(dp_transpose)<- gsub("-", "_", names(dp_transpose))

# Open a list called Compound
Compound <- c()
#Open a data frame to store all the mean calculations in
dp_ALL_mn <- as.data.frame(t(sort(dp_uniq)))

# Calculate means and then append those as rows to dp_ALL_mn and save compound names in Compound
list
for (i in colnames(dp_transpose[- c(1,2)])){
  # First calculate the mean of each compound for each experimental group
  dp_subset <- subset(dp_transpose, select = c(Sample, Label, get(i)))
  colnames(dp_subset)[3] <- "Compound"
  dp_mn <- ddply(dp_subset, "Label", summarise, mean = mean(Compound),  sd = sd(Compound))
  # Also save the compound name in a separate list
  Compound <- append(Compound, paste0(i, "__mean"))
  Compound <- append(Compound, paste0(i, "__SD"))
  # Transposing dp_mn so that it can be used properly later
  dp_mnt <- as.data.frame(t(dp_mn[,-1]))
  # Then transform the data to numeric values
  dp_mnt<-data.frame(lapply(dp_mnt, as.numeric))

  dp_ALL_mn <- rbind.data.frame(dp_ALL_mn, dp_mnt)
}

# Get labels from top row of dp_ALL_mn, which is the different experimental groups
Label_names <- dp_ALL_mn[1,]
# Rename the summary table with those experimental group names
colnames(dp_ALL_mn)<-Label_names
# Remove the top row, which is now no longer necessary
dp_ALL_mn <- dp_ALL_mn[-1,]
#Append the list Compound as a column, it will now say what compound is in which row
dp_ALL_mn <- cbind(Compound, dp_ALL_mn)

# Write new file
write_csv(dp_ALL_mn, file = filn_ms, append = FALSE, col_names = TRUE)
```

FOLD CHANGE ANS STATISTICAL TESTS

Uses dp_transpose from normalised data output

```
##### SECTION 1: SET VARIABLES #####
# Choose whether you want to calculate fold-change as a ratio (A/B) or as fraction ((A-B)/B)
#"rat" for ratio and "frac" for fraction
clc <- "rat"

# Significance test parameters
# Ls1 is the group you want to compare the groups in Ls2 to -- this can also be a (short) list, then write c("Name of Group 1", ..., "Name of Group2")
# NB! I recommend keeping ls1 to a single group and the running the code again with a different ls1. Too many groups in ls1 will severely slow down the code
ls1 = c("")
# Ls2 are the groups that you want to test relative to ls1, this can be longer (e.g. all the treatment groups)
ls2 <- c("" )

# Identifier to add to the file name for the FDR test output
idF = ""
# Identifier to add to the file name for the Tukey's test output
idT = ""

## FOLD CHANGE CALCULATIONS ##
# Open a list called Compound
Compound <- c()
# Open a data frame to store all the mean calculations in
dp_ALL_mn <- as.data.frame(t(sort(dp_uniq)))

# Calculate means and then append those as rows to dp_ALL_mn and save compound names in Compound list
for (i in colnames(dp_transpose[- c(1,2)])){
  # First calculate the mean of each compound for each experimental group
  dp_subset <- subset(dp_transpose, select = c(Sample, Label, get(i)))
  colnames(dp_subset)[3] <- "Compound"
  dp_mn <- ddply(dp_subset, "Label", summarise, mean = mean(Compound))
  #  Also save the compound name in a separate list
  Compound <- append(Compound, i)

  # Transposing dp_mn so that it can be used properly later
  dp_mnt <- as.data.frame(t(dp_mn[,-1]))
  #Then transform the data to numeric values
  dp_mnt<-data.frame(lapply(dp_mnt, as.numeric))

  dp_ALL_mn <- rbind.data.frame(dp_ALL_mn, dp_mnt)
}

# Get labels from top row of dp_ALL_mn, which is the different experimental groups
Label_names <- dp_ALL_mn[1,]
# Rename the summary table with those experimental group names
colnames(dp_ALL_mn)<-Label_names
# Remove the top row, which is now no longer necessary
dp_ALL_mn <- dp_ALL_mn[-1,]
# Append the list Compound as a column, it will now say what compound is in which row
dp_ALL_mn <- cbind(Compound, dp_ALL_mn)

#Compare each experimental group with another, writing out a .csv file for each group of comparisons
# The for-loop includes an if/else statement calculating either ratios or fractions
```

```
for (m in colnames(dp_ALL_mn[,-1])){
 # Define the group you are comparing to
 Ctr = m

 # Open a new data frame for storing the ratios by pasting in the Compound names; rename the column Compound
 dp_ALL_clc <- as.data.frame(dp_ALL_mn$Compound)
 colnames(dp_ALL_clc)[1] <- "Compound"

 # Calculate ratios or fractions
 if (clc == "rat"){
  #  Loop through dp_ALL_mn and use that to calculate ratios (stored in dp_ALL_clc) of Ctr vs the other experimental groups
  for (n in colnames(dp_ALL_mn[,-1])){
   dp_ALL_clc$ratio <- as.numeric(dp_ALL_mn[[Ctr]])/as.numeric(dp_ALL_mn[[n]])
   comb <- paste("Ratio", paste(Ctr, "/", n, sep = ""), sep = " ")
   names(dp_ALL_clc)[names(dp_ALL_clc) == "ratio"] <- comb
  }
 } else if (clc == "frac"){
  #Loop through dp_ALL_mn and use that to calculate fractions (stored in dp_ALL_clc) of Ctr vs the other experimental groups
  for (n in colnames(dp_ALL_mn[,-1])){
   dp_ALL_clc$ratio <- (as.numeric(dp_ALL_mn[[n]])-as.numeric(dp_ALL_mn[[Ctr]])/as.numeric(dp_ALL_mn[[Ctr]]))
   comb <- paste("Fraction", paste(Ctr, "/", n, sep = ""), sep = " ")
   names(dp_ALL_clc)[names(dp_ALL_clc) == "ratio"] <- comb
  }
 } else {
  print("Define what kind of calculation you want to do (see section 1)")
 }

 # Delete the column containing Ctr/Ctr
 dp_ALL_clc <- dplyr:::select(dp_ALL_clc, -ends_with(Ctr))

 # Save file as .csv
 wd_temp <- wd
 # Save file with Ratio or Fraction in file name, depending on what has been specified
 if (clc == "rat"){
  filnm_temp <- paste("/", "Ratio of ", Ctr, " to other groups", ".csv", sep = "")
 } else if (clc == "frac"){
  filnm_temp <- paste("/", "Fraction of ", Ctr, " to other groups", ".csv", sep = "")
 } else {print("Check that clc has been defined in section 1")}
 wd_temp <- paste(wd_temp, filnm_temp, sep = "")
 write_excel_csv(dp_ALL_clc, wd_temp, delim = ";", append = FALSE, col_names = TRUE)
}
```

```
## TUKEY'S TEST ##
#Open a new data frame to store all of the results
dp_tukey <- setNames(data.frame(matrix(ncol = 10, nrow = 0)), c("Metabolites", "term", "group1",
          "group2", "null.value", "estimate", "conf.low", "conf.high", "p.adj",
          "p.adj.signif"))

# For loop in which Tukey's test is done to binary comparisons, not across the whole data set, to avoid for
"over correction" of p-values
for (g in ls1){
 for (r in ls2){
  if (g == r) next
  # Make a temporary data frame with only two groups
  dp_tmp_filt <- filter(dp_transpose, Label == g | Label == r)

  # Pivot to make a long table with only 3 columns
  dp_long <- dp_tmp_filt %>%
   select(-Sample) %>%
   pivot_longer(-Label, names_to = "Metabolites", values_to = "Value")

  # Tidy up dp_long names
  dp_long <- dp_long %>%
   mutate(across(.cols = Label,
          .fns = ~ str_replace_all(.,
                  pattern = "-",
                  replacement= "."))) %>%
   mutate(across(.cols = Metabolites,
          .fns = ~ str_replace_all(.,
                  pattern = "-",
                  replacement= "_")))

  # Calculate p-values, using Tukey as a multiple comparison correction
  dp_tukey_tmp <- dp_long %>%
   group_by(Metabolites) %>%
   rstatix:::tukey_hsd(Value ~ Label)

  # Remove all of the ns from dp_tukey
  dp_tukey_SDonly <- dp_tukey_tmp %>%
   filter(!str_detect(p.adj.signif, "ns"))

  #Append to dp_tukey, which will hold all of the results in the end
  dp_tukey <- rbind(dp_tukey, dp_tukey_SDonly)
 }
}

# Save the Tukey output as a .csv file
write_csv(dp_tukey, file = idT, append = FALSE, col_names = TRUE)
```

```
# fdr CORRECTED T-TEST
#Open a new data frame to store all of the results
dp_FDR <- setNames(data.frame(matrix(ncol = 11, nrow = 0)),
c("Metabolites",".y.","group1","group2","n1","n2","statistic","df","p","p.adj","p.adj.signif"))

# For-loop
for (g in ls1){
 for (r in ls2){
  if (g == r) next
  # Make a temporary data frame with only two groups
  dp_tmp_filt <- filter(dp_transpose, Label == g | Label == r)

  # Pivot to make a long table with only 3 columns
  dp_long <- dp_tmp_filt %>%
   select(-Sample) %>%
   pivot_longer(-Label, names_to = "Metabolites", values_to = "Value")

  # Tidy up dp_long names
  dp_long <- dp_long %>%
   mutate(across(.cols = Label,
          .fns = ~ str_replace_all(.,
                   pattern = "-",
                   replacement= "."))) %>%
   mutate(across(.cols = Metabolites,
          .fns = ~ str_replace_all(.,
                   pattern = "-",
                   replacement= "_")))

  # Calculate p-values, using Tukey as a multiple comparison correction
  dp_FDR_tmp <- dp_long %>%
   group_by(Metabolites) %>%
   t_test(Value ~ Label) %>%
   adjust_pvalue(method = "fdr") %>%
   add_significance()

  # Remove all of the ns from dp_tukey
  dp_FDR_SDonly <- dp_FDR_tmp %>%
   filter(!str_detect(p.adj.signif, "ns"))

  #Append to dp_tukey, which will hold all of the results in the end
  dp_FDR <- rbind(dp_FDR, dp_FDR_SDonly)
 }
}

# Save the FDR output as a .csv file
write_csv(dp_FDR, file = idF, append = FALSE, col_names = TRUE)
```

LINE PLOTS

Uses dp_transpose from normalised data output

```
## DEFINING COLORS ###
# Before plotting: colour palette must be defined. Everything is in HEX code.
# A list of hex codes and their colour description is given at the very end.
# Palette1: Line colour between points
palette1 <- c("")
# Palette2: Line colour of error bars
palette2 <- c("black")
# Palette3: Point colour, add enough for the number of experimental groups
palette3 <- c("black")
# Palette4: color of grid and frame around plot
palette4 <- c("grey")

### DEFINING PLOT SHAPES ###
# Depending on what you are plotting it can be helpful to define different shapes
# See ggplot2_shapes.png for the numbers and corresponding shapes
# NB! You must provide the same number of defined shapes as you have experimental groups
# Swap out the numbers between the brackets of c()
shp = c()
# Data point size
psz=1
# Line width between points
lsz=0.75
# Line width of error bars
eblsz=0.5

### DEFINING FONT, FONT SIZE AND OTHER PLOT PARAMETERS ###
# Defaults/recommendations are given in the supporting document
# Plot title size, font face type (plain, italic, bold, bold.italic) and font type (sans, mono or serif)
tisz=20; tifc="plain"; fnt="sans"
# Title for the y-axis
yti = "Normalised Ion Abundance"
# Title for the x-axis -- here with a unicode for the Greek letter mu
xti = paste0("Time (hours)")
# Plot font size
plsz=16
# DPI/Image resolution
dpisz=300
# xang is angle of data labels on x-axis. Number = degress rotation. Default 0 degree.
# hjx = adjustment of placement of x label, for xang = 0 or 90, hjx = 0.5. For xang = 45, hjx = 1.
xang=45; hjx = 1
# Y-axis minimum (ymi) and maximum (yma). This ensures that all plots are easy to compare. Can use NA
for open ended min/max
ymi=0; yma=NA
# Numeric x-axis? "Y" or "N"
xx = "Y"
# X-axis minimum and maximum
xmi = 20; xma = 100
```

```
# MAKING THE PLOTS #
# The for-loop first makes a sub-setted data frame of a single metabolite/compound ion,
# Then the mean and standard deviation of that is calculated and used to make the plot.
if (xx == "N"){
 for (i in colnames(dp_transpose[- c(1,2)])){
   # Make a sub-setted table of one data column and then calculate mean and standard deviation
   dp_subset <- subset(dp_transpose, select = c(Sample, Label, get(i)))
   colnames(dp_subset)[3] <- 'Compound'
   dp_mn <- ddply(dp_subset, "Label", summarise, mean = mean(Compound), sd = sd(Compound))

   # Plot line and point plot with standard deviation
   p<-ggplot(dp_mn, mapping = aes(x=Label, y=mean, group=1)) +
    geom_line(size=lsz, color=palette1) +
    geom_errorbar(aes(ymin=mean-sd, ymax=mean+sd), width=.2, position=position_dodge(0.05),
size=eblsz, color=palette2) +
    geom_point(aes(shape=Label), size=psz, color=palette3) +
    scale_shape_manual(values=shp)+
    ylim(ymi, yma) +
    theme(
     # Background left blank with grey grid lines and border
     panel.grid.major = element_line(colour = palette4),
     panel.background = element_blank(),
     panel.border = element_rect(colour = palette4, fill = NA, size = 1),

     # x-axis label adjustments
     axis.title.x = element_blank(),
     axis.text.x = element_text(angle=xang, hjust=hjx),

     # Plot title adjustments
     plot.title = element_text(size = tisz, hjust=0.5, face=tifc),

     # Overall text adjustments
     text = element_text(family=fnt, size = plsz),

     # Remove the annoying key box
     legend.position = "none") +

    ggtitle(label=i) +
    ylab(paste(yti, "\n")) +
    xlab(xti)

   # Save the plot as compound_name.png, with dpi specified
   ggsave(paste0(i, ".png"), p, dpi=dpisz)
   }
} else if (xx == "Y"){
 for (i in colnames(dp_transpose[- c(1,2)])){
   # Make a sub-setted table of one data column and then calculate mean and standard deviation
   dp_subset <- subset(dp_transpose, select = c(Sample, Label, get(i)))
   colnames(dp_subset)[3] <- 'Compound'
   dp_mn <- ddply(dp_subset, "Label", summarise, mean = mean(Compound), sd = sd(Compound))
   # Split "Label" into "Label" and "X-axis"/xis
   dp_mn <- dp_mn %>%
    separate(col = Label, into = c("Label", "Time"), sep="_")

   # Plot line and point plot with standard deviation
   p<-ggplot(dp_mn, mapping = aes(x=as.numeric(Time), y=mean, group=Label)) +
    geom_line(size=lsz, color=palette1) +
```

```
    geom_errorbar(aes(ymin=mean-sd, ymax=mean+sd), width=.2, position=position_dodge(0.05),
size=eblsz, color=palette2) +
    geom_point(aes(shape=Label), size=psz, color=palette3) +
    scale_shape_manual(values=shp)+
    ylim(ymi, yma) +
    xlim(xmi, xma) +
    theme(
     # Background left blank with grey grid lines and border
     panel.grid.major = element_line(colour = palette4),
     panel.background = element_blank(),
     panel.border = element_rect(colour = palette4, fill = NA, size = 1),

     # x-axis label adjustments
     axis.title.x = element_blank(),
     axis.text.x = element_text(angle=xang, hjust=hjx),

     # Plot title adjustments
     plot.title = element_text(size = tisz, hjust=0.5, face=tifc),

     # Overall text adjustments
     text = element_text(family=fnt, size = plsz),

     # Remove the annoying key box
     legend.position = "none") +

    ggtitle(label=i) +
    ylab(paste(yti, "\n")) +
    xlab(xti)

  # Save the plot as compound_name.png, with dpi specified
  ggsave(paste0(i, ".png"), p, dpi=dpisz)
  }
}
```

UNTARGETED PATHWAYS ANALTSIS: PREPARATION AND GENERATION OF DATA

```
##### SECTION 1: SET VARIABLES #####
# Fill in the path to the correct folder and NB! You need FORWARD slashes, not backward slashes
wd = ""
# Separator used in .csv files (usually a comma)
sp = ","
# File to be uploaded (must have one column with m/z values (titled m.z) and one with retention time (titled RT))
filnm = " example.csv "
# File name of tidied file (can be same as previous, but that will overwrite the uploaded file and I don't recommend that)
newfilnm = "example_tidy.csv"

## Functional analysis parameters ##
# File name of file used for functional analysis -- e.g. the tidied file newfilnm
filnm2 = "EXAMPLE.csv"

# Mass error of MS instrument used (usually set to 5.0, but lower or higher is fine)
ppm = 5.0
# MS mode: "positive" or "negative"
md = "negative"
# Is the retention time in "seconds" or "minutes" (the assumption is that retention time is included -- the pre-processing of the file ensures that this is easy to include)
RT = "minutes"

# Multiple comparison correct applied: "Y" or "N"
mcc = "N"
# Type of multiple comparison correction applied: "holm","hochberg", "hommel", "bonferroni", "BH", "BY", "fdr"
crr = "fdr"

# Choice of algorithm, mummichog ("mum") or GSEA ("gsea")
alg = "mum"
# P-value cut off (default 0.25 or top 10% of peaks)
pval = 0.05

# Parameters for Peak Set Enrichment Analysis (PSEA)
# Organism library: "hsa_mfn" (default), "hsa_biocyc" and "hsa_kegg" (hsa = human) -- see metaboanalyst.ca for further options.
orgLb = "hsa_mfn"
# Number of metabolites needed to consider a pathway a metabolite set (usual minimum is 3)
minLb = 3
# Number of permutations, standard is 100 (more = slower)
prmNum = 100

# Main group to compare to (e.g. the treatment control)
mngrp = "MUT-Co"
# List of groups you want to compare to the main group (e.g. treated). Can be the remaining ones in allgrp, but needs to be written a second time here please
subgrp <- "WT-Co"
```

```
######################################################################
# SET WORKING DIRECTORY #
# Working directory is also where generated files will be saved
setwd(wd)

# INSTALL AND LOAD PACKAGES #
#Pacman for various plotting stuff -- tidyverse for piping (%>%)
pacman::p_load(pacman, rio, tidyverse, tibble)

# Load various libraries that will/might be useful
library(MetaboAnalystR); library(qpcR); library(tidyr); library(dplyr);
library(stringr); library(fs); library(janitor); library(purrr); library(rstatix)

## PREPARING THE DATAFILE ##
# Read the new .csv file -- it should just be in the working directory, so no need to specify location
# dp = processed data
dp <- as.data.frame(read.csv(filnm, sep = sp))

# Save the m.z and RT columns as a separate data frame to manipulate
smpl <- dp %>% dplyr:::select(m.z, RT)
# Remove any empty rows
smpl <- smpl[complete.cases(smpl), ]
# Swap order of m.z and RT
smpl <- smpl %>% relocate(RT)

# Combine into one column with the correct separation
smpl_tidy <- smpl %>% unite(., col = "Sample", sep = "__")
# Add "Label" in as top row
smpl_tidy <- rbind(data.frame(Sample = "Label"), smpl_tidy)

# Make a new data frame without the singular m.z and RT columns
dp_func <- dp %>%
  dplyr:::select(-(c(m.z, RT)))
# Add in the new column instead
dp_func <- cbind(smpl_tidy, dp_func)
# Print out as a new file
wd_temp <- paste0(wd, "/", newfilnm)
write_csv(dp_func, wd_temp, append = FALSE, col_names = TRUE)

### FUNCTIONAL ANALYSIS ###
# Transpose dp_func so that we can calculate the p-values and test statistics necessary
# Read the new file with normalised data
dp2 <- as.data.frame(read.csv(filnm2, sep = sp))

nm = as.data.frame(names(dp2))
if (nm[2,] != "Label"){
  print("Transposing the data, one sec...")
  #First, save the compound ion/metabolite names and check that it's correct
  metabo_names<-dp2[,1]
  metabo_names<-metabo_names[-c(1)]
  #Second save the sample names
  Sample<-as.data.frame(colnames(dp2))
  Sample<-Sample[-c(1),]

  #To avoid row-name issues after transposing, we will add a row of numbers to the top
  #First, make the numbers. Go from 1 to n, n = ncol(dp)
  nrcol <- ncol(dp2)
```

```
 rf <- as.data.frame(matrix(ncol=nrcol, nrow=1))
 for(i in 1:nrcol) {rf[1,i] = as.character(i)}
 #Rename the columns after the rows, i.e. numbers as characters
 names(rf)<-rf
 #Then we change the column names of dp to match rf, so that they can merge without R throwing a fit
 names(dp2) <- names(rf)
 #Finally, save the first row as a data frame, so this can be added back as a column later
 Label<-as.data.frame(t(dp2[1,]))
 Label<-Label[-c(1),]

 #Then transpose the data frame, except for the first column
 dp_transpose<- as.data.frame(t((dp2[,-1])))
 #Then transform the data to numeric values
 dp_transpose<-data.frame(lapply(dp_transpose[,-1], as.numeric))
 #Add back the correct compound ion/metabolite names and then check to see that the file looks correct
 colnames(dp_transpose)<-metabo_names
 #Add back the column containing "sample" information
 dp_transpose<-cbind(Label, Sample, dp_transpose)

} else {
 #Re-load dp, but such that it doesn't mess up the column names
 dp_transpose<-as.data.frame(read.csv(filnm2, check.names=FALSE, sep = sp))
 Label<-dp[,2]
}


# Make a list of files to be moved
FA.filnms <- c("peaks_to_paths_0_dpi300.png", "mummichog_pathway_enrichment.csv",
"mummichog_matched_compound_all.csv", "Ttest-for-FA.txt")

# Another unholy for-loop in which a binary comparison is done one by one and the results are stored in
separate folders
for (g in mngrp){
 for (r in subgrp){
  if (g == r) next
  # Make a temporary data frame with only two groups
  dp_tmp_filt <- filter(dp_transpose,  Label == g | Label == r)

  # Pivot that data frame (dp_filter) to a long format
  dp_long <- dp_tmp_filt %>%
   dplyr:::select(-Sample) %>%
   pivot_longer(-Label, names_to = "Metabolites", values_to = "Value")

  # Run a t-test
  if(mcc == "N"){
   dp_ttest <- dp_long %>%
    group_by(Metabolites) %>%
    t_test(Value ~ Label)
  } else if(mcc == "Y"){
   dp_ttest <- dp_long %>%
    group_by(Metabolites) %>%
    t_test(Value ~ Label) %>%
    adjust_pvalue(p.col = NULL, output.col = NULL, method = crr)
   dp_ttest <- dp_ttest %>%
    select(-p) %>%
    rename(p = p.adj)}
```

```
  # Tidy up dp_ttest so that it only includes m/z, p-value, t-score (statistic) and retention time.
  # Ranked by p-value
  dp_tidy <- dp_ttest %>%
   select(c(Metabolites, statistic, p)) %>%
   dplyr::rename(p.value = p, t.score = statistic) %>%
   separate(., col = "Metabolites", into = c("m.z", "rt"), sep = "__") %>%
   relocate("rt", .after = last_col()) %>%
   relocate("p.value", .before = t.score) %>%
   arrange(p.value)

  # Write a file that saves this
  filnm.txt = paste0("Ttest-for-FA.txt")
  wd_temp2 <- paste0(wd, "/", filnm.txt)
  write_delim(dp_tidy, wd_temp2, append = FALSE, col_names = TRUE)

  # Now, feed this .txt file back into MetaboANalystR code
  # Initialize the data object
  mSet<-InitDataObjects("mass_all", "mummichog", FALSE)
  mSet<-SetPeakFormat(mSet)
  # Set the "instrument" parameters
  mSet<-UpdateInstrumentParameters(mSet, ppm, md, "yes", 0.02);
  # Load peak list that was just created and sanity check it
  mSet<-Read.PeakListData(mSet, filnm.txt);
  mSet<-SanityCheckMummichogData(mSet)
  # Set the method for peak enrichment, keep v2 because retention time is always included
  mSet<-SetPeakEnrichMethod(mSet, algOpt = alg, "v2")
  # Set p-value cutoff
  mSet<-SetMummichogPval(mSet, pval)
  # Perform Peak Set Enrichment Analysis
  mSet<-PerformPSEA(mSet, orgLb, "current", minLb , prmNum)
  mSet<-PlotPeaks2Paths(mSet, "peaks_to_paths_0_", "png", 300, width=NA)

  # Open new folder to store results in
  wd_tmp3 <- paste0(wd, "/", g, " and ", r, " Functional Analysis")
  dir_create(wd_tmp3)

  # Move the files to the new directory
  for (f in FA.filnms){file_move(path = paste0(wd, "/", f), new_path = paste0(wd_tmp3, "/", f))}
 }
}
```

MATCH EC TO KEGG CODES

```
##### SECTION 1: SET VARIABLES #####
# Fill in the path to the correct folder and NB! You need FORWARD slashes, not backward slashes
wd = "C:/Users/ingvi/OneDrive - Nexus365/RStudio Scripts"

# Pathway enrichment data file name
# NB! Remove any "/" from any of the pathway names (usually "urea cycle/amino group metabolism" that causes an issue)
pth = "mummichog_pathway_enrichment.csv"
# Matched compound data file name
mc = "mummichog_matched_compound_all.csv"
# KEGG compounds list and pathways list
kggcmp = "KEGG codes and names.csv"
kggpth = "KEGG pathways .csv"
# Separator used in the .csv file (, or ;)
sp = ","

#The p-value cut off for which pathways are chosen to match compound names to enriched pathways (using the FET score)
pval = 0.05

########################################################################
##### SECTION 2 #####

# SET WORKING DIRECTORY #
# Working directory is also where generated files will be saved
setwd(wd)

# INSTALL AND LOAD PACKAGES #
#Pacman for various plotting stuff -- tidyverse for piping (%>%)
pacman::p_load(pacman, rio, tidyverse, tibble)

# Load various libraries that will/might be useful
library(MetaboAnalystR); library(qpcR); library(tidyr); library(dplyr); library(stringr)
library(fs); library(janitor); library(purrr); library(rstatix); library(rlist)

## PREPARING THE DATAFILE ##
# Read the new .csv file -- it should just be in the working directory, so no need to specify location
# dp = processed data
dp_pth_tmp <- as.data.frame(read.csv(pth, sep = sp))
dp_mc <- as.data.frame(read.csv(mc, sep = sp))
kg_pth <- as.data.frame(read.csv(kggpth, sep = ","))
kg_cmp <- as.data.frame(read.csv(kggcmp, sep = ","))

# Rename FET to p.val for ease-of-use
dp_pth <- dp_pth_tmp %>%
  dplyr:::rename(p.val = FET, path.name = X)
# Tidy the path.name content to better match the data base later on
dp_pth <- dp_pth %>%
  mutate(across(.cols = path.name,
                .fns = ~ str_replace_all(.,
                                         pattern = " ",
                                         replacement= "."))) %>%
  mutate(across(.cols = path.name,
                .fns = ~ str_replace_all(.,
                                         pattern = ",",
                                         replacement= ".")))
```

```
# Make a subset data frame with one pathway from dp_pth
# Find the pathways below the p-value cut off
dp_pcut <- dp_pth %>%
  dplyr:::select(p.val, path.name) %>%
  filter(p.val < pval) %>%
  mutate(., path.name = str_replace_all(path.name,
                        pattern = "/",
                        replacement= " "))

# Match ECs codes in each pathway with compounds in the mummichog matched compound list
for (m in dp_pcut[["path.name"]]){
  dp_tmp <- dp_pth %>%
    dplyr:::select(path.name, EC.Hits) %>%
    pivot_wider(names_from = path.name, values_from = EC.Hits) %>%
    dplyr:::select(m) %>%
    separate_rows(m, sep = ";")

  # Open a generic data frame with the correct number of columns and column names
  p <- data.frame(matrix(nrow = 1, ncol = ncol(dp_mc)))
  names(p) <- colnames(dp_mc)

  # Now fill that data frame with specific information
  for (v in dp_tmp[[1]]){
    # Use filter() on Empirical.Compound in dp_mc with the information from vec_tmp (i.e. the ECs tied to a
specific pathway)
    dp_sub <- filter(dp_mc, Empirical.Compound == v)
    # Take the rows in dp_sub and bind it to a data frame specifically named after a pathway
    p <- rbind(p, dp_sub)
  }

  # Remove any empty rows
  p <- p[complete.cases(p), ]

  # Save p as a .txt file with the name of the pathway name
  wd_temp <- paste0(wd, "/", "pathway ", m, ".txt")
  write_delim(p, wd_temp, append = FALSE, col_names = TRUE)
}
```